

72nd annual meeting of the Italian society of physiology: New perspectives in physiological research

Edited by

Giovanna Valenti, Fiorenzo Conti, Andrea Gerbino
and Grazia Tamma

Published in

Frontiers in Physiology
Frontiers in Immunology
Frontiers in Medicine
Frontiers in Neuroscience



FRONTIERS EBOOK COPYRIGHT STATEMENT

The copyright in the text of individual articles in this ebook is the property of their respective authors or their respective institutions or funders. The copyright in graphics and images within each article may be subject to copyright of other parties. In both cases this is subject to a license granted to Frontiers.

The compilation of articles constituting this ebook is the property of Frontiers.

Each article within this ebook, and the ebook itself, are published under the most recent version of the Creative Commons CC-BY licence. The version current at the date of publication of this ebook is CC-BY 4.0. If the CC-BY licence is updated, the licence granted by Frontiers is automatically updated to the new version.

When exercising any right under the CC-BY licence, Frontiers must be attributed as the original publisher of the article or ebook, as applicable.

Authors have the responsibility of ensuring that any graphics or other materials which are the property of others may be included in the CC-BY licence, but this should be checked before relying on the CC-BY licence to reproduce those materials. Any copyright notices relating to those materials must be complied with.

Copyright and source acknowledgement notices may not be removed and must be displayed in any copy, derivative work or partial copy which includes the elements in question.

All copyright, and all rights therein, are protected by national and international copyright laws. The above represents a summary only. For further information please read Frontiers' Conditions for Website Use and Copyright Statement, and the applicable CC-BY licence.

ISSN 1664-8714
ISBN 978-2-8325-4783-0
DOI 10.3389/978-2-8325-4783-0

About Frontiers

Frontiers is more than just an open access publisher of scholarly articles: it is a pioneering approach to the world of academia, radically improving the way scholarly research is managed. The grand vision of Frontiers is a world where all people have an equal opportunity to seek, share and generate knowledge. Frontiers provides immediate and permanent online open access to all its publications, but this alone is not enough to realize our grand goals.

Frontiers journal series

The Frontiers journal series is a multi-tier and interdisciplinary set of open-access, online journals, promising a paradigm shift from the current review, selection and dissemination processes in academic publishing. All Frontiers journals are driven by researchers for researchers; therefore, they constitute a service to the scholarly community. At the same time, the *Frontiers journal series* operates on a revolutionary invention, the tiered publishing system, initially addressing specific communities of scholars, and gradually climbing up to broader public understanding, thus serving the interests of the lay society, too.

Dedication to quality

Each Frontiers article is a landmark of the highest quality, thanks to genuinely collaborative interactions between authors and review editors, who include some of the world's best academicians. Research must be certified by peers before entering a stream of knowledge that may eventually reach the public - and shape society; therefore, Frontiers only applies the most rigorous and unbiased reviews. Frontiers revolutionizes research publishing by freely delivering the most outstanding research, evaluated with no bias from both the academic and social point of view. By applying the most advanced information technologies, Frontiers is catapulting scholarly publishing into a new generation.

What are Frontiers Research Topics?

Frontiers Research Topics are very popular trademarks of the *Frontiers journals series*: they are collections of at least ten articles, all centered on a particular subject. With their unique mix of varied contributions from Original Research to Review Articles, Frontiers Research Topics unify the most influential researchers, the latest key findings and historical advances in a hot research area.

Find out more on how to host your own Frontiers Research Topic or contribute to one as an author by contacting the Frontiers editorial office: frontiersin.org/about/contact

72nd annual meeting of the Italian society of physiology: New perspectives in physiological research

Topic editors

Giovanna Valenti — University of Bari Aldo Moro, Italy
Fiorenzo Conti — Marche Polytechnic University, Italy
Andrea Gerbino — University of Bari Aldo Moro, Italy
Grazia Tamma — University of Bari Aldo Moro, Italy

Citation

Valenti, G., Conti, F., Gerbino, A., Tamma, G., eds. (2024). *72nd annual meeting of the Italian society of physiology: New perspectives in physiological research*. Lausanne: Frontiers Media SA. doi: 10.3389/978-2-8325-4783-0

Table of contents

- 05 **Editorial: 72nd annual meeting of the Italian society of physiology: new perspectives in physiological research**
Andrea Gerbino, Grazia Tamma, Fiorenzo Conti and Giovanna Valenti
- 08 **Biological effects of sub-lethal doses of glyphosate and AMPA on cardiac myoblasts**
Elisa Arrigo, Sara Gilardi, Luisa Muratori, Stefania Raimondo and Daniele Mancardi
- 20 **A novel estimate of biological aging by multiple fitness tests is associated with risk scores for age-related diseases**
A. Manca, G. Fiorito, M. Morrone, A. Boi, B. Mercante, G. Martinez, L. Ventura, A. P. Delitala, A. Cano, M. G. Catte, G. Solinas, F. Melis, F. Ginatempo and F. Deriu
- 29 **Alterations of the Ca^{2+} clearing mechanisms by type 2 diabetes in aortic smooth muscle cells of Zucker diabetic fatty rat**
Adriana Moreno-Salgado, Nayeli Coyotl-Santiago, Roberto Moreno-Vazquez, Mayte Lopez-Teyssier, Mario Garcia-Carrasco, Francesco Moccia and Roberto Berra-Romani
- 48 **Mechanisms underlying the anti-aging activity of bergamot (*Citrus bergamia*) extract in human red blood cells**
Alessia Remigante, Sara Spinelli, Elisabetta Straface, Lucrezia Gambardella, Marina Russo, Giovanna Cafeo, Daniele Caruso, Giuseppe Falliti, Paola Dugo, Silvia Dossena, Angela Marino and Rossana Morabito
- 63 **Apoptotic volume decrease (AVD) in A_{549} cells exposed to water-soluble fraction of particulate matter (PM_{10})**
M. E. Giordano, G. Udayan, M. R. Guascito, A. R. De Bartolomeo, A. Carlino, M. Conte, D. Contini and M. G. Lionetto
- 74 **Microglial crosstalk with astrocytes and immune cells in amyotrophic lateral sclerosis**
Matteo Calafatti, Germana Coccozza, Cristina Limatola and Stefano Garofalo
- 86 **Intracellular Ca^{2+} signalling: unexpected new roles for the usual suspect**
Francesco Moccia, Alessandra Fiorio Pla, Dmitry Lim, Francesco Lodola and Andrea Gerbino
- 102 **Intercellular crosstalk mediated by tunneling nanotubes between central nervous system cells. What we need to advance**
D. L. Capobianco, L. Simone, M. Svelto and F. Pisani
- 109 **Restored retinal physiology after administration of niacin with citicoline in a mouse model of hypertensive glaucoma**
Alberto Melecchi, Rosario Amato, Massimo Dal Monte, Dario Rusciano, Paola Bagnoli and Maurizio Cammalleri

- 122 **Restoring autophagic function: a case for type 2 diabetes mellitus drug repurposing in Parkinson's disease**
Marco Greco, Anas Munir, Debora Musarò, Chiara Coppola and Michele Maffia
- 134 **AAPH-induced oxidative damage reduced anion exchanger 1 (SLC4A1/AE1) activity in human red blood cells: protective effect of an anthocyanin-rich extract**
Alessia Remigante, Sara Spinelli, Giuseppe Tancredi Patanè, Davide Barreca, Elisabetta Straface, Lucrezia Gambardella, Giuseppina Bozzuto, Daniele Caruso, Giuseppe Falliti, Silvia Dossena, Angela Marino and Rossana Morabito
- 154 **Autophagy machinery plays an essential role in traumatic brain injury-induced apoptosis and its related behavioral abnormalities in mice: focus on *Boswellia* Sacra gum resin**
Livia Interdonato, Ylenia Marino, Daniela Impellizzeri, Ramona D'Amico, Rosalba Siracusa, Roberta Fusco, Gaetano Cammilleri, Licia Pantano, Sergio Modafferi, Ali S. Abdelhameed, Tilman Fritsch, Luay J. Rashan, Salvatore Cuzzocrea, Vittorio Calabrese, Marika Cordaro and Rosanna Di Paola



OPEN ACCESS

EDITED AND REVIEWED BY

Geoffrey A. Head,
Baker Heart and Diabetes Institute, Australia

*CORRESPONDENCE

Andrea Gerbino,
✉ andrea.gerbino@uniba.it

RECEIVED 19 March 2024

ACCEPTED 25 March 2024

PUBLISHED 05 April 2024

CITATION

Gerbino A, Tamma G, Conti F and Valenti G (2024), Editorial: 72nd annual meeting of the Italian society of physiology: new perspectives in physiological research.
Front. Physiol. 15:1403715.
doi: 10.3389/fphys.2024.1403715

COPYRIGHT

© 2024 Gerbino, Tamma, Conti and Valenti. This is an open-access article distributed under the terms of the [Creative Commons Attribution License \(CC BY\)](#). The use, distribution or reproduction in other forums is permitted, provided the original author(s) and the copyright owner(s) are credited and that the original publication in this journal is cited, in accordance with accepted academic practice. No use, distribution or reproduction is permitted which does not comply with these terms.

Editorial: 72nd annual meeting of the Italian society of physiology: new perspectives in physiological research

Andrea Gerbino^{1*}, Grazia Tamma¹, Fiorenzo Conti² and Giovanna Valenti¹

¹Department of Biosciences, Biotechnologies and Environment, Università di Bari Aldo Moro, Bari, Italy,

²Section of Neuroscience and Cell Biology, Department of Experimental and Clinical Medicine, Università Politecnica delle Marche, Ancona, Italy

KEYWORDS

autophagy, aging, Ca²⁺ signaling, herbal extracts, intercellular signaling, oxidative stress

Editorial on the Research Topic

72nd Annual meeting of the Italian society of physiology: new perspectives in physiological research

The 72nd Annual Meeting of the Italian Society of Physiology, held in Bari in September 2022, provided a vibrant platform for the convergence of leading physiologists, fostering interdisciplinary dialogue, and paving the way for innovative research directions. This Research Topic encompasses a diverse array of topics that emerged from the rich texture of discussions and presentations at the conference. Gathering insights from esteemed researchers across Italy, the Research Topic delves into groundbreaking studies that shed light on various facets of physiological research. Covering a spectrum of themes ranging from cell physiology to neurobiology and cardiovascular health, each article offers a unique perspective, contributing to the collective understanding of complex biological processes.

In exploring novel therapeutic approaches for neurological disorders, the spotlight on autophagy emerges as a promising avenue. Traumatic brain injury (TBI) poses significant challenges in treatment, often leaving limited options due to its complex pathophysiology. However, recent investigations into the role of autophagy machinery, particularly in post-TBI neuronal responses, shed light on potential interventions. Boswellia Sacra gum resin (BSR) emerges as a notable candidate, exhibiting modulatory effects on neuronal autophagy and demonstrating substantial improvements in functional recovery within a mouse model of TBI (Interdonato et al.). This aligns with a broader narrative within the field of neurodegenerative diseases, notably Parkinson's disease (PD), where a repurposing strategy involving Type 2 Diabetes Mellitus (T2DM) drugs gains support. The interplay between T2DM and PD pathogenesis, marked by disruptions in autophagic processes, underscores the therapeutic potential of antidiabetic medications (Greco et al.). By restoring autophagic function, these drugs offer a glimmer of hope in mitigating neurodegenerative processes and enhancing neuronal resilience. Thus, the convergence of research efforts in different fields highlights the pivotal role of autophagy modulation in addressing multifaceted challenges within the complex scenario of neurological disorders. As the population ages, the incidence of neurological diseases tends to increase. This demographic

trend underscores the importance of developing accurate and reliable instruments for monitoring individual health, particularly among the elderly. A recent study developed a composite measure of fitness status based on multiple tests, including the six-minute walking test. Data from eight fitness tests were collected from 176 participants aged 51–80. The newly developed biomarker for biological aging showed strong associations with cardiovascular risk scores and mortality predictions, outperforming previous methods (Manca et al.). This approach has potential for clinical screening and monitoring but requires further validation.

Exploring the therapeutic potential of botanical extracts and dietary supplements unveils a compelling narrative in addressing various health challenges. An anthocyanin-rich fraction extracted from *Callistemon citrinus* flowers emerges as a protective shield against oxidative stress-induced damage in human red blood cells (RBCs). By preserving RBC morphology and anion exchanger 1 (band 3, SLC4A1/AE1) activity, this extract underscores the importance of dietary interventions in fighting oxidative stress-related pathologies (Remigante et al.). Similarly, niacin combined with citicoline demonstrates promise in restoring retinal physiology preventing retinal ganglion cell loss, offering a glimmer of hope in the management of hypertensive glaucoma (Melecchi et al.). Furthermore, bergamot extract emerges as a potent anti-aging agent, exhibiting profound effects on human RBCs exposed to D-Galactose-induced aging (Remigante et al.). Through its multifaceted antioxidant and metabolic regulatory properties, bergamot extract holds potential in mitigating age-related changes, thus presenting a novel avenue in anti-aging therapeutics. Collectively, these findings underscore the burgeoning interest in harnessing the therapeutic power of botanical extracts and dietary supplements in addressing a spectrum of health disorders.

Resolving the intricate web of cellular communication unveils a captivating narrative in understanding disease pathogenesis and therapeutic interventions. In the context of neurodegenerative disorders like Amyotrophic Lateral Sclerosis (ALS), the crosstalk between microglia, astrocytes, and infiltrating immune cells emerges as a pivotal player in shaping the neuroinflammatory milieu (Calafatti et al.). By orchestrating a pro-inflammatory microenvironment, this intricate interplay exacerbates neuronal damage, further fueling disease progression. Meanwhile, tunneling nanotubes (TNTs) offer a novel avenue for long-range intercellular communication within the central nervous system (CNS), yet this area remains largely unexplored (Capobianco et al.). Serving as conduits for the exchange of small signals and large cargo between CNS cells, TNTs redefine our understanding of cellular interactions in controlling CNS functions. As we delve deeper into these intercellular dialogues, new therapeutic strategies aiming to modulate microglial phenotypes and restore CNS homeostasis are on the horizon, holding promise in mitigating neurodegenerative processes and improving patient outcomes.

The deleterious impact of environmental pollutants on human health is a growing concern, with airborne particulate matter less than 10 μm in size (PM 10) emerging as a significant risk factor. Investigations into the cellular mechanisms underlying PM-induced cytotoxicity shed light on its role in triggering apoptotic volume decrease (AVD), a hallmark of early apoptosis, in A549 pulmonary cells (Giordano et al.). Furthermore, chronic exposure to glyphosate,

a common herbicide, and its metabolite AMPA, raises questions about their potential cardiovascular effects. Studies elucidating the biological effects of sub-lethal doses of these agrochemicals on H9c2 cardiac myoblasts uncover a complex interplay between these agrochemicals and cytotoxicity (reduction in cell viability, increased ROS production, morphological alterations, and mitochondrial dysfunction), highlighting the need for further research to inform regulatory policies and public health interventions (Arrigo et al.).

Finally, the dynamic orchestration of intracellular signaling pathways lies at the heart of cellular function and disease pathogenesis. Despite decades of research, the spatiotemporal analysis of Ca^{2+} signaling events continues to surprise, revealing previously unexplored facets of cellular function. The experimental exploitation of classic and newly developed genetically encoded fluorescent probes is opening new windows, shedding light on unexpected roles for this ubiquitous ion (Moccia et al.). Recent investigations have elucidated four such roles: 1) the transient receptor potential mucolipin 1 (TRPML1) channel plays a crucial role in modulating water reabsorption in the kidney; 2) dysregulation of endoplasmic reticulum-to-mitochondria Ca^{2+} transfer contributes to astroglial dysfunction in Alzheimer's Disease; 3) TRP Melastatin 8 (TRPM8) plays a non-canonical role as a Rap1A inhibitor in cancer progression; and 4) non-genetic optical stimulation might serve as a new tool to enable precise manipulation of Ca^{2+} signals in cardiovascular function. In addition, investigations into the effects of Type 2 Diabetes Mellitus (T2DM) on vascular smooth muscle cells (VSMCs) have uncovered significant alterations in intracellular Ca^{2+} handling (Moreno-Salgado et al.). Studies conducted in Zucker Diabetic Fatty rats have shown that T2DM leads to decreased Ca^{2+} release from the sarcoplasmic reticulum (SR) and increased activity of store-operated channels (SOCs) in VSMCs. Furthermore, enhanced cytosolic Ca^{2+} activity during the early stage of ATP-induced Ca^{2+} transient decay, along with alterations in the activity of Ca^{2+} extrusion mechanisms, suggests a potential link between dysregulated Ca^{2+} homeostasis in VSMCs and vascular dysfunction associated with T2DM.

As we navigate the ever-expanding landscape of physiological research, it is essential to acknowledge the collaborative efforts of scientists, clinicians, and educators driving scientific innovation forward. The 72nd Annual Meeting of the Italian Society of Physiology exemplifies the spirit of inquiry and collaboration that fuels progress in biomedical sciences. We extend our heartfelt gratitude to all the authors, reviewers, and contributors who have made this Research Topic possible.

In conclusion, this Research Topic serves as a demonstration to the boundless curiosity and collective endeavor of the scientific community. May the discoveries unveiled within these pages inspire future generations of physiologists and propel us closer to unraveling the mysteries of human biology and health.

Author contributions

AG: Writing—original draft, Writing—review and editing. GT: Writing—original draft, Writing—review and editing. FC: Writing—original draft, Writing—review and editing. GV: Writing—original draft, Writing—review and editing.

Funding

The author(s) declare that no financial support was received for the research, authorship, and/or publication of this article.

Conflict of interest

The authors declare that the research was conducted in the absence of any commercial or financial relationships that could be construed as a potential conflict of interest.

The author(s) declared that they were an editorial board member of Frontiers, at the time of submission. This had no impact on the peer review process and the final decision.

Publisher's note

All claims expressed in this article are solely those of the authors and do not necessarily represent those of their affiliated organizations, or those of the publisher, the editors and the reviewers. Any product that may be evaluated in this article, or claim that may be made by its manufacturer, is not guaranteed or endorsed by the publisher.



OPEN ACCESS

EDITED BY

Andrea Gerbino,
University of Bari Aldo Moro, Italy

REVIEWED BY

Teresa Soda,
University Magna Graecia of Catanzaro,
Italy
Zaid Altaany,
Yarmouk University, Jordan

*CORRESPONDENCE

Daniele Mancardi,
✉ daniele.mancardi@unito.it
Elisa Arrigo,
✉ elisa.arrigo@unito.it

RECEIVED 14 February 2023

ACCEPTED 10 April 2023

PUBLISHED 24 April 2023

CITATION

Arrigo E, Gilardi S, Muratori L, Raimondo S
and Mancardi D (2023), Biological effects
of sub-lethal doses of glyphosate and
AMPA on cardiac myoblasts.
Front. Physiol. 14:1165868.
doi: 10.3389/fphys.2023.1165868

COPYRIGHT

© 2023 Arrigo, Gilardi, Muratori,
Raimondo and Mancardi. This is an open-
access article distributed under the terms
of the [Creative Commons Attribution
License \(CC BY\)](#). The use, distribution or
reproduction in other forums is
permitted, provided the original author(s)
and the copyright owner(s) are credited
and that the original publication in this
journal is cited, in accordance with
accepted academic practice. No use,
distribution or reproduction is permitted
which does not comply with these terms.

Biological effects of sub-lethal doses of glyphosate and AMPA on cardiac myoblasts

Elisa Arrigo^{1*}, Sara Gilardi¹, Luisa Muratori^{1,2}, Stefania Raimondo^{1,2}
and Daniele Mancardi^{1*}

¹Department of Clinical and Biological Sciences, University of Torino, Turin, Italy, ²Neuroscience Institute Cavalieri Ottolenghi (NICO), University of Torino, Turin, Italy

Introduction: Glyphosate is the active compound of different non-selective herbicides, being the most used agriculture pesticide worldwide. Glyphosate and AMPA (one of its main metabolites) are common pollutants of water, soil, and food sources such as crops. They can be detected in biological samples from both exposed workers and general population. Despite glyphosate acts as inhibitor of the shikimate pathway, present only in plants and some microorganisms, its safety in mammals is still debated. Acute glyphosate intoxications are correlated to cardiovascular/neuronal damages, but little is known about the effects of the chronic exposure.

Methods: We evaluated the direct biological effects of different concentrations of pure glyphosate/AMPA on a rat-derived cell line of cardiomyoblasts (H9c2) in acute (1–2 h) or sub-chronic (24–48 h) settings. We analyzed cell viability/morphology, ROS production and mitochondrial dynamics.

Results: Acute exposure to high doses (above 10 mM) of glyphosate and AMPA triggers immediate cytotoxic effects: reduction in cell viability, increased ROS production, morphological alterations and mitochondrial function. When exposed to lower glyphosate concentrations (1 μ M–1 mM), H9c2 cells showed only a slight variation in cell viability and ROS production, while mitochondrial dynamic was unvaried. Moreover, the phenotype was completely restored after 48 h of treatment. Surprisingly, the sub-chronic (48 h) treatment with low concentrations (1 μ M–1 mM) of AMPA led to a late cytotoxic response, reflected in a reduction in H9c2 viability.

Conclusion: The comprehension of the extent of human exposure to these molecules remains pivotal to have a better critical view of the available data.

KEYWORDS

AMPA, ROS, cardiac myoblasts, mitochondria, glyphosate, H9c2

1 Introduction

Glyphosate [IUPAC name N-(phosphonomethyl) glycine] is a synthetic phosphonic amino derivative of glycine, which disrupts the shikimate pathway by inhibiting the activity of 5-enolpyruvylshikimate-3-phosphatase (EPSP) synthase. This metabolic pathway is used by plants and several microorganisms for the biosynthesis of folate and aromatic aminoacids (Bai and Ogbourne, 2016). Glyphosate (Gly) is the active compound of a large part of non-selective herbicidal (glyphosate-based herbicidal, GBHs), being the most used worldwide since middle 70s (Torretta et al., 2018).

Gly is absorbed through leaves and stems and it is transported from roots to edible parts (Tong et al., 2017). In agriculture, genetically modified Gly-resistant crops (as soybean, cotton, corn, etc.) are extensively used and, because of their resistance they accumulate Gly at high concentrations (Xu et al., 2019). Once applied, Gly undergoes degradation mainly by a process known as mineralization, which leads to different byproducts, with aminomethyl phosphonic acid (AMPA) as the main metabolite. The kinetic of this mechanism is highly dependent on soil pH and minerals concentration. Other processes that determine Gly fate are immobilization and leaching: the first one leads to soil adsorption/accumulation, while the second results in water contamination (Bai and Ogbourne, 2016). Gly and AMPA are highly soluble in water and their persistence is variable depending on water conditions with half-lives ranging from few days to several weeks (Tomlin, 2009; Grandcoin et al., 2017; ATSDR, 2020; Goncalyes et al., 2020). In soil, Gly and AMPA accumulate with a discrete persistence with half-lives depending on factors such as pH, salinity, microbial composition, spanning from few days up to about a year (Bai and Ogbourne, 2016; Bento et al., 2016; Domínguez et al., 2016; Grandcoin et al., 2017; ATSDR, 2020).

Given the massive use of GBHs, Gly and AMPA are frequently detected in different water and food samples and classified as pollutants (Bai and Ogbourne, 2016; Bonansea et al., 2017; Silva et al., 2018; Xu et al., 2019; Okada et al., 2020; Marques et al., 2021; Pelosi et al., 2022). The constant presence represents not only an ecological burden but also a potential indirect threat to both animal and human health. Gly and AMPA were, in fact, found in urines of both occupationally or para-occupationally exposed workers (from 0.26 to 73.5 µg/L) and in general population (from 0.16 to 7.6 µg/L) (Krüger et al., 2014; Niemann et al., 2015; Gillezeau et al., 2019; Perry et al., 2019; Mesnage et al., 2022a). Indeed, this type of report suffers from inconstant technical approaches that fail to allow a reliable comparison, mostly because the available studies are based on very different methodologies for Gly and AMPA quantification (gas chromatography, liquid chromatography or ELISA) (Valle et al., 2019). Liquid chromatography is the elective analytical technique for glyphosate determination because of its flexibility and availability in different types of laboratories. This technique can be coupled with different detector types (i.e., ultraviolet-visible, fluorescence, mass spectrometry, etc.) many of which are applicable to Gly quantification. Every technique needs various degrees of technical skills to be performed and requires substantially different investments, and each of them can reach different levels of sensitivity (Moldovan et al., 2023). Hence, more accurate and standardized procedures are needed to reliable and repeatable measurements of Gly and AMPA concentration in biological samples and, therefore, an accurate evaluation of exposure extent.

Despite its selective mechanism of action, Gly has been proven to have either acute or chronic toxicity in different off-target non-mammals animal species, such as amphibians, annelids, arthropods, fishes and birds (Antón et al., 1994; Contardo-Jara et al., 2009; Roy et al., 2016; Gill et al., 2018; Jin et al., 2018). However, these effects were more severe when animals were exposed to Gly formulation than the molecule alone, suggesting that the adjuvants (such as surfactants) act in synergy, amplifying the toxicity.

As of today, the safety of Gly in mammals is still under debate. Acute intoxications due to GBHs ingestion are reported to strongly affect cardiovascular system (Bradberry et al., 2004; Gress et al., 2015;

Brunetti et al., 2020; Hu et al., 2021), as well as to cause gastrointestinal and respiratory symptoms, hypotension and consciousness alteration (Lee et al., 2000; Bradberry et al., 2004); however, these effects are due to very high levels of Gly and adjuvants and are in line with accidental intake and does not reflect the low, although daily, exposure of the general population. The long-term effects of a chronic exposure to Gly and AMPA are not clear. Some *in vitro* studies on different mammalian cell lines showed Gly (or its formulations) to be genotoxic (Benachour and Séralini, 2009; Martini et al., 2012; Mesnage et al., 2013; Townsend et al., 2017; Santovito et al., 2018; Mesnage et al., 2022b), cytotoxic (Townsend et al., 2017; Vanlaeys et al., 2018; Hao et al., 2020; Martínez et al., 2020) and reprotoxic (Gasnier et al., 2009; Clair et al., 2012; De Liz Oliveira Cavalli et al., 2013; Anifandis et al., 2017; Stur et al., 2019; Hao et al., 2020; Jarrell et al., 2020; Cao et al., 2021; Mohammadi et al., 2022). Gly toxicity is usually associated with oxidative stress, dysfunctional mitochondria dynamics and bioenergetics. The sensibility to Gly seems to be cell specific; only few studies demonstrated Gly toxicity in concentrations below the human Acceptable Daily Intake (1.0 mg/kg) (Santovito et al., 2018) and not related to the adjuvants present in its formulations.

In the present work, we evaluate the direct biological effects of different concentrations of pure Gly or AMPA on a rat-derived immortalized cell line of cardiomyoblasts (H9c2), recognized as a valuable tool for investigating *in vitro* effect of toxic factors on myocardial and muscle-skeletal immortalized cells (Branco et al., 2015; Boulefour et al., 2021; Onódi et al., 2022).

In the first part of the study, we simulated an acute exposure to high levels (10–20 mM) of Gly or AMPA. We eventually shifted to lower concentrations (1 µM–1 mM) in order to identify a sub-lethal range to mimic the biological effects of acute and sub-chronic treatments. We evaluated changes in cell viability, morphology, ROS production and mitochondrial distribution and mass.

2 Materials and methods

2.1 Solutions & reagents

MTT (3-(4,5-dimethylthiazol-2-yl)-2,5-diphenyl-2H-tetrazolium) bromide), Glyphosate, AMPA (amino methyl phosphonic acid), DCF-DA (2,2'-dichlorofluorescein diacetate), NAC (N-Acetyl cysteine) were purchased from Sigma-Aldrich.

2.1.1 MTT

The solution was freshly prepared the day of the experiment by dissolving 5 mg/mL of powder in sterile Phosphate Buffered Saline (PBS—Sigma Aldrich).

2.1.2 Glyphosate, AMPA and NAC

Stock solutions were freshly made the day of the experiments by dissolving the powder in serum-free cell culture medium. Then, stock solutions were diluted in complete cell culture medium to reach the working concentrations.

2.1.3 DCF-DA

Stock solution was made by dissolving the powder in sterile dimethyl sulphoxide (DMSO—Sigma-Aldrich) and stored at −20°C,

in the dark. Stock solution was diluted in sterile PBS with $\text{Ca}^{2+}/\text{Mg}^{2+}$ to reach the working concentration.

2.2 Cell culture

H9c2 cells (ATCC® CRL-1446™) were purchased from Sigma-Aldrich. Cell culture was performed in Dulbecco's Modified Eagle's Medium (DMEM) with phenol red (Sigma-Aldrich) supplemented with 10% Fetal Bovine Serum (FBS - Sigma-Aldrich), 1% 200 mM L-Glutamine (Microgem), 1% penicillin/streptomycin (Sigma-Aldrich) at 37°C, 5% CO_2 , 25% O_2 . Cells were split at 80% confluence.

2.3 Cell viability

H9c2 cells were seeded in 96-well plates at 5×10^4 cells/well and kept in incubator 24 h. Then, cells were starved O/N in DMEM 2% FBS and treated with different Gly or AMPA concentrations for different times. When necessary, cells were pretreated 1 h with NAC (100 μM). After the treatments, the medium was replaced, 10 μl MTT were added to each well and the plates were incubated 3 h at 37°C. Then, medium was discarded and the purple formazan crystals were dissolved in 100 μl DMSO. The optical density was measured in a microplate reader (Model 680—BioRad) at 570 nm. The experiment was performed on technical and biological triplicates.

2.4 Morphology

Cells were plated into Petri dishes and kept in complete medium for 24 h to allow cell adhesion. After the desired confluence (70%–90%) was reached, samples were treated with 10 or 20 mM of glyphosate or AMPA for 24 h (t24) or kept in culture medium. After the treatments, cells were washed with warm sterile PBS with $\text{Ca}^{2+}/\text{Mg}^{2+}$ and medium was replaced with a fresh one. All samples were observed under an optical microscope (Axiovert 200—Zeiss) at t0 or t24 with a 63X lens. Images were acquired through Infinity Analyze Software (Lumenera Corporation). At least five fields/sample have been analyzed. The experiment was performed on technical triplicates.

2.5 Transmission electron microscopy

H9c2 cells were plated into Petri dishes and kept in culture until reaching 80% confluence. Then, cells were treated with Gly 10 mM for 1 h or kept in culture medium (Control). Cells were gently washed with warm sterile PBS without $\text{Ca}^{2+}/\text{Mg}^{2+}$, detached with trypsin/EDTA 0.05%/0.02% (PAN Biotech), collected in tubes and centrifuged 5' at 3000 rpm. Supernatant was discarded and pellet was fixed in 1% paraformaldehyde (Merck, Darmstadt, Germany), 1.25% glutaraldehyde (Fluka, St Louis, MO, United States) and 0.5% saccharose in 0.1 M Sörensen phosphate buffer (pH 7.2) for 2 h. For resin embedding, samples were post-fixed in 2% osmium tetroxide (SIC, Società Italiana Chimici) for 2 h and dehydrated in ethanol (Sigma Aldrich) from 30% to 100% (5 min each passage). After two

passages of 7 min in propylene oxide, one passage of 1 h in a 1:1 mixture of propylene oxide (Sigma Aldrich) and Glauert's mixture of resins, samples were embedded in Glauert's mixture of resins (made of equal parts of Araldite M and the Araldite Harter, HY 964, Sigma Aldrich). In the resin mixture, 0.5% of the plasticizer dibutyl phthalate (Sigma Aldrich) was added. For the final step, 2% of accelerator 964 was added to the resin in order to promote resin polymerization at 60°C. Ultra-thin serial sections (70 nm thick) were cut using an Ultracut UCT ultramicrotome (Leica Microsystems, Wetzlar, Germany), stained with a solution of 4% UAR-EMS uranyl acetate replacement in distilled water and analysed using a JEM-1010 transmission electron microscope (JEOL, Tokyo, Japan) equipped with a Mega-View-III digital camera and a Soft-Imaging-System (SIS, Münster, Germany) for computerized acquisition of the images.

For mitochondria quantification, 4 ultra-thin sections 50 μm distant each other were considered for each experimental group with a magnification of 30000X. A total of 50 cells for experimental group were analysed and the number of impaired and unimpaired mitochondria was estimated in % based on their morphological features such as the shape of mitochondria, the morphology of the cristae and evidence of swelling.

2.6 ROS measurements

DCFH-DA is a non-fluorescent molecule permeable to cells. It is hydrolyzed at the intracellular level in dichlorofluorescein (DCFH), which is retained in the cell as it is no longer able to cross cell membranes. In the presence of H_2O_2 , DCFH is oxidized forming the highly fluorescent DCF.

4×10^3 cells/well were seeded in 96-well plates and kept in incubator O/N to allow adhesion. Cells were treated with different concentrations of Gly or AMPA for 1 or 2 h. After the treatments, cells were gently washed two times with warm PBS with $\text{Ca}^{2+}/\text{Mg}^{2+}$. 100 μl /well of 10 μM DCF-DA were added and the plates were incubated for 45 min at 37°C, covered by an aluminum foil. Cells were washed two times with warm PBS with $\text{Ca}^{2+}/\text{Mg}^{2+}$. The fluorescence intensity was measured at the wavelengths ex: 485 nm and em: 535 nm with a microplate reader (Infinite 200—Tecan). The experiment was performed on technical and biological triplicates. A control lane with only cells (NO DCF) was always included to subtract cellular auto-fluorescence.

2.7 Mitochondrial staining

MitoTracker Green FM™ (MTG—Thermo Fisher) is a fluorescent probe, which stains mitochondria independently from their metabolic activity.

5×10^3 cells/well were plated in 24-well plates in complete DMEM and kept O/N in the incubator. Cells were washed with sterile warm PBS with $\text{Ca}^{2+}/\text{Mg}^{2+}$ and treated with different concentrations of Gly or AMPA for 2 or 24 h. After the treatments, cells were gently washed with sterile warm PBS with $\text{Ca}^{2+}/\text{Mg}^{2+}$. 100 nM MTG was added to each well and plates were incubated 30' in the dark at 37°C. Samples were washed with warm sterile PBS with $\text{Ca}^{2+}/\text{Mg}^{2+}$ and observed under a fluorescence microscope (Axiovert 200—Zeiss) with a $\times 40$ magnification lens.

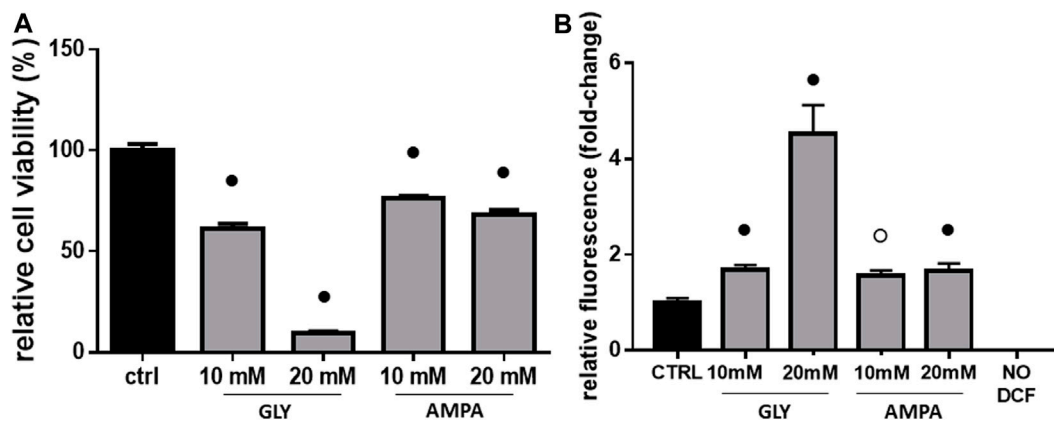


FIGURE 1

Cell viability & ROS production. The figure shows the relative histograms obtained from: (A) MTT and (B) DCF-DA assays. H9c2 cells were treated with 10 or 20 mM of glyphosate (GLY) or AMPA for 2 h. After the treatments, cell viability and ROS production were assessed, respectively, through MTT and DCF-DA assays. Mean \pm SD; p -values: ○ < 0.0005; ● < 0.001 vs. control. NO DCF: control lane without the fluorescent probe.

Images were acquired through Infinity Analyze Software (Lumenera Corporation) with a resolution of 480 × 360 pixels. At least five fields/sample have been analyzed. The experiment was performed on technical triplicates.

2.8 Statistical and computer analysis

Statistical analysis was performed using Graphpad Prism Software® (version 9.00, GraphPad Software). Data are expressed as a mean \pm SD. The differences between the groups were analyzed through statistical tests: ANOVA, one-way or two-way, or Kruskal-Wallis or Mann-Whitney t -test. Statistical significance has been set at $p < 0.05$.

3 Results

3.1 Effects of high doses of glyphosate and AMPA—Acute exposure

In order to evaluate whether an acute exposure to Gly or AMPA determines changes in cell viability in our cell model, we performed an MTT assay.

After 2 h, Gly treatment diminished H9c2 viability in a concentration-dependent manner, with the most dramatic effect given by the highest dose. As shown in Figure 1, 10 and 20 mM treatment determined, respectively, 30% and 90% decrease in cell viability (Figure 1A). At equal doses, AMPA decreased cell viability from 20% to 30% (Figure 1A).

In light of the observed cytotoxic effects and considering that Gly, in the literature, is often associated with oxidative stress (Sardão et al., 2009; Kwiatkowska et al., 2014; Anifandis et al., 2017; Burchfield et al., 2019; Cao et al., 2021), we performed ROS measurements on H9c2 cells.

At 10 mM, there was a slight increase in ROS production compared to the control, without substantial differences between Gly and AMPA

groups (Figure 1B). Treatment with 20 mM of Gly, instead, determined a 4-fold increase in ROS production (Figure 1B), which can explain the dramatic loss in cell viability (Figure 1A). This potent effect was not observed in 20 mM AMPA treated group, which ROS levels are comparable to 10 mM one (Figure 1B).

After 24 h (t24), signs of membrane blebbing and cell shrinkage are still present in Gly-treated group (Figure 2, bottom panels); many rounded and floating cells were clearly visible in the plates at 20 mM, together with strong signs of cytoplasmic cavitation. The same morphological alterations were not observed in AMPA treated group (Figure 2, bottom panels).

After analysis of phenotypical changes (Figures 1, 2), additional MTT and DCF-DA assays were performed in a shorter time-range, focusing on 10 mM Gly treatment, which effects were not too deleterious on the selected cell model.

Interestingly, cell viability did not change when comparing 1 h and 2 hours-treatment groups (Figure 3A), while ROS production was significantly higher after 1 h (Figure 3B), confirming an early response of H9c2 cells to these levels of Gly exposure.

As additional confirmation, both a decrease in cell viability (\approx 20%, Figure 4A) and an increase in ROS production (\approx 1.5 fold-change, Figure 4B) were significant in H9c2 cells already after 5 min of 10 mM Gly. However, the most appreciable effect was reached after 1 h (Figures 3, 4).

Given the significant and rapid production of ROS, an involvement of Gly-driven mitochondrial functional impairment was postulated. Therefore, H9c2 cells were treated with Gly 10 mM for 1 h and analyzed using transmission electron microscopy. The morphology of mitochondria was further investigated by transmission electron microscopy that allowed to access healthy mitochondria with intact double membrane structure, cristae and cristae space easily detectable in the control group (Figures 5A, C); several swollen mitochondria without cristae, instead, are detected in Gly-treated group (Figures 5B, D). Furthermore, the number of perinuclear mitochondria was quantified. We determined two populations: 1) “healthy mitochondria” (HM) showing normal morphology, cristae structure and intact membrane; 2) “damaged

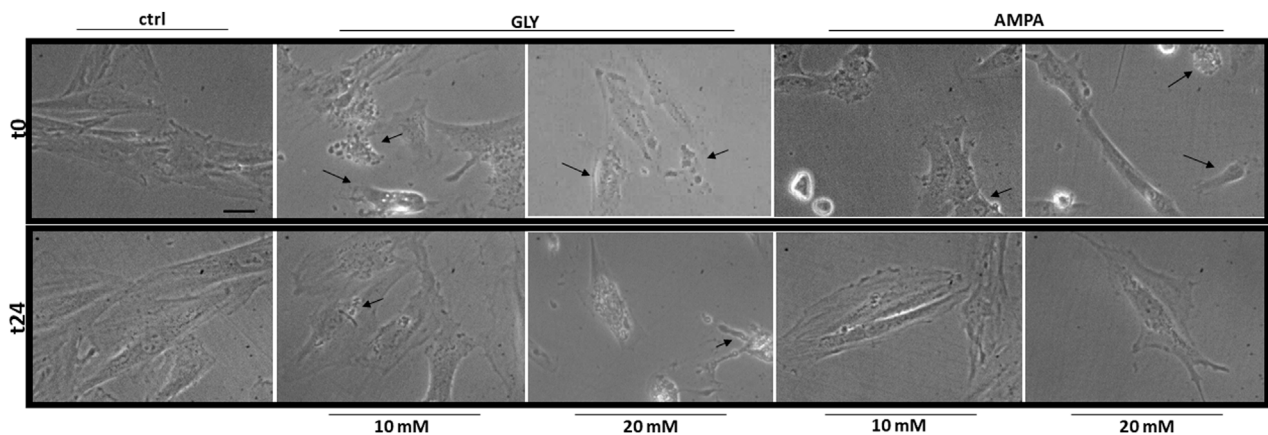


FIGURE 2

Morphology. The figure shows representative fields of H9c2 cells treated with 10 or 20 mM of glyphosate (GLY) or AMPA for 24 h. Images were acquired through a camera connected to an inverted microscope at the start (t0—top panels) and at the end (t24—bottom panels) of the treatments with a 63X lens (scale bar = 10 μm).

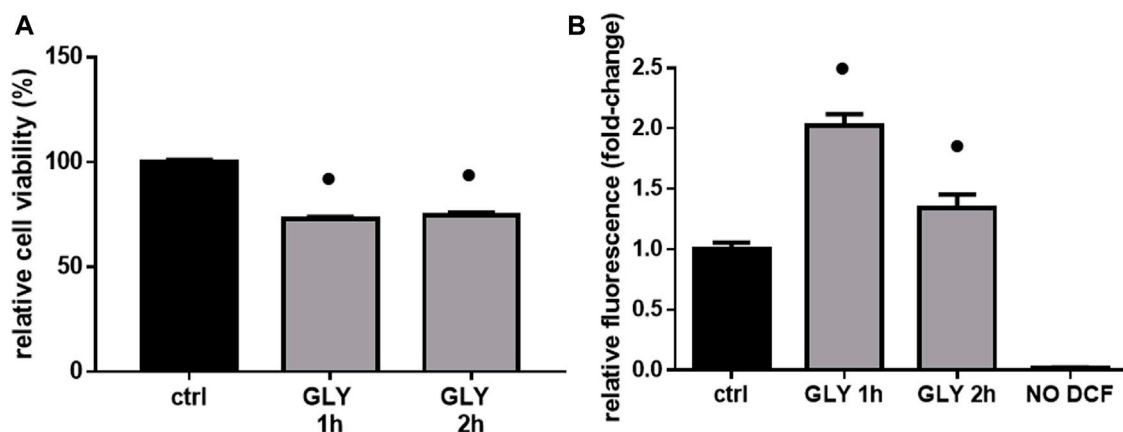


FIGURE 3

Cell viability & ROS production. The figure shows the relative histograms obtained from: (A) MTT and (B) DCF-DA assays. H9c2 cells were treated with 10 mM of glyphosate (GLY) for 1 or 2 h. After the treatments, cell viability and ROS production were assessed, respectively, through MTT and DCF-DA assays. Mean ± SD; p-values: ● < 0.0001 vs. control. NO DCF: control lane without the fluorescent probe.

mitochondria" (DM) with degenerated or swollen *cristae*. To calculate the percentage of DM, we used the formula:

$$\% \text{ of DM} = \frac{\text{DM}}{(\text{HM} + \text{DM})} \times 100$$

As shown in Figure 5E, the percentage of damaged mitochondria was significantly higher in Gly-treated group compared to control, potentially explaining the observed cytotoxic effects.

3.2 Effects of medium-to-low doses of glyphosate and AMPA—Acute exposure

The acute exposure of H9c2 cells from medium (1 mM) to very low (1 μM) doses of Gly, produced similar effects seen before

(Figure 1), although to a lesser extent. In terms of cell viability and ROS production, the treatments determined, respectively, a decrease from 10% to 15% (Figure 6A) and an increase from 1.1 to 1.2 fold-change (Figure 6B).

The use of the antioxidant NAC, even if effective in lowering ROS production (Figure 6B), was not able to totally restore cell viability (Figure 6A).

After the observation of Gly- and AMPA-induced production of reactive oxygen species, we wanted to test if there were variations in mitochondrial mass and distribution. To do so, we probed mitochondria with the fluorescent molecule MitoTracker Green FM™ after 2 or 24 h of Gly or AMPA treatment.

Mitochondrial distribution, as shown in Figures 7A, B, appeared homogeneous and no variations in fluorescence intensity were detected, suggesting that both mitochondrial dynamics and mass

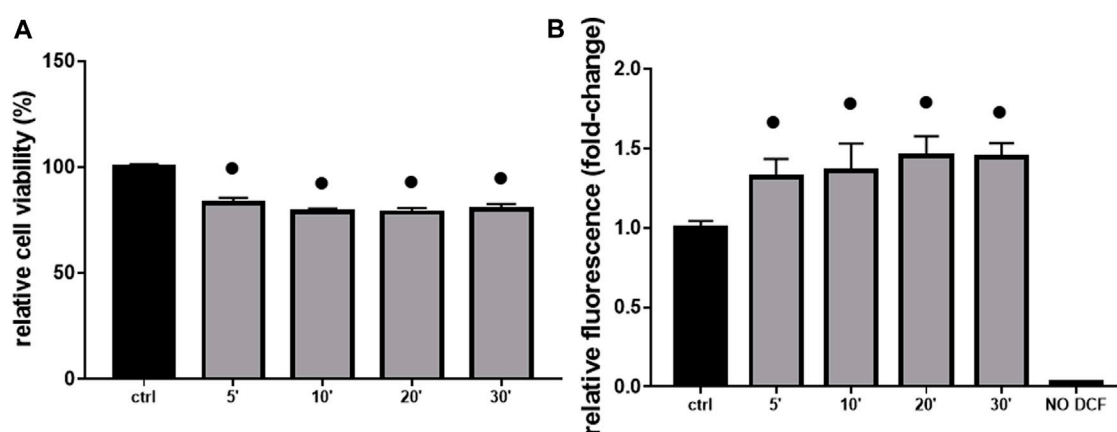


FIGURE 4

Cell viability & ROS production. The figure shows the relative histograms obtained from: (A) MTT and (B) DCF-DA assays. H9c2 cells were treated with 10 mM of glyphosate at different time points (from 5 to 30 min). After the treatments, cell viability and ROS production were assessed, respectively, through MTT and DCF-DA assays. Mean \pm SD; p -values: \bullet < 0.0001 vs. control. NO DCF: control lane without the fluorescent probe.

were preserved. However, we cannot totally exclude that the inability to find any relevant change, could be associated with a limitation of the technique used, which has, indeed, a limited resolution. Moreover, the probe stains all mitochondria independently from their activity, so it was not possible to distinguish healthy and damaged populations.

3.3 Effects of medium-to-low doses of glyphosate and AMPA—Sub-chronic exposure

Given the scarce effects of Gly on ROS production (Figures 6A, B) and since there were not changes in mitochondrial distribution and mass after 24 h of Gly (Figure 7A) or AMPA (Figure 7B) exposure, we hypothesized that H9c2 cells were able to overcome the injury. To verify this hypothesis, we tested cell viability of H9c2 cells after prolonged exposure (24 and 48 h) to low doses (1 μ M–1 mM) of Gly or AMPA.

As expected, after 24 h of low doses of Gly exposure, cell viability is totally rescued, except for the 1 mM dose (Figure 8A). After 48 h, the control phenotype was restored under all doses (Figure 8B).

As regards to AMPA treated-group, after 24 h, cell viability was comparable to control cells (Figure 8A). Surprisingly, after 48 h of exposure, cell viability decreased by \approx 40% at all doses (Figure 8B).

4 Discussion

Gly is considered an environmental pollutant as active compound of a large part of non-selective herbicidal largely used worldwide in the last 50 years (Torretta et al., 2018). As a matter of fact, traces of Gly and AMPA (its main degradation product) are commonly detected in samples of water, soil and food (Bai and Ogbourne, 2016; Bonansea et al., 2017; Silva et al., 2018; Xu et al., 2019). This diffuse contamination leads to a constant exposure, representing both an ecological and a health concern for humans

and animals. Despite its plant-specific mechanism of action, Gly has been proven to have either acute or chronic toxicity in different animal species, including mammals.

4.1 Glyphosate effects

At high doses, Gly treatment determines a great reduction in myoblasts viability after 2 h (Figure 1A). The response appears very early, since 10 mM treatment is able to reduce cell viability already after 5 min (Figure 4A). Furthermore, cell shrinkage and membrane blebbing are already visible soon after the application of the treatments (Figure 2, top panels). Signs of cell damage are still present after 24 h (Figure 2, bottom panels). Coupled to the reduction in cell viability, these morphologic alterations suggest an involvement of apoptotic pathways (Sardão et al., 2009; Gui et al., 2012; Zhang et al., 2018; Noritake et al., 2020). Benachour and Séralini (2009) showed that *in vitro* pure Gly treatment caused apoptosis via caspase (cas)-3 and -7 activation, already after 6 h, in three different human cell lines. Gly-dependent increase in cas-3, -8 and -9 activity was also recently confirmed in human peripheral blood mononuclear cells (hPBMCs) (Kwiatkowska et al., 2020). Moreover, in a neuroblastoma cell line (SHSY-5Y), 5 mM Gly treatment altered the expression of different apoptosis-related genes such as BAX, BCL2, CASP3 and CASP9 (Martínez et al., 2020).

The toxic effects we observed were related, at least in part, to ROS production and mitochondrial abnormalities. Mitochondria are, in fact, key players in maintaining cellular redox status and homeostasis. Upon a toxic stimulus, mitochondria may trigger an apoptotic response through cytochrome c release followed by the activation of cas-9-dependent pathway (Orrenius, 2004). A dose of 10 mM Gly determined a great production of ROS already after 5 min (Figure 4B), reaching the peak after 1 h (Figure 3B). In addition, 1 h of Gly treatment rapidly provoked mitochondrial disruption (Figures 5A, B). This is in line with what shown in hPBMCs, in which 4 h *in vitro* Gly treatment, from 0.05 mM, caused

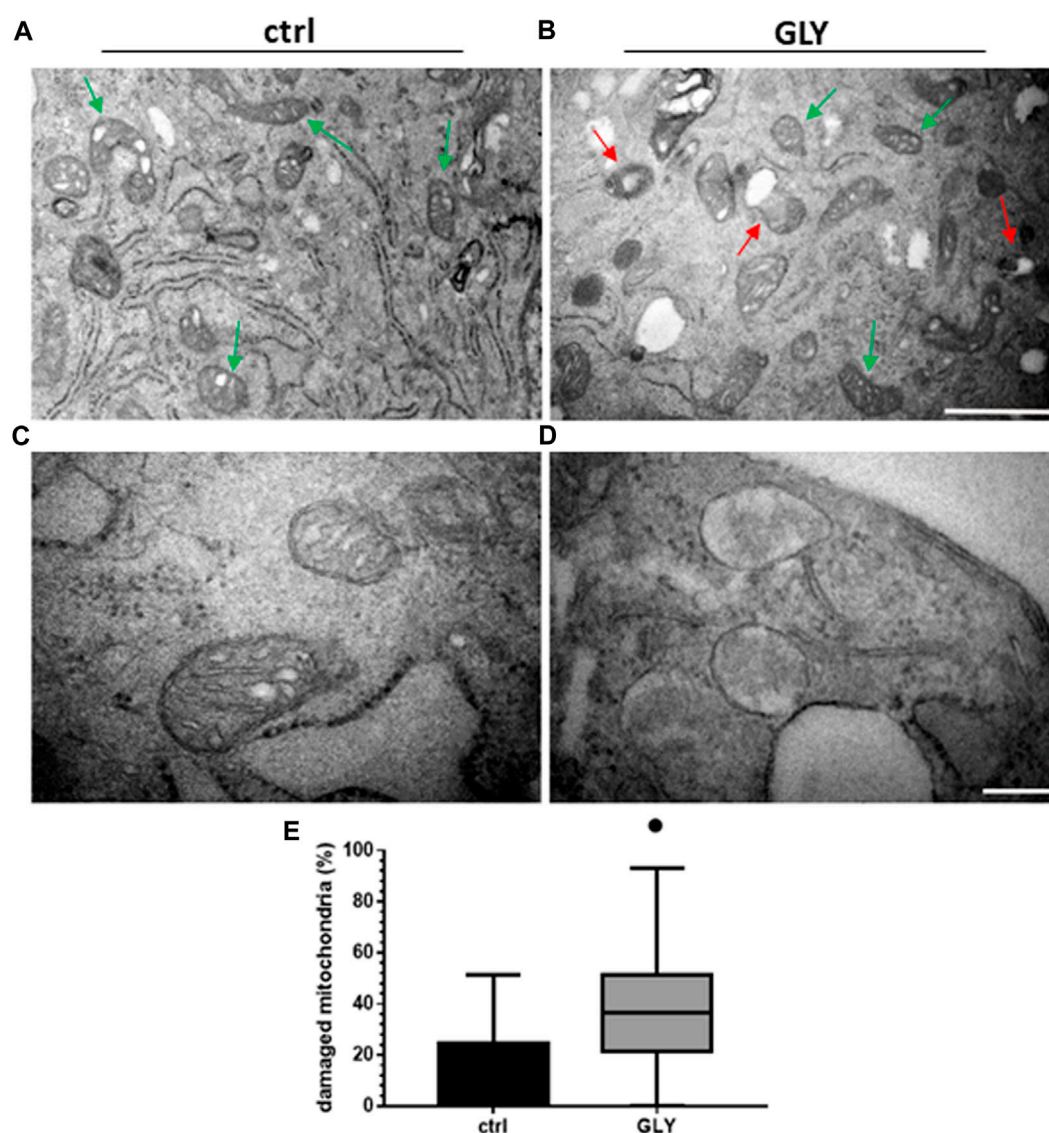


FIGURE 5

Ultrastructural analysis and mitochondria quantification. The figure shows: (A) Ultrastructure of HM in H9c2 cells control group (green arrows); (B) morphology of DM (red arrows) and HM (green arrows) in GLY group (10 mM, 1 h of treatment) (Scale bar = 1 μ m); (C) higher magnification of HM in control group and (D) higher magnification of DM in GLY group (Scale bar = 0.2 μ m). In (E) the relative boxplots of the mitochondrial count are shown. *p*-values: ● < 0.0001 vs. control.

a significant reduction in mitochondrial membrane potential ($\Delta\Psi_m$) and a consistent ROS production. These effects were markedly increased at 5 mM concentration (Kwiatkowska et al., 2020). H9c2 viability after 1 or 2 h of Gly exposure was comparable (Figure 3A), altogether suggesting that the damage could occur during the first hour. However, it remains a speculation since we did not checked these data in a longest time-window for this range of Gly concentration.

The same drastic effects were not detected at lower concentrations (1 μ M–1 mM), in which there was only a slight (although significant) variation in cell viability (Figure 6A) and ROS production (Figure 6B) after acute treatment. Similar results were obtained from Kim et al. (2013): the researchers found that the treatment with pure Gly up to 10 μ M was not able not alter

H9c2 features in terms of caspases activation, cell morphology and $\Delta\Psi_m$. As a further confirmation of the low toxicity, the sub-chronic exposure (24 or 48 h) of H9c2 to low doses of Gly showed a total rescue of the phenotype in terms of cell viability (Figures 8A, B) and no variations in mitochondrial dynamics (Figure 7A) or cell morphology (data not shown), suggesting that the cells were able to recover from the damage. A similar type of behaviour has been already reported by Townsend et al. (2017), which demonstrated that Gly is lethal to Raji cells (a line of lymphoblast-like cells) at concentrations above 10 mM, while no cytotoxic effects were observable at concentrations at or below 100 μ M. Furthermore, in their study, acute (from 30 to 60 min) Gly treatment in concentrations between 1 and 5 mM induced significant DNA damage, which was totally recovered after 2 h.

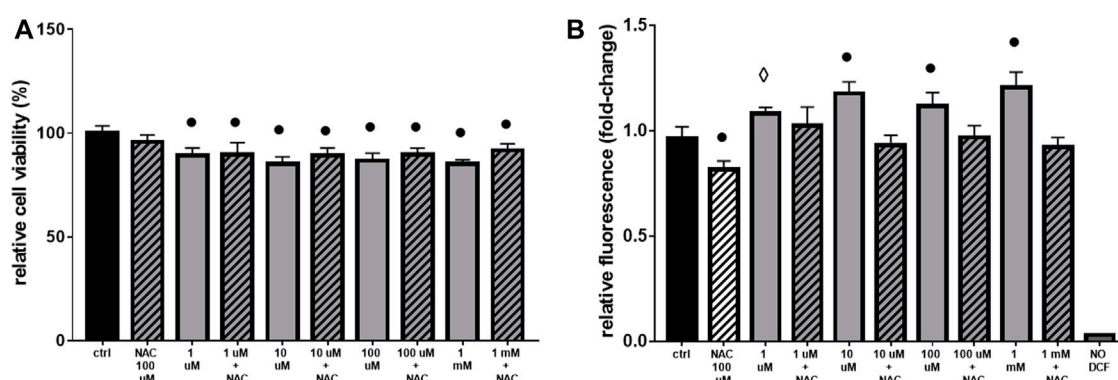


FIGURE 6

Cell viability and ROS production. The figure shows the histograms obtained from: (A) MTT and (B) DCF-DA assays. H9c2 cells were treated with 1 μ M to 1 mM of glyphosate and/or 100 μ M of NAC for 2 h. After the treatments, cell viability and ROS production were assessed, respectively, through MTT and DCF-DA assays. Mean \pm SD; p -values: $\diamond < 0.005$; $\circ < 0.0005$; $\bullet < 0.0001$ vs. control. NO DCF: control lane without the fluorescent probe.

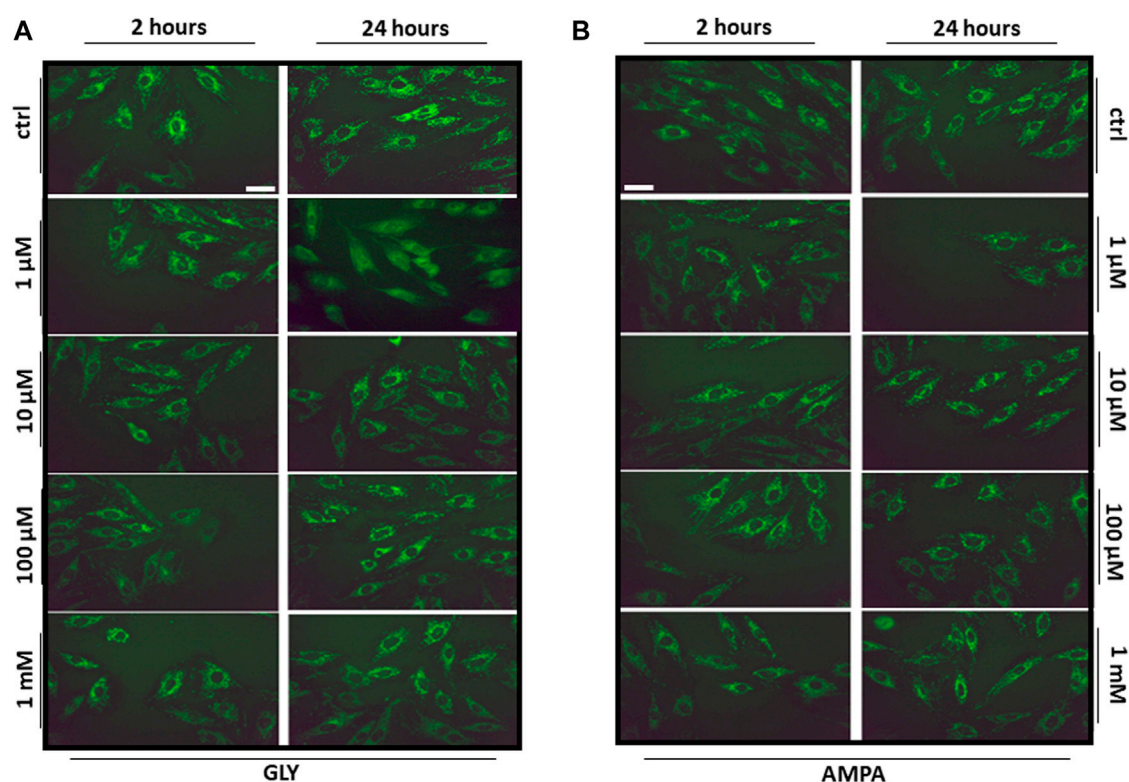


FIGURE 7

Mitochondrial distribution. The figure shows the representative images (40X, scale bar = 10 μ m) of H9c2 cells stained with the mitochondrial fluorescent dye MitoTracker Green FM. H9c2 cells were treated with 100 nM to 1 mM of (A) glyphosate (GLY) or (B) AMPA for 2 or 24 h.

Overall, our original results are not in contrast with what previously reported in literature. Gly appears toxic, on average, at- or above 1 mM in different mammalian and non-mammalian cell types, while at low doses it is relatively safe. The toxicity mechanisms seem to be related to oxidative stress, induced by mitochondrial dysfunctions or disruption of antioxidant systems (Contardo-Jara et al., 2009; Kwiatkowska et al., 2014; Lopes et al.,

2014; Jin et al., 2018; Vanlaeys et al., 2018; Martínez et al., 2020; Nerozzi et al., 2020; Madani and Carpenter, 2022; Strilbyska et al., 2022).

It remains unclear whether Gly exerts its toxicity by acting in an intra- or extra-cellular manner. Unfortunately, as of today, it is not known whether glyphosate is transported into mammalian cells and how it may vary across different cell lines. A 2016 study performed

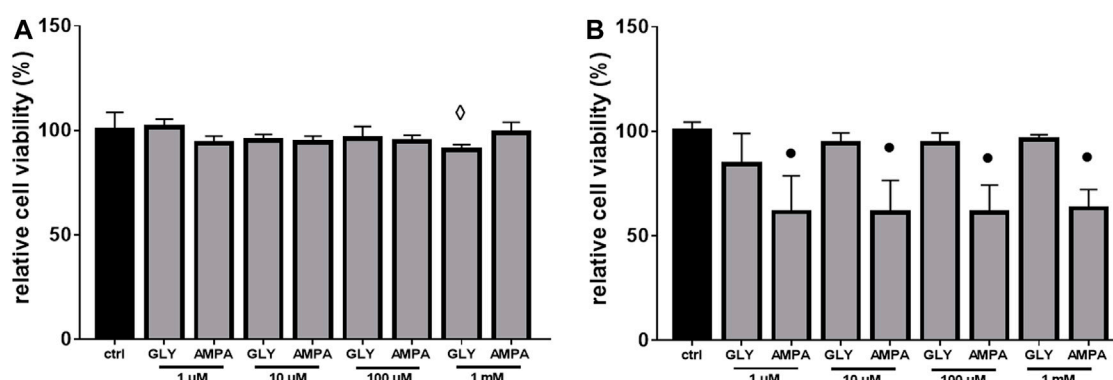


FIGURE 8

Cell viability. The figure shows the relative histograms obtained from MTT assays. H9c2 cells were treated with 1 μ M to 1 mM of glyphosate (GLY) or AMPA for (A) 24 h or (B) 48 h. Mean \pm SD; p -values: $\diamond < 0.005$; $\bullet < 0.0001$ vs. control.

on a human epithelial cell line suggests an active uptake mediated by the L-type aminoacid transporter (LAT) (Xu et al., 2016). We evaluated whether our cells could use this carrier for Gly uptake. To do so, we co-treated the cells with different doses of glyphosate (5, 10 and 20 mM) and a specific LAT-1 inhibitor (2-aminobicyclo-(2,2,1)-heptane-2-carboxylic acid, BCH) in acute settings (1 and 2 h). We, then, assessed cell viability and ROS production through MTT and DCF-DA assays, respectively, that did not show any changes in Gly-driven cytotoxicity (data not shown), suggesting that cardiac myoblasts use a different type of transport system and/or that Gly toxicity relies on a receptor-mediated signalling.

4.2 AMPA effects

Cells exposure to AMPA showed two types of responses. There was an acute cytotoxic response to high doses (10 or 20 mM), as demonstrated by a reduction in cell viability (Figure 1A) and an increase in ROS production (Figure 1B). Membrane blebbing, cell shrinkage and cytoplasmic cavitation were observable at t0 (Figure 2, top panels), but not after 24 h of treatment (Figure 2, bottom panels). Overall, in this range of concentrations, AMPA treatment was less toxic than Gly. Kwiatkowska et al. (2020) observed an analogous behavior: in hPBMcs, the treatment with AMPA induced hydroxyl radical formation only at the highest concentration (5 mM), while Gly treatment was effective already at 0.05 mM. Similarly, in a study from 2018, it was observed an increase in ROS levels in hPBMcs exposed to 1 mM Gly, but not to the same concentration of AMPA (Woźniak et al., 2018). In SHSY-5Y cells, after 48 h of exposure to 10 mM AMPA there was a significant increase in ROS production, while Gly exerted the same effect at 5 mM (Martínez et al., 2020).

Conversely, when treated sub-chronically at low doses (from 1 to 1 mM), H9c2 cells showed a late cytotoxic response to AMPA. After 48 h, there was a decrease in cell viability about 40% at all doses (Figure 8B). This was somehow unexpected, given the scarce amount of data about AMPA effects (especially in mammals) (Grandcoin et al., 2017; Bailey et al., 2018; Stur et al., 2019),

and represents a result that need to be explored with more detail. A non-monotonic response to sub-lethal doses of AMPA was recently reported in amphibians. In such experimental model, the chronic treatment with low (0.07 μ g/L) and medium (0.32 μ g/L) doses of AMPA determined a significant dysfunction of the antioxidant machinery, which authors suggest to be linked to a hyper-stimulation of catalase activity, while high doses (3.57 μ g/L) did not recapitulate the same effect (Cheron et al., 2022). We hypothesize that the early response could be due to a direct extracellular damage (as the binding with a receptor), while the late one could be secondary to bioaccumulation. Accordingly, it was demonstrated that, in hPBMcs, AMPA treatment determined an increase in both cas-8 [generally associated with the death receptors-mediated apoptotic pathway (Orrenius, 2004)] and cas-9 [involved in the mitochondrial-mediated apoptotic pathway (Orrenius, 2004)] activity (Kwiatkowska et al., 2020), supporting the hypothesis that the molecule is able to trigger both types of response. The activation of cas-3 and cas-9 pathways, following 48 h of AMPA treatment, was also reported by Martínez et al. (2020) in SHSY-5Y cells.

The fact that Gly treatment did not determine the same effects, could have two means: (I) Gly is not actively metabolized in AMPA neither inside nor outside our cells; (II) the kinetic of Gly to AMPA biotransformation is very slow, so more time is necessary to start to see the effects (Bailey et al., 2018).

4.3 Conclusion

Overall, we confirmed in our model previous *in vitro* studies indicating that pure Gly is toxic when administered at high concentrations, causing alterations in cell viability, morphology and mitochondrial health. At low doses, Gly causes only a slight cytotoxic response and the phenotype is rescued within 24 h. AMPA recreates almost the same effects, but with a lesser extent. Moreover, we provided new evidences about a late cytotoxic response to low doses of sub-chronically administered AMPA. In each condition, mitochondria and the antioxidant machinery are likely to be key mediators, a finding which is largely supported by the literature.

Unfortunately, the comprehension of the mechanisms by which Gly is possibly imported into mammalian cells is very limited, nor is clear if it is actively or inactively metabolized within the cells. Unveiling these aspects would help to clarify whether the damage is receptor-mediated or if it occurs after the internalization of the molecules. Furthermore, it is of pivotal importance to have a reliable measure of the real human exposure to glyphosate and AMPA, in order to critically evaluate all the scientific data obtained as of today. Since the main route of exposure of the general population to Gly is through the diet, it is pivotal to perform quality control of the agro-food chain. In particular, on those foods which are more likely to contain Gly such as fish/meat and derivatives, cereals and derivatives, honey and beverages such as tea, beer and wine. Some studies have been already conducted and are reported in a recent review by Soares et al. (2021). To do so, there is the urge to develop standardized quantification systems with good sensitivity (that should be well below the maximum residue limit established) but also affordable in terms of technical equipment and costs, a goal achievable with HPLC-related methodologies. Last, in order to shed light on the debate about Gly safety, it would be helpful to distinguish between the damages directly related to the pure molecules and its metabolites and the ones mediated (or amplified) by the adjuvants, i.e., the surfactants, present in the different GBH formulations.

This study needs further research to address additional scientific concerns: first, we did not include AMPA in all of the experiments, since we did not expect to observe any appreciable effect (especially at low doses); second, we did not examine in depth the effects of the chronic exposure of the two substances. However, the evaluation of a chronic treatment in an *in vitro* environment is limited and this study was intended as a pilot to identify a sub-toxic range, coherent with the environmental exposure, to evaluate the chronic toxicity of Gly *in vivo*.

References

- Anifandis, G., Amiridis, G., Konstantinos, D., Daponte, A., Dovolou, E., Gavril, E., et al. (2017). The *in vitro* impact of the herbicide roundup on human sperm motility and sperm mitochondria. *Toxics* 6, 2. doi:10.3390/toxics6010002
- Antón, F. A., Laborda, E., and De Ariz, M. (1994). Acute toxicity of the herbicide glyphosate to fish. *Chemosphere* 28, 745–753.
- ATSDR (Agency for Toxic Substances and Disease Registry). (2020). Toxicological profile for glyphosate - draft for public comment. Available at: <https://www.atsdr.cdc.gov/ToxProfiles/tp214.pdf>
- Bai, S. H., and Ogbourne, S. M. (2016). Glyphosate: Environmental contamination, toxicity and potential risks to human health via food contamination. *Environ. Sci. Pollut. Res.* 23, 18988–19001. doi:10.1007/s11356-016-7425-3
- Bailey, D. C., Todt, C. E., Burchfield, S. L., Pressley, A. S., Denney, R. D., Snapp, I. B., et al. (2018). Chronic exposure to a glyphosate-containing pesticide leads to mitochondrial dysfunction and increased reactive oxygen species production in *Caenorhabditis elegans*. *Environ. Toxicol. Pharmacol.* 57, 46–52. doi:10.1016/j.etap.2017.11.005
- Benachour, N., and Séralini, G.-É. (2009). Glyphosate formulations induce apoptosis and necrosis in human umbilical, embryonic, and placental cells. *Chem. Res. Toxicol.* 22, 97–105. doi:10.1021/tx800218n
- Bento, C. P. M., Yang, X., Gort, G., Xue, S., Van Dam, R., Zomer, P., et al. (2016). Persistence of glyphosate and aminomethylphosphonic acid in loess soil under different combinations of temperature, soil moisture and light/darkness. *Sci. Total Environ.* 572, 301–311. doi:10.1016/j.scitotenv.2016.07.215
- Bonanse, R. I., Filippi, I., Wunderlin, D. A., Marino, D. J. G., and Amé, M. V. (2017). The fate of glyphosate and AMPA in a freshwater endorheic basin: An ecotoxicological risk assessment. *Toxics* 6, 3. doi:10.3390/toxics6010003
- Boulefour, W., Mery, B., Rowinski, E., Rivier, C., Daguene, E., and Magne, N. (2021). Cardio-oncology preclinical models: A comprehensive review. *Anticancer Res.* 41, 5355–5364. doi:10.21873/anticancer.15348
- Bradberry, S. M., Proudfoot, A. T., and Vale, J. A. (2004). Glyphosate poisoning. *Toxicol. Rev.* 23, 159–167. doi:10.2165/00139709-200423030-00003
- Branco, A. F., Pereira, S. P., Gonzalez, S., Gusev, O., Rizvanov, A. A., and Oliveira, P. J. (2015). Gene expression profiling of H9c2 myoblast differentiation towards a cardiac-like phenotype. *PLoS ONE* 10, e0129303. doi:10.1371/journal.pone.0129303
- Brunetti, R., Maradey, J. A., Dearmin, R. S., Belford, P. M., and Bhav, P. D. (2020). Electrocardiographic abnormalities associated with acute glyphosate toxicity. *Hear. Case Rep.* 6, 63–66. doi:10.1016/j.hrcr.2019.10.014
- Burchfield, S. L., Bailey, D. C., Todt, C. E., Denney, R. D., Negga, R., and Fitsanakis, V. A. (2019). Acute exposure to a glyphosate-containing herbicide formulation inhibits Complex II and increases hydrogen peroxide in the model organism *Caenorhabditis elegans*. *Environ. Toxicol. Pharmacol.* 66, 36–42. doi:10.1016/j.etap.2018.12.019
- Cao, M., Wang, Y., Yang, F., Li, J., and Qin, X. (2021). Melatonin rescues the reproductive toxicity of low-dose glyphosate-based herbicide during mouse oocyte maturation via the GPER signaling pathway. *J. Pineal Res.* 70, e12718. doi:10.1111/jpi.12718
- Cheron, M., Costantini, D., Angelier, F., Ribout, C., and Brischoux, F. (2022). Aminomethylphosphonic acid (AMPA) alters oxidative status during embryonic development in an amphibian species. *Chemosphere* 287 (2), 131882. doi:10.1016/j.chemosphere.2021.131882
- Clair, É., Mesnage, R., Travert, C., and Séralini, G.-É. (2012). A glyphosate-based herbicide induces necrosis and apoptosis in mature rat testicular cells *in vitro*, and testosterone decrease at lower levels. *Toxicol. Vitro* 26, 269–279. doi:10.1016/j.tiv.2011.12.009

Author contributions

DM and EA contributed to conception and design of the study. EA and SG performed the experiment. EA, LM and SR performed ultrastructural TEM analysis. EA organized the database. EA performed the statistical analysis. EA wrote the first draft of the manuscript. DM, EA, SG, LM and SR wrote sections of the manuscript. All authors contributed to manuscript revision, read, and approved the submitted version.

Funding

This study was supported by Fondo di Beneficenza Intesa San Paolo and RILO 2020/2021 granted to DM, and RILO 2021/2022 granted to SR.

Conflict of interest

The authors declare that the research was conducted in the absence of any commercial or financial relationships that could be construed as a potential conflict of interest.

Publisher's note

All claims expressed in this article are solely those of the authors and do not necessarily represent those of their affiliated organizations, or those of the publisher, the editors and the reviewers. Any product that may be evaluated in this article, or claim that may be made by its manufacturer, is not guaranteed or endorsed by the publisher.

- Contardo-Jara, V., Klingelmann, E., and Wiegand, C. (2009). Bioaccumulation of glyphosate and its formulation Roundup Ultra in *Lumbriculus variegatus* and its effects on biotransformation and antioxidant enzymes. *Environ. Pollut.* 157, 57–63. doi:10.1016/j.envpol.2008.07.027
- De Liz Oliveira Cavalli, V. L., Cattani, D., Heinz Reig, C. E., Pierozan, P., Zanatta, L., Parisotto, E. B., et al. (2013). Roundup disrupts male reproductive functions by triggering calcium-mediated cell death in rat testis and Sertoli cells. *Free Radic. Biol. Med.* 65, 335–346. doi:10.1016/j.freeradbiomed.2013.06.043
- Dominguez, A., Brown, G. G., Sautter, K. D., Ribas de Oliveira, C. M., Carvalho de Vesconcelos, E., Niva, C. C., et al. (2016). Toxicity of AMPA to the earthworm *Eisenia andrei* Bouché, 1972 in tropical artificial soil. *Sci. Rep.* 6, 19731–19738. doi:10.1038/srep19731
- Gasnier, C., Dumont, C., Benachour, N., Clair, E., Chagnon, M.-C., and Séralini, G.-É. (2009). Glyphosate-based herbicides are toxic and endocrine disruptors in human cell lines. *Toxicology* 262, 184–191. doi:10.1016/j.tox.2009.06.006
- Gill, J. P. K., Sethi, N., Mohan, A., Datta, S., and Girdhar, M. (2018). Glyphosate toxicity for animals. *Environ. Chem. Lett.* 16, 401–426. doi:10.1007/s10311-017-0689-0
- Gillezeau, C., Van Gerwen, M., Shaffer, R. M., Rana, I., Zhang, L., Sheppard, L., et al. (2019). The evidence of human exposure to glyphosate: A review. *Environ. Health* 18, 2. doi:10.1186/s12940-018-0435-5
- Gonçalves, B. B., Giaquinto, P. C., Dos Santos Silva, D., Silva Neto, C. C. M., Alves De Lima, A., Darosci, A. A. B., et al. (2020). “Ecotoxicology of glyphosate-based herbicides on aquatic environment,” in *Biochemical toxicology - heavy metals and nanomaterials* (London, UK: IntechOpen). doi:10.5772/intechopen.85157
- Grandcoin, A., Piel, S., and Baurès, E. (2017). AminoMethylPhosphonic acid (AMPA) in natural waters: Its sources, behavior and environmental fate. *Water Res.* 117, 187–197. doi:10.1016/j.watres.2017.03.055
- Gress, S., Lemoine, S., Séralini, G.-É., and Puddu, P. E. (2015). Glyphosate-based herbicides potentially affect cardiovascular system in mammals: Review of the literature. *Cardiovasc. Toxicol.* 15, 117–126. doi:10.1007/s12012-014-9282-y
- Gui, Y.-X., Fan, X.-N., Wang, H.-M., Wang, G., and Chen, S. (2012). Glyphosate induced cell death through apoptotic and autophagic mechanisms. *Neurotoxicology Teratol.* 34, 344–349. doi:10.1016/j.ntt.2012.03.005
- Hao, Y., Zhang, Y., Cheng, J., Xu, W., Gao, J., Tao, L., et al. (2020). Adjuvant contributes Roundup's unexpected effects on A549 cells. *Environ. Res.* 184, 109306. doi:10.1016/j.envres.2020.109306
- Hu, J., Leseur, C., Miao, Y., Manservigi, F., Panzacchi, S., Mandrioli, D., et al. (2021). Low-dose exposure of glyphosate-based herbicides disrupt the urine metabolome and its interaction with gut microbiota. *Sci. Rep.* 11, 3265. doi:10.1038/s41598-021-82552-2
- Jarrell, Z. R., Ahmmad, M. U., and Benson, A. P. (2020). Glyphosate-based herbicide formulations and reproductive toxicity in animals. *Veterinary Animal Sci.* 10, 100126. doi:10.1016/j.vas.2020.100126
- Jin, J., Kurobe, T., Ramírez-Duarte, W. F., Bolotaolo, M. B., Lam, C. H., Pandey, P. K., et al. (2018). Sub-lethal effects of herbicides penoxsulam, imazamox, fluridone and glyphosate on Delta Smelt (*Hypomesus transpacificus*). *Aquat. Toxicol.* 197, 79–88. doi:10.1016/j.aquatox.2018.01.019
- Kim, Y., Hong, J., Gil, H., Song, H., and Hong, S. (2013). Mixtures of glyphosate and surfactant TN20 accelerate cell death via mitochondrial damage-induced apoptosis and necrosis. *Toxicol. Vitro* 27, 191–197. doi:10.1016/j.tiv.2012.09.021
- Krüger, M., Schiedorn, P., Schrödl, W., Hoppe, H.-W., Lutz, W., and Shehata, A. A. (2014). Detection of glyphosate residues in animals and humans. *J. Environ. Anal. Toxicol.* 4, 210. doi:10.4172/2161-0525.1000210
- Kwiatkowska, M., Huras, B., and Bukowska, B. (2014). The effect of metabolites and impurities of glyphosate on human erythrocytes (*in vitro*). *Pesticide Biochem. Physiology* 109, 34–43. doi:10.1016/j.pestbp.2014.01.003
- Kwiatkowska, M., Michałowicz, J., Jarosiewicz, P., Pingot, D., Sicińska, P., Huras, B., et al. (2020). Evaluation of apoptotic potential of glyphosate metabolites and impurities in human peripheral blood mononuclear cells (*in vitro* study). *Food Chem. Toxicol.* 135, 110888. doi:10.1016/j.fct.2019.110888
- Lee, H. L., Chen, K. W., Chi, C. H., Huang, J. J., and Tsai, L. M. (2000). Clinical presentations and prognostic factors of a glyphosate — surfactant herbicide intoxication: A review of 131 cases. *Acad. Emerg. Med.* 7, 906–910. doi:10.1111/j.1553-2712.2000.tb02069.x
- Lopes, F. M., Varela Junior, A. S., Dahl Corcini, C., Cardoso Da Silva, A., Gasperin Guazzelli, V., Tavares, G., et al. (2014). Effect of glyphosate on the sperm quality of zebrafish *Danio rerio*. *Aquat. Toxicol.* 155, 322–326. doi:10.1016/j.aquatox.2014.07.006
- Madani, N. A., and Carpenter, D. O. (2022). Effects of glyphosate and glyphosate-based herbicides like Roundup™ on the mammalian nervous system: A review. *Environ. Res.* 214 (4), 113933. doi:10.1016/j.envres.2022.113933
- Marques, J. G. C., Verissimo, K. J. S., Fernandes, B. S., Ferreira, S. R. M., Montenegro, S. M. G. L., and Motteran, F. (2021). Glyphosate: A review on the current environmental impacts from a Brazilian perspective. *Bull. Environ. Contam. Toxicol.* 107, 385–397. doi:10.1007/s00128-021-03295-4
- Martinez, M.-A., Rodriguez, J.-L., Lopez-Torres, B., Martinez, M., Martinez-Larrañaga, M. R., Maximiliano, J.-E., et al. (2020). Use of human neuroblastoma SH-SY5Y cells to evaluate glyphosate-induced effects on oxidative stress, neuronal development and cell death signaling pathways. *Environ. Int.* 135, 105414. doi:10.1016/j.envint.2019.105414
- Martini, C. N., Gabrielli, M., and Vila, M. D. C. (2012). A commercial formulation of glyphosate inhibits proliferation and differentiation to adipocytes and induces apoptosis in 3T3-L1 fibroblasts. *Toxicol. Vitro* 26, 1007–1013. doi:10.1016/j.tiv.2012.04.017
- Mesnage, R., Bernay, B., and Séralini, G.-É. (2013). Ethoxylated adjuvants of glyphosate-based herbicides are active principles of human cell toxicity. *Toxicology* 313, 122–128. doi:10.1016/j.tox.2012.09.006
- Mesnage, R., Bowyer, R. C. E., El Balkhi, S., Saint-Marcoux, F., Gardere, A., Quinten Raymond Ducarmon, Q. R., et al. (2022a). Impacts of dietary exposure to pesticides on faecal microbiome metabolism in adult twins. *Environ. Health* 21, 46. doi:10.1186/s12940-022-00860-0
- Mesnage, R., Ibragim, M., Mandrioli, D., Falcioni, L., Tibaldi, E., Belpoggi, F., et al. (2022b). Comparative toxicogenomics of glyphosate and roundup herbicides by mammalian stem cell-based genotoxicity assays and molecular profiling in sprague-dawley rats. *Toxicol. Sci.* 186 (1), 83–101. doi:10.1093/toxsci/kfab143
- Mohammadi, K., Sani, M. A., Safaei, P., Rahmani, J., Molaei-Aghaee, E., and Mahdi Jafari, S. (2022). A systematic review and meta-analysis of the impacts of glyphosate on the reproductive hormones. *Environ. Sci. Pollut. Res.* 29, 62030–62041. doi:10.1007/s11356-021-16145-x
- Moldovan, H., Imre, S., Duca, R. C., and Farczádi, L. (2023). Methods and strategies for biomonitoring in occupational exposure to plant protection products containing glyphosate. *Int. J. Environ. Res. Public Health* 20 (4), 3314. doi:10.3390/ijerph20043314
- Nerozzi, C., Recuero, S., Galeati, G., Bucci, D., Spinaci, M., and Yeste, M. (2020). Effects of Roundup and its main component, glyphosate, upon mammalian sperm function and survival. *Sci. Rep.* 10, 11026. doi:10.1038/s41598-020-67538-w
- Niemann, L., Sieke, C., Pfeil, R., and Solecki, R. (2015). A critical review of glyphosate findings in human urine samples and comparison with the exposure of operators and consumers. *J. für Verbraucherschutz und Lebensmittelsicherheit* 10, 3–12. doi:10.1007/s00003-014-0927-3
- Noritake, K., Aki, T., Isa, S., and Uemura, K. (2020). Pyroptotic cell death by exposure to 1-butanol in H9c2 cardiomyoblastoma cells. *Heliyon* 6, e05503. doi:10.1016/j.heliyon.2020.e05503
- Okada, E., Allinson, M., Barral, M. P., Clarke, B., and Allinson, G. (2020). Glyphosate and aminomethylphosphonic acid (AMPA) are commonly found in urban streams and wetlands of Melbourne, Australia. *Water Res.* 168, 115139. doi:10.1016/j.watres.2019.115139
- Onódi, Z., Visnovitz, T., Kiss, B., Hambalkó, S., Koncz, A., Ágg, B., et al. (2022). Systematic transcriptomic and phenotypic characterization of human and murine cardiac myocyte cell lines and primary cardiomyocytes reveals serious limitations and low resemblances to adult cardiac phenotype. *J. Mol. Cell. Cardiol.* 165, 19–30. doi:10.1016/j.yjmcc.2021.12.007
- Orrenius, S. (2004). Mitochondrial regulation of apoptotic cell death. *Toxicol. Lett.* 149, 19–23. doi:10.1016/j.toxlet.2003.12.017
- Pelosi, C., Bertrand, C., Bretagnolle, V., Coeurdassier, M., Delhomme, O., Deschamps, M., et al. (2022). Glyphosate, AMPA and glufosinate in soils and earthworms in a French arable landscape. *Chemosphere* 301, 134672. doi:10.1016/j.chemosphere.2022.134672
- Perry, M. J., Mandrioli, D., Belpoggi, F., Manservigi, F., Panzacchi, S., and Irwin, C. (2019). Historical evidence of glyphosate exposure from a US agricultural cohort. *Environ. Health* 18, 42. doi:10.1186/s12940-019-0474-6
- Roy, N. M., Ochs, J., Zambrycka, E., and Anderson, A. (2016). Glyphosate induces cardiovascular toxicity in *Danio rerio*. *Environ. Toxicol. Pharmacol.* 46, 292–300. doi:10.1016/j.etap.2016.08.010
- Santovito, A., Ruberto, S., Gendusa, C., and Cervella, P. (2018). *In vitro* evaluation of genomic damage induced by glyphosate on human lymphocytes. *Environ. Sci. Pollut. Res.* 25, 34693–34700. doi:10.1007/s11356-018-3417-9
- Sardão, V. A., Oliveira, P. J., Holy, J., Oliveira, C. R., and Wallace, K. B. (2009). Morphological alterations induced by doxorubicin on H9c2 myoblasts: Nuclear, mitochondrial, and cytoskeletal targets. *Cell Biol. Toxicol.* 25, 227–243. doi:10.1007/s10565-008-9070-1
- Silva, V., Montanarella, L., Jones, A., Fernández-Ugalde, O., Mol, H. G. J., Ritsema, C. J., et al. (2018). Distribution of glyphosate and aminomethylphosphonic acid (AMPA) in agricultural topsoils of the European Union. *Sci. Total Environ.* 621, 1352–1359. doi:10.1016/j.scitotenv.2017.10.093
- Soares, D., Silva, L., Duarte, S., Pena, A., and Pereira, A. (2021). Glyphosate use, toxicity and occurrence in food. *Foods* 10 (11), 2785. doi:10.3390/foods10112785
- Strilbyaska, O. M., Tsiumpala, S. A., Kozachyshyn, I. I., Strutynska, T., Burdyliuk, N., Lushchak, V. I., et al. (2022). The effects of low-toxic herbicide Roundup and glyphosate on mitochondria. *Exp. Clin. Sci.* 21, 183–196. doi:10.17179/excli2021-4478
- Stur, E., Aristizabal-Pachon, A. F., Peronni, K. C., Agostini, L. P., Waigel, S., Chariker, J., et al. (2019). Glyphosate-based herbicides at low doses affect canonical pathways in estrogen positive and negative breast cancer cell lines. *PLoS ONE* 14 (7), e0219610. doi:10.1371/journal.pone.0219610

- Tomlin, C. (2009). *The pesticide manual: A world compendium*. UK: British Crop Protection Council.
- Tong, M., Gao, W., Jiao, W., Zhou, J., Li, Y., He, L., et al. (2017). Uptake, translocation, metabolism, and distribution of glyphosate in nontarget tea plant (*camellia sinensis* L.). *J. Agric. Food Chem.* 65, 7638–7646. doi:10.1021/acs.jafc.7b02474
- Torretta, V., Katsoyiannis, I., Viotti, P., and Rada, E. (2018). Critical review of the effects of glyphosate exposure to the environment and humans through the food supply chain. *Sustainability* 10, 950. doi:10.3390/su10040950
- Townsend, M., Peck, C., Meng, W., Heaton, M., Robinson, R., and O'Neill, K. (2017). Evaluation of various glyphosate concentrations on DNA damage in human Raji cells and its impact on cytotoxicity. *Regul. Toxicol. Pharmacol.* 85, 79–85. doi:10.1016/j.yrtph.2017.02.002
- Valle, A. L., Mello, F. C. C., Alves-Balvedi, R. P., Rodrigues, L. P., and Goulart, L. R. (2019). Glyphosate detection: Methods, needs and challenges. *Environ. Chem. Lett.* 17, 291–317. doi:10.1007/s10311-018-0789-5
- Vanlaeys, A., Dubuisson, F., Séralini, G.-É., and Travert, C. (2018). Formulants of glyphosate-based herbicides have more deleterious impact than glyphosate on TM4 Sertoli cells. *Toxicol. Vitro* 52, 14–22. doi:10.1016/j.tiv.2018.01.002
- Woźniak, E., Sicińska, P., Michałowicz, J., Woźniak, K., Reszka, E., Huras, B., et al. (2018). The mechanism of DNA damage induced by Roundup 360 PLUS, glyphosate and AMPA in human peripheral blood mononuclear cells - genotoxic risk assessment. *Food Chem. Toxicol.* 120, 510–522. doi:10.1016/j.fct.2018.07.035
- Xu, J., Gao, L., Wang, Z., Si, L., He, S., Cai, J., et al. (2016). The role of L-type amino acid transporters in the uptake of glyphosate across mammalian epithelial tissues. *Chemosphere* 145, 487–494. doi:10.1016/j.chemosphere.2015.11.062
- Xu, J., Smith, S., Smith, G., Wang, W., and Li, Y. (2019). Glyphosate contamination in grains and foods: An overview. *Food control.* 106, 106710. doi:10.1016/j.foodcont.2019.106710
- Zhang, Y., Chen, X., Gueydan, C., and Han, J. (2018). Plasma membrane changes during programmed cell deaths. *Cell Res.* 28, 9–21. doi:10.1038/cr.2017.133



OPEN ACCESS

EDITED BY

Giovanna Valenti,
University of Bari Aldo Moro, Italy

REVIEWED BY

Elisa Grazioli,
Foro Italico University of Rome, Italy
Emiliano Cè,
University of Milan, Italy

*CORRESPONDENCE

F. Deriu,
✉ deriuf@uniss.it

[†]These authors have contributed equally to this work

RECEIVED 23 February 2023

ACCEPTED 25 April 2023

PUBLISHED 09 May 2023


CITATION

Manca A, Fiorito G, Morrone M, Boi A, Mercante B, Martinez G, Ventura L, Delitala AP, Cano A, Catte MG, Solinas G, Melis F, Ginatempo F and Deriu F (2023), A novel estimate of biological aging by multiple fitness tests is associated with risk scores for age-related diseases. *Front. Physiol.* 14:1164943. doi: 10.3389/fphys.2023.1164943

COPYRIGHT

© 2023 Manca, Fiorito, Morrone, Boi, Mercante, Martinez, Ventura, Delitala, Cano, Catte, Solinas, Melis, Ginatempo and Deriu. This is an open-access article distributed under the terms of the [Creative Commons Attribution License \(CC BY\)](#). The use, distribution or reproduction in other forums is permitted, provided the original author(s) and the copyright owner(s) are credited and that the original publication in this journal is cited, in accordance with accepted academic practice. No use, distribution or reproduction is permitted which does not comply with these terms.

A novel estimate of biological aging by multiple fitness tests is associated with risk scores for age-related diseases

A. Manca^{1†}, G. Fiorito^{1†}, M. Morrone¹, A. Boi¹, B. Mercante¹, G. Martinez¹, L. Ventura¹, A. P. Delitala², A. Cano¹, M. G. Catte¹, G. Solinas¹, F. Melis¹, F. Ginatempo¹ and F. Deriu^{1,3*} 

¹Department of Biomedical Sciences, University of Sassari, Sassari, Italy, ²Department of Medicine, Surgery and Pharmacy, University of Sassari, Sassari, Italy, ³Unit of Endocrinology, Nutritional and Metabolic Disorders, AOU Sassari, Sassari, Italy

Introduction: Recent research highlights the need for a correct instrument for monitoring the individual health status, especially in the elderly. Different definitions of biological aging have been proposed, with a consistent positive association of physical activity and physical fitness with decelerated aging trajectories. The six-minute walking test is considered the current gold standard for estimating the individual fitness status in the elderly.

Methods: In this study, we investigated the possibility of overcoming the main limitations of assessing fitness status based on a single measure. As a result, we developed a novel measure of fitness status based on multiple fitness tests. In 176 Sardinian individuals aged 51–80 years we collected the results of eight fitness tests to measure participants' functional mobility, gait, aerobic condition, endurance, upper and lower limb strength, and static and dynamic balance. In addition, the participants' state of health was estimated through validated risk scores for cardiovascular diseases, diabetes, mortality, and a comorbidity index.

Results: Six measures contributing to fitness age were extracted, with TUG showing the largest contribution (beta = 2.23 SDs), followed by handgrip strength (beta = −1.98 SDs) and 6MWT distance (beta = −1.11 SDs). Based on fitness age estimates, we developed a biological aging measure using an elastic net model regression as a linear combination of the results of the fitness tests described above. Our newly developed biomarker was significantly associated with risk scores for cardiovascular events (ACC-AHA: $r = 0.61$; $p = 0.0006$; MESA: $r = 0.21$; $p = 0.002$) and mortality (Levine mortality score: $r = 0.90$; $p = 0.0002$) and outperformed the previous definition of fitness status based on the six-minute walking test in predicting an individual health status.

Discussion: Our results indicate that a composite measure of biological age based on multiple fitness tests may be helpful for screening and monitoring strategies in clinical practice. However, additional studies are needed to test standardisation and to calibrate and validate the present results.

KEYWORDS

biological age-chronological age, aging, cardiovascular diseases, 6-min walking test, timed "up and go" test, ten meter walk test, handgrip test

Introduction

Persons of the same chronological age may vary in their pace of aging, suggesting that chronological age is an inadequate proxy of biological aging (Liu et al., 2018). Most researchers agree that biological or phenotypic aging can be described as the accumulation of damages at the cellular, molecular, tissue and organ levels, which lead to “age-related changes in an organism that adversely affect its vitality and functions” (Finch, 1994; Gilbert, 2000). The characteristics of biological aging, as distinguished from diseases of aging, affect all the individuals of a species.

The current gold standard for quantifying biological aging is DNA methylation (DNAm), which allows estimating chronological and biological ages through epigenetic clocks that can also predict a variety of aging outcomes, including all-cause mortality, cancers, health span, and physical functioning (Levine et al., 2018). Biological age can also be estimated via a newly introduced tool, the Phenotypic Age calculator, which considers a combination of blood-measured biomarkers associated with longevity (Levine et al., 2018). Only very recently, epigenetic clocks have started to incorporate physical fitness (PF) parameters into their calculations (e.g., the DNAm FitAge) (McGreevy et al., 2022). These measures have been shown to correlate with changes in molecular signs of decline and can provide further insights into the effect of lifestyle on the aging process.

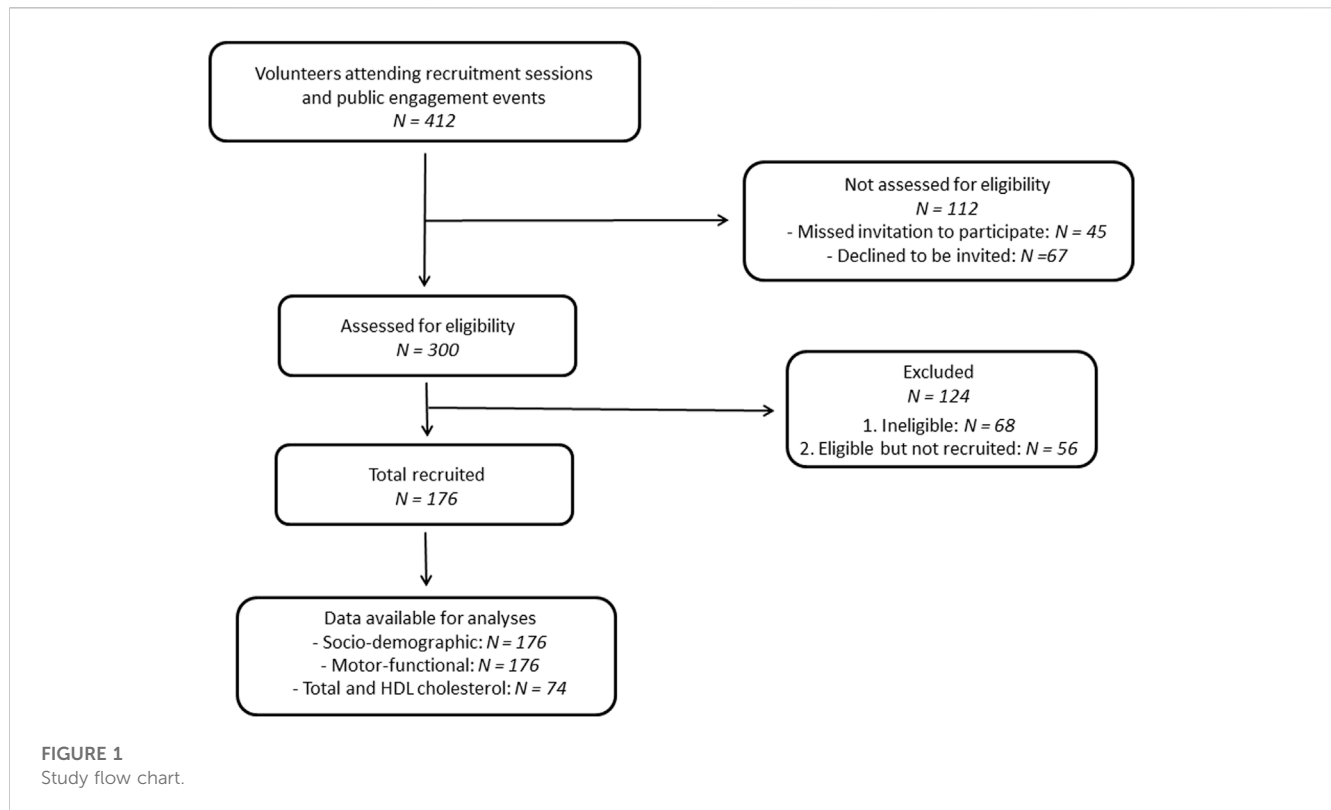
The American College of Sports Medicine defines PF as “a set of attributes that people have or achieve that relates to the ability to perform physical activity. It is also characterized by 1) an ability to perform daily activities with vigor, and 2) a demonstration of traits and capacities that are associated with a low risk of premature development of hypokinetic diseases (e.g., those associated with physical inactivity)” (Wilder et al., 2006). Indeed, maintaining good levels of PF during adulthood and later life, i.e., active aging, helps preserve autonomy and functional abilities and decelerate aging trajectories (Pareja-Galeano et al., 2015; Fiuza-Luces et al., 2018). Adequate PF is considered an established protective factor against chronic diseases and age-related disabilities (Sanchez-Sanchez et al., 2020). Importantly, the amount of physical activity accomplished in the transition from adult to older age is crucial to fostering successful ageing and has been shown to surpass other cardiovascular or sociodemographic risk factors that are classically associated with adverse health outcomes (Sanchez-Sanchez et al., 2020). Health benefits of active aging include reduced hospitalization and mortality rates, increased lifespan, and quality of life (Ekelund et al., 2019; Sanchez-Sanchez et al., 2020). It has been pointed out that preventing loss of physical and cognitive function and improving mental health and social engagement are the main benefits whereby physical activity would mostly contribute to improved chances of successful and healthy aging (Szychowska and Drygas, 2022). Older adults who maintain a regular physically active lifestyle have been extensively reported to display estimated biological ages considerably younger than their chronological ages (Nakamura et al., 1989; Levine et al., 2018; Sanchez-Sanchez et al., 2020; World Health Organization, 2015). The World Health Organization (WHO, 2002) defines healthy aging, “as the process of developing and maintaining the functional ability that enables wellbeing in older age” (Beard

et al., 2016). Within such multidimensional framework, where the aging person needs to stay active to remain a resource to families, communities and economies, PF has proved among the most important contributors to healthy aging (Tucker, 2017).

In light of the above background, defining PF levels accurately and reliably is, therefore, of critical importance. Even though PF can be determined by multiple components—the main ones being body composition, cardiorespiratory endurance, muscular strength, flexibility, and balance (Caspersen et al., 1985), the cardiorespiratory domain is by far the most examined. This is generally accomplished by means of the gold standard for cardiorespiratory fitness assessment, which is the maximum oxygen uptake obtained at the end of a cardiorespiratory exercise testing. In low-resource environments or the clinical setting, submaximal and field exercise tests are more feasible and generally preferred (Ross et al., 2016). Among these, the Six-Minute Walk test (6MWT) has emerged as the most employed test for cardiorespiratory fitness and overall functional capacity (Matos Casano and Anjum, 2022). The 6MWT was introduced by the American Thoracic Society in 2002 as a sub-maximal exercise test to assess aerobic capacity, endurance, and PF (ATS Committee on Proficiency Standards for Clinical Pulmonary Function Laboratories, 2002). Beyond assessing PF and the individual's functional capacity, it also provides information regarding the systems involved in physical activity, including pulmonary and cardiovascular systems, blood circulation, body metabolism, and peripheral circulation (ATS Committee on Proficiency Standards for Clinical Pulmonary Function Laboratories, 2002). This has led to consider the 6MWT as a global mobility and PF test for both, healthy and diseased populations (Wiener et al., 2019; Soares-Miranda et al., 2021; Elshafey and Alsakhawi, 2022; Matos Casano and Anjum, 2022).

In the clinical setting, the 6MWT still provides the main definition of PF, despite this outcome is increasingly being assessed in research over different components (aerobic fitness, muscular strength and endurance, flexibility, and body composition). Some studies have recently attempted to overcome this limitation by employing more comprehensive testing procedures to determine PF in the elderly. Mack-Inocentio et al. (2020) evaluated PF in 590 older adults aged 60+ years through a multi-domain battery of as many as ten motor-functional tests and found that a smaller set of these (trunk strength, handgrip strength, 6MWT, sit-to-stand, sit-and-reach) could explain the largest amount of variation in physical performance and functional capacity of persons older than 60 years.

Based on the above background, we hypothesized that the new multi-domain definition of PF would outperform the mono-dimensional definition based on the 6MWT in predicting the abovementioned health risk scores of our mixed cohort of middle-aged and older adults. Therefore, the present study aimed at 1) profiling biological aging in a group in the 50–80 years through multiple fitness tests; 2) overcoming the main limits of the 6MWT and identifying a comprehensive and novel measure of biological aging based on different components of fitness; 3) identifying the best motor predictors of biological aging, and 4) testing their ability to estimate an individual state of health, though investigation of their association with cardiovascular, morbidity and mortality risk scores.



Materials and methods

Participants

The current study was advertised via social networks and public engagement events to find participants. The group facilitator also gave a public lecture previewing the study project at the University of Sassari, Italy. Participants were required to be 50 years old or over at the time of the examination (from February 2021 to December 2021) and have no medical, physical, or cognitive condition that would interfere with participation in the functional assessments. We selected the first 300 respondents deemed apparently eligible after a preliminary telephone interview. After thoroughly screening for eligibility, 176 volunteers participated in the study. **Figure 1** presents the study flow chart according to the Strengthening the Reporting of Observational Studies in Epidemiology (STROBE) checklist (Vandenbroucke et al., 2007). The Institutional Review Board and the Clinical Research Ethics Committee approved all procedures involving human subjects (ID: PG/2020/16846). Following the Declaration of Helsinki, written informed consent was obtained from each participant before inclusion and participation in the tests.

Clinical examination

The subjects were evaluated by a geriatric specialist to ensure that they met the eligibility criteria. The patient's heart rate and blood pressure were measured during the examination. At the same time, respiratory, rheumatologic, neurological,

cardiovascular, musculoskeletal, neoplastic, and metabolic conditions were thoroughly investigated. Additional factors that may influence health outcomes, such as the participant's smoking history, level of education, and current pharmacological therapy, were evaluated and recorded. The Italian validated version of the Geriatric Depression Scale was used to assess the subject's depression (Galeoto et al., 2018). Lastly, adherence to the Mediterranean diet was evaluated using the MEDIET questionnaire, with scores ranging from low (0–5 points), medium (6–8 points), to maximal adherence (>9 points) (Ros et al., 2014).

Motor-functional tests

Eight different tests were administered to examine the participant's functional mobility, gait, aerobic condition, endurance, upper and lower limb strength and static and dynamic balance: 1) the Four Square Step Test (4SST) (Cleary and Skorniyakov, 2017); 2) the Timed Up and Go test (TUG) (Podsiadlo and Richardson, 1991); the 10 m Walk Test (10MWT) evaluating both the 3) self-selected and comfortable walking speed and 4) fastest walking speed (Perera et al., 2006); 5) the Short Physical Performance Battery (SPPB) (Perera et al., 2006); 6) 6MWT (ATS Committee on Proficiency Standards for Clinical Pulmonary Function Laboratories, 2002); maximum voluntary isometric contraction of both the dominant 7) forearm (Handgrip test) and 8) quadriceps (Abizanda et al., 2012). Dynamometric measurements were performed with a Handgrip Dynamometer (G200, Biometrics LTD., Newport, United Kingdom)

and with a hand-held dynamometer (MyoMeter M550, Biometrics LTD., Newport, United Kingdom) connected to a laptop via the same data collection tools.

Between each test repetition, a 1-min rest was given to recover, and a 2-min rest between one test and the next. The time taken to complete the tests was monitored using a stopwatch.

Statistical analyses

Biological age definition

We defined the biological age of study participants based on the results of the motor-functional tests described above using a statistical approach previously employed to define the epigenetic age (Horvath, 2013). Specifically, we employed a linear regression model with elastic net regularization, where chronological age was the dependent variable (y), and the standardised results of the motor tests were the predictors (x_1, x_2, \dots). The elastic net model, including λ_1 and λ_2 penalizations, allows extracting relevant predictors of y and avoids overfitting simultaneously. The optimal values of the λ_1 and λ_2 parameters were derived as those minimising the root mean squared error (RMSQ) averaging from 100 permutations in which 80% of the sample was used (*glmnet R package*). The model-predicted age was defined as the biological/fitness age. By definition, individuals with higher predicted than chronological age are experiencing accelerated ageing and *vice versa*. Further, we determined the fitness age acceleration measure (fitAA) as the residuals of the regression of fitness age on chronological age.

State of health/risk scores

We computed three composite risk scores predictive of 10-year risk of cardiovascular diseases:

- the Framingham Risk Score (FRS) (D'Agostino et al., 2008),
- the Cardiovascular disease (CVD) risk from the American College of Cardiology (ACC) and American Heart Association (AHA) (Goff et al., 2013),
- the CHD risk prediction based on the MESA cohort (Budoff et al., 2018).

The three CVD scores include measures of total and HDL cholesterol, available for a subgroup of the whole study sample ($N = 74$). In this subsample, we computed the three CVD scores and a reduced version without using total and HDL cholesterol values. The CVD score calculated without cholesterol values had a Pearson correlation higher than 0.99 with the original measure for all three measures. Based on the above, we used the CVD risk score without cholesterol for subsequent analyses to increase the sample size. Also, we computed a composite score for the risk of diabetes within 7.5 years according to the algorithm described by Stern et al. (Stern et al., 2002). Similarly to what was described for CVD risk, the diabetes score version computed without cholesterol measures strongly correlated ($R > 0.99$) with the original one. Finally, we calculated the 10-year mortality score according to Levine et al. (Levine et al., 2018) and the Charlson Comorbidity Index (CCI) (Roffman et al., 2016).

Results

This study sample included 176 volunteers (60.2% women) aged 51–80. Table 1 summarizes study sample characteristics, including anthropometric variables, health lifestyle variables such as smoking history, dietary status and polypharmacy and the maximum education attained as a proxy for the socio-economic status, and lifestyle. The average age was 66.5 years ($SD = 7.8$). Most of the study participants hold a high-school diploma (45%), whereas 5% attended primary school only; the average body mass index (BMI) was 26.9 kg/m^2 ($SD = 3.9$); 56% were never smokers; finally, the average adherence to the Mediterranean diet score was moderate in women (median = 6, IQR = 2) and low in men (median = 5, IQR = 2).

Fitness age definition and components

Our elastic net model extracted six features, as described in Table 2. A precise ranking was identified in how much each test contributed to fitness age. The weights in Table 2 can be interpreted as the increase in biological age for each increase by one standard deviation of the corresponding test result. Positive coefficients/weights indicate motor tests whose results are higher in an individual with higher fitness age and *vice versa*. Accordingly, TUG had the largest contribution, followed by handgrip strength and 6MWT distance.

As expected, the predicted (fitness) age correlated with the chronological age (Pearson 0.75, $p < 0.0001$; Figure 2). This applied both to women and men. Based on this relationship, the novel measure fitAA was derived as the residual of the linear regression of fitness age on chronological age.

Association of fitAA with risk scores

In Table 3 we showed the results of the linear regressions of risk scores with fitAA adjusted for covariates as described in Methods. The results are presented in Table 3. Increased value of the fitAA was significantly associated with ACC-AHA and MESA scores for CVD risk, and with the Levine mortality score.

FitAA vs. previous definition of physical fitness in predicting risk scores

Based on the results above, we propose to classify individual fitness status according to the newly developed fitAA measure. Specifically, we defined individuals with fitAA scores lower than -2.5 as “FIT”; individuals with fitAA scores ranging from -2.5 to 2.5 as “NORMAL”; and those with fitAA higher than 2.5 as “UNFIT”. Then, we compared the newly developed classification of fitness status with that commonly used in the literature based on the 6MWT (Matos Casano and Anjum, 2022) in the ability to predict risk scores for CVD, diabetes and mortality. Table 4 reports the results of the association of the categorical fitness status vs. risk scores, according to the two definitions described above.

TABLE 1 Anthropometric and demographic characteristics of the participants.

Variable (units of measurement)		Women N = 106	Men N = 70	Total N = 176
Age (years)		66.97 ± 7.46	65.74 ± 8.2	66.48 ± 7.77
		(65.53, 68.41)	(63.79, 67.7)	(65.33, 67.64)
Weight (kg)		63.55 ± 10.41	78.35 ± 12.22	69.44 ± 13.29
		(61.55, 65.56)	(75.43, 81.26)	(67.46, 71.41)
Height (m)		1.53 ± 0.09	1.69 ± 0.07	1.59 ± 0.11
		(1.51, 1.55)	(1.67, 1.71)	(1.58, 1.61)
Body mass index (kg/m ²)		26.77 ± 4.17	27.27 ± 3.61	26.97 ± 3.95
		(25.97, 27.58)	(26.41, 28.13)	(26.38, 27.56)
Mediterranean diet adherence [pts: median (IQR)]		6 (2)	5 (2)	6 (2)
Comorbidity index (pts)		3.12 ± 1.68	2.71 ± 1.31	2.96 ± 1.55
		(2.8, 3.45)	(2.4, 3.03)	(2.73, 3.19)
Geriatric depression scale (pts)		4.65 ± 2.68	4.07 ± 2.72	4.42 ± 2.7
		(4.13, 5.17)	(3.42, 4.73)	(4.02, 4.83)
Polypharmacy (count)		2 (2)	1 (3)	1 (2)
Smoking history	Not smoking	n = 85	n = 62	n = 147
	Smoking	n = 18	n = 7	n = 25
	Never smoked	n = 57	n = 40	n = 97
	Have smoked	n = 46	n = 29	n = 75
Education level	Primary school	n = 6	n = 3	n = 9
	Middle school	n = 28	n = 12	n = 40
	High school	n = 44	n = 35	n = 79
	Tertiary +	n = 25	n = 17	n = 42

All data are presented as mean ± standard deviation and 95% confidence interval, except for polypharmacy data (expressed as median and IQR, interquartile range). Abbreviations: kg, kilograms; m, meters; pts, points.

TABLE 2 Coefficients of the elastic net model for selected variables contributing to the biological age (FitAge).

FitAge coefficients	
Variable	Coefficient (SDs)
TUG time	2.23
Handgrip strength	−1.98
6MWT distance	−1.11
Fast walking 10MWT time	0.95
4SST time	0.23
Quadriceps strength	−0.19

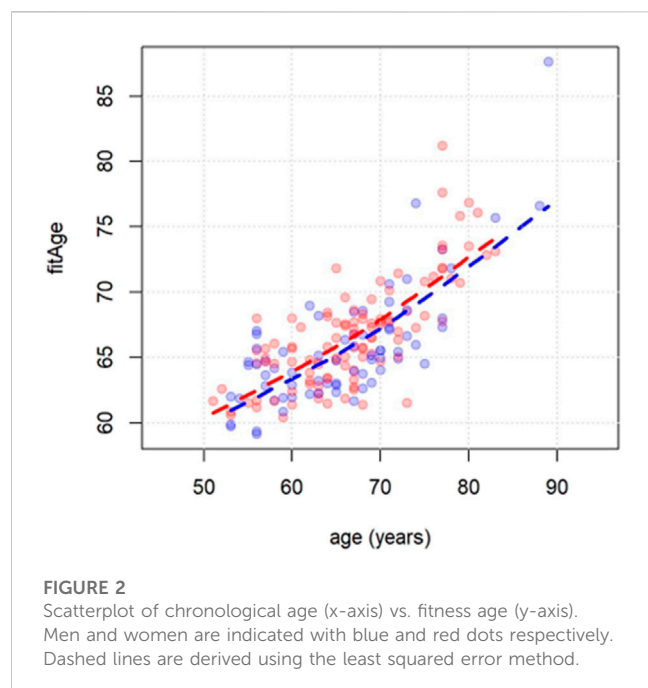
Abbreviations: SDs, standard deviations; TUG, timed up and go test; 6MWT, 6-min walk test; 10MWT, 10-m walk test; 4SST, four square step test. Coefficients indicate the standardized weight of each motor test in the construction of the biological/fitness age. Coefficients equal to zero indicate no contribution to the biological aging measure.

The fitness status definition based on fitAA outperformed the previous classification based on the results of the “6 min walking test” in estimating CVD and mortality scores, as shown in [Table 4](#). In

fact, no significant associations of risk scores with fitness status based on the 6MWT were detected, whereas fitness status based on fitAA was significantly associated with ACC-AHA and MESA CVD scores, and the Levine mortality score.

Discussion

In this exploratory study we provide evidence that the individual biological age of our sample can be efficiently estimated by the comprehensive set of motor tests assessed here. The elastic net regression model identified the variables mostly contributing to biological age: the time needed to complete the TUG, and maximal handgrip strength, suggesting that in clinical practice, the results of these two tests deserve more attention for assessing an individual state of health. The strong association of these physical tests with biological age was not unexpected. Low grip strength at midlife may indicate subclinical disease, which later develops into clinical disease and disability, whereas good grip strength may mark some general intrinsic midlife vitality or motivation that tracks into good functional ability in old age ([Rantanen et al., 1999](#)). Handgrip strength, gait speed and ability to independently rise from a chair



(the latter two being essential components of the TUG) are tests of muscle strength and function that have been recommended by international study groups on sarcopenia, including the European Working Group on Sarcopenia in Older People (EWGSOP) (Cruz-Jentoft et al., 2010), the Asian Working Group for Sarcopenia (Chen et al., 2014), and the International Working Group on Sarcopenia (Fielding et al., 2011) for the screening and diagnosis of sarcopenia. In this regard, handgrip strength is an established and powerful predictor of healthy aging beginning from midlife (Rantanen et al., 1999). Our findings on the relevance of TUG and handgrip also align with a more recent study where these tests were found to be the best predictors of short-term mortality in the elderly (Chua et al., 2020). They also agree with a pertinent consensus of experts, who proposed a panel of biomarkers of healthy ageing, which include the TUG and handgrip strength among the five biomarkers of physical capability (Lara et al., 2015). Interestingly, the other biomarkers are balance, gait speed and chair rising, all three being key components of the TUG.

Although preliminary, this finding suggests that these simple and well-known physical tests are strong and useful markers for predicting healthy aging trajectories. We also observed that the universally employed 6MWT was not a major contributor to age prediction. This disagrees with a relatively large and recent body of literature referring to this test as a measure of physical functioning and fitness (Wiener et al., 2019; Soares-Miranda et al., 2021; Elshafey and Alsakhawi, 2022). The gold-standard for demonstrating the physical fitness of an individual is the direct determination of peak oxygen uptake, which is considered the best indicator of cardiovascular fitness and aerobic endurance (Edvardsen et al., 2013). Due to the high costs and low feasibility of this approach in settings other than research, the walking distance covered in 6 min has been progressively supported as a low-cost, more applicable alternative to estimate fitness status, particularly in the elderly and diseased populations (Matos Casano and Anjum, 2022). However, age prediction models based on multiple domains are increasingly being favored over unidimensional measures as they can predict the individual health status in a more comprehensive manner. In this regard, Mack-Inocentio and colleagues introduced the Vitality Test Battery as a relatively simple tool that can be used to assess the physical condition of senior men and women outside a laboratory (Mack-Inocentio et al., 2020). Compared to their tool, which consists of a battery of 10 tests (6-min walk, trunk strength, hand grip strength, medicine ball throwing, 30-s chair stand, flexibility, balance, plate tapping, ruler drop, and dual task), our novel measure of fitness status based on the biological age, i.e., the fitness age acceleration (fitAA) that we developed, relies on two major contributors to fitness age, i.e., TUG test and handgrip strength, and to a minor extent, on the 6MWT. This measure was calculated into two steps: 1) an elastic net penalised regression model is trained to predict the chronological age of individuals; 2) the residuals of the regression of predicted (biological) on observed (chronological) age is defined as the age acceleration (or deceleration in the case of negative values) according to the physical fitness revealed by the set of physical tests administered. In this context, fitAA may be used as a quantitative measure of the difference between biological and chronological age, allowing the identification of individuals experience accelerated (or decelerated) aging.

When we measured the ability of this newly introduced measure to predict health status in terms of its association

TABLE 3 Results of the linear models in which each risk score was used as the outcome (dependent variable) and fitness age acceleration (fitAA) as the predictor, adjusting for covariates.

	Estimate	95% CI	p
Framingham CVD score	0.26	(-0.04; 0.56)	0.0903
ACC AHA CVD score	0.61	(0.27; 0.95)	0.0006
MESA CVD score	0.21	(0.08; 0.35)	0.0023
Stern diabetes risk score	-0.25	(-1.14; 0.63)	0.5763
Comorbidity index	0.02	(-0.05; 0.08)	0.6469
Levine mortality score	0.90	(0.43; 1.37)	0.0002

Abbreviations: fitAA, fitness age acceleration; CI, confidence interval; CVD, cardiovascular diseases; ACC, American College of Cardiology; AHA, American heart association; MESA, multi-ethnic study of atherosclerosis. Estimates can be interpreted as the increase in the percentage risk score for each year increase in fitAA. Only significant p values should be in bold.

TABLE 4 Results of the linear models in which each risk score was used as the outcome (dependent variable) and categorization of the fitness status as the predictor, adjusting for covariates. Estimates can be interpreted as the increase in the percentage risk score for individual in the NORMAL and UNFIT categories compared to the FIT (reference) group.

	Fitness status based on the 6 min walking test			Fitness status based on the fitAA measure		
	Estimate	95% CI	p	Estimate	95% CI	p
Framingham CVD score						
Normal	0.91	(−2.45; 4.28)	0.60	0.83	(−3.05; 4.71)	0.68
Unfit	−0.83	(−4.23; 2.57)	0.63	4.15	(−0.74; 9.04)	0.10
ACC AHA CVD score						
Normal	0.28	(−3.40; 3.95)	0.88	0.90	(−1.78; 3.57)	0.51
Unfit	−1.77	(−5.48; 1.94)	0.35	4.51	(1.13; 7.89)	0.01
MESA CVD score						
Normal	0.77	(−0.76; 2.30)	0.33	0.24	(−0.82; 1.31)	0.66
Unfit	0.42	(−1.13; 1.97)	0.60	1.40	(0.05; 2.74)	0.04
Stern diabetes risk score						
Normal	−6.33	(−15.39; 2.72)	0.17	−1.99	(−8.87; 4.88)	0.57
Unfit	−6.52	(−15.68; 2.64)	0.17	−2.07	(−10.87; 6.72)	0.64
Comorbidity index						
Normal	0.13	(−0.48; 0.74)	0.67	0.16	(−0.36; 0.68)	0.55
Unfit	0.15	(−0.46; 0.77)	0.63	0.06	(−0.60; 0.71)	0.87
Levine Mortality score						
Normal	−0.34	(−4.82; 4.14)	0.88	0.27	(−3.50; 4.05)	0.89
Unfit	1.49	(−3.02; 6.01)	0.52	4.80	(0.01; 9.60)	0.04

Abbreviations: fitAA, fitness age acceleration; CVD, cardiovascular diseases; ACC, American College of Cardiology; AHA, American heart association; MESA, multi-ethnic study of atherosclerosis. Only significant p values should be in bold.

with risk scores for CVD and mortality and compared it with the conventional definition of fitness based on the 6MWT, we found that fitAA, unlike 6MWT, was significantly associated with major health risk scores calculated according to established formulae (D'Agostino et al., 2008; Goff et al., 2013; Budoff et al., 2018; Levine et al., 2018; Roffman et al., 2016): the higher fitAA, the higher the short term risk of cardiovascular events and death.

To improve the interpretability of our results we categorized individuals into three groups according to their fitAA value: individuals with fitAA lower than −2.5 years (labelled as “FIT”) showed the highest fitness and lowest risk scores, suggesting that they experience slower and healthier ageing. Conversely, individuals with fitAA higher than +2.5 years showed the lowest fitness and highest risk scores, suggesting accelerated and less healthy ageing. Scores between these two cut-offs characterise individuals whose biological age is close to their chronological age and with intermediate risk scores.

Such estimates can be interpreted as the increase in the risk score of “NORMAL” and “UNFIT” individuals compared to the “FIT” group used as the reference. Accordingly, we estimated that an “UNFIT” individual has, on average, around 5% higher probability

of dying or experiencing a CVD event within the next 10 years than a “FIT” individual. This categorization allowed us to compare our multi-level measure with that based on the conventional 6MWT. This study's results highlight that a composite measure of fitness status outperforms 6MWT in estimating the state of health of an individual.

This work has limitations. First, we collected data from a mixed cohort of middle-aged and older adults. Further, the available sample size does not allow us to generalise these results to the whole population over 50 years and does not allow setting-up cut-offs for the definition of accelerated, normal, or decelerated aging. However, we provided proof of the advantages of using multiple fitness tests to assess the health status of the elderly. The weights defined in this study through the elastic net regression model must be calibrated and validated in larger population studies before they can be used in clinical practice.

Further, additional studies are needed to assess fitness status separately in women and men, as the measures to evaluate it in the elderly and the transition from adult age to elderly may behave differently in the two sexes, even though our data consistently ranked the TUG as the major contributor to biological age in both men and women.

Conclusion

Our results suggest that a proper evaluation of fitness status should favor a set of physical motor tests that include the TUG, which reflects the essential components of mobility, and handgrip strength, which is a valid indicator of overall strength. These two simple tests proved the best predictors of fitness age and could represent robust and feasible tools to monitor the ageing process according to the fitness level displayed. In conjunction with this finding, the newly introduced measure—fitAA—that quantifies the difference between biological and chronological age—can help to identify individuals at high risk for non-communicable diseases in the short period, with important advantages for public health and screening policies. Although we examined well-validated measures of risk to assess the individual state of health, further investigation using a longitudinal design is needed to assess risk measures associated with accelerated fitAA more precisely and to validate our findings.

Data availability statement

The raw data supporting the conclusion of this article will be made available by the authors, without undue reservation.

Ethics statement

The studies involving human participants were reviewed and approved by Institutional Review Board and the Clinical Research Ethics Committee approved all procedures involving human subjects (ID: PG/2020/16846). The patients/participants provided their written informed consent to participate in this study.

References

- Abizanda, P., Navarro, J. L., García-Tomás, M. I., López-Jiménez, E., Martínez-Sánchez, E., and Paterna, G. (2012). Validity and usefulness of hand-held dynamometry for measuring muscle strength in community-dwelling older persons. *Arch. Gerontol. Geriatr.* 54 (1), 21–27. doi:10.1016/j.archger.2011.02.006
- Arango-Lopera, V. E., Arroyo, P., Gutierrez-Robledo, L. M., Perez-Zepeda, M. U., and Cesari, M. (2013). Mortality as an adverse outcome of sarcopenia. *J. Nutr. Health Aging* 17 (3), 259–262. doi:10.1007/s12603-012-0434-0
- ATS Committee on Proficiency Standards for Clinical Pulmonary Function Laboratories (2002). ATS statement: Guidelines for the six-minute walk test. *Am. J. Respir. Crit. Care Med.* 166 (1), 111–117. doi:10.1164/ajrccm.166.1.at1102
- Beard, J. R., Officer, A., de Carvalho, I. A., Sadana, R., Pot, A. M., Michel, J. P., et al. (2016). The world report on ageing and health: A policy framework for healthy ageing. *Lancet* 387 (10033), 2145–2154. doi:10.1016/S0140-6736(15)00516-4
- Budoff, M. J., Young, R., Burke, G., Carr, J. J., Detrano, R. C., Folsom, A. R., et al. (2018). Ten-year association of coronary artery calcium with atherosclerotic cardiovascular disease (ASCVD) events: The multi-ethnic study of atherosclerosis (MESA). *Eur. Heart J.* 39, 2401–2408. doi:10.1093/eurheartj/ehy217
- Caspersen, C. J., Powell, K. E., and Christenson, G. M. (1985). Physical activity, exercise, and physical fitness: Definitions and distinctions for health-related research. *Public Health Rep.* 100, 126–131.
- Chen, L. K., Liu, L. K., Woo, J., Assantachai, P., Auyeung, T. W., Bahyah, K. S., et al. (2014). Sarcopenia in asia: Consensus report of the asian working group for sarcopenia. *J. Am. Med. Dir. Assoc.* 15 (2), 95–101. doi:10.1016/j.jamda.2013.11.025
- Chua, K. Y., Lim, W. S., Lin, X., Yuan, J. M., and Koh, W. P. (2020). Handgrip strength and timed up-and-go (TUG) test are predictors of short-term mortality among elderly in a population-based cohort in Singapore. *J. Nutr. Health Aging* 24 (4), 371–378. doi:10.1007/s12603-020-1337-0
- Cleary, K., and Skorniyakov, E. (2017). Predicting falls in older adults using the four square step test. *Physiother. Theory Pract.* 33 (10), 766–771. doi:10.1080/09593985.2017.1354951
- Cruz-Jentoft, A. J., Baeyens, J. P., Bauer, J. M., Boirie, Y., Cederholm, T., Landi, F., et al. (2010). Sarcopenia: European consensus on definition and diagnosis: Report of the European working group on sarcopenia in older people. *Age Ageing* 39 (4), 412–423. doi:10.1093/ageing/afq034
- D'Agostino, R. B., Vasan, R. S., Pencina, M. J., Wolf, P. A., Cobain, M., Massaro, J. M., et al. (2008). General cardiovascular risk profile for use in primary care: The Framingham heart study. *Circulation* 117 (6), 743–753. doi:10.1161/CIRCULATIONAHA.107.699579
- Edvardsen, E., Hansen, B. H., Holme, I. M., Dyrstad, S. M., and Anderssen, S. A. (2013). Reference values for cardiorespiratory response and fitness on the treadmill in a 20- to 85-year-old population. *Chest* 144 (1), 241–248. doi:10.1378/chest.12-1458
- Ekelund, U., Tarp, J., Steene-Johannessen, J., Hansen, B. H., Jefferis, B., Fagerland, M. W., et al. (2019). Dose-response associations between accelerometry measured physical activity and sedentary time and all cause mortality: Systematic review and harmonised meta-analysis. *BMJ* 366, l4570. doi:10.1136/bmj.l4570
- Elshafey, M. A., and Alsakhawi, R. S. (2022). Inspiratory muscle training and physical fitness in children with down syndrome: A randomized controlled trial. *Arch. Phys. Med. Rehabil.* 22, 00363–02287. doi:10.1016/j.apmr.2022.04.005
- Fielding, R. A., Vellas, B., Evans, W. J., Bhasin, S., Morley, J. E., Newman, A. B., et al. (2011). Sarcopenia: An undiagnosed condition in older adults. Current consensus definition: Prevalence, etiology, and consequences. International working group on sarcopenia. *J. Am. Med. Dir. Assoc.* 12 (4), 249–256. doi:10.1016/j.jamda.2011.01.003
- Finch, C. E. (1994). *Longevity, senescence, and the genome*. Chicago: University of Chicago Press.
- Fiuza-Luces, C., Santos-Lozano, A., Joyner, M., Carrera-Bastos, P., Picazo, O., Zugaza, J. L., et al. (2018). Exercise benefits in cardiovascular disease: Beyond attenuation of

Author contributions

AM, GF, and FD conceived the study. MM, AB, GM, LV, AC, and MC conducted the experiments. AM, GF, and FD drafted the manuscript. All authors reviewed the manuscript and approved the final version for submission.

Funding

FD is the recipient of a 3-year grant from MUR PON-AIM 2014–2020 (Grant No.: PONBIOMEDAIM2). BM was supported by the same grant. FM was supported by Fondi di Ateneo per la Ricerca (FAR 2020). Additional support was provided by Fondazione di Sardegna (FdS 2020).

Conflict of interest

The authors declare that the research was conducted in the absence of any commercial or financial relationships that could be construed as a potential conflict of interest.

Publisher's note

All claims expressed in this article are solely those of the authors and do not necessarily represent those of their affiliated organizations, or those of the publisher, the editors and the reviewers. Any product that may be evaluated in this article, or claim that may be made by its manufacturer, is not guaranteed or endorsed by the publisher.

- traditional risk factors. *Nat. Rev. Cardiol.* 15 (12), 731–743. doi:10.1038/s41569-018-0065-1
- Galeoto, G., Sansoni, J., Scuccimarri, M., Bruni, V., De Santis, R., Colucci, M., et al. (2018). A psychometric properties evaluation of the Italian version of the geriatric depression Scale. *Depress Res. Treat.* 2018, 1797536. doi:10.1155/2018/1797536
- Gilbert, S. F. (2000). *Developmental biology 6th edition*. Sunderland (MA): Sinauer Associates.
- Goff, D. C., Lloyd-Jones, D. M., Bennett, G., Coady, S., D'Agostino, R. B., Gibbons, R., et al. (2013). ACC/AHA guideline on the assessment of cardiovascular risk. *Circulation* 2014, 129.
- Horvath, S. (2013). DNA methylation age of human tissues and cell types. *Genome Biol.* 14 (10), R115. doi:10.1186/gb-2013-14-10-r115
- Lara, J., Cooper, R., Nissan, J., Ginty, A. T., Khaw, K. T., Deary, I. J., et al. (2015). A proposed panel of biomarkers of healthy ageing. *BMC Med.* 13, 222. doi:10.1186/s12916-015-0470-9
- Levine, M. E., Lu, A. T., Quach, A., Chen, B. H., Assimes, T. L., Bandinelli, S., et al. (2018). An epigenetic biomarker of aging for lifespan and healthspan. *Aging (Albany NY)* 10 (4), 573–591. doi:10.18632/aging.101414
- Liu, Z., Kuo, P. L., Horvath, S., Crimmins, E., Ferrucci, L., and Levine, M. (2018). A new aging measure captures morbidity and mortality risk across diverse subpopulations from nhanes IV: A cohort study. *PLoS Med.* 15 (12), e1002718. doi:10.1371/journal.pmed.1002718
- Mack-Inocentio, D., Menai, M., Doré, E., Doreau, B., Gaillard, C., Finaud, J., et al. (2020). Large-scale assessment of health-related physical fitness in French older adults: Feasibility and validity. *Front. Public Health* 8, 487308. doi:10.3389/fpubh.2020.487308
- Matos Casano, H. A., and Anjum, F. (2022). *Six minute walk test*. Treasure Island (FL): StatPearls Publishing. [Updated 2022 Oct 17]. In: StatPearls.
- McGreevy, K. M., Radak, Z., Torma, F., Lu, A. T., Belsky, D. W., Binder, A., et al. (2022). *DNAFitAge: Biological age indicator incorporating physical fitness*. medRxiv.
- Nakamura, E., Moritani, T., and Kanetaka, A. (1989). Biological age versus physical fitness age. *Eur. J. Appl. Physiol. Occup. Physiol.* 58 (7), 778–785. doi:10.1007/BF00637391
- Pareja-Galeano, H., Garatachea, N., and Lucia, A. (2015). Exercise as a polypill for chronic diseases. *Prog. Mol. Biol. Transl. Sci.* 135, 497–526. doi:10.1016/bs.pmbts.2015.07.019
- Perera, S., Mody, S. H., Woodman, R. C., and Studenski, S. A. (2006). Meaningful change and responsiveness in common physical performance measures in older adults. *J. Am. Geriatr. Soc.* 54 (5), 743–749. doi:10.1111/j.1532-5415.2006.00701.x
- Podsiadlo, D., and Richardson, S. (1991). The timed "up and go": A test of basic functional mobility for frail elderly persons. *J. Am. Geriatr. Soc.* 39 (2), 142–148. doi:10.1111/j.1532-5415.1991.tb01616.x
- Rantanen, T., Guralnik, J. M., Foley, D., Masaki, K., Leveille, S., Curb, J. D., et al. (1999). Midlife hand grip strength as a predictor of old age disability. *JAMA* 281 (6), 558–560. doi:10.1001/jama.281.6.558
- Roffman, C. E., Buchanan, J., and Allison, G. T. (2016). Charlson comorbidities index. *J. Physiother.* 62 (3), 171. doi:10.1016/j.jphys.2016.05.008
- Ros, E., Martínez-González, M. A., Estruch, R., Salas-Salvadó, J., Fitó, M., Martínez, J. A., et al. (2014). Mediterranean diet and cardiovascular health: Teachings of the PREDIMED study. *Adv. Nutr.* 5 (3), 330S–6S. doi:10.3945/an.113.005389
- Ross, R., Blair, S. N., Arena, R., Church, T. S., Després, J. P., Franklin, B. A., et al. (2016). Importance of assessing cardiorespiratory fitness in clinical practice: A case for fitness as a clinical vital sign: A scientific statement from the American heart association. *Circulation* 134 (24), e653–e699. doi:10.1161/CIR.0000000000000461
- Sanchez-Sanchez, J. L., Izquierdo, M., Carnicero-Carreño, J. A., García-García, F. J., and Rodríguez-Mañas, L. (2020). Physical activity trajectories, mortality, hospitalization, and disability in the Toledo Study of Healthy Aging. *J. Cachexia Sarcopenia Muscle* 11 (4), 1007–1017. doi:10.1002/jcsm.12566
- Soares-Miranda, L., Lucia, A., Silva, M., Peixoto, A., Ramalho, R., da Silva, P. C., et al. (2021). Physical fitness and health-related quality of life in patients with colorectal cancer. *Int. J. Sports Med.* 42 (10), 924–929. doi:10.1055/a-1342-7347
- Stern, M. P., Williams, K., and Haffner, S. M. (2002). Identification of persons at high risk for type 2 diabetes mellitus: Do we need the oral glucose tolerance test? *Ann. Intern. Med.* 136, 575–581. doi:10.7326/0003-4819-136-8-200204160-00006
- Szychowska, A., and Drygas, W. (2022). Physical activity as a determinant of successful aging: A narrative review article. *Aging Clin. Exp. Res.* 34 (6), 1209–1214. doi:10.1007/s40520-021-02037-0
- Tucker, L. A. (2017). Physical activity and telomere length in U.S. men and women: An NHANES investigation. *Prev. Med.* 100, 145–151. doi:10.1016/j.ypmed.2017.04.027
- Vandenbroucke, J. P., von Elm, E., Altman, D. G., Gøtzsche, P. C., Mulrow, C. D., Pocock, S. J., et al. (2007). Strengthening the reporting of observational studies in Epidemiology (STROBE): Explanation and elaboration. *PLoS Med.* 4 (10), e297. doi:10.1371/journal.pmed.0040297
- Wiener, J., McIntyre, A., Janssen, S., Chow, J. T., Batey, C., and Teasell, R. (2019). Effectiveness of high-intensity interval training for fitness and mobility post stroke: A systematic review. *PM R* 11 (8), 868–878. doi:10.1002/pmrj.12154
- Wilder, R. P., Greene, J. A., Winters, K. L., Long, W. B., 3rd, Gubler, K., and Edlich, R. F. (2006). Physical fitness assessment: An update. *J. Long. Term. Eff. Med. Implants* 16 (2), 193–204. doi:10.1615/jlongtermeffmedimplants.v16.i2.90
- World Health Organization. (2015). World report on ageing and health. World Health Organization. Available at: <https://apps.who.int/iris/handle/10665/186463>.



OPEN ACCESS

EDITED BY

Grazia Tamma,
University of Bari Aldo Moro, Italy

REVIEWED BY

Alessia Remigante,
University of Messina, Italy
Anna De Bartolo,
University of Calabria, Italy
Daniele Mancardi,
University of Turin, Italy

*CORRESPONDENCE

Roberto Berra-Romani,
✉ rberra001@hotmail.com
Francesco Moccia,
✉ francesco.moccia@unipv.it

RECEIVED 04 April 2023

ACCEPTED 27 April 2023

PUBLISHED 11 May 2023

CITATION

Moreno-Salgado A, Coyotl-Santiago N,
Moreno-Vazquez R, Lopez-Teyssier M,
Garcia-Carrasco M, Moccia F and
Berra-Romani R (2023), Alterations of the
Ca²⁺ clearing mechanisms by type
2 diabetes in aortic smooth muscle cells
of Zucker diabetic fatty rat.
Front. Physiol. 14:1200115.
doi: 10.3389/fphys.2023.1200115

COPYRIGHT

© 2023 Moreno-Salgado, Coyotl-Santiago,
Moreno-Vazquez, Lopez-Teyssier,
Garcia-Carrasco, Moccia and
Berra-Romani. This is an open-access
article distributed under the terms of the
[Creative Commons Attribution License \(CC BY\)](#). The use, distribution or
reproduction in other forums is
permitted, provided the original author(s)
and the copyright owner(s) are credited
and that the original publication in this
journal is cited, in accordance with
accepted academic practice. No use,
distribution or reproduction is permitted
which does not comply with these terms.

Alterations of the Ca²⁺ clearing mechanisms by type 2 diabetes in aortic smooth muscle cells of Zucker diabetic fatty rat

Adriana Moreno-Salgado¹, Nayeli Coyotl-Santiago¹,
Roberto Moreno-Vazquez¹, Mayte Lopez-Teyssier¹,
Mario Garcia-Carrasco², Francesco Moccia^{3*} and
Roberto Berra-Romani^{1*}

¹Department of Biomedicine, School of Medicine, Benemerita Universidad Autonoma de Puebla, Puebla, Mexico, ²Department of Immunology, School of Medicine, Benemerita Universidad Autonoma de Puebla, Puebla, Mexico, ³Department of Biology and Biotechnology "Lazzaro Spallanzani", University of Pavia, Pavia, Italy

Type 2 Diabetes Mellitus (T2DM) is a rapidly rising disease with cardiovascular complications constituting the most common cause of death among diabetic patients. Chronic hyperglycemia can induce vascular dysfunction through damage of the components of the vascular wall, such as vascular smooth muscle cells (VSMCs), which regulate vascular tone and contribute to vascular repair and remodeling. These functions are dependent on intracellular Ca²⁺ changes. The mechanisms by which T2DM affects Ca²⁺ handling in VSMCs still remain poorly understood. Therefore, the objective of this study was to determine whether and how T2DM affects Ca²⁺ homeostasis in VSMCs. We evaluated intracellular Ca²⁺ signaling in VSMCs from Zucker Diabetic Fatty rats using Ca²⁺ imaging with Fura-2/AM. Our results indicate that T2DM decreases Ca²⁺ release from the sarcoplasmic reticulum (SR) and increases the activity of store-operated channels (SOCs). Moreover, we were able to identify an enhancement of the activity of the main Ca²⁺ extrusion mechanisms (SERCA, PMCA and NCX) during the early stage of the decay of the ATP-induced Ca²⁺ transient. In addition, we found an increase in Ca²⁺ entry through the reverse mode of NCX and a decrease in SERCA and PMCA activity during the late stage of the signal decay. These effects were appreciated as a shortening of ATP-induced Ca²⁺ transient during the early stage of the decay, as well as an increase in the amplitude of the following plateau. Enhanced cytosolic Ca²⁺ activity in VSMCs could contribute to vascular dysfunction associated with T2DM.

KEYWORDS

type 2 diabetes mellitus, intracellular Ca²⁺, Fura-2, freshly isolated vascular smooth muscle cells, Zucker diabetic fatty

1 Introduction

Diabetes mellitus (DM) comprises a group of metabolic diseases characterized by an increase in plasma glucose levels (hyperglycemia) due to defects in the secretion (type 1 DM or T1DM) or action (type 2 DM or T2DM) of insulin (ElSayed et al., 2023). T2DM is the most common form of DM as it constitutes 90% of all diabetic cases worldwide

(IDF Diabetes Atlas, 2021). The most common cause of death among diabetic patients is represented by cardiovascular disorders with heart disease causing approximately 70% of patients' deaths (Gu et al., 1998; Einarson et al., 2018). Other causes of mortality include cerebrovascular disease, myocardial infarction, hypertension and atherosclerosis (Kennedy, 2017).

It has long been known that hyperglycemia, dyslipidemia and insulin resistance, all of which accompany T2DM, are related to an increase in cardiovascular risk by affecting the structural components of blood vessels through multiple mechanisms, such as protein glycosylation and oxidative stress, which lead to vascular dysfunction (Szuszkiewicz-Garcia and Davidson, 2014; Mao et al., 2022). Vascular dysfunction is a complex and multifactorial process; however, there is strong evidence showing that T2DM alters intracellular Ca^{2+} handling in vascular smooth muscle cells (VSMCs) (Fernandez-Velasco et al., 2014; Nieves-Cintrón et al., 2021). Remodeling of Ca^{2+} handling in VSMCs may dramatically alter vascular reactivity as well other processes, such as migration and proliferation, which are involved in vascular repair and angiogenesis (Fernandez-Velasco et al., 2014). Alterations in these processes may favor the development of pathologies such as hypertension and atherosclerosis. Although most of the studies performed in animal models of T2DM hint at an increase in the bioavailability of intracellular Ca^{2+} that enhances vascular reactivity or cell migration and proliferation, depending on the VSMC phenotype (Fernandez-Velasco et al., 2014), the cellular and molecular mechanisms involved still remain poorly understood. Several reports suggest that T2DM induces an increase in the expression or activity of Ca^{2+} -permeable channels, such as the store-operated calcium entry (SOCE) pathway and transient receptor potential canonical channels (TRPC) on the sarcolemma (Chung et al., 2009; Nieves-Cintrón et al., 2021), and inositol 1,4,5-trisphosphate receptor (IP_3R) Ca^{2+} release channels in the sarcoplasmic reticulum (SR) (Velmurugan and White, 2012; Nieves-Cintrón et al., 2021). For instance, a recent study suggested that SOCE is enhanced in diabetic VSMCs and exacerbates vasoconstriction in the aorta of Zucker Diabetic Fatty (ZDF) rats, a model widely used for the study of T2DM (Yang et al., 2020). In addition, hyperglycemia stimulates expression of ORAI1, thus, augmenting store-operated Ca^{2+} -entry in primary human aortic smooth muscle cells (Ma et al., 2020).

Only scarce information is available about the alteration of Ca^{2+} removal mechanisms, which significantly contribute to maintain intracellular Ca^{2+} homeostasis under physiological conditions, in VSMCs during T2DM. A study carried out on cultured A7r5 cells showed that hyperglycemia causes an increase in the activity of Plasma Membrane Ca^{2+} -ATPase (PMCA), which extrudes Ca^{2+} across the sarcolemma, as well as a decrease in the activity of Sarco-Endoplasmic Reticulum Ca^{2+} -ATPase (SERCA), which sequesters cytosolic Ca^{2+} into the SR (El-Najjar et al., 2017). Similarly, it has been suggested that SERCA activity is downregulated by oxidative stress in rat aortic VSMCs from ZDF rats, although the impact of SERCA oxidation of Ca^{2+} clearance has not been directly assessed (Tong et al., 2010). $\text{Na}^+/\text{Ca}^{2+}$ exchanger (NCX) represents an alternative pathway for Ca^{2+} extrusion across the plasma membrane in VSMCs, but it is still unknown whether it is affected by T2DM. Therefore, it is mandatory to gain further insights about the remodeling of the Ca^{2+} handling machinery in

an experimental model that effectively recapitulates the pathophysiology of T2DM, such as ZDF rats. The present investigation sought to exhaustively assess whether and how T2DM alters the intracellular Ca^{2+} signaling in VSMCs from the aorta of ZDF rats, loaded with the Ca^{2+} -sensitive indicator, Fura-2-acetoxymethyl ester (Fura-2/AM).

2 Materials and methods

2.1 Zucker diabetic fatty rat model

All the experiments were carried out according to the *Norma Oficial Mexicana* (NOM-062-ZOO-1999, 9.4.2.1.3.) for the care and handling of laboratory animals. The protocols were reviewed and approved by the Animal Care and Use Committee of the Benemerita Universidad Autonoma de Puebla, identification code: BERRSAL71, 18-05-2017. Experiments were carried out in male ZDF rats (3 months old) from Charles River Laboratories, California, U.S.A. Throughout the text, diabetic-obese ZDF rats (ZDF-Lepr^{fa/fa}) will be designated as OZDF rats, and lean controls, non-obese non-diabetic ZDF (ZDF-Lepr^{+/+}) as LZDF. The rats were kept at the University Animal Core Facilities under controlled environmental temperature and, exposed to light-dark cycles of 12 h, with *ad libitum* consumption of water and high energy diet, Purina 5,008 chow.

2.2 Somatic and biochemical parameters

To determine if OZDF rats did indeed develop T2DM, 5 days prior to the experiment, a glucose tolerance test was performed. The animals were fasted for 6 h in metabolic cages with free access to water. Immediately after, a glucose dose (2 g/kg of weight) was administered intraperitoneally. Two hours later, a blood sample was obtained by puncture of the caudal vein to measure glucose levels using the Accucheck® system (Roche, Mannheim, Germany). The day of the experiment, we proceeded to measure the body mass (weight), length (distance from the tip of the nose to the base of the tail) and the abdominal circumference using a measuring tape.

The body mass index (BMI) was calculated using the following equation:

$$\text{BMI} = \frac{\text{Body mass (g)}}{\text{Length}^2 (\text{cm})^2}$$

Finally, all the epididymal fat surrounding both testes was accurately removed and weighed.

2.3 Isolation and culture rat aortic VSMC and dissection of epididymal fat samples

Isolation and culture of rat VSMCs were carried out according to the protocol previously described by Berra-Romani et al. to isolate proliferating, non-contracting VSMCs (Berra-Romani et al., 2008). ZDF rats were anesthetized with intraperitoneal ketamine-xylazine solution, 0.2 mL per 100 g of weight. The thoracic aorta was

dissected out and perfused with low- Ca^{2+} physiological salt solution (PSS1, see composition in [Section 2.5](#)). Under sterile conditions the artery was cleaned of fat and connective tissue and then incubated for ~40 min at 37°C in PSS1 containing 1 mg/mL collagenase type 2. After the incubation, the aorta was washed three times with PSS1 and the adventitia was carefully stripped. The aorta was cut longitudinally in order to expose the *tunica intima* and the endothelium was mechanically removed by rubbing a microdissection scissor against the endothelial layer. Aortic tissue was cut in a proximately 2 mm pieces and enzymatically digested for 40 min at 37°C in PSS1 containing 2 mg/mL collagenase type XI, 0.16 mg/mL elastase type IV and 2 mg/mL bovine serum albumin (BSA; fat free). After de digestion, VSMCs were resuspended by gently triturating the tissue with a fire-polished Pasteur pipette. To stop enzymatic digestion, 10 mL of Dulbecco's modified Eagle's medium (DMEM) supplemented with 10% fetal bovine serum (FBS) was added. VSMCs were centrifugated for 10 min at 300g. The supernatant was discarded, and the resulting cell pellet was re-suspended in 1 mL complete medium (DMEM with 10% FBS and 1% antibiotic antimycotic solution (100x)). VSMC were plated on 35 mm culture dishes under a humidified atmosphere of 5% CO_2 - 95% O_2 at 37°C. Culture medium was changed on days 4 and 7 and Ca^{2+} imaging experiments were performed on subconfluent cultures on days 7 and 8. The aortic VSMCs identity was confirmed by α -actin labelling, as shown in ([Berra-Romani et al., 2008](#)).

2.4 $[\text{Ca}^{2+}]_i$ measurements

Cultured VSMCs were loaded with 3 μM Ca^{2+} indicator, Fura-2/AM in PSS2 (see composition in [Section 2.5](#)) for 35 min at controlled room temperature (22–23 °C). After 20 min washing in PSS2, the culture dish was mounted onto the stage of an upright epifluorescence Axiolab microscope (Carl Zeiss, Oberkochen, Germany) equipped with a $\times 40$ Achromplan objective (water-immersion, 2.05 mm working distance, 1.0 numerical aperture) to observe the cells. VSMCs were excited alternately at 340 and 380 nm, and the emitted light was detected at 510 nm. A neutral density filter (optical density = 1.0) was coupled to the 380 nm filter to approach the intensity of the 340 nm light. A round diaphragm was used to increase the contrast. The exciting filters were mounted on a filter wheel equipped with a shutter (Lambda 10, Sutter Instrument, Novato, CA, United States). Custom software, working in the LINUX environment, was used to drive the camera (Extended-ISIS Camera, Photonic Science, Millham, United Kingdom) and the filter wheel, and to measure and plot on-line the fluorescence from a number of 20–50 rectangular “regions of interest” (ROI) enclosing 20–50 single cells. Each ROI was identified by a number. The intracellular Ca^{2+} concentration ($[\text{Ca}^{2+}]_i$) was monitored by measuring, for each ROI, the ratio of the mean fluorescence emitted at 510 nm when exciting alternatively at 340 and 380 nm (shortly termed “Ratio (F_{340}/F_{380})”). An increase in $[\text{Ca}^{2+}]_i$ causes an increase in the Ratio (F_{340}/F_{380}). Ratio measurements were performed and plotted on-line every 3 s. Ratio (F_{340}/F_{380}) values are expressed as arbitrary units (a.u.). Images were stored on the hard disk and converted offline to Ratio (F_{340}/F_{380}) images by ImageJ software (National Institutes of Health, United States, <http://rsbweb.nih.gov/ij/>). The experiments were carried out at

controlled room temperature (22–23°C) to limit time-dependent decreases in the intensity of the fluorescence signal.

Mn^{2+} has been shown to quench Fura-2 fluorescence. Since Mn^{2+} and Ca^{2+} share common entry pathways in the plasma membrane, Fura-2 quenching by Mn^{2+} is regarded as an index of divalent cation influx. Experiments were carried out at the 360 nm wavelength, the isosbestic wavelength for Fura-2, and in Ca^{2+} -free medium supplemented with 0.5 mM EGTA, as previously described ([Zuccolo et al., 2019](#)). This avoids Ca^{2+} competition for Mn^{2+} entry and, therefore, enhances Mn^{2+} quenching.

2.5 Solutions

Low- Ca^{2+} physiological salt solution (PSS1) had the following composition (in mM): 140 NaCl, 5.36 KCl, 0.34 Na_2HPO_4 , 0.44 KH_2PO_4 , 10 HEPES, 1.2 MgCl_2 , 10 D-glucose and 0.05 CaCl_2 . Physiological salt solution (PSS2) composition (in mM) was: 140 NaCl, 5 KCl, 1.2 NaH_2PO_4 , 5 NaHCO_3 , 10 HEPES, 1.4 MgCl_2 , 1.8 CaCl_2 and 11.5 D-glucose. In Ca^{2+} free solution (0Ca^{2+}), 0.05 EGTA was added. In Mn^{2+} -quenching experiments, 200 μM MnCl_2 was added to the 0Ca^{2+} external solution. Solutions were titrated to pH 7.2 for PSS1 and 7.4 for PSS2 with NaOH. The osmolality of PSS as measured with an osmometer (Wescor 5,500, Logan, UT) was 338 mmol/kg.

2.6 Data analysis

For each protocol, data were collected from at least four rats under each condition. The amplitude of the peak Ca^{2+} response to either cyclopiazonic acid (CPA) or adenosine-trisphosphate (ATP) was measured as the difference between the Ratio (F_{340}/F_{380}) at the peak and the mean Ratio (F_{340}/F_{380}) of 500 s baseline before the peak ([Supplementary Figure S1](#)). Amplitude of the late stage of the decay (Amp600) was calculated as the difference between the Ratio (F_{340}/F_{380}) 600 s after adding the agonist and the mean Ratio (F_{340}/F_{380}) of 200 s baseline before the peak of the Ca^{2+} response ([Supplementary Figure S1](#)). The duration of the Ca^{2+} response to ATP was measured as the time it takes the Ca^{2+} signal to be reduced at 90% (early) ([Supplementary Figure S1](#)), 60% (intermediate) ([Supplementary Figure S1](#)) and 30% (late) ([Supplementary Figure S1](#)) of the initial Ca^{2+} peak amplitude (considered as 100%), shortly termed as “decay time” (DT) ([Supplementary Figure S1](#)). The area under the curve (AUC) was measured by calculating the integral of each Ca^{2+} tracing from when the ATP is applied until it is removed. In order to perform the statistical comparison between the experimental groups in the presence of selective inhibitors of Ca^{2+} -clearing mechanisms, we proceeded to normalize the measures to the mean value of each parameter determined in the absence of the inhibitor within the same experimental group (shortly termed “ Δ ”). For mean traces, fluorescence levels (F) were normalized to resting fluorescence (F_0) to compare the height of the Ca^{2+} responses produced by cells displaying different basal fluorescence levels (F/F_0). The rate of Mn^{2+} influx was evaluated by measuring the slope of the fluorescence intensity curve after Mn^{2+} addition ([Zuccolo et al., 2019](#)). Data are expressed as mean \pm standard error (SE). Normal data (identified using the D'Agostino and Pearson omnibus normality test ($p < 0.05$)), were statistically analyzed using an unpaired

TABLE 1 Zucker Diabetic Fatty rat characteristics. Mean \pm SE of somatic and biochemical parameters measured in Zucker Diabetic Fatty (LZDF and OZDF) rats at the age of 12 weeks. Body mass index (BMI) was calculated according to the equation described in materials and Methods. Blood glucose levels were measured using the Accucheck[®] system, 2 h after the intraperitoneal administration of glucose (2 g/kg of weight) in 6 h fasted animals. * indicates $p \leq 0.05$ (Student's t-test, $n = 5$ per group; for glucose values $n = 14$ per group).

	LZDF	OZDF
Body weight (g)	297.8 \pm 3.87	494.3 \pm 5.86*
Length (cm)	22.19 \pm 0.25	23.64 \pm 0.36*
BMI (g/cm ²)	0.60 \pm 0.01	0.88 \pm 0.02*
Abdominal circumference (cm)	13.35 \pm 0.15	17.13 \pm 0.27*
Epididymal fat (g)	2.50 \pm 0.15	12.63 \pm 0.72*
Glucose 2h (gr/dl)	126.06 \pm 5.49	239.5 \pm 24.54*

Student's t-test. A p -value < 0.05 was considered statistically significant.

2.7 Chemicals

SEA0400 was obtained from Tocris Bioscience (Bristol, United Kingdom). Collagenase type 2 and FBS were obtained from Gibco (GIBCO BRL, Life Technologies, Grand Island, NY). All other chemicals were purchased from Sigma-Aldrich.

3 Results

3.1 Zucker diabetic fatty rat characteristics

Somatic parameter obtained from 3 months old littermate LZDF and OZDF rats are shown in Table 1. OZDF rats presented an increase of around 66% in body mass weight ($p \leq 0.05$) and of around 6.5% of the nose-tail length ($p \leq 0.05$) compared with their control, LZDF rats. Given that the increase in weight could be attributed to an increase in the rat size (to its length), we proceeded to calculate the body mass index (BMI) to rule out that the differences seen in the weight were due to the difference in length between both groups. Likewise, the mean BMI value was statistically higher (46.6%) in the OZDF rats compared to the LZDF group ($p \leq 0.05$), suggesting that the weight gain is due to obesity that has been widely reported in the literature in this strain of rats (Shiota and Printz, 2012; Wang et al., 2013; Al-Awar et al., 2016; King and Bowe, 2016; Berra-Romani et al., 2019). The presence of obesity in the OZDF rats was demonstrated by the 28% and 405% increase in abdominal circumference ($p \leq 0.05$) and epididymal fat weight ($p \leq 0.05$), respectively, in OZDF vs. LZDF rats. To confirm T2DM presence in OZDF rats, a glucose tolerance test was performed as described in Materials and Methods section. The mean \pm SE of blood glucose levels measured 2 h after the intraperitoneal administration of glucose (2 g/kg of weight), was approximately 90% higher ($p \leq 0.05$) in the OZDF rats compared to the LZDF rats (Table 1). Altogether the results confirm that OZDF rats present obesity and diabetes. In addition, a deeper biochemical analysis of LZDF rats and OZDF rats has been presented in (Berra-Romani et al., 2019), showing that OZDF rats present: 1)

hyperlipidemia (increased total cholesterol, very low-density lipoproteins, and triglyceride levels); 2) hyperinsulinemia both in fasting and glucose-fed animals; and 3) insulin resistance. All together these results confirm the presence in OZDF rats of the main characteristics of human T2DM.

3.2 T2DM shortens the early phase of the decay and increases the plateau amplitude of ATP-induced Ca^{2+} signals in rat aortic VSMCs

Preliminary recordings revealed that resting Ca^{2+} levels were similar (Supplementary Figure S2A) and that spontaneous Ca^{2+} oscillations (Supplementary Figure S2B) did not occur in VSMCs from the two animal groups. Moreover, 20 μM ATP was found to induce only a Ca^{2+} transient in rat aortic VSMCs from both OZDF and LZDF rats (Supplementary Figure S3). Since we were also interested in the impact of T2DM on the plateau phase of the Ca^{2+} response to physiological autacoids (Berra-Romani et al., 2019), ATP concentration was raised to 300 μM . In resting VSMCs from both LZDF and OZDF rats, the application of 300 μM ATP induced an intracellular Ca^{2+} signal that consisted in a rapid Ca^{2+} spike followed by a slow decay phase to a sustained plateau phase, which returned to the baseline upon agonist removal (Figure 1A). When comparing both groups, we did not find any statistical difference in both the peak amplitude (Figure 1B, left panel) and area under the curve (AUC) (Figure 1D). However, decay time (DT) at 90% and 60% of total amplitude were decreased ($p \leq 0.05$) in VSMCs from OZDF rats (Figure 1C). In addition, we found an increase in the amplitude of the plateau phase in VSMCs from OZDF rats compared to LZDF rats, as shown by the increase in Amp600 value ($p \leq 0.05$) (Figure 1B, right panel). Conversely, the decay time at 30% was not different between both groups (Figure 1C). The fastest decline of the initial Ca^{2+} peak could explain why the increase in Amp600 does not result in an increased AUC.

3.3 Effect of the removal of extracellular Ca^{2+} (0Ca^{2+}) on ATP-induced Ca^{2+} signals in rat aortic VSMCs

Figure 2 shows the average of Ca^{2+} signals recorded from cultured VSMCs obtained from LZDF (Figure 2A) and OZDF (Figure 2D) rat aortas challenged with ATP (300 μM) in presence (dotted line; + Ca^{2+}) and absence (continuous line; + 0Ca^{2+}) of Ca^{2+} in the extracellular medium. Removal of extracellular Ca^{2+} (0Ca^{2+}) caused a decrease in peak amplitude, AUC, and decay time, as well as the disappearance of the plateau phase, in ATP-induced Ca^{2+} transients in both LZDF (Figures 2A-C) and OZDF VSMCs (Figures 2D-F). These findings confirm that both endogenous Ca^{2+} release through ER-resident IP_3Rs and extracellular Ca^{2+} entry via store-operated channels (SOCs) support the Ca^{2+} response to ATP in proliferating rat aortic VSMCs (Berra-Romani et al., 2008). In accord, depletion of the ER Ca^{2+} store with cyclopiazonic acid (CPA; 10 μM) prevented the subsequent Ca^{2+} response to ATP (300 μM) (Supplementary Figure S4). Of note, caffeine (10 mM), a selective agonist of ryanodine receptors (RyR) (Pulina et al., 2010) failed to elicit an increase in $[\text{Ca}^{2+}]_i$ in rat aortic VSMCs from LZDF rats (Supplementary Figure S3), which is consistent with the notion that proliferating VSMCs lack RyRs (Berra-Romani

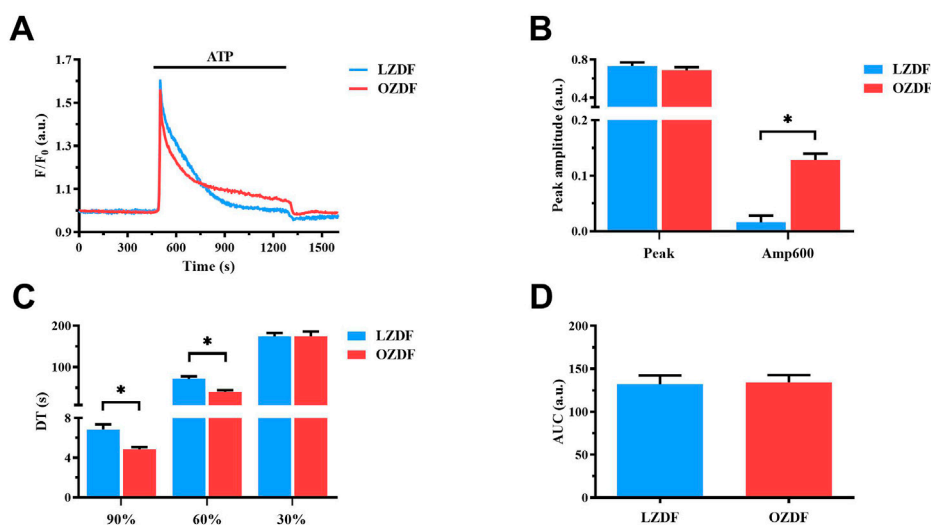


FIGURE 1

T2DM shortens the ATP-induced Ca^{2+} signal during the early phase of the decay and increases the plateau amplitude in rat aortic VSMCs. Mean traces of the Ca^{2+} signal evoked by ATP (300 μM) in VSMCs from LZDF (blue tracing) and OZDF (red tracing) rats (A). Peak amplitude [(B), left], amplitude 600 s after the application of the agonist (Amp600) [(B), right], decay time at 90, 60% and 30% of total amplitude (DT) (C) and area under the curve (AUC) (D) are expressed as mean \pm SE. Statistical comparison between groups was performed using Student's t-test. * indicates $p < 0.05$. Analysis was performed in 121 cells obtained from 6 rats for the LZDF group ($n = 6$; 121 cells) and 179 cells obtained from 6 rats for the OZDF group ($n = 6$; 179 cells).

et al., 2008). Therefore, IP_3Rs drive ATP-dependent SR Ca^{2+} mobilization under 0Ca^{2+} conditions. Furthermore, the Mn^{2+} -quenching assay, which has been widely employed to measure SOCE in both vascular endothelial cells (Zuccolo et al., 2019) and VSMCs (Smani et al., 2007), showed that CPA caused an increase in the rate of Fura-2 fluorescence quenching by extracellular Mn^{2+} (Supplementary Figure S5). However, the rate of CPA-evoked Mn^{2+} entry was significantly ($p < 0.05$) enhanced in rat aortic VSMCs from OZDF rats (Supplementary Figure S5), thereby confirming SOCE upregulation by T2DM.

3.4 T2DM reduces agonist-induced SR Ca^{2+} release in rat aortic VSMCs

In order to assess whether IP_3 -induced SR Ca^{2+} release is affected by T2DM, we compared intracellular Ca^{2+} release evoked by the IP_3 -synthesizing autacoid, ATP (300 μM), in the absence of extracellular Ca^{2+} (0Ca^{2+}) in rat aortic VSMCs from LZDF and OZDF rats (Figure 3A) (Berra-Romani et al., 2008; Berra-Romani et al., 2019). Under these conditions, we found a reduction in both the peak Ca^{2+} amplitude and AUC of the Ca^{2+} transient in OZDF as compared to LZDF VSMCs (Figure 3B). Of note, the peak Ca^{2+} response to ATP was lower in rat aortic OZDF VSMCs in the absence, but not in the presence, of extracellular Ca^{2+} (see Figure 1B). We did not find any statistical difference in the decay time to 90% and 60% of the total amplitude; however, the decay time to 30% of the Ca^{2+} response was significantly ($p < 0.05$) increased in VSMCs from OZDF rats (Figure 3C). Conversely, in the presence of extracellular Ca^{2+} , the early phase of the decay was faster in OZDF VSMCs and there was no difference in the decay time at 30% between the two animal groups (see Figure 1C). These observations suggest that: 1) endogenous Ca^{2+} release is reduced and/or 2) the

Ca^{2+} -transporting mechanisms clearing the initial Ca^{2+} peak are altered by T2DM, although this dysregulation is unmasked by removing extracellular Ca^{2+} . The fastest decline of the initial Ca^{2+} peak recorded in the presence of external Ca^{2+} (Figure 1C) suggests that extracellular Ca^{2+} entry could stimulate SERCA, PMCA and/or NCX, as previously demonstrated in rat aortic VSMCs (Baryshnikov et al., 2009), and thereby accelerate cytosolic Ca^{2+} clearance (see Discussion). In addition, enhanced SOCE is also likely to compensate for the lower IP_3 -induced SR Ca^{2+} release and bring the amplitude of the initial Ca^{2+} peak to the same value as that measured in LZDF rats.

3.5 T2DM does not alter SR Ca^{2+} content in rat aortic VSMCs

The lower ER Ca^{2+} release evoked by the physiological stimulation of IP_3Rs with ATP could be due to a reduction in the free Ca^{2+} concentration within the ER. Therefore, we evaluated the amount of releasable free Ca^{2+} in the SR by inhibiting SERCA activity with CPA in the absence of extracellular Ca^{2+} (Berra-Romani et al., 2008; Berra-Romani et al., 2019). The application of CPA (10 μM) induced a slow Ca^{2+} transient corresponding to the passive leak of free SR Ca^{2+} into the cytoplasm through leakage channels that remain to be identified (Figure 4A). Subsequently, the intracellular Ca^{2+} concentration returned to the baseline because of Ca^{2+} extrusion across the sarcolemma by PMCA and NCX. CPA is routinely employed to compare SR or endoplasmic reticulum Ca^{2+} content between different cell types (Lodola et al., 2017; Berra-Romani et al., 2019), including VSMCs (Berra-Romani et al., 2008; Liu et al., 2019). No differences were found in the peak Ca^{2+} amplitude and AUC of the Ca^{2+} response to CPA (Figure 4B). These data indicate that there is no detectable

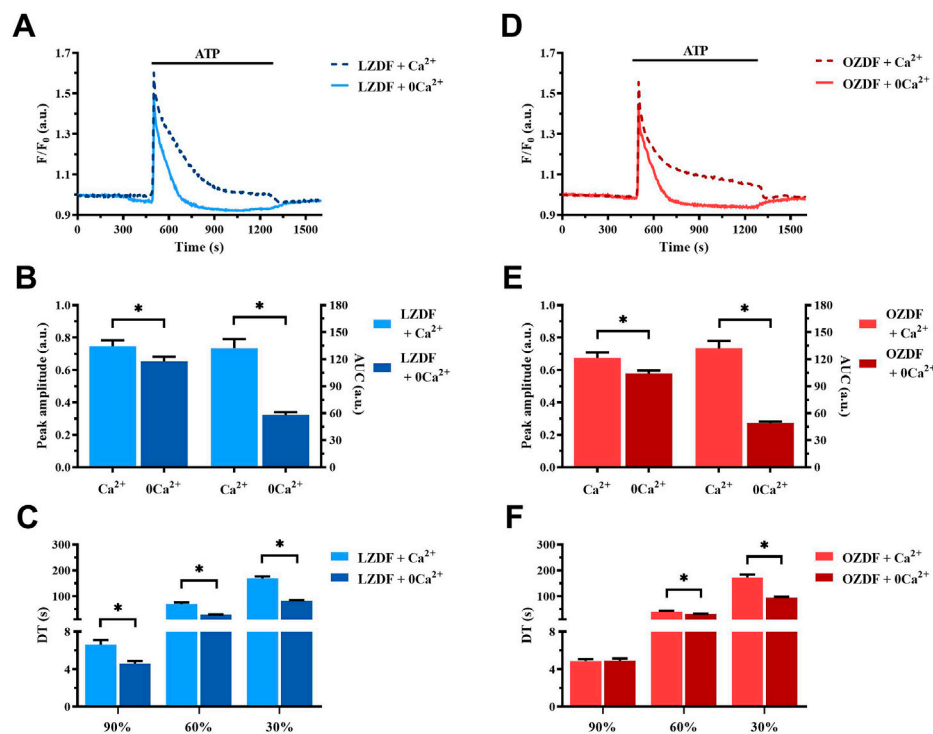


FIGURE 2

Effect of the removal of extracellular Ca^{2+} (0Ca^{2+}) on the ATP-induced Ca^{2+} signal in rat aortic VSMCs. Mean traces of the Ca^{2+} signal evoked by ATP ($300\ \mu\text{M}$) in the absence (continuous light-blue line; 0Ca^{2+}) and presence (dashed dark-blue line; Ca^{2+}) of extracellular Ca^{2+} in VSMCs from LZDF rats (A). Peak amplitude [(B), left], area under the curve (AUC) [(B), right] and decay time (DT) (C) of the Ca^{2+} signal in VSMCs from LZDF rats, in presence (light blue bars; Ca^{2+}) and absence (dark blue bars; 0Ca^{2+}). Mean traces of the Ca^{2+} signal evoked by ATP ($300\ \mu\text{M}$) in the absence (continuous light-red line; 0Ca^{2+}) and presence (dashed dark-red line; Ca^{2+}) of extracellular Ca^{2+} in VSMCs from OZDF rats (D). Peak amplitude [(E), left], AUC [(E), right] and DT (F) of the Ca^{2+} signal in VSMCs from OZDF rats. All parameters are expressed as mean \pm SE. Statistical comparison between groups was performed using Student's *t*-test. * indicates $p < 0.05$ ($n = 6$; 127 cells for LZDF Ca^{2+} , $n = 6$; 191 cells for LZDF 0Ca^{2+} , $n = 6$; 182 cells for OZDF Ca^{2+} , $n = 6$; 204 cells for OZDF 0Ca^{2+}).

difference in the SR free Ca^{2+} concentration between LZDF and OZDF VSMCs. Overall, these findings suggest that IP_3 -induced SR Ca^{2+} release is somehow tempered in rat aortic VSMCs from OZDF rats and that there are no major differences in PMCA and NCX activity under 0Ca^{2+} conditions between the two animal groups (Figures 4A, B).

3.6 T2DM alters SERCA activity in rat aortic VSMCs from OZDF rats

In order to assess whether the Ca^{2+} -transporting mechanisms clearing the initial Ca^{2+} peak are altered by T2DM, we separately evaluated the contribution of SERCA, PMCA and NCX to ATP-induced increase in $[\text{Ca}^{2+}]_i$ in the presence and absence of extracellular Ca^{2+} . In accord, as anticipated above, extracellular Ca^{2+} entry could change the rate of cytosolic Ca^{2+} clearance from the cytosol. Therefore, the Ca^{2+} -removal mechanisms at play during the physiological stimulation with ATP could differ depending on whether Ca^{2+} influx is activated or not.

We first evaluated whether and how T2DM alters SERCA activity by measuring the Ca^{2+} response to ATP ($300\ \mu\text{M}$) in the presence of a selective SERCA inhibitor, CPA ($10\ \mu\text{M}$).

3.6.1 SERCA activity changes during the decay of the Ca^{2+} response to ATP in the presence of extracellular Ca^{2+}

In aortic VSMCs from LZDF and OZDF rats, the inhibition of SERCA activity with CPA in the presence of extracellular Ca^{2+} did not cause any significant change in the amplitude of the initial Ca^{2+} peak evoked by ATP ($300\ \mu\text{M}$), although there was a trend towards a reduction in LZDF rats and a trend toward an increase in OZDF rats (Figures 5A, B). However, SERCA inhibition with CPA caused a significant ($p < 0.05$) increase in ATP-induced ΔAmp600 in both LZDF and OZDF rats (Figure 5C). Nevertheless, the increase in the ΔAmp600 value induced by CPA was significantly ($p < 0.05$) larger in VSMCs from LZDF as compared to OZDF rats (Figure 5D). Additionally, the pharmacological blockade of SERCA activity induced a significant ($p < 0.05$) increase in the decay time to 90% and 60% in VSMCs from both LZDF and OZDF rats (Figure 5E). However, the increase in the normalized decay time (termed as ΔDT) to both 90% and 60% was significantly ($p < 0.05$) larger in aortic VSMCs from OZDF rats (Figure 5F). In the presence of CPA, the Ca^{2+} response to $300\ \mu\text{M}$ ATP was maintained at such a high plateau level (Figure 5A) that it was not possible to measure the late (30%) clearing rates in both lean and obese animals (Figures 5E, F). Consequently, CPA caused a significant increase ($p < 0.05$) in

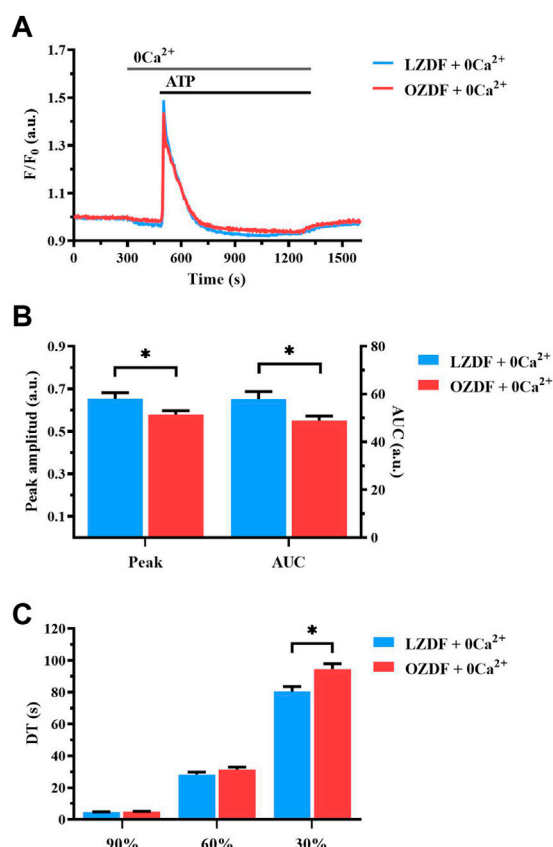


FIGURE 3
T2DM reduces agonist-induced Ca^{2+} release from SR in rat aortic VSMCs. Mean traces of the Ca^{2+} signal evoked by ATP (300 μM) in the absence of extracellular Ca^{2+} (0Ca^{2+}) in VSMCs from LZDF (blue tracing) and OZDF (red tracing) rats (A). Peak amplitude [(B), left], area under the curve (AUC) [(B), right] and DT (C) of the Ca^{2+} signal in VSMCs from LZDF (blue bars) and OZDF (red bars) rats. All parameters are expressed as mean \pm SE. Statistical comparison between groups was performed using Student's t-test. * indicates $p < 0.05$ ($n = 6$; 191 cells for LZDF 0Ca^{2+} , $n = 6$; 204 cells for OZDF 0Ca^{2+}).

the AUC value in VSMCs from both LZDF and OZDF rats (Figure 5G), but its elevation (termed as ΔAUC) was significantly ($p < 0.05$) larger in diabetic VSMCs (Figure 5H). These data suggest that SERCA activity is increased in OZDF as compared to LZDF rats during the early stage of decay of the Ca^{2+} transient. However, this effect is dramatically reversed during the late stage of the decay. In accord, in rat aortic VSMCs from OZDF rats stimulated with ATP in the presence of extracellular Ca^{2+} , the initial Ca^{2+} peak is sharper due to the faster Ca^{2+} clearance by SERCA, whereas the plateau achieves a larger value because of SOCE upregulation [see Supplementary Figure S5 and (Yan et al., 2020)] and of slower Ca^{2+} clearance by SERCA.

3.6.2 SERCA activity is reduced during the late stage of the decay of the ATP-induced Ca^{2+} transient in the absence of extracellular Ca^{2+}

In rat aortic VSMCs from LZDF rats, SERCA inhibition with CPA under 0Ca^{2+} conditions significantly ($p < 0.05$) reduced the

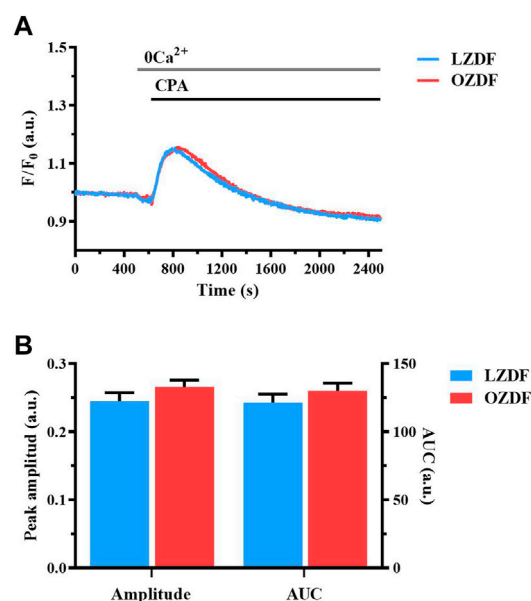


FIGURE 4
T2DM does not alter SR Ca^{2+} content in rat aortic VSMCs. Mean traces of the Ca^{2+} signal evoked by SERCA inhibitor, CPA in the absence of extracellular Ca^{2+} in VSMCs from LZDF (blue tracing) and OZDF (red tracing) rats (A). Peak amplitude [(B), left], area under the curve (AUC) [(B), right] in VSMCs from LZDF (blue bars) and OZDF (red bars) rats. All parameters are expressed as mean \pm SE. Statistical comparison between groups was performed using Student's t-test. * indicates $p < 0.05$ ($n = 6$; 167 cells for LZDF, $n = 6$; 189 cells for OZDF).

Ca^{2+} peak amplitude of ATP-induced Ca^{2+} transient as compared to the control Ca^{2+} trace recorded without the inhibitor (Figure 6A, B). In addition, CPA caused a remarkable slowing down of the decay phase, thereby significantly ($p < 0.05$) increasing the decay time to 90%, 60% and 30% and the AUC (Figures 6C, E). As for the OZDF group, SERCA inhibition under 0Ca^{2+} conditions induced a tiny, but not significant decrease in the Ca^{2+} peak amplitude (Figure 6B). However, the decay time to 90%, 60% and 30% and the AUC were again significantly ($p < 0.05$) increased as compared to the control Ca^{2+} trace obtained in the absence of CPA (Figures 6C, E). When the Ca^{2+} response to ATP in both rat groups was normalized, there was no difference in the increase in the decay time (ΔDT) to 90% and 60% (Figure 6D), while the increases in the decay time to 30% (Figure 6D) and in the AUC (ΔAUC ; Figure 6F) were significantly ($p < 0.05$) larger in LZDF rats. These findings support the notion that, in rat aortic VSMCs from OZDF rats, SERCA activity is reduced during the late stage of the decay phase (i.e., when the $[\text{Ca}^{2+}]_i$ returns to the 30% of the initial Ca^{2+} peak). In line with this hypothesis, blocking Ca^{2+} clearance with CPA converted the Ca^{2+} transient into a biphasic Ca^{2+} elevation in LZDF but not OZDF rats (Figure 6A). This means that Ca^{2+} pumping by SERCA is reduced during the late stage of the decay phase in diabetic VSMCs and does not significantly contribute to remove cytosolic Ca^{2+} . Intriguingly, the larger inhibition of ATP-induced Ca^{2+} release unmasked by 0Ca^{2+} conditions in LZDF VSMCs treated with CPA suggests that SERCA activity can control the rise in $[\text{Ca}^{2+}]_i$ rise in lean but not diabetic animals.

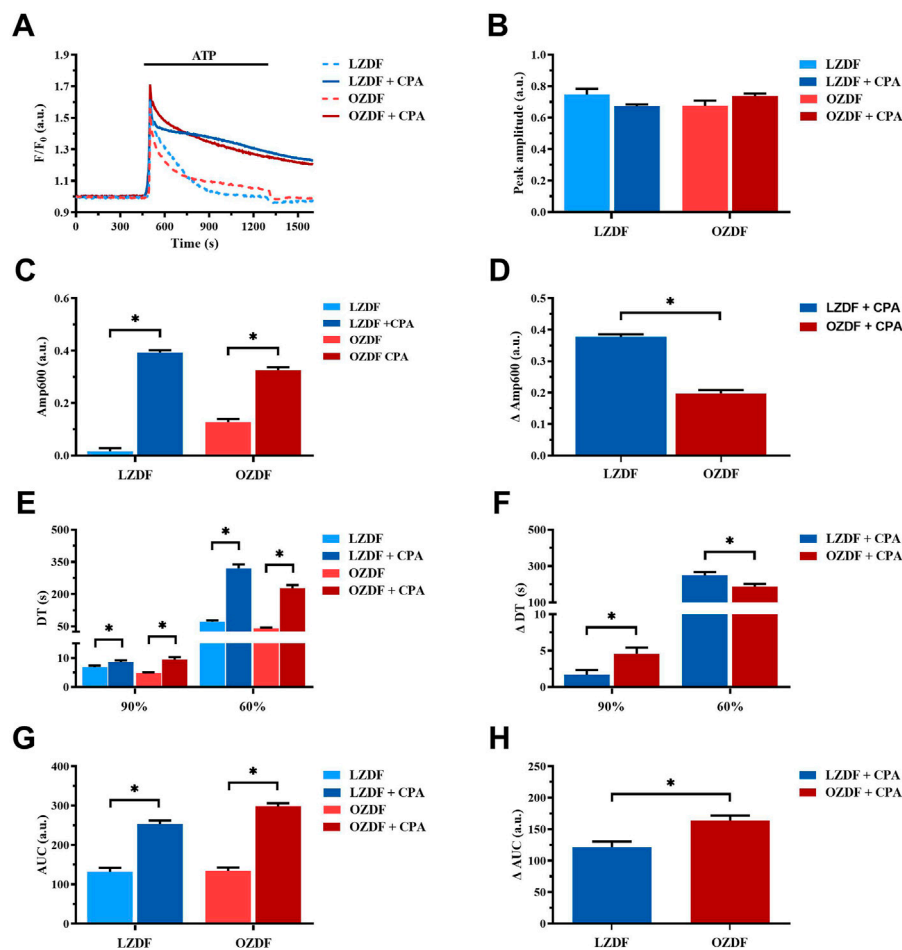


FIGURE 5

SERCA activity changes during the decay of the Ca^{2+} response to ATP in the presence of extracellular Ca^{2+} . Mean traces of the ATP-induced Ca^{2+} transient in the absence (dashed blue line for LZDF and dashed red line for OZDF) and presence (continuous blue line for LZDF and continuous red line for OZDF) of SERCA inhibitor, CPA (10 μM), in VSMCs (A). Peak amplitude (B), amplitude of the late stage of the decay (Amp600) (C), decay time (DT) (E) and area under the curve (AUC) (G) of the ATP-evoked Ca^{2+} signal in the presence and absence (control) of CPA. Normalized values of Amp600 (ΔAmp600) (D), decay time (ΔDT) (F) and AUC (ΔAUC) (F) for comparison purposes between LZDF and OZDF groups. All parameters are expressed as mean \pm SE. Statistical comparison between groups was performed using Student's t-test. * indicates $p < 0.05$. $n = 6$; 121 cells for LZDF control, $n = 6$; 127 cells for LZDF + CPA, $n = 6$; 179 cells for OZDF control, $n = 6$; 182 cells for OZDF + CPA.

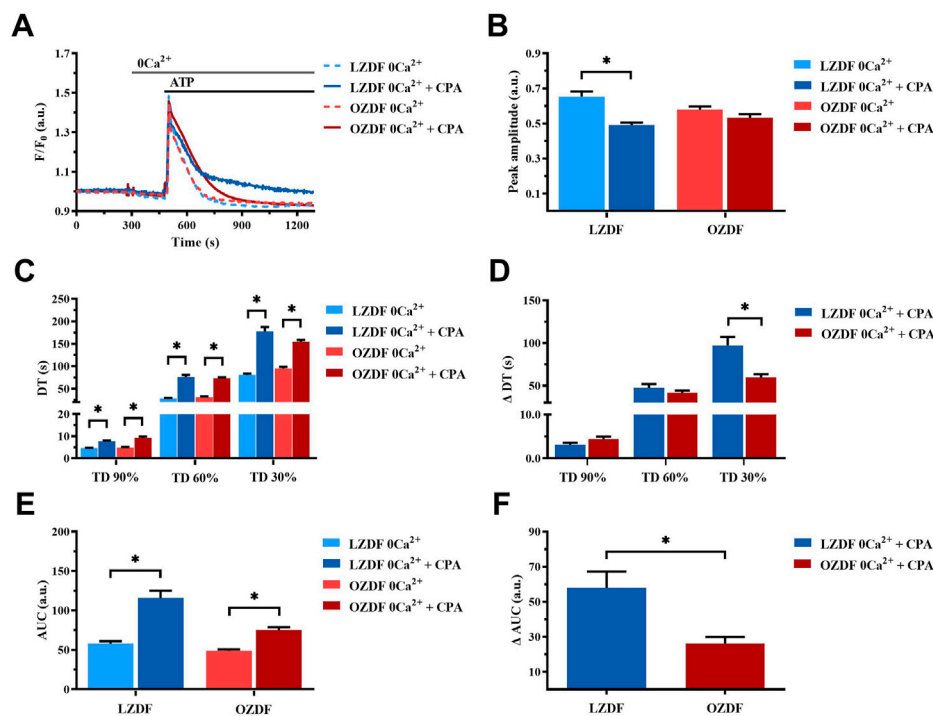
3.7 T2DM alters PMCA activity in rat aortic VSMCs

To evaluate PMCA activity in rat aortic VSMCs during T2DM, we used orthovanadate (OV; 500 μM) to inhibit this mechanism during the stimulation with ATP in the presence and absence of extracellular Ca^{2+} .

3.7.1 PMCA-dependent Ca^{2+} extrusion is increased during the decay of ATP-induced Ca^{2+} transient in VSMCs from OZDF rats in the presence of extracellular Ca^{2+}

The inhibition of PMCA activity by using OV in the presence of extracellular Ca^{2+} (Figure 7A) did not affect either the Ca^{2+} peak amplitude (Figure 7B) or the decay time to 90% and 60% of the Ca^{2+} response to ATP in VSMCs from LZDF rats (Figure 7E). Conversely, the value of Amp600 (Figure 7C), the decay time to 30% (Figure 7E)

and the AUC (Figure 7G) were significantly ($p < 0.05$) increased in the presence of OV. As to the OZDF group, the inhibition of PMCA activity with OV caused a significant ($p < 0.05$) reduction in the Ca^{2+} peak amplitude (Figure 7B), whereas all the remaining parameters (i.e., Amp600, decay time and AUC) were significantly ($p < 0.05$) increased (Figure 7, panels C, E and G). When the Ca^{2+} response to ATP in both groups of rats was normalized, we found that the increase in the Amp600 value (Figure 7D; ΔAmp600) and in the AUC (ΔAUC ; Figure 7H) caused by PMCA inhibition were significantly ($p < 0.05$) larger in VSMCs from LZDF rats as compared to the OZDF group. However, the increase in the decay time to 90% and 60% (ΔDT) was significantly ($p < 0.05$) larger in OZDF rats (Figure 7F). Altogether, these findings suggest that, in the presence of extracellular Ca^{2+} , PMCA plays a major role in clearing cytosolic Ca^{2+} at the beginning of the Ca^{2+} response to ATP, while its contribution decreases during the plateau phase, in VSMCs from OZDF rats. In accord, the increase in ΔDT to 90% and

**FIGURE 6**

SERCA activity is reduced during the late stage of the decay of the ATP-induced Ca²⁺ transient in 0Ca²⁺. Mean traces of the ATP-induced Ca²⁺ transient in the absence (dashed blue line for LZDF and dashed red line for OZDF) and presence (continuous blue line for LZDF and continuous red line for OZDF) of SERCA inhibitor, CPA (10 μ M), in VSMCs (A). Peak amplitude (B), decay time (C) and area under the curve (AUC) (E) of the ATP-evoked Ca²⁺ signal in the presence and absence (control) of CPA. Normalized values of decay time (Δ DT) (D) and AUC (Δ AUC) (F) for comparison purposes between LZDF and OZDF groups. All parameters are expressed as mean \pm SE. Statistical comparison between groups was performed using Student's t-test. * indicates $p < 0.05$. $n = 6$; 191 cells for LZDF control, $n = 7$; 242 cells for LZDF CPA 0Ca²⁺, $n = 6$; 204 cells for OZDF control, $n = 6$; 221 cells for OZDF CPA 0Ca²⁺).

60% induced by OV indicates that the Ca²⁺ pumping rate of PMCA after the initial elevation in [Ca²⁺]_i is faster in OZDF VSMCs. Conversely, the lower increase in Δ Amp600 suggests that SERCA plays a minor role in removing Ca²⁺ during the plateau phase and, consequently, its inhibition causes a lower elevation in plateau amplitude. In addition, OV-induced inhibition of ATP-induced ER Ca²⁺ release suggests that PMCA contributes to the propagation of the rise in [Ca²⁺]_i following agonist stimulation in diabetic VSMCs. This finding is consistent with the higher activity of PMCA at the beginning of the Ca²⁺ signal discussed above.

3.7.2 PMCA-dependent Ca²⁺ extrusion is reduced during the early stage of the decay of the ATP-induced Ca²⁺ transient in VSMCs from OZDF rats in the absence of extracellular Ca²⁺

In rat aortic VSMCs from LZDF rats, the inhibition of PMCA with OV in the absence of extracellular Ca²⁺ (0Ca²⁺) caused a significant ($p < 0.05$) reduction in the Ca²⁺ peak amplitude (Figures 8A, B). Likewise, the decay time to 90%, 60%, and 30% (Figure 8C) and the AUC (Figure 8E) were significantly ($p < 0.05$) reduced. In VSMCs from OZDF rats, pretreatment with OV also caused a significant decrease in the peak amplitude of the Ca²⁺ transient (Figures 8A, B). Similar to LZDF rats, we observed a decrease in the decay time to 90%, 60%, and 30% (Figure 8C), while the AUC was increased in OZDF VSMCs (Figure 8E). When the

Ca²⁺ response to ATP in both groups of rats was normalized, the reduction in the decay time to 90% and 60% of the initial Ca²⁺ peak (Δ DT) were significantly larger in OZDF as compared to LZDF rats (Figure 8D). Conversely, the Δ AUC was significantly ($p < 0.05$) larger in the OZDF group compared to LZDF (Figure 8F). These findings confirm that PMCA activity increases during the initial phase of the Ca²⁺ response to ATP in VSMCs from OZDF rats, and that such increase in Ca²⁺ extrusion via PMCA is unmasked by OV.

3.8 T2DM alters NCX activity in rat aortic VSMCs

Finally, in order to assess whether and how T2DM alters NCX activity in rat aortic VSMCs, we inhibited this mechanism using the selective inhibitor, SEA0400 (3 μ M), in the presence and absence of extracellular Ca²⁺ (0Ca²⁺).

3.8.1 NCX activity changes during Ca²⁺ response evoked by ATP in the presence of extracellular Ca²⁺ in rat aortic VSMCs from OZDF rats

In VSMCs from LZDF rats (Figure 9A), blockade of NCX with SEA0400 significantly ($p < 0.05$) reduced the Ca²⁺ peak amplitude (Figure 9B) and increased the Amp600 (Figure 9C) of the Ca²⁺ response to ATP. There were no differences in decay time to 90%

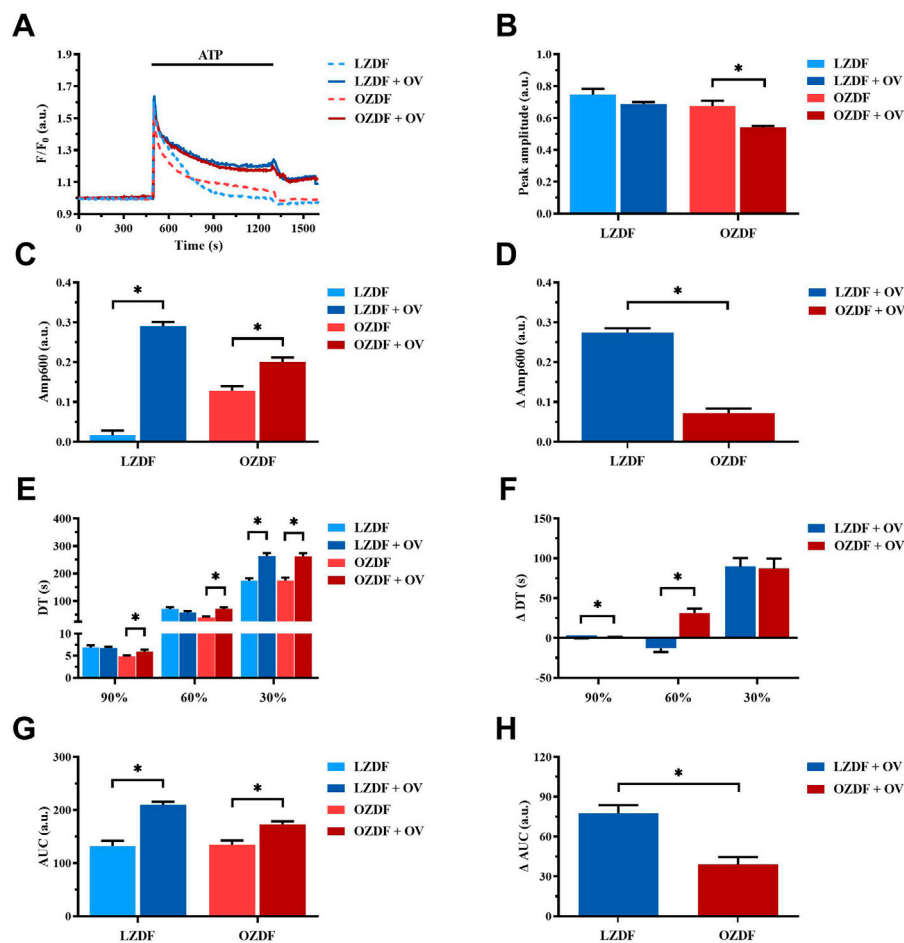


FIGURE 7

PMCA-dependent Ca^{2+} extrusion is increased during the decay of ATP-induced elevation in $[Ca^{2+}]_i$ in VSMCs from OZDF rats in the presence of extracellular Ca^{2+} . Mean traces of the ATP-induced Ca^{2+} transient in the absence (dashed blue line for LZDF and dashed red line for OZDF) and presence (continuous blue line for LZDF and continuous red line for OZDF) of PMCA inhibitor, sodium orthovanadate (OV, 500 μ M) (A). Peak amplitude (B), amplitude of the late stage of the decay (Amp600) (C), decay time (E) and area under the curve (AUC) (G) of the ATP-evoked Ca^{2+} signal in the presence and absence (control) of OV. Normalized values of Amp600 (Δ Amp600) (D), decay time (Δ DT) (F) and AUC (Δ AUC) (H) for comparison purposes between LZDF and OZDF groups. All parameters are expressed as mean \pm SE. Statistical comparison between groups was performed using Student's t-test. * indicates $p < 0.05$. ($n = 6$; 121 cells for LZDF control, $n = 6$; 240 cells for LZDF OV, $n = 6$; 179 cells for OZDF control, $n = 6$; 251 cells for OZDF OV.

and 30% of the total amplitude (Figure 9E), whereas the decay time to 60% (Figure 9E), as well as the AUC (Figure 9G), were significantly ($p < 0.05$) reduced. In OZDF VSMCs (Figure 9A), SEA0400 did not significantly ($p < 0.05$) affect the Ca^{2+} peak amplitude (Figure 9B), although it significantly ($p < 0.05$) reduced the Amp600 (Figure 9C). Conversely, the decay time to 90%, 60%, and 30% were significantly ($p < 0.05$) increased (Figure 9E), while the AUC remained unaltered (Figure 9G). Clearly, there was a significant ($p < 0.05$) difference in the Δ Amp600 (Figure 9D), Δ DT (Figure 9F) Δ AUC between OZDF and LZDF rats (Figure 9H). These findings suggest that NCX modulates the amplitude of the initial Ca^{2+} peak and contributes to extrude cytosolic Ca^{2+} during the plateau phase, but not the early decay phase of the Ca^{2+} response to ATP in LZDF rats. Conversely, NCX is crucial to remove cytosolic Ca^{2+} by acting in the forward mode during all the decay of the initial rise in $[Ca^{2+}]_i$ but supports Ca^{2+} entry by switching into the reverse mode during the plateau phase, in OZDF rats.

3.8.2 NCX activity is reduced during the early stage of the decay of ATP-induced Ca^{2+} transient in rat aortic VSMCs from OZDF rats in the absence of extracellular Ca^{2+}

Under $0Ca^{2+}$ conditions (Figure 10A), the inhibition of NCX with SEA0400 induced a decrease in the Ca^{2+} peak amplitude (Figure 10B) and in the AUC (Figure 10E) of the ATP-evoked Ca^{2+} transient in rat aortic VSMCs from LZDF rats. Conversely, all the decay time were significantly increased as compared to their control values measured in the absence of the inhibitor (Figure 10C). Likewise, in VSMCs from OZDF rats, NCX inhibition under $0Ca^{2+}$ conditions caused a decrease in the Ca^{2+} peak amplitude of the ATP-induced Ca^{2+} response (Figure 10B) and in the decay time to 90% and 60% (Figure 10C). The decay time to 30% (Figure 10C) increased, while the AUC (Figure 10E) remained unchanged under these conditions. Because of these changes the increase in Δ DT to 90% and 60% was significantly ($p < 0.05$) larger in LZDF VSMCs (Figure 10D), as well as there was a significant ($p < 0.05$)

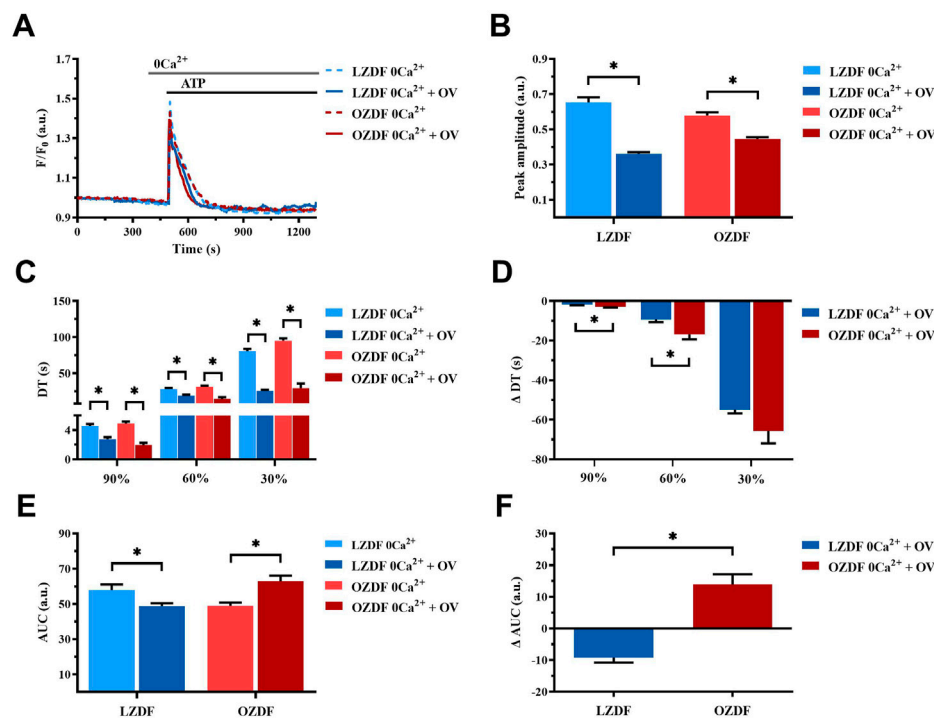


FIGURE 8

PMCA-dependent Ca^{2+} extrusion is reduced during the early stage of the decay of ATP-induced Ca^{2+} transient in VSMCs from OZDF rats in the absence of extracellular Ca^{2+} . Mean traces of the ATP-induced Ca^{2+} transient in the absence (dashed blue line for LZDF and dashed red line for OZDF) and presence (continuous blue line for LZDF and continuous red line for OZDF) of PMCA inhibitor, sodium orthovanadate (OV, 500 μM) in 0Ca^{2+} (A). Peak amplitude (B), decay time (C) and area under the curve (AUC) (E) of the ATP-evoked Ca^{2+} signal in the presence and absence (control) of OV. Normalized values of decay time (ΔDT) (D) and AUC (ΔAUC) (F) for comparison purposes between LZDF and OZDF groups. All parameters are expressed as mean \pm SE. Statistical comparison between groups was performed using Student's t-test. * indicates $p < 0.05$. $n = 6$; 191 cells for LZDF control, $n = 6$; 308 cells for LZDF OV 0Ca^{2+} , $n = 6$; 204 cells for OZDF control, $n = 4$; 153 cells for OZDF OV 0Ca^{2+} .

difference in the ΔAUC between OZDF and LZDF rats (Figure 10F). These findings reveal that, under 0Ca^{2+} conditions, NCX modulates the amplitude of the initial Ca^{2+} peak in both LZDF and OZDF rats. Conversely, NCX supports the decline of the Ca^{2+} response to the baseline in LZDF, but not in OZDF VSMCs.

Simultaneous inhibition of SERCA, PMCA and NCX differently alters the Ca^{2+} response to ATP in OZDF as compared to LZDF rat aortic VSMCs.

Finally, we assessed whether and how the simultaneous inhibition of SERCA, PMCA and NCX affects the Ca^{2+} response to ATP both in the presence and absence of extracellular Ca^{2+} .

3.8.3 Simultaneous inhibition of SERCA, PMCA and NCX in the presence of extracellular Ca^{2+}

In the presence of extracellular Ca^{2+} (Figure 11A), the Ca^{2+} response elicited by ATP (300 μM) in the presence of CPA (10 μM) + OV (500 μM) + SEA0400 (3 μM) presented a significant ($p < 0.05$) decrease in peak amplitude (Figure 11B) and in Amp600 (Figure 11C) in VSMCs from both LZDF and OZDF rats. These data are consistent with the inhibitory effect exerted by OV (Figure 7B) and SEA0400 (Figure 9B) on peak Ca^{2+} amplitude in aortic VSMCs from, respectively, OZDF and LZDF rats. Likewise, these data are consistent with the evidence that blocking either SERCA (Figure 5C) or PMCA (Figure 7C) activity prevents the recovery of the initial increase in $[\text{Ca}^{2+}]_i$ and enhances the amplitude

of the subsequent plateau phase in both animal groups, while blocking NCX activity enhances Amp600 only in LZDF VSMCs (Figure 9C). However, the ΔAmp600 recorded in OZDF VSMCs under these experimental conditions is significantly ($p < 0.05$) lower than in LZDF VSMCs (Figure 11D), which is consistent with a reduction in SERCA and PMCA activity by T2DM. Because of this complex remodelling of the Ca^{2+} handling machinery in obese diabetic rats, the AUC of the Ca^{2+} response undergoes a significant ($p < 0.05$) increase only in VSMCs from OZDF rats (Figures 11E, F).

3.8.4 Simultaneous inhibition of SERCA, PMCA and NCX in the absence of extracellular Ca^{2+}

In the absence of extracellular Ca^{2+} (0Ca^{2+}) (Figure 12A), the Ca^{2+} response elicited by ATP (300 μM) in the presence of CPA (10 μM) + OV (500 μM) + SEA0400 (3 μM) still presented a significant ($p < 0.05$) decrease in peak amplitude (Figure 12B) in both groups of animals. As expected, under these experimental conditions, the initial increase in $[\text{Ca}^{2+}]_i$ failed to fully recover to the baseline (Figure 12A), thereby resulting in a plateau-like signal that did not return to pre-stimulation levels. Intriguingly, the ΔAmp600 recorded in OZDF VSMCs upon simultaneous blockade of SERCA, PMCA and NCX was significantly ($p < 0.05$) lower than in LZDF VSMCs (Figure 12C). This finding is consistent with the reduction in the activity of all these Ca^{2+} -

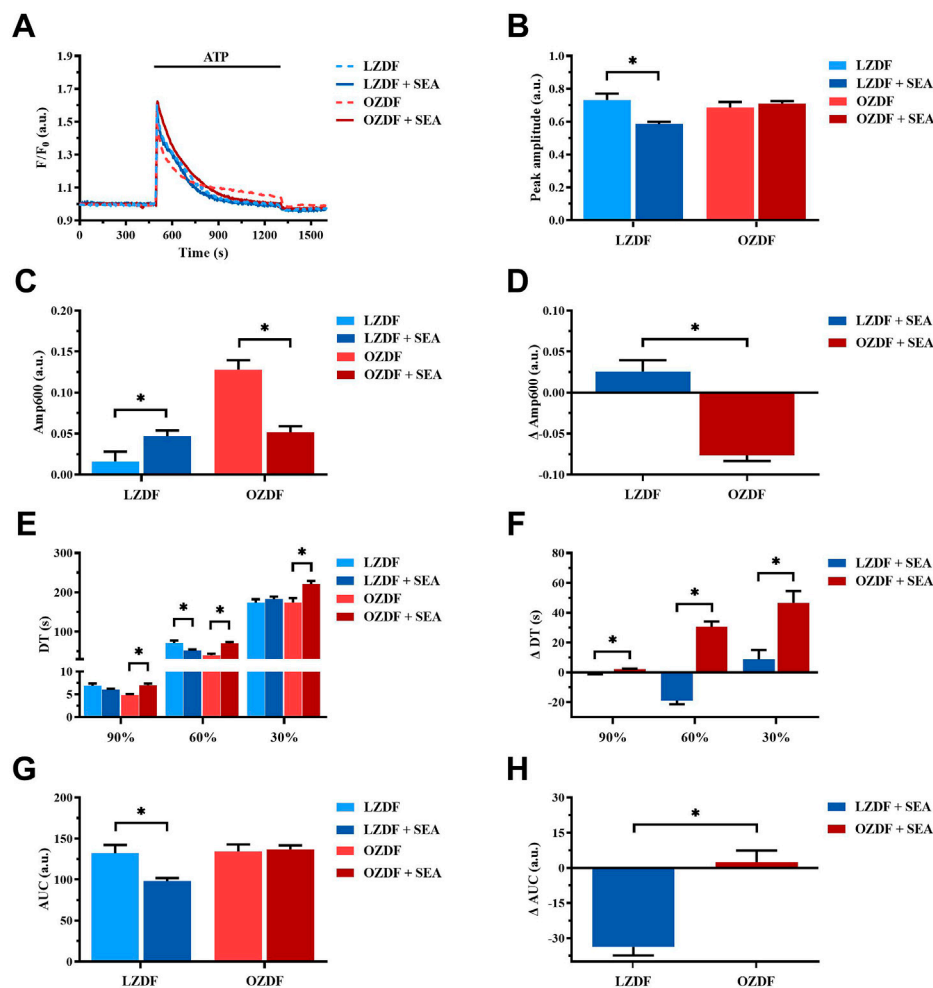


FIGURE 9

NCX activity changes during the Ca^{2+} response evoked by ATP in the presence of extracellular Ca^{2+} in rat aortic VSMCs from OZDF rats. Mean traces of the ATP-induced Ca^{2+} transient in the absence (dashed blue line for LZDF and dashed red line for OZDF) and presence (continuous blue line for LZDF and continuous red line for OZDF) of NCX inhibitor, SEA0400 (3 μM) (A). Peak amplitude (B), amplitude of the late stage of the decay (Amp600) (C), decay time (E) and area under the curve (AUC) (G) of the ATP-evoked Ca^{2+} signal in the presence and absence (control) of SEA0400. Normalized values of Amp600 (ΔAmp600) (D), decay time (ΔDT) (F) and AUC (ΔAUC) (H) for comparison purposes between LZDF and OZDF groups. All parameters are expressed as mean \pm SE. Statistical comparison between groups was performed using Student's t-test. * indicates $p < 0.05$, $n = 6$; 121 cells for LZDF control, $n = 6$; 272 cells for LZDF SEA0400, $n = 6$; 179 cells for OZDF control, $n = 6$; 290 cells for OZDF SEA0400.

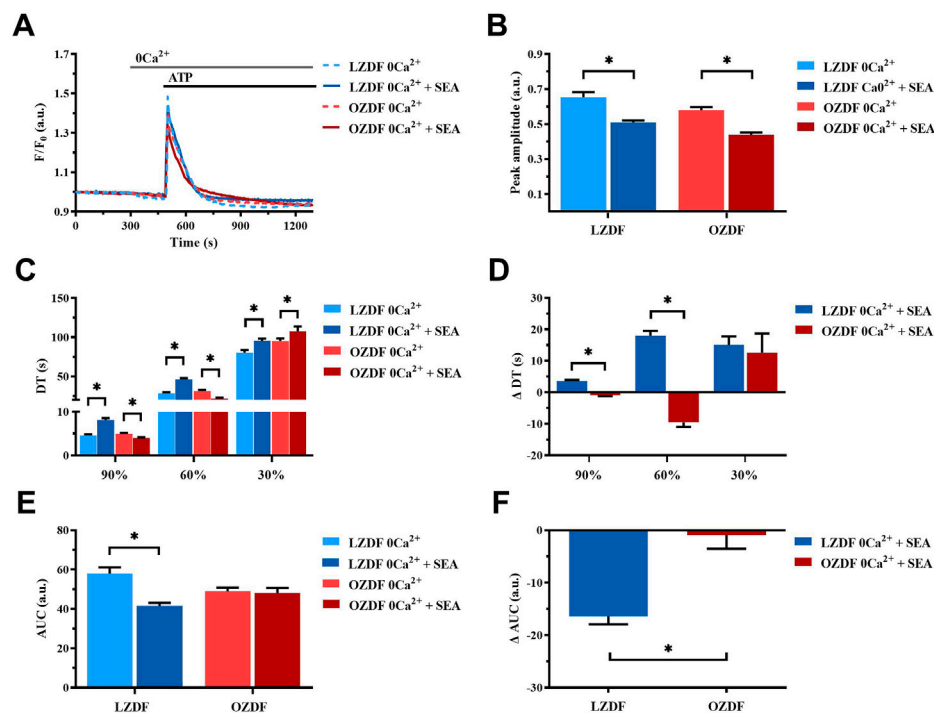
transporting systems under 0Ca^{2+} conditions. Because of this complex remodelling of the Ca^{2+} handling machinery in obese diabetic rats, the AUC of the Ca^{2+} response undergoes a significant ($p < 0.05$) increase only in VSMCs from LZDF rats (Figures 12D, E).

4 Discussion

4.1 Animal model

As shown in Table 1, at the age of 12 weeks, all the morphological parameters measured (body weight, length, abdominal circumference and epididymal fat) were significantly increased in the OZDF rats in comparison to the LZDF group. The increment in weight concurs with the data previously

reported by other research groups (Fridlyand and Philipson, 2006; Tirmenstein et al., 2015; Berra-Romani et al., 2019). Since this could be attributed to an increase in the length of the rat, we calculated the BMI to rule out the possibility that differences in length would interfere with our results. BMI was statistically higher in OZDF rats compared to the LZDF group, evidencing that weight gain is indeed due to obesity, as also reported by other studies (Shiota and Printz, 2012; Wang et al., 2013; Al-Awar et al., 2016; King and Bowe, 2016). The presence of obesity in OZDF rats was also demonstrated by a 405% increase in the amount of adipose tissue formed around the epididymis (epididymal fat). These results confirm that OZDF rats present obesity at the age of 12–16 weeks. Confirming that the animals used for the experimental protocols did indeed develop T2DM, plasma glucose levels 2 hours after intraperitoneally glucose administration (2 g/kg of weight) were more elevated in OZDF rats. This information indicates that OZDF rats are glucose intolerant,

**FIGURE 10**

NCX activity is reduced during the early stage of the decay of ATP-induced Ca²⁺ transient in rat aortic VSMCs from OZDF rats in the absence of extracellular Ca²⁺. Mean traces of the ATP-induced Ca²⁺ transient in the absence (dashed blue line for LZDF and dashed red line for OZDF) and presence (continuous blue line for LZDF and continuous red line for OZDF) of NCX inhibitor, SEA0400 (3 μM) in 0Ca²⁺ (A). Peak amplitude (B), decay time (C) and area under the curve (AUC) (E) of the ATP-evoked Ca²⁺ signal in the presence and absence (control) of SEA0400. Normalized values decay time (ΔDT) (D) and AUC (ΔAUC) (F) for comparison purposes between LZDF and OZDF groups. All parameters are expressed as mean ± SE. Statistical comparison between groups was performed using Student's t-test. * indicates $p < 0.05$. $n = 6$; 121 cells for LZDF control, $n = 6$; 199 cells for LZDF SEA0400 0Ca²⁺, $n = 6$; 179 cells for OZDF control, $n = 6$; 162 cells for OZDF SEA0400 0Ca²⁺.

which constitutes one of the criteria that according to the ADA, are sufficient to diagnose T2DM in humans (ElSayed et al., 2023).

4.2 T2DM shortens the early phase of the decay and increases the plateau amplitude of ATP-induced Ca²⁺ signals in rat aortic VSMCs

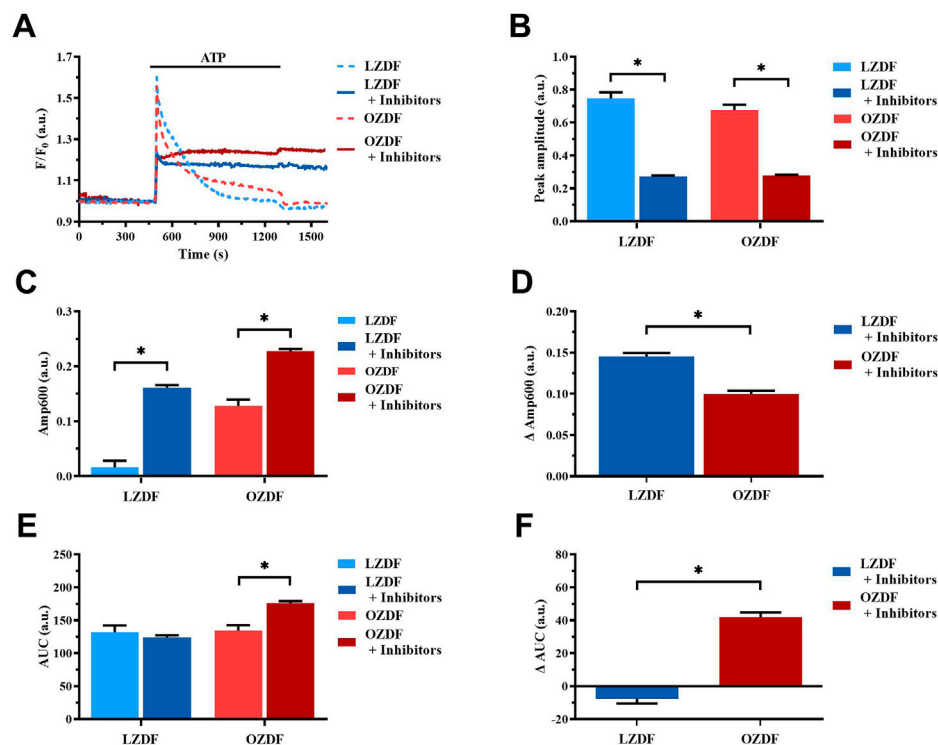
The experiments carried out in this study demonstrate that Ca²⁺ handling is altered in VSMCs from OZDF rats. In particular, T2DM causes two important effects on the ATP-evoked biphasic elevation in [Ca²⁺]_i: 1) a significant reduction in decay time to 90% and 60% of the initial Ca²⁺ peak amplitude (early stage of the decay of [Ca²⁺]_i to resting levels) and 2) a significant increase in the amplitude of the plateau (late stage of the decay of [Ca²⁺]_i and SOCE activation). Shortening of the early phase of decay could be due to alterations in the activity of the Ca²⁺-clearing mechanisms, such as SERCA, PMCA and NCX.

The role of SERCA (Zhang et al., 2018; Pereira et al., 2022); PMCA (Pande et al., 2006; Baryshnikov et al., 2009) and NCX (Liu et al., 2016; Yang et al., 2020) in clearing cytosolic Ca²⁺ upon agonist stimulation in aortic VSMCs has extensively been reported. However, few studies are available above the effect of DM on the activity of these Ca²⁺-clearing mechanisms VSMCs. In A7r5 cells, hyperglycemia was reported to induce a reduction in SERCA expression and activity

(Searls et al., 2010; Tong et al., 2010) and an increase in PMCA and NCX activity (Han et al., 2022). However, our data showing that the decay phase of the initial increase in [Ca²⁺]_i evoked by ATP is accelerated in OZDF rat aortic VSMCs suggests that T2DM increases the activity of the Ca²⁺-clearing machinery. As to the increase in plateau amplitude observed in OZDF rat aortic VSMCs, this could clearly be due to SOCE upregulation, as recently shown in (Ma et al., 2020; Zhu et al., 2021). A recent report confirmed that SOCE was enhanced in aortic VSMCs deriving from Zucker diabetic fatty rats due to upregulation of Orai1 protein (Yang et al., 2020). In accord, the Mn²⁺-quenching assay confirmed that extracellular Ca²⁺ entry evoked by the pharmacological depletion of the ER Ca²⁺ store with CPA was remarkably larger in OZDF VSMCs as compared to LZDF. However, the increase in plateau amplitude could also reflect a reduction in the activity of Ca²⁺-extruding mechanisms and/or an increase in Ca²⁺ entry through the reverse mode of NCX (Zhang et al., 2005; Pulina et al., 2010; Liu et al., 2016; Berra-Romani et al., 2019).

4.3 T2DM reduces ATP-induced SR Ca²⁺ release in rat aortic VSMCs

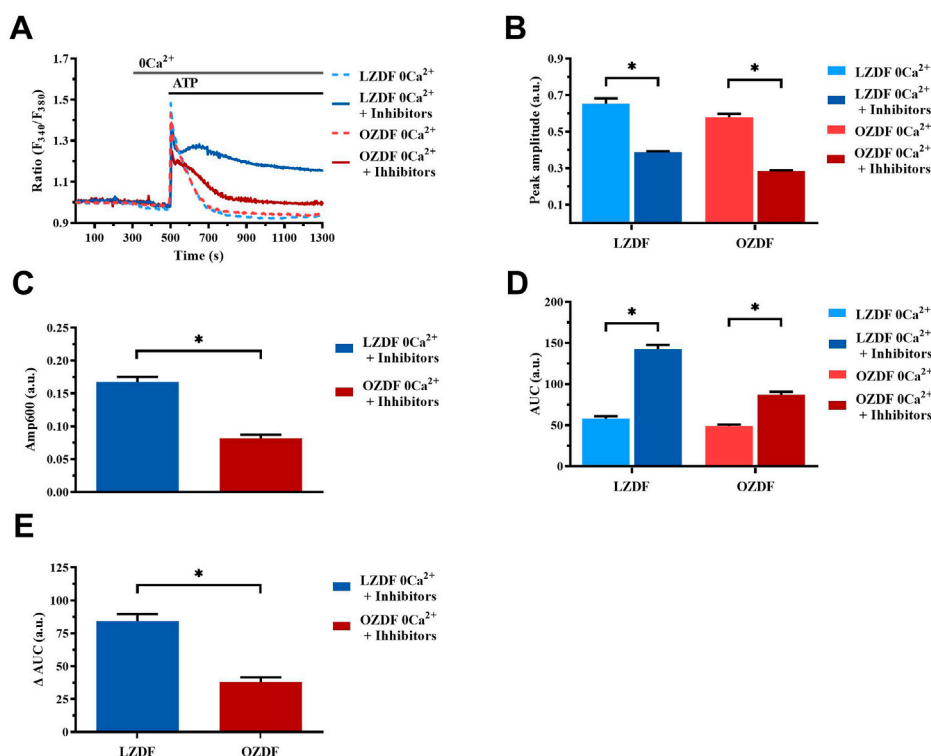
In order to elucidate the mechanism(s) whereby T2DM alters the Ca²⁺ response to ATP in rat aortic VSMCs, we first stimulated

**FIGURE 11**

Simultaneous inhibition of SERCA, PMCA and NCX in the presence of extracellular Ca^{2+} . Mean traces of ATP-induced Ca^{2+} signals in the absence (dashed blue line for LZDF and dashed red line for OZDF) and presence (continuous blue line for LZDF and continuous red line for OZDF) of CPA (10 μM) + OV (500 μM) + SEA0400 (3 μM) (+inhibitors) in normal extracellular Ca^{2+} concentration (A). Peak amplitude (B), amplitude of the late stage of the decay (Amp600) (C) and area under the curve (AUC) (E) of the ATP-evoked Ca^{2+} signal in the presence (+inhibitors) and absence (control) of CPA + OV + SEA0400. Normalized values decay time (ΔDT) (D) and AUC (ΔAUC) (F) for comparison purposes between LZDF and OZDF groups. All parameters are expressed as mean \pm SE. Statistical comparison between groups was performed using Student's t-test. * indicates $p < 0.05$. $n = 6$; 121 cells for LZDF control, $n = 4$; 245 cells for LZDF + Inhibitors, $n = 6$; 179 cells for OZDF control, $n = 5$; 360 cells for OZDF + Inhibitors.

the cells under 0Ca^{2+} conditions. This condition is widely employed to assess the role played by extracellular Ca^{2+} in shaping peak amplitude, decay phase and plateau amplitude of the Ca^{2+} response to extracellular stimulation (Urena et al., 2007; Berra-Romani et al., 2008; Linde et al., 2012). Ca^{2+} removal from the extracellular solution caused a significant decrease in Ca^{2+} peak amplitude and abolished the plateau phase, thus converting the biphasic Ca^{2+} response to ATP in a transient elevation in $[\text{Ca}^{2+}]_i$ in VSMCs from both animal groups. However, ATP-induced SR Ca^{2+} release was remarkably lower in rat aortic VSMCs from OZDF rats. Enhanced SOCE could therefore shift the amplitude of the initial Ca^{2+} peak evoked by ATP in OZDF VSMCs to the same amplitude as that induced in LZDF cells, which present a larger IP_3 -induced SR Ca^{2+} release but lower SOCE. The reduced Ca^{2+} peak observed under 0Ca^{2+} conditions can be attributed to multiple factors, including downregulation of P2Y receptors, reduced phospholipase C (PLC) activation, lower IP_3R and RyR expression and/or activity, and a decrease in SR Ca^{2+} content. However, CPA-induced intracellular Ca^{2+} release, which is a widely employed readout of SR Ca^{2+} content, was not altered in OZDF VSMCs, as also reported in VSMCs from diabetic mice (Velmurugan and White, 2012). In contrast, ATP-evoked intracellular Ca^{2+} release, which is mainly dependent on IP_3Rs (see below), was significantly reduced in OZDF rat aortic VSMCs. This finding suggests that either P2Y receptors are

downregulated or their downstream signalling pathways, such as those culminating in PLC engagement and IP_3R activation, are compromised by T2DM. A study performed in systemic arterial smooth muscle cells deriving from rat models of T1DM, as well as in VSMCs exposed to high glucose, showed a reduction in IP_3R expression that attenuated vasopressin-induced Ca^{2+} response (Searls et al., 2010). Conversely, Velmurugan et al. found that, in aortic VSMCs from mice with T2DM, IP_3R excitability was augmented through the direct interaction with the anti-apoptotic Bcl-2 proteins (Velmurugan and White, 2012). The discrepancy in these results could be due to several factors, such as heterogeneity in the vascular district, animal model, type of DM and progress of the disease. However, the evidence that T2DM increases IP_3R activity in mouse VSMCs strongly suggests that IP_3 -dependent Ca^{2+} release is also enhanced in rat VSMCs. On the other hand, although DM alters RyR function in contractile VSMCs (Fernandez-Velasco et al., 2014), dedifferentiation induces RyR downregulation in the proliferative phenotype of VSMCs (Berra-Romani et al., 2008; House et al., 2008). Consistently, our Ca^{2+} imaging recordings confirmed that caffeine did not induce Ca^{2+} signals in cultured rat aortic VSMCs. Therefore, RyRs are unlikely to contribute to ATP-induced endogenous Ca^{2+} mobilization in the VSMCs employed in the present investigation. Likewise, ionotropic P2X receptors are lost during the dedifferentiation of VSMCs and cannot

**FIGURE 12**

Simultaneous inhibition of SERCA, PMCA and NCX in the absence of extracellular Ca²⁺. Mean traces of the ATP-induced Ca²⁺ signals in the absence (dashed blue line for LZDF and dashed red line for OZDF) and presence (continuous blue line for LZDF and continuous red line for OZDF) of CPA (10 μM) + OV (500 μM) + SEA0400 (3 μM) (+inhibitors) in absence of extracellular Ca²⁺ (0Ca²⁺) (A). Peak amplitude (B), amplitude of the late stage of the decay (Amp600) (C) and area under the curve (AUC) (D) of the ATP-evoked Ca²⁺ signal in the presence (+inhibitors) and absence (control) of CPA + OV + SEA0400. Normalized values of AUC (ΔAUC) (E) for comparison purposes between LZDF and OZDF groups. All parameters are expressed as mean ± SE. Statistical comparison between groups was performed using Student's t-test. * indicates $p < 0.05$. $n = 6$; 121 cells for LZDF control, $n = 7$; 426 cells for LZDF + Inhibitors, $n = 6$; 179 cells for OZDF control, $n = 6$; 410 cells for OZDF + Inhibitors.

contribute to the initial Ca²⁺ peak induced by ATP in the presence of extracellular Ca²⁺ (Erlinge et al., 1998). The evidence discussed below that PMCA inhibition reduces the amplitude of the initial Ca²⁺ peak and that PMCA is engaged by Ca²⁺ entry strongly suggest that PMCA activity is required to promote full IP₃R activation in T2DM.

4.4 T2DM alters SERCA activity in rat aortic VSMCs

The inhibition of SERCA activity with CPA in the presence of extracellular Ca²⁺ elongated the decay phase of the Ca²⁺ transient induced by ATP in both experimental groups. However, this effect was greater during the early phases of decay (i.e., 90% and 60%) in OZDF rats. This observation suggests that Ca²⁺ sequestration by SERCA is enhanced during the initial stage of the Ca²⁺ transient and affects the early phase of decay in OZDF VSMCs. Furthermore, SERCA inhibition by CPA caused a larger increase in Amp600, which is a readout of plateau amplitude, in LZDF as compared to OZDF rats. This finding indicates that SERCA activity could decrease during the later stages of the decay phase, which would result in less removal of Ca²⁺ during the plateau phase. Therefore, the larger Amp600 recorded in OZDV VSMCs could be underlain

by the combination of enhanced SOCE and reduced SERCA activity. Both an increase and a decrease in SERCA activity in the presence of DM have been reported. Particularly, in dyslipidemic diabetic pigs, Hill et al. found an increase in Ca²⁺ buffering by SERCA2 in coronary artery VSMCs isolated from dyslipidemic diabetic pigs (Hill et al., 2003). Conversely, in rat aortic VSMCs harvested from two different models of T1DM, Searls et al. found a decrease in the expression of SERCA2 and SERCA3, thereby reducing Ca²⁺ and attenuating the Ca²⁺ response to vasopressin (Searls et al., 2010). Downregulation of SERCA was also observed in cultured rat VSMCs exposed to high glucose, although this did not produce any significant alteration in the Ca²⁺ response to phenylephrine (El-Najjar et al., 2017). Interestingly, the protein expression of SERCA2B, which represents the main SERCA isoform in proliferating VSMCs (Berra-Romani et al., 2008) can be significantly enhanced in the thoracic and abdominal aortas of OZDF rats (Berra-Romani et al., 2019). Conversely, SERCA2B activity can be negatively modulated by oxidative stress (Berra-Romani et al., 2019; Negri et al., 2021), which is dramatically enhanced in OZDF rats (Chinen et al., 2007). It has been recently proposed that an early increase in [Ca²⁺]_i can stimulate the production of reactive oxygen species (ROS) via the Ca²⁺-dependent recruitment of NADPH oxidase 5 (NOX5) (Negri et al., 2021). Additionally, ROS could be generated upon

NOX2 activation by Gq-protein Coupled Receptors (Negri et al., 2021), such as purinergic P2Y receptors. Therefore, we hypothesize that the initial increase in $[Ca^{2+}]_i$ evoked by ATP is rapidly cleared by SERCA2B in rat aortic VSMCs from OZDF rats due to its increased expression as compared to LZDF animals. However, ATP stimulation could also result in NOX2 and/or NOX5 activation, thereby exacerbating the ongoing oxidative stress and inhibiting SERCA2B activity during the plateau phase. Overall, our findings suggest that SERCA activity is increased during the initial phase of the Ca^{2+} response to an IP_3 -producing autacoid, such as ATP, but the decreases during the later stages of the increase in $[Ca^{2+}]_i$ in aortic VSMCs from OZDF rats.

4.5 T2DM alters PMCA activity in rat aortic VSMCs

The next Ca^{2+} -clearing mechanism evaluated in the present investigation was PMCA. In both experimental groups, OV caused a larger increase in Amp600 in LZDF as compared to OZDF rats. This finding indicates that also PMCA activity is reduced during the plateau phase of the Ca^{2+} response to ATP in diabetic animals. It turns out that blocking Ca^{2+} extrusion via PMCA with OV causes a larger accumulation of cytosolic Ca^{2+} in LZDF as compared to OZDF VSMCs. It is, therefore, plausible to conclude that the increase in plateau amplitude observed in diabetic rat aortic VSMCs is also due to a decrease in PMCA activity. As to the early phase of the Ca^{2+} signal, the decay time to 90% and 60% of the initial Ca^{2+} peak were significantly increased in OZDF, but not in LZDF VSMCs. This finding suggests that Ca^{2+} extrusion through PMCA is increased by T2DM at the onset of ATP-evoked increase in $[Ca^{2+}]_i$. Notably, OV reduced the Ca^{2+} peak amplitude in diabetic but not lean VSMCs. This finding suggests that enhanced PMCA activity is somehow required to propagate the rise in $[Ca^{2+}]_i$ following agonist stimulation, as described in human platelets (Jones et al., 2010). The increase in PMCA activation could be attributed to enhanced SOCE, which can engage PMCA with high spatio-temporal efficiency and thereby finely tune IP_3 -evoked SR Ca^{2+} release during the rising phase of the Ca^{2+} signal.

Conversely, when PMCA was inhibited in the absence of extracellular Ca^{2+} , the decay time at 90%, 60% and 30% were significantly reduced in both animal groups. This finding strongly suggests that PMCA plays a minor role in buffering the initial increase in $[Ca^{2+}]_i$ under $0Ca^{2+}$ conditions. Furthermore, the amplitude of the initial Ca^{2+} peak was significantly decreased also in LZDF rat aortic VSMCs, which means that extracellular Ca^{2+} entry can substitute PMCA to regulate IP_3 -dependent SR Ca^{2+} release in lean animals. Interestingly, also CPA reduced the amplitude of the initial Ca^{2+} peak in LZDF VSMCs stimulated with ATP only under $0Ca^{2+}$ conditions, thereby indicating that SERCA interacts with PMCA to finely tune IP_3 -induced SR Ca^{2+} mobilization in non-diabetic VSMCs in the absence of Ca^{2+} entry.

These results, therefore, set extracellular Ca^{2+} as a regulator of PMCA in rat aortic VSMCs. PMCA activity is likely to be increased during the early phase of Ca^{2+} response evoked by ATP in the presence of extracellular Ca^{2+} in OZDF rat aortic VSMCs, while it declines during the subsequent plateau phase. In contrast, PMCA does not seem to have a relevant role under $0Ca^{2+}$ conditions in both

animal groups. A functional coupling between SOCE and PMCA has long been known. Extracellular Ca^{2+} incoming through Orai1 channels can stimulate adjacent PMCA in a calmodulin-dependent manner and promote Ca^{2+} extrusion across the plasma membrane (Klishin et al., 1998; Snitsarev and Taylor, 1999). PMCA might not be engaged under $0Ca^{2+}$ conditions, so that IP_3 -released Ca^{2+} is removed by alternative Ca^{2+} -clearing mechanisms that present a higher extrusion rate and therefore accelerate the decay phase of the Ca^{2+} transient in both animal groups. The subsequent inhibition of PMCA activity during the late phase of decay even in the presence of extracellular Ca^{2+} could again reflect the enhanced oxidative stress imposed to diabetic VSMCs during the development of the Ca^{2+} signal. In accord, it has been demonstrated that ROS inhibit PMCA activity and thereby favour the accumulation of cytosolic Ca^{2+} (Kim et al., 2018), which is consistent with the increase in plateau amplitude in OZDF VSMCs.

Scarce information is available regarding the mechanisms by which T2DM affects PMCA in VSMCs; however, our results resemble those reported by El-Najjar et al., who showed that PMCA activity in rat aortic VSMCs exposed to high extracellular glucose is enhanced due to the increase in PMCA4 expression (El-Najjar et al., 2017). Similar results were observed in VSMCs from coronary arteries of diabetic and dyslipidemic pigs (Hill et al., 2003). Nevertheless, neither study evaluated whether PMCA activity decreases during the Ca^{2+} response to an IP_3 -producing autacoid.

4.6 T2DM alters NCX activity in rat aortic VSMCs

The last Ca^{2+} -clearing mechanism evaluated in the present investigation was NCX. As described for SERCA and PMCA, NCX inhibition elicited different effects in lean vs. diabetic rats. In the presence of extracellular Ca^{2+} , SEA0400 reduced the amplitude of the initial Ca^{2+} peak in LZDF but not OZDF VSMCs. Therefore, NCX is likely to regulate IP_3 -induced SR Ca^{2+} release in rat aortic VSMCs from lean animals. Furthermore, blocking NCX activity did not remarkably affect the decay phase, but increased Amp600, of the Ca^{2+} response evoked by ATP in LZDF rats. Conversely, SEA0400 slowed down all the decay time and inhibited the plateau phase in OZDF VSMCs. These findings indicate that: 1) NCX operates in the forward (i.e., Ca^{2+} out) mode during the late phase of the Ca^{2+} response to ATP in lean VSMCs and 2) NCX switches from the forward to the reverse-mode (i.e., Ca^{2+} in) during the decay phase of the Ca^{2+} response evoked by ATP in diabetic VSMCs. The Ca^{2+} -clearing activity of NCX during the early phase of the ATP-evoked increase in $[Ca^{2+}]_i$ could contribute to explain its sharper decline in OZDF VSMCs. Conversely, under $0Ca^{2+}$ conditions, Ca^{2+} extrusion via NCX seems to be decreased in diabetic VSMCs. In accord, blocking NCX activity accelerated the decay rate, which means that NCX is unlikely to clear cytosolic Ca^{2+} in the absence of Ca^{2+} entry. On the other hand, SEA0400 slows down the clearing rate in LZDF VSMCs, which indicates that in lean animals NCX drives the recovery of the Ca^{2+} transient to the baseline only under $0Ca^{2+}$ conditions.

Five Similar to SERCA, it is still unclear how T2DM affects NCX activity in VSMCs. A study performed by El-najjar et al. showed that, in VSMCs exposed to high glucose, there were no alterations in

NCX expression or activity (El-najjar et al., 2017). Conversely, NCX activity was enhanced in cardiomyocytes isolated from db/db obese type 2 diabetic mice (Pereira et al., 2006). Future studies are required to understand whether NCX and PMCA expression are altered in aortic VSMCs from OZDF rats. Conclusion.

Herein, we provided the first demonstration that the Ca^{2+} -transporting machinery is deranged in aortic VSMCs from diabetic obese rats. The Ca^{2+} pumping activity of SERCA and PMCA is increased by T2DM during the early phase of the Ca^{2+} transient, whereas it is remarkably slowed down during the following plateau phase. Similarly, NCX contributes to buffer the initial increase in $[\text{Ca}^{2+}]_i$ by operating in the reverse-mode, but it then reverses into the Ca^{2+} -entry mode during the plateau phase. Therefore, the larger plateau observed in rat aortic VSMCs from OZDF rats is not only due to SOCE upregulation, as shown by others and confirmed in the present study, but also to the lower Ca^{2+} extrusion via PMCA and SERCA and to the activation of the reverse-mode of NCX. This latter observation suggests that a Na^+ -permeable channel is recruited or enhances its activity in diabetic VSMCs challenged with ATP. The non-selective cation channel, TRP Canonical 6 (TRPC6), can be gated by diacylglycerol produced upon PLC activation and generates local cytosolic Na^+ transients beneath the plasma membrane that drive NCX-mediated Ca^{2+} entry in purinergically stimulated rat aortic VSMCs (Poburko et al., 2007). Future work will have to assess whether TRPC6 activation is enhanced by T2DM and contributes to further elevate the $[\text{Ca}^{2+}]_i$ during the plateau phase. Preliminary evidence showed that TRPC6 protein was upregulated in caudal artery smooth muscle from Type 2 diabetic Goto-Kakizaki rats (Mita et al., 2010), whereas TRPC3 protein expression was increased in platelets of patients affected by T2DM (Zbidi et al., 2009).

Intriguingly, extracellular Ca^{2+} entry is required to engage PMCA and the forward mode of NCX during the decay phase. The functional coupling between Orai1, i.e., the pore-forming subunit of SOCs, and PMCA has been firmly established, while a straight-forward relationship between SOCE and NCX-mediated Ca^{2+} extrusion is yet to be reported. The faster decay of $[\text{Ca}^{2+}]_i$ observed in diabetic rat aortic VSMCs challenged with ATP in the absence of extracellular Ca^{2+} and upon inhibition of either PMCA or NCX activity suggests the involvement of an alternative Ca^{2+} -clearing mechanism. Mitochondrial have been shown to rapidly buffer Ca^{2+} at high $[\text{Ca}^{2+}]_i$ in rat systemic arterial smooth muscle cells (McCarron and Muir, 1999; Kamishima et al., 2000). Although this issue remains highly controversial, the rate of mitochondrial Ca^{2+} uptake could be increased by T2DM (Belosludtsev et al., 2020). Intriguingly, the simultaneous blockade of SERCA, PMCA and NCX activity in the absence of extracellular Ca^{2+} results in a plateau-like elevation in $[\text{Ca}^{2+}]_i$ that presents a higher Amp600 in VSMCs from LZDF rats. This finding implies that an additional Ca^{2+} -removal mechanism intervene to buffer, at least partially, the initial rise in $[\text{Ca}^{2+}]_i$ elicited by ATP in rat aortic VSMCs from OZDF rats. These alterations in the Ca^{2+} clearing machine in aortic VSMCs could exacerbate vascular dysfunction in diabetes. For instance, the aberrant increase in $[\text{Ca}^{2+}]_i$ observed could enhance VSMC proliferation and migration, thereby favoring atherosclerotic plaques and vascular calcification. In addition, cytosolic Ca^{2+}

overload in VSMCs could exacerbate oxidative stress within the vascular wall (Negri et al., 2021).

Data availability statement

The raw data supporting the conclusion of this article will be made available by the authors, without undue reservation.

Ethics statement

The animal study was reviewed and approved by the Animal Care and Use Committee of the Benemerita Universidad Autonoma de Puebla, identification code: BERRSAL71, 18-05-2017.

Author contributions

RB-R and FM were responsible for the study design and write the manuscript. AM-S, NC-S, RM-V, and ML-T were responsible for data collection, data analysis and interpretation. MG-C assisted with data interpretation. All authors read the manuscript critically and approved the submitted version.

Funding

This research was funded by Facultad de Medicina de la Benemérita Universidad Autónoma de Puebla to pay for publication expenses. RB-R is supported by the National Council of Science and Technology (CONACYT), Identification Number: CVU121216.

Conflict of interest

The authors declare that the research was conducted in the absence of any commercial or financial relationships that could be construed as a potential conflict of interest.

Publisher's note

All claims expressed in this article are solely those of the authors and do not necessarily represent those of their affiliated organizations, or those of the publisher, the editors and the reviewers. Any product that may be evaluated in this article, or claim that may be made by its manufacturer, is not guaranteed or endorsed by the publisher.

Supplementary material

The Supplementary Material for this article can be found online at: <https://www.frontiersin.org/articles/10.3389/fphys.2023.1200115/full#supplementary-material>

References

- Al-Awar, A., Kupai, K., Veszelka, M., Szucs, G., Attieh, Z., Murlasits, Z., et al. (2016). Experimental diabetes mellitus in different animal models. *J. Diabetes Res.* 2016, 9051426. doi:10.1155/2016/9051426
- Baryshnikov, S. G., Pulina, M. V., Zulian, A., Linde, C. I., and Golovina, V. A. (2009). Orail, a critical component of store-operated Ca²⁺ entry, is functionally associated with Na⁺/Ca²⁺ exchanger and plasma membrane Ca²⁺ pump in proliferating human arterial myocytes. *Am. J. Physiol. Cell Physiol.* 297 (5), C1103–C1112. doi:10.1152/ajpcell.00283.2009
- Belosludtsev, K. N., Belosludtseva, N. V., and Dubinin, M. V. (2020). Diabetes mellitus, mitochondrial dysfunction and Ca(2+)-dependent permeability transition pore. *Int. J. Mol. Sci.* 21 (18), 6559. doi:10.3390/ijms21186559
- Berra-Romani, R., Guzman-Silva, A., Vargaz-Guadarrama, A., Flores-Alonso, J. C., Alonso-Romero, J., Trevino, S., et al. (2019). Type 2 diabetes alters intracellular Ca(2+) handling in native endothelium of excised rat aorta. *Int. J. Mol. Sci.* 21 (1), 250. doi:10.3390/ijms21010250
- Berra-Romani, R., Mazzocco-Spezia, A., Pulina, M. V., and Golovina, V. A. (2008). Ca²⁺ handling is altered when arterial myocytes progress from a contractile to a proliferative phenotype in culture. *Am. J. Physiol. Cell Physiol.* 295 (3), C779–C790. doi:10.1152/ajpcell.00173.2008
- Chinen, I., Shimabukuro, M., Yamakawa, K., Higa, N., Matsuzaki, T., Noguchi, K., et al. (2007). Vascular lipotoxicity: Endothelial dysfunction via fatty-acid-induced reactive oxygen species overproduction in obese Zucker diabetic fatty rats. *Endocrinology* 148 (1), 160–165. doi:10.1210/en.2006-1132
- Chung, A. W., Au Yeung, K., Chum, E., Okon, E. B., and van Breemen, C. (2009). Diabetes modulates capacitative calcium entry and expression of transient receptor potential canonical channels in human saphenous vein. *Eur. J. Pharmacol.* 613 (1–3), 114–118. doi:10.1016/j.ejphar.2009.04.029
- Einarson, T. R., Acs, A., Ludwig, C., and Panton, U. H. (2018). Prevalence of cardiovascular disease in type 2 diabetes: A systematic literature review of scientific evidence from across the world in 2007–2017. *Cardiovasc Diabetol.* 17 (1), 83. doi:10.1186/s12933-018-0728-6
- El-Najjar, N., Kulkarni, R. P., Nader, N., Hodeify, R., and Machaca, K. (2017). Effects of hyperglycemia on vascular smooth muscle Ca(2+) signaling. *Biomed. Res. Int.*, 2017, 3691349. doi:10.1155/2017/3691349
- ElSayed, N. A., Aleppo, G., Aroda, V. R., Bannuru, R. R., Brown, F. M., Bruemmer, D., et al. (2023). 2. Classification and diagnosis of diabetes: Standards of care in diabetes-2023. *Diabetes Care* 46 (1), S19–S40. doi:10.2337/dc23-S002
- Erlinge, D., Hou, M., Webb, T. E., Barnard, E. A., and Moller, S. (1998). Phenotype changes of the vascular smooth muscle cell regulate P2 receptor expression as measured by quantitative RT-PCR. *Biochem. Biophys. Res. Commun.* 248 (3), 864–870. doi:10.1006/bbrc.1998.9083
- Fernandez-Velasco, M., Ruiz-Hurtado, G., Gomez, A. M., and Rueda, A. (2014). Ca(2+) handling alterations and vascular dysfunction in diabetes. *Cell Calcium* 56 (5), 397–407. doi:10.1016/j.ceca.2014.08.007
- Fridlyand, L. E., and Philipson, L. H. (2006). Reactive species and early manifestation of insulin resistance in type 2 diabetes. *Diabetes Obes. Metab.* 8 (2), 136–145. doi:10.1111/j.1463-1326.2005.00496.x
- Gu, K., Cowie, C. C., and Harris, M. I. (1998). Mortality in adults with and without diabetes in a national cohort of the U.S. population, 1971–1993. *Diabetes Care* 21 (7), 1138–1145. doi:10.2337/diacare.21.7.1138
- Han, A. Y., Ha, S. M., Shin, Y. K., and Seol, G. H. (2022). Ginsenoside Rg-1 prevents elevated cytosolic Ca(2+) via store-operated Ca(2+) entry in high-glucose-stimulated vascular endothelial and smooth muscle cells. *BMC Complement. Med. Ther.* 22 (1), 166. doi:10.1186/s12906-022-03647-5
- Hill, B. J., Price, E. M., Dixon, J. L., and Sturek, M. (2003). Increased calcium buffering in coronary smooth muscle cells from diabetic dyslipidemic pigs. *Atherosclerosis* 167 (1), 15–23. doi:10.1016/s0021-9150(02)00381-7
- House, S. J., Potier, M., Bisaillon, J., Singer, H. A., and Trebak, M. (2008). The non-excitable smooth muscle: Calcium signaling and phenotypic switching during vascular disease. *Pflugers Arch.* 456 (5), 769–785. doi:10.1007/s00424-008-0491-8
- IDF Diabetes Atlas (2021). *IDF diabetes Atlas*. Available at: <https://www.idf diabetesatlas.org>.
- Jones, S., Solomon, A., Sanz-Rosa, D., Moore, C., Holbrook, L., Cartwright, E. J., et al. (2010). The plasma membrane calcium ATPase modulates calcium homeostasis, intracellular signaling events and function in platelets. *J. Thromb. Haemost.* 8 (12), 2766–2774. doi:10.1111/j.1538-7836.2010.04076.x
- Kamishima, T., Davies, N. W., and Standen, N. B. (2000). Mechanisms that regulate [Ca²⁺]_i following depolarization in rat systemic arterial smooth muscle cells. *J. Physiol.* 522 (2), 285–295. doi:10.1111/j.1469-7793.2000.t01-2-00285.x
- Kennedy, M. W. (2017). *Intracoronary insights in diabetes mellitus*. Nijmegen, Holland: Radboud University. Available at: <https://hdl.handle.net/2066/176469>.
- Kim, M. J., Choi, K. J., Yoon, M. N., Oh, S. H., Kim, D. K., Kim, S. H., et al. (2018). Hydrogen peroxide inhibits Ca(2+) efflux through plasma membrane Ca(2+)-ATPase in mouse parotid acinar cells. *Korean J. Physiol. Pharmacol.* 22 (2), 215–223. doi:10.4196/kjpp.2018.22.2.215
- King, A., and Bowe, J. (2016). Animal models for diabetes: Understanding the pathogenesis and finding new treatments. *Biochem. Pharmacol.* 99, 1–10. doi:10.1016/j.bcp.2015.08.108
- Klishin, A., Sedova, M., and Blatter, L. A. (1998). Time-dependent modulation of capacitative Ca²⁺ entry signals by plasma membrane Ca²⁺ pump in endothelium. *Am. J. Physiol.* 274 (4), C1117–C1128. doi:10.1152/ajpcell.1998.274.4.C1117
- Linde, C. I., Karashima, E., Raina, H., Zulian, A., Wier, W. G., Hamlyn, J. M., et al. (2012). Increased arterial smooth muscle Ca²⁺ signaling, vasoconstriction, and myogenic reactivity in Milan hypertensive rats. *Am. J. Physiol. Heart Circ. Physiol.* 302 (3), H611–H620. doi:10.1152/ajpheart.00950.2011
- Liu, B., Wang, D., Luo, E., Hou, J., Qiao, Y., Yan, G., et al. (2019). Role of TG2-mediated SERCA2 serotonylation on hypoxic pulmonary vein remodeling. *Front. Pharmacol.* 10, 1611. doi:10.3389/fphar.2019.01611
- Liu, B., Yang, L., Zhang, B., Kuang, C., Huang, S., and Guo, R. (2016). NF-κB-Dependent upregulation of NCX1 induced by angiotensin II contributes to calcium influx in rat aortic smooth muscle cells. *Can. J. Cardiol.* 32 (11), e11. doi:10.1016/j.cjca.2016.02.060
- Lodola, F., Laforenza, U., Cattaneo, F., Ruffinatti, F. A., Poletto, V., Massa, M., et al. (2017). VEGF-induced intracellular Ca(2+) oscillations are down-regulated and do not stimulate angiogenesis in breast cancer-derived endothelial colony forming cells. *Oncotarget* 8 (56), 95223–95246. doi:10.18632/oncotarget.20255
- Ma, K., Sukkar, B., Zhu, X., Zhou, K., Cao, H., Voelkl, J., et al. (2020). Stimulation of ORAI1 expression, store-operated Ca(2+) entry, and osteogenic signaling by high glucose exposure of human aortic smooth muscle cells. *Pflugers Arch.* 472 (8), 1093–1102. doi:10.1007/s00424-020-02405-1
- Mao, L., Yin, R., Yang, L., and Zhao, D. (2022). Role of advanced glycation end products on vascular smooth muscle cells under diabetic atherosclerosis. *Front. Endocrinol. (Lausanne)* 13, 983723. doi:10.3389/fendo.2022.983723
- McCarron, J. G., and Muir, T. C. (1999). Mitochondrial regulation of the cytosolic Ca²⁺ concentration and the InsP₃-sensitive Ca²⁺ store in Guinea-pig colonic smooth muscle. *J. Physiol.* 516, 149–161. doi:10.1111/j.1469-7793.1999.149aa.x
- Mita, M., Ito, K., Taira, K., Nakagawa, J., Walsh, M. P., and Shoji, M. (2010). Attenuation of store-operated Ca²⁺ entry and enhanced expression of TRPC channels in caudal artery smooth muscle from Type 2 diabetic Goto-Kakizaki rats. *Clin. Exp. Pharmacol. Physiol.* 37 (7), 670–678. doi:10.1111/j.1440-1681.2010.05373.x
- Negri, S., Faris, P., and Moccia, F. (2021). Reactive oxygen species and endothelial Ca(2+) signaling: Brothers in arms or partners in crime? *Int. J. Mol. Sci.* 22 (18), 9821. doi:10.3390/ijms22189821
- Nieves-Cintrón, M., Flores-Tamez, V. A., Le, T., Baudel, M. M., and Navedo, M. F. (2021). Cellular and molecular effects of hyperglycemia on ion channels in vascular smooth muscle. *Cell Mol. Life Sci.* 78 (1), 31–61. doi:10.1007/s00018-020-03582-z
- Pande, J., Mallhi, K. K., Sawh, A., Szewczyk, M. M., Simpson, F., and Grover, A. K. (2006). Aortic smooth muscle and endothelial plasma membrane Ca²⁺ pump isoforms are inhibited differently by the extracellular inhibitor caloxin 1b1. *Am. J. Physiol. Cell Physiol.* 290 (5), C1341–C1349. doi:10.1152/ajpcell.00573.2005
- Pereira, A. C., Araujo, A. V., Paulo, M., da Silva, R. S., and Bendhack, L. M. (2022). RuBPY decreases intracellular calcium by decreasing influx and increasing storage. *Clin. Exp. Pharmacol. Physiol.* 49 (7), 759–766. doi:10.1111/1440-1681.13652
- Pereira, L., Matthes, J., Schuster, I., Valdivia, H. H., Herzig, S., Richard, S., et al. (2006). Mechanisms of [Ca²⁺]_i transient decrease in cardiomyopathy of db/db type 2 diabetic mice. *Diabetes* 55 (3), 608–615. doi:10.2337/diabetes.55.03.06.db05-1284
- Poburko, D., Liao, C. H., Lemos, V. S., Lin, E., Maruyama, Y., Cole, W. C., et al. (2007). Transient receptor potential channel 6-mediated, localized cytosolic [Na⁺] transients drive Na⁺/Ca²⁺ exchanger-mediated Ca²⁺ entry in purinergically stimulated aorta smooth muscle cells. *Circ. Res.* 101 (10), 1030–1038. doi:10.1161/CIRCRESAHA.107.155531
- Pulina, M. V., Zulian, A., Berra-Romani, R., Beskina, O., Mazzocco-Spezia, A., Baryshnikov, S. G., et al. (2010). Upregulation of Na⁺ and Ca²⁺ transporters in arterial smooth muscle from ouabain-induced hypertensive rats. *Am. J. Physiol. Heart Circ. Physiol.* 298 (1), H263–H274. doi:10.1152/ajpheart.00784.2009
- Searls, Y. M., Loganathan, R., Smirnova, I. V., and Stehno-Bittel, L. (2010). Intracellular Ca²⁺ regulating proteins in vascular smooth muscle cells are altered with type 1 diabetes due to the direct effects of hyperglycemia. *Cardiovasc Diabetol.* 9, 8. doi:10.1186/1475-2840-9-8
- Shiota, M., and Printz, R. L. (2012). Diabetes in Zucker diabetic fatty rat. *Methods Mol. Biol.* 933, 103–123. doi:10.1007/978-1-62703-068-7_8
- Smani, T., Dominguez-Rodriguez, A., Hmadcha, A., Calderon-Sanchez, E., Horrillo-Ledesma, A., and Ordóñez, A. (2007). Role of Ca²⁺-independent phospholipase A2 and store-operated pathway in urocortin-induced vasodilatation of rat coronary artery. *Circ. Res.* 101 (11), 1194–1203. doi:10.1161/CIRCRESAHA.107.159053

- Snitsarev, V. A., and Taylor, C. W. (1999). Overshooting cytosolic Ca^{2+} signals evoked by capacitative Ca^{2+} entry result from delayed stimulation of a plasma membrane Ca^{2+} pump. *Cell Calcium* 25 (6), 409–417. doi:10.1054/ceca.1999.0041
- Szuskiewicz-Garcia, M. M., and Davidson, J. A. (2014). Cardiovascular disease in diabetes mellitus: Risk factors and medical therapy. *Endocrinol. Metab. Clin. North Am.* 43 (1), 25–40. doi:10.1016/j.ecl.2013.09.001
- Tirmenstein, M., Horvath, J., Graziano, M., Mangipudy, R., Dorr, T., Colman, K., et al. (2015). Utilization of the Zucker diabetic fatty (ZDF) rat model for investigating hypoglycemia-related toxicities. *Toxicol. Pathol.* 43 (6), 825–837. doi:10.1177/0192623315581020
- Tong, X., Hou, X., Jourdeuil, D., Weisbrod, R. M., and Cohen, R. A. (2010). Upregulation of Nox4 by TGF β 1 oxidizes SERCA and inhibits NO in arterial smooth muscle of the prediabetic Zucker rat. *Circ. Res.* 107 (8), 975–983. doi:10.1161/CIRCRESAHA.110.221242
- Urena, J., del Valle-Rodriguez, A., and Lopez-Barneo, J. (2007). Metabotropic Ca^{2+} channel-induced calcium release in vascular smooth muscle. *Cell Calcium* 42 (4–5), 513–520. doi:10.1016/j.ceca.2007.04.010
- Velmurugan, G. V., and White, C. (2012). Calcium homeostasis in vascular smooth muscle cells is altered in type 2 diabetes by Bcl-2 protein modulation of InsP3R calcium release channels. *Am. J. Physiol. Heart Circ. Physiol.* 302 (1), H124–H134. doi:10.1152/ajpheart.00218.2011
- Wang, Y. W., Sun, G. D., Sun, J., Liu, S. J., Wang, J., Xu, X. H., et al. (2013). Spontaneous type 2 diabetic rodent models. *J. Diabetes Res.* 2013, 401723. doi:10.1155/2013/401723
- Yan, F., Lu, J., Zhang, Y., Li, X., Chan, W. H., Zhao, Q., et al. (2020). Resveratrol stimulates the Na^{+} - Ca^{2+} exchanger on the plasma membrane to reduce cytosolic Ca^{2+} in rat aortic smooth muscle cells. *J. Cardiovasc. Pharmacol.* 76 (5), 610–616. doi:10.1097/FJC.0000000000000897
- Yang, H., Chen, X. Y., Kuang, S. J., Zhou, M. Y., Zhang, L., Zeng, Z., et al. (2020). Abnormal Ca^{2+} handling contributes to the impairment of aortic smooth muscle contractility in Zucker diabetic fatty rats. *J. Mol. Cell Cardiol.* 141, 82–92. doi:10.1016/j.yjmcc.2020.03.009
- Zbidi, H., Lopez, J. J., Amor, N. B., Bartegi, A., Salido, G. M., and Rosado, J. A. (2009). Enhanced expression of STIM1/Orai1 and TRPC3 in platelets from patients with type 2 diabetes mellitus. *Blood Cells Mol. Dis.* 43 (2), 211–213. doi:10.1016/j.bcmd.2009.04.005
- Zhang, J., Lee, M. Y., Cavalli, M., Chen, L., Berra-Romani, R., Balke, C. W., et al. (2005). Sodium pump α 2 subunits control myogenic tone and blood pressure in mice. *J. Physiol.* 569 (1), 243–256. doi:10.1113/jphysiol.2005.091801
- Zhang, R., Peng, L., Ran, H., Fan, Y., Zhao, Y., and Cao, F. (2018). Farnesoid X receptor activation modulates calcium homeostasis in rat aortic vascular smooth muscle cells. *Chin. J. Physiol.* 61 (4), 210–220. doi:10.4077/CJP.2018.BAG554
- Zhu, X., Ma, K., Zhou, K., Liu, J., Nurnberg, B., and Lang, F. (2021). Vasopressin-stimulated ORAI1 expression and store-operated Ca^{2+} entry in aortic smooth muscle cells. *J. Mol. Med. Berl.* 99 (3), 373–382. doi:10.1007/s00109-020-02016-4
- Zuccolo, E., Laforenza, U., Negri, S., Botta, L., Berra-Romani, R., Faris, P., et al. (2019). Muscarinic M5 receptors trigger acetylcholine-induced Ca^{2+} signals and nitric oxide release in human brain microvascular endothelial cells. *J. Cell Physiol.* 234 (4), 4540–4562. doi:10.1002/jcp.27234



OPEN ACCESS

EDITED BY

Andrea Gerbino,
University of Bari Aldo Moro, Italy

REVIEWED BY

Francisco O. Silva,
University of Texas Southwestern Medical
Center, United States
Francesco Moccia,
University of Pavia, Italy
Antonella Pantaleo,
University of Sassari, Italy

*CORRESPONDENCE

Alessia Remigante,
✉ aremigante@unime.it

[†]These authors have contributed equally
to this work

[†]These authors share senior authorship

RECEIVED 19 May 2023

ACCEPTED 22 June 2023

PUBLISHED 30 June 2023

CITATION

Remigante A, Spinelli S, Straface E,
Gambardella L, Russo M, Cafeo G,
Caruso D, Falliti G, Dugo P, Dossena S,
Marino A and Morabito R (2023),
Mechanisms underlying the anti-aging
activity of bergamot (*Citrus bergamia*)
extract in human red blood cells.
Front. Physiol. 14:1225552.
doi: 10.3389/fphys.2023.1225552

COPYRIGHT

© 2023 Remigante, Spinelli, Straface,
Gambardella, Russo, Cafeo, Caruso,
Falliti, Dugo, Dossena, Marino and
Morabito. This is an open-access article
distributed under the terms of the
[Creative Commons Attribution License
\(CC BY\)](https://creativecommons.org/licenses/by/4.0/). The use, distribution or
reproduction in other forums is
permitted, provided the original author(s)
and the copyright owner(s) are credited
and that the original publication in this
journal is cited, in accordance with
accepted academic practice. No use,
distribution or reproduction is permitted
which does not comply with these terms.

Mechanisms underlying the anti-aging activity of bergamot (*Citrus bergamia*) extract in human red blood cells

Alessia Remigante^{1*†}, Sara Spinelli^{1†}, Elisabetta Straface²,
Lucrezia Gambardella², Marina Russo¹, Giovanna Cafeo¹,
Daniele Caruso³, Giuseppe Falliti³, Paola Dugo¹, Silvia Dossena⁴,
Angela Marino^{1†} and Rossana Morabito^{1†}

¹Department of Chemical and Biological, Pharmaceutical and Environmental Sciences, University of Messina, Messina, Italy, ²Biomarkers Unit, Center for Gender-Specific Medicine, Istituto Superiore di Sanità, Rome, Italy, ³Complex Operational Unit of Clinical Pathology of Papardo Hospital, Messina, Italy, ⁴Institute of Pharmacology and Toxicology, Paracelsus Medical University, Salzburg, Austria

Introduction: Aging is a process characterised by a decline in physiological functions. Reactive species play a crucial role in the aging rate. Due to the close relationship between aging and oxidative stress, functional foods rich in phytochemicals are excellent candidates to neutralise age-related changes.

Aim: This investigation aims to verify the potential protective role of bergamot (*Citrus bergamia*, *Femminello* cultivar) peel and juice extract in a model of aging represented by human red blood cells (RBCs) exposed to D-Galactose (DGal).

Methods: Bergamot peel and juice extracts were subjected to RP-HPLC/PDA/MS for determination of their composition in bioactive compounds. Markers of oxidative stress, including ROS production, thiobarbituric acid reactive substances (TBARS) levels –a marker of lipid peroxidation, oxidation of total protein sulfhydryl groups, as well as the expression and anion exchange capability of band 3 and glycated haemoglobin (A1c) production have been investigated in RBCs treated with D-Gal for 24 h, with or without pre-incubation for 15 min with 5 µg/mL peel or juice extract. In addition, the activity of the endogenous antioxidant system, including catalase (CAT) and superoxide dismutase (SOD), as well as the diversion of the RBC metabolism from glycolysis towards the pentose phosphate pathway shunt, as denoted by activation of glucose-6-phosphate dehydrogenase (G6PDH), have been explored.

Results: Data shown here suggest that bergamot peel and juice extract i) prevented the D-Gal-induced ROS production, and consequently, oxidative stress injury to biological macromolecules including membrane lipids and proteins; ii) significantly restored D-Gal-induced alterations in the distribution and ion transport kinetics of band 3; iii) blunted A1c production; iv) effectively impeded the over-activation of the endogenous antioxidant enzymes CAT and SOD; and v) significantly prevented the activation of G6PDH.

Discussion: These results further contribute to shed light on aging mechanisms in human RBCs and identify bergamot as a functional food rich in natural antioxidants useful for prevention and treatment of oxidative stress-related changes, which may lead to pathological states during aging.

KEYWORDS

flavonoid fraction, bergamot (*Citrus bergamia*), peel and/or juice extract, oxidative stress, aging, red blood cells, band 3 anion exchanger

1 Introduction

Aging is a biological process that results in a progressive and non-reversible decline in the physiological functions of all body organs and is caused by damage accumulation with concomitant elevation of oxidative stress (Fukagawa, 1999; Akki et al, 2018; Akki et al, 2019; Ferrera et al, 2021). In 1972, Denham Harman (Harman, 1972) postulated the free radical theory of aging, which points to accumulation of reactive species as the underlying reason for the oxidation of the biological macromolecules and consequent cell injury, thereby explaining the alterations in cell functions during natural aging (Junqueira et al, 2004; Remigante and Morabito, 2022).

Aerobic cell metabolism requires oxygen as the final electron acceptor of oxidation reactions and reactive oxygen species (ROS) represent a byproduct of this process. The physiological role of red blood cells (RBCs) is the transport of respiratory gases from the lungs to the tissues and *vice versa*, in order to supply the cells with oxygen. In the blood stream, RBCs are continuously exposed to both endogenous and exogenous reactive species able to injury their structure, thus impairing their physiology and functionality (Rizvi and Maurya, 2007; Remigante et al, 2021a; Fujii et al, 2021; Arrigo et al, 2023). Un-neutralized reactive species react with both RBC plasma membrane lipids and proteins and promote oxidative alterations at level of lipids (lipid peroxidation) and proteins (protein oxidation) and/or fragmentation, respectively (Avitabile et al, 2020). Alternatively, the accumulation of reactive species results in the induction of glycation reactions, which leads to the increased endogenous production of advanced glycation end products (AGEs) (Moldogazieva et al, 2019). Non-enzymatic glycation of membrane glycoproteins and/or haemoglobin as well as their gradual accumulation within RBCs can account for altered rheologic properties of RBCs (Turk et al, 1998). In RBCs, oxidative stress-related aging is accompanied by a decrease in cell volume and hemoglobin content and an increase in cell density (Pandey and Rizvi, 2010). These alterations are correlated with a loss of cholesterol and phospholipids, resulting in a decrease in the surface area that reflects a loss of membrane lipids and protein constituents. The reduction of surface area could be explained by a gradual membrane blebbing and vesiculation (Willekens et al, 2008), both accelerated in aged RBCs (Pandey and Rizvi, 2011). In addition, these changes might limit the ability of the RBCs to maintain the highly deformable biconcave shape necessary to pass through the narrow capillaries, thus contributing to their removal from circulation (Shiga et al, 1990; Pretorius, 2018).

One of the major goals of RBC redox regulation results in protection of their main plasma membrane protein, band 3 (SLC4A1/AE1) (Abbas et al, 2018). Band 3 is an integral trans-membrane protein that plays different functions: 1) the maintenance of anion homeostasis (Reithmeier et al, 2016); 2) the binding between plasma membrane lipids and cytoskeletal proteins, reflecting on cell shape (De Franceschi et al, 2012; Vallese et al, 2022; Spinelli et al, 2023); 3) the docking, at level of the N-terminal cytosolic domain that protrudes into the cytosol, of a series of structural proteins and glycolytic enzymes (e.g., glyceraldehyde 3-phosphate dehydrogenases: GAPDH) (Campanella et al, 2008; Puchulu-Campanella et al, 2013), as well as cytosolic proteins such as haemoglobin (Zhang et al, 2003). Moreover, haemoglobin, in addition to

its central role of carrying oxygen from the lungs to peripheral tissues, may serve as oxygen sensor, in order to appropriately link band 3 to regulation of the RBC metabolism (Ellsworth, 2000; Puchulu-Campanella et al, 2013). In fact, several studies have provided compelling, albeit indirect, evidence that, when not encumbered by deoxy-hemoglobin, the N-terminal of band 3 can bind to and, in turn, inhibit the glycolytic enzyme GAPDH (Issaian et al, 2021). Oxygen-dependent metabolic modulation is mediated by the competitive binding of deoxy-hemoglobin and glycolytic enzymes to the band 3 cytosolic domain. When oxidant stress is high, GAPDH enzyme is bound to band 3 and thereby inhibited (Reisz et al, 2016). In this context, RBCs favor glucose oxidation through the pentose phosphate pathway (PPP), in order to generate the reducing cofactor NADPH and fuel endogenous antioxidant systems. On the other hand, when oxidant stress is low, haemoglobin is deoxygenated and binds to the band 3 N-terminus, which in turn favors the release of glycolytic enzymes from the membrane to promote the generation of energy in the form of ATP and NADH through glycolysis (Castagnola et al, 2010). This balance may be dysregulated by early RBCs aging and/or increased reactive oxygen species (ROS) levels, thus depriving RBCs of their crucial metabolic plasticity and leading to their removal from the blood circulation (Kuhn et al, 2017). Therefore, the regulation of the balance between glycolysis and PPP is essential and enables RBCs to counteract oxidative insults impacting on their cell structures/functions. In addition, unusual levels of reactive species could be the common denominator in the development and progression of different aging-related acute and/or chronic pathologies, although the precise mechanisms contributing to oxidative stress-induced injury are still poorly clarified (Radi et al, 2014; Bo-Htay et al, 2018; Martinelli et al, 2020; Emanuelli et al, 2022; Guo et al, 2022; Remigante and Morabito, 2022).

To contain oxidative stress effects, RBCs possess an excellent cytosolic antioxidant machinery composed of non-enzymatic as well as enzymatic antioxidants, which represent an effective antioxidant equipment to protect RBCs themselves along with other body cells and tissues (Zabinski et al, 2000; Inal et al, 2001). The use of natural secondary metabolites such as polyphenol-rich extracts with antioxidant properties could be an excellent and workable alternative for supporting the integrated antioxidant system (Jacob, 1995; Lunceford and Gugliucci, 2005; Dorta et al, 2008; Kouka et al, 2017; Xu et al, 2019; Remigante et al, 2022a; Remigante et al, 2022b). In this regards, special attention has been paid to the potential health benefits of the flavonoid fraction of the bergamot (*Citrus bergamia*) (Russo et al, 2016).

Bergamot is a small tree belonging to Rutaceae family that is mainly cultivated in a specific area of the region of Calabria (Italy) known to ensure a microclimate suitable for its growth. The essential oil of bergamot, which is obtained from the fruit peel, has been extensively characterized and used in cosmetic and food industries, whereas the bergamot by-products, such as the pulp and juice, have been only recently evaluated for their beneficial properties, which include cholesterol reduction, antioxidant and anti-inflammatory effects (Ferlazzo et al, 2015; Russo et al, 2015; Carresi et al, 2016; Lauro et al, 2016; Musolino et al, 2019). This reassessment may lead to reduction in the disposal costs of industrial processes and gain of a good source of nutraceuticals, thus representing an economic

advantage (Russo et al, 2021). To date, no scientific study evaluating the anti-aging properties of peel and/or juice extracts from bergamot in human RBCs has been reported.

The long-term exposure to high doses of D-Galactose (D-Gal) represents a good experimental model of natural aging (Azman and Zakaria, 2019). Thus, the present investigation aims to identify the potential beneficial effects of bergamot peel and juice extracts from *Femminello* cultivar on the molecular mechanisms underlying natural aging in RBCs, including oxidative damage, glycation events and activation of the endogenous enzymatic defense system. To this aim, juice and peel extracts from bergamot fruits belonging to *Femminello* cultivar were subjected to RP-HPLC/PDA/MS for determination of their precise composition in bioactive compounds and their effects were evaluated in a D-Gal-induced model of aging in human RBCs.

2 Materials and methods

2.1 Materials and samples for analytical determination of bioactive molecules

Water, formic acid, ethanol, acetonitrile and methanol were obtained from Merck Life Science (Merck KGaA, Darmstadt, Germany). The standard compounds ferulic acid, synapic acid, eriocitrin, narirutin, and neohesperidin were obtained from Extrasynthese (Genay Cedex, France). Apigenin 6,8-di-C-glucoside, diosmetin 6,8-di-C-glucoside, naringin, brutieridin, limonin glucoside, nomilin glucoside, nomilinic acid glucoside, limonin, melitidin, nomilin and neoeriocitrin were previously isolated in our laboratory. Bergamot (*Citrus bergamia*) peels used in this research belong to *Femminello* cultivar and the experimental protocol has been performed with peels obtained from two fruits. Fruits were collected at the same stage of ripeness from trees grown in Calabria (Melito di Porto Salvo, Reggio Calabria, Italy) on January 2023. Fruits were washed, dried and stored at +4°C, then peeled and squeezed. Peels were dried at 25°C for 48 h.

The juice was subjected to RP-HPLC analysis without any pre-treatment. On the other hand, a solvent extraction procedure was performed on peel samples before RP-HPLC analysis. The bioactive compounds extraction procedure was previously validated by our group (Russo et al, 2015). Briefly, 10 g of samples were extracted with 100 mL of methanol for three times. The extract was subjected to chromatographic analysis. The juice and the peel extract were analysed in triplicate.

2.2 Determination of bioactive compounds using RP-HPLC/PDA/MS

A Shimadzu Prominence LC-20A system (Shimadzu, Milan, Italy) was employed to carry out HPLC analyses. The HPLC instrument was equipped with SPD-M20A UV and HPLCMS-2020 detectors. The analytical procedure was previously validated by our group (Russo et al, 2014). This analytical method allowed to quantify the bioactive molecule content in juice and bergamot peel samples. Figure of merits were calculated in accordance with the EURACHEM guidelines (Group, 1998).

2.3 Solutions and chemicals used to RBC sample processing

Chemicals used to perform experiments were purchased from Sigma (Milan, Italy). With regard to stock solutions, 4, 4'-diisothiocyanatostilbene-2, 2'-disulfonate (DIDS, 10 mM) was prepared in dimethyl sulfoxide (DMSO); D-Galactose (D-Gal, 1 M) was prepared in distilled water and N-ethylmaleimide (NEM, 310 mM) was prepared in ethanol. H₂O₂ experimental solution was obtained by dilution in distilled water from a 30% w/w stock solution. Ethanol never exceeded 0.001% v/v in the experimental solutions and was previously tested on RBCs to exclude haemolysis. Peel extract obtained as described above and juice devoid of the fibrous part were poured into freeze-drying flasks and placed into the vacuum chamber, frozen at -50°C, and then freeze-dried for 72 h (BenchTop K Series Freeze Dryers, VirTis Gardiner, United States). The concentrated peel extract required a dilution 1:100 w/v with distilled water prior to use in experiments.

2.4 Preparation of RBCs

Blood needed for the planned experiments was withdrawn from healthy volunteers (age 25–45 years) upon their informed consent. Whole blood samples, put in test tubes containing ethylenediaminetetraacetic acid (EDTA) as anticoagulant, were repeatedly washed in isotonic solution (NaCl 150 mM, 4-(2-hydroxyethyl)-1-piperazineethanesulfonic acid (HEPES) 5 mM, glucose 5 mM, pH 7.4, osmotic pressure 300 mOsm/kgH₂O; centrifugation with Neya 16R, 1,200 × g, 5 min) to eliminate plasma along with buffy coat. As a further step, thus obtained RBCs were put in isotonic solution at the haematocrit index requested by each protocol.

2.5 Haemolysis measurement

To determine the % haemolysis, RBCs (35% haematocrit) were treated with or without peel or juice extract in isotonic solution for 15 min at 37°C and then processed according to Remigante and collaborators (Remigante et al, 2022b). Haemoglobin absorbance was determined at 405 nm wavelength after subtracting the absorbance of blank (0.9% v/v NaCl solution).

2.6 Determination of intracellular reactive oxygen species (ROS)

The ROS levels were evaluated by the cell-permeable indicator 2', 7'-dichlorofluorescein diacetate (H2DCFDA, D6883, Sigma-Aldrich), according to the manufacturer's instructions, with slight modifications. Red blood cells were exposed to 100 mM D-Gal for 24 h at 25°C with or without pre-incubation with different concentrations of peel or juice extract. As the positive control, RBCs were incubated with H₂O₂. ROS formation was determined by a fluorescence microplate reader (Onda Spectrophotometer, UV-21) at excitation and emission wavelengths of 485 nm and 535 nm, respectively, after subtracting the background fluorescence. Results are expressed in %.

2.7 Measurement of thiobarbituric-acid-reactive substances (TBARS) levels

TBARS levels were detected as described by Mendanha and co-authors (Mendanha et al, 2012), with minor modifications. Red blood cells were suspended at 20% haematocrit and incubated with or without different concentrations of peel or juice extract. Next, samples were incubated in 100 mM D-Gal-containing solution and then addressed to quantification of TBARS levels obtained by subtracting 20% of the absorbance at 453 nm from that one at 532 nm (Onda Spectrophotometer, UV-21). Finally, the results were reported as μM TBARS levels.

2.8 Measurement of total sulfhydryl group (-SH) content

Measurement of total -SH groups was performed according to Aksenov and Markesbery technique (Aksenov and Markesbery, 2001) with minor modifications. Red blood cells, suspended at 35% haematocrit, were incubated with or without peel or juice extract at different concentrations and successively exposed to D-Gal. To obtain a complete oxidation of total -SH groups, the treatment with NEM was used as the positive control. After that, samples were spectrophotometrically read at 412 nm (Onda spectrophotometer, UV-21). Data were normalised to protein content and results reported as μM TNB/mg protein.

2.9 Analytical cytology

Band 3 expression levels were detected according to Straface and collaborators (Straface et al, 2011). The analysis was performed by an Olympus BX51 Microphot fluorescence microscope or by a FACScan flow cytometer (Becton Dickinson, Mountain View, CA, United States) equipped with a 488 nm argon laser on left untreated RBCs or after their exposure to D-Gal, with or without pre-incubation with peel or juice extract. The median values of fluorescence intensity histograms were used to provide a semi-quantitative analysis.

2.10 SO_4^{2-} uptake measurement

2.10.1 Control condition

To establish the anion exchange via band 3, SO_4^{2-} uptake was measured as formerly described (Romano and Passow, 1984; Galtieri et al, 2002; Romano et al, 2002; Morabito et al, 2013; Morabito et al, 2016; Morabito et al, 2018; Morabito et al, 2019a; Morabito et al, 2020a; Remigante et al, 2020; Perrone et al, 2023). Shortly, this procedure allows for the determination of the kinetic of transport and amount of SO_4^{2-} internalized by RBCs by turbidimetric analysis after precipitation of the cell content with BaCl_2 . In particular, each sample was addressed to the spectrophotometer (UV-21, Onda Spectrophotometer, Carpi, Modena, Italy, 425 nm wavelength) and the obtained absorbance was successively converted to $(\text{SO}_4^{2-}) \text{ L cells} \times 10^{-2}$ based on a calibrated standard curve previously established by precipitating known SO_4^{2-}

concentrations. Sulphate concentration was needed to quantify the rate constant of SO_4^{2-} uptake (min^{-1}). To this end the following equation was used: $C_t = C_{\infty} (1 - e^{-rt}) + C_0$ (C_t , C_{∞} , and C_0 indicate the intracellular SO_4^{2-} concentrations measured at time t , ∞ , and 0, respectively, e indicate the Neper number (2.7182818), r indicates the rate constant accounting for the process velocity, t is the time at which the SO_4^{2-} concentration was measured). The rate constant is useful to monitor the anion exchange process, as it specifically represents the inverse of the time needed to reach ~63% of total SO_4^{2-} intracellular concentration. The parameter $(\text{SO}_4^{2-}) \text{ L cells} \times 10^{-2}$ reported in figures corresponds to the micromolar concentration of SO_4^{2-} internalized by 5 mL RBCs at 3% haematocrit.

2.10.2 Experimental conditions

After 15 min pre-incubation with or without peel or juice extract, RBCs (3% haematocrit) were incubated with D-Gal and then centrifuged (Neya 16R, 4°C, $1,200 \times g$, 5 min) to discard the supernatant and to suspend RBCs in SO_4^{2-} medium. Similarly to what described for control conditions, the rate constant for SO_4^{2-} uptake was quantified.

2.11 Advanced glycation end products (AGEs): measurement of glycated haemoglobin (A1c) levels

The glycated haemoglobin content (%A1c) was measured as described by Sompong and collaborators (Sompong et al, 2015) with minor modifications. To this end, RBCs pre-exposed or not to peel or juice extract, were incubated with D-Gal and successively addressed to spectrophotometrically analysis (BioPhotometer Plus, Eppendorf, Manchester, United Kingdom, 610 nm wavelength). Finally, A1c levels (%) were determined from a standard curve obtained from known A1c doses.

2.12 Assessment of the endogenous antioxidant activity

2.12.1 Superoxide dismutase (SOD) activity assay

Superoxide dismutase (SOD) activity was evaluated by a specific assay kit (CS0009, Sigma-Aldrich, Milan, Italy), according to the manufacturer's instructions, with slight modifications. Red blood cells were treated with D-Gal, with or without pre-incubation with peel or juice extract. As the positive control, cells were incubated with H_2O_2 . Superoxide dismutase activity was determined by reading the absorbance at 450 nm wavelength (Fluostar Omega, BMG Labtech, Ortenberg, Germany) after subtracting the background.

2.12.2 Catalase (CAT) activity assay

Catalase activity was evaluated by the catalase assay kit (MAK381, Sigma-Aldrich, Milan, Italy), according to the manufacturer's instructions, with slight modifications. Red blood cells were treated with D-Gal with or without pre-incubation with peel or juice extract. As the positive control, cells were treated with H_2O_2 . Catalase activity was determined by reading the absorbance at

570 nm wavelength (Fluostar Omega, BMG Labtech, Ortenberg, Germany) after subtracting the background.

2.12.3 Glucose-6-phosphate dehydrogenase (G6PDH) activity assay

RBCs were left untreated or treated with D-Gal, with or without pre-incubation with peel or juice extract. Glucose-6-phosphate dehydrogenase (G6PDH) activity was assessed using a commercial G6PDH activity assay kit (Sigma-Aldrich, Milan, Italy), according to the manufacturer's instructions. The fluorescence intensity is proportional to the G6PDH activity in the samples. Determination of the reaction rate was performed by a plate spectrophotometer (Onda Spectrophotometer, UV-21) to monitor NADPH rate of production, such molecule absorbs light at 340 nm, over a 30 min time course. Then the obtained reaction rate, presented as %, was normalized to total protein content by spectrophotometrically analysis at 540 nm wavelength needed to detect haemoglobin absorbance.

2.12.4 Reduced glutathione (GSH) content measurement

GSH levels were quantified according to Teti and collaborators (Teti et al, 2005). Blood samples (20% hematocrit), which were left untreated or exposed to D-Gal with or without pre-incubation, were centrifuged (Neya 16R, 4°C, 1,200× g, 5 min) and resuspended in isotonic solution. After treatments, the content of GSH was measured by Cayman's GSH assay kit using an enzymatic recycling method with glutathione reductase. Sample absorbance was measured at 412 nm (Onda spectrophotometer, UV-21). The amount of GSSG was calculated by the following formula: $1/2 \text{ GSSG} = \text{GSH total-GSH reduced}$. Results are expressed as a GSH/GSSG ratio.

2.13 Analysis and statistics

All data are expressed as arithmetic means \pm standard error of the mean. GraphPad Prism (version 9.0, GraphPad Software, San Diego, CA, United States) and Excel (Version 2021, Microsoft, Redmond, WA, United States) software were used to perform statistical analysis and graphics. One-way analysis of variance (ANOVA) followed by Bonferroni's multiple comparison or Dunnet's post-test as appropriate, unless otherwise specified, was used to determine significant differences between mean values. Statistically significant differences between data sets were assumed at $p < 0.05$; (n) corresponds to the number of independent measurements.

3 Results

3.1 Determination of bioactive compounds

Table 1 reports qualitative and quantitative features of bioactive molecules deriving from bergamot juice and peel samples. In particular, thanks to the RP-HPLC/PDA/MS analyses, 26 bioactive molecules, of which three are phenolic acids, six limonoids and seventeen flavonoids, were identified and

quantified. As seen in Table 1, the two sample sources showed the same qualitative profile.

On the other hand, juice and peels differed from a quantitative point of view. Peel sample was richer in bioactive molecules ($16,132.3 \text{ mg kg}^{-1}$) than juice sample (498.1 mg kg^{-1}). For both sources, the most abundant class of bioactive molecules (88%–94% of the total content) was represented by flavonoids. Neohesperidin was the most abundant bioactive compound in these samples.

3.2 Antioxidant capacity estimation of peel and juice extract

A series of experiments were conducted with increasing concentrations (1–250 $\mu\text{g/mL}$) of peel or juice extracts and incubation times (15 min–3 h) to exclude a possible hemolytic and pro-oxidant effect and estimate the antioxidant capacity of the peel or juice extract. Incubation with 1–5 $\mu\text{g/mL}$ of peel or juice extract for 15 min at 37°C failed to induce hemolysis, increase TBARS levels, and reduce SH group content in RBCs (Supplementary Figures S1, S2). As expected, incubation of RBCs with 100 mM D-Gal for 24 h at 25°C led to a substantial increase in ROS and TBARS levels as well as a reduction in -SH group content compared to untreated RBCs (Supplementary Figure S3), which denotes induction of oxidative stress and is consistent our former findings (Remigante et al, 2022c). However, pre-incubation with 1 $\mu\text{g/mL}$ of peel or juice extract for 15 min at 37°C did not significantly reduced ROS levels in D-Gal treated RBCs, while leading to minor effects on TBARS levels and -SH group content (Supplementary Figures S3A–C). Increasing concentration and pre-incubation times revealed a clear antioxidant effect of the peel and juice extracts, as denoted by a significant reduction in ROS and TBARS levels, as well as increase in total SH group content compared to D-Gal treated RBCs (Supplementary Figures S3D–I). Based on these data, we selected the most effective antioxidant concentration as well as the shortest effective time of incubation and pre-treatment with 5 $\mu\text{g/mL}$ of peel or juice extract for 15 min has been chosen to carry out the following experiments.

3.2.1 Evaluation of intracellular ROS levels

Reactive oxygen species were detected in RBCs left untreated or, alternatively, exposed to 100 mM D-Gal for 24 h at 25°C with or without pre-exposure to 5 $\mu\text{g/mL}$ peel or juice extract for 15 min at 37°C. Figure 1A displays the intracellular ROS levels at 0 and 24 h after exposure to D-Gal. As seen, 100 mM D-Gal treated samples showed a significant increase of ROS levels compared to left untreated samples. In samples pre-exposed to 5 $\mu\text{g/mL}$ peel or juice extract, the incubation with 100 mM D-Gal failed to significantly increase ROS levels, which remained unchanged when compared to control values (Figure 1A). As expected, ROS levels of RBCs treated with 20 mM H_2O_2 for 30 min were significantly higher with respect to those of RBCs left untreated (control). In addition, peel or juice extract alone did not significantly alter the intracellular ROS levels (data not shown).

TABLE 1 Concentration (mg Kg⁻¹ ± standard deviation) of bioactive molecules in Femminello bergamot juice and peel. Each sample was analyzed in triplicate.

n°	Compound	Class ^a	Juice	Peel
1	Ferulic acid 4-O-glucoside ^b	PA	<LoD ^c	74.3 ± 0.27
2	Sinapoyl glucoside ^d	PA	<LoD ^c	208.8 ± 1.40
3	Apigenin 6,8-di-C-β-D-glucoside	F	4.2 ± 0.01	63.4 ± 0.80
4	Diosmetin-6,8-di-C-glucoside	F	3.9 ± 0.02	83.9 ± 0.78
5	Eriocitrin	F	16.0 ± 0.21	303.1 ± 3.38
6	Limonin glucoside	L	<LoD ^c	10.7 ± 0.52
7	Neocitrin	F	15.5 ± 0.04	947.3 ± 4.97
8	5-Sinapoyquinic acid ^d	PA	<LoD ^c	19.7 ± 0.94
9	Poncirin ^e	F	24.9 ± 0.07	1811.6 ± 5.32
10	Diosmetin 8-C-glucoside ^f	F	<LoD ^c	155.4 ± 0.05
11	Narirutin	F	61.2 ± 0.21	853.4 ± 6.60
12	Naringin	F	12.2 ± 0.05	383.6 ± 2.93
13	Apigenin 7-O-neohesperidoside ^e	F	2.0 ± 0.05	65.6 ± 1.40
14	Deacetyl nomilin glucoside ^g	L	<LoD ^c	793.4 ± 1.94
15	Neodiosmin ^e	F	14.1 ± 0.46	1,533.9 ± 1.33
16	Apigenin 7-O-neohesperidoside-4-glucoside ^e	F	<LoD ^c	52.5 ± 1.22
17	Neohesperidin	F	300.0 ± 3.72	6,410.6 ± 11.04
18	Nomilin glucoside	F	<LoD ^c	964.4 ± 0.58
19	Nomilinic acid glucoside	F	<LoD ^c	445.4 ± 0.16
20	Apigenin 7-O-diglucuronide ^e	F	<LoD ^c	13.5 ± 0.34
21	Melitidin	F	10.4 ± 0.07	154.5 ± 2.08
22	Brutieridin	F	33.3 ± 0.09	494.4 ± 1.11
23	Ichangin ^h	L	<LoD ^c	39.3 ± 0.55
24	Obacunoic acid ^h	L	<LoD ^c	33.7 ± 0.22
25	Limonin	L	<LoD ^c	73.9 ± 0.03
26	Nomilin	L	<LoD ^c	123.8 ± 0.03
	All		498.1	16,132.3

Bioactive molecules were quantitatively determined based on calibration curves obtained with the corresponding standard compound, i.e.

^aPA, phenolic acid; F, flavonoid; L, limonoid.

^bferulic acid.

^cLoD values ranged from 0.004 mg kg⁻¹–1.10 mg kg⁻¹.

^dsynapic acid.

^eapigenin 6,8-di-C-glucoside.

^fdiosmetin 6,8-di-C-glucoside.

^gnomilin glucoside.

^hlimonin. (Russo et al, 2015; Russo et al, 2016; Russo et al, 2021).

3.2.2 Measurement of thiobarbituric acid reactive substances (TBARS) levels

Thiobarbituric-acid-reactive substances (TBARS) levels measured in RBCs are reported in **Figure 1B**. As expected, TBARS levels after treatment with 20 mM H₂O₂ for 1 h were significantly higher than those detected in control (left untreated RBCs). Similarly, after 24 h treatment with 100 mM D-Gal, TBARS levels were significantly increased with respect to control. Importantly, in RBCs pre-treated with 5 µg/mL of peel or juice

extract and then exposed to 100 mM D-Gal, TBARS levels were significantly lower than those measured in 100 mM D-Gal-treated RBCs. Of note, peel or juice extract alone did not significantly alter TBARS levels (**Supplementary Figures S1D, S2D**).

3.2.3 Total sulfhydryl group content measurement

Figure 1C shows the total content of sulfhydryl groups in left untreated RBCs or treated with either the oxidizing molecule NEM as positive control (2 mM for 1 h) or D-Gal (100 mM for 24 h) with

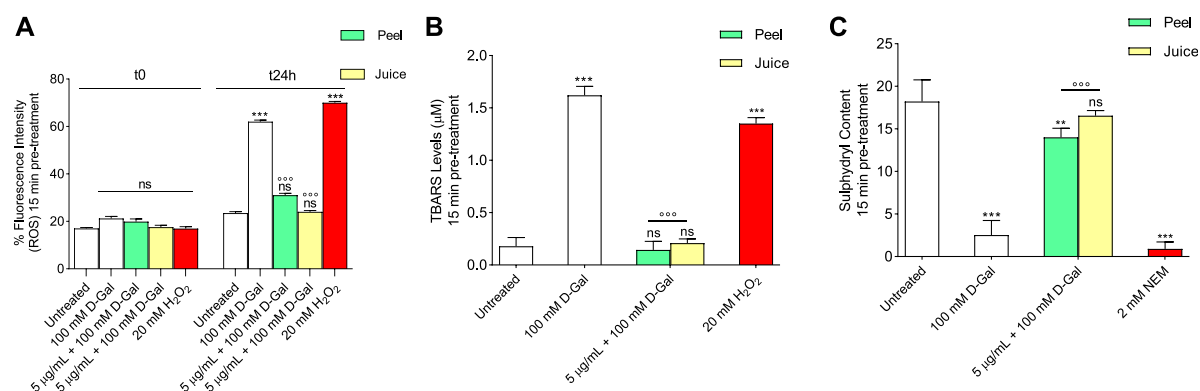


FIGURE 1

Antioxidant capacity estimation of peel and juice extract. human RBCs have been left untreated or exposed to 20 mM H₂O₂ or 2 mM NEM for 1 h or 100 mM D-Gal for 24 h at 25°C with or without pre-exposure to peel or juice extract for 15 min at 37°C. (A) estimation of ROS levels; (B) estimation of TBARS levels; (C) estimation of total sulphydryl group content (µM TNB/µg protein). ns, not statistically significant versus control (untreated); ***p* < 0.01 and ****p* < 0.001 versus control, °°° *p* < 0.001 versus 100 mM D-Gal, ANOVA followed by Bonferroni's multiple comparison post-test (*n* = 12).

or without pre-treatment with peel or juice extract (5 µg/mL). As expected, treatment with NEM led to a significant reduction in the content of the sulphydryl groups compared to untreated RBCs (control). Sulphydryl groups in - RBCs treated with 100 mM D-Gal were also significantly lower than control. The total content of the sulphydryl groups in 100 mM D-Gal-treated RBCs was significantly restored in case of pre-treatment with peel or juice extract (5 µg/mL) (Figure 1C). Additionally, peel or juice extract alone did not significantly alter the total content of the sulphydryl groups (Supplementary Figures S1G, S2G).

3.3 Determination of band 3 expression levels

The levels of band 3 expression were significantly decreased in human RBCs incubated with 100 mM D-Gal for 24 h with respect to control (Figure 2A). Pre-treatment with 5 µg/mL peel extract partially restored band 3 expression in RBCs treated with 100 mM D-Gal. Also, band 3 expression was totally restored in RBCs pre-exposed to 5 µg/mL juice extract. Moreover, Band 3 distribution was assessed by immunofluorescence technique. In particular, band 3 was mainly clustered (arrows) in leptocytes after 100 mM D-Gal exposure, with respect to untreated RBCs (Figure 2B). These changes were attenuated by pre-treatment with 5 µg/mL or juice extract. Of note, band 3 expression was altered neither by peel nor by juice extracts given alone (data not shown).

3.4 SO₄²⁻ uptake measurement

To evaluate the band 3 activity, the SO₄²⁻ uptake during the time was determined in RBCs left untreated (control) or treated with 100 mM D-Gal for 24 h at 25°C, with or without pre-exposure to 5 µg/mL peel or juice extract for 15 min at 37°C (Figure 3). In left untreated RBCs, SO₄²⁻ uptake is seen to progressively increase

reaching equilibrium in 16.68 min (rate constant of SO₄²⁻ uptake = 0.059 ± 0.001 min⁻¹, Table 2). The transport rate constant in RBCs treated with 100 mM D-Gal (0.092 ± 0.001 min⁻¹) was significantly increased with respect to control, thus denoting an accelerated transport kinetics, which was in agreement with former findings (Remigante et al, 2022c). Pre-exposure to 5 µg/mL peel or juice extract significantly reduced the rate constant of SO₄²⁻ uptake, which did not differ from control in the case of pre-treatment with peel extract. The SO₄²⁻ amount internalized by RBCs after 45 min of incubation in SO₄²⁻ medium was not significantly altered by D-Gal with or without peel or juice extract. In DIDS-treated cells, rate constant of SO₄²⁻ uptake and the SO₄²⁻ amount internalized were substantially reduced compared to control, consistent with a SO₄²⁻ transport via band 3 (Table 2). Red blood cells treated with 5 µg/mL peel or juice extract alone showed a time course of SO₄²⁻ uptake that was not significantly altered compared to control (Supplementary Figure S4).

3.5 Advanced glycation end products (AGEs): measurement of glycated haemoglobin (A1c) levels

Figure 4 displays the % A1c determined in left untreated RBCs or treated with 100 mM D-Gal for 24 h, with or without pre-exposure to 5 µg/mL peel or juice extract for 15 min at 37°C. The data obtained showed that %A1c levels measured after exposure to 100 mM D-Gal were significantly higher than those of RBCs left untreated (control). Instead, in RBCs pre-treated with 5 µg/mL peel or juice extract, a trend towards a decrease in %A1c levels was seen, which was statistically significant although %A1c levels remained elevated compared to control. In Figure 4, A1c levels measured in diabetes patients -used as the positive control- are also reported (Chandalia and Krishnaswamy, 2002). As expected, a significant increase in the A1c levels were measured in RBCs from diabetic patients. Lastly, %A1c content was not significantly altered by peel or juice extract when applied alone (data not shown).

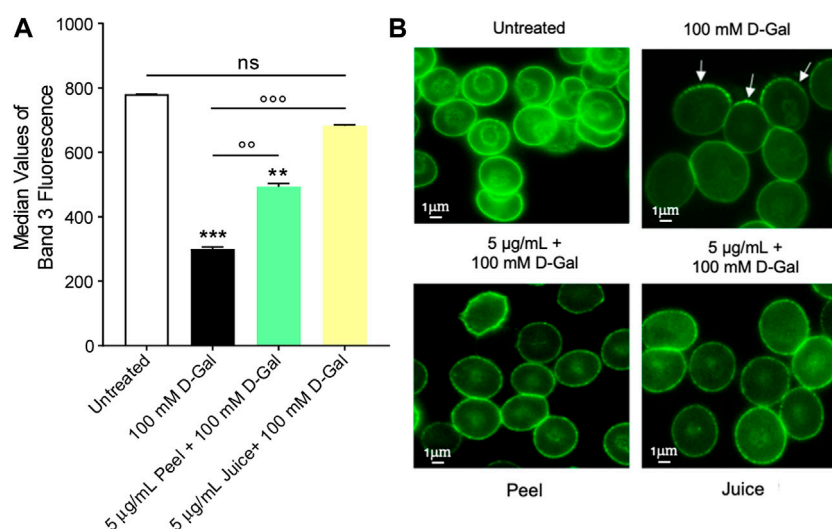


FIGURE 2

Flow cytometry immunofluorescence of band 3 expression. Red blood cells were left untreated or treated with 100 mM D-Gal for 24 h at 25°C, with or without pre-exposure to 5 µg/mL peel or juice extract for 15 min at 37°C. **(A)** Histograms report median values of fluorescence intensity. **(B)** Flow cytometry immunofluorescence representative micrographs showing band 3 distribution in left untreated RBCs, treated with 100 D-Gal, or alternatively, pre-incubated with 5 µg/mL peel or juice extract, and then exposed to 100 mM D-Gal. Samples were observed with a $\times 100$ objective. Note the significant morphological changes in 100 mM D-Gal (arrows). ns, not statistically significant versus control (untreated); ** $p < 0.01$ and *** $p < 0.001$ versus control, °° $p < 0.01$ and °°° $p < 0.001$ versus 100 mM D-Gal, ANOVA followed by Bonferroni's multiple comparison post-test ($n = 3$).

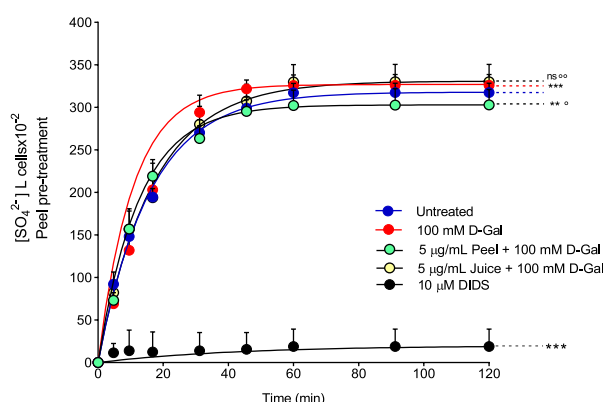


FIGURE 3

Time course of SO_4^{2-} uptake. Red blood cells were left untreated (control) or treated with 100 mM D-Gal (24 h, at 25°C) with or without pre-incubation with 5 µg/mL peel or juice extract (15 min at 37°C). Red blood cells were also exposed to a specific inhibitor of band 3 (10 µM DIDS). ns, not statistically significant versus untreated (control); ** $p < 0.01$ and *** $p < 0.001$ versus control; ° $p < 0.05$ and °° $p < 0.01$ versus 100 mM D-Gal, one-way ANOVA followed by Bonferroni's multiple comparison *post hoc* test ($n = 15$).

3.6 Assessment of the endogenous antioxidant activity

3.6.1 Activity of superoxide dismutase (SOD)

In **Figure 5A**, the SOD activity was evaluated in RBCs left untreated or treated with D-Gal (100 mM for 24 h at 25°C) with or without pre-exposure to 5 µg/mL peel or juice extract for 15 min at 37°C. In RBCs exposed to D-Gal, the SOD activity was found

significantly increased compared to the untreated cells. Conversely, pre-incubation with peel or juice extract resulted in a significant recovery of SOD activity with respect to D-Gal-treated cells. As expected, SOD activity in RBCs treated with 20 mM H_2O_2 for 30 min at 25°C as the positive control was significantly higher than that of control RBCs. Of note, peel and juice extracts did not significantly alter SOD activity when given alone (data not shown).

3.6.2 Activity of catalase (CAT)

Catalase was assayed in RBCs left untreated or treated with D-Gal (100 mM for 24 h at 25°C), with or without pre-treatment with 5 µg/mL peel or juice extract (15 min at 37°C). D-Gal treatment caused an increased CAT activity compared to control cells, which was consistent with an elevated oxidative stress (**Figure 5B**). Unlike, the pre-incubation with peel and/or juice extract (5 µg/mL for 15 min at 37°C) showed a CAT activity almost comparable to that of control (**Figure 5B**). Exposure to 20 mM H_2O_2 for 30 min (25°C) has been considered as the positive control. As expected, CAT activity in RBCs treated with H_2O_2 was significantly higher than those of control RBCs. Moreover, the extracts of peel and juice alone did not significantly alter CAT activity (data not shown).

3.6.3 Activity of glucose-6-phosphate dehydrogenase (G6PDH)

In **Figure 5C**, G6PDH activity was measured in RBC left untreated or treated with D-Gal (100 mM for 24 h at 25°C), with or without pretreatment with 5 µg/mL peel or juice extract (15 min at 37°C). G6PDH activity was severely stimulated by an increased oxidative stress in the D-Gal-treated cells compared to control RBCs. On the contrary, in cells pre-exposed to peel or juice extract, G6PDH activity was brought back to the control levels. As expected, G6PDH activity of RBCs treated with G6PDH positive

TABLE 2 Rate constant of SO_4^{2-} uptake, time needed to reach equilibrium, and SO_4^{2-} quantity internalized by either RBCs untreated or treated as indicated. Data are presented as means \pm S.E.M. from (n) separate experiments. ns not statistically significant *versus* untreated (control); *** $p < 0.001$ *versus* untreated; ° $p < 0.01$ *versus* 100 mM D-Gal, as attested by one-way ANOVA followed by Bonferroni's multiple comparison *post hoc* test.

Experimental conditions	Rate constant (min^{-1})	Time (min)	n	SO_4^{2-} amount trapped after 45 min of incubation in SO_4^{2-} medium (SO_4^{2-}) I cells $\times 10^{-2}$
Untreated	0.059 ± 0.001	16.68	15	299.08 ± 9.95
100 mM D-Gal	$0.092 \pm 0.001^{***}$	10.74	15	321.75 ± 10.57^{ns}
5 $\mu\text{g/mL}$ Peel Extract +100 mM D-Gal	$0.059 \pm 0.001^{ns,°}$	16.70	15	307.50 ± 19.75^{ns}
5 $\mu\text{g/mL}$ Juice Extract +100 mM D-Gal	$0.079 \pm 0.001^{ns,°}$	12.52	15	295.25 ± 10.37^{ns}
10 μM DIDS	$0.023 \pm 0.001^{***}$	42.17	15	$15.5 \pm 0.37^{***}$

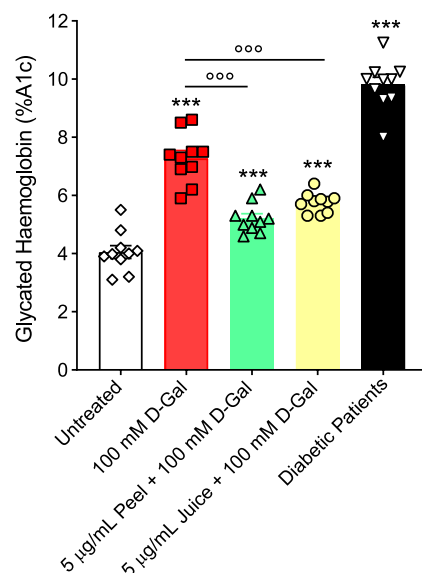


FIGURE 4

Glycated haemoglobin levels (%A1c). Red blood cells were left untreated or treated with 100 mM D-Gal (24 h, at 25°C) with or without pre-incubation with 5 $\mu\text{g/mL}$ peel or juice extract (15 min at 37°C). ns, not statistically significant *versus* untreated; *** $p < 0.001$ *versus* untreated; °°° $p < 0.01$ *versus* 100 mM D-Gal, one-way ANOVA followed by Bonferroni's multiple comparison *post hoc* test ($n = 10$).

control supplied by the manufacturer for 30 min at 25°C was significantly higher than that of RBCs left untreated. In addition, both peel and juice extracts did not significantly alter G6PDH activity (data not shown).

3.6.4 Estimation of GSH/GSSG ratio

Figure 6 displays the GSH/GSSG ratio measured in RBCs treated with 100 mM D-Gal for 24 h at 25°C with or without pre-treatment with 5 $\mu\text{g/mL}$ peel and juice extract for 15 min at 37°C. The GSH/GSSG ratio measured after treatment with D-Gal was significantly lower than that detected in left untreated RBCs. This effect could be associated with an increased GSSG levels and/or decreased GSH levels, both of which are indicative of an increased intracellular

oxidative stress. However, pre-incubation with peel and juice extract restored GSH levels. As expected, incubation with 2 mM NEM for 1 h (used as the positive control) led to a significant reduction in the GSH/GSSG content compared to left untreated RBCs. On the contrary, both peel and juice extract alone did not significantly alter the GSH/GSSG content (data not shown).

4 Discussion

Recently, an increasing body of evidence has supported the hypothesis that natural molecules -referred to as antioxidants-may have a protective role in retarding or reversing the course of age-related diseases (Tan et al, 2018; Singh et al, 2020; Lu et al, 2021; Remigante et al, 2022b; Cui et al, 2022). These compounds are able to compete with substrates which are sensitive to oxidation, thus inhibiting or delaying the reactions between reactive species and biological macromolecules (Pisoschi and Pop, 2015). Even though reactive species are involved in several biological processes, their over-production can lead to cell damage and consequently, development of chronic diseases (Costa et al, 2020; Luo et al, 2020; Bertelli et al, 2021; Remigante et al, 2021b; Forman and Zhang, 2021; Zuccolini et al, 2022). Thus, dietary intake of natural antioxidant compounds could work as a boost to the endogenous antioxidant machinery against reactive species and/or free radicals, thus playing an important role in the prevention of pathological states (Pingitore et al, 2015; Gantenbein and Kanaka-Gantenbein, 2021). Herein, the composition in bioactive molecules of bergamot peel and juice (Table 1) and their effects on oxidative-stress induced aging were described in a cell-based model represented by human RBCs subjected to prolonged (24 h) exposure to 100 mM D-Gal. This cell-based model, which was validated in our former studies (Remigante et al, 2022c; Remigante et al, 2022d; Spinelli et al, 2023), recapitulates the cellular and molecular mechanisms of natural aging, i.e., oxidative stress and haemoglobin glycation.

Though various investigations described the numerous activities of bioactive compounds of bergamot extracts, their effects on aging RBCs have not yet been fully analysed. Then, the first step of the present investigation was to test a broad range of concentrations (from 1 $\mu\text{g/mL}$ to 250 $\mu\text{g/mL}$) of bergamot peel and juice extract, as well as increasing incubation time intervals (15 min, 1 and 3 h), to

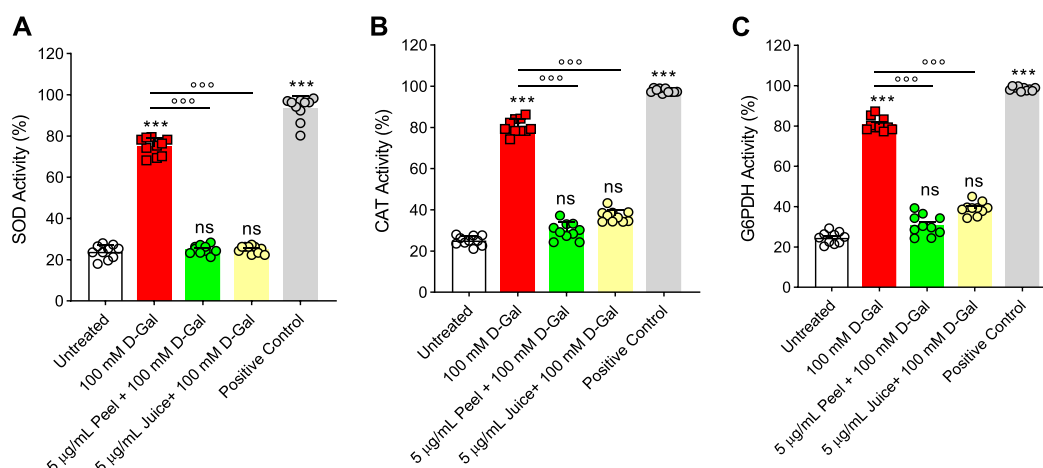


FIGURE 5

Effects of D-Gal (100 mM) exposure with or without pre-treatment with peel or juice extract for 15 min in RBCs. (A) SOD activity, (B) CAT activity, and (C) G6PDH activity. ns, not significant versus untreated (control); *** $p < 0.001$ versus untreated; °°° $p < 0.001$ versus 100 mM D-Gal, as determined by one-way ANOVA followed by Bonferroni's multiple comparison *post hoc* test ($n = 10$).

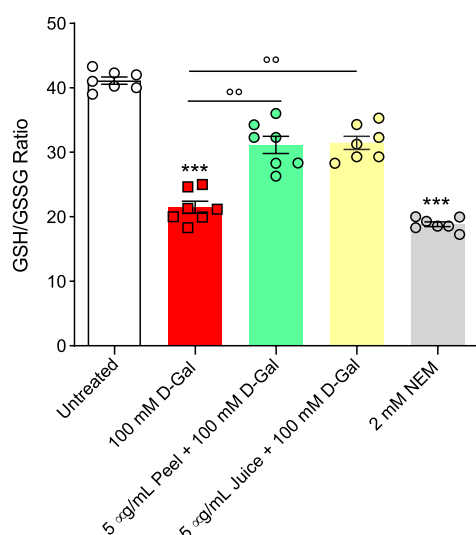


FIGURE 6

Assessment of the GSH/GSSG ratio measured in RBCs incubated for 24 h at 25°C with D-Gal with or without pre-treatment with peel or juice extract (15 min at 37°C). GSH, reduced glutathione; GSSG, oxidized glutathione. *** $p < 0.001$ versus left untreated RBCs; °° $p < 0.01$ versus D-Gal, one-way ANOVA followed by Bonferroni's multiple comparison *post hoc* test ($n = 7$).

exclude any damage in terms of haemolysis, lipid peroxidation and protein oxidation that could potentially be caused by direct exposure of RBCs to peel or juice extracts (Supplementary Figures S1, S2). Indeed, concentrations of peel or juice extract equal to or greater than 10 µg/mL could induce haemolysis and exhibited a pro-oxidant effect, especially following prolonged incubation times. This is not surprising, given that various antioxidants may act as pro-oxidants depending on their concentration (Osseni et al, 2000; Sahebkar, 2015; Giordano et al, 2020). These and our findings point to the

importance of carefully assessing concentration and incubation time when novel potential antioxidant compounds are tested in cell-based assays. Based on these considerations, we selected a 15 min pre-treatment with 5 µg/mL peel or juice extract in order to estimate the antioxidant capacity by measuring ROS and TBARS levels, and total content of sulfhydryl groups in RBCs incubated for 24 h with 100 mM D-Gal (Figure 1).

Red blood cells are susceptible to ROS-induced damage because of their high polyunsaturated fatty acid content and their abundance in iron (Fe^{2+})-rich haemoglobin. This latter acts as a catalyst in redox reactions and lipid peroxidation, resulting in TBARS production as the final product (Pandey and Rizvi, 2010). Also, RBCs often undergo membrane protein oxidation and/or carbonylation. Therefore, the oxidation of protein sulfhydryl groups (-SH) and/or the formation of carbonyl groups are indicators of oxidative injury to proteins in human RBCs. Since ROS generated during cellular metabolism cause the oxidation of biological macromolecules, the effect of peel and juice extract on the intracellular ROS levels has been evaluated as a first step of the investigation. A 15 min pre-exposure of RBCs to 5 µg/mL peel or juice extract could effectively prevent the ROS production caused by exposure to D-Gal (Figure 1A).

To better elucidate the process of oxidation of plasma membrane macromolecules, the estimation of both TBARS level and sulfhydryl group content of total proteins, which in RBCs mainly belong to band 3 protein (Rao and Reithmeier, 1979), have been investigated. Our findings show that pre-exposure (15 min) to 5 µg/mL peel or juice extract completely prevented TBARS levels increase in RBCs treated with 100 D-Gal (Figure 1B) and could at least partially (peel) or completely (juice) restore sulfhydryl group content (Figure 1C). These findings denote that peel or juice extract could effectively protect both the lipid and protein component of the RBC plasma membrane from oxidation. Data related to oxidative stress assessment are in line with what previously showed by other researchers and suggest that polyphenols and phytochemicals could play scavenger activity by directly neutralizing reactive

species and free radicals and avoid their detrimental impact on biological macromolecules (Zhao et al, 2006; Kelen and Tepe, 2007; Luo et al, 2021; Kruk et al, 2022).

One of the most interesting and still unknown implications of oxidative stress-related aging is its impact on plasma membrane transport systems. In this regard, several investigations demonstrated that the aging process may impact the anion ($\text{Cl}^-/\text{HCO}_3^-$) exchange, mediated by band 3, on the RBC plasma membrane. The structure of this protein consists of two rather different domains of a similar size (Arakawa et al, 2015). The C-terminal domain carries out $\text{Cl}^-/\text{HCO}_3^-$ exchange across the plasma membrane (Reithmeier et al, 2016; Remigante et al, 2022e). This function can be monitored by the rate constant for sulphate (SO_4^{2-}) uptake (Morabito et al, 2016; Morabito et al, 2017a; Morabito et al, 2017b), which is slower and more easily detectable than Cl^- or HCO_3^- uptake (Jennings, 1976; Romano and Passow, 1984; Morabito et al, 2019b; Crupi et al, 2019). SO_4^{2-} uptake measurement has been firmly confirmed as an efficient tool to investigate the impact of redox conditions on RBCs homeostasis (Morabito et al, 2016; Morabito et al, 2019b; Remigante et al, 2019). Hence, the SO_4^{2-} uptake through band 3 was measured in RBCs after treatment with D-Gal (100 mM) with or without pre-exposure (15 min) to 5 $\mu\text{g}/\text{mL}$ of bergamot peel or juice extract. In RBCs treated with D-Gal (100 mM), the rate constant for SO_4^{2-} uptake was accelerated compared to the control (Figure 3; Table 2). The evidence that oxidative stress provokes functional modifications of band 3 in human RBCs has been provided also in other cell-based models of oxidative stress. In particular, acute H_2O_2 -induced oxidative stress provoked a reduction in the rate constant for SO_4^{2-} uptake (Morabito et al, 2016; Morabito et al, 2017b), whereas in an oxidative stress model induced by high glucose concentrations an accelerated rate of anion exchanging has been seen (Morabito et al, 2020b). Thus, a possible a two-faced effect on the velocity of anion exchange could depend on specific cell component (lipids, proteins, as well as enzymes) affected by both the stressors and the related pathways. In this context, although no functional alteration was reported in RBCs treated exclusively with 5 $\mu\text{g}/\text{mL}$ peel or juice extract (Supplementary Figure S4), a 15 min pre-treatment of RBCs formerly exposed to D-Gal partially or totally recovered the rate constant for SO_4^{2-} uptake (Figure 3; Table 2). Based on data hitherto obtained, we can point out that both extracts show a similar protective effect on anionic exchange and could, therefore, act a key role in counteracting oxidative stress-induced functional changes in human RBCs.

The binding sites for cytoskeletal and cytoplasmic proteins, including haemoglobin, are located on the N-terminal cytoplasmic domain of band 3 (Anong et al, 2009; Wu et al, 2011). Haemoglobin glycation represents a case of non-enzymatic protein glycation associated with production of AGEs (Luevano-Contreras and Chapman-Novakofski, 2010). To better explore the molecular interaction between band 3 and haemoglobin, levels of both proteins were evaluated. The data obtained show that 100 mM D-Gal treatment caused both a loss and a redistribution of band 3, most probably due to the shedding of protein-containing vesicles (Kuo et al, 2017) (Figures 2A, B). Yet, despite this, band 3 expression levels were partially or totally restored in RBCs pre-treated with 5 $\mu\text{g}/\text{mL}$

peel or juice extract, respectively (Figures 2A, B). The shedding of membrane area is a critical point for cell fate, since a reduced surface-to-volume ratio is thought to correlate with the early phagocytosis of aged RBCs (Kuo et al, 2017). Consequently to membrane shedding, the cytoskeleton reduces to a 3- to 5-fold smaller area (Li and Lykotrafitis, 2015). The proteins affected are mainly band 3, ankyrin, spectrin, and occasionally protein 4.2 and the Rh protein. These proteins are all part of one of the complexes by which the cytoskeleton is anchored to the lipid bilayer (Gardel et al, 2008; Anong et al, 2009; Vallese et al, 2022). Presumably, damage of these proteins is responsible for the impaired cellular deformability associated with oxidative stress (Mohanty et al, 2014). A decrease in RBC deformability leads to impaired microcirculation and tissue oxygenation (Schwartz et al, 1991; Silva-Herdade et al, 2016). For example, Spinelli and co-authors have shown that both band 3 phosphorylation and rearrangements in cytoskeleton proteins can lead to cell deformation and structural alteration of human RBCs during the aging processes (Spinelli et al, 2023).

As mentioned above, haemoglobin is anchored to band 3 cytoplasmic domain. In this regard, our findings indicated that exposure of RBCs to 100 mM D-Gal for 24 h increased the content of A1c levels (Figure 4), contributing to both biochemical and structural changes, including clustering of band 3 regions. At a more advanced stage of aging, such clusters could represent a recognition site for antibodies directed against aged RBCs, thus triggering the early removal of RBCs from the blood circulation (Briglia et al, 2017). Importantly, in RBCs pre-treated with 5 $\mu\text{g}/\text{mL}$ peel or juice extract, a clear trend towards a decrease in %A1c production was seen (Figure 4). Collectively, these findings (Figures 2, 4) suggest that the active biomolecules of the bergamot juice or peel extract might efficiently prevent RBCs membrane shedding, formation of glycated haemoglobin, and RBCs structural instability, all of which are hallmarks of aging.

At last, we investigated the activity of endogenous antioxidant enzymes CAT and SOD (Figures 5A, B). These antioxidant enzymes own outstanding free radical scavenging capacities and play vital roles in human RBCs (Ulanczyk et al, 2020). The SOD and CAT activity in RBCs incubated with 100 mM D-Gal was much higher than in control cells, which could reflect the activation of the endogenous antioxidant defense system to suppress the formation of free radicals (Figure 1A). Nevertheless, the increase in SOD and CAT activity failed to compensate for the increase in free radicals (Figure 1A), as also demonstrated by the increase in lipid peroxidation levels as well as total protein oxidation (Figures 1B, C). Upregulation in CAT and SOD activity with concomitant substantial elevation of oxidative stress markers might reflect exhaustion of the endogenous antioxidant system. These biochemical changes may provoke injury to the membrane proteins and lipid structure. As a result, the membrane mechanical properties could be modified, resulting in deformability and fluidity reduction or altered permeability of the phospholipid bilayer, which, in turn, reduce the ability of the membrane to withstand osmotic changes (Spinelli et al, 2023). In this context, pre-exposure of RBCs to peel and juice extracts could significantly prevent the upregulation in both SOD and

CAT activity observed in D-Gal-treated cells (Figures 5A, B). These findings denote that the active biomolecules of the bergamot juice or peel extract might act synergistically with endogenous antioxidant system to counteract oxidative stress in RBCs and preserve cell integrity.

RBCs are unable to generate ATP using molecular oxygen because of lack of mitochondria. Glycolysis is the only source of ATP generation in mature RBCs. It has been found that under normal conditions about 90% of total imported glucose is used to generate ATP through glycolysis and the remaining 10% of glucose is addressed to PPP (Reisz et al, 2016). Glucose-6-phosphate dehydrogenase (G6PDH) is a crucial enzyme of this latter pathway, which produces reduced NADPH and represents the most important defense mechanism for RBCs in case of excessive oxidant generation, or of ineffective antioxidant defense (Maha, 2009). In these conditions, glycolysis and its key enzyme GAPDH are inhibited (Reisz et al, 2016). In addition to its importance in the RBC as a major metabolic determinant during oxidative stress, G6PDH activity is also employed as an indication of cell aging (Subasinghe and Spence, 2008). The G6PDH activity was severely stimulated - presumably by an increased oxidative stress - in D-Gal-treated cells compared to control RBC cells (Figure 5C), which was consistent with inhibition of glycolysis and activation of the PPP shunt. Vice versa, in cells pre-exposed to peel and/or juice extract the G6PDH activity was brought back to the control levels (Figure 5C). In addition, as already mentioned, the underlying mechanisms of aging can severely alter enzyme activities, including glutathione (Maher, 2005). Glutathione is an important endogenous non-enzymatic antioxidant that neutralizes ROS production (Ahmad and Mahmood, 2019). Its depletion makes cells more prone to oxidative damage. Then, the GSH/GSSG ratio was assayed. The obtained results confirmed that 100 mM D-Gal treatment reduced the GSH/GSSG ratio. However, the pre-incubation of RBCs with peel and juice extract partially restored the redox balance (Figure 6). In summary, our findings suggest that the active biomolecules of the bergamot juice or peel extract might prevent metabolic alterations in RBCs exposed to oxidative stress.

5 Conclusion

Here we characterize the precise composition in bioactive compounds of the bergamot (*Citrus bergamia*, Femminello cultivar) peel and juice extracts and we assess their protective effect in an oxidative stress-related model of cellular aging in RBCs. The data presented here indicate, for the first time, that polyphenol-rich extracts of peel and juice from bergamot fruit may act on oxidative stress-induced alterations of the lipid and protein cellular components, including the endogenous antioxidant system as well as proteins with ion transport activity and enzymatic metabolic activity, thus protecting the structural and functional integrity of human RBCs. This study identifies bergamot as an antioxidant functional food and further suggests that diet supplementation with bergamot or its derivatives might contribute to the prevention or attenuation of pathophysiological events linked to RBCs dysfunction during aging.

Data availability statement

The raw data supporting the conclusion of this article will be made available by the authors, without undue reservation.

Ethics statement

The studies involving human participants were reviewed and approved by the study was conducted in accordance with the Declaration of Helsinki and approved by the Institutional Review Board (or Ethics Committee) of University of Messina (prot.52-22). The patients/participants provided their written informed consent to participate in this study.

Author contributions

AR and RM conceived and designed the research; SS, MR, GC, ES, LG, DC, GF, and PD performed the experiments and analyzed the data; AR and RM interpreted the results of the experiments; SS and AR prepared the figures; AR drafted the manuscript; AM, AR, and SD edited and revised the manuscript. All authors contributed to the article and approved the submitted version.

Acknowledgments

The authors thank 1) Azienda Agricola Cilea Rosaria for kindly providing us bergamot fruits, 2) Shimadzu and Merck Life Science corporations for the continuous support, 3) Professor Caterina Faggio (from University of Messina) for helpful discussion, and iv) Dr. Federica De Gaetano (from University of Messina) for technical assistance.

Conflict of interest

The authors declare that the research was conducted in the absence of any commercial or financial relationships that could be construed as a potential conflict of interest.

Publisher's note

All claims expressed in this article are solely those of the authors and do not necessarily represent those of their affiliated organizations, or those of the publisher, the editors and the reviewers. Any product that may be evaluated in this article, or claim that may be made by its manufacturer, is not guaranteed or endorsed by the publisher.

Supplementary material

The Supplementary Material for this article can be found online at: <https://www.frontiersin.org/articles/10.3389/fphys.2023.1225552/full#supplementary-material>

References

- Abbas, Y. M., Toye, A. M., Rubinstein, J. L., and Reithmeier, R. A. F. (2018). Band 3 function and dysfunction in a structural context. *Curr. Opin. Hematol.* 25, 163–170. doi:10.1097/MOH.0000000000000418
- Ahmad, S., and Mahmood, R. (2019). Mercury chloride toxicity in human erythrocytes: Enhanced generation of ROS and RNS, hemoglobin oxidation, impaired antioxidant power, and inhibition of plasma membrane redox system. *Environ. Sci. Pollut. Res. Int.* 26, 5645–5657. doi:10.1007/s11356-018-04062-5
- Akki, R., Siracusa, R., Cordaro, M., Remigante, A., Morabito, R., Errami, M., et al. (2019). Adaptation to oxidative stress at cellular and tissue level. *Arch. Physiol. Biochem.* 128, 521–531. doi:10.1080/13813455.2019.1702059
- Akki, R., Siracusa, R., Morabito, R., Remigante, A., Campolo, M., Errami, M., et al. (2018). Neuronal-like differentiated SH-SY5Y cells adaptation to a mild and transient H₂O₂-induced oxidative stress. *Cell Biochem. Funct.* 36, 56–64. doi:10.1002/cbf.3317
- Aksenov, M. Y., and Markesbery, W. R. (2001). Changes in thiol content and expression of glutathione redox system genes in the hippocampus and cerebellum in Alzheimer's disease. *Neurosci. Lett.* 302, 141–145. doi:10.1016/S0304-3940(01)01636-6
- Anong, W. A., Franco, T., Chu, H., Weis, T. L., Devlin, E. E., Bodine, D. M., et al. (2009). Adducin forms a bridge between the erythrocyte membrane and its cytoskeleton and regulates membrane cohesion. *Blood* 114, 1904–1912. doi:10.1182/blood-2009-02-203216
- Arakawa, T., Kobayashi-Yurugi, T., Alguel, Y., Iwanari, H., Hatae, H., Iwata, M., et al. (2015). Crystal structure of the anion exchanger domain of human erythrocyte band 3. *Science* 350, 680–684. doi:10.1126/science.aaa4335
- Arrigo, F., Impellitteri, F., Piccione, G., and Faggio, C. (2023). Phthalates and their effects on human health: Focus on erythrocytes and the reproductive system. *Comp. Biochem. Physiol. C Toxicol. Pharmacol.* 270, 109645. doi:10.1016/j.cbpc.2023.109645
- Avitabile, E., Senes, N., D'Avino, C., Tsamesidis, I., Pinna, A., Medici, S., et al. (2020). The potential antimalarial efficacy of hemocompatible silver nanoparticles from *Artemisia* species against *P. falciparum* parasite. *PLoS One* 15, e0238532. doi:10.1371/journal.pone.0238532
- Azman, K. F., and Zakaria, R. (2019). D-Galactose-induced accelerated aging model: An overview. *Biogerontology* 20, 763–782. doi:10.1007/s10522-019-09837-y
- Bertelli, S., Remigante, A., Zuccolini, P., Barbieri, R., Ferrera, L., Picco, C., et al. (2021). Mechanisms of activation of LRRC8 volume regulated anion channels. *Cell Physiol. Biochem.* 55, 41–56. doi:10.33594/000000329
- Bo-Htay, C., Palee, S., Apaijai, N., Chattipakorn, S. C., and Chattipakorn, N. (2018). Effects of d-galactose-induced ageing on the heart and its potential interventions. *J. Cell Mol. Med.* 22, 1392–1410. doi:10.1111/jcmm.13472
- Briglia, M., Rossi, M. A., Faggio, C., and Eryptosis, C. (2017). Eryptosis: Ally or enemy. *Curr. Med. Chem.* 24, 937–942. doi:10.2174/092986732466616118142425
- Campanella, M. E., Chu, H., Wandersee, N. J., Peters, L. L., Mohandas, N., Gilligan, D. M., et al. (2008). Characterization of glycolytic enzyme interactions with murine erythrocyte membranes in wild-type and membrane protein knockout mice. *Blood* 112, 3900–3906. doi:10.1182/blood-2008-03-146159
- Carresi, C., Gliozzi, M., Giancotta, C., Scarcella, A., Scarano, F., Bosco, F., et al. (2016). Studies on the protective role of Bergamot polyphenols in doxorubicin-induced cardiotoxicity. *PharmaNutrition* 4, S19–S26. doi:10.1016/j.phanu.2015.11.005
- Castagnola, M., Messana, I., Sanna, M. T., and Giardina, B. (2010). Oxygen-linked modulation of erythrocyte metabolism: State of the art. *Blood Transfus.* 8, s53–s58. Suppl 3. doi:10.2450/2010.009S
- Chandalia, H., and Krishnaswamy, P. (2002). Glycated hemoglobin. *Curr. Sci.* 1522–1532.
- Costa, R., Remigante, A., Civello, D. A., Bernardinelli, E., Szabo, Z., Morabito, R., et al. (2020). O-GlcNAcylation suppresses the ion current ICLswell by preventing the binding of the protein ICLn to alpha-integrin. *Front. Cell Dev. Biol.* 8, 607080. doi:10.3389/fcell.2020.607080
- Crupi, R., Morabito, R., Remigante, A., Gugliandolo, E., Britti, D., Cuzzocrea, S., et al. (2019). Susceptibility of erythrocytes from different sources to xenobiotics-induced lysis. *Comp. Biochem. Physiol. C Toxicol. Pharmacol.* 221, 68–72. doi:10.1016/j.cbpc.2019.03.008
- Cui, Z., Zhao, X., Amevor, F. K., Du, X., Wang, Y., Li, D., et al. (2022). Therapeutic application of quercetin in aging-related diseases: SIRT1 as a potential mechanism. *Front. Immunol.* 13, 943321. doi:10.3389/fimmu.2022.943321
- De Franceschi, L., Scardoni, G., Tomelleri, C., Danek, A., Walker, R. H., Jung, H. H., et al. (2012). Computational identification of phospho-tyrosine sub-networks related to acanthocyte generation in neuroacanthocytosis. *PLoS One* 7, e31015. doi:10.1371/journal.pone.0031015
- Dorta, D. J., Pigoso, A. A., Mingatto, F. E., Rodrigues, T., Pestana, C. R., Uyemura, S. A., et al. (2008). Antioxidant activity of flavonoids in isolated mitochondria. *Phytother. Res.* 22, 1213–1218. doi:10.1002/ptr.2441
- Ellsworth, M. L. (2000). The red blood cell as an oxygen sensor: What is the evidence? *Acta Physiol. Scand.* 168, 551–559. doi:10.1046/j.1365-201x.2000.00708.x
- Emanuelli, M., Sartini, D., Molinelli, E., Campagna, R., Pozzi, V., Salvolini, E., et al. (2022). The double-edged sword of oxidative stress in skin damage and melanoma: From physiopathology to therapeutic approaches. *Antioxidants (Basel)* 11, 612. doi:10.3390/antiox11040612
- Ferrera, L., Barbieri, R., Picco, C., Zuccolini, P., Remigante, A., Bertelli, S., et al. (2021). TRPM2 oxidation activates two distinct potassium channels in melanoma cells through intracellular calcium increase. *Int. J. Mol. Sci.* 22, 8359. doi:10.3390/ijms22168359
- Ferlazzo, N., Visalli, G., Smeriglio, A., Cirmi, S., Lombardo, G. E., Campiglia, P., et al. (2015). Flavonoid fraction of orange and bergamot juices protect human lung epithelial cells from hydrogen peroxide-induced oxidative stress. *Evidence-Based Complementary Altern. Med.* 2015, 1–14. doi:10.1155/2015/957031
- Forman, H. J., and Zhang, H. (2021). Targeting oxidative stress in disease: Promise and limitations of antioxidant therapy. *Nat. Rev. Drug Discov.* 20, 689–709. doi:10.1038/s41573-021-00233-1
- Fujii, J., Homma, T., Kobayashi, S., Warang, P., Madkaikar, M., and Mukherjee, M. B. (2021). Erythrocytes as a preferential target of oxidative stress in blood. *Free Radic. Res.* 55, 781–799. doi:10.1080/10715762.2021.1873318
- Fukagawa, N. K. (1999). Aging: Is oxidative stress a marker or is it causal? *Proc. Soc. Exp. Biol. Med.* 222, 293–298. doi:10.1046/j.1525-1373.1999.d01-146.x
- Galtieri, A., Tellone, E., Romano, L., Misiti, F., Bellocchio, E., Ficarra, S., et al. (2002). Band-3 protein function in human erythrocytes: Effect of oxygenation-deoxygenation. *Biochim. Biophys. Acta* 1564, 214–218. doi:10.1016/S0005-2736(02)00454-6
- Gantenbein, K. V., and Kanaka-Gantenbein, C. (2021). Mediterranean diet as an antioxidant: The impact on metabolic health and overall wellbeing. *Nutrients* 13, 1951. doi:10.3390/nu13061951
- Gardel, M. L., Kasza, K. E., Brangwynne, C. P., Liu, J., and Weitz, D. A. (2008). Chapter 19: Mechanical response of cytoskeletal networks. *Methods Cell Biol.* 89, 487–519. doi:10.1016/S0091-679X(08)00619-5
- Giordano, M. E., Caricato, R., and Lionetto, M. G. (2020). Concentration dependence of the antioxidant and prooxidant activity of trolox in HeLa cells: Involvement in the induction of apoptotic volume decrease. *Antioxidants (Basel)* 9, 1058. doi:10.3390/antiox9111058
- Group, E. W. (1998). The fitness for purpose of analytical methods: A laboratory guide to method validation and related topics. Available at: <http://www.eurachem.org/guides/pdf/valid.pdf> 1998.
- Guo, J., Huang, X., Dou, L., Yan, M., Shen, T., Tang, W., et al. (2022). Aging and aging-related diseases: From molecular mechanisms to interventions and treatments. *Signal Transduct. Target Ther.* 7, 391. doi:10.1038/s41392-022-01251-0
- Harman, D. (1972). Free radical theory of aging: Dietary implications. *Am. J. Clin. Nutr.* 25, 839–843. doi:10.1093/ajcn/25.8.839
- Inal, M. E., Kanbak, G., and Sunal, E. (2001). Antioxidant enzyme activities and malondialdehyde levels related to aging. *Clin. Chim. Acta* 305, 75–80. doi:10.1016/S0009-8981(00)00422-8
- Issaian, A., Hay, A., Dzieciatkowska, M., Roberti, D., Perrotta, S., Darula, Z., et al. (2021). The interactome of the N-terminus of band 3 regulates red blood cell metabolism and storage quality. *Haematologica* 106, 2971–2985. doi:10.3324/haematol.2020.278252
- Jacob, R. A. (1995). The integrated antioxidant system. *Nutr. Res.* 15, 755–766. doi:10.1016/0271-5317(95)00041-g
- Jennings, M. L. (1976). Proton fluxes associated with erythrocyte membrane anion exchange. *J. Membr. Biol.* 28, 187–205. doi:10.1007/bf01869697
- Junqueira, V. B., Barros, S. B., Chan, S. S., Rodrigues, L., Giavarotti, L., Abud, R. L., et al. (2004). Aging and oxidative stress. *Mol. Asp. Med.* 25, 5–16. doi:10.1016/j.mam.2004.02.003
- Kelen, M., and Tepe, B. (2007). Screening of antioxidative properties and total phenolic compounds of various extracts of three different seed of grape varieties (*Vitis vinifera* L.) from Turkish flora. *Pak. J. Biol. Sci.* 10, 403–408. doi:10.3923/pjbs.2007.403.408
- Kouka, P., Priftis, A., Stagos, D., Angelis, A., Stathopoulos, P., Xinos, N., et al. (2017). Assessment of the antioxidant activity of an olive oil total polyphenolic fraction and hydroxytyrosol from a Greek Olea europaea variety in endothelial cells and myoblasts. *Int. J. Mol. Med.* 40, 703–712. doi:10.3892/ijmm.2017.3078
- Kruk, J., Aboul-Enein, B. H., Duchnik, E., and Marchlewicz, M. (2022). Antioxidative properties of phenolic compounds and their effect on oxidative stress induced by severe physical exercise. *J. Physiol. Sci.* 72, 19. doi:10.1186/s12576-022-00845-1
- Kuhn, V., Diederich, L., Keller IV, T. S., Kramer, C. M., Lückstädt, W., Panknin, C., et al. (2017). Red blood cell function and dysfunction: Redox regulation, nitric oxide metabolism, anemia. *Antioxidants redox Signal.* 26, 718–742. doi:10.1089/ars.2016.6954
- Kuo, W. P., Tigges, J. C., Toxavidis, V., and Ghiran, I. (2017). Red blood cells: A source of extracellular vesicles. *Methods Mol. Biol.* 1660, 15–22. doi:10.1007/978-1-4939-7253-1_2

- Lauro, F., Giacchetti, L. A., Ilari, S., Dagostino, C., Gliozzi, M., Morabito, C., et al. (2016). Inhibition of spinal oxidative stress by bergamot polyphenolic fraction attenuates the development of morphine induced tolerance and hyperalgesia in mice. *PLoS One* 11, e0156039. doi:10.1371/journal.pone.0156039
- Li, H., and Lykotrafitis, G. (2015). Vesiculation of healthy and defective red blood cells. *Phys. Rev. E Stat. Nonlin Soft Matter Phys.* 92, 012715. doi:10.1103/PhysRevE.92.012715
- Lu, W., Shi, Y., Wang, R., Su, D., Tang, M., Liu, Y., et al. (2021). Antioxidant activity and healthy benefits of natural pigments in fruits: A review. *Int. J. Mol. Sci.* 22, 4945. doi:10.3390/ijms22094945
- Luevano-Contreras, C., and Chapman-Novakofski, K. (2010). Dietary advanced glycation end products and aging. *Nutrients* 2, 1247–1265. doi:10.3390/nu2121247
- Lunceford, N., and Gugliucci, A. (2005). Ilex paraguariensis extracts inhibit AGE formation more efficiently than green tea. *Fitoterapia* 76, 419–427. doi:10.1016/j.fitote.2005.03.021
- Luo, J., Mills, K., le Cessie, S., Noordam, R., and van Heemst, D. (2020). Ageing, age-related diseases and oxidative stress: What to do next? *Ageing Res. Rev.* 57, 100982. doi:10.1016/j.arr.2019.100982
- Luo, J., Si, H., Jia, Z., and Liu, D. (2021). Dietary anti-aging polyphenols and potential mechanisms. *Antioxidants (Basel)* 10, 283. doi:10.3390/antiox10020283
- Maher, P. (2005). The effects of stress and aging on glutathione metabolism. *Ageing Res. Rev.* 4, 288–314. doi:10.1016/j.arr.2005.02.005
- Maha, A. A. (2009). Effect of glucose-6-phosphate dehydrogenase deficiency on some biophysical properties of human erythrocytes. *Hematology* 14, 38–45. doi:10.1179/102453309X385061
- Martinelli, L., Tomassoni, D., Moruzzi, M., Roy, P., Cifani, C., Amenta, F., et al. (2020). Cardiovascular changes related to metabolic syndrome: Evidence in obese Zucker rats. *Int. J. Mol. Sci.* 21, 2035. doi:10.3390/ijms21062035
- Mendanha, S. A., Anjos, J. L., Silva, A. H., and Alonso, A. (2012). Electron paramagnetic resonance study of lipid and protein membrane components of erythrocytes oxidized with hydrogen peroxide. *Braz. J. Med. Biol. Res.* 45, 473–481. doi:10.1590/s0100-879x2012007500050
- Mohanty, J. G., Nagababu, E., and Rifkind, J. M. (2014). Red blood cell oxidative stress impairs oxygen delivery and induces red blood cell aging. *Front. Physiol.* 5, 84. doi:10.3389/fphys.2014.00084
- Moldogazieva, N. T., Mokhosoev, I. M., Mel'nikova, T. I., Porozov, Y. B., and Terentiev, A. A. (2019). Oxidative stress and advanced lipoxidation and glycation end products (ALEs and AGEs) in aging and age-related diseases. *Oxid. Med. Cell Longev.* 2019, 3085756. doi:10.1155/2019/3085756
- Morabito, R., Marino, A., Romano, P., Rigano, C., and La Spada, G. (2013). Sulphate and chloride-dependent potassium transport in human erythrocytes are affected by crude venom from nematocysts of the jellyfish *pelagia noctiluca*. *Cell Physiol. Biochem.* 32, 86–95. doi:10.1159/000356630
- Morabito, R. R., Arcuri, B., Marino, A., Giammanco, M., La Spada, G. M., et al. (2018). Effect of cadmium on anion exchange capability through Band 3 protein in human erythrocytes. *J. Biol. Res.* 91, 1–7. doi:10.4081/jbr.2018.7203
- Morabito, R., Remigante, A., and Marino, A. (2019b). Melatonin protects band 3 protein in human erythrocytes against H₂O₂-induced oxidative stress. *Molecules* 24, 2741. doi:10.3390/molecules24152741
- Morabito, R., Remigante, A., Cavallaro, M., Taormina, A., La Spada, G., and Marino, A. (2017a). Anion exchange through band 3 protein in canine leishmaniasis at different stages of disease. *Pflügers Arch.* 469, 713–724. doi:10.1007/s00424-017-1974-2
- Morabito, R., Remigante, A., Cordaro, M., Trichilo, V., Loddo, S., Dossena, S., et al. (2020a). Impact of acute inflammation on Band 3 protein anion exchange capability in human erythrocytes. *Arch. Physiol. Biochem.* 128, 1242–1248. doi:10.1080/13813455.2020.1764048
- Morabito, R., Remigante, A., Di Pietro, M. L., Giannetto, A., La Spada, G., and Marino, A. (2017b). SO₄(=) uptake and catalase role in preconditioning after H₂O₂-induced oxidative stress in human erythrocytes. *Pflügers Arch.* 469, 235–250. doi:10.1007/s00424-016-1927-1
- Morabito, R., Remigante, A., and Marino, A. (2019a). Protective role of magnesium against oxidative stress on SO₄(=) uptake through band 3 protein in human erythrocytes. *Cell Physiol. Biochem.* 52, 1292–1308. doi:10.33594/0000000091
- Morabito, R., Remigante, A., Spinelli, S., Vitale, G., Trichilo, V., Loddo, S., et al. (2020b). High glucose concentrations affect band 3 protein in human erythrocytes. *Antioxidants (Basel)* 9, 365. doi:10.3390/antiox9050365
- Morabito, R., Romano, O., La Spada, G., and Marino, A. (2016). H₂O₂-Induced oxidative stress affects SO₄ transport in human erythrocytes. *PLoS One* 11, e0146485. doi:10.1371/journal.pone.0146485
- Musolino, V., Gliozzi, M., Nucera, S., Carresi, C., Maiuolo, J., Mollace, R., et al. (2019). The effect of bergamot polyphenolic fraction on lipid transfer protein system and vascular oxidative stress in a rat model of hyperlipemia. *Lipids Health Dis.* 18, 115–118. doi:10.1186/s12944-019-1061-0
- Ossen, R. A., Rat, P., Bogdan, A., Warnet, J. M., and Touitou, Y. (2000). Evidence of prooxidant and antioxidant action of melatonin on human liver cell line HepG2. *Life Sci.* 68, 387–399. doi:10.1016/s0024-3205(00)00955-3
- Pandey, K. B., and Rizvi, S. I. (2011). Biomarkers of oxidative stress in red blood cells. *Biomed. Pap. Med. Fac. Univ. Palacky. Olomouc Czech Repub.* 155, 131–136. doi:10.5507/bp.2011.027
- Pandey, K. B., and Rizvi, S. I. (2010). Markers of oxidative stress in erythrocytes and plasma during aging in humans. *Oxid. Med. Cell Longev.* 3, 2–12. doi:10.4161/oxim.3.1.10476
- Perrone, P., Spinelli, S., Mantegna, G., Notarale, R., Straface, E., Caruso, D., et al. (2023). Mercury chloride affects band 3 protein-mediated anionic transport in red blood cells: Role of oxidative stress and protective effect of olive oil polyphenols. *Cells* 12, 424. doi:10.3390/cells12030424
- Pingitore, A., Lima, G. P., Mastorci, F., Quinones, A., Iervasi, G., and Vassalle, C. (2015). Exercise and oxidative stress: Potential effects of antioxidant dietary strategies in sports. *Nutrition* 31, 916–922. doi:10.1016/j.nut.2015.02.005
- Pisoschi, A. M., and Pop, A. (2015). The role of antioxidants in the chemistry of oxidative stress: A review. *Eur. J. Med. Chem.* 97, 55–74. doi:10.1016/j.ejmech.2015.04.040
- Pretorius, E. (2018). Erythrocyte deformability and eryptosis during inflammation, and impaired blood rheology. *Clin. Hemorheol. Microcirc.* 69, 545–550. doi:10.3233/CH-189205
- Puchulu-Campanella, E., Chu, H., Anstee, D. J., Galan, J. A., Tao, W. A., and Low, P. S. (2013). Identification of the components of a glycolytic enzyme metabolon on the human red blood cell membrane. *J. Biol. Chem.* 288, 848–858. doi:10.1074/jbc.M112.428573
- Radi, E., Formichi, P., Battisti, C., and Federico, A. (2014). Apoptosis and oxidative stress in neurodegenerative diseases. *J. Alzheimers Dis.* 42, S125–S152. Suppl 3. doi:10.3233/JAD-132738
- Rao, A., and Reithmeier, R. (1979). Reactive sulfhydryl groups of the band 3 polypeptide from human erythrocyte membranes. Location in the primary structure. *J. Biol. Chem.* 254, 6144–6150. doi:10.1016/s0021-9258(18)50530-5
- Reisz, J. A., Wither, M. J., Dzieciatkowska, M., Nemkov, T., Issaian, A., Yoshida, T., et al. (2016). Oxidative modifications of glyceraldehyde 3-phosphate dehydrogenase regulate metabolic reprogramming of stored red blood cells. *Blood* 128, e32–e42. doi:10.1182/blood-2016-05-714816
- Reithmeier, R. A., Casey, J. R., Kalli, A. C., Sansom, M. S., Alguel, Y., and Iwata, S. (2016). Band 3, the human red cell chloride/bicarbonate anion exchanger (AE1, SLC4A1), in a structural context. *Biochim. Biophys. Acta* 1858, 1507–1532. doi:10.1016/j.bbame.2016.03.030
- Remigante, A., Morabito, R., and Marino, A. (2021a). Band 3 protein function and oxidative stress in erythrocytes. *J. Cell Physiol.* 236, 6225–6234. doi:10.1002/jcp.30322
- Remigante, A., and Morabito, R. (2022). Cellular and molecular mechanisms in oxidative stress-related diseases. *Int. J. Mol. Sci.* 23, 8017. doi:10.3390/ijms23148017
- Remigante, A., Morabito, R., and Marino, A. (2019). Natural antioxidants beneficial effects on anion exchange through band 3 protein in human erythrocytes. *Antioxidants (Basel)* 9, 25. doi:10.3390/antiox9010025
- Remigante, A., Morabito, R., Spinelli, S., Trichilo, V., Loddo, S., Sarikas, A., et al. (2020). D-Galactose decreases anion exchange capability through band 3 protein in human erythrocytes. *Antioxidants (Basel)* 9, 689. doi:10.3390/antiox9080689
- Remigante, A., Spinelli, S., Straface, E., Gambardella, L., Caruso, D., Falliti, G., et al. (2022a). Antioxidant activity of quercetin in a H₂O₂-induced oxidative stress model in red blood cells: Functional role of band 3 protein. *Int. J. Mol. Sci.* 23, 10991. doi:10.3390/ijms231910991
- Remigante, A., Spinelli, S., Basile, N., Caruso, D., Falliti, G., Dossena, S., et al. (2022d). Oxidation stress as a mechanism of aging in human erythrocytes: Protective effect of quercetin. *Int. J. Mol. Sci.* 23, 7781. doi:10.3390/ijms23147781
- Remigante, A., Spinelli, S., Pusch, M., Sarikas, A., Morabito, R., Marino, A., et al. (2022e). Role of SLC4 and SLC26 solute carriers during oxidative stress. *Acta Physiol. (Oxf)* 235, e13796. doi:10.1111/apha.13796
- Remigante, A., Spinelli, S., Straface, E., Gambardella, L., Caruso, D., Falliti, G., et al. (2022b). Acai (euterpe oleracea) extract protects human erythrocytes from age-related oxidative stress. *Cells* 11, 2391. doi:10.3390/cells11152391
- Remigante, A., Spinelli, S., Trichilo, V., Loddo, S., Sarikas, A., Pusch, M., et al. (2022c). d-Galactose induced early aging in human erythrocytes: Role of band 3 protein. *J. Cell Physiol.* 237, 1586–1596. doi:10.1002/jcp.30632
- Remigante, A., Zuccolini, P., Barbieri, R., Ferrera, L., Morabito, R., Gavazzo, P., et al. (2021b). NS-11021 modulates cancer-associated processes independently of BK channels in melanoma and pancreatic duct adenocarcinoma cell lines. *Cancers (Basel)* 13, 6144. doi:10.3390/cancers13236144
- Rizvi, S. I., and Maurya, P. K. (2007). Markers of oxidative stress in erythrocytes during aging in humans. *Ann. N. Y. Acad. Sci.* 1100, 373–382. doi:10.1196/annals.1395.041
- Romano, L., and Passow, H. (1984). Characterization of anion transport system in trout red blood cell. *Am. J. Physiol.* 246, C330–C338. doi:10.1152/ajpcell.1984.246.3.C330
- Romano, L., Scuteri, A., Gugliotta, T., Romano, P., de Luca, G., Sidoti, A., et al. (2002). Sulphate influx in the erythrocytes of normotensive, diabetic and hypertensive patients. *Cell Biol. Int.* 26, 421–426. doi:10.1006/cbir.2002.0874

- Russo, C., Maugeri, A., Lombardo, G. E., Musumeci, L., Barreca, D., Rapisarda, A., et al. (2021). The second life of citrus fruit waste: A valuable source of bioactive compounds. *Molecules* 26, 5991. doi:10.3390/molecules26195991
- Russo, M., Arigò, A., Calabrò, M. L., Farnetti, S., Mondello, L., and Dugo, P. (2016). Bergamot (citrus bergamia risso) as a source of nutraceuticals: Limonoids and flavonoids. *J. Funct. Foods* 20, 10–19. doi:10.1016/j.jff.2015.10.005
- Russo, M., Bonaccorsi, I., Torre, G., Sarò, M., Dugo, P., and Mondello, L. (2014). Underestimated sources of flavonoids, limonoids and dietary fibre: Availability in lemon's by-products. *J. Funct. foods* 9, 18–26. doi:10.1016/j.jff.2014.04.004
- Russo, M., Dugo, P., Marzocco, S., Inferrera, V., and Mondello, L. (2015). Multidimensional preparative liquid chromatography to isolate flavonoids from bergamot juice and evaluation of their anti-inflammatory potential. *J. Sep. Sci.* 38, 4196–4203. doi:10.1002/jssc.201500878
- Sahebkar, A. (2015). Dual effect of curcumin in preventing atherosclerosis: The potential role of pro-oxidant-antioxidant mechanisms. *Nat. Prod. Res.* 29, 491–492. doi:10.1080/14786419.2014.956212
- Schwartz, R. S., Madsen, J. W., Rybicki, A. C., and Nagel, R. L. (1991). Oxidation of spectrin and deformability defects in diabetic erythrocytes. *Diabetes* 40, 701–708. doi:10.2337/diab.40.6.701
- Shiga, T., Maeda, N., and Kon, K. (1990). Erythrocyte rheology. *Crit. Rev. Oncol. Hematol.* 10, 9–48. doi:10.1016/1040-8428(90)90020-s
- Silva-Herdade, A. S., Andolina, G., Faggio, C., Calado, A., and Saldanha, C. (2016). Erythrocyte deformability - a partner of the inflammatory response. *Microvasc. Res.* 107, 34–38. doi:10.1016/j.mvr.2016.04.011
- Singh, B., Singh, J. P., Kaur, A., and Singh, N. (2020). Phenolic composition, antioxidant potential and health benefits of citrus peel. *Food Res. Int.* 132, 109114. doi:10.1016/j.foodres.2020.109114
- Sompong, W., Cheng, H., and Adisakwattana, S. (2015). Protective effects of ferulic acid on high glucose-induced protein glycation, lipid peroxidation, and membrane ion pump activity in human erythrocytes. *PLoS One* 10, e0129495. doi:10.1371/journal.pone.0129495
- Spinelli, S., Straface, E., Gambardella, L., Caruso, D., Falliti, G., Remigante, A., et al. (2023). Aging injury impairs structural properties and cell signaling in human red blood cells; acai berry is a keystone. *Antioxidants (Basel)* 12, 848. doi:10.3390/antiox12040848
- Straface, E., Gambardella, L., Mattatelli, A., Canali, E., Boccalini, F., Agati, L., et al. (2011). The red blood cell as a gender-associated biomarker in metabolic syndrome: A pilot study. *Int. J. Cell Biol.* 2011, 1–7. doi:10.1155/2011/204157
- Subasinghe, W., and Spence, D. M. (2008). Simultaneous determination of cell aging and ATP release from erythrocytes and its implications in type 2 diabetes. *Anal. Chim. Acta* 618, 227–233. doi:10.1016/j.aca.2008.04.061
- Tan, B. L., Norhaizan, M. E., and Liew, W. P. (2018). Nutrients and oxidative stress: Friend or foe? *Oxid. Med. Cell Longev.* 2018, 1–24. doi:10.1155/2018/9719584
- Teti, D., Crupi, M., Busa, M., Valenti, A., Loddo, S., Mondello, M., et al. (2005). Chemical and pathological oxidative influences on band 3 protein anion-exchanger. *Cell Physiol. Biochem.* 16, 77–86. doi:10.1159/000087734
- Turk, Z., Mesić, R., and Benko, B. (1998). Comparison of advanced glycation endproducts on haemoglobin (Hb-AGE) and haemoglobin A1c for the assessment of diabetic control. *Clin. Chim. acta* 277, 159–170. doi:10.1016/s0009-8981(98)00128-4
- Ulanczyk, Z., Grabowicz, A., Cecerska-Heryc, E., Sleboda-Taront, D., Krytkowska, E., Mozolewska-Piotrowska, K., et al. (2020). Dietary and lifestyle factors modulate the activity of the endogenous antioxidant system in patients with age-related macular degeneration: Correlations with disease severity. *Antioxidants (Basel)* 9, 954. doi:10.3390/antiox9100954
- Vallese, F., Kim, K., Yen, L. Y., Johnston, J. D., Noble, A. J., Cali, T., et al. (2022). Architecture of the human erythrocyte ankyrin-1 complex. *Nat. Struct. Mol. Biol.* 29, 706–718. doi:10.1038/s41594-022-00792-w
- Willekens, F. L., Werre, J. M., Groenen-Dopp, Y. A., Roerdinkholder-Stoelwinder, B., de Pauw, B., and Bosman, G. J. (2008). Erythrocyte vesiculation: A self-protective mechanism? *Br. J. Haematol.* 141, 549–556. doi:10.1111/j.1365-2141.2008.07055.x
- Wu, F., Sachwell, T. J., and Toye, A. M. (2011). Anion exchanger 1 in red blood cells and kidney: Band 3's in a podThis paper is one of a selection of papers published in a Special Issue entitled CSBMCB 53rd Annual Meeting — membrane Proteins in Health and Disease, and has undergone the Journal's usual peer review process. *Biochem. Cell Biol.* 89, 106–114. doi:10.1139/o10-146
- Xu, D., Hu, M. J., Wang, Y. Q., and Cui, Y. L. (2019). Antioxidant activities of quercetin and its complexes for medicinal application. *Molecules* 24, 1123. doi:10.3390/molecules24061123
- Zabinski, Z., Dabrowski, Z., Moszczynski, P., and Rutowski, J. (2000). The activity of erythrocyte enzymes and basic indices of peripheral blood erythrocytes from workers chronically exposed to mercury vapours. *Toxicol. Ind. Health* 16, 58–64. doi:10.1191/074823300678827663
- Zhang, Y., Manning, L. R., Falcone, J., Platt, O., and Manning, J. M. (2003). Human erythrocyte membrane band 3 protein influences hemoglobin cooperativity. *J. Biol. Chem.* 278, 39565–39571. doi:10.1074/jbc.M303352200
- Zhao, H., Dong, J., Lu, J., Chen, J., Li, Y., Shan, L., et al. (2006). Effects of extraction solvent mixtures on antioxidant activity evaluation and their extraction capacity and selectivity for free phenolic compounds in barley (*Hordeum vulgare* L.). *J. Agric. Food Chem.* 54, 7277–7286. doi:10.1021/jf061087w
- Zuccolini, P., Ferrera, L., Remigante, A., Picco, C., Barbieri, R., Bertelli, S., et al. (2022). The VRAC blocker DCPIB directly gates the BK channels and increases intracellular Ca²⁺ in melanoma and pancreatic duct adenocarcinoma cell lines. *Br. J. Pharmacol.* 179, 3452–3469. doi:10.1111/bph.15810



OPEN ACCESS

EDITED BY

Grazia Tamma,
University of Bari Aldo Moro, Italy

REVIEWED BY

Alessia Remigante,
University of Messina, Italy
Piotr Bednarczyk,
Warsaw University of Life Sciences,
Poland

*CORRESPONDENCE

M. E. Giordano,
✉ elena.giordano@unisalento
M. G. Lionetto,
✉ giulia.lionetto@unisalento

RECEIVED 07 May 2023

ACCEPTED 21 June 2023

PUBLISHED 10 July 2023

CITATION

Giordano ME, Udayan G, Guascito MR,
De Bartolomeo AR, Carlino A, Conte M,
Contini D and Lionetto MG (2023),
Apoptotic volume decrease (AVD) in A₅₄₉
cells exposed to water-soluble fraction of
particulate matter (PM₁₀).
Front. Physiol. 14:1218687.
doi: 10.3389/fphys.2023.1218687

COPYRIGHT

© 2023 Giordano, Udayan, Guascito, De
Bartolomeo, Carlino, Conte, Contini and
Lionetto. This is an open-access article
distributed under the terms of the
[Creative Commons Attribution License
\(CC BY\)](#). The use, distribution or
reproduction in other forums is
permitted, provided the original author(s)
and the copyright owner(s) are credited
and that the original publication in this
journal is cited, in accordance with
accepted academic practice. No use,
distribution or reproduction is permitted
which does not comply with these terms.

Apoptotic volume decrease (AVD) in A₅₄₉ cells exposed to water-soluble fraction of particulate matter (PM₁₀)

M. E. Giordano^{1*}, G. Udayan¹, M. R. Guascito¹,
A. R. De Bartolomeo¹, A. Carlino¹, M. Conte², D. Contini³ and
M. G. Lionetto^{1,4*}

¹Department Biological and Environmental Sciences and Technologies (DiSTeBA), Salento University, Lecce, Italy, ²Institute of Atmospheric Sciences and Climate, ISAC-CNR, Rome, Italy, ³Institute of Atmospheric Sciences and Climate, ISAC-CNR, Lecce, Italy, ⁴NBFC, National Biodiversity Future Center, Palermo, Italy

Exposure to atmospheric particulate matter (PM) is recognized as a human health risk factor of great concern. The present work aimed to study the cellular mechanisms underlying cytotoxic effects of airborne particulate matter <10 µm in size (PM₁₀), sampled in an urban background site from January to May 2020, on A549 cells. In particular, the study addressed if PM₁₀ exposure can be a main factor in the induction of the Apoptotic Volume Decrease (AVD), which is one of the first events of apoptosis, and if the generation of intracellular oxidative stress can be involved in the PM₁₀ induction of apoptosis in A549 cells. The cytotoxicity of PM₁₀ samples was measured by MTT test on cells exposed for 24 h to the PM₁₀ aqueous extracts, cell volume changes were monitored by morphometric analysis of the cells, apoptosis appearance was detected by annexin V and the induction of intracellular oxidative stress was evaluated by the ROS sensitive CM-H₂DCFDA fluorescent probe. The results showed cytotoxic effects ascribable to apoptotic death in A549 cells exposed for 24 h to aqueous extracts of airborne winter PM₁₀ samples characterized by high PM₁₀ value and organic carbon content. The detected reduced cell viability in winter samples ranged from 55% to 100%. Normotonic cell volume reduction (ranging from about 60% to 30% cell volume decrease) after PM₁₀ exposure was already detectable after the first 30 min clearly indicating the ability of PM₁₀, mainly arising from biomass burning, to induce Apoptotic Volume Decrease (AVD) in A549 cells. AVD was prevented by the pre-treatment with 0.5 mM SITS indicating the activation of Cl⁻ efflux presumably through the activation of VRAC channels. The exposure of A549 cells to PM₁₀ aqueous extracts was able to induce intracellular oxidative stress detected by using the ROS-sensitive probe CM-H₂DCFDA. The PM₁₀-induced oxidative stress was statistically significantly correlated with cell viability inhibition and with apoptotic cell shrinkage. It was already evident after 15 min exposure representing one of the first cellular effects caused by PM exposure. This result suggests the role of oxidative stress in the PM₁₀ induction of AVD as one of the first steps in cytotoxicity.

KEYWORDS

AVD, particulate matter, apoptosis, A549 cells, oxidative stress, air pollution

1 Introduction

World Health Organization (WHO) recognizes that air pollution is a critical risk factor for noncommunicable diseases (NCDs) all over the world. It is estimated that air pollution is causing 24% of global adult deaths from heart disease, 25% from stroke, 43% from chronic obstructive pulmonary disease, and 29% from lung cancer. Air pollution is a major risk factor for pneumonia, being the leading cause of death in under 5 years aged children (WHO, 2019). In particular, the particulate component of air pollution poses a major risk to health. Atmospheric particulate matter (PM) is a complex mixture of components with great variability in their physical-chemical properties according to climatic, geographical, and source-specific variables (Amato et al., 2016; Chirizzi et al., 2017). The size of particles is directly linked to their potential for causing health problems. Small particles less than 10 μm in diameter pose the greatest problems because they can get deep into the respiratory tract, and some may even get into the bloodstream, in particular fine inhalable particles. According to WHO, exposure to PM has been identified as an important risk factor for mortality (WHO, 2019). The International Agency for Research on Cancer (IARC) has classified particulate matter from outdoor air pollution as carcinogenic to humans (IARC Group 1) (Loomis et al., 2013).

Although exposure to PM is recognized as a human health risk factor, the causal relationship between PM exposure and the genesis of pathological conditions and the underlying toxicological mechanisms are to date not completely understood. Several studies outlined the oxidative potential of PM (Chirizzi et al., 2017; Romano et al., 2020) and its capability to induce intracellular oxidative stress (Lionetto et al., 2019; Lionetto et al., 2021), as an important property for the outcome of adverse health effects (Cheng et al., 2016). In general, oxidative stress has been associated with cell homeostasis imbalance, mitochondrial damage, and apoptosis – (Yang et al., 2018; Zhang et al., 2018). Though numerous studies have focused on the cytotoxic effects of PM so far, several issues remain unclarified, particularly those related to the cell death pathways and underlying mechanisms (Chen et al., 2023).

Exposure to PM is known to be associated with apoptosis induction in several cell types including bone marrow (BM)-derived endothelial progenitor cells (Cui et al., 2015) through oxidative stress induction, human epithelial lung cells (L132) through activation of both TNF- α induced pathway and mitochondrial pathway (Dagher et al., 2006), mice bronchial epithelium cells via PI3K/AKT/mTOR signaling pathway (Han and Zhuang, 2021), GC-2spd cells by activation of RIPK1 apoptotic signaling pathway (Zhang et al., 2018), alveolar macrophages (Wei et al., 2021), and human cardiomyocytes (AC16 cell) (Yang et al., 2018) through mitochondria-mediated apoptosis pathway.

The apoptotic process is associated with a distinct set of molecular and cellular changes involving the cytoplasm, nucleus, and plasma membrane, which include cell shrinkage, formation of apoptotic bodies, chromatin condensation, and DNA degradation. The apoptotic cell shrinkage is a universal prominent feature of the cell under apoptosis and arises in two distinct phases: The first phase starts before cell fragmentation or formation of the apoptotic body, while the second phase is associated with cell fragmentation (Benson et al.,

1996). The early phase, called Apoptotic Volume Decrease (AVD) (Maeno et al., 2000), is represented by an isotonic cell shrinkage that occurs early after apoptotic stimuli, before the activation of caspases, the release of cytochrome c from mitochondria and DNA fragmentation, and seems to be a prerequisite for apoptosis (Okada et al., 2001). In a variety of cell types, prevention of AVD inhibits subsequent apoptotic biochemical and morphological events, and cells are rescued from death (Maeno et al., 2000; Antico et al., 2023).

The cell volume reduction during apoptosis occurs under normotonic conditions, independent of changes in the osmolarity of the extracellular environment, and is the consequence of an exit of Cl^- and K^+ from the cells (Bortner and Cidlowski, 2002; Lionetto et al., 2010; Poulsen et al., 2010; Antico et al., 2023) through the activation of specific channels. Concerning Cl^- exit from the cell, volume-regulated anion channels (VRAC) are considered the players in vertebrate cells (Maeno et al., 2000; D'Anglemont de Tassigny et al., 2004). These channels are formed by a hexameric assembly of members of the LRRC8 gene family and are ubiquitously expressed in all vertebrate cells being involved in cell volume homeostasis (Bertelli et al., 2021). The molecular mechanisms underlying their activation have not yet been completely understood. The proposed molecular mechanisms include low intracellular ionic strength, membrane unfolding, oxidation, phosphorylation, and G-protein coupling (Bertelli et al., 2021). It is known that VRAC activation is crucial to AVD happening and it occurs rapidly in a wide variety of cell types in both mitochondrion-mediated intrinsic, and death receptor-mediated extrinsic apoptosis (Maeno et al., 2000; Shimizu et al., 2004; Lee et al., 2007). Inhibition of these channels was found to prevent AVD and subsequent downstream apoptotic steps (Okada et al., 2006).

The present work aimed to study the mechanisms underlying cytotoxic effects of airborne particulate matter <10 μm in size (PM_{10}) in A549 cells, used as a model, focusing on one of the earliest events of apoptosis, the Apoptotic Volume Decrease (AVD). A549 cells are representative of the human lung Alveolar Type II pneumocytes (Foster et al., 1998), and are being widely used as a cellular model for respiratory research and assessment of adverse effects of PM on human health (Yi et al., 2012; Wang et al., 2013). Type II cells are the only cells involved in surfactant secretion in the respiratory epithelium and their damage can affect the lung defense system against environmental stressors (Akella and Deshpande, 2013).

For the study, we used aqueous extracts of eight airborne PM_{10} samples, collected in an urban site (Aradeo, province of Lecce, Puglia, Italy) potentially influenced by the local urban activities, biomass burning, agricultural activities, and the nearby industrial activities during the period from 14-01-2020 to 28-05-2020. Guascito et al. (2023) described that the larger contribution of PM_{10} in the study site originated from biomass burning.

The choice of water-soluble extracts of sampled PM_{10} arises from the experimental need to reproduce experimental conditions similar to the physiological exposure at the level of respiratory epithelium, where the surface of the respiratory epithelial cells is covered by a thin fluid layer, in which PM_{10} dissolves.

To the best of our knowledge, this is the first work focusing on airborne PM and AVD induction and aims to contribute to improving the knowledge about the mechanisms underlying the effects of PM at the airway epithelium.

2 Materials and methods

2.1 Sampling campaign, PM₁₀ gravimetric determination and chemical composition

The study was performed on eight PM₁₀ samples chosen from the whole sampling campaign carried out from December to May 2020 in a site located in southeastern Italy (Aradeo, Puglia, Italy) already described in a previous work (Guascito et al., 2023). The sampling site was located in the center of the municipality of Aradeo (Lecce, Italy) (40°07'47" N; 18°07'56" E) with a population of about 10,000 inhabitants. The site is an urban background site potentially influenced by the local urban activities, biomass burning and agricultural activities, and the nearby industrial activities including a cement production plant located at about 7.2 km in the northeast direction. Daily PM₁₀ samples (starting from midnight) were collected by an automatic low-volume sampler at 38.3 L·min⁻¹ (Zambelli Explorer Plus) on PTFE filters (Whatman, 47 mm in diameter) located on the roof of the City Hall at about 14 m above the ground.

As widely described by Guascito et al. (2023), the larger contribution of PM₁₀ in the study site originated from biomass burning.

Gravimetric determination of PM₁₀ samples was done according to UNI EN 12341 (2014) by weighing the filters (three replicates before and after sampling), following stabilization for 48 h in a conditioned room (for details see Guascito et al., 2023). The weighing was performed using a microbalance Sartorius Cubis (model MSx6.6S, ±1 µg resolution). Quality control of gravimetric results was done using field blanks and periodic (once per week) control of the inlet flow rate of the samplers with external flow meters. Organic (OC) and elemental carbon (EC) were determined by a Sunset laboratory carbon analyser (Sunset Laboratory Inc., Tigard OR, United States) using thermo-optical transmittance (TOT) with the EUSAAR2 protocol (Cesari et al., 2018). The analyser was calibrated using a sucrose solution as an external standard (2.198 g/L in water, CPChem Ltd., Bulgaria). Linear calibration had a slope of 0.97 (±0.01), a negligible intercept, (0.1 ± 0.2), and a determination coefficient $R^2 = 0.99$.

The chemical composition of PM₁₀ sampled was determined via ICP-MS (PerkinElmer NexION 1000 and NexION 300x) for the main metals and ion chromatography (ICS1100, Thermo Scientific) for the water-soluble ions according to Guascito et al. (2023).

2.2 Cell viability measurement by MTT assay

Cell viability was evaluated by MTT test on A549 cells exposed for 24 h to the water-soluble fractions of PM₁₀ extracted from the whole PTFE filter for each of the eight samples according to Lionetto et al. (2021). Extraction was carried out in 10 mL ultrapure water (Milli-Q) using an ultrasonic bath. Four cycles of sonication for a total of 80 min were performed and each cycle was followed by 1 min vortex agitation (according to Lionetto et al., 2021). Then, the extracts were filtered using PTFE (polytetrafluoroethylene) 0.45 µm pore syringe filters. The assay measures the metabolic activity of the cells as an indicator of cell viability, assessing the mitochondrial NAD(P)H-dependent oxidoreductase enzyme activity which

reduces a yellow tetrazolium salt (3-(4,5-dimethylthiazol-2-yl)-2,5-diphenyltetrazolium bromide (MTT) 3-(4, 5-dimethylthiazol-2-yl)-2, 5-diphenyltetrazolium bromide to formazan that accumulates as crystals within healthy cells. These are dissolved with DMSO and the absorbance of the resulting colored solution is spectrophotometrically analyzed at 570 nm (Cytation 5, BioTek Instruments, Winooski, VT, United States). Six replicates per sample were carried out. The relative viability of the cells was calculated as follows:

$$\text{Relative viability of cells (\%)} = \left[\frac{(\text{treated cells OD})}{(\text{untreated cells OD})} \right] \times 100$$

2.3 Morphological analysis of the cells and cell volume change determination

A549 cells adherent to the bottom of a 96 multiwell were exposed to the PM₁₀ aqueous extracts for 24 h and visualized by Cytation 5 cell imaging multimode reader (Agilent, Santa Clara, CA, United States) (observation objective: ×40). Cell volume changes were monitored by morphometric analysis of the cells and were expressed as a percentage of the cell area of 2-D cell images after PM₁₀ exposure vs. the cell area of control cells (cells not exposed to the PM₁₀ extracts) according to Giordano et al. (2020) and Lionetto et al. (2010). At least a minimum of 100 cells/field and 5 fields per well were analyzed.

2.4 Detection of apoptosis by annexin V

One of the earliest events of apoptosis is the translocation of the membrane phospholipid from the inner to the outer leaflet of the plasma membrane. Once exposed to the extracellular environment, binding sites on phosphatidylserine become available for Annexin V, a 36 kDa Ca²⁺-dependent phospholipid-binding protein that has a high affinity for the anionic phospholipid phosphatidylserine (Leventis and Grinstein, 2010).

A549 cells exposed to PM₁₀ aqueous extracts for 24 h were incubated with 1 µg/mL annexin V (Alexa Fluor® 488) for 15 min and viewed by Cytation 5 cell imaging multimode reader according to Gelles et al. (2019).

2.5 Intracellular oxidative stress detection assay and confocal visualization

The intracellular oxidative stress was assessed using the ROS-sensitive cell-permeant probe 5-(6)-Chloromethyl-2',7'-dichlorodihydrofluorescein diacetate, acetyl ester (CMH₂DCFDA) (Ex/Em: 492–495/517–527 nm) (Thermo Fisher Scientific, Waltham, MA, United States) according to Lionetto et al. (2021); Giordano et al. (2020). The probe, once in the intracellular compartment, loses its acetate group, which is cleaved by cellular esterases, and undergoes hydrolysis. The resulting DCFH carboxylate anion is trapped inside the cell and once oxidized by intracellular ROS produces the fluorescent product DCF

TABLE 1 Values of PM₁₀ concentrations and carbon content (organic carbon OC and elemental carbon EC) of the eight samples used for the study.

Sampling data	PM ₁₀ (µg/m ³)	OC (µg/m ³)	EC (µg/m ³)
14/1/2020	47.9 ± 2.4	29.6 ± 1.5	3.2 ± 0.2
18/1/2020	50.8 ± 2.5	21.8 ± 1.1	2.0 ± 0.1
21/1/2020	37.9 ± 1.9	17.8 ± 0.9	1.9 ± 0.1
23/1/2020	35.4 ± 1.8	4.6 ± 0.3	0.4 ± 0.1
11/2/2020	27.1 ± 1.3	4.7 ± 0.3	0.5 ± 0.1
5/3/2020	27.9 ± 1.4	11.6 ± 0.6	1.3 ± 0.1
9/5/2020	14.1 ± 0.7	3.3 ± 0.2	0.4 ± 0.1
28/5/2020	12.9 ± 0.6	2.6 ± 0.2	0.3 ± 0.1

(Ameziane-El-Hassani and Dupuy, 2013). Fluorescence intensity was measured using the Cytation 5 cell imaging multimode reader. The results were expressed as a fold increase in the fluorescence intensity compared to the negative control (untreated cells). More details of the methodology are reported in Giordano et al. (2020).

Cells charged with CM-H₂DCFDA were also visualized by confocal microscopy. Briefly, A549 cells were plated at a density of 1×10^5 cells per mL into a chambered coverslip (IBIDI, Gräfelfing, Germany), incubated for 24 h for the adhesion of the cells to the bottom of the plate, then exposed for 24 h with the aqueous PM₁₀ extracts and finally charged with CM-H₂DCFDA as reported above. The cells were viewed using a $\times 100$ NA plan apochromatic objective mounted on a NIKON TE300 inverted microscope coupled to a NIKON C1 confocal laser scanning unit (Nikon, Tokyo, Japan). The Argon 488-nm laser line was used. Unlabeled cells did not exhibit any detectable fluorescence under the conditions used. Images were acquired and analyzed by EZ-C1 NIKON software.

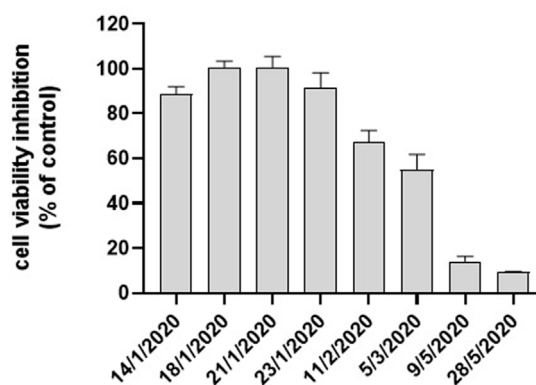
2.6 Statistics

Data are given as the mean \pm S.E.M. The statistical significance was analyzed by one-way ANOVA, and Dunnett's multiple comparison test.

3 Results

3.1 Effect of PM₁₀ exposure on cell viability

The average values of PM₁₀ concentration and carbon content of the 8 samples used in the present study are reported in Table 1. The sample set included six winter samples characterized by higher PM₁₀ concentrations and two spring samples characterized by lower PM₁₀ values in agreement with the typical seasonal PM₁₀ concentration of the area (Cesari et al., 2018). On average the same trend was also observed for carbon content. Moreover, it must be considered that the sampling campaign was carried out in 2020, when Italy was subjected to a national lockdown and limitation to the movement of people because of the COVID-19 pandemic. The first six samples were collected before the lockdown period, while the other two May

**FIGURE 1**

Cytotoxicity of PM₁₀ expressed as % cell viability inhibition assessed by the MTT test on A549 cells exposed for 24 h to PM₁₀ aqueous extracts.

samples were collected just after the lockdown when the restart of activities was slow. Some previous evidence indicated that the lockdown has slightly reduced the PM₁₀ concentration in the air at least in this region of Italy (Dinoi et al., 2021). The mean chemical composition of the PM₁₀ in the study site is reported in Supplementary Table S1.

Cell viability after 24 h exposure to water-soluble extract of the airborne PM₁₀ samples was assessed by MTT assay on A549 cells. In Figure 1 the MTT results obtained on the eight PM₁₀ samples chosen for the objective of the present study are reported. Inhibition of the mitochondrial NAD(P)H-dependent cellular oxidoreductase enzymatic activity after exposure of A549 cells for 24 h to the aqueous extracts of PM₁₀ compared to control cells was observed in the sample data set in agreement with a previous study on the whole sampling campaign (Guascito et al., 2023). The entity of the inhibition varied from about 100% (detected in January samples) to values of about 9% recorded in May samples. The dose-dependence response of the assay for each aqueous extract was preliminarily checked by exposure of A549 cells to increasing dilutions of the same extract, as reported in our previous studies (Lionetto et al., 2019; Lionetto et al., 2021). On average, winter samples showed a higher cytotoxic potential as indicated by the high percentage reduction of cell viability, particularly in January and February, compared to the two May samples according to Guascito et al. (2023) in parallel to PM₁₀ concentration.

3.2 Cell volume alteration and apoptosis detection in A549 cells exposed to PM₁₀

To deepen the analysis of the mechanisms involved in PM₁₀-induced cytotoxicity on A549 cells, cell morphology was analyzed on PM₁₀ exposed cells in parallel to MTT assay using Cytation 5 cell imaging multimode reader on the same samples.

After 24 h exposure to PM₁₀ aqueous extracts, A549 cells showed typical cell shrinkage detected as a percentage decrease of the cell area of 2-D images compared to not exposed (control) cells (Figure 2A). Cell shrinkage levels were in agreement with the

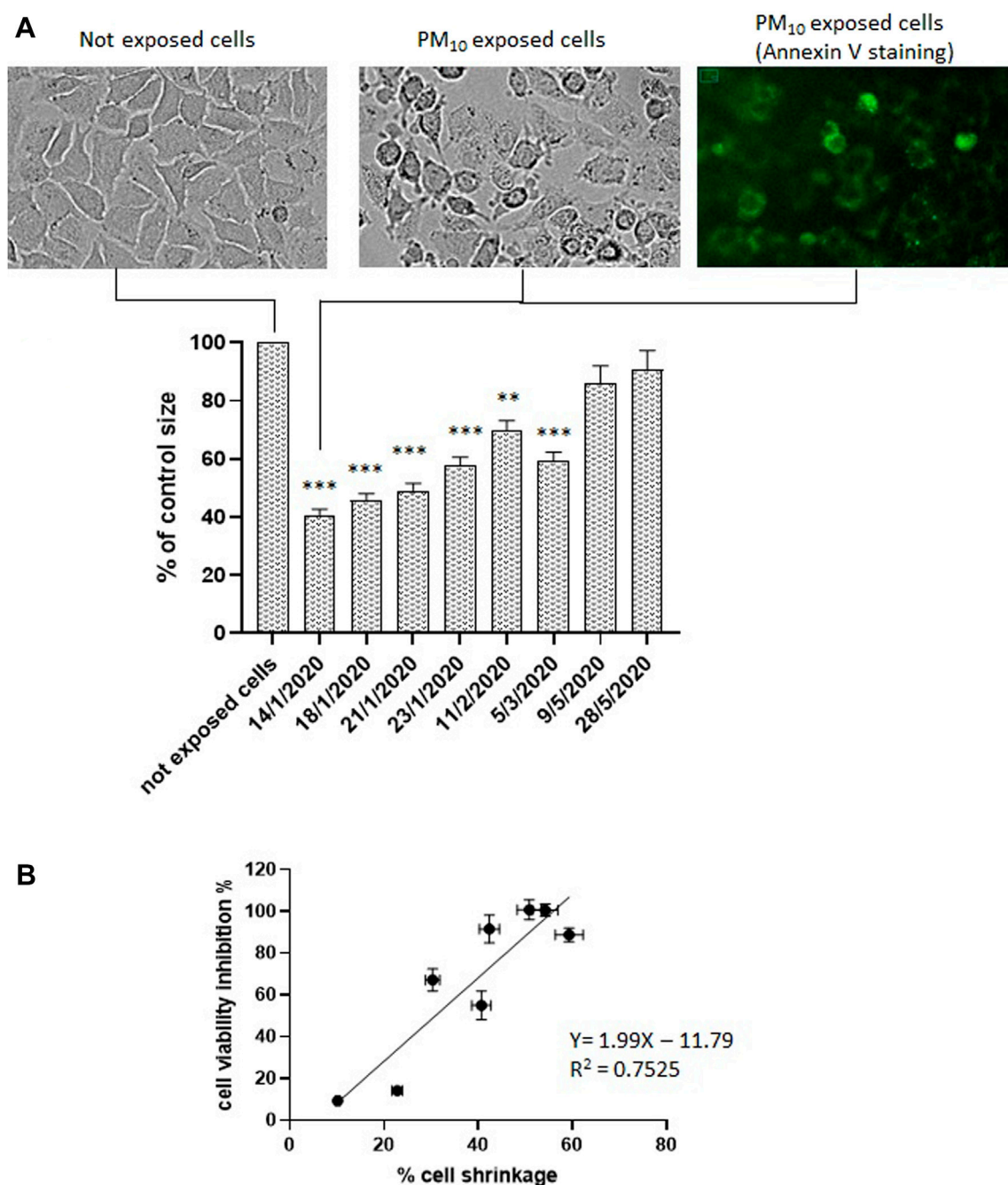
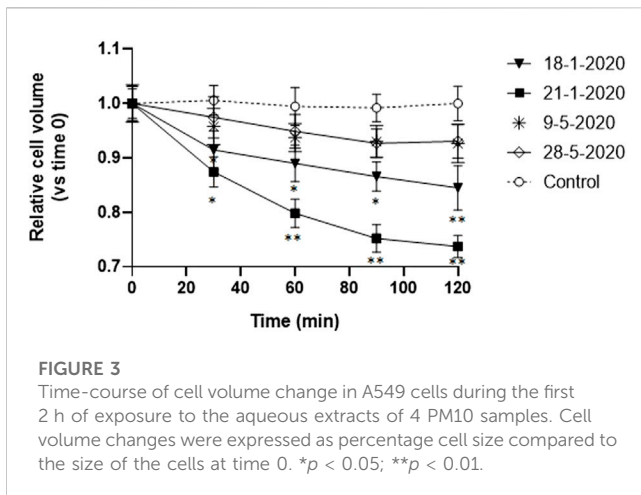


FIGURE 2

(A, B) Cell volume change in A549 cells exposed to the aqueous extracts of the 8 PM₁₀ samples expressed as percentage cell size compared to not exposed cells (control). Representative brightfield image of not exposed cells; representative images of PM₁₀ exposed cells (sample of 14-1-2020). brightfield and annexin V stained. (B) Correlation analysis between cell viability inhibition and % of cell shrinkage.

NAD(P)H-dependent cellular oxidoreductase enzymatic activity reduction, as indicated by the correlation analysis (Figure 2B). Particularly high cell volume reduction, above 50%, was observed in the samples which showed the highest inhibition of mitochondrial NAD(P)H-dependent oxidoreductase activity. Cell shrinkage was also accompanied by other typical morphological signs of apoptosis such as cell rounding, surface roughness, blebs formation, and annexin V positivity, visualized by the detectable green contour

of the cell plasma membrane of cells treated with 1 µg/mL annexin V (Alexa Fluor® 488) following exposure to PM₁₀ extract as shown in Figure 2A. This figure reports representative images obtained from the sample of 14-1-2020. Similar apoptotic positive evidence (cell rounding, surface roughness, blebs formation, and annexin V positivity) were obtained also for the other 5 winter samples but was not detectable for the two May samples (not shown).



3.3 Apoptotic volume decrease in A549 cells exposed to PM₁₀ aqueous extracts

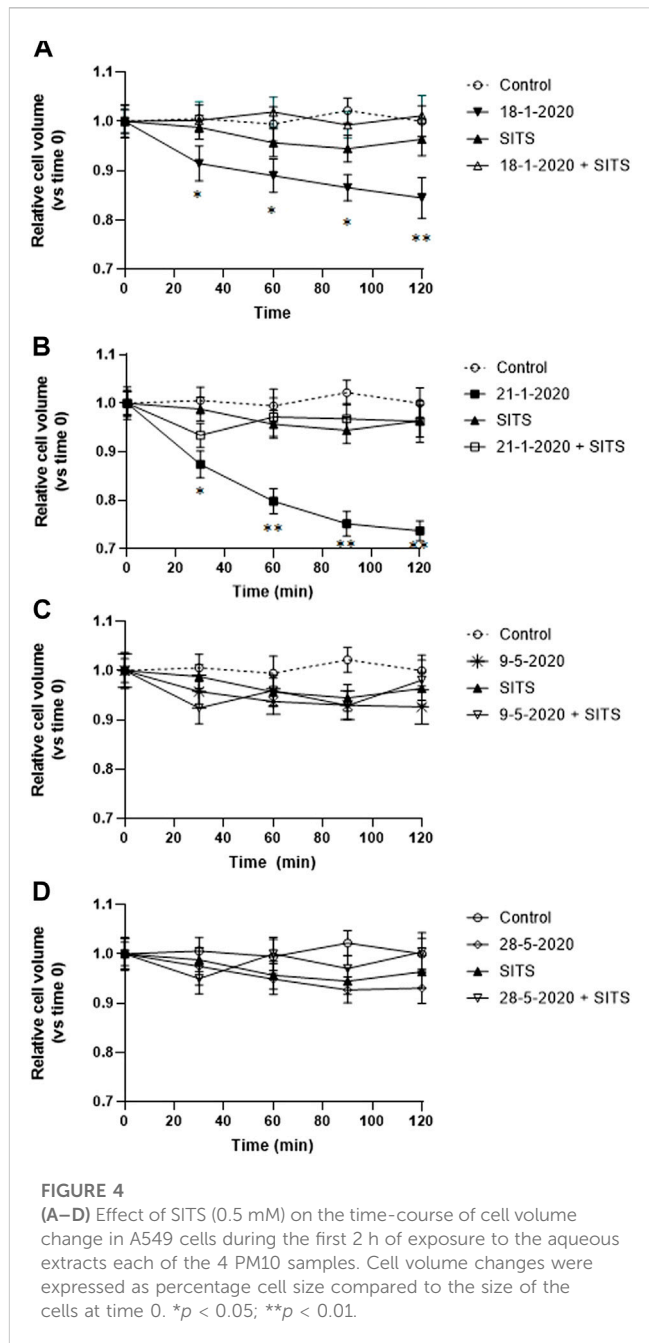
After detecting reduced vitality and apoptosis appearance in A549 cells following 24 h exposure to PM₁₀ aqueous extracts, we tested the hypothesis of the possible involvement of PM₁₀ exposure in the induction of the Apoptotic Volume Decrease (AVD), which is one of the first events of apoptosis, occurring early in the first 1–2 h (Chang et al., 2000; Maeno et al., 2000). Therefore, the time course of the volume changes was monitored in A549 cells during the first 2 h of exposure to PM₁₀ aqueous extracts by time-lapse imaging of the cells every 30 min. The AVD analysis was focused on 4 representative samples, two January samples, characterized by the highest values of vitality reduction and a marked cell shrinkage after 24 h exposure, and the two samples of May, characterized by a reduction of the NAD(P)H-dependent cellular oxidoreductase activity below 15% and without apparent apoptotic signs. For each of the four filter extracts, three independent experiments were performed.

The cells exposed to the aqueous extracts of January 18 and 21 showed a significant reduction of cell volume compared to control cells already after 30 min exposure and the decrease continued in the 2 h observation reaching 16% and 27% respectively (Figure 3). If these results are compared with the overall apoptotic cell volume reduction observed after 24 h in the same extracts, the AVD response observed in the first 2 h corresponds to one-third and one-half respectively of the overall cell shrinkage produced.

On the other hand, the cells exposed to the other two spring extracts (9-5-2022 and 28-5-2022) did not show any significant cell size reduction compared to the control cells.

3.4 Effect of SITS in the PM₁₀-induced apoptotic volume decrease

AVD is known to be caused by the loss of K⁺ and Cl⁻ from the cell (Yu and Choi, 2000). Therefore, in order to investigate the nature of the PM₁₀-induced early isotonic cell shrinkage, A549 cells were preincubated with 0.5 mM disulfonic stilbene



derivative (4-Acetamido-40-isothiocyanato-stilbene-2,20-disulfonic acid), a known inhibitor of Cl⁻ channels (Kokubun et al., 1991) including the ubiquitously expressed volume-regulated anion channels (VRACs) (Maeno et al., 2000; Hoffman et al., 2015; Okada et al., 2021), which have been demonstrated to be involved in AVD in other cell types (Maeno et al., 2000). The cells were viewed by time-lapse microscopy. After (4-Acetamido-40-isothiocyanato-stilbene-2,20-disulfonic acid) preincubation, the cells were exposed to the PM₁₀ aqueous extracts of 18-1-2020 and 21-1-2020 for 2 h and in this case, the PM-induced isotonic shrinkage was completely prevented (Figures 4A, B). On the other hand, (4-Acetamido-40-isothiocyanato-stilbene-2,20-disulfonic acid)

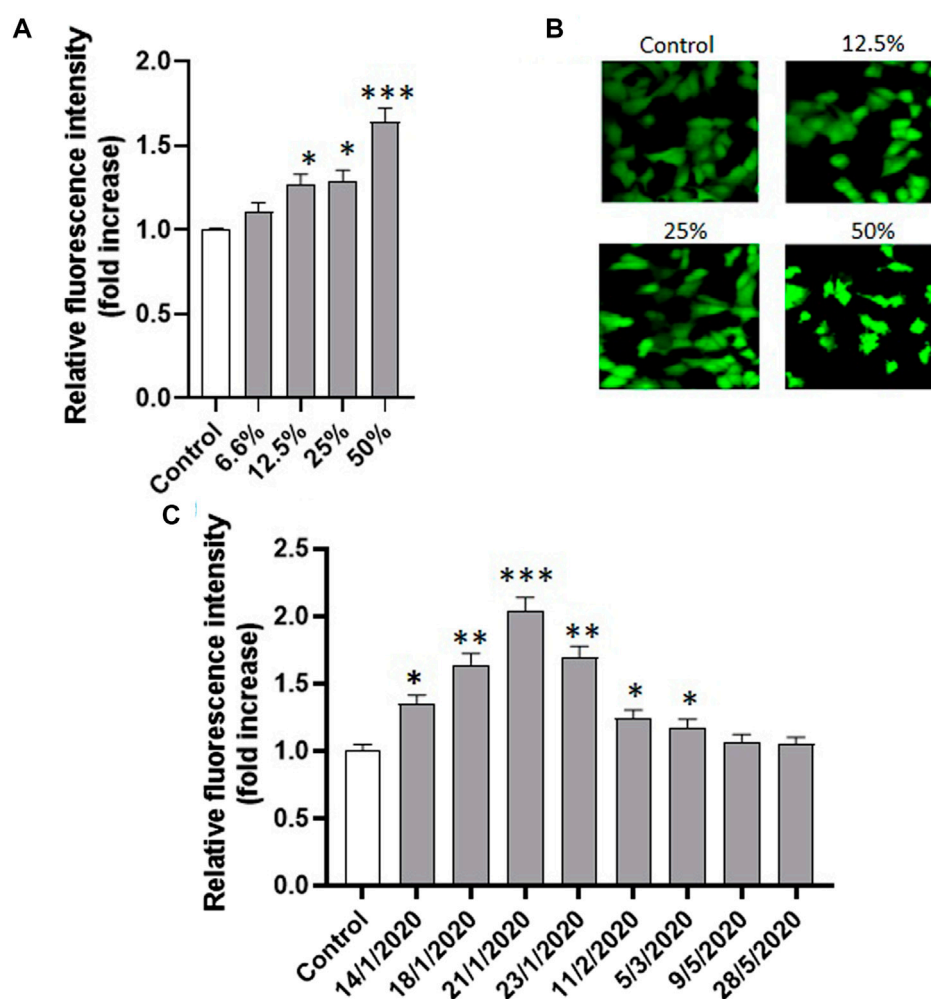


FIGURE 5

(A) Effect of the exposure (24 h) to increasing concentrations of the same PM₁₀ extract (representative experiment on the sample of 21-1-2020) on the intracellular fluorescence intensity of A549 cells charged with the ROS-sensitive probe CM-H₂DCFDA and the corresponding confocal images (B); (C) Intracellular fluorescence of A549 cells exposed to the eight PM₁₀ aqueous extracts for 24 h and charged with the ROS sensitive probe CM-H₂DCFDA (extract dilution used for all the samples: 50%).

alone was not able to produce any significant alteration in cell size. The other two extracts, not showing AVD, were also tested and no significant effect of (4-Acetamido-40-isothiocyanato-stilbene-2,20-disulfonic acid) treatment was observed (Figures 4C, D).

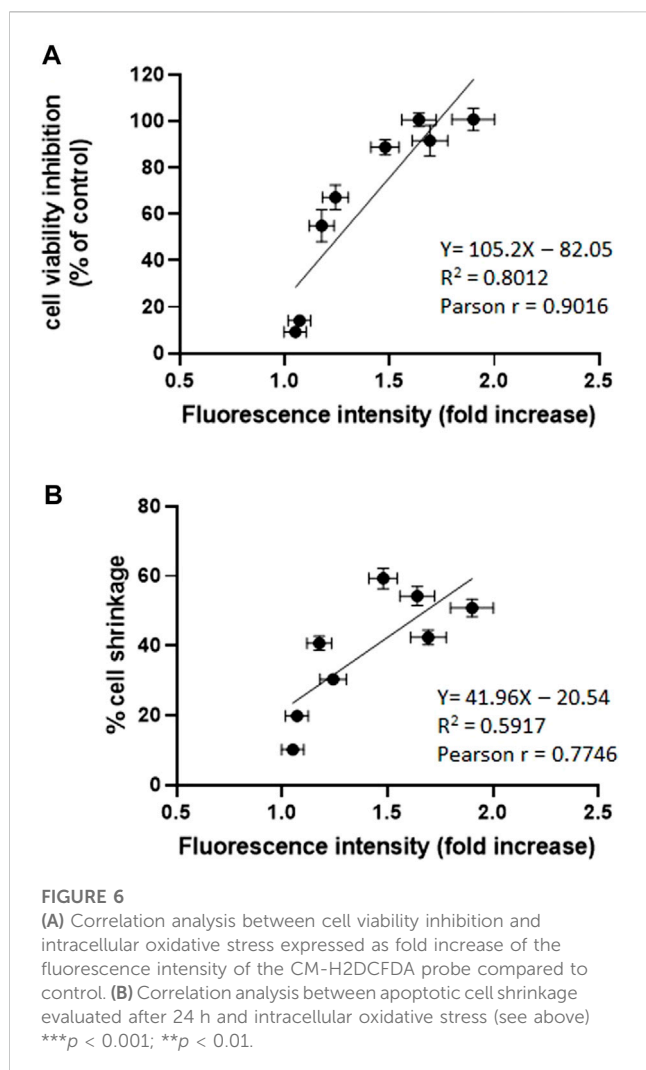
3.5 Oxidative stress induction in A549 cells exposed to PM₁₀

It is known that reactive oxygen species and oxidative stress play a pivotal role in apoptosis induction in several cell types (Kannan and Jain, 2000; Redza-Dutordoir and Averill-Bates, 2016).

In order to test whether oxidative stress was involved in PM₁₀-induced apoptosis in A549 cells, intracellular oxidative stress levels were measured in A549 exposed for 24 h to all the

eight PM₁₀ aqueous extracts of the study using the cell-permeable probe CM-H₂DCFDA. Preliminarily, the cells were exposed to different dilutions of the same extract. Figure 5A shows the representative dose response for one of the tested samples (21-1-2021) revealing that PM₁₀ was able to induce the generation of intracellular oxidative stress in a dose-dependent way. The confocal representative images of cells exposed to different dilutions of the PM₁₀ extracts and then charged with the fluorescent probe are reported in Figure 5B. The intracellular fluorescence intensity of the exposed cells increases with the concentration of the PM₁₀ aqueous extract. At the highest dilution tested the appearance of apoptotic blebs is clearly evident.

The analysis of the PM₁₀-induced intracellular oxidative stress was applied to the eight extracts revealing a highly significant fluorescence increase compared to control in the six winter samples after 24 h, while no significant effect was observed in the

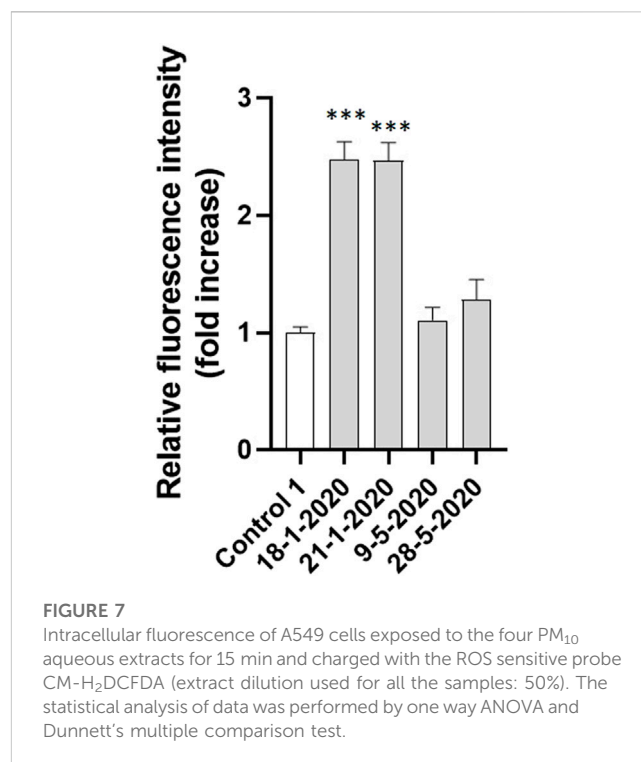


two spring samples (Figure 5C). The oxidative stress data were statistically correlated with vitality inhibition data and cell shrinkage results (Figures 6A, B) suggesting that the generation of intracellular oxidative stress can be one of the main underlying mechanisms of the PM₁₀ induction of apoptosis in A549 cells.

The investigation of the effect of PM₁₀ exposure on intracellular oxidative stress induction was deepened with a short-term analysis of the intracellular fluorescence of A549 cells charged with CM-H₂DCFDA and exposed for 15 min to the 4 aqueous PM₁₀ extracts used for AVD analysis. As reported in Figure 7, the cells exposed to the aqueous extracts of 18-1-2020 and 21-1-2020 expressed a significantly increased fluorescence compared to control cells already after 15 min exposure, suggesting that the induction of oxidative stress by PM₁₀ was an early event, timely correspondent with the AVD induction sustained by VRAC channels.

4 Discussion

The impact of air pollution on public health has become a great concern worldwide, in particular, PM is considered one of



the main risk factors for human health (Loomies et al., 2013; WHO, 2019). Cell death has been used as a hallmark of cell injury induced by PM (Peixoto et al., 2017) representing a general toxic outcome since it results from the integration of the multiple toxic effects that PM can induce at the cellular level. Cell death has been recognized as one important underlying mechanism of the development or exacerbation of respiratory diseases, such as emphysema and chronic obstructive pulmonary diseases (Peixoto et al., 2017).

The present work wants to contribute to the knowledge about the mechanisms underlying the cytotoxic effects of PM at the airway epithelium using A549 cells as a model and focuses on the induction of apoptotic volume decrease, one of the early events in the apoptotic process. The study was carried out on water extracts of airborne PM coming from an urban site in the South of Italy (Aradeo, province of Lecce, Apulia, Italy) whose dominant PM source was represented by biomass burning during the sampling period of the study as previously assessed by Guascito et al. (2023). The used samples included winter samples with high PM₁₀ values, high carbon content values (mainly linked to biomass combustion, as previously assessed), and high cytotoxicity, and spring samples, collected in the post-COVID-lockdown period, characterized by low PM₁₀ values, low carbon content values, and low or negligible cytotoxicity.

Cell death has a central role in homeostasis and it is also responsible for the onset of several pathological conditions. In recent years, various types of cell death, such as apoptosis, autophagy, necrosis, pyroptosis, ferroptosis, and cuproptosis, have been elucidated (Chen et al., 2023), and an increasing number of works have focused on the cellular death pathways related to PM exposure. Among the death cell types, apoptosis is the most widely

investigated in PM-induced cytotoxicity and it has been related to the appearance of pulmonary fibrosis (Yang et al., 2020).

In our study, cytotoxic effects induced by PM₁₀ ascribable to apoptotic death were observed in winter samples which are characterized by the higher PM₁₀ and organic carbon content, as revealed by the typical apoptotic sign appearance such as cell volume reduction, cell rounding, surface roughness, blebs formation, and annexin V positivity. Apoptotic volume reduction was observed early, since a significant cell shrinkage was already detectable after the first 30 min exposure to the winter PM₁₀ samples, while no significant changes in cell volume were observed in spring samples which did not show the typical sign of apoptosis. These results clearly indicate the ability of PM₁₀, mainly arising from biomass burning, to induce AVD in A549 cells. AVD was triggered by the activation of Cl⁻ efflux, since the pretreatment with SITS, a known inhibitor of Cl⁻ channels including the VRAC channels, completely inhibited the PM-induced activation of AVD. The pretreatment with SITS did not exert any effect on cell volume in control conditions suggesting that the channels responsible for the PM₁₀-induced Cl⁻ efflux were not activated in basal conditions.

A549 cells are known to express the ubiquitous volume-regulated anion channels (VRAC) composed of members of the leucine-rich repeat-containing protein 8 family (LRRC8A-E) (He et al., 2010; Canella et al., 2017; Bach et al., 2018; Centeio et al., 2020). Normally, these channels are closed and underwent activation following hypotonic swelling playing a key role in the Regulatory Volume Decrease response which allows the cells to recover their volume through the release of osmolytes (mainly K⁺ and Cl⁻) followed by loss of osmotically obliged water. In addition, VRAC channels have been previously demonstrated to be activated in A549 cells in normotonicity under apoptosis-related stressful conditions such as carboplatin and ozone exposure (He et al., 2010; Canella et al., 2017; Bach et al., 2018) being responsible for the induction of AVD. In light of this knowledge, our results indicate the ability of biomass-burning-related PM₁₀ to activate AVD in A549 cells through the activation of VRAC channels.

As regards the PM₁₀ components able to induce the activation of VRAC channels, it is known that these channels are activated by ROS in various cell types (Jiao et al., 2006; Matsuda et al., 2010; Shen et al., 2014; Friard et al., 2021). PM is known to express an intrinsic oxidant-generating capacity that is related with the physical-chemical properties of the particles, such as their surface characteristics and their chemical composition, related to the pollutants adsorbed (such as metals, polycyclic aromatic hydrocarbons, quinones) expressed by the PM oxidative potential (Chirizzi et al., 2017; Carlino et al., 2023). Besides its intrinsic oxidant-generating capacity, PM also exhibits a cell-mediated oxidant-generating capacity once in the cells, including the activation of intracellular signaling pathways leading to the formation of ROS, the interference with the endogenous production of ROS at the mitochondrial level, the release of radical metabolites arising from the biotransformation of the chemical contaminants of PM (Ghio et al., 2012), and the inhibition of intracellular antioxidant defenses (Chirino et al., 2010). The two types of PM oxidant properties (endogenous and cell-mediated) are statistically correlated as previously demonstrated (Lionetto et al., 2021; Guascito et al., 2023).

In our study, we found that exposure of A549 to PM₁₀ aqueous extracts was able to induce intracellular oxidative stress detected by the ROS-sensitive probe CM-H₂DCFDA. The oxidative stress induction, expressed as a fold increase of the intracellular probe fluorescence, was statistically significantly correlated with cell viability inhibition and with apoptotic cell shrinkage. The oxidative stress induction was already evident after 15 min exposure suggesting that the appearance of PM₁₀ induced AVD through the activity of VRAC channels is mediated by the PM₁₀ induced intracellular oxidative stress, which in turn represents one of the first PM-induced cellular effects leading to cytotoxicity.

5 Conclusion

In conclusion, obtained results demonstrated for the first time that exposure to airborne PM₁₀ aqueous extracts, mainly influenced by biomass burning, induces Apoptotic Volume Decrease in A549 cells. AVD was prevented by the pretreatment with SITS suggesting the activation of Cl⁻ efflux presumably through the activation of VRAC channels. The exposure of A549 cells to PM₁₀ aqueous extracts was able to induce intracellular oxidative stress detected by using the ROS-sensitive probe CM-H₂DCFDA. The PM₁₀ oxidative stress induction was statistically significantly correlated with cell viability inhibition and with apoptotic cell shrinkage. The oxidative stress induction was already evident after 15 min exposure representing one of the first cellular effects induced by PM exposure leading to cytotoxicity. Its early appearance suggests its role in the PM₁₀ mediated AVD induction. This finding deserves to be in more detail evaluated in future works addressing the efficiency of the endogenous antioxidant system in PM treated A549 cells.

Although future studies are needed to better clarify important aspects of the research such as the signaling pathway accounting for AVD activation through VRAC opening and the role played by ROS in these pathways also in relation to the chemical composition of PM₁₀, the manuscript contributes to improving the knowledge about the cellular mechanisms responsible for the effects of PM at the airway epithelium.

Data availability statement

The raw data supporting the conclusion of this article will be made available by the authors, without undue reservation.

Author contributions

Conceptualization: MEG and MGL; Methodology: MEG, and MGL; Investigation: MEG, GU, MRG, AC, MC, DC, and MGL; resources: MGL, MRG, and DC; data curation: MEG, GU, MRG, AC, MC, DC, and ML; writing—original draft preparation: MEG and ML; writing—review and editing: MEG, GU, MRG, AC, MC, DC, and ML; supervision: ML. All authors contributed to the article and approved the submitted version.

Funding

This research was funded by project PAPER (Paper Analyzer for Particulate Exposure Risk), funded within POR Puglia FESR-FSE 2014-2020—Asse prioritario 1—Azione 1.6—Bando Innonetwork—Aiuti a sostegno delle attività di R&S, grant number PH3B166. Moreover, the research was funded also by the project “Dipartimento di Eccellenza” awarded to DiSTeBA, CUP: F85D18000130001, and by Regione Puglia through the Programma Regionale “RIPARTI” (asegni di Ricerca per riPARTire con le Imprese). AVVISO PUBBLICO n. 3/FSE/2021 POC PUGLIA FESR-FSE 2014/2020. Project n. C0d473c3, CUP: F87G22000260002.

Acknowledgments

Authors wish to thank Dr. Franco Papadia (Aradeo Municipality) and Mr. Lucio Perrone (University of Salento) for their help in logistics and for hosting the instruments during the measurement campaigns.

References

- Akella, A., and Deshpande, S. B. (2013). Pulmonary surfactants and their role in pathophysiology of lung disorders. *Indian J. Exp. Biol.* 51, 5–22.
- Amato, F., Alastuey, A., Karanasiou, A., Lucarelli, F., Nava, S., Calzolari, G., et al. (2016). AIRUSE-LIFE+: A harmonized PM speciation and source apportionment in five southern European cities. *Atmos. Chem. Phys.* 16, 3289–3309. doi:10.5194/acp-16-3289-2016
- Ameziane-El-Hassani, R., and Dupuy, C. (2013). Detection of intracellular reactive oxygen species (CM-H₂DCFDA). *Bio-protocol* 3, e313. doi:10.21769/bioprotoc.313
- Antico, S., Lionetto, M. G., Giordano, M. E., Caricato, R., and Schettino, T. (2023). Cell volume regulation and apoptotic volume decrease in rat distal colon superficial enterocytes. *Cell. Physiol. biochem.* 32, 1551–1565. doi:10.1159/000356592
- Bach, M. D., Sørensen, B. H., and Lambert, I. H. (2018). Stress-induced modulation of volume-regulated anions channels in human alveolar carcinoma cells. *Physiol. Rep.* 6, e13869. doi:10.14814/phy2.13869
- Benson, R. S. P., Heer, S., Dive, C., and Watson, A. J. M. (1996). Characterization of cell volume loss in CEM-C7A cells during dexamethasone-induced apoptosis. *Am. J. Physiol.* 270, C1190–C1203. doi:10.1152/ajpcell.1996.270.4.C1190
- Bertelli, S., Remigante, A., Zuccolini, P., Barbieri, R., Ferrera, L., Picco, C., et al. (2021). Mechanisms of activation of LRRC8 volume regulated anion channels. *Cell Physiol. Biochem.* 55 (S1), 41–56. doi:10.33594/00000329
- Bortner, C. D., and Cidlowski, J. A. (2002). Apoptotic volume decrease and the incredible shrinking cell. *Cell Death Differ.* 9, 1307–1310. doi:10.1038/sj.cdd.4401126
- Canella, R., Martini, M., Borriello, R., Cavicchio, C., Muresan, X. M., Benedusi, M., et al. (2017). Modulation of chloride currents in human lung epithelial cells exposed to exogenous oxidative stress. *J. Cell Physiol.* 232, 1817–1825. doi:10.1002/jcp.25705
- Carlino, A., Romano, M. P., Lionetto, M. G., Contini, D., and Guascito, M. R. (2023). An overview of the automated and on-line systems to assess the oxidative potential of particulate matter. *Atmosphere* 14, 256. doi.org/doi:10.3390/atmos14020256
- Centeio, R., Ousingsawat, J., Schreiber, R., and Kunzelmann, K. (2020). Ca²⁺ dependence of volume-regulated VRAC/LRRC8 and TMEM16A Cl[−] channels. *Front. Cell. Dev. Biol.* 8, 596879. doi:10.3389/fcell.2020.596879
- Cesari, D., De Benedetto, G. E., Bonasoni, P., Busetto, M., Dinioi, A., Merico, E., et al. (2018). Seasonal variability of PM_{2.5} and PM₁₀ composition and sources in an urban background site in Southern Italy. *Sci. Total Environ.* 612, 202–213. doi:10.1016/j.scitotenv.2017.08.230
- Chang, Y. H., Phelps, P. C., Berezsky, I. K., Ebersberger, M. L., and Trump, B. F., Jr. (2000). Studies on the mechanisms and kinetics of apoptosis induced by microinjection of cytochrome c in rat kidney tubule epithelial cells (NRK-52E). *Am. J. Pathol.* 156, 637–649. doi:10.1016/S0002-9440(10)64768-2
- Chen, Y., Wu, Y., Qi, Y., and Liu, S. (2023). Cell death pathways: The variable mechanisms underlying fine particulate matter-induced cytotoxicity. *Nanosci* 3, 130–139. doi:10.1021/acsnanoscienceau.2c00059
- Cheng, H., Saffari, A., Sioutas, C., Forman, H. J., Morgan, T. E., and Finch, C. E. (2016). Nanoscale particulate matter from urban traffic rapidly induces oxidative stress and inflammation in olfactory epithelium with concomitant effects on brain. *Environ. Health Perspect.* 124, 1537–1546. doi:10.1289/EHP134
- Chirino, Y. I., Sánchez-Pérez, Y., Osornio-Vargas, Á. R., Morales-Bárceñas, R., Gutiérrez-Ruiz, M. C., Segura-García, Y., et al. (2010). PM₁₀ impairs the antioxidant defense system and exacerbates oxidative stress driven cell death. *Toxicol. Lett.* 193, 209–216. doi:10.1016/j.toxlet.2010.01.009
- Chirizzi, D., Cesari, D., Guascito, M. R., Dinioi, A., Giotta, L., Donato, A., et al. (2017). Influence of Saharan dust outbreaks and carbon content on oxidative potential of water-soluble fractions of PM_{2.5} and PM₁₀. *Atmos. Environ.* 163, 1–8. doi:10.1016/j.atmosenv.2017.05.021
- Cui, Y., Xie, X., Jia, F., He, J., Li, Z., Fu, M., et al. (2015). Ambient fine particulate matter induces apoptosis of endothelial progenitor cells through reactive oxygen species formation. *Cell. Physiol. biochem.* 35, 353–363. doi:10.1159/000369701
- Dagher, Z., Garçon, G., Billet, S., Gosset, P., Ledoux, F., Courcot, D., et al. (2006). Activation of different pathways of apoptosis by air pollution particulate matter (PM_{2.5}) in human epithelial lung cells (L132) in culture. *Toxicology* 225, 12–24. doi:10.1016/j.tox.2006.04.038
- D’Anglemont de Tassigny, A., Souktani, R., Henry, P., Ghaleh, B., and Berdeaux, A. (2004). Volume-sensitive chloride channels (ICl_{vol}) mediate doxorubicin-induced apoptosis through apoptotic volume decrease in cardiomyocytes. *Fundam. Clin. Pharm.* 18, 531–538. doi:10.1111/j.1472-8206.2004.00273.x
- Dinno, A., Gulli, D., Ammoscato, I., Calidonna, C. R., and Contini, D. (2021). Impact of the coronavirus pandemic lockdown on atmospheric nanoparticle concentrations in two sites of Southern Italy. *Atmosphere* 12, 352. doi:10.3390/atmos12030352
- Foster, K. A., Oster, C. G., Mayer, M. M., Avery, M. L., and Audus, K. L. (1998). Characterization of the A549 cell line as a type II pulmonary epithelial cell model for drug metabolism. *Exp. Cell Res.* 243, 359–366. doi:10.1006/excr.1998.4172
- Friard, J., Laurain, A., Rubera, I., and Duranton, C. (2021). LRRC8/VRAC channels and the redox balance: A complex relationship. *Cell. Physiol. biochem.* 55, 106–118. doi:10.33594/000000341
- Gelles, J. D., Mohammed, J. N., Santos, L. C., Legarda, D., Ting, A. T., and Chipuk, J. E. (2019). Single-cell and population-level analyses using real-time kinetic labeling couples proliferation and cell death mechanisms. *Dev. Cell* 51, 277–291.e4. doi:10.1016/j.devcel.2019.08.016
- Ghio, A. J., Carraway, M. S., and Madden, M. C. (2012). Composition of air pollution particles and oxidative stress in cells, tissues, and living systems. *J. Toxicol. Environ. Health B Crit. Rev.* 15, 1–21. doi:10.1080/10937404.2012.632359
- Giordano, M. E., Caricato, R., and Lionetto, M. G. (2020). Concentration dependence of the antioxidant and prooxidant activity of trolox in HeLa cells: Involvement in the

Conflict of interest

The authors declare that the research was conducted in the absence of any commercial or financial relationships that could be construed as a potential conflict of interest.

Publisher’s note

All claims expressed in this article are solely those of the authors and do not necessarily represent those of their affiliated organizations, or those of the publisher, the editors and the reviewers. Any product that may be evaluated in this article, or claim that may be made by its manufacturer, is not guaranteed or endorsed by the publisher.

Supplementary material

The Supplementary Material for this article can be found online at: <https://www.frontiersin.org/articles/10.3389/fphys.2023.1218687/full#supplementary-material>

induction of apoptotic volume decrease. *Antioxidants* 2020, 1058. doi:10.3390/antiox9111058

Guascito, M. R., Lionetto, M. G., Mazzotta, F., Conte, M., Giordano, M. E., Caricato, R., et al. (2023). Characterisation of the correlations between oxidative potential and *in vitro* biological effects of PM10 at three sites in the central Mediterranean. *J. Hazard. Mat.* 448, 130872. doi:10.1016/j.jhazmat.2023.130872

Han, X., and Zhuang, Y. (2021). PM_{2.5} induces autophagy-mediated cell apoptosis via PI3K/AKT/mTOR signaling pathway in mice bronchial epithelium cells. *Exp. Ther. Med.* 21, 1. doi:10.3892/etm.2020.9433

He, W., Li, H., Min, X., Liu, J., Hu, B., Hou, S., et al. (2010). Activation of volume-sensitive Cl⁻ channel is involved in carboplatin-induced apoptosis in human lung adenocarcinoma cells. *Cancer Biol. Ther.* 9, 885–891. doi:10.4161/cbt.9.11.11666

Hoffmann, E. K., Sørensen, B. H., Sauter, D. P., and Lambert, I. H. (2015). Role of volume-regulated and calcium-activated anion channels in cell volume homeostasis, cancer and drug resistance. *Channels* 9, 380–396. doi:10.1080/19336950.2015.1089007

Jiao, J. D., Xu, C. Q., Yue, P., Dong, D. L., Li, Z., Du, Z. M., et al. (2006). Volume-sensitive outwardly rectifying chloride channels are involved in oxidative stress-induced apoptosis of mesangial cells. *Biochem. Biophys. Res. Commun.* 340, 277–285. doi:10.1016/j.bbrc.2005.11.175

Kannan, K., and Jain, S. K. (2000). Oxidative stress and apoptosis. *Pathophysiology* 7, 153–163. doi:10.1016/s0928-4680(00)00053-5

Kokubun, S., Saigusa, A., and Tamura, T. (1991). Blockade of Cl⁻ channels by organic and inorganic blockers in vascular smooth muscle cells. *Pflügers Arch.* 418, 204–213. doi:10.1007/BF00370515

Lee, E. L., Shimizu, T., Ise, T., Numata, T., Kohno, K., and Okada, Y. (2007). Impaired activity of volume-sensitive Cl⁻ channel is involved in cisplatin resistance of cancer cells. *J. Cell Physiol.* 211, 513–521. doi:10.1002/jcp.20961

Leventis, P. A., and Grinstein, S. (2010). The distribution and function of phosphatidylserine in cellular membranes. *Annu. Rev. Biophys.* 39, 407–427. doi:10.1146/annurev.biophys.093008.131234

Lionetto, M. G., Giordano, M. E., Calisi, A., Caricato, R., Hoffmann, E., and Schettino, T. (2010). Role of BK channels in the apoptotic volume decrease in native eel intestinal cells. *Cell. Physiol. biochem.* 25, 733–744. doi:10.1159/000315093

Lionetto, M. G., Guascito, M. R., Caricato, R., Giordano, M. E., De Bartolomeo, A. R., Romano, M. P., et al. (2019). Correlation of oxidative potential with ecotoxicological and cytotoxicological potential of PM₁₀ at an urban background site in Italy. *Atmosphere*, 10, 733. doi.org/doi:10.3390/atmos10120733

Lionetto, M. G., Guascito, M. R., Giordano, M. E., Caricato, R., De Bartolomeo, A. R., Romano, M. P., et al. (2021). Oxidative potential, cytotoxicity, and intracellular oxidative stress generating capacity of PM₁₀: A case study in South of Italy. *Atmosphere*, 12, 464. doi.org/doi:10.3390/atmos12040464

Loomis, D., Grosse, Y., Lauby-Secretan, B., Ghissassi, F. E., Bouvard, V., Benbrahim-Tallaa, L., et al. (2013). The carcinogenicity of outdoor air pollution. *Lancet Oncol.* 14, 1262–1263. doi:10.1016/s1470-2045(13)70487-x

Maeno, E., Ishizaki, Y., Kanaseki, T., Hazama, A., and Okada, Y. (2000). Normotonic cell shrinkage because of disordered volume regulation is an early prerequisite to apoptosis. *Proc. Natl. Acad. Sci. U. S. A.* 97, 9487–9492. doi:10.1073/pnas.140216197

Matsuda, J. J., Filali, M. S., Moreland, J. G., Miller, F. J., and Lamb, F. S. (2010). Activation of swelling-activated chloride current by tumor necrosis factor- α requires ClC-3-dependent endosomal reactive oxygen production. *J. Biol. Chem.* 285, 22864–22873. doi:10.1074/jbc.M109.099838

Okada, Y., Shimizu, T., Maeno, E., Tanabe, S., Wang, X., and Takahashi, N. (2006). Volume-sensitive chloride channels involved in apoptotic volume decrease and cell death. *J. Membr. Biol.* 209, 21–29. doi:10.1007/s00232-005-0836-6

Okada, Y., Maeno, E., Shimizu, T., Dezaki, K., Wang, J., and Morishima, S. (2001). Receptor-mediated control of regulatory volume decrease (RVD) and apoptotic volume decrease (AVD). *J. Physiol.* 532, 3–16. doi:10.1111/j.1469-7793.2001.0003g.x

Okada, Y., Sabirov, R. Z., Sato-Numata, K., and Numata, T. (2021). Cell death induction and protection by activation of ubiquitously expressed anion/cation channels. Part I: Roles of VSOR/VRAC in cell volume regulation, release of double-edged signals and apoptotic/necrotic cell death. *Front. Cell Dev. Biol.* 8, 614040. doi:10.3389/fcell.2020.614040

Peixoto, M. S., de Oliveira Galvão, M. F., and Batistuzzo de Medeiros, S. R. (2017). Cell death pathways of particulate matter toxicity. *Chemosphere* 188, 32–48. doi:10.1016/j.chemosphere.2017.08.076

Poulsen, K. A., Andersen, E. C., Klausen, T. K., Hougaard, C., Lambert, I. H., and Hoffmann, E. K. (2010). Deregulation of apoptotic volume decrease and ionic movements in multidrug resistant tumor cells: Role of the chloride permeability. *Am. J. Physiol.* 298, C14–C25. doi:10.1152/ajpcell.00654.2008

Redza-Dutordoir, M., and Averill-Bates, D. A. (2016). Activation of apoptosis signalling pathways by reactive oxygen species. *Biochim. Biophys. Acta* 1863, 2977–2992. doi:10.1016/j.bbamcr.2016.09.012

Romano, S., Perrone, M. R., Becagli, S., Pietrogrande, M. C., Russo, M., Caricato, R., et al. (2020). Ecotoxicity, genotoxicity, and oxidative potential tests of atmospheric PM10 particles. *Atmos. Environ.* 221, 117085. doi:10.1016/j.atmosenv.2019.117085

Shen, M., Wang, L., Wang, B., Wang, T., Yang, G., Shen, L., et al. (2014). Activation of volume-sensitive outwardly rectifying chloride channel by ROS contributes to ER stress and cardiac contractile dysfunction: Involvement of CHOP through wnt. *Cell Death Dis.* 5, e1528. doi.org/doi:10.1038/cddis.2014.479

Shimizu, T., Numata, T., and Okada, Y. (2004). A role of reactive oxygen species in apoptotic activation of volumesensitive Cl⁻ channel. *Proc. Natl. Acad. Sci. U. S. A.* 101, 6770–6773. doi:10.1073/pnas.0401604101

Wang, B., Li, K., Jin, W., Lu, Y., Zhang, Y., Shen, G., et al. (2013). Properties and inflammatory effects of various size fractions of ambient particulate matter from Beijing on A549 and J774A.1 cells. *Cells. Environ. Sci. Technol.* 47, 10583–10590. doi:10.1021/es401394g

Wei, H., Yuan, W., Yu, H., and Geng, H. (2021). Cytotoxicity induced by fine particulate matter (PM_{2.5}) via mitochondria-mediated apoptosis pathway in rat alveolar macrophages. *Environ. Sci. Pollut. Res. Int.* 28, 25819–25829. doi:10.1007/s11356-021-12431-w

WHO (2019). *Noncommunicable disease and air pollution. WHO European high-level conference on noncommunicable diseases*. Copenhagen, Denmark: WHO Regional Office for Europe.

Yang, L., Liu, G., Fu, L., Zhong, W., Li, X., and Pan, Q. (2020). DNA repair enzyme OGG1 promotes alveolar progenitor cell renewal and relieves PM_{2.5}-induced lung injury and fibrosis. *Ecotoxicol. Environ. Saf.* 205, 111283. doi:10.1016/j.ecoenv.2020.111283

Yang, X., Feng, L., Zhang, Y., Hu, H., Shi, Y., Liang, S., et al. (2018). Cytotoxicity induced by fine particulate matter (PM_{2.5}) via mitochondria-mediated apoptosis pathway in human cardiomyocytes. *Ecotoxicol. Environ. Saf.* 161, 198–207. doi:10.1016/j.ecoenv.2018.05.092

Yi, S., Zhang, F., Qu, F., and Ding, W. (2012). Water-insoluble fraction of airborne particulate matter (PM10) induces oxidative stress in human lung epithelial A549 cells. *Environ. Toxicol.* 29, 226–233. doi:10.1002/tox.21750

Yu, S. P., and Choi, D. W. (2000). Ions, cell volume, and apoptosis. *Proc. Natl. Acad. Sci. U. S. A.* 97, 9360–9362. doi:10.1073/pnas.97.17.9360

Zhang, J., Liu, J., Ren, L., Wei, J., Duan, J., Zhang, L., et al. (2018). PM_{2.5} induces male reproductive toxicity via mitochondrial dysfunction, DNA damage and RIPK1 mediated apoptotic signaling pathway. *Sci. Total Environ.* 634, 1435–1444. doi:10.1016/j.scitotenv.2018.03.383



OPEN ACCESS

EDITED BY

Andrea Gerbino,
University of Bari Aldo Moro, Italy

REVIEWED BY

Savina Apolloni,
University of Rome Tor Vergata, Italy
Barbara Barile,
University of Bari Aldo Moro, Italy

*CORRESPONDENCE

Stefano Garofalo
✉ stefano.garofalo@uniroma1.it

[†]These authors have contributed
equally to this work and share
first authorship

RECEIVED 16 May 2023

ACCEPTED 03 July 2023

PUBLISHED 26 July 2023

CITATION

Calafatti M, Coccozza G, Limatola C and
Garofalo S (2023) Microglial crosstalk with
astrocytes and immune cells in
amyotrophic lateral sclerosis.
Front. Immunol. 14:1223096.
doi: 10.3389/fimmu.2023.1223096

COPYRIGHT

© 2023 Calafatti, Coccozza, Limatola and
Garofalo. This is an open-access article
distributed under the terms of the [Creative
Commons Attribution License \(CC BY\)](#). The
use, distribution or reproduction in other
forums is permitted, provided the original
author(s) and the copyright owner(s) are
credited and that the original publication in
this journal is cited, in accordance with
accepted academic practice. No use,
distribution or reproduction is permitted
which does not comply with these terms.

Microglial crosstalk with astrocytes and immune cells in amyotrophic lateral sclerosis

Matteo Calafatti^{1†}, Germana Coccozza^{1†}, Cristina Limatola^{2,3}
and Stefano Garofalo^{1*}

¹Department of Physiology and Pharmacology, Sapienza University of Rome, Rome, Italy, ²Istituto di Ricovero e Cura a Carattere Scientifico (IRCCS) Neuromed, Pozzilli, Italy, ³Department of Physiology and Pharmacology, Sapienza University, Laboratory Affiliated to Istituto Pasteur, Rome, Italy

In recent years, biomedical research efforts aimed to unravel the mechanisms involved in motor neuron death that occurs in amyotrophic lateral sclerosis (ALS). While the main causes of disease progression were first sought in the motor neurons, more recent studies highlight the gliocentric theory demonstrating the pivotal role of microglia and astrocyte, but also of infiltrating immune cells, in the pathological processes that take place in the central nervous system microenvironment. From this point of view, microglia-astrocytes-lymphocytes crosstalk is fundamental to shape the microenvironment toward a pro-inflammatory one, enhancing neuronal damage. In this review, we dissect the current state-of-the-art knowledge of the microglial dialogue with other cell populations as one of the principal hallmarks of ALS progression. Particularly, we deeply investigate the microglia crosstalk with astrocytes and immune cells reporting *in vitro* and *in vivo* studies related to ALS mouse models and human patients. At last, we highlight the current experimental therapeutic approaches that aim to modulate microglial phenotype to revert the microenvironment, thus counteracting ALS progression.

KEYWORDS

amyotrophic lateral sclerosis (ALS), Astrocytes, immune cell, inflammation, microglia

1 Mechanisms of neurodegeneration in ALS

ALS is the most common adult-onset motor neuron disease, affecting the upper and lower motor neurons (MN) in the brain and spinal cord. People with ALS develop muscle weakness and atrophy, leading to paralysis and death from neuromuscular respiratory failure, within 3 to 5 years after onset. Riluzole and the free-radical scavenger edaravone are the only treatments approved to treat ALS patients, which act on survival and rate of progression, respectively.

Traditionally, ALS has been classified as either the sporadic or familial form. Sporadic ALS (sALS) is the most common form, accounting for around 90% of all cases (1–5). Familial, or inherited, ALS (fALS) runs in families and accounts for the remaining 5–10% of cases. Mutations in several genes have been implicated in fALS and contribute to the

development of sALS (e.g. superoxide dismutase 1 (SOD1), fused in sarcoma (FUS), TAR DNA binding protein (TARDBP) and chromosome 9 open reading frame 72 (C9orf72) (6–8). Proteins encoded by these genes are involved in several aspects of MN function and in ALS pathogenesis, including protein homeostasis, axonal transport, DNA repair, RNA metabolism, vesicle transport, inflammation, mitochondrial dysfunction, and glial cell function (9–11). In 1994, Gurney et al. developed the first mouse model of ALS, a transgenic model that over-expressed the ALS-associated mutant SOD1^{G93A} and recapitulate some of the key clinical features of human ALS (12). These mice showed evident progressive motor abnormalities and paralysis, microglia acquire an inflammatory phenotype affecting MN death, and myeloid cells expressing mutated SOD1 promote neurotoxicity (8, 13, 14). In another ALS mouse model based on TDP-43 mutations, the TDP-43^{A315T} mice showed pathological aggregates of ubiquitinated proteins in specific neurons and reactive gliosis, with the loss of both upper and lower MNs (15, 16). Abnormal expansion of an intronic hexanucleotide GGGGCC (G4C2) repeat of the C9orf72 gene is ALS's most frequently reported genetic cause (17–20). Several transgenic mouse models containing the full-length C9orf72 gene show decreased survival, paralysis, muscle denervation, MN loss, and cortical neurodegeneration (21).

Despite the advance of knowledge of the ALS pathogenesis, most of the molecular and cellular mechanisms involved in the progression and development of the disease remain largely unexplored. Recently, a majority of the evidence indicates that ALS is a non-neuronal-autonomous disease (1, 2, 13). Indeed, in this scenario, glia and immune cells build up a complex regulatory network involved in ALS disease, exerting both neurotoxic and neuroprotective effects on neurons. In this review, we summarize the role of non-neuronal cells in ALS pathology, with a particular focus on microglia interplay with astrocytes and peripheral immune cells that orchestrates the ALS microenvironment. We discuss the current therapeutic approaches that aim to modulate microglial crosstalk with non-neuronal cells, and finally look to the future of new therapeutic trials.

2 Microglial functions in health and disease

Microglia, which represent ~5–12% of the Central Nervous System (CNS) cells, are the resident macrophages of the CNS (22, 23), that originate from myeloid precursor cells which enter into the CNS during embryogenesis (24), becoming independent self-renewing population (25, 26). The general definition of microglial role describes them as able to perform three essential functions: sensing their environment, maintaining physiological homeostasis, and protecting from self and exogenous stimuli. Microglia are able to adopt a plethora of phenotypes, depending on the surrounding environment, which can differ in the healthy CNS and in various disease states (27–30). Recent *in vivo* imaging studies clearly demonstrate that microglial thin processes continually explore and sample the local environment at steady state (31, 32). Consistently, in the healthy CNS, microglia are necessary for

proper brain development, providing trophic support to neurons, removing apoptotic cell debris, regulating neuronal and synaptic plasticity, developmental myelination, and tissue regeneration (33–37). In several pathological conditions, microglia lose their homeostatic molecular signature, resulting in rapid modification of their morphology, transcriptional profile, and phagocytic activity, acquiring a pro-inflammatory profile (38–44); the persistent inflammation can lead to neurotoxicity, and ultimately to neurodegeneration (45–47). Microglia have also been described as active participants in host defense against pathogens and protein aggregates, such as β -Amyloid (A β), mutant huntingtin, prions (PrP^{Sc}), α -synuclein, oxidized or SOD1 (48–50). In response to CNS insults, microglia initiate a defense program to restore brain homeostasis, through different pattern recognition receptors (PRRs), including toll-like receptors (TLRs), scavenger receptors (SRs), and complement receptor 3 (CR3) (51–58). Furthermore, neurotoxicity dysregulates microglial immunological checkpoints (such as Trem2 and CX3CR1) that normally prevent their overreaction and may help to control inflammation (52). Dysregulation of these pathways increases the risk for Alzheimer's disease (AD), frontotemporal lobar degeneration (FTLD), frontotemporal dementia (FTD), and ALS (59). Dysregulation of the host-defense pathway further, may also be caused by mutations in specific genes, such as Trem2, HTT, and TDP43, further, resulting in an inflammatory response and neuronal damage (60–62).

2.1 Microglia in ALS

Evidence that detrimental microglia contribute to sustaining the inflammation in ALS is observed in imaging studies in patients with ALS, human post-mortem samples, and rodent models of ALS (63–65). Microglia increase the expression of CD14, CD18, SR-A, and CD68 in ALS spinal cord, and CD68⁺ microglial cells are detected in close proximity to MNs (66), and in the brain of ALS patients using Positron emission tomography (PET) imaging (67, 68). Notably, microglia modify their phenotype with disease progression: adult microglia isolated from ALS mouse models at disease onset show a protective/anti-inflammatory phenotype, while microglia isolated from end-stage disease are toxic/pro-inflammatory (69–74). Consistently, in familial ALS (fALS) patients with SOD1 mutations, and in the SOD1-ALS mouse models, microglia affect MN death (75) and promote neurotoxicity (76), as well as regulate the feeding behavior and overall metabolism (77). Microglial-mediated MN death in ALS occurs through an NF- κ B-dependent mechanism (75) and by secreting reactive oxygen species and pro-inflammatory cytokines (such as interleukin (IL)-1, IL-6, tumour necrosis factor (TNF)- α) (78, 79). Although a number of studies are in line with the neuroinflammatory and neurotoxic microglial role observed in SOD1 mutated ALS patients and mouse models (8, 13, 14), the functional role of microglia in familial ALS or mouse models with mutated TDP-43 is not clear. In post-mortem human brain tissue from ALS patients and mouse models expressing mutated TDP43, were observed aggregates of ubiquitinated proteins in MNs, astrocytes and microglia, loss of both upper and lower MN and intestinal dysmotility that could induce premature death (15). On the contrary, the suppression of mutated human(h) TDP-43 protein in neurons, dramatically increased the microglial proliferation and changed their morphology and

phagocytic activity against neuronal hTDP-43 (15). The partial depletion of microglia using PLX3397, a CSF1R and c-kit inhibitor, failed to recover motor functions in hTDP-43 mice, revealing an important neuroprotective role for microglia (80).

Recent work showed that C9orf72 expression is highest in myeloid cells, and loss of function of the C9ORF72 protein in mice disrupts microglial function and may contribute to neurodegeneration in C9orf72 expansion patients (18, 20, 81–87). Other disease mechanisms that occur in the ALS/FTD with C9orf72 gene mutation include a gain of toxicity mediated through either the RNA itself (88, 89) and/or the translation of aberrant dipeptide repeat (DPR) proteins by a non-canonical translation mechanism called repeat associated non-AUG dependent (RAN) translation (90, 91). Immunoreactive microglia and upregulation of inflammatory pathways have been confirmed in patients with mutated C9orf72 and correlate with rapid disease progression (87). Anyway, since most C9orf72 mouse models do not show ALS motor symptoms, neurodegeneration, or inflammatory response, it is difficult to determine the relationship between C9orf72-specific molecular pathology and ALS.

3 Microglial dialogue with non-neuronal cells in ALS

In the CNS, non-neuronal cells play crucial homeostatic functions both in health and diseases. The involvement of these cells in the pathophysiology of ALS is being increasingly characterized. Microglia crosstalk with peripheral immune cells and astrocytes to exert either neuroprotective or adverse effects through a broad range of cell-to-cell interactions.

3.1 Microglia – Astrocytes crosstalk

Similar to microglia, during ALS progression, astrocytes adopt neurotoxic properties which actively contribute to disease pathogenesis (92). In fact, both *in vitro* and *in vivo* studies demonstrated that in ALS mouse models, astrocytes with mutated mSOD1 protein exert neurotoxic effects on motor neurons, by releasing pro-inflammatory factors (93). Moreover, reactive astrocytes were described in the post-mortem CNS tissue obtained from ALS patients (94–96). This finding was confirmed further *in vivo* via diagnostic imaging using PET scanning demonstrating cerebral white matter and pontine astrogliosis in ALS patients (97).

In recent years, the crosstalk between astrocytes and other non-neuronal cells has been studied in more detail. The astrocytic transition from neuroprotective to neurotoxic was accompanied by a shift in microglial phenotype, suggesting that astrocytes may be important regulators of microglia activation and neuroinflammation in ALS (98). To date, several studies demonstrated that the detrimental microglia shape astrocyte phenotype in ALS driving disease progression. Both in human and mouse ALS tissues it was found the presence of neurotoxic reactive (A1-like) astrocytes since the early phase of the disease (92, 99–101). Moreover, microglia modify their phenotype as the disease progression: indeed, adult microglia isolated from ALS mouse

models at disease onset show a protective/anti-inflammatory phenotype, while microglia isolated from end-stage disease are toxic/pro-inflammatory (67–72).

However, controversial results have been obtained on which cell population, between microglia and astrocytes, acquires a pro-inflammatory/neurotoxic phenotype during ALS progression. Indeed, Alexianu et al. reported that microglia activation precedes astrocyte reactivity (102). On the contrary, another study suggested that astrogliosis is present since the early symptomatic stage, while prominent microgliosis is only evident at the late phase (103).

Astrocytes have been shown to shape the microglial phenotype according to disease stage, modulating neuroprotective and neurotoxic functions in the pre-symptomatic and symptomatic phases of ALS, respectively (98). In the SOD1^{G93A} ALS mouse model, astrocytic NF- κ B activation drove microglial proliferation and leukocyte infiltration in the CNS (98). This response was initially beneficial by prolonging the pre-symptomatic phase, but it became detrimental in the symptomatic phase, accelerating disease progression. Specifically, in the pre-symptomatic phase astrocytic NF- κ B activation in SOD1 mouse models induced a Wntless-related integration site (Wnt)-dependent anti-inflammatory microglial response via nuclear factor kappa-B kinase subunit beta (IKK2), resulting in neuroprotective effects on motor neurons which translated into a delay of motor symptoms (98). However, in the symptomatic phase, NF- κ B activation in astrocytes promoted pro-inflammatory microglial responses (via CD68, TGF- β , TNF- α) which accelerated disease progression (98). A recent study indicated astrocytic TGF- β 1 as a major molecule modulating microglial phenotype toward detrimental one (104). Astrocyte-specific overproduction of TGF- β 1 in SOD1^{G93A} mice interfered with the neuroprotective effects of microglia during the pre- and early symptomatic stages and accelerated disease progression in a non-cell-autonomous manner. This interference resulted in reduced production of neurotrophic factors from microglia and a reduced number of CNS infiltrating T cells. Consistently, the expression levels of endogenous TGF- β 1 in SOD1^{G93A} mice negatively correlated with overall life expectancy, while the administration of a TGF- β signaling inhibitor extended it (104). These findings raise TGF- β 1 to an important determinant of disease progression in ALS.

On the other hand, many pieces of evidence suggest that the activation of microglia precedes the reactivity of astrocytes in ALS (105). Brites and colleagues demonstrated that microglia respond earlier than astrocytes to cell stress or damage by activating NF- κ B and mitogen-activated protein kinase (MAPK) signaling pathways, thus leading to the release of pro-inflammatory cytokines (e.g., TNF- α and IL-1 β) (105). These cytokines were shown to exert an inhibitory effect on Cx-43 expression, the main constitutive protein of astrocytes' gap junctions, therefore hampering communication between astrocytes, and possibly interfering with their neuroprotective role (106). In addition, cell-cell contacts and microglial-derived soluble mediators are necessary for astrocytes to fully respond to lipopolysaccharide (LPS) insult and Toll-Like Receptor (TLR) ligation (11413), suggesting that microglia may exert a permissive effect on astrocyte pro-inflammatory activation. Liddel et al. demonstrated that the microglial derived-pro-inflammatory cytokines IL-1 α , TNF α and complement component C1q42 are necessary and sufficient to induce pro-

inflammatory astrocytes in mice (92). Consistently, a triple knock-out of these factors in $IL-1\alpha^{-/-} TNF\alpha^{-/-} C1qa^{-/-} SOD1^{G93A}$ mice led to a drastic reduction in the number of reactive astrocytes, improving lifespan and delaying motor neuron loss and disease progression (92). This finding further supports the hypothesis of a microglia-to-astrocyte polarization.

Since an intimate interaction/communication between microglia and astrocytes occurs in ALS, a better understanding of their crosstalk could help to define potential therapeutic strategies targeting the glia in ALS.

3.2 Microglia – Natural killer cells crosstalk

NK cells contribute to ALS progression by interacting with CNS resident cells and peripheral immune cells. Increased numbers of NK cells have been found in the peripheral blood and CNS of ALS patients (107), and a rich infiltrate of NK cells has been described in the CNS of $SOD1^{G93A}$ mouse models (5). The NK cells - microglia crosstalk has been recently characterized, highlighting the importance of this interaction in the pathogenesis of ALS. Indeed, in NK cell-depleted $hSOD1^{G93A}$ and $TDP43^{A315T}$ microglia acquired a typical neuroprotective morphology, covering a wider parenchymal region and increasing the branches number (108). Moreover, NK cell-depleted $hSOD1^{G93A}$ mice showed a reduction in microgliosis, indicated as the number of microglia in the ventral horns of the spinal cord (108). In the absence of NK cells, microglia reduced the expression of genes associated to a pro-inflammatory phenotype, including $IL-6$, $IL-1\beta$, $TNF-\alpha$, with the simultaneous increase of expression of the anti-inflammatory ($Chil3$, $Arg-1$, and $TGF-\beta$), antioxidant ($Msod1$) and neuroprotective ($P2yr12$, $Trem2$, $Kcnn4$, $Bdnf$, $IL-15$) markers (108). The molecular link that drives the crosstalk between microglia and NK cells in ALS is the $IFN-\gamma$ produced by infiltrated NK cells during the pre-symptomatic stage of disease. Accordingly, the $IFN-\gamma$ immunodepletion (via $IFN-\gamma$ -blocking antibody XMG1.2 administration) had consequences similar to NK cell depletion on microglial phenotype, switching them toward an anti-inflammatory phenotype (108). Lastly, this NK cell-mediated modulation of microglia resulted in an increased number of motor neurons in the ventral horn of spinal cord, and affected survival and onset time both in $SOD1^{G93A}$ and $TDP43^{A315T}$ mouse models (108). These results were further validated in an elegant study (109) exploiting Natalizumab, a blocking antibody for the $\alpha 4$ integrin (anti-VLA-4) (110, 111), to reduce the transfer of peripheral immune cells to the CNS of the $hSOD1^{G93A}$ ALS mouse model. In the lumbar spinal cord of Natalizumab-treated mice was found a reduced number of NK cells and, accordingly, microglial cells reduced the expression of pro-inflammatory markers ($IL-6$, $IL-1\beta$ and $tnf-\alpha$), and $IFN-\gamma$ level was significantly reduced compared to vehicle-treated $hSOD1^{G93A}$ mice (108). However, Natalizumab treatment showed more effects on the modulation of the inflammation in the ALS microenvironment, suggesting a more complex scenario due to the role of different peripheral immune cells infiltrated in the CNS. Overall, these results point toward the importance of microglia-NK cells crosstalk modulation to reduce motor neuron loss in ALS.

3.3 Microglia - T lymphocytes crosstalk

Activated T cells are present in the CNS at a steady state to perform immunological surveillance (112) and provide immunological responses that are modulated by cell to cell signaling (113). Infiltration of $CD4^{+}$ and $CD8^{+}$ T lymphocytes has been documented in the brain and spinal cord of ALS patients (114, 115). Specifically, perivascular and intraparenchymal $CD4^{+}$ helper T cells were found to surround degenerating corticospinal tracts, while ventral horns were enriched with both $CD4^{+}$ helper and $CD8^{+}$ cytotoxic T cells. The lymphocytic infiltration did not correlate with the rate of progression or stage of the disease in ALS patients (115); on the contrary, in transgenic mice expressing mutant $SOD1^{G93A}$, the number of $CD4^{+}$ and $CD8^{+}$ T cells infiltrating the spinal cord increased as the disease progressed (116, 117). Multiple levels of evidence suggest that $CD4^{+}$ helper T cells exert neuroprotective functions, especially in the initial phases of the disease process (116, 118), while $CD8^{+}$ cytotoxic T cells present at later phases of the disease are possibly neurotoxic (119, 120). T cell functional profiles are, at least in part, shaped by a complex dialogue with microglia and neurons, as explained below.

3.3.1 Microglia - $CD4^{+}$ T lymphocytes crosstalk

$CD4^{+}$ T cells comprise multiple functionally distinct cell populations that regulate different functions, classified as Th1, Th2, regulatory T cells (Tregs), and Th17 cells (121). Although the role of $CD4^{+}$ T cells in ALS remains controversial, the putatively protective effect of these cells on MNs is widely accepted (122–124). A major insight into the role of $CD4^{+}$ T cells came from Beers & al., who bred immunodeficient mice lacking functional lymphocytes or functional $CD4^{+}$ T cells with $mSOD1^{G93A}$ transgenic mice and performed selective reconstitution experiments with bone marrow transplants (116). The lack of functional $CD4^{+}$ T lymphocytes resulted in a faster disease progression characterized at the molecular level by the upregulated expression of pro-inflammatory functional markers like NOX2 and pro-inflammatory cytokines, while reconstitution of $CD4^{+}$ T lymphocytes prolonged survival and inhibited the acquisition of pro-inflammatory phenotype in microglia (116). The absence of functional $CD4^{+}$ T cells in $mSOD1^{G93A}$ mice reduced the mean survival time, supporting the neuroprotective role of these lymphocytes. The fractalkine receptor (CX3CR1), a chemokine receptor expressed by microglia, monocytes, dendritic cells, and subsets of T cells, was involved in microglial neurotoxicity (125), and consistently, was reduced in mice lacking $CD4^{+}$ T cells and increased following bone marrow reconstitution (125).

Within the $CD4^{+}$ T lymphocyte subsets, endogenous Tregs are particularly associated to neuroprotection in ALS, with a time-specific effect (122, 123). Tregs were found to be increased in spinal cords of $mSOD1$ mice after disease onset, accompanied further by increased expression of $IL-4$ and higher number of neuroprotective/anti-inflammatory microglia (122). During the progression of the disease, there was a loss of Forkhead box P3 (FoxP3) expression in Tregs, with a concomitant reduction of $IL-4$ level (122). Passive transfer of Tregs from donor $mSOD1^{G93A}$ mice in the early phase of the disease, sustained $IL-4$ levels and anti-inflammatory microglia,

delaying the onset of symptoms and increasing the survival of recipient mSOD1^{G93A} mice (116, 122).

In ALS patients, neuroinflammation can be attributed to the impaired suppressive function of Tregs in addition to their decreased numbers (123, 126). Indeed, mutated SOD1 Tregs were less effective in suppressing effector T cells (Teff) proliferation (123). With the progress of diagnostic imaging, PET of activated microglia in ALS patients offers a potential opportunity to assess Treg-mediated neuroprotection (63, 67, 127). While Treg and anti-inflammatory microglia increase in the early stage of ALS (128–130), Th1 and pro-inflammatory microglia increased the inflammation in the microenvironment in the later stage of ALS (131, 132). Accordingly, a parallel shift from a neuroprotective Treg/anti-inflammatory response to a neurotoxic Th1/pro-inflammatory response has been postulated during ALS progression by Zhao et al. (132). In the mSOD1 mouse model, a Treg/anti-inflammatory response dominates the initial slowly progressing phase of the disease, as Tregs suppress microglial toxicity and SOD1 T effector cells through IL-4, IL-10 and TGF- β (132). During ALS progresses, the immune response switches to a deleterious Th1/pro-inflammatory response, where the interaction between Th1 and microglia enhances pro-inflammatory responses, including the release of TNF- α , IL-6, and IL-1 β , and downregulates Treg suppressive functions (132).

Overall, these data support the concept of a well-orchestrated and complex dialog among microglia and CD4⁺ T cells, suggesting that different CD4⁺ T lymphocyte subsets play different roles in shaping microglial functions during ALS progression.

3.3.2 Microglia – CD8⁺ T lymphocytes crosstalk

In the peripheral blood of ALS patients, cytotoxic CD8⁺ T cells number was found to be significantly increased, suggesting a systemic immune activation (133). However, the role of these cells in the progression of ALS remains difficult to decipher (134).

Particularly, microglia-CD8⁺ T cell crosstalk is fundamental to drive the inflammation in ALS affected regions (120). Specifically, major histocompatibility complex I (MHCI) depletion in resident microglia or the lack of CD8⁺ T cell infiltration in the spinal cord of β 2 microglobulin-deficient hSOD1^{G93A} mice (which express little if any MHCI on the cell surface and are defective for CD8⁺ T cells) delayed motor symptoms and prolonged the survival mean time, suggesting that microglia interact with infiltrated CD8⁺ T cells through MHC complex, promoting MN death in ALS. Moreover, the level of CD68⁺ microglia was lower in the spinal cord of β 2 microglobulin-deficient hSOD1^{G93A} mice suggesting that the MN preservation is due to a lack of interaction with CD8⁺ T cells (120). Interestingly, β 2 microglobulin-deficiency in the peripheral nervous system (i.e. sciatic nerve) impaired motor axon stability and anticipated the onset of muscle atrophy, delineating regional differences in the role of MHCI and CD8⁺ T cells in the pathogenesis of ALS (120).

3.4 Microglia – Monocytes/macrophages crosstalk

In ALS patients, peripheral monocytes infiltrate the CNS (66), and the monocytes isolated from peripheral blood of ALS patients show a

pro-inflammatory profile (135). Furthermore, the degree of systemic monocyte/macrophage activation directly correlates to the rate of disease progression (136). In the hSOD1^{G93A} mouse model, inflammatory monocytes infiltrate the ALS affected regions (137), and their progressive recruitment to the spinal cord correlates with neuronal loss (137). Prior to disease onset, monocytes expressed a polarized macrophage pro-inflammatory phenotype (M1 signature), which included increased levels of chemokine receptor CCR2. This receptor normally interacts with the ligand CCL2, controlling the migration and infiltration of CCR2-expressing monocytes/macrophages in a process implicated in multiple neurodegenerative diseases. Butovsky et al. demonstrated that CCL2 expression by microglia increases as ALS progresses (138). Mouse monocytes fall into two phenotypically distinct subsets: Ly-6C^{hi} (which are CCR2⁺) and Ly-6C^{lo} (which are CCR2⁻), corresponding to human CD14^{hi}CD16⁻ and CD14⁺CD16⁺ monocytes, respectively (138). Ly6C is a GPI-linked protein of the Ly6 family, which is found mostly in inflammatory monocytes (139). Accordingly, hSOD1^{G93A} mouse treatment with anti-Ly6C monoclonal antibody reduced the number of monocytes recruited to the spinal cord, diminished neuronal loss, and extended survival (137).

Recently, a study by Chiot et al. (140) investigated the crosstalk between peripheral macrophages and microglia in ALS. Targeted gene modulation of the reactive oxygen species pathway in peripheral myeloid cells of hSOD1^{G93A} mice, reduced both peripheral macrophage and microglial activation, and delayed the onset of motor symptoms (140). Specifically, the chemotherapy agent busulfan was used to induce myeloablation, followed by bone marrow transplantation in which mutant SOD1-expressing macrophages were replaced with macrophages genetically modified with less neurotoxic properties (via downregulating of Nox2 or overexpression of wild-type Sod1). In this model, resident microglial cells acquired an anti-inflammatory/protective phenotype and a reduction was found in microgliosis in the spinal cord (140). These results indicate that the modification of infiltrating monocytes/macrophages suppresses neurotoxic microglial responses in ALS, suggesting direct or indirect crosstalk between these two cell populations. The mechanisms underlying this crosstalk are not yet clear, but the authors suggested that replacing of inflammatory peripheral monocytes/macrophages could pave the way for a new therapeutic approach for ALS patients.

4 Currently approved therapies in ALS

The complex pathogenesis in ALS, coupled with its clinical and molecular heterogeneity, resulted in too many failed attempts at drug discovery and development. The foundation for failure includes the wrong target, route of administration, outcome measures, and the many different pathogenic mechanisms at play in different patients (141). Drugs undergoing clinical trials are available on the ALS Association website (<https://www.neals.org/als-trials/search-for-a-trial/>). To date, there are two FDA-approved drugs for ALS: riluzole and edaravone. Both drugs have a relatively small efficacy in delaying motor function deterioration, and their effectiveness is limited during early stages of the disease (142).

Riluzole was the first FDA drug approved for clinical use in 1995. This drug blocks glutamate release and therefore glutamatergic neurotransmission in the CNS, exerting neuroprotective function as it dampens pathological excitotoxicity in ALS (143). Additional proposed mechanisms of action include an indirect antagonism of glutamate receptors in addition to the inactivation of neuronal voltage-gated Na⁺ channel (144). Edaravone was the second FDA approved ALS-specific drug, in 2017. Edaravone is a neuroprotective drug with broad free radical scavenging activity that protect neurons, glia, and vascular endothelial cells against oxidative stress (145).

4.1 Therapies targeting neuroinflammation and microglial crosstalk with peripheral immune cells

Multiple compounds with immune-modulatory properties have been reported to affect the crosstalk between microglia and immune cells. Although promising in the mouse models of ALS, preclinical results have so far failed to translate into meaningful clinical outcomes (146, 147). Most efforts in the development and application of immune-modulatory drugs in ALS aimed at reducing pro-inflammatory and neurotoxic immune responses. Among the therapies recently developed to target neuroinflammation and microglia phenotype in ALS, the following demonstrated significant benefits in preclinical studies and have already or are soon to be translated to clinical trials (Table 1).

- dl-3-*n*-Butylphthalide (NBP) is a small molecule compound showing neuroprotective effects via multiple mechanisms, including modulation of mitochondrial oxidative stress, apoptosis and autophagy (148). In hSOD1^{G93A} mice, treatment with NBP extended survival by attenuating microglial activation and motor neuron loss (149, 150). A randomized trial (ChiCTR.org.cn Identifier: ChiCTR-IPR-15007365) of NBP in the treatment of ALS patients was conducted in China. The preliminary results indicated that

NBP did not improve the ALS Functional Rating Scale (ALSFRS)-R score in patients with ALS (151).

- Cannabinoids exert anti-glutamatergic, anti-oxidant and anti-inflammatory actions through activation of the CB (1) and CB(2) receptors, whereby receptor activation reduces pro-inflammatory microglia, decreasing the microglial secretion of neurotoxic mediators (152, 153). In hSOD1^{G93A} mice, treatment with WIN-55,212-2, a cannabinoid agonist with higher affinity to the CB2 than the CB1 receptor (154), and the Selective CB2 receptor agonist AM-1241 significantly delayed disease progression and increased mean survival time (155, 156). Although these promising results, a meta-analysis of the studies conducted on murine models concluded that animal studies have moderate to high risk of bias and are highly heterogeneous. Therefore, more standardized studies on cannabinoids are necessary before bringing these compounds to the clinic (157).
- Ibudilast (MN-166) is a non-selective phosphodiesterase 4 inhibitor with a neuroprotective effect primarily mediated by the inhibition of inflammatory mediators and the upregulation of neurotrophic factors in pro-inflammatory microglia (158). Two clinical trials with ibudilast have been completed in ALS patients, and one is currently ongoing. The first Phase II trial (ClinicalTrials.gov Identifier: NCT02238626) evaluated the safety, tolerability and clinical responsiveness of ibudilast co-administered with riluzole. The study showed good safety and tolerability but no overall difference in disease progression between ibudilast and placebo treatment arms. Subgroup analysis suggested that patients with bulbar or upper limb onset might have more benefit from the compound (159). A Phase IIb/III study, the COMBAT-ALS study is currently recruiting on North America in order to evaluate the pharmacokinetics, safety and tolerability and assess the efficacy of ibudilast on function, muscle strength, quality of life and survival in ALS (ClinicalTrials.gov Identifier: NCT04057898).

TABLE 1 Therapies targeting neuroinflammation and microglial crosstalk with peripheral immune cells in ALS.

Drug	Mechanism	Target cells	Trial number	Phase
dl-3- <i>n</i> -Butylphthalide (NBP)	Modulation of mitochondrial oxidative stress, apoptosis and autophagy	Microglia, Motor Neurons	ChiCTR-IPR-15007365	II
Cannabinoids	Anti-glutamatergic, antioxidant and anti-inflammatory actions	Microglia	N/A	N/A
Ibudilast (MN-166)	Anti-inflammatory and neurotrophic actions	Microglia	NCT02238626 NCT04057898	II IIb/III
Masitinib	Anti-inflammatory; modulation of aberrant microgliosis	Microglia	NCT02588677 NCT03127267	II/III III
Minocycline	Anti-inflammatory	Microglia, Motor Neurons	NCT00047723	III
NP001	Anti-inflammatory	Microglia	NCT01091142 NCT01281631 NCT02794857	I II II

N/A, not applicable.

- Masitinib is a tyrosine-kinase inhibitor whose oral administration was shown to control aberrant microgliosis, abrogate neuroinflammation and slow disease progression in the hSOD1^{G93A} mice (160). The primary analysis of a randomized Phase II/III trial testing masitinib in combination with riluzole for the treatment of ALS patients ([ClinicalTrials.gov](https://clinicaltrials.gov/ct2/show/study?term=NCT02588677) Identifier: NCT02588677) showed a significantly slowed functional decline, although there was no discernible difference in overall survival between the two arms (161). Long-term survival analysis indicated that oral masitinib prolonged survival by over

2 years as compared with placebo, provided that treatment started prior to severe impairment of functionality (162). A subsequent phase III clinical trial is currently ongoing ([ClinicalTrials.gov](https://clinicaltrials.gov/ct2/show/study?term=NCT03127267) Identifier: NCT03127267).

- Minocycline is a second-generation tetracycline antibiotic, capable to penetrate the blood-brain barrier, with anti-inflammatory effects independent of its antimicrobial activity. The compound has been demonstrated to dampen microglial activation (163) and apoptosis by inhibiting mitochondrial permeability-transition-mediated cytochrome c release (164). The compound delayed disease onset and extended survival in the

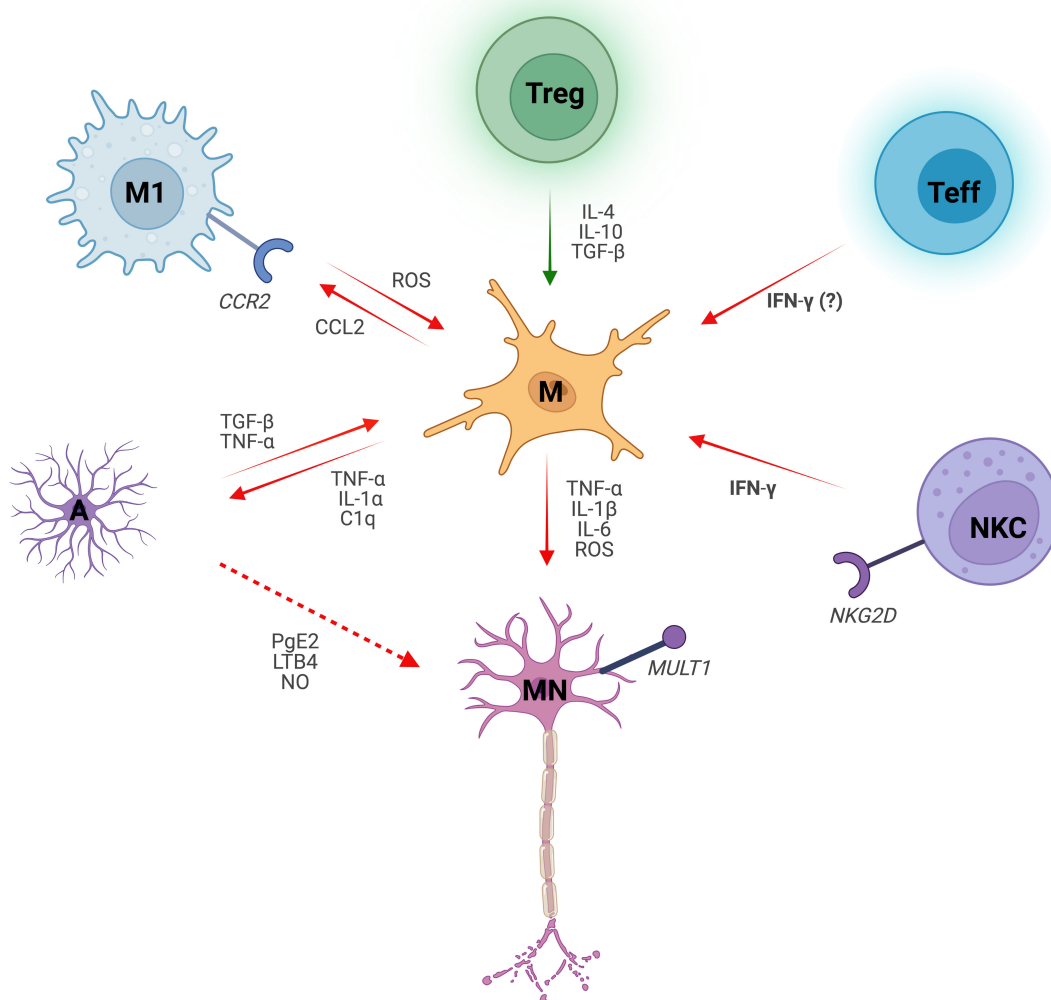


FIGURE 1

Microglial dialogue with non-neuronal cells in Amyotrophic Lateral Sclerosis. Microglia (M) induce motor neuron (MN) degeneration in ALS by secreting reactive oxygen species (ROS) and pro-inflammatory cytokines, such as Interleukin 1 beta (IL-1β), Interleukin 6 (IL-6) and Tumor Necrosis Factor (TNF-α). Microglial crosstalk with non-neuronal cells shapes their phenotype, either skewing it towards a pro-inflammatory (red arrows) or anti-inflammatory (green arrows) phenotype. Microglial-derived pro-inflammatory cytokines Interleukin 1 alpha (IL-1α), TNFα and complement component C1q induce pro-inflammatory astrocytes (A). Conversely, activated astrocytes promote inflammatory microglial responses via Transforming Growth Factor β (TGF-β) and TNF-α. Reactive astrocytes also exert toxic effects on MNs by secreting inflammatory mediators such as Prostaglandin E2 (PgE2), Leukotriene B4 (LTB4) and nitric oxide (NO). Chemokine ligand 2 receptor (CCR2)-expressing macrophages (M1) are recruited by the Chemokine Ligand 2 (CCL2) released by microglia. ROS pathway in classically activated macrophages induces microglial activation. Regulatory T cells (Treg) suppress microglial toxicity as well as other immune cells (not shown) through Interleukin 4 (IL-4), Interleukin 10 (IL-10) and TGF-β. Notably, TGF-β effect on microglia is context- and cell-dependent. Microglia-CD8+ Effector T cell (Teff) crosstalk drives neuroinflammation in ALS, with Interferon gamma (IFN-γ) secreted by the latter likely playing a role. Infiltrated Natural Killer Cells (NKC) instruct microglia towards an inflammatory profile by the release of IFN-γ. Additionally, NKCs are neurotoxic to MNs via NKG2D - NKG2D ligand (MULT1) interaction.

hSOD1^{G93A} and hSOD1^{G37R} transgenic models of ALS (164–166). However, a subsequent randomized placebo-controlled phase III trial (ClinicalTrials.gov Identifier: NCT00047723) disproved any efficacy of the compound in patients, reporting an ALSFRS-R score deterioration faster in the minocycline group than in the placebo group, along with a higher incidence of adverse events (167).

- NP001 is a highly purified form of sodium chlorite, targeting inflammatory macrophages by down-regulating the Nuclear Factor κ B (NF- κ B) inflammatory pathways (168). Preliminary studies in hSOD1^{G93A} mice showed a significant increase in life expectancy compared to control (169). A phase I trial in ALS patients (ClinicalTrials.gov Identifier: NCT01091142) showed that NP001 was generally safe and well tolerated, and caused a dose-dependent reduction in expression of the pro-inflammatory marker CD16 (170). Two subsequent randomized phase II trials (ClinicalTrials.gov Identifier NCT01281631, NCT02794857) suggested that NP001 slowed the progression of ALS symptoms in a subset of patients with marked neuroinflammation (171). Combined *post hoc* analysis did not show significant differences between placebo and active treatment but identified a 40- to 65-y-old subset in which NP001-treated patients demonstrated slower declines in ALSFRS-R score compared with placebo (172).

5 Conclusions

The crosstalk between immune cells and glia contribute to MN degeneration in ALS. Despite the advance in the scientific findings aimed to unravel the molecular and cellular mechanisms that induce MN to death, ALS persists without effective therapy that improves motor symptoms and increases the life of patients. In ALS microglia promote a pro-inflammatory microenvironment, supported by neurotoxic astrocytes and infiltrated lymphocytes and macrophages that exert an effective immune reaction against MNs (Figure 1) (92, 96–108, 120, 140, 173).

Here we review the state-of-art regarding this fascinating cellular communication, highlighting the current hypothesis that modulating the interaction of microglia with astrocytes and immune cells could represent a promising therapy. It is crucial to keep improving the biological knowledge of ALS and the interplay with resident and infiltrating immune cells in order to understand the cell-to-cell

communication mechanisms and their role in driving disease pathogenesis. At last, we discuss the current experimental approaches that aim to modulate microglial phenotype to modulate the inflammation in the CNS counteracting ALS progression.

The possibility to integrate these exciting discoveries with new combination therapies will open new tools to treat this devastating disease.

Author contributions

MC and GC wrote review. CL and SG supervised, wrote and edited the review. All authors contributed to the article and approved the submitted version.

Funding

SG was supported by A0112E0073 Funding Source: Regione Lazio POR FSE 2014–2020 PRATT25118; NextGenerationEU” DD. 3175/2021 E DD. 3138/2021 CN_3: National Center for Gene Therapy and Drugs based on RNA Technology Codice Progetto CN 00000041; RF GR-2021-12372494. G.C. was supported by NextGenerationEU” DD. 3175/2021 E DD. 3138/2021 CN_3: National Center for Gene Therapy and Drugs based on RNA Technology Codice Progetto CN 00000041. C.L. was supported by RF-2018-12366215; Next Generation EU PNRR Rome Technopole Flagship 7; Ateneo Sapienza “SEED” PNR 2022.

Conflict of interest

The authors declare that the research was conducted in the absence of any commercial or financial relationships that could be construed as a potential conflict of interest.

Publisher’s note

All claims expressed in this article are solely those of the authors and do not necessarily represent those of their affiliated organizations, or those of the publisher, the editors and the reviewers. Any product that may be evaluated in this article, or claim that may be made by its manufacturer, is not guaranteed or endorsed by the publisher.

References

1. Goutman SA, Hardiman O, Al-Chalabi A, Chió A, Savelieff MG, Kiernan MC, et al. Emerging insights into the complex genetics and pathophysiology of amyotrophic lateral sclerosis. *Lancet Neurol* (2022) 21:465–79. doi: 10.1016/S1474-4422(21)00414-2
2. Renton AE, Chio A, Traynor BJ. State of play in amyotrophic lateral sclerosis genetics. *Nat Neurosci* (2014) 17:17–23. doi: 10.1038/nn.3584
3. Keller MF, Ferrucci L, Singleton AB, Tienari PJ, Laaksovirta H, Restagno G, et al. Genome-wide analysis of the heritability of amyotrophic lateral sclerosis. *JAMA Neurol* (2014) 71:1123–34. doi: 10.1001/jamaneurol.2014.1184
4. Al-Chalabi A, Fang F, Hanby MF, Leigh PN, Shaw CE, Ye W, et al. An estimate of amyotrophic lateral sclerosis heritability using twin data. *J Neurol Neurosurg Psychiatry* (2010) 81:1324–6. doi: 10.1136/jnnp.2010.207464

5. Fang F, Kamel F, Lichtenstein P, Bellocco R, Sparén P, Sandler DP, et al. Familial aggregation of amyotrophic lateral sclerosis. *Ann Neurol* (2009) 66:94–9. doi: 10.1002/ana.21580
6. Rosen DR, Siddique T, Patterson D, Figlewicz DA, Sapp P, Hentati A, et al. Mutations in Cu/Zn superoxide dismutase gene are associated with familial amyotrophic lateral sclerosis. *Nature* (1993) 362:59–62. doi: 10.1038/362059a0
7. Chia R, Chio A, Traynor BJ. Novel genes associated with amyotrophic lateral sclerosis: diagnostic and clinical implications. *Lancet Neurol* (2018) 17:94–102. doi: 10.1016/S1474-4422(17)30401-5
8. Hayashi Y, Homma K, Ichijo H. SOD1 in neurotoxicity and its controversial roles in SOD1 mutation-negative ALS. *Adv Biol Regul* (2016) 60:95–104. doi: 10.1016/j.jbior.2015.10.006
9. McGeer PL, McGeer EG. Inflammatory processes in amyotrophic lateral sclerosis. *Muscle Nerve* (2002) 26:459–70. doi: 10.1002/mus.10191
10. Ferraiuolo L, Kirby J, Grierson AJ, Sendtner M, Shaw PJ. Molecular pathways of motor neuron injury in amyotrophic lateral sclerosis. *Nat Rev Neurol* (2011) 7:616–30. doi: 10.1038/nrneurol.2011.152
11. Hop PJ, Zwamborn RAJ, Hannon E, Shireby GL, Nabais MF, Walker EM, et al. Genome-wide study of DNA methylation shows alterations in metabolic, inflammatory, and cholesterol pathways in ALS. *Sci Transl Med* (2022) 14:eabj0264. doi: 10.1126/scitranslmed.abj0264
12. Dal Canto MC, Gurney ME. Development of central nervous system pathology in a murine transgenic model of human amyotrophic lateral sclerosis. *Am J Pathol* (1994) 145:1271–9.
13. Boillée S. Onset and progression in inherited ALS determined by motor neurons and microglia. *Science* (2006) 312:1389–92. doi: 10.1126/science.1123511
14. Bosco DA, Morfini G, Karabacak N.M, Song Y, Gros-Louis F, Pasinelli P, et al. Wild-type and mutant SOD1 share an aberrant conformation and a common pathogenic pathway in ALS. *Nat Neurosci* (2010) 13:1396–403. doi: 10.1038/nn.2660
15. Wegorzewska I. TDP-43 mutant mice develop features of ALS and frontotemporal lobar degeneration. *Proc Natl Acad Sci* (2009) 106:18809–14. doi: 10.1073/pnas.0908767106
16. Suk TR, Rousseaux MWC. The role of TDP-43 mislocalization in amyotrophic lateral sclerosis. *Mol Neurodegener* (2020) 15:45. doi: 10.1186/s13024-020-00397-1
17. Renton AE, Rousseaux MWC. A hexanucleotide repeat expansion in C9ORF72 is the cause of chromosome 9p21-linked ALS-FTD. *Neuron* (2011) 72:257–68. doi: 10.1016/j.neuron.2011.09.010
18. DeJesus-Hernandez M, Mackenzie IR, Boeve BF, Boxer AL, Baker M, Rutherford NJ, et al. Expanded GGGGCC hexanucleotide repeat in noncoding region of C9ORF72 causes chromosome 9p-linked FTD and ALS. *Neuron* (2011) 72:245–56. doi: 10.1016/j.neuron.2011.09.011
19. Ebbert MTW, Farrugia SL, Sens JP, Jansen-West K, Gendron TF, Prudencio M, et al. Long-read sequencing across the C9orf72 ‘GGGGCC’ repeat expansion: implications for clinical use and genetic discovery efforts in human disease. *Mol Neurodegener* (2018) 13:46. doi: 10.1186/s13024-018-0274-4
20. Ciura S, Lattante S, Le Ber I, Latouche M, Tostivint H, Brice A, et al. Loss of function of C9orf72 causes motor deficits in a zebrafish model of amyotrophic lateral sclerosis. *Ann Neurol* (2013) 74:180–7. doi: 10.1002/ana.23946
21. Therrien M, Rouleau GA, Dion PA, Parker JA. Deletion of C9ORF72 results in motor neuron degeneration and stress sensitivity in *C. elegans*. *PLoS One* (2013) 8:e83450. doi: 10.1371/journal.pone.0083450
22. Pelvig DP, Pakkenberg H, Stark AK, Pakkenberg B. Neocortical glial cell numbers in human brains. *Neurobiol Aging* (2008) 29:1754–62. doi: 10.1016/j.neurobiolaging.2007.04.013
23. Masuda T, Amann L, Monaco G, Sankowski R, Staszewski O, Krueger M, et al. Specification of CNS macrophage subsets occurs postnatally in defined niches. *Nature* (2022) 604:740–8. doi: 10.1038/s41586-022-04596-2
24. Lawson LJ, Perry VH, Dri P, Gordon S. Heterogeneity in the distribution and morphology of microglia in the normal adult mouse brain. *Neuroscience* (1990) 39:151–70. doi: 10.1016/0306-4522(90)90229-W
25. Ransohoff RM, Perry VH. Microglial physiology: unique stimuli, specialized responses. *Annu Rev Immunol* (2009) 27:119–45. doi: 10.1146/annurev.immunol.021908.132528
26. Bruttger J, Karraam K, Wörtge S, Regen T, Marini F, Hoppmann N, et al. Genetic cell ablation reveals clusters of local self-renewing microglia in the mammalian central nervous system. *Immunity* (2015) 43:92–106. doi: 10.1016/j.immuni.2015.06.012
27. Ransohoff RM. A polarizing question: do M1 and M2 microglia exist? *nat. Neurosci.* (2016) 19:987–91. doi: 10.1038/nn.4338
28. Hammond BP, Manek R, Kerr BJ, Macauley MS, Plemel JR. Regulation of microglia population dynamics throughout development, health, and disease. *Glia* (2021) 69(12):2771–97. doi: 10.1002/glia.24047
29. Hammond TR, Robinton D, Stevens B. Microglia and the brain: complementary partners in development and disease. *Annu Rev Cell Dev Biol* (2018) 34:523–44. doi: 10.1146/annurev-cellbio-100616-060509
30. Zia S, Rawji KS, Michaels NJ, Burr M, Kerr BJ, Healy LM, et al. Microglia diversity in health and multiple sclerosis. *Front Immunol* (2020) 11:588021. doi: 10.3389/fimmu.2020.588021
31. Masuda T, Sankowski R, Staszewski O, Prinz M. Microglia heterogeneity in the single-cell era. *Cell Rep* (2020) 30:1271–81. doi: 10.1016/j.celrep.2020.01.010
32. Deczkowska A, Amit I, Schwartz M. Microglial immune checkpoint mechanisms. *Nat Neurosci* (2018) 21:6. doi: 10.1038/s41593-018-0145-x
33. Brown GC, Neher JJ. Microglial phagocytosis of live neurons. *Nat Rev Neurosci* (2014) 15:209–16. doi: 10.1038/nrn3710
34. Schafer DP, Stevens B. Phagocytic glial cells: sculpting synaptic circuits in the developing nervous system. *Curr Opin Neurobiol* (2013) 23:1034–40. doi: 10.1016/j.conb.2013.09.012
35. Tremblay ME, Lowery RL, Majewska AK. Microglial interactions with synapses are modulated by visual experience. *PLoS Biol* (2010) 8:e1000527. doi: 10.1371/journal.pbio.1000527
36. Paolicelli RC, Bolas G, Pagani F, Maggi L, Scianni M, Panzanelli P, et al. Synaptic pruning by microglia is necessary for normal brain development. *Science* (2011) 333:1456–8. doi: 10.1126/science.1202529
37. Hughes AN, Appel B. Microglia phagocytose myelin sheaths to modify developmental myelination. *Nat Neurosci* (2020) 23(9):1055–1066. doi: 10.1038/s41593-020-0654-2
38. Lloyd AF, Davies CL, Holloway RK, Labrak Y, Ireland G, Carradori D, et al. Central nervous system regeneration is driven by microglia necroptosis and repopulation. *Nat Neurosci* (2021) 22(7):1046–1052. doi: 10.1038/s41593-019-0418-z
39. Moore CS, Ase AR, Kinsara A, Rao VTS, Michell-Robinson M, Leong SY, et al. P2Y12 expression and function in alternatively activated human microglia. *Neuro Immunoinflamm* (2015) 2:e80. doi: 10.1212/NXI.0000000000000080
40. Riaz K, Galic MA, Kentner AC, Reid AY, Sharkey KA, Pittman QJ, et al. Microglia-dependent alteration of glutamatergic synaptic transmission and plasticity in the hippocampus during peripheral inflammation. *J Neurosci* (2015) 35:4942–52. doi: 10.1523/JNEUROSCI.4485-14.2015
41. Naj AC, Naj AC, Jun G, Reitz C, Kunkle BW, Perry W, et al. Effects of multiple genetic loci on age at onset in late-onset Alzheimer disease: a genome-wide association study. *JAMA Neurol* (2014) 71:1394–404. doi: 10.1001/jamaneurol.2014.1491
42. Butovsky O, Weiner HL. Microglial signatures and their role in health and disease. *Nat Rev Neurosci* (2018) 19:622–35. doi: 10.1038/s41583-018-0057-5
43. Masuda T, Sankowski R, Staszewski O, Bottcher C, Amann LSagar, et al. Spatial and temporal heterogeneity of mouse and human microglia at single-cell resolution. *Nature* (2019) 566(7744):388–392. doi: 10.1038/s41586-019-0924-x
44. Krasemann S, Madore C, Cialic R, Baufeld C, Calcagno N, El Fatimy R, et al. The TREM2-APOE pathway drives the transcriptional phenotype of dysfunctional microglia in neurodegenerative diseases. *Immunity* (2017) 47(3):566–581 e569. doi: 10.1016/j.immuni.2017.08.008
45. Wyss-Coray T, Rogers J. Inflammation in Alzheimer disease—a brief review of the basic science and clinical literature. *Cold Spring Harb Perspect Med* (2012) 2:a006346. doi: 10.1101/cshperspect.a006346
46. Leng F, Edison P. Neuroinflammation and microglial activation in Alzheimer disease: where do we go from here? *Nat Rev Neurol* (2020) 17:157–172. doi: 10.1038/s41582-020-00435-y
47. Gushchina S, Pryce G, Yip PK, Wu D, Pallier P, Giovannoni G, et al. Increased expression of colony-stimulating factor-1 in mouse spinal cord with experimental autoimmune encephalomyelitis correlates with microglial activation and neuronal loss. *Glia* (2018) 66(10):2108–2125. doi: 10.1002/glia.23464
48. Hickman SE, Allison EK, El Khoury J. Microglial dysfunction and defective beta-amyloid clearance pathways in aging Alzheimer’s disease mice. *J Neurosci* (2008) 28:8354–60. doi: 10.1523/JNEUROSCI.0616-08.2008
49. Liao B, Zhao W, Beers DR, Henkel JS, Appel SH. Transformation from a neuroprotective to a neurotoxic microglial phenotype in a mouse model of ALS. *Exp Neurol* (2012) 237:147–52. doi: 10.1016/j.expneurol.2012.06.011
50. Muzio L, Martino G, Furlan R. Multifaceted aspects of inflammation in multiple sclerosis: the role of microglia. *J Neuroimmunol* (2007) 191:39–44. doi: 10.1016/j.jneuroim.2007.09.016
51. El Khoury J, Hickman SE, Thomas CA, Cao L, Silverstein SC, Loike JD. Scavenger receptor-mediated adhesion of microglia to beta-amyloid fibrils. *Nature* (1996) 382:716–9. doi: 10.1038/382716a0
52. Hickman SE, Kingery ND, Ohsumi TK, Borowsky ML, Wang L, Means TK, et al. The microglial sensome revealed by direct RNA sequencing. *Nat Neurosci* (2013) 16:1896–905. doi: 10.1038/nn.3554
53. Saijo K, Crotti A, Glass CK. Regulation of microglia activation and deactivation by nuclear receptors. *Glia* (2013) 61:104–11. doi: 10.1002/glia.22423
54. Heneka MT, Golenbock DT, Latz E. Innate immunity in Alzheimer’s disease. *Nat Immunol* (2015) 16:229–36. doi: 10.1038/ni.3102
55. Wu J, Chen ZJ. Innate immune sensing and signaling of cytosolic nucleic acids. *Annu Rev Immunol* (2014) 32:461–88. doi: 10.1146/annurev-immunol-032713-120156
56. Areschoug T, Gordon S. Scavenger receptors: role in innate immunity and microbial pathogenesis. *Cell Microbiol* (2009) 11:1160–9. doi: 10.1111/j.1462-5822.2009.01326.x
57. Appel SH, Zhao W, Beers DR, Henkel JS. The microglial-motoneuron dialogue in ALS. *Acta Myol* (2011) 30:4–8.

58. Ransohof RM, El Khoury J. Microglia in health and disease. *Cold Spring Harb Perspect Biol* (2015) 8:a020560. doi: 10.1101/cshperspect.a020560
59. Hickman S, Izzy S, Sen P, Morsett L, El Khoury J. Microglia in neurodegeneration. *Nat Neurosci* (2018) 21:1359–69. doi: 10.1038/s41593-018-0242-x
60. Bemiller SM, McCray TJ, Allan K, Formica SV, Xu G, Wilson G, et al. TREM2 deficiency exacerbates tau pathology through dysregulated kinase signaling in a mouse model of tauopathy. *Mol Neurodegener* (2017) 12:74. doi: 10.1186/s13024-017-0216-6
61. Jonsson T, Stefansson H, Steinberg S, Jonsdottir I, Jonsson PV, Snaedal J, et al. Variant of TREM2 associated with the risk of alzheimer's disease. *N Engl J Med* (2013) 368:107–16. doi: 10.1056/NEJMoa1211103
62. Ghosh R, Tabrizi SJ. Huntington disease. *Handb Clin Neurol* (2018) 147:255–78. doi: 10.1016/B978-0-444-63233-3.00017-8
63. Corcia P, Tauber C, Vercoullie J, Arlicot N, Prunier C, Praline J, et al. Molecular imaging of microglial activation in amyotrophic lateral sclerosis. *PLoS One* (2012) 7: e52941. doi: 10.1371/journal.pone.0052941
64. Brites D, Vaz AR. Microglia centered pathogenesis in ALS: insights in cell interconnectivity. *Front Cell Neurosci* (2014) 8:117. doi: 10.3389/fncel.2014.00117
65. Ransohoff RM, Schafer D, Vincent A, Blachere NE, Bar-Or A. Neuroinflammation: ways in which the immune system affects the brain. *Neurotherapeutics* (2015) 12:896–909. doi: 10.1007/s13311-015-0385-3
66. Henkel JS, Engelhardt JJ, Siklos L, Simpson EP, Kim SH, Pan T, et al. Presence of dendritic cells, MCP-1, and activated microglia/macrophages in amyotrophic lateral sclerosis spinal cord tissue. *Ann Neurol* (2004) 55:221–35. doi: 10.1002/ana.10805
67. Turner MR, Cagnin A, Turkheimer FE, Miller CC, Shaw CE, Brooks DJ, et al. Evidence of widespread cerebral microglial activation in amyotrophic lateral sclerosis: an [¹¹C](R)-PK11195 positron emission tomography study. *Neurobiol Dis* (2004) 15:601–9. doi: 10.1016/j.nbd.2003.12.012
68. Zurcher NR, Loggia ML, Lawson R, Chonde DB, Izquierdo-Garcia D, et al. Increased in vivo glial activation in patients with amyotrophic lateral sclerosis: assessed with [¹¹C]-PBR28. *NeuroImage Clin* (2015) 7:409–14. doi: 10.1016/j.nicl.2015.01.009
69. Chiu I, Morimoto EA, Goodarzi H, Liao J, O'Keefe S, Phatnani H, et al. A neurodegeneration-specific gene-expression signature of acutely isolated microglia from an amyotrophic lateral sclerosis mouse model. *Cell Rep* (2013) 4(2):385–401. doi: 10.1016/j.celrep.2013.06.018
70. Clarke BE, Patani R. The microglial component of amyotrophic lateral sclerosis. *Brain* (2020) 123:3526–39. doi: 10.1093/brain/awaa309
71. Beers DR. Neuroinflammation modulates distinct regional and temporal clinical responses in ALS mice. *Brain Behav Immun* (2011) 25:1025–35. doi: 10.1016/j.bbi.2010.12.008
72. Beers DR, Henkel JS, Xiao Q, Zhao W, Wang J, Yen AA, et al. Wild-type microglia extend survival in PU.1 knockout mice with familial amyotrophic lateral sclerosis. *Proc Natl Acad Sci U.S.A.* (2006) 103(43):16021–6.
73. Salter MW. Microglia emerge as central players in brain disease. *Nat Med* (2017) 23:1018–27. doi: 10.1038/nm.4397
74. Deczkowska A. Disease-associated microglia: a universal immune sensor of neurodegeneration. *Cell* (2018) 173:1073–81. doi: 10.1016/j.cell.2018.05.003
75. Frakes AE, Ferraiuolo L, Haidet-Phillips AM, Schmelzer L, Braun L, Miranda CJ, et al. Microglia induce motor neuron death via the classical NF- κ B pathway in amyotrophic lateral sclerosis. *Neuron* (2014) 81:1009–23. doi: 10.1016/j.neuron.2014.01.013
76. Thonhoff JR, Gao J, Dunn TJ, Ojeda L, Wu P. Mutant SOD1 microglia-generated nitrooxidative stress promotes toxicity to human fetal neural stem cell-derived motor neurons through direct damage and noxious interactions with astrocytes. *Am J Stem Cells* (2011) 19:2–21.
77. Coccoza G, Garofalo S, Morotti M, Chece G, Grimaldi A, Lecce M, et al. The feeding behaviour of amyotrophic lateral sclerosis mouse models is modulated by the Ca²⁺-activated K⁺ channels modulate microglia affecting motor neuron survival in hSOD1G93A mice. *Brain Behav Immun* (2021) 178(24):4891–906. doi: 10.1111/bph.15665
78. Parisi C, Arisi I, D'Ambrosi N, Storti AE, Brandi R, D'Onofrio M, et al. Dysregulated microRNAs in amyotrophic lateral sclerosis microglia modulate genes linked to neuroinflammation. *Cell Death Dis* (2013) 12:e959. doi: 10.1038/cddis.2013.491
79. Coccoza G, di Castro MA, Carbonari L, Grimaldi A, Antonangeli F, Garofalo S, et al. Ca²⁺-activated K⁺ channels modulate microglia affecting motor neuron survival in hSOD1G93A mice. *Brain Behav Immun* (2018) 73:584–95. doi: 10.1016/j.bbi.2018.07.002
80. Spiller KJ, Restrepo CR, Khan T, Dominique MA, Fang TC, Canter RG, et al. Microglia-mediated recovery from ALS-relevant motor neuron degeneration in a mouse model of TDP-43 proteinopathy. *Nat Neurosci* (2018) 21:329–40. doi: 10.1038/s41593-018-0083-7
81. Majounie E, Renton AE, Mok K, Doppler EG, Waite A, Rollinson S, et al. Frequency of the C9orf72 hexanucleotide repeat expansion in patients with amyotrophic lateral sclerosis and frontotemporal dementia: a cross-sectional study. *Lancet Neurol* (2012) 11:323–30. doi: 10.1016/S1474-4422(12)70043-1
82. Belzil VV, Bauer PO, Prudencio M, Gendron TF, Stetler CT, Yan IK, et al. Reduced C9orf72 gene expression in c9FTD/ALS is caused by histone trimethylation, an epigenetic event detectable in blood. *Acta Neuropathol* (2013) 126:895–905. doi: 10.1007/s00401-013-1199-1
83. Gijssels I, Van Langenhove T, van der Zee J, Slegers K, Philtjens S, Kleinberger G, et al. A C9orf72 promoter repeat expansion in a Flanders-Belgian cohort with disorders of the frontotemporal lobar degeneration-amyotrophic lateral sclerosis spectrum: a gene identification study. *Lancet Neurol* (2012) 11:54–65. doi: 10.1016/S1474-4422(11)70261-7
84. Fratta P, Poulter M, Lashley T, Rohrer JD, Polke J, Beck J, et al. Homozygosity for the C9orf72 GGGGCC repeat expansion in frontotemporal dementia. *Acta Neuropathol* (2013) 126:401–9. doi: 10.1007/s00401-013-1147-0
85. Xi Z, Zinman L, Moreno D, Schymick J, Liang Y, Sato C, et al. Hypermethylation of the CpG island near the G4C2 repeat in ALS with a C9orf72 expansion. *Am J Hum Genet* (2013) 92:981–9. doi: 10.1016/j.ajhg.2013.04.017
86. Waite AJ, Baumer D, East S, Neal J, Morris HR, Ansorge O, et al. Reduced C9orf72 protein levels in frontal cortex of amyotrophic lateral sclerosis and frontotemporal degeneration brain with the C9ORF72 hexanucleotide repeat expansion. *Neurobiol Aging* (2014) 35:1779.e5–1779.e13. doi: 10.1016/j.neurobiolaging.2014.01.016
87. O'Rourke JG, Bogdanik L, Yáñez A, Lall D, Wolf AJ, Muhammad AKMG, et al. C9orf72 is required for proper macrophage and microglial function in mice. *Science* (2016) 351:1324–9. doi: 10.1126/science.aaf1064
88. Donnelly CJ, Zhang PW, Pham JT, Haeusler AR, Mistry NA, Videny S, et al. RNA Toxicity from the ALS/FTD C9ORF72 expansion is mitigated by antisense intervention. *Neuron* (2013) 80:415–28. doi: 10.1016/j.neuron.2013.10.015
89. Sareen D, O'Rourke JG, Meera P, Muhammad AKMG, Grant S, Simpkinson M, et al. Targeting RNA foci in iPSC-derived motor neurons from ALS patients with a C9ORF72 repeat expansion. *Sci Trans Med* (2013) 5:208ra149. doi: 10.1126/scitranslmed.3007529
90. Ash PEA, Bieniek KF, Gendron TF, Caulfield T, Lin WL, DeJesus-Hernandez M, et al. Unconventional translation of C9ORF72 GGGGCC expansion generates insoluble polypeptides specific to c9FTD/ALS. *Neuron* (2013) 77:639–46. doi: 10.1016/j.neuron.2013.02.004
91. Zu T, Liu Y, Banez-Coronel M, Reid T, Pletnikova O, Lewis J, et al. RAN proteins and RNA foci from antisense transcripts in C9ORF72 ALS and frontotemporal dementia. *Proc Natl Acad Sci USA* (2013) 110:E4968–77. doi: 10.1073/pnas.1315438110
92. Liddelow SA, Guttenplan KA, Clarke LE, Bennett FC, Bohlen CJ, Schirmer L, et al. Neurotoxic reactive astrocytes are induced by activated microglia. *Nature* (2017) 541:481–7. doi: 10.1038/nature21029
93. Phani S, Re DB, Przedborski S. The role of the innate immune system in ALS. *Front Pharmacol* (2012) 3:150. doi: 10.3389/fphar.2012.00150
94. Kawamata T, Akiyama H, Yamada T, McGee PL. Immunologic reactions in amyotrophic lateral sclerosis brain and spinal cord tissue. *Am J Pathol* (1992) 140:691–707.
95. Schiffer D, Cordera S, Cavalla P, Migheli A. Reactive astrogliosis of the spinal cord in amyotrophic lateral sclerosis. *J Neurol Sci* (1996) 139:27–33. doi: 10.1016/0022-510X(96)00073-1
96. Nagy D, Kato T, Kushner PD. Reactive astrocytes are widespread in the cortical gray matter of amyotrophic lateral sclerosis. *J Neurosci Res* (1994) 38:336–47. doi: 10.1002/jnr.490380312
97. Johansson A, Engler H, Blomquist G, Scott B, Wall A, et al. Evidence for astrogliosis in ALS demonstrated by [¹¹C](L)-deprenyl-D2 PET. *J Neurol Sci* (2007) 255:17–22. doi: 10.1016/j.jns.2007.01.057
98. Ouali Alami N, Schurr C, Olde Heuvel F, Tang L, Li Q, Tasdogan A, et al. NF- κ B activation in astrocytes drives a stage-specific beneficial neuroimmunological response in ALS. *EMBO J* (2018) 37:e98697. doi: 10.15252/embj.201798697
99. Guttenplan KA, Weigel MK, Adler DI, Couthouis J, Liddelow SA, Gitler AD, et al. Knockout of reactive astrocyte activating factors slows disease progression in an ALS mouse model. *Nat Commun* (2020) 11:3753. doi: 10.1038/s41467-020-17514-9
100. Peng AYT, et al. Loss of TDP-43 in astrocytes leads to motor deficits by triggering A1-like reactive phenotype and triglia dysfunction. *Proc Natl Acad Sci USA* (2020) 117:29101–12. doi: 10.1073/pnas.2007806117
101. Liang LL, Zhu B, Zhao Y, Li X, Liu T, Pina-Crespo J, et al. Membralin deficiency dysregulates astrocytic glutamate homeostasis leading to ALS-like impairment. *J Clin Invest* (2019) 129:3103–20. doi: 10.1172/JCI127695
102. Alexianu ME, Kozovska M, Appel SH. Immune reactivity in a mouse model of familial ALS correlates with disease progression. *Neurology* (2001) 57:1282–9. doi: 10.1212/WNL.57.7.1282
103. Yang WW, Sidman RL, Taksir TV, Treleaven CM, Fidler JA, Cheng SH. Relationship between neuropathology and disease progression in the SOD1(G93A) ALS mouse. *Exp Neurol* (2011) 227:287–95. doi: 10.1016/j.expneurol.2010.11.019
104. Endo F, Komine O, Fujimori-Tonou N, Katsuno M, Jin S, Watanabe S, et al. Astrocyte-derived TGF- β 1 accelerates disease progression in ALS mice by interfering with the neuroprotective functions of microglia and T cells. *Cell Rep* (2015) 11(4):592–604. doi: 10.1016/j.celrep.2015.03.053
105. Brites D. The evolving landscape of neurotoxicity by unconjugated bilirubin: role of glial cells and inflammation. *Front Pharmacol* (2012) 3:88. doi: 10.3389/fphar.2012.00088
106. Meme W, Calvo CF, Froger N, Ezan P, Amigou E, Koulakoff A, et al. Proinflammatory cytokines released from microglia inhibit gap junctions in astrocytes: potentiation by beta-amyloid. *FASEB J* (2006) 20:494–6. doi: 10.1096/fj.05-4297fje

107. Murdock BJ, Zhou T, Kashlan SR, Little RJ, Goutman SA, Feldman EL. Correlation of peripheral immunity with rapid amyotrophic lateral sclerosis progression. *JAMA Neurol* (2017) 74(12):1446–54. doi: 10.1001/jamaneurol.2017.2255
108. Garofalo S, Coccoza G, Porzia A, Inghilleri M, Raspa M, Scavizzi F, et al. Natural killer cells modulate motor neuron-immune cell cross talk in models of amyotrophic lateral sclerosis. *Nat Commun* (2020) 11(1):1773. doi: 10.1038/s41467-020-15644-8
109. Garofalo S, Coccoza G, Bernardini G, Savage J, Raspa M, Aronica E, et al. Blocking immune cell infiltration of the central nervous system to tame neuroinflammation in amyotrophic lateral sclerosis. *Brain Behav Immun* (2022) 105:1–14. doi: 10.1016/j.bbi.2022.06.004
110. Yu Y, Schürpf T, Springer TA. How natalizumab binds and antagonizes $\alpha 4$ integrins. *J Biol Chem* (2013) 288(1):23214–25. doi: 10.1074/jbc.M113.501668
111. Gan Y, Liu R, Wu W, Bompreszi R, Shi FD. Antibody to $\alpha 4$ integrin suppresses natural killer cells infiltration in central nervous system in experimental autoimmune encephalomyelitis. *J Neuroimmunol* (2012) 247:9–15. doi: 10.1016/j.jneuroim.2012.03.011
112. Engelhardt B, Ransohoff RM. The ins and outs of T-lymphocyte trafficking to the CNS: anatomical sites and molecular mechanisms. *Trends Immunol* (2005) 26(9):485–95. doi: 10.1016/j.it.2005.07.004
113. Matejuk A, Vandenbark AA, Offner H. Cross-talk of the CNS with immune cells and functions in health and disease. *Front Neurol* (2021) 12:672455. doi: 10.3389/fneur.2021.672455
114. Engelhardt JI, Tajti J, Appel SH. Lymphocytic infiltrates in the spinal cord in amyotrophic lateral sclerosis. *Arch Neurol* (1993) 50:30–6. doi: 10.1001/archneur.1993.00540010026013
115. Fiala M, Chattopadhyay M, La Cava A, Tse E, Liu G, Lourenco E, et al. IL-17A is increased in the serum and in spinal cord CD8 and mast cells of ALS patients. *J Neuroinflammation* (2010) 7:76. doi: 10.1186/1742-2094-7-76
116. Beers DR, Henkel JS, Zhao W, Wang J, Appel SH. CD4+ T cells support glial neuroprotection, slow disease progression, and modify glial morphology in an animal model of inherited ALS. *Proc Natl Acad Sci USA* (2008) 105:15558–63. doi: 10.1073/pnas.0807419105
117. Chiu IM, Chen A, Zheng Y, Kosaras B, Tsiftoglou SA, et al. T Lymphocytes potentiate endogenous neuroprotective inflammation in a mouse model of ALS. *Proc Natl Acad Sci USA* (2008) 105:17913–8. doi: 10.1073/pnas.0804610105
118. Kipnis J, Schwartz M. Controlled autoimmunity in CNS maintenance and repair: naturally occurring CD4+CD25+ regulatory T cells at the crossroads of health and disease. *Neuromol Med* (2005) 7:197–206. doi: 10.1385/NMM:7:3:197
119. Coque E, Salsac C, Espinosa-Carrasco G, Varga B, Degauque N, Cadoux M, et al. Cytotoxic CD8+ T lymphocytes expressing ALS-causing SOD1 mutant selectively trigger death of spinal motoneurons. *Proc Natl Acad Sci U S A* (2019) 116(6):2312–7. doi: 10.1073/pnas.1815961116
120. Nardo G, Trolese MC, Verderio M, Mariani A, De Paola M, Riva N, et al. Counteracting roles of MHCI and CD8+ T cells in the peripheral and central nervous system of ALS SOD1G93A mice. *Mol Neurodegener* (2018) 13(1):42. doi: 10.1186/s13024-018-0271-7
121. Hirahara K, Nakayama T. CD4+ T-cell subsets in inflammatory diseases: beyond the Th1/Th2 paradigm. *Int Immunol* (2016) 28(4):163–71. doi: 10.1093/intimm/dxw006
122. Beers DR, Henkel JS, Zhao W, Wang J, Huang A, Wen S, et al. Endogenous regulatory T lymphocytes ameliorate amyotrophic lateral sclerosis in mice and correlate with disease progression in patients with amyotrophic lateral sclerosis. *Brain* (2011) 134(Pt 5):1293–314. doi: 10.1093/brain/awr074
123. Beers DR, Zhao W, Wang J, Zhang X, Wen S, Neal D, et al. ALS patients' regulatory T lymphocytes are dysfunctional, and correlate with disease progression rate and severity. *JCI Insight* (2017) 2:e89530. doi: 10.1172/jci.insight.89530
124. Henkel JS, Beers DR, Zhao W, Appel SH. Microglia in ALS: the good, the bad, and the resting. *J Neuroimmune Pharmacol* (2009) 4:389–98. doi: 10.1007/s11481-009-9171-5
125. Cardona AE, Pioro EP, Sasse ME, Kostenko V, Cardona SM, Dijkstra IM, et al. Control of microglial neurotoxicity by the fractalkine receptor. *Nat Neurosci* (2006) 9:917–24. doi: 10.1038/nn1715
126. Henkel JS, Beers DR, Wen S, Rivera AL, Toennis KM, Appel JE, et al. Regulatory T-lymphocytes mediate amyotrophic lateral sclerosis progression and survival. *EMBO Mol Med* (2013) 5(1):64–79. doi: 10.1002/emmm.201201544
127. Thonhoff JR, Simpson EP, Appel SH. Neuroinflammatory mechanisms in amyotrophic lateral sclerosis pathogenesis. *Curr Opin Neurol* (2018) 31(5):635–9. doi: 10.1097/WCO.0000000000000599
128. Liu G, Ma H, Qiu L, Li L, Cao Y, Ma J, et al. Phenotypic and functional switch of macrophages induced by regulatory CD4+CD25+ T cells in mice. *Immunol Cell Biol* (2011) 89:130–42. doi: 10.1038/icb.2010.70
129. Tiemessen MM, Jagger AL, Evans HG, van Herwijnen MJ, John S, Taams LS. CD4+CD25+Foxp3+ regulatory T cells induce alternative activation of human monocytes/macrophages. *Proc Natl Acad Sci USA* (2007) 104:19446–51. doi: 10.1073/pnas.0706832104
130. Savage NDL, de Boer T, Walburg KV, Joosten SA, van Meijgaarden K, Geluk A, et al. Human anti-inflammatory macrophages induce Foxp3+GITR+CD25+ regulatory T cells, which suppress via membrane-bound TGF- β 1. *J Immunol* (2008) 181:2220–6. doi: 10.4049/jimmunol.181.3.2220
131. Gao Z, Tsirka SE. Animal models of MS reveal multiple roles of microglia in disease pathogenesis. *Neurol Res Int* (2011) 2011:383087. doi: 10.1155/2011/383087
132. Zhao W, Beers DR, Appel SH. Immune-mediated mechanisms in the pathogenesis of amyotrophic lateral sclerosis. *J Neuroimmune Pharmacol* (2013) 8:888–99. doi: 10.1007/s11481-013-9489-x
133. Rentzos M, Evangelopoulos E, Sereti E, Zouvelou V, Marmara S, Alexakis T, et al. Alterations of T cell subsets in ALS: a systemic immune activation? *Acta Neurol Scand* (2012) 125(4):260–4. doi: 10.1111/j.1600-0404.2011.01528.x
134. Liu Z, Cheng X, Zhong S, Zhang X, Liu C, Liu F, et al. Peripheral and central nervous system immune response crosstalk in amyotrophic lateral sclerosis. *Front Neurosci* (2020) 14:575. doi: 10.3389/fnins.2020.00575
135. Zhao W, Beers DR, Hooten KG, Sieglaff DH, Zhang A, Kalyana-Sundaram S, et al. Characterization of gene expression phenotype in amyotrophic lateral sclerosis monocytes. *JAMA Neurol* (2017) 74:677–85. doi: 10.1001/jamaneurol.2017.0357
136. Zhang R, Gascon R, Miller RG, Gelinas DF, Mass J, Hadlock K, et al. Evidence for systemic immune system alterations in sporadic amyotrophic lateral sclerosis (sALS). *J Neuroimmunol* (2005) 159(1–2):215–24. doi: 10.1016/j.jneuroim.2004.10.009
137. Butovsky O, Siddiqui S, Gabrieli G, Lanser AJ, Dake B, Murugaiyan G, et al. Modulating inflammatory monocytes with a unique microRNA gene signature ameliorates murine ALS. *J Clin Invest* (2012) 122:3063–87. doi: 10.1172/jci62636
138. Geissmann F, Jung S, Littman DR. Blood monocytes consist of two principal subsets with distinct migratory properties. *Immunity* (2003) 19:71–82. doi: 10.1016/S1074-7613(03)00174-2
139. Mosser DM, Edwards JP. Exploring the full spectrum of macrophage activation. *Nat Rev Immunol* (2008) 8(12):958–69. doi: 10.1038/nri2448
140. Chiot A, Zaidi S, Iltis C, Ribon M, Berriat F, Schiaffino L, et al. Modifying macrophages at the periphery has the capacity to change microglial reactivity and to extend ALS survival. *Nat Neurosci* (2020) 23(11):1339–51. doi: 10.1038/s41593-020-00718-z
141. Morgan S, Orrell RW. Pathogenesis of amyotrophic lateral sclerosis. *Br Med Bull* (2016) 119(1):87–98. doi: 10.1093/bmb/ldw026
142. Liscic RM, Alberici A, Cairns NJ, Romano M, Buratti E. From basic research to the clinic: innovative therapies for ALS and FTD in the pipeline. *Mol Neurodegener* (2020) 15(1):31. doi: 10.1186/s13024-020-00373-9
143. Doble A. The pharmacology and mechanism of action of riluzole. *Neurology* (1996) 47(6 Suppl 4):S233–41. doi: 10.1212/wnl.47.6_suppl_4.233s
144. Cheah BC, Vucic S, Krishnan AV, Kiernan MC. Riluzole, neuroprotection and amyotrophic lateral sclerosis. *Curr Med Chem* (2010) 17(18):1942–199. doi: 10.2174/092986710791163939
145. Takei K, Watanabe K, Yuki S, Akimoto M, Sakata T, Palumbo J. Ederavone and its clinical development for amyotrophic lateral sclerosis. *Amyotroph Lateral Scler Frontotemporal Degener* (2017) 18(sup1):5–10. doi: 10.1080/21678421.2017.1353101
146. Petrov D, Mansfield C, Moussy A, Hermine O. ALS clinical trials review: 20 years of failure. are we any closer to registering a new treatment? *Front Aging Neurosci* (2017) 9:68. doi: 10.3389/fnagi.2017.00068
147. Liu J, Wang F. Role of neuroinflammation in amyotrophic lateral sclerosis: cellular mechanisms and therapeutic implications. *Front Immunol* (2017) 8:1005. doi: 10.3389/fimmu.2017.01005
148. Luo R, Wangqin R, Zhu L, Bi W. Neuroprotective mechanisms of 3-n-butylphthalide in neurodegenerative diseases. *BioMed Rep* (2019) 11(6):235–40. doi: 10.3892/br.2019.1246
149. Feng X, Peng Y, Liu M, Cui L. DL-3-n-butylphthalide extends survival by attenuating glial activation in a mouse model of amyotrophic lateral sclerosis. *Neuropharmacology* (2012) 62(2):1004–10. doi: 10.1016/j.neuropharm.2011.10.009
150. Zhou QM, Zhang JJ, Li S, Chen S, Le WD. N-butylidenephthalide treatment prolongs life span and attenuates motor neuron loss in SOD1G93A mouse model of amyotrophic lateral sclerosis. *CNS Neurosci Ther* (2017) 23(5):375–85. doi: 10.1111/cns.12681
151. Liu M, Yao X, Huang X, Shang H, Fan D, He J, et al. A multicenter, randomized, double blind, placebo-controlled clinical trial of DL-3-n-butylphthalide in treatment of amyotrophic lateral sclerosis. *Randomized Controlled Trial Chin Med J (Engl)* 136(3):354–356. doi: 10.1097/CM9.00000000000002442
152. Bilsland LG, Greensmith L. The endocannabinoid system in amyotrophic lateral sclerosis. *Curr Pharm Des* (2008) 14(23):2306–16. doi: 10.2174/138161208785740081
153. Giacompo S, Mazzon E. Can cannabinoids be a potential therapeutic tool in amyotrophic lateral sclerosis? *Neural Regener Res* (2016) 11(12):1896–9. doi: 10.4103/1673-5374.197125
154. Felder CC, Joyce KE, Briley EM, Mansouri J, Mackie K, Blond O, et al. Comparison of the pharmacology and signal transduction of the human cannabinoid CB1 and CB2 receptors. *Mol Pharmacol* (1995) 48(3):443–50.
155. Bilsland LG, Dick JR, Pryce G, Petrosino S, Di Marzo D, Baker D, et al. Increasing cannabinoid levels by pharmacological and genetic manipulation delays disease progression in SOD1 mice. *FASEB J* (2006) 20(7):1003–5. doi: 10.1096/fj.05-4743fj
156. Shoemaker JL, Seely KA, Reed RL, Crow JP, Prather PL. The CB2 cannabinoid agonist AM-1241 prolongs survival in a transgenic mouse model of amyotrophic lateral

sclerosis when initiated at symptom onset. *J Neurochem* (2007) 101(1):87–98. doi: 10.1111/j.1471-4159.2006.04346.x

157. Urbi B, Owusu MA, Hughes I, Katz M, Broadley S, Sabet A. Effects of cannabinoids in amyotrophic lateral sclerosis (ALS) murine models: a systematic review and meta-analysis. *J Neurochem* (2019) 149(2):284–97. doi: 10.1111/jnc.14639

158. Mizuno T, Kurotani T, Komatsu Y, Kawanokuchi J, Kato H, Mitsuma N, et al. Neuroprotective role of phosphodiesterase inhibitor ibudilast on neuronal cell death induced by activated microglia. *Neuropharmacology*. (2004) 46(3):404–11. doi: 10.1016/j.neuropharm.2003.09.009

159. Oskarsson B, Maragakis N, Bedlack RS, Goyal N, Meyer JA, Gengeet A, et al. MN-166 (ibudilast) in amyotrophic lateral sclerosis in a phase IIb/III study: COMBAT-ALS study design. *Neurodegener Dis Manage* (2021) 11(6):431–43. doi: 10.2217/nmt-2021-0042

160. Trias E, Ibarburu S, Barreto-Núñez R, Babdor J, Maciel TT, Guillo M, et al. Post-paralysis tyrosine kinase inhibition with masitinib abrogates neuroinflammation and slows disease progression in inherited amyotrophic lateral sclerosis. *J Neuroinflammation* (2016) 13(1):177. doi: 10.1186/s12974-016-0620-9

161. Mora JS, Genge A, Chio A, Estol CJ, Chaverri D, Hernández M, et al. Masitinib as an add-on therapy to riluzole in patients with amyotrophic lateral sclerosis: a randomized clinical trial. *Amyotroph Lateral Scler Frontotemporal Degener* (2020) 21(1–2):5–14. doi: 10.1080/21678421.2019.1632346

162. Mora JS, Bradley WG, Chaverri D, Hernández-Barral M, Mascias J, Gamez J, et al. Long-term survival analysis of masitinib in amyotrophic lateral sclerosis. *Ther Adv Neurol Disord* (2021) 14:17562864211030365. doi: 10.1177/17562864211030365

163. Yrjänheikki J, Keinänen R, Pellikka M, Hökfelt T, Koistinaho J. Tetracyclines inhibit microglial activation and are neuroprotective in global brain ischemia. *Proc Natl Acad Sci U S A* (1998) 95(26):15769–74. doi: 10.1073/pnas.95.26.15769

164. Zhu S, Stavrovskaya IG, Drozda M, Kim BYS, Ona V, Li M, et al. Minocycline inhibits cytochrome c release and delays progression of amyotrophic lateral sclerosis in mice. *Nature*. (2002) 417(6884):74–8. doi: 10.1038/417074a

165. Van Den Bosch L, Tilkin P, Lemmens G, Robberecht W. Minocycline delays disease onset and mortality in a transgenic model of ALS. *Neuroreport* (2002) 13:1067–70. doi: 10.1097/00001756-200206120-00018

166. Kriz J, Nguyen MD, Julien JP. Minocycline slows disease progression in a mouse model of amyotrophic lateral sclerosis. *Neurobiol Dis* (2002) 10(3):268–78. doi: 10.1006/nbdi.2002.0487

167. Gordon PH, Moore DH, Miller RG, Florence JM, Verheijde JL, Doorish C, et al. Efficacy of minocycline in patients with amyotrophic lateral sclerosis: a phase III randomised trial. *Lancet Neurol* (2007) 6(12):1045–53. doi: 10.1016/S1474-4422(07)70270-3

168. McGrath MS, Kahn JO, Herndier BG. Development of WF10, a novel macrophage-regulating agent. *Curr Opin Investig Drugs* (2002) 3:365–73.

169. McGrath MS, Miller RG. Development of macrophage activation regulator NP001 for ALS. proceedings of the 21st international symposium on ALS/MND, in: *Clinical Work in Progress*, Orlando, USA, 2010 Dec 11–13.

170. Miller RG, Zhang R, Block G, Katz J, Barohn R, Kasarskis E, et al. NP001 regulation of macrophage activation markers in ALS: a phase I clinical and biomarker study. *Amyotroph Lateral Scler Frontotemporal Degener* (2014) 15(7–8):601–9. doi: 10.3109/21678421.2014.951940

171. Miller RG, Block G, Katz JS, Barohn RJ, Gopalakrishnan V, Cudkowicz M, et al. Randomized phase 2 trial of NP001-a novel immune regulator: safety and early efficacy in ALS. *Neurol Neuroimmunol Neuroinflamm* (2015) 2(3):e100. doi: 10.1212/NXI.0000000000000100

172. Miller RG, Zhang R, Bracci PM, Azhir A, Richard Barohn R, Bedlack R, et al. Phase 2B randomized controlled trial of NP001 in amyotrophic lateral sclerosis: pre-specified and *post hoc* analyses. *Muscle Nerve* (2022) 66(1):39–49. doi: 10.1002/mus.27511

173. Holm TH, Draeby D, Owens T. Microglia are required for astroglial toll-like receptor 4 response and for optimal TLR2 and TLR3 response. *Glia* (2012) 60:630–8. doi: 10.1002/glia.22296



OPEN ACCESS

EDITED BY

Fátima Regina Mena Barreto Silva,
Federal University of Santa Catarina,
Brazil

REVIEWED BY

Roberta Gualdani,
Université catholique de Louvain,
Belgium
Dimitra Gkika,
Plasticité et Résistance aux Thérapies
Anticancéreuses (CANTHER), France

*CORRESPONDENCE

Andrea Gerbino,
✉ andrea.gerbino@uniba.it

[†]These authors have contributed equally
to this work and share last authorship

RECEIVED 21 April 2023

ACCEPTED 18 July 2023

PUBLISHED 27 July 2023

CITATION

Moccia F, Fiorio Pla A, Lim D, Lodola F and
Gerbino A (2023), Intracellular Ca²⁺
signalling: unexpected new roles for the
usual suspect.
Front. Physiol. 14:1210085.
doi: 10.3389/fphys.2023.1210085

COPYRIGHT

© 2023 Moccia, Fiorio Pla, Lim, Lodola
and Gerbino. This is an open-access
article distributed under the terms of the
[Creative Commons Attribution License
\(CC BY\)](#). The use, distribution or
reproduction in other forums is
permitted, provided the original author(s)
and the copyright owner(s) are credited
and that the original publication in this
journal is cited, in accordance with
accepted academic practice. No use,
distribution or reproduction is permitted
which does not comply with these terms.

Intracellular Ca²⁺ signalling: unexpected new roles for the usual suspect

Francesco Moccia^{1†}, Alessandra Fiorio Pla^{2†}, Dmitry Lim^{3†},
Francesco Lodola^{4,5†} and Andrea Gerbino^{6*†}

¹Laboratory of General Physiology, Department of Biology and Biotechnology "L. Spallanzani", University of Pavia, Pavia, Italy, ²Department of Life Sciences and Systems Biology, University of Torino, Turin, Italy, ³Department of Pharmaceutical Sciences, Università del Piemonte Orientale "Amedeo Avogadro", Novara, Italy, ⁴Department of Biotechnology and Biosciences, University of Milan-Bicocca, Milan, Italy, ⁵Center for Nano Science and Technology @PoliMi, Istituto Italiano di Tecnologia, Milan, Italy, ⁶Department of Biosciences, Biotechnologies and Environment, University of Bari Aldo Moro, Bari, Italy

Cytosolic Ca²⁺ signals are organized in complex spatial and temporal patterns that underlie their unique ability to regulate multiple cellular functions. Changes in intracellular Ca²⁺ concentration ([Ca²⁺]_i) are finely tuned by the concerted interaction of membrane receptors and ion channels that introduce Ca²⁺ into the cytosol, Ca²⁺-dependent sensors and effectors that translate the elevation in [Ca²⁺]_i into a biological output, and Ca²⁺-clearing mechanisms that return the [Ca²⁺]_i to pre-stimulation levels and prevent cytotoxic Ca²⁺ overload. The assortment of the Ca²⁺ handling machinery varies among different cell types to generate intracellular Ca²⁺ signals that are selectively tailored to subserve specific functions. The advent of novel high-speed, 2D and 3D time-lapse imaging techniques, single-wavelength and genetic Ca²⁺ indicators, as well as the development of novel genetic engineering tools to manipulate single cells and whole animals, has shed novel light on the regulation of cellular activity by the Ca²⁺ handling machinery. A symposium organized within the framework of the 72nd Annual Meeting of the Italian Society of Physiology, held in Bari on 14–16th September 2022, has recently addressed many of the unexpected mechanisms whereby intracellular Ca²⁺ signalling regulates cellular fate in healthy and disease states. Herein, we present a report of this symposium, in which the following emerging topics were discussed: 1) Regulation of water reabsorption in the kidney by lysosomal Ca²⁺ release through Transient Receptor Potential Mucolipin 1 (TRPML1); 2) Endoplasmic reticulum-to-mitochondria Ca²⁺ transfer in Alzheimer's disease-related astroglial dysfunction; 3) The non-canonical role of TRP Melastatin 8 (TRPM8) as a Rap1A inhibitor in the definition of some cancer hallmarks; and 4) Non-genetic optical stimulation of Ca²⁺ signals in the cardiovascular system.

KEYWORDS

Ca²⁺ signalling, lysosomal Ca²⁺, mitochondria-ER contact sites, TRP channels, non-canonical signalling, optical stimulation

1 Introduction

An increase in intracellular Ca²⁺ concentration ([Ca²⁺]_i) can operate over a very wide dynamic range to specifically regulate a multitude of cellular functions (Berridge et al., 2003). Neurotransmitter release from presynaptic terminals, as well as insulin exocytosis from pancreatic β-cells, occur within microseconds on the elevation in [Ca²⁺]_i, while the

intracellular Ca^{2+} oscillations that drive gene expression may last for a few hours (Berridge et al., 2003; Clapham, 2007). An additional mechanism that enriches the versatility of intracellular Ca^{2+} signalling is represented by the spatial location of the Ca^{2+} sources, which can be physically coupled to different Ca^{2+} -dependent decoders (Berridge et al., 2003; Bagur and Hajnóczky, 2017; Ong et al., 2019; Barak and Parekh, 2020). Environmental cues generate a complex choreography of intracellular Ca^{2+} signals (Berridge et al., 2003; Clapham, 2007), whose spatio-temporal malleability enables one single ion messenger to control as many different functions as fertilization (Moccia et al., 2006), cell cycle (Lim et al., 2003) and proliferation (Faris et al., 2019; Faris et al., 2022), migration (Fiorio Pla et al., 2012; Zuccolo et al., 2018b), differentiation (Maione et al., 2022), contraction (Bers, 2008; Landstrom et al., 2017), metabolism (Patella et al., 2015), angiogenesis (Bernardini et al., 2019; Moccia et al., 2019b; Scarpellino et al., 2020), vasculogenesis (Moccia et al., 2012; Moccia et al., 2013; Zuccolo et al., 2018a), and, more recently, neurovascular coupling (Negri et al., 2021c; Soda et al., 2023). The multifaceted nature of intracellular Ca^{2+} signalling can be further appreciated by recalling that, depending on the Ca^{2+} source and on the Ca^{2+} -dependent target, an increase in $[\text{Ca}^{2+}]_i$ may induce opposing cellular responses, e.g., proliferation (Faris et al., 2022) and apoptosis (Astesana et al., 2021; Faris et al., 2023), vascular smooth muscle cell contraction (Knot and Nelson, 1998) and relaxation (Nelson et al., 1995), neuronal depolarization (Menigoz et al., 2016) and hyperpolarization (Tiwari et al., 2018), long-term potentiation (Ezra-Nevo et al., 2018; Soda et al., 2019; Locatelli et al., 2021) and long-term depression (Hirano, 2013). Dysregulation of the sophisticated machinery that orchestrates the Ca^{2+} response to physiological signals can, therefore, trigger or exacerbate a growing list of life-threatening disorders, such as neurodegenerative (Lim et al., 2014; Lim et al., 2021a) and cardiovascular (Venetucci et al., 2012; Moccia et al., 2019a) disorders, severe combined immunodeficiency (SCID) (Vaeth et al., 2020), and cancer (Moccia, 2018; Prevarskaya et al., 2018).

The Ca^{2+} response to environmental cues in non-excitabile cells is usually triggered by the phospholipase C-dependent production of inositol-1,4,5-trisphosphate (InsP_3), which mobilizes Ca^{2+} from what is regarded the most abundant intracellular Ca^{2+} reservoir, namely, the endoplasmic reticulum (ER) (Berridge et al., 2003; Clapham, 2007). InsP_3 gates the ionotropic InsP_3 receptors (InsP_3Rs), which are non-selective cation channel located on ER cisternae, in the presence of a permissive concentration of ambient Ca^{2+} (Prole and Taylor, 2019). Repetitive events of InsP_3 -evoked Ca^{2+} release may be spatially confined to peripheral InsP_3Rs , which are located in close proximity to plasmalemmal G_q -Protein Coupled Receptors (G_qPCRs) (Keebler and Taylor, 2017; Thillaiappan et al., 2017), or can propagate as regenerative Ca^{2+} waves through the mechanism of Ca^{2+} -induced Ca^{2+} release (CICR) (Bootman et al., 1997). Ryanodine receptors (RyRs), which represent the main Ca^{2+} -releasing channel in the sarcoplasmic reticulum (SR) and may also be present in the ER, support InsP_3 -evoked regenerative Ca^{2+} waves in some, but not all (Moccia et al., 2019b), cell types (Santulli et al., 2018). Depletion of the ER/SR Ca^{2+} content due to cyclic Ca^{2+} extrusion in the extracellular milieu by plasma membrane Ca^{2+} -ATPase or $\text{Na}^+/\text{Ca}^{2+}$ exchanger (NCX) (Moccia et al., 2002; Berra-Romani et al., 2023) is prevented by the activation of store-operated Ca^{2+} entry

(SOCE) (Lewis, 2020; Moccia et al., 2023). SOCE requires the dynamic interplay between Stromal Interaction Molecules 1 and 2 (STIM1 and STIM2, respectively), which serve as sensor of ER Ca^{2+} concentration ($[\text{Ca}^{2+}]_{\text{ER}}$), and the Ca^{2+} -selective channels, Orai1-3, on the plasma membrane (Lewis, 2020; Moccia et al., 2023). In excitable cells, membrane depolarization evoked by excitatory synaptic transmission (Locatelli et al., 2021) or spontaneous diastolic depolarization (Eisner et al., 2017) can lead to extracellular Ca^{2+} entry through multiple types of voltage-operated Ca^{2+} channels (VOCCs), which can be followed by CICR through RyRs and/or InsP_3Rs (Bading, 2013; Eisner et al., 2017). In both excitable and non-excitabile cells, extracellular Ca^{2+} entry is further mediated by the Transient Receptor Potential (TRP) family of non-selective cation channels, most of which are polymodal Ca^{2+} -permeable channels able to sense chemical, thermal and mechanical signals and thereby execute the most appropriate cellular response (Curcic et al., 2019; Vangeel and Voets, 2019; Diver et al., 2022). The advent of novel high-speed, 2D and 3D time-lapse imaging techniques, single-wavelength and genetic Ca^{2+} indicators, as well as the development of novel genetic engineering tools to manipulate single cells and whole animals, has shed novel light on the regulation of cellular activity by the Ca^{2+} handling machinery (Lim et al., 2016a; Bagur and Hajnóczky, 2017; Tapella et al., 2020; Berra-Romani et al., 2021; Leoni et al., 2021; Longden et al., 2021; Marta et al., 2022). For instance, it has been recognized that ER cisternae may establish dynamic contacts with other intracellular organelles, such as mitochondria (Csordas et al., 2010; Csordas et al., 2018; Bartok et al., 2019; Lim et al., 2021a; Sanchez-Vazquez et al., 2023) and lysosomes (Kilpatrick et al., 2013; Atakpa et al., 2018; Faris et al., 2022), to shape intracellular Ca^{2+} signals. The Ca^{2+} -dependent inter-organellar communication between ER and mitochondria has long been known to dictate cellular fate (Loncke et al., 2021; Bonora et al., 2022). We now know that, although both InsP_3Rs in ER cisternae and mitochondria in the cytosol are quite motile, they can establish temporary interactions at mitochondria-associated ER membranes (MAMs) to increase mitochondrial Ca^{2+} in an InsP_3 -dependent manner and stimulate cellular bioenergetics (Gherardi et al., 2020; Katona et al., 2022). However, stress conditions, such as those that can lead to neurodegenerative disorders, can alter the distance between the ER and mitochondria and, thereby, impair mitochondrial Ca^{2+} uptake and cellular bioenergetics that contributes to cell dysfunction (Lim et al., 2021a; Lim et al., 2023). An unexpected mode of Ca^{2+} -dependent inter-organellar communication has also been described at the membrane contact sites between ER and lysosomes (Kilpatrick et al., 2013; Ronco et al., 2015). Herein, the second messenger nicotinic acid adenine dinucleotide phosphate (NAADP), which can also be synthesized upon G_qPCR or tyrosine kinase receptor (TKR) activation, gates two pore channels (TPCs) to mediate lysosomal Ca^{2+} release and prime ER-embedded InsP_3Rs for InsP_3 -dependent activation (Patel, 2015; Galione et al., 2023). Lysosomal Ca^{2+} can also be mobilized by TRP Mucolipin 1 (TRPML1), which plays a crucial role in autophagic progression (Medina et al., 2015; Di Paola et al., 2018). TRPML1-mediated Ca^{2+} signals were thought to be confined to the perilyosomal Ca^{2+} space (Medina et al., 2015), but recent studies unexpectedly reported TRPML1-induced global Ca^{2+} signals via the Ca^{2+} -dependent recruitment of RyRs and InsP_3Rs (Kilpatrick et al., 2016; Thakore

et al., 2020). An additional dogma that has recently turned into a signalling revolution regards the same operation mode of ion channels. Channel proteins do more than simply conducting biologically relevant ions (Montes de Oca Balderas, 2022). Indeed, emerging evidence indicates that ion channels can signal in a flux-independent mode, thereby widening their potential impact on cell physiology (Borowiec et al., 2014; Vrenken et al., 2016; Chinigo et al., 2020; Pressey and Woodin, 2021; Arcangeli et al., 2023). For instance, the intracellular domains of some VOCCs, i.e., $\text{Ca}_v1.2$ (Gomez-Ospina et al., 2006) and $\text{Ca}_v2.1$ (Kordasiewicz et al., 2006), as well as some isoforms of the accessory $\text{Ca}_v\beta$ subunit (Hibino et al., 2003), can translocate into the nucleus and induce Ca^{2+} -independent gene expression. Furthermore, some ionotropic receptors, such as N-methyl-D-aspartate (NMDA) receptors (Montes de Oca Balderas and Aguilera, 2015; Negri et al., 2021a) and type A γ -aminobutyric acid (GABA) receptors (Negri et al., 2022b), can signal an increase in $[\text{Ca}^{2+}]_i$ in a flux-independent manner due to their ability to interact with their corresponding metabotropic receptors. Several members of the TRP superfamily can also function in a non-canonical mode. For instance, TRP Melastatin type 7 (TRPM7) channel promotes most of its effect through the intrinsic kinase activity that is located within its COOH-terminus (Desai et al., 2012; Faouzi et al., 2017; Cai et al., 2018), whereas TRP Canonical type 1 (TRPC1) does not need to mediate Ca^{2+} to induce proliferation in human umbilical cord vein endothelial cells (Abdullaev et al., 2008). Finally, the versatility of the Ca^{2+} handling machinery has been exploited to design alternative therapeutic avenues for many diseases that are still waiting for an effective treatment. For instance, a light-operated Ca^{2+} permeable channel (LOC) has been generated by introducing plant-derived photosensory domain into a cytoplasmic loop of the Orai1 channel (He et al., 2021). Optogenetic intervention by this novel LOC proved effective to suppress excessive hematopoietic stem cell self-renewal and to alleviate neurodegeneration in a model of amyloidosis (He et al., 2021).

A symposium organized within the framework of the 72nd Annual Meeting of the Italian Society of Physiology, held in Bari on 14–16th September 2022, has recently addressed many of the unexpected mechanisms whereby intracellular Ca^{2+} signalling regulates cellular fate in healthy and disease. The symposium, named “ Ca^{2+} signalling: unexpected new roles for the usual suspect”, gathered together four renowned Italian physiologists, who informed a numerous and very interested audience about their novel findings regarding the following topics: 1) the role of TRPML1 in Ca^{2+} -mediated water reabsorption in the kidney (Prof. Andrea Gerbino, University of Bari Aldo Moro); 2) the modulation of the ER-mitochondria distance to fuel cellular metabolism in astrocytes and prevent neurodegeneration in Alzheimer's disease (Prof. Dmitry Lim, University of Piemonte Orientale, Novara); 3) the non-canonical role of TRP Melastatin 8 (TRPM8) in the definition of some cancer hallmarks (Prof. Alessandra Fiorio Pla, University of Turin); and 4) the use of novel light-sensitive organic actuators to stimulate angiogenesis and control cardiac cells pacing (Prof. Francesco Lodola, University of Milan-Bicocca). Herein, we present a full report of the symposium and discuss the implications for the Ca^{2+} signalling field of the novel findings that were presented during each lecture.

2 TRPML1 and aquaporin 2: the secret liaison mediated by lysosomal Ca^{2+}

Lysosomes are multifunctional organelles: apart from well-defined digestive tasks (Xu and Ren, 2015), lysosomes act as a regulatory hub integrating multiple cues to modulate a wide spectrum of intracellular signaling pathways (Ballabio, 2016). Lysosomal vesicles are emerging as a novel Ca^{2+} reservoir that can finely modulate cellular fate through local or global Ca^{2+} signals (Patel and Cai, 2015; Galione, 2019; Galione et al., 2023). Throughout the whole process, lysosomes can freely diffuse and deliver/reuptake Ca^{2+} in the close proximity of target organelles such as ER, mitochondria and secretory vesicles. Understanding how lysosomes establish the Ca^{2+} -dependent cross-talk with surrounding organelles that orchestrate the Ca^{2+} response to physiological cues is crucial to appreciate how defective lysosomal Ca^{2+} signalling underpins life-threatening diseases, such as cancer (Faris et al., 2018), viral infections (Moccia et al., 2021a), hypertension (Negri et al., 2021b) and arrhythmias (Negri et al., 2021b), and lysosomal storage disorders (Kiselyov et al., 2010; Lloyd-Evans et al., 2010; Morgan et al., 2011).

The lysosomal matrix is strongly acidic with a pH of around 4.6 originated by the continuous activity of a vesicular H^+ -proton pump ATPase (V-ATPase) (Xu and Ren, 2015). Lysosomes can actively accumulate large amount of free Ca^{2+} (0.5 mM) through a mechanism that is still highly debated (Yang et al., 2019). Refilling with the Ca^{2+} of the lysosomal matrix could be driven either by a putative $\text{H}^+/\text{Ca}^{2+}$ exchanger in a pH-dependent manner (Christensen et al., 2002; Ronco et al., 2015; Melchionda et al., 2016) or by extracellular Ca^{2+} entry through endocytosis or SOCE (Gerasimenko et al., 1998; Sbrano et al., 2017). Lysosomal Ca^{2+} can be released into the cytosol through TPCs (Patel, 2015), of which two isoforms exist in mammals (i.e., TPC1 and TPC2), and TRPML1 (Faris et al., 2018). TPCs are gated by NAADP, which can be produced upon G_qPCR or TKR activation on the plasma membrane, and phosphatidylinositol-3, 5-bisphosphate (PIP_2) (Patel, 2015; Galione et al., 2023). Intriguingly, planar lysosomal patch-clamp recording showed that NAADP evoked TPC2-mediated currents that were equally mediated by Na^+ and Ca^{2+} , while those gated by PIP_2 were relatively Na^+ -selective (Gerndt et al., 2020). TPCs can be located at membrane contact sites (MCSs) between lysosomes and ER (Kilpatrick et al., 2017; Faris et al., 2022), where they are physiologically activated by NAADP to release lysosomal Ca^{2+} and evoke global Ca^{2+} signals via Ca^{2+} -induced Ca^{2+} release through InsP_3Rs and/or ryanodine receptors (Patel, 2015; Galione et al., 2023). According to the “trigger-hypothesis” (Galione, 2019; Galione et al., 2023), the InsP_3 -induced Ca^{2+} response to a plethora of extracellular stimuli, including glutamate (Foster et al., 2018; Zuccolo et al., 2019), acetylcholine (Aley et al., 2013), foetal bovine serum (Faris et al., 2019), and vascular endothelial growth factor (VEGF) (Moccia et al., 2021b), is initiated by the NAADP-sensitive lysosomal TPCs. TRPML1 is a non-selective cation permeable channel that mediates lysosomal Ca^{2+} , Fe^{2+} , and Zn^{2+} release into the cytosol in response by either endogenous agonists, such as phosphatidylinositol 3,5-bisphosphate [$\text{PI}(3,5)\text{P}_2$] (Gan et al., 2022) and reactive oxygen species (ROS) (Zhang et al., 2016) or synthetic ligands, such as ML-SA1 (Kilpatrick et al., 2016). TRPML1 usually mediates local events of Ca^{2+} release

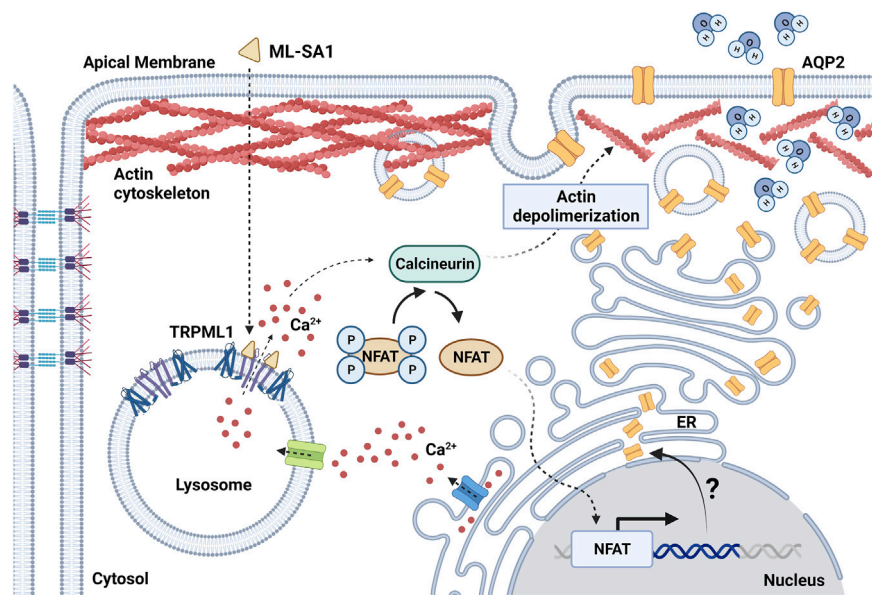


FIGURE 1

Schematic diagram showing the effect of TRPML1 activation on AQP2-mediated water reabsorption in mouse renal collecting duct cells. ML-SA1 triggers TRPML1-dependent local Ca^{2+} events that are sustained by the endoplasmic reticulum (ER) Ca^{2+} content. Activation of the Ca^{2+} /calcineurin/NFAT pathway determines depolymerization of the actin cytoskeleton, thus leading to accumulation of AQP2 at the apical plasma membrane and enhancing water membrane permeability. The putative role of lysosomal Ca^{2+} signaling events as switch for changes in AQP2 expression level through the modulation of the transcriptional activity of NFAT needs further investigation (question mark). Created with [BioRender.com](https://www.biorender.com) (agreement number: FY259UYCKW).

that stimulate autophagy by inducing the nuclear translocation of the Ca^{2+} -sensitive transcription factor, TFEB (Medina et al., 2015; Di Paola et al., 2018). Furthermore, TRPML1-induced local Ca^{2+} release modulates additional lysosomal functions, including lysosomal exocytosis, membrane trafficking and biogenesis (Di Paola et al., 2018; Medina, 2021). Recent evidence, however, showed that local lysosomal Ca^{2+} release through TRPML1 can also lead to global elevations in $[\text{Ca}^{2+}]_i$ via CICR through InsP_3Rs (Kilpatrick et al., 2016) or RyRs (Thakore et al., 2020). The Ca^{2+} -dependent crosstalk between TRPML1 and ER/SR-resident Ca^{2+} -permeable channels is, however, seemingly looser as compared to TPCs. In agreement with this evidence, a recent investigation showed that local Ca^{2+} release events through TRPML1 control water homeostasis in the renal collecting duct (CD, Figure 1) (Scorza et al., 2023).

Facultative water reabsorption in CD cells is finely tuned by a plethora of intracellular signaling mediators and transcription factors (Knepper et al., 2015). Antidiuresis is activated upon the release of the antidiuretic hormone (ADH) by the posterior pituitary gland. Specific binding of ADH with the vasopressin type 2 receptor (V2R), which is localized in principal cells of the CD, stimulates the cAMP/protein kinase A (PKA) axis leading to the apical fusion of the water channel aquaporin 2 (AQP2)-harboring vesicles (Zhao et al., 2023). The rapid apical accumulation of AQP2 boosts water permeability that, in the presence of the strong osmotic gradient in the kidney medulla, is responsible for water reabsorption in the interstitium. The ADH-dependent increase in $[\text{Ca}^{2+}]_i$ is likewise important to enable the proper fusion of AQP2 vesicles with the plasma membrane. Therefore, it does not come as a surprise that Ca^{2+} signaling events can independently influence AQP2 expression

and translocation even in the absence of cAMP-mediated cues (Chou et al., 2000; Procino et al., 2015; Mamenko et al., 2016; Tomilin et al., 2019). For instance, the antidiabetic drug rosiglitazone facilitates AQP2 apical accumulation and water reabsorption by inducing massive Ca^{2+} influx upon the specific activation of Transient Receptor Potential Vanilloid 6 (TRPV6) channel (Procino et al., 2015). In addition, a wide variety of TRP channels have been reported in CD cells and CD-derived cultures (Woudenberg-Vrenken et al., 2009). The activation of these channels orchestrates Ca^{2+} responses that are mainly driven by remarkable Ca^{2+} influx often associated with additional Ca^{2+} release from the ER. These robust Ca^{2+} signals can rapidly invade the bulk of the cytosol thus engaging a number of Ca^{2+} -dependent molecular effectors localized throughout the cell. Conversely, only scarce information is currently available regarding the role of local Ca^{2+} signals in AQP2-mediated water homeostasis. A recent investigation provided the first evaluation of lysosomal Ca^{2+} signaling events in renal CD cells, which were evoked by either blocking the vacuolar H-ATPase (V-ATPase) with bafilomycin A1 to deplete the lysosomal Ca^{2+} pool (Morgan et al., 2015) or activating TRPML1 with the synthetic agonist ML-SA1 (Kilpatrick et al., 2016) (Figure 1). In CD cells, both lysosomal agonists induced robust and long-lasting cytosolic Ca^{2+} oscillations sustained by tonic ER Ca^{2+} release through InsP_3Rs but not directly associated to lysosomal Ca^{2+} -triggered CICR (Scorza et al., 2023), as widely reported for TPCs (Macgregor et al., 2007; Brailoiu et al., 2009; Kilpatrick et al., 2013; Faris et al., 2019; Moccia et al., 2021b; Faris et al., 2022). This finding strongly suggests that InsP_3 -mediated ER Ca^{2+} release drives lysosomal Ca^{2+} refilling in CD cells. ML-SA1 and

bafilomycin A1 differentially modulated AQP2 translocation to the apical membrane and actin polymerization in the cytosol, since only ML-SA1 specifically elicited submaximal water reabsorption in collecting duct cells (Scorza et al., 2023) (Figure 1). Even though ML-SA1 increased water permeability to the same extent as submaximal doses of the cAMP increasing agents forskolin and IBMX, TRPML1 activation was unable to switch on the cAMP/PKA pathway. Currently, the cytosolic Ca^{2+} effectors translating TRPML1-mediated Ca^{2+} release into an increase in AQP2-containing vesicle translocation to the apical membrane remain to be deciphered. However, TRPML1-dependent AQP2 translocation and actin depolymerization were inhibited by blocking the Ca^{2+} -dependent phosphatase calcineurin (CaN) with cyclosporine A (Scorza et al., 2023). Intriguingly, CaN is selectively engaged by TRPML1-mediated lysosomal Ca^{2+} release to drive the nuclear translocation of TFEB (Medina et al., 2015), the master regulator of lysosomal function and autophagy (Di Paola et al., 2018; Medina, 2021) (Figure 1). CaN activation tightly bridges lysosomal Ca^{2+} signaling events and water reabsorption by directly dephosphorylating cytoskeletal organizing proteins (cofilin, WAVE-1 and synaptopodin) or eliciting long-lasting transcriptional effects mediated by NFAT (Descasez et al., 2012). Therefore, it is reasonable to assume that TRPML1 can regulate water balance by influencing the polymerization state of the actin cytoskeleton thus facilitating the fusion of AQP2-harboring vesicles with the apical plasma membrane (Figure 1). Noteworthy, TRPML1 induced Ca^{2+} events have been associated with fusion of gastric tubulovesicles carrying the H^+/K^+ -ATPase that pumps H^+ into the gastric lumen (Sahoo et al., 2017).

3 Ca^{2+} handling at the mitochondria-ER contact sites: role in Alzheimer's disease-related astroglial dysfunction and beyond

Mitochondrial enzymes and F_0F_1 ATP synthase require Ca^{2+} for activation and maintenance of bioenergetic activity and production of ATP. Mitochondria uptake Ca^{2+} with a high affinity directly from juxtaposed InsP_3Rs located in mitochondria-associated ER membranes (MAMs) (Rizzuto et al., 1993). The morpho-functional complex that holds together interacting ER and mitochondria is referred to as mitochondria-ER contact sites (MERCS) (Herrera-Cruz and Simmen, 2017). Ca^{2+} transfer at MERCS occurs through a complex composed of InsP_3Rs , voltage-dependent anion channel 1 (VDAC1) and the associated protein Grp75, and then, into mitochondrial matrix, via a low affinity mitochondrial Ca^{2+} uniporter. Besides Ca^{2+} fluxes, MERCS are responsible for a number of key cellular processes, such as lipid and steroid biogenesis, mitochondrial fission and dynamics, autophagosome formation, apoptosis induction, and others (Barazzuol et al., 2021). Disruption of MERCS has been observed in several neurodegenerative diseases, including Parkinson's disease, amyotrophic lateral sclerosis and Alzheimer's disease (AD) (Paillusson et al., 2016; Area-Gomez and Schon, 2017; Lim et al., 2021a; Leal and Martins, 2021). In AD, a strengthening of the interaction between ER and mitochondria has been found in human brains and in animal and cellular AD models (Lim et al., 2021a).

Although such increase has been associated with mitochondrial dysfunction and with aberrant processing of amyloid precursor protein (APP), mechanistic aspects MERCS alterations and cause-effect relationships with AD-related cellular pathology remain poorly understood (Lim et al., 2021a; Lim et al., 2023).

AD, a major, yet incurable, age-related neurological disorder, has a long-lasting pathogenesis with poorly characterized preclinical and prodromal phases. Cellular dysfunctions, such as alterations of protein synthesis and degradation with associated accumulation of misfolded/aggregated proteins, mitochondrial dysfunction with concomitant bioenergetic deficit and oxidative stress, and derangement of Ca^{2+} homeostasis and signalling, represent early signs of AD pathology (De Strooper and Karran, 2016). Yet, these dysfunctions have mainly been studied and interpreted from the point of view of neuronal pathology, while alterations in glial cells, specifically in astrocytes, have been largely overlooked (Verkhratsky et al., 2019; Merlo et al., 2021). Astrocytes are homeostatic and supportive cells in the central nervous system (CNS), which warrant correct development, function and adaptation of neurons and other cells in the CNS to activity and stress (Verkhratsky and Nedergaard, 2016; Santello et al., 2019; Tapella et al., 2020). They participate in formation of morpho-functional units in the brain, such as blood-brain barrier (BBB) and neurovascular unit (Schaeffer and Iadecola, 2021), and are responsible for metabolic, structural and functional support to neurons. In AD pathogenesis, astrocytes undergo complex biphasic alterations, first becoming asthenic and atrophic, to turn to hypertrophy and reactivity at later AD stages in concomitance with the development of senile plaques and neurofibrillary tangles accompanied by remodelling of astrocytic Ca^{2+} signalling (Lim et al., 2014; Lim et al., 2016b; Verkhratsky et al., 2019). Reactive astrocytes, in association with microglial cells, participate in the development of neuroinflammatory reaction. During these transformations, astrocytes lose their homeostatic and defensive functions and leave neurons to suffer damage, lose synaptic connectivity and die. Little is known about astrocytic cell pathology during early AD pathogenesis.

Unexpectedly, recent findings suggest that the alterations of MERCS and ER-mitochondrial Ca^{2+} transport may be responsible for a number of cellular dysfunctions, which may explain the loss of homeostatic function by AD astrocytes. These studies took advantage of a novel model of immortalized hippocampal astrocytes from 3xTg mouse model of AD, which faithfully reproduce transcriptional and functional alterations of primary AD astrocytes (Ruffinatti et al., 2018; Rocchio et al., 2019). Moreover, they produce and release β -amyloid peptide and have impaired autophagic and proteasomal protein degradation, which are signs of early cellular dysfunction in AD (Gong et al., 2023). Immortalized WT and 3xTg-AD astrocytes, referred to as WT-iAstro and 3Tg-iAstro, represent versatile and easy-to-handle astrocytic AD model, well suited for comprehensive investigation from single cell imaging and transfection to omics analyses and sub-cellular fractionation requiring large amount of material (Tapella et al., 2023). First, it was assessed whether 3Tg-iAstro present mitochondrial alterations characteristic for AD cells. 3Tg-iAstro cells have a lower basal mitochondrial respiration and severely impaired respiratory reserve, significantly lower mitochondrial ATP production and significantly higher mitochondrial ROS.

Glycolytic activity was also impaired in 3Tg-iAstro compared with WT-iAstro cells. This was in line with recent reports on AD-derived human iPSC-differentiated astrocytes (Oksanen et al., 2017; Oksanen et al., 2019). Proteomics analysis on isolated mitochondria and associated ER membranes were also conducted. Surprisingly, differentially expressed proteins were found to be mainly responsible for ER functions and ribosomal proteins synthesis (Dematteis et al., 2020). Validation of these results showed that 3Tg-iAstro cells presented a lower rate of basal protein synthesis and low-grade chronic ER stress accompanied by an increased phosphorylation of eukaryotic initiation factor 2 α (p-eIF2 α). Gong et al. (2023) found that proteasomal and autophagic activities are impaired in 3Tg-iAstro cells. Moreover, 3Tg-iAstro, but not WT-iAstro cells, were unable to promote the formation of the bidimensional tubular network, which is the *in vitro* surrogate of *in vivo* blood vessel formation (Balbi et al., 2019; Balducci et al., 2021), in an *in vitro* astrocyte/pericyte/endothelial 3D co-culture due to a loss of secreted factors, thereby suggesting the impairment of key homeostatic functions (Tapella et al., 2022). These alterations were also found in hippocampus of 3xTg-AD mice *in vivo* (Tapella et al., 2022).

Next, it was investigated if 3Tg-iAstro presented alterations of Ca²⁺ homeostasis (Lim et al., 2021b). A significant increase of steady-state ER Ca²⁺ level and higher ATP-induced Ca²⁺ signals in the cytosolic compartment, indicating a higher Ca²⁺ ER load and higher InsP₃-mediated Ca²⁺ release, were reported. This was in accord with previous reports (Grolla et al., 2013a; Grolla et al., 2013b; Lim et al., 2013; Ronco et al., 2014). However, unexpectedly, ATP-induced Ca²⁺ transients, measured in mitochondrial matrix, were significantly lower in 3Tg-iAstro compared with WT-iAstro cells, indicating on the alterations with ER-mitochondrial Ca²⁺ transport. This was in line with the increased ER-mitochondrial interaction at a distance of 8–10 nm, which we have demonstrated using a split-GFP ER-mitochondrial contact site sensor (SPLICS) (Cieri et al., 2018; Dematteis et al., 2020). To investigate if the increased ER-mitochondrial interaction and the impaired mitochondrial Ca²⁺ signals were responsible for alterations of cellular proteostasis, an artificial linker that fixes the ER and the outer mitochondrial membrane at a short distance of about 10 nm was overexpressed in WT-iAstro cells, thereby reproducing MERCS and Ca²⁺ alterations found in 3Tg-iAstro cells. Strikingly, fixing MERCS at 10 nm reproduced the impairment of ribosomal protein synthesis and increased p-eIF2 α levels. Moreover, as reported for 3Tg-iAstro cells, WT-iAstro cells overexpressing 10 nm linker were unable to support tubulogenesis *in vitro* in 3D co-culture with pericytes and endothelial cells (Tapella et al., 2022).

Taken together, these results provide proof of principle that the shortening of ER-mitochondrial distance, observed in AD, may be causative for a number of cellular AD-related alterations. Furthermore, our results suggest that the altered MERCS function in AD astrocytes may result in impairment of CNS homeostasis, BBB and neuronal dysfunction (Figure 2). Further experiments are necessary to elucidate molecular mechanisms of MERCS dysfunction and dissect the role of impaired ER-mitochondrial Ca²⁺ transfer in AD pathogenesis.

4 Non-canonical role of TRP Melastatin 8 (TRPM8) in the definition of some cancer hallmark

TRPM8 is a member of the TRP family primarily known for its classical cold receptor function in sensory neurons required for cold thermal transduction and response as well as pain sensation in mammals (McKemy et al., 2002; Madrid et al., 2006; Dhaka et al., 2008; Knowlton et al., 2013). The first identified “full-length” isoform of TRPM8 consists of a homotetrameric protein of 1,104 amino acid (128 kDa) organized into six hydrophobic transmembrane α -helices (S1–S6) with a transmembrane loop between S5 and S6, and cytosolic tetrameric coiled-coil COOH-terminal domain (C-term) and a large hydrophilic NH₂-terminal domain (N-term) containing “TRPM homology regions” (MHR) involved in channel assembly and trafficking (Kraft and Harteneck, 2005; Fujiwara and Minor, 2008; Yin et al., 2018). The voltage sensor-like domain (VSLD) is defined by the first 4 TM helices (S1–S4) and also contains the binding sites for menthol and icilin at the cavity formed with the TRP domain (Bandell et al., 2006; Yin et al., 2019). The pore module of TRPM8 is, instead, formed by the last 2 TM helices (S5–S6) and it is characterized by a highly conserved hydrophobic region and a conserved aspartate residue, responsible for ion selectivity ($P_{Ca}/P_{Na} = 3.3$) (Zholos et al., 2011). Interestingly, this full length TRPM8 is mainly localized in the plasma membrane but is also partly present at the ER level where it functions by releasing Ca²⁺ from the store (Chinigo et al., 2022).

Beside this well known role in thermal transduction, the human *TRPM8* gene was first identified and cloned from prostate tissues and described as a new prostate-specific gene due to the peculiar expression pattern shown during prostate cancer (PCa) progression (Tsavaler et al., 2001). In particular, TRPM8 is upregulated in benign hyperplasia (BPH) and during the early androgen-dependent stages of PCa, and then downregulated in the more advanced androgen-independent metastatic stages of the tumor. Consistent with its unique deregulation during PCa progression, alterations in TRPM8 channel activity have been linked to several cancer hallmarks, including tumor cell proliferation and survival, cell migration, and angiogenesis (Alaimo et al., 2020; Grolez et al., 2022).

However, the impact of TRPM8 in the development and progression of PCa is subject to complex modulation mechanisms that also underlie the expression of different isoforms with distinct subcellular localization and activity depending on tumor stage and androgen sensitivity. Indeed, the expression of the full-length isoform of TRPM8 located on the plasma membrane (TRPM8_{PM}) is highly subject to androgen regulation and thus is significantly downregulated in androgen deprivation and androgen receptor (AR) loss during the late androgen-independent phase of PCa (Zhang and Barritt, 2004; Bidaux et al., 2005; Grolez et al., 2019). This regulation occurs through both genomic and non-genomic mechanisms involving the AR (Figure 3) (Bidaux et al., 2005; Grolez et al., 2019). As regarding in particular the non-genomic action, the role of AR-TRPM8 interaction is tightly regulated by testosterone in a dose-dependent manner: low doses of testosterone (10 nM) are associated with AR-TRPM8 localization at the level of lipid rafts and a significant inhibition of TRPM8 activity which in turn lead to an increase in cell motility as compared with the absence of

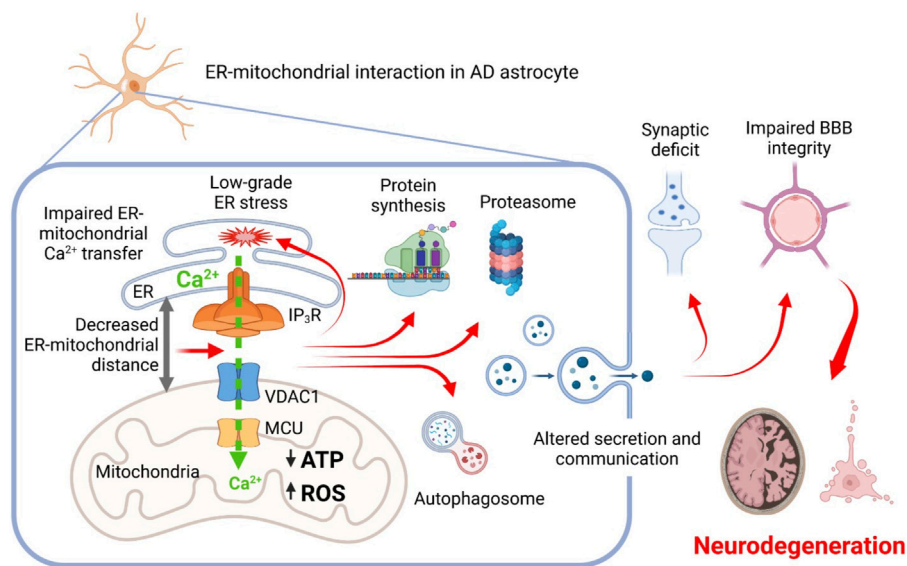


FIGURE 2

Proposed scheme relationships between AD-related mutations, mitochondrial-ER interaction, mitochondrial and ER Ca^{2+} signaling, and cellular dysfunctions in astrocytes. Altered ER-mitochondrial interaction impairs ER-mitochondrial Ca^{2+} transfer, resulting in mitochondrial bioenergetic deficit and increased production of ROS, induction of a low-grade chronic ER stress and derangement of proteins synthesis and degradation. Cellular dysproteostasis results in an impaired secretion of factors including adhesion molecules, components of extracellular matrix, pro-neurogenic and neuroprotective molecules. Altogether, this impairs homeostatic and signaling activity of AD astrocytes eventually leading to impairment of synaptic functions, blood-brain barrier integrity and to development of neurodegeneration.

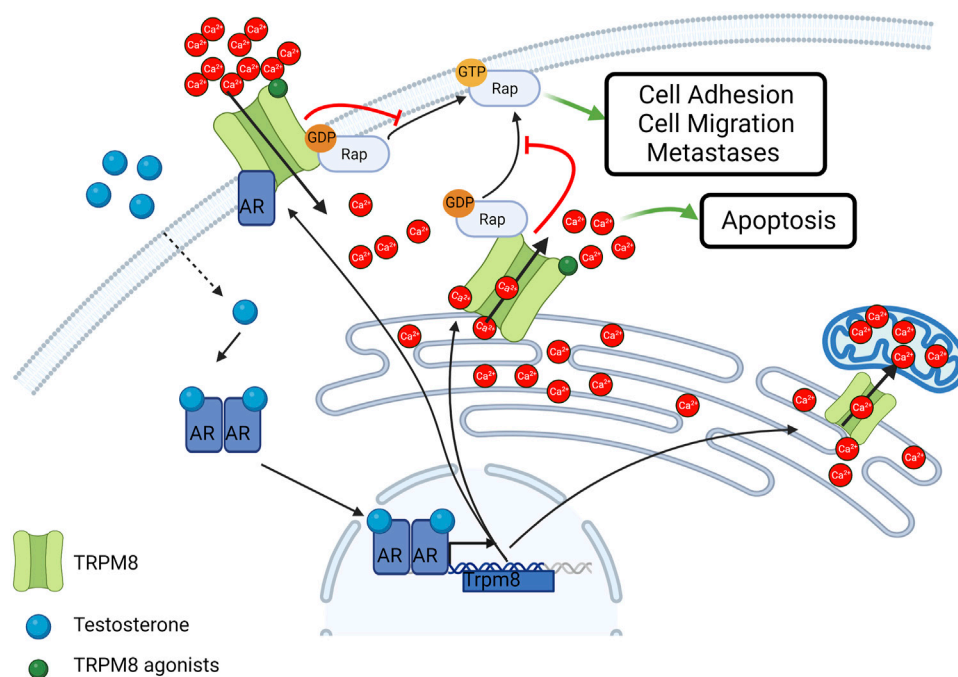


FIGURE 3

Schematic representation of TRPM8 subcellular localization and activity in cancer cells. TRPM8 Full length isoform localizes at the plasma membrane and is subjected to androgen regulation. Smaller isoforms typically localize in the ER and mediate Ca^{2+} release in the cytosol or Ca^{2+} transfer in the mitochondria. TRPM8 also act independently from its channel activity as an inhibitor of the small GTPase Rap1A thus inhibiting cell adhesion and migration. Created with BioRender.com (agreement number: AT259UYHZ3).

testosterone; on the other hand, high doses of testosterone (100 nM) lead to a decrease of TRPM8-AR interaction thus reverting the inhibitory effect of AR on TRPM8 activity (Grolez et al., 2019). This loss of interaction and delocalization of TRPM8 outside of lipid rafts, significantly increases prostate cancer cell motility (Grolez et al., 2019).

Beside the role of the full-length TRPM, during the transition from androgen-dependent to androgen-independent phases of PCa, through an alternative splicing mechanism, the “full-length” isoform of TRPM8 gives way to a shorter isoform with typical ER localization, known as TRPM8_{ER} (Bidaux et al., 2007). The TRPM8_{ER} isoform, being able to directly release ER Ca²⁺ and thereby activate SOCE on the plasma membrane, is mainly involved in the control of Ca²⁺-dependent pro-apoptotic mechanisms (Figure 3) (Thebault et al., 2005; Prevarskaya et al., 2007). Interestingly, the pro-apoptotic role of TRPM8 has also been confirmed in PCa cells treated with sub-lethal doses of radio, hormonal, or chemo therapies (Alaimo et al., 2020; Genovesi et al., 2022). Furthermore, other isoforms of the channel have been identified to date in the prostate. A functional TRPM8_{ER} characterized by only 4 rather than 7 transmembrane domains (TMDs) has been identified and characterized as a mediator of the Ca²⁺ transfer from the ER to the mitochondria in PCa epithelial cells (Figure 2) (Bidaux et al., 2018), while short non-channel TRPM8 isoforms (sM8s) with ubiquitous cytosolic localization in PCa were found to exert antagonist functions towards the full-length isoform (Peng et al., 2015; Bidaux et al., 2016). sM8s are a first example of non-channel function of TRPM8 that influences cell behavior independently of pore function and Ca²⁺ mobilization (Fernandez et al., 2012). Therefore, the growth of primary PCa as a result of the equilibrium between proliferation and apoptosis may depend on the relative expression levels of the different TRPM8 isoforms with channel and non-channel functioning.

In addition, TRPM8 regulates cell migration through both Ca²⁺-dependent and Ca²⁺-independent mechanisms. TRPM8-mediated Ca²⁺ signals induce an increase in the expression and activity of some proteins that are crucial in the epithelial-to-mesenchymal transition (EMT), in focal adhesion dynamics and consequently in the control of cell adhesion and migration (Noren et al., 2000; Millar et al., 2017). In particular, Cdc42, Rac1, ERK, and FAK are stimulated in a Ca²⁺-dependent manner by TRPM8 activity in PCa cells (Yang et al., 2009; Zhu et al., 2011; Wang et al., 2012; Grolez et al., 2022). On the other hand, the involvement of TRPM8 in the migratory machinery goes beyond its channel function. Indeed, a novel facet of TRPM8 as an inhibitor of the small GTPase Rap1A that is completely independent of its cation channel activity has recently been unveiled (Figure 3) (Genova et al., 2017; Chinigo et al., 2022). More specifically, a direct physical interaction between TRPM8 and Rap1A has been characterized in both PCa-derived endothelial cells and epithelial PCa cells (Genova et al., 2017; Chinigo et al., 2022). The interaction site is located on the NH₂-terminus of the channel and involves the glutamate 207 and the tyrosine 240, which directly interact with some residues (including tyrosine 32) located within the switch I region of Rap1A, responsible for the transition from the inactive to the active form of the small GTPase (Chinigo et al., 2022). Indeed, Rap1A, as a small GTPase, co-exists in two different forms: an active form when bound to GTP and an inactive form when bound to the GDP (Vetter and Wittinghofer,

2001). Specific guanine exchange factors (GEFs) catalyze the exchange between GDP and GTP thereby inducing small GTPase activation, which normally results in the promotion of cell adhesion through the activation of the β 1-integrin signaling at the plasma membrane (Chrzanowska-Wodnicka et al., 2008; Boettner and Van Aelst, 2009; Carmona et al., 2009; Cherfils and Zeghouf, 2013). Recent work demonstrated that TRPM8 intracellularly binds Rap1A mainly at the ER in its inactive form, thus hindering its translocation to the plasma membrane and its subsequent activation (Genova et al., 2017; Chinigo et al., 2022). This mechanism results in the inhibition of cell adhesion and migration in PCa-derived endothelial cells and in epithelial PCa cells, thus making TRPM8 an appealing candidate to block both tumor invasiveness and angiogenesis (Genova et al., 2017; Chinigo et al., 2022). Although TRPM8 expression is sufficient to exert these functional effects, stimulation with TRPM8 agonists, such as icilin and WS12, further potentiates these effects not only by recruiting Ca²⁺-dependent pathways, such as Cdc42, Rac1, ERK, and FAK, but also by probably promoting TRPM8-Rap1 interaction. This could be explained by global conformational rearrangements triggered by agonist binding in the TRPM8 TMDs that are propagated to the cytosolic domain where interaction with Rap1A occurs (Yin et al., 2018; Yin et al., 2019). Rap1A is not the only GTPase involved in the TRPM8 interactome. Indeed, TRPM8 was found to interact with the inactive form of the G-protein subunit G α_q , which leads to the inhibition of TRPM8 gating and, in turn, may be subject to TRPM8-mediated metabotropic regulation (Klasen et al., 2012; Zhang et al., 2012). These data fit into the broader context of a bidirectional close interplay between TRP channels and small GTPases at all stages of the metastatic cascade through both Ca²⁺-dependent and Ca²⁺-independent pathways (Chinigo et al., 2020).

All these recent mechanistic findings on TRPM8 provide new insights for the development of innovative and effective tools targeting TRPM8 to block PCa progression and improve the prognosis of the currently incurable metastatic castration-resistant prostate cancer (mCRPC) phenotypes. In addition to supporting a potential use of TRPM8 in anti-tumor therapy as a dual target to simultaneously counteract metastatic dissemination and angiogenesis, they also shed new light on the possibility of using TRP channels as targets for the development of peptidomimetics in cancer therapy. In fact, the administration of therapeutic peptide mimicking the channel or part of its structure would further reduce any side effects associated with the wide tissue distribution of TRP channels and the multitude of intracellular signalling pathways regulated by them, directly targeting a specific protein-protein interaction and consequently impairing only its associated cellular pathways (Mabonga and Kappo, 2019; Tsagareli and Nozadze, 2020). As to TRPM8-Rap1A interaction, the applicability of a peptide that reproduces the N-terminus of the channel in patients in androgen-independent late stages of PCa seems to be further supported by the fact that none of the residues involved in this interaction were mutated in the analyzed patient cohorts (Chinigo et al., 2022). Of note, validation of TRPM8-Rap1A interaction in more than 1 cell line (Genova et al., 2017; Chinigo et al., 2022), including prostate, breast, and cervical cancer cells as well as endothelial cells, suggests a broader spectrum of action of TRPM8 as an inhibitor of Rap1, albeit with a different impact in terms of control of cell adhesion and migration according to the cell

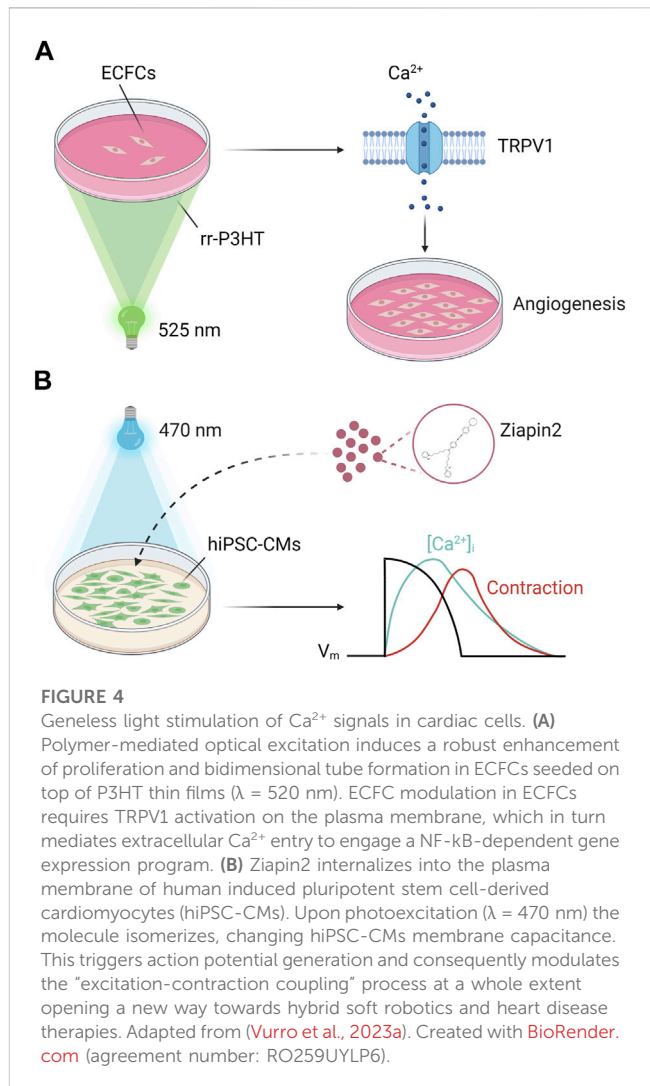
type. Therefore, this protein-protein interaction could prove to be an interesting target in the treatment of a much wider range of pathologies.

5 Non-genetic light stimulation of Ca^{2+} signals in cardiovascular research: methodology and possible applications

The idea to use light to trigger specific biological pathways, including Ca^{2+} signalling, represents one of the most fascinating insights in modern science (Lodola and Moccia, 2022). In recent years, photostimulation of cells and living systems has received great interest from the scientific community due to several unique advantages. Indeed, light is a minimally invasive biophysical tool that can overcome the limitations of more conventional stimulation approaches based on electrical, chemical, mechanical, or magnetic cues (i.e., limited spatial and temporal resolution) (Di Maria et al., 2018). The potential revolutionary role of light has been originally suggested by Sir Francis Crick. The Nobel Prize for Physiology or Medicine, discussing the need to achieve a selective control of individual neurons to understand the complexity of the brain, asserted that “*The ideal signal would be light, probably at an infrared wavelength to allow the light to penetrate far enough. This seems rather farfetched, but it is conceivable that molecular biologists could engineer a particular cell type to be sensitive to light in this way*” (Crick, 1999). This revolutionary concept became reality few years later with the implementation of Optogenetics, which consists in the expression of light-sensitive ion channels into the cellular plasma membrane to control the activity of neurons or other cell types with light (Deisseroth, 2011). However, the standard method to deliver the light-sensitive sensors-actuators to the target cells membrane impinges on viral constructs and this, combined with the fact that the exogenous proteins are isolated from very distant species (i.e., bacteria, algae, or unicellular fungi), open a series of issues in the therapeutic translatability of the approach.

An alternative strategy to still preserve the advantages of optical stimulation, but avoiding genetic modification, relies on the use of photosensitive transducers (Di Maria et al., 2018; Hopkins et al., 2019). The foundation of this approach is built on the convergence of various cutting-edge expertise ranging from biology, material science and photonics. In recent years, both inorganic and organic semiconductors have been used with excellent results (Di Maria et al., 2018; Hopkins et al., 2019). In particular, the organic one has aroused considerable interest within the scientific community due to their unique characteristics. In fact, these materials support both ionic and charge transfer, are soft and conformable, cost-effective and solution processable, but most importantly their absorption range is in the visible region, and they present a high biocompatibility, thus proving capable of interfacing with living matter to transduce light into a biological signal. Regioregular polymer poly(3-hexylthiophene-2,5-diyl), referred as P3HT, is probably the workhorse material among the organic semiconductors and the widely studied for biological purposes (Antognazza et al., 2015; Di Maria et al., 2018; Moccia et al., 2020).

The main photophysical mechanisms that occur at the polymer/cell interface could be capacitive, electrochemical, or thermally



mediated. These phenomena in turn generate different cellular response. For example, at the cellular level, planar P3HT has been proven effective in the modulation of the membrane potential of non-excitatory cells (i.e., HEK-293 cells and astrocytes) up to the optical stimulation/silencing of neuronal firing (Ghezzi et al., 2011; Benfenati et al., 2014; Antognazza et al., 2015; Feyen et al., 2016; Di Maria et al., 2018). Notably, its efficacy is not limited to *in vitro* applications. Indeed P3HT-based hybrid interfaces (Ghezzi et al., 2013; Antognazza et al., 2016; Maya-Vetencourt et al., 2017), and more recently also nanoparticles (Maya-Vetencourt et al., 2020), were also shown to restore light-sensitivity and visual acuity in animal models of retinal degeneration evidencing novel potential biomedical implications of conjugated polymers.

The modulation of cellular fate via electrochemical and/or thermal signals could be achieved by modulation of $[\text{Ca}^{2+}]_i$ (Bossio et al., 2018; Moccia et al., 2022). Recently, it has been demonstrated that P3HT photoexcitation led to the activation of the non-selective cation channel Transient Receptor Potential Vanilloid 1 (TRPV1) channel (Lodola et al., 2017b; Moccia et al., 2020; Moccia et al., 2022). TRPV1 is a non-selective cation channel

that can integrate a variety of extracellular cues (Moccia et al., 2020; Moccia et al., 2022), including an increase in ROS (Guarini et al., 2012), an increase in temperature $>40^{\circ}\text{C}$ (Caterina et al., 1997), and by a reduction in extracellular pH (Jordt et al., 2000). In accord, P3HT photoexcitation can stimulate TRPV1-mediated membrane depolarization via the local increase in temperature and ROS concentration at the interface between P3HT thin films and cell membrane (Lodola et al., 2017b). Further studies showed that optical excitation of P3HT thin films induced intracellular Ca^{2+} oscillations in human circulating endothelial colony forming cells ECFCs (Negri et al., 2022a), a truly endothelial progenitor population that is mobilized in peripheral circulation upon an ischemic insult to regenerate the damaged vascular networks (Moccia et al., 2018). TRPV1-mediated Ca^{2+} signals were mainly elicited by local ROS generation and were supported by InsP_3 -induced ER Ca^{2+} release and SOCE (Negri et al., 2022a). Of note, light-induced intracellular Ca^{2+} oscillations were reminiscent of the repetitive Ca^{2+} spikes whereby vascular endothelial growth factor (Dragoni et al., 2011; Dragoni et al., 2015; Lodola et al., 2017a) and the human amniotic fluid stem cell secretome (Balducci et al., 2021) induce the nuclear translocation of NF- κB to stimulate ECFC proliferation and tube formation. In agreement with these observations, optical excitation of P3HT thin films was found to boost ECFC pro-angiogenic activity by activating TRPV1 and thereby promoting a NF- κB -dependent gene expression program (Figure 4A) (Lodola et al., 2019a). These findings pave the way towards the use of these materials as a reliable tool for precise and reversible optically-driven modulation of ECFC physiological activity (Zhang et al., 2014; Lodola et al., 2019a; Moccia et al., 2020; Moccia et al., 2022).

The same interface has been applied also to optical increase the contractile activity of human induced pluripotent stem cell-derived cardiomyocytes (hiPSC-CMs), a process where Ca^{2+} is the actual coupling between excitation occurring in the sarcolemma and the onset of mechanical contraction (Bers and Guo, 2005). Although in this experimental setting the physical process was photothermal, P3HT still presents advantages over more traditional stimulation methods, thereby opening interesting perspectives for the control of cardiac pacing (Lodola et al., 2019b).

Within this context, an alternative approach involves photochromic compounds (Wang and Li, 2018). These organic molecules undergo reversible transformation between two metastable states following the absorption of an electromagnetic radiation and provide a conceptually simple and convenient way to control cellular activity. Indeed, photoswitches can bind covalently to ion channels/receptors or be targeted directly to the plasma membrane bilayer, thus modifying, upon photoisomerization, the ion channel dynamics and/or the electrical properties of the membrane (Gorostiza and Isacoff, 2008; Izquierdo-Serra et al., 2016; Leippe et al., 2017). Recently, a newly synthesized amphiphilic azobenzene-based photo-transducer (Ziapi2), successfully tested in bacteria, HEK-293 cells and neurons (Paterno et al., 2020a; Paterno et al., 2020b; DiFrancesco et al., 2020; Magni et al., 2022), has been used as a non-invasive optical tool to trigger hiPSC-CMs contraction behavior (Vurro et al., 2023a). Thanks to its peculiar chemical properties Ziapi2 has the capability to dwell within the hiPSC-CMs sarcolemma. In this environment the molecule

photoisomerization induces a heatless mechanical perturbation upon millisecond pulse of visible light that leads to a dynamic modulation of membrane capacitance. This change in the passive electrical property of the cell results in a transient hyperpolarization followed by a delayed depolarization able to elicit an action potential. The electrical activity correlates with changes in Ca^{2+} dynamics and ultimately with an increase in the contraction rate (Figure 4B). The photopacing efficacy of the approach has been further extended to a cardiac microphysiological model that mimics the cellular organization and substrate mechanical properties of native cardiac tissue (Vurro et al., 2023b), thus proving that Ziapi2 could be a viable tool for the modulation of the excitation-contraction coupling with a precise spatial and temporal punctuality.

6 Conclusion

The Symposium “ Ca^{2+} signalling: unexpected new roles for the usual suspect” has been one of the most attended events of the 72nd Annual Meeting of the Italian Society of Physiology. In our opinion, this was not only due to the widespread function of the Ca^{2+} handling machinery, which plays fundamental and diversified roles in human physiology that could of course gather vast interest by the audience. We believe that the Symposium gathered such a large audience since it aimed at a presenting one of the oldest signalling messengers known, i.e., Ca^{2+} , from a novel perspective. It is now clear that the Ca^{2+} handling machinery is no longer limited, to quote a few paradigmatic examples, to intracellular Ca^{2+} stores that exclusively located in the ER or to voltage-gated Ca^{2+} channels and ligand-gated channels on the plasma membrane. Lysosomes and mitochondria are also crucial to shape the physiological Ca^{2+} response to extracellular cues by, respectively, amplifying, or modulating ER Ca^{2+} release. Altering this delicate balance of inter-organellar Ca^{2+} fluxes can lead to life-threatening disorders, such as AD, cancer, and lysosomal storage disorders, and many more are likely to be discovered in the next future. The non-canonical function of ion channels, exemplified by TRPM8-Rap1A interaction, represents another revolutionary field of research showing that classical omics technologies, such as single-cell RNA sequencing or mass spectrometry, need to be integrated by a physiological approach to truly understand the signalling mode of a channel transcript/protein. These emerging pieces of information on the heterogeneity and versatility of the Ca^{2+} handling machinery can be exploited to design alternative strategies to selectively rescue the function of diseased cells by combining novel nanotechnologies with a proper knowledge of molecular physiology. Due to its polymodal nature, TRPV1 is certainly the best molecular switch to translate optical stimulation of photosensitive conjugated polymers into a biologically relevant signal. But other candidates presenting similar sensitivity to heat and ROS, such as TRP Ankyrin 1, are likely to be rapidly integrated in the arsenal of Ca^{2+} -permeable channels that could be probed for their therapeutic potential. In conclusion, this Symposium, which also engendered may fruitful discussions and opened the way to new collaborations among the participants (including many foreigner guests), confirmed that Italian Physiology is at the forefront of research in Ca^{2+} signalling, as also proven by many other oral and poster presentations of the meeting

(Martinotti et al., 2019; Nesher et al., 2019; Badone et al., 2021; Lazzarini et al., 2022; Michelucci et al., 2022; Sforza et al., 2022; Arici et al., 2023; Lia et al., 2023).

Author contributions

All authors listed have made a substantial, direct, and intellectual contribution to the work and approved it for publication.

Funding

The authors gratefully acknowledge financial support from: Fondo Ricerca Giovani from the University of Pavia (FM); #NEXTGENERATIONEU (NGEU) and funded by the Ministry of University and Research (MUR), National Recovery and Resilience Plan (NRRP), project MNESYS (PE0000006)—A Multiscale integrated approach to the study of the nervous system in health and disease (DN. 1553 11.10.2022) (FM); EU Horizon 2020 FETOPEN-2018-2020 Programme “LION-HEARTED”, grant agreement n. 828984 (FM and FL); PRIN-2017 “Lioness” project (#GA 754345) from Italian Ministry for Education, University and Research (MIUR) (AF); FAR-2019 from the Università del Piemonte Orientale (DL); Fondo di Ateneo (2020-ATE-0044) from the University of Milano-Bicocca (FL).

References

- Abdullaev, I. F., Bisaillon, J. M., Potier, M., Gonzalez, J. C., Motiani, R. K., and Trebak, M. (2008). Stim1 and Orai1 mediate CRAC currents and store-operated calcium entry important for endothelial cell proliferation. *Circ. Res.* 103, 1289–1299. doi:10.1161/01.RES.0000338496.95579.56
- Alaimo, A., Lorenzoni, M., Ambrosino, P., Bertossi, A., Bisio, A., Macchia, A., et al. (2020). Calcium cytotoxicity sensitizes prostate cancer cells to standard-of-care treatments for locally advanced tumors. *Cell Death Dis.* 11, 1039. doi:10.1038/s41419-020-03256-5
- Aley, P. K., Singh, N., Brailoiu, G. C., Brailoiu, E., and Churchill, G. C. (2013). Nicotinic acid adenine dinucleotide phosphate (NAADP) is a second messenger in muscarinic receptor-induced contraction of Guinea pig trachea. *J. Biol. Chem.* 288, 10986–10993. doi:10.1074/jbc.M113.458620
- Antognazza, M. R., Di Paolo, M., Ghezzi, D., Mete, M., Di Marco, S., Maya-Vetencourt, J. F., et al. (2016). Characterization of a polymer-based, fully organic prosthesis for implantation into the subretinal space of the rat. *Adv. Healthc. Mater.* 5, 2271–2282. doi:10.1002/adhm.201600318
- Antognazza, M. R., Martino, N., Ghezzi, D., Feyen, P., Colombo, E., Endeman, D., et al. (2015). Shedding light on living cells. *Adv. Mater.* 27, 7662–7669. doi:10.1002/adma.201403513
- Arcangeli, A., Duranti, C., Iorio, J., and Lastraoli, E. (2023). The role of potassium channels in tumours of the gastrointestinal tract: A focus on the human ether-a-go-go related gene 1 channels. *J. Physiol.* 601, 1597–1610. doi:10.1113/JP282310
- Area-Gomez, E., and Schon, E. A. (2017). On the pathogenesis of alzheimer's disease: The MAM hypothesis. *FASEB J.* 31, 864–867. doi:10.1096/fj.201601309
- Arici, M., Ferrandi, M., Barassi, P., Hsu, S. C., Torre, E., Luraghi, A., et al. (2023). Istaroxime metabolite PST3093 selectively stimulates SERCA2a and reverses disease-induced changes in cardiac function. *J. Pharmacol. Exp. Ther.* 384, 231–244. doi:10.1124/jpet.122.001335
- Asesana, V., Faris, P., Ferrari, B., Siciliani, S., Lim, D., Biggiogera, M., et al. (2021). [Pt(O,O'-acac)(γ-acac)(DMS)]: Alternative strategies to overcome cisplatin-induced side effects and resistance in T98G glioma cells. *Cell Mol. Neurobiol.* 41, 563–587. doi:10.1007/s10571-020-00873-8
- Atakpa, P., Thillaiappan, N. B., Mataragka, S., Prole, D. L., and Taylor, C. W. (2018). IP3 receptors preferentially associate with ER-lysosome contact sites and selectively deliver Ca(2+) to lysosomes. *Cell Rep.* 25, 3180–3193.e7. doi:10.1016/j.celrep.2018.11.064
- Bading, H. (2013). Nuclear calcium signalling in the regulation of brain function. *Nat. Rev. Neurosci.* 14, 593–608. doi:10.1038/nrn3531
- Badone, B., Ronchi, C., Lodola, F., Knaust, A. E., Hansen, A., Eschenhagen, T., et al. (2021). Characterization of the PLN p.Arg14del Mutation in Human Induced Pluripotent Stem Cell-Derived Cardiomyocytes. *Int. J. Mol. Sci.* 22, 13500. doi:10.3390/ijms222413500
- Bagur, R., and Hajnoczky, G. (2017). Intracellular Ca(2+) sensing: Its role in calcium homeostasis and signaling. *Mol. Cell* 66, 780–788. doi:10.1016/j.molcel.2017.05.028
- Balbi, C., Lodder, K., Costa, A., Moimas, S., Moccia, F., Van Herwaarden, T., et al. (2019). Reactivating endogenous mechanisms of cardiac regeneration via paracrine boosting using the human amniotic fluid stem cell secretome. *Int. J. Cardiol.* 287, 87–95. doi:10.1016/j.ijcard.2019.04.011
- Balducci, V., Faris, P., Balbi, C., Costa, A., Negri, S., Rosti, V., et al. (2021). The human amniotic fluid stem cell secretome triggers intracellular Ca²⁺ oscillations, NF-κB nuclear translocation and tube formation in human endothelial colony-forming cells. *J. Cell Mol. Med.* 25, 8074–8086. doi:10.1111/jcmm.16739
- Ballabio, A. (2016). The awesome lysosome. *EMBO Mol. Med.* 8, 73–76. doi:10.15252/emmm.201505966
- Bandell, M., Dubin, A. E., Petrus, M. J., Orth, A., Mathur, J., Hwang, S. W., et al. (2006). High-throughput random mutagenesis screen reveals TRPM8 residues specifically required for activation by menthol. *Nat. Neurosci.* 9, 493–500. doi:10.1038/nn1665
- Barak, P., and Parekh, A. B. (2020). Signaling through Ca(2+) microdomains from store-operated CRAC channels. *Cold Spring Harb. Perspect. Biol.* 12, a035097. doi:10.1101/cshperspect.a035097
- Barazzuol, L., Giamogante, F., and Cali, T. (2021). Mitochondria associated membranes (MAMs): Architecture and physiopathological role. *Cell Calcium* 94, 102343. doi:10.1016/j.ceca.2020.102343
- Bartok, A., Weaver, D., Golenar, T., Nichtova, Z., Katona, M., Bansaghi, S., et al. (2019). IP(3) receptor isoforms differently regulate ER-mitochondrial contacts and local calcium transfer. *Nat. Commun.* 10, 3726. doi:10.1038/s41467-019-11646-3
- Benfenati, V., Martino, N., Antognazza, M. R., Pistone, A., Toffanin, S., Ferroni, S., et al. (2014). Photostimulation of whole-cell conductance in primary rat neocortical astrocytes mediated by organic semiconducting thin films. *Adv. Healthc. Mater.* 3, 392–399. doi:10.1002/adhm.201300179
- Bernardini, M., Brossa, A., Chinigo, G., Grolez, G. P., Trimaglio, G., Allart, L., et al. (2019). Transient receptor potential channel expression signatures in tumor-derived endothelial cells: Functional roles in prostate cancer angiogenesis. *Cancers (Basel)* 11, E956. doi:10.3390/cancers11070956

Acknowledgments

The authors gratefully acknowledge all their coworkers for the enthusiasm and incredible commitment to their research projects on Ca²⁺ signalling. The Article Processing Charge has been paid by the Italian Society of Physiology, which we gratefully acknowledge.

Conflict of interest

The authors declare that the research was conducted in the absence of any commercial or financial relationships that could be construed as a potential conflict of interest.

The reviewer DG declared a past collaboration with the author AFP to the handling editor.

Publisher's note

All claims expressed in this article are solely those of the authors and do not necessarily represent those of their affiliated organizations, or those of the publisher, the editors and the reviewers. Any product that may be evaluated in this article, or claim that may be made by its manufacturer, is not guaranteed or endorsed by the publisher.

- Berra-Romani, R., Brunetti, V., Pellavio, G., Soda, T., Laforenza, U., Scarpellino, G., et al. (2023). Allyl isothiocyanate induces Ca(2+) signals and nitric oxide release by inducing reactive oxygen species production in the human cerebrovascular endothelial cell line hCMEC/D3. *Cells* 12, 1732. doi:10.3390/cells12131732
- Berra-Romani, R., Guerra, G., and Moccia, F. (2021). Editorial: Advances and current challenges in calcium signaling within the cardiovascular system. *Front. Physiol.* 12, 696315. doi:10.3389/fphys.2021.696315
- Berridge, M. J., Bootman, M. D., and Roderick, H. L. (2003). Calcium signalling: Dynamics, homeostasis and remodelling. *Nat. Rev. Mol. Cell Biol.* 4, 517–529. doi:10.1038/nrm1155
- Bers, D. M. (2008). Calcium cycling and signaling in cardiac myocytes. *Annu. Rev. Physiol.* 70, 23–49. doi:10.1146/annurev.physiol.70.113006.100455
- Bers, D. M., and Guo, T. (2005). Calcium signaling in cardiac ventricular myocytes. *Ann. N. Y. Acad. Sci.* 1047, 86–98. doi:10.1196/annals.1341.008
- Bidaux, G., Borowiec, A. S., Dubois, C., Delcourt, P., Schulz, C., Vanden Abeele, F., et al. (2016). Targeting of short TRPM8 isoforms induces 4TM-TRPM8-dependent apoptosis in prostate cancer cells. *Oncotarget* 7, 29063–29080. doi:10.18632/oncotarget.8666
- Bidaux, G., Flourakis, M., Thebault, S., Zholos, A., Beck, B., Gkika, D., et al. (2007). Prostate cell differentiation status determines transient receptor potential melastatin member 8 channel subcellular localization and function. *J. Clin. Invest.* 117, 1647–1657. doi:10.1172/JCI30168
- Bidaux, G., Gordienko, D., Shapovalov, G., Farfariello, V., Borowiec, A. S., Iamshanova, O., et al. (2018). 4TM-TRPM8 channels are new gatekeepers of the ER-mitochondria Ca(2+) transfer. *Biochim. Biophys. Acta Mol. Cell Res.* 1865, 981–994. doi:10.1016/j.bbamcr.2018.04.007
- Bidaux, G., Roudbaraki, M., Merle, C., Crepin, A., Delcourt, P., Slomianny, C., et al. (2005). Evidence for specific TRPM8 expression in human prostate secretory epithelial cells: Functional androgen receptor requirement. *Endocr. Relat. Cancer* 12, 367–382. doi:10.1677/erc.1.00969
- Boettner, B., and Van Aelst, L. (2009). Control of cell adhesion dynamics by Rap1 signaling. *Curr. Opin. Cell Biol.* 21, 684–693. doi:10.1016/j.ccb.2009.06.004
- Bonora, M., Giorgi, C., and Pinton, P. (2022). Molecular mechanisms and consequences of mitochondrial permeability transition. *Nat. Rev. Mol. Cell Biol.* 23, 266–285. doi:10.1038/s41580-021-00433-y
- Bootman, M. D., Berridge, M. J., and Lipp, P. (1997). Cooking with calcium: The recipes for composing global signals from elementary events. *Cell* 91, 367–373. doi:10.1016/s0092-8674(00)80420-1
- Borowiec, A. S., Bidaux, G., Tacine, R., Dubar, P., Pigat, N., Delcourt, P., et al. (2014). Are Orail and Orail3 channels more important than calcium influx for cell proliferation? *Biochim. Biophys. Acta* 1843, 464–472. doi:10.1016/j.bbamcr.2013.11.023
- Bossio, C., Abdel Aziz, I., Tullii, G., Zucchetti, E., Debellis, D., Zangoli, M., et al. (2018). Photocatalytic activity of polymer nanoparticles modulates intracellular calcium dynamics and reactive oxygen species in HEK-293 cells. *Front. Bioeng. Biotechnol.* 6, 114. doi:10.3389/fbioe.2018.00114
- Brailoiu, G. C., Brailoiu, E., Parkesh, R., Galione, A., Churchill, G. C., Patel, S., et al. (2009). NAADP-mediated channel 'chatter' in neurons of the rat medulla oblongata. *Biochem. J.* 419 (91–97), 91–97. doi:10.1042/BJ20081138
- Cai, N., Lou, L., Al-Saadi, N., Tetteh, S., and Runnels, L. W. (2018). The kinase activity of the channel-kinase protein TRPM7 regulates stability and localization of the TRPM7 channel in polarized epithelial cells. *J. Biol. Chem.* 293, 11491–11504. doi:10.1074/jbc.RA118.001925
- Carmona, G., Gottig, S., Orlandi, A., Scheele, J., Bauerle, T., Jugold, M., et al. (2009). Role of the small GTPase Rap1 for integrin activity regulation in endothelial cells and angiogenesis. *Blood* 113, 488–497. doi:10.1182/blood-2008-02-138438
- Caterina, M. J., Schumacher, M. A., Tominaga, M., Rosen, T. A., Levine, J. D., and Julius, D. (1997). The capsaicin receptor: A heat-activated ion channel in the pain pathway. *Nature* 389, 816–824. doi:10.1038/39807
- Cherfils, J., and Zeghouf, M. (2013). Regulation of small GTPases by GEFs, GAPs, and GDIs. *Physiol. Rev.* 93, 269–309. doi:10.1152/physrev.00003.2012
- Chinigo, G., Fiorio Pla, A., and Gkika, D. (2020). TRP channels and small GTPases interplay in the main hallmarks of metastatic cancer. *Front. Pharmacol.* 11, 581455. doi:10.3389/fphar.2020.581455
- Chinigo, G., Grolez, G. P., Audero, M., Bokhobza, A., Bernardini, M., Cicero, J., et al. (2022). TRPM8-Rap1A interaction sites as critical determinants for adhesion and migration of prostate and other epithelial cancer cells. *Cancers (Basel)* 14, 2261. doi:10.3390/cancers14092261
- Chou, C. L., Yip, K. P., Michea, L., Kador, K., Ferraris, J. D., Wade, J. B., et al. (2000). Regulation of aquaporin-2 trafficking by vasopressin in the renal collecting duct. Roles of ryanodine-sensitive Ca2+ stores and calmodulin. *J. Biol. Chem.* 275, 36839–36846. doi:10.1074/jbc.M00552200
- Christensen, K. A., Myers, J. T., and Swanson, J. A. (2002). pH-dependent regulation of lysosomal calcium in macrophages. *J. Cell Sci.* 115, 599–607. doi:10.1242/jcs.115.3.599
- Chrzanowska-Wodnicka, M., Kraus, A. E., Gale, D., White, G. C., and Vansluis, J. (2008). Defective angiogenesis, endothelial migration, proliferation, and MAPK signaling in Rap1b-deficient mice. *Blood* 111, 2647–2656. doi:10.1182/blood-2007-08-109710
- Cieri, D., Vicario, M., Giacomello, M., Vallesse, F., Filadi, R., Wagner, T., et al. (2018). Splic: A split green fluorescent protein-based contact site sensor for narrow and wide heterotypic organelle juxtaposition. *Cell Death Differ.* 25, 1131–1145. doi:10.1038/s41418-017-0033-z
- Clapham, D. E. (2007). Calcium signaling. *Cell* 131, 1047–1058. doi:10.1016/j.cell.2007.11.028
- Crick, F. (1999). The impact of molecular biology on neuroscience. *Philos. Trans. R. Soc. Lond. B Biol. Sci.* 354, 2021–2025. doi:10.1098/rstb.1999.0541
- Csordas, G., Varnai, P., Golenar, T., Roy, S., Purkins, G., Schneider, T. G., et al. (2010). Imaging interorganelle contacts and local calcium dynamics at the ER-mitochondrial interface. *Mol. Cell* 39, 121–132. doi:10.1016/j.molcel.2010.06.029
- Csordas, G., Weaver, D., and Hajnoczky, G. (2018). Endoplasmic reticulum-mitochondrial contactology: Structure and signaling functions. *Trends Cell Biol.* 28, 523–540. doi:10.1016/j.tcb.2018.02.009
- Curcio, S., Schober, R., Schindl, R., and Groschner, K. (2019). TRPC-mediated Ca(2+) signaling and control of cellular functions. *Semin. Cell Dev. Biol.* 94, 28–39. doi:10.1016/j.semdcb.2019.02.001
- De Strooper, B., and Karran, E. (2016). The cellular phase of alzheimer's disease. *Cell* 164, 603–615. doi:10.1016/j.cell.2015.12.056
- Deisseroth, K. (2011). Optogenetics. *Nat. Methods* 8, 26–29. doi:10.1038/nmeth.f.324
- Demattei, G., Vydymantaite, G., Ruffinatti, F. A., Chahin, M., Farruggio, S., Barberis, E., et al. (2020). Proteomic analysis links alterations of bioenergetics, mitochondria-ER interactions and proteostasis in hippocampal astrocytes from 3xTg-AD mice. *Cell Death Dis.* 11, 645. doi:10.1038/s41419-020-02911-1
- Desai, B. N., Krapivinsky, G., Navarro, B., Krapivinsky, L., Carter, B. C., Febvay, S., et al. (2012). Cleavage of TRPM7 releases the kinase domain from the ion channel and regulates its participation in Fas-induced apoptosis. *Dev. Cell* 22, 1149–1162. doi:10.1016/j.devcel.2012.04.006
- Descasez, V., Mestre, E., Marquet, P., and Essig, M. (2012). Calcineurin regulation of cytoskeleton organization: A new paradigm to analyse the effects of calcineurin inhibitors on the kidney. *J. Cell Mol. Med.* 16, 218–227. doi:10.1111/j.1582-4934.2011.01398.x
- Dhaka, A., Earley, T. J., Watson, J., and Patapoutian, A. (2008). Visualizing cold spots: TRPM8-expressing sensory neurons and their projections. *J. Neurosci.* 28, 566–575. doi:10.1523/JNEUROSCI.3976-07.2008
- Di Maria, F., Lodola, F., Zucchetti, E., Benfenati, F., and Lanzani, G. (2018). The evolution of artificial light actuators in living systems: From planar to nanostructured interfaces. *Chem. Soc. Rev.* 47, 4757–4780. doi:10.1039/c7cs00860k
- Di Paola, S., Scotto-Rosato, A., and Medina, D. L. (2018). TRPML1: The Ca(2+) retractor of the lysosome. *Cell Calcium* 69, 112–121. doi:10.1016/j.ceca.2017.06.006
- Difrancesco, M. L., Lodola, F., Colombo, E., Maragiano, L., Bramini, M., Paterno, G. M., et al. (2020). Neuronal firing modulation by a membrane-targeted photoswitch. *Nat. Nanotechnol.* 15, 296–306. doi:10.1038/s41565-019-0632-6
- Diver, M. M., Lin King, J. V., Julius, D., and Cheng, Y. (2022). Sensory TRP channels in three dimensions. *Annu. Rev. Biochem.* 91, 629–649. doi:10.1146/annurev-biochem-032620-105738
- Dragoni, S., Laforenza, U., Bonetti, E., Lodola, F., Bottino, C., Berra-Romani, R., et al. (2011). Vascular endothelial growth factor stimulates endothelial colony forming cells proliferation and tubulogenesis by inducing oscillations in intracellular Ca2+ concentration. *Stem Cells* 29, 1898–1907. doi:10.1002/stem.734
- Dragoni, S., Reforgiato, M., Zuccolo, E., Poletto, V., Lodola, F., Ruffinatti, F. A., et al. (2015). Dysregulation of VEGF-induced proangiogenic Ca2+ oscillations in primary myelofibrosis-derived endothelial colony-forming cells. *Exp. Hematol.* 43, 1019–1030.e3. doi:10.1016/j.exphem.2015.09.002
- Eisner, D. A., Caldwell, J. L., Kistamas, K., and Trafford, A. W. (2017). Calcium and excitation-contraction coupling in the heart. *Circ. Res.* 121, 181–195. doi:10.1161/CIRCRESAHA.117.310230
- Ezra-Nevo, G., Prestori, F., Locatelli, F., Soda, T., Ten Brinke, M. M., Engel, M., et al. (2018). Cerebellar learning properties are modulated by the CRF receptor. *J. Neurosci.* 38, 6751–6765. doi:10.1523/JNEUROSCI.3106-15.2018
- Faouzi, M., Kilch, T., Horgen, F. D., Fleig, A., and Penner, R. (2017). The TRPM7 channel kinase regulates store-operated calcium entry. *J. Physiol.* 595, 3165–3180. doi:10.1113/jp274006
- Faris, P., Casali, C., Negri, S., Iengo, L., Biggiogera, M., Maione, A. S., et al. (2022). Nicotinic acid adenine dinucleotide phosphate induces intracellular Ca(2+) signalling and stimulates proliferation in human cardiac mesenchymal stromal cells. *Front. Cell Dev. Biol.* 10, 874043. doi:10.3389/fcell.2022.874043
- Faris, P., Pellavio, G., Ferulli, F., Di Nezza, F., Shekha, M., Lim, D., et al. (2019). Nicotinic acid adenine dinucleotide phosphate (NAADP) induces intracellular Ca(2+) release through the two-pore channel TPC1 in metastatic colorectal cancer cells. *Cancers (Basel)* 11, 542. doi:10.3390/cancers11040542
- Faris, P., Rumolo, A., Pellavio, G., Tanzi, M., Vismara, M., Berra-Romani, R., et al. (2023). Transient receptor potential ankyrin 1 (TRPA1) mediates reactive oxygen

species-induced Ca(2+) entry, mitochondrial dysfunction, and caspase-3/7 activation in primary cultures of metastatic colorectal carcinoma cells. *Cell Death Discov.* 9, 213. doi:10.1038/s41420-023-01530-x

Faris, P., Shekha, M., Montagna, D., Guerra, G., and Moccia, F. (2018). Endolysosomal Ca(2+) signalling and cancer hallmarks: Two-pore channels on the move, TRPML1 lags behind. *Cancers (Basel)* 11, 27. doi:10.3390/cancers11010027

Fernandez, J. A., Skryma, R., Bidaux, G., Magleby, K. L., Scholfield, C. N., McGeown, J. G., et al. (2012). Short isoforms of the cold receptor TRPM8 inhibit channel gating by mimicking heat action rather than chemical inhibitors. *J. Biol. Chem.* 287, 2963–2970. doi:10.1074/jbc.M111.272823

Feyen, P., Colombo, E., Endeman, D., Nova, M., Laudato, L., Martino, N., et al. (2016). Light-evoked hyperpolarization and silencing of neurons by conjugated polymers. *Sci. Rep.* 6, 22718. doi:10.1038/srep22718

Fiorio Pla, A., Ong, H. L., Cheng, K. T., Brossa, A., Bussolati, B., Lockwich, T., et al. (2012). TRPV4 mediates tumor-derived endothelial cell migration via arachidonic acid-activated actin remodeling. *Oncogene* 31, 200–212. doi:10.1038/ncr.2011.231

Foster, W. J., Taylor, H. B. C., Padamsey, Z., Jeans, A. F., Galione, A., and Emptage, N. J. (2018). Hippocampal mGluR1-dependent long-term potentiation requires NAADP-mediated acidic store Ca(2+) signaling. *Sci. Signal* 11, eaat9093. doi:10.1126/scisignal.aat9093

Fujiwara, Y., and Minor, D. L., Jr. (2008). X-ray crystal structure of a TRPM assembly domain reveals an antiparallel four-stranded coiled-coil. *J. Mol. Biol.* 383, 854–870. doi:10.1016/j.jmb.2008.08.059

Galione, A., Davis, L. C., Martucci, L. L., and Morgan, A. J. (2023). NAADP-mediated Ca(2+) signalling. *Handb. Exp. Pharmacol.* 278, 3–34. doi:10.1007/164_2022_607

Galione, A. (2019). NAADP receptors. *Cold Spring Harb. Perspect. Biol.* 11, a035071. doi:10.1101/cshperspect.a035071

Gan, N., Han, Y., Zeng, W., Wang, Y., Xue, J., and Jiang, Y. (2022). Structural mechanism of allosteric activation of TRPML1 by PI(3,5)P(2) and rapamycin. *Proc. Natl. Acad. Sci. U. S. A.* 119, e2120404119. doi:10.1073/pnas.2120404119

Genova, T., Grolez, G. P., Camillo, C., Bernardini, M., Bokhobza, A., Richard, E., et al. (2017). TRPM8 inhibits endothelial cell migration via a non-channel function by trapping the small GTPase Rap1. *J. Cell Biol.* 216, 2107–2130. doi:10.1083/jcb.201506024

Genovesi, S., Moro, R., Vignoli, B., De Felice, D., Canossa, M., Montironi, R., et al. (2022). Trpm8 expression in human and mouse castration resistant prostate adenocarcinoma paves the way for the preclinical development of TRPM8-based targeted therapies. *Biomolecules* 12, 193. doi:10.3390/biom12020193

Gerasimenko, J. V., Tepikin, A. V., Petersen, O. H., and Gerasimenko, O. V. (1998). Calcium uptake via endocytosis with rapid release from acidifying endosomes. *Curr. Biol.* 8, 1335–1338. doi:10.1016/s0960-9822(07)00565-9

Gerndt, S., Chen, C. C., Chao, Y. K., Yuan, Y., Burgstaller, S., Scotto Rosato, A., et al. (2020). Agonist-mediated switching of ion selectivity in TPC2 differentially promotes lysosomal function. *Life* 9, e54712. doi:10.7554/eLife.54712

Gherardi, G., Monticelli, H., Rizzuto, R., and Mammucari, C. (2020). The mitochondrial Ca(2+) uptake and the fine-tuning of aerobic metabolism. *Front. Physiol.* 11, 554904. doi:10.3389/fphys.2020.554904

Ghezzi, D., Antognazza, M. R., Dal Maschio, M., Lanzarini, E., Benfenati, F., and Lanzani, G. (2011). A hybrid bioorganic interface for neuronal photoactivation. *Nat. Commun.* 2, 166. doi:10.1038/ncomms1164

Ghezzi, D., Antognazza, M. R., Maccarone, R., Bellani, S., Lanzarini, E., Martino, N., et al. (2013). A polymer optoelectronic interface restores light sensitivity in blind rat retinas. *Nat. Photonics* 7, 400–406. doi:10.1038/nphoton.2013.34

Gomez-Ospina, N., Tsuruta, F., Barreto-Chang, O., Hu, L., and Dolmetsch, R. (2006). The C terminus of the L-type voltage-gated calcium channel Ca(V)1.2 encodes a transcription factor. *Cell* 127, 591–606. doi:10.1016/j.cell.2006.10.017

Gong, C., Bonfilii, L., Zheng, Y., Cecarini, V., Cuccioloni, M., Angeletti, M., et al. (2023). Immortalized alzheimer's disease astrocytes: Characterization of their proteolytic systems. *Mol. Neurobiol.* 60, 2787–2800. doi:10.1007/s12035-023-03231-z

Gorostiza, P., and Isacoff, E. Y. (2008). Optical switches for remote and noninvasive control of cell signaling. *Science* 322, 395–399. doi:10.1126/science.1166022

Grolez, G. P., Chinigo, G., Barras, A., Hammadi, M., Noyer, L., Kondratska, K., et al. (2022). TRPM8 as an anti-tumoral target in prostate cancer growth and metastasis dissemination. *Int. J. Mol. Sci.* 23, 6672. doi:10.3390/ijms23126672

Grolez, G. P., Gordiendko, D. V., Clarisse, M., Hammadi, M., Desruelles, E., Fromont, G., et al. (2019). TRPM8-androgen receptor association within lipid rafts promotes prostate cancer cell migration. *Cell Death Dis.* 10, 652. doi:10.1038/s41419-019-1891-8

Grolla, A. A., Fakhfour, G., Balzaretto, G., Marcello, E., Gardoni, F., Canonico, P. L., et al. (2013a). Aβ leads to Ca²⁺ signaling alterations and transcriptional changes in glial cells. *Neurobiol. Aging* 34, 511–522. doi:10.1016/j.neurobiolaging.2012.05.005

Grolla, A. A., Sim, J. A., Lim, D., Rodriguez, J. J., Genazzani, A. A., and Verkhratsky, A. (2013b). Amyloid-beta and Alzheimer's disease type pathology differentially affects the calcium signalling toolkit in astrocytes from different brain regions. *Cell Death Dis.* 4, e623. doi:10.1038/cddis.2013.145

Guarini, G., Ohanyan, V. A., Kmetz, J. G., Dellostretto, D. J., Thoppil, R. J., Thodeti, C. K., et al. (2012). Disruption of TRPV1-mediated coupling of coronary blood flow to cardiac metabolism in diabetic mice: Role of nitric oxide and BK channels. *Am. J. Physiol. Heart Circ. Physiol.* 303, H216–H223. doi:10.1152/ajpheart.00011.2012

He, L., Wang, L., Zeng, H., Tan, P., Ma, G., Zheng, S., et al. (2021). Engineering of a bona fide light-operated calcium channel. *Nat. Commun.* 12, 164. doi:10.1038/s41467-020-20425-4

Herrera-Cruz, M. S., and Simmen, T. (2017). Over six decades of discovery and characterization of the architecture at mitochondria-associated membranes (MAMs). *Adv. Exp. Med. Biol.* 997, 13–31. doi:10.1007/978-981-10-4567-7_2

Hibino, H., Pironkova, R., Onwumere, O., Rousset, M., Charnet, P., Hudspeth, A. J., et al. (2003). Direct interaction with a nuclear protein and regulation of gene silencing by a variant of the Ca2+-channel beta 4 subunit. *Proc. Natl. Acad. Sci. U. S. A.* 100, 307–312. doi:10.1073/pnas.0136791100

Hirano, T. (2013). Long-term depression and other synaptic plasticity in the cerebellum. *Proc. Jpn. Acad. Ser. B Phys. Biol. Sci.* 89, 183–195. doi:10.2183/pjab.89.183

Hopkins, J., Travaglini, R., Lauto, A., Cramer, T., Fraboni, B., Seidel, J., et al. (2019). Photoactive organic substrates for cell stimulation: Progress and perspectives. *Adv. Mat. Technol.* 4, 1800744. doi:10.1002/admt.201800744

Izquierdo-Serra, M., Bautista-Barrufet, A., Trapero, A., Garrido-Charles, A., Diaz-Tahoces, A., Camarero, N., et al. (2016). Optical control of endogenous receptors and cellular excitability using targeted covalent photoswitches. *Nat. Commun.* 7, 12221. doi:10.1038/ncomms12221

Jordt, S. E., Tominaga, M., and Julius, D. (2000). Acid potentiation of the capsaicin receptor determined by a key extracellular site. *Proc. Natl. Acad. Sci. U. S. A.* 97, 8134–8139. doi:10.1073/pnas.100129497

Katona, M., Bartok, A., Nichtova, Z., Csordas, G., Berezhnaya, E., Weaver, D., et al. (2022). Capture at the ER-mitochondrial contacts licenses IP(3) receptors to stimulate local Ca(2+) transfer and oxidative metabolism. *Nat. Commun.* 13, 6779. doi:10.1038/s41467-022-34365-8

Keebler, M. V., and Taylor, C. W. (2017). Endogenous signalling pathways and caged IP3 evoke Ca(2+) puffs at the same abundant immobile intracellular sites. *J. Cell Sci.* 130, 3728–3739. doi:10.1242/jcs.208520

Kilpatrick, B. S., Eden, E. R., Hockey, L. N., Yates, E., Futter, C. E., and Patel, S. (2017). An endosomal NAADP-sensitive two-pore Ca(2+) channel regulates ER-endosome membrane contact sites to control growth factor signaling. *Cell Rep.* 18, 1636–1645. doi:10.1016/j.celrep.2017.01.052

Kilpatrick, B. S., Eden, E. R., Schapira, A. H., Futter, C. E., and Patel, S. (2013). Direct mobilisation of lysosomal Ca2+ triggers complex Ca2+ signals. *J. Cell Sci.* 126, 60–66. doi:10.1242/jcs.118836

Kilpatrick, B. S., Yates, E., Grimm, C., Schapira, A. H., and Patel, S. (2016). Endolysosomal TRP mucolipin-1 channels trigger global ER Ca2+ release and Ca2+ influx. *J. Cell Sci.* 129, 3859–3867. doi:10.1242/jcs.190322

Kiselyov, K., Yamaguchi, S., Lyons, C. W., and Muallem, S. (2010). Aberrant Ca2+ handling in lysosomal storage disorders. *Cell Calcium* 47, 103–111. doi:10.1016/j.ceca.2009.12.007

Klasen, K., Hollatz, D., Zielke, S., Gisselmann, G., Hatt, H., and Wetzel, C. H. (2012). The TRPM8 ion channel comprises direct Gq protein-activating capacity. *Pflugers Arch.* 463, 779–797. doi:10.1007/s00424-012-1098-7

Knepper, M. A., Kwon, T. H., and Nielsen, S. (2015). Molecular physiology of water balance. *N. Engl. J. Med.* 372, 1349–1358. doi:10.1056/NEJMra1404726

Knot, H. J., and Nelson, M. T. (1998). Regulation of arterial diameter and wall [Ca2+] in cerebral arteries of rat by membrane potential and intravascular pressure. *J. Physiol.* 508 (Pt 1), 199–209. doi:10.1111/j.1469-7793.1998.199br.x

Knowlton, W. M., Palkar, R., Lippoldt, E. K., McCoy, D. D., Baluch, F., Chen, J., et al. (2013). A sensory-labeled line for cold: TRPM8-expressing sensory neurons define the cellular basis for cold, cold pain, and cooling-mediated analgesia. *J. Neurosci.* 33, 2837–2848. doi:10.1523/JNEUROSCI.1943-12.2013

Kordasiewicz, H. B., Thompson, R. M., Clark, H. B., and Gomez, C. M. (2006). C-termini of P/Q-type Ca2+ channel alpha1A subunits translocate to nuclei and promote polyglutamine-mediated toxicity. *Hum. Mol. Genet.* 15, 1587–1599. doi:10.1093/hmg/ddl080

Kraft, R., and Harteneck, C. (2005). The mammalian melastatin-related transient receptor potential channel channels: An overview. *Pflugers Arch.* 451, 204–211. doi:10.1007/s00424-005-1428-0

Landstrom, A. P., Dobrev, D., and Wehrens, X. H. T. (2017). Calcium signaling and cardiac arrhythmias. *Circ. Res.* 120, 1969–1993. doi:10.1161/CIRCRESAHA.117.310083

Lazzarini, E., Lodrini, A. M., Arici, M., Bolis, S., Vagni, S., Panella, S., et al. (2022). Stress-induced premature senescence is associated with a prolonged QT interval and recapitulates features of cardiac aging. *Theranostics* 12, 5237–5257. doi:10.7150/thno.70884

Leal, N. S., and Martins, L. M. (2021). Mind the gap: Mitochondria and the endoplasmic reticulum in neurodegenerative diseases. *Biomedicine* 9, 227. doi:10.3390/biomedicine9020227

- Leippe, P., Koehler Leman, J., and Trauner, D. (2017). Specificity and speed: Tethered photopharmacology. *Biochemistry* 56, 5214–5220. doi:10.1021/acs.biochem.7b00687
- Leoni, L., Tonelli, F., Besio, R., Gioia, R., Moccia, F., Rossi, A., et al. (2021). Knocking out TMEM38B in human foetal osteoblasts hFOB 1.19 by CRISPR/cas9: A model for recessive OI type xiv. *PLoS One* 16, e0257254. doi:10.1371/journal.pone.0257254
- Lewis, R. S. (2020). Store-operated calcium channels: From function to structure and back again. *Cold Spring Harb. Perspect. Biol.* 12, a035055. doi:10.1101/cshperspect.a035055
- Lia, A., Sansevero, G., Chiavagato, A., Sbrissa, M., Pendin, D., Mariotti, L., et al. (2023). Rescue of astrocyte activity by the calcium sensor STIM1 restores long-term synaptic plasticity in female mice modelling Alzheimer's disease. *Nat. Commun.* 14, 1590. doi:10.1038/s41467-023-37240-2
- Lim, D., Bertoli, A., Sorgato, M. C., and Moccia, F. (2016a). Generation and usage of aequorin lentiviral vectors for Ca(2+) measurement in sub-cellular compartments of hard-to-transfect cells. *Cell Calcium* 59, 228–239. doi:10.1016/j.ceca.2016.03.001
- Lim, D., Dematteis, G., Tapella, L., Genazzani, A. A., Cali, T., Brini, M., et al. (2021a). Ca(2+) handling at the mitochondria-ER contact sites in neurodegeneration. *Cell Calcium* 98, 102453. doi:10.1016/j.ceca.2021.102453
- Lim, D., Ercolano, E., Kyoizuka, K., Nusco, G. A., Moccia, F., Lange, K., et al. (2003). The M-phase-promoting factor modulates the sensitivity of the Ca2+ stores to inositol 1,4,5-trisphosphate via the actin cytoskeleton. *J. Biol. Chem.* 278, 42505–42514. doi:10.1074/jbc.M301851200
- Lim, D., Iyer, A., Ronco, V., Grolla, A. A., Canonico, P. L., Aronica, E., et al. (2013). Amyloid beta deregulates astroglial mGluR5-mediated calcium signaling via calcineurin and Nf-kB. *Glia* 61, 1134–1145. doi:10.1002/glia.22502
- Lim, D., Rodriguez-Arellano, J. J., Parpura, V., Zorec, R., Zeidan-Chulia, F., Genazzani, A. A., et al. (2016b). Calcium signalling toolkits in astrocytes and spatio-temporal progression of Alzheimer's disease. *Curr. Alzheimer Res.* 13, 359–369. doi:10.2174/156720501366615116130104
- Lim, D., Ronco, V., Grolla, A. A., Verkhatsky, A., and Genazzani, A. A. (2014). Glial calcium signalling in Alzheimer's disease. *Rev. Physiol. Biochem. Pharmacol.* 167, 45–65. doi:10.1007/112_2014_19
- Lim, D., Semyanov, A., Genazzani, A., and Verkhatsky, A. (2021b). Calcium signaling in neuroglia. *Int. Rev. Cell Mol. Biol.* 362, 1–53. doi:10.1016/bs.ircmb.2021.01.003
- Lim, D., Tapella, L., Dematteis, G., Genazzani, A. A., Corazzari, M., and Verkhatsky, A. (2023). The endoplasmic reticulum stress and unfolded protein response in Alzheimer's disease: A calcium dyshomeostasis perspective. *Ageing Res. Rev.* 87, 101914. doi:10.1016/j.arr.2023.101914
- Lloyd-Evans, E., Waller-Evans, H., Peterneva, K., and Platt, F. M. (2010). Endolysosomal calcium regulation and disease. *Biochem. Soc. Trans.* 38, 1458–1464. doi:10.1042/BST0381458
- Locatelli, F., Soda, T., Montagna, I., Tritto, S., Botta, L., Prestori, F., et al. (2021). Calcium Channel-dependent induction of long-term synaptic plasticity at excitatory golgi cell synapses of cerebellum. *J. Neurosci.* 41, 3307–3319. doi:10.1523/JNEUROSCI.3013-19.2020
- Lodola, F., Laforenza, U., Cattaneo, F., Ruffinatti, F. A., Poletto, V., Massa, M., et al. (2017a). VEGF-induced intracellular Ca2+ oscillations are down-regulated and do not stimulate angiogenesis in breast cancer-derived endothelial colony forming cells. *Oncotarget* 8, 95223–95246. doi:10.18632/oncotarget.20255
- Lodola, F., Martino, N., Tullii, G., Lanzani, G., and Antognazza, M. R. (2017b). Conjugated polymers mediate effective activation of the mammalian ion channel Transient receptor potential vanilloid 1. *Sci. Rep.* 7, 8477. doi:10.1038/s41598-017-08541-6
- Lodola, F., and Moccia, F. (2022). Fiat lux - light at the service of cardiac physiology. *pH* 2, 39–46.
- Lodola, F., Rosti, V., Tullii, G., Desii, A., Tapella, L., Catarsi, P., et al. (2019a). Conjugated polymers optically regulate the fate of endothelial colony-forming cells. *Sci. Adv.* 5, eaav4620. doi:10.1126/sciadv.aav4620
- Lodola, F., Vurro, V., Crasto, S., Di Pasquale, E., and Lanzani, G. (2019b). Optical pacing of human-induced pluripotent stem cell-derived cardiomyocytes mediated by a conjugated polymer interface. *Adv. Healthc. Mater.* 8, e1900198. doi:10.1002/adhm.201900198
- Loncke, J., Kaasik, A., Bezprozvanny, I., Parys, J. B., Kerkhofs, M., and Bultynck, G. (2021). Balancing ER-mitochondrial Ca(2+) fluxes in health and disease. *Trends Cell Biol.* 31, 598–612. doi:10.1016/j.tcb.2021.02.003
- Longden, T. A., Mughal, A., Hennig, G. W., Harraz, O. F., Shui, B., Lee, F. K., et al. (2021). Local IP3 receptor-mediated Ca(2+) signals compound to direct blood flow in brain capillaries. *Sci. Adv.* 7, eab0101. doi:10.1126/sciadv.ab0101
- Mabonga, L., and Kappo, A. P. (2019). Protein-protein interaction modulators: Advances, successes and remaining challenges. *Biophys. Rev.* 11, 559–581. doi:10.1007/s12551-019-00570-x
- Macgregor, A., Yamasaki, M., Rakovic, S., Sanders, L., Parkesh, R., Churchill, G. C., et al. (2007). NAADP controls cross-talk between distinct Ca2+ stores in the heart. *J. Biol. Chem.* 282, 15302–15311. doi:10.1074/jbc.M611167200
- Madrid, R., Donovan-Rodriguez, T., Meseguer, V., Acosta, M. C., Belmonte, C., and Viana, F. (2006). Contribution of TRPM8 channels to cold transduction in primary sensory neurons and peripheral nerve terminals. *J. Neurosci.* 26, 12512–12525. doi:10.1523/JNEUROSCI.3752-06.2006
- Magni, A., Bondelli, G., Paterno, G. M., Sardar, S., Sesti, V., D'andrea, C., et al. (2022). Azobenzene photoisomerization probes cell membrane viscosity. *Phys. Chem. Chem. Phys.* 24, 8716–8723. doi:10.1039/d1cp05881a
- Maione, A. S., Faris, P., Iengo, L., Catto, V., Bisonni, L., Lodola, F., et al. (2022). Ca(2+) dysregulation in cardiac stromal cells sustains fibro-adipose remodeling in Arrhythmogenic Cardiomyopathy and can be modulated by flecainide. *J. Transl. Med.* 20, 522. doi:10.1186/s12967-022-03742-8
- Mamenko, M., Dhande, I., Tomilin, V., Zaika, O., Boukelmoune, N., Zhu, Y., et al. (2016). Defective store-operated calcium entry causes partial nephrogenic diabetes insipidus. *J. Am. Soc. Nephrol.* 27, 2035–2048. doi:10.1681/ASN.2014121200
- Marta, K., Booth, D., Csordas, G., and Hajnoczy, G. (2022). Fluorescent protein transgenic mice for the study of Ca(2+) and redox signaling. *Free Radic. Biol. Med.* 181, 241–250. doi:10.1016/j.freeradbiomed.2022.02.011
- Martinotti, S., Laforenza, U., Patrone, M., Moccia, F., and Ranzato, E. (2019). Honey-mediated wound healing: H2O2 entry through AQP3 determines extracellular Ca2+ influx. *Int. J. Mol. Sci.* 20, 764. doi:10.3390/ijms20030764
- Maya-Vetencourt, J. F., Ghezzi, D., Antognazza, M. R., Colombo, E., Mete, M., Feyen, P., et al. (2017). A fully organic retinal prosthesis restores vision in a rat model of degenerative blindness. *Nat. Mater.* 16, 681–689. doi:10.1038/nmat4874
- Maya-Vetencourt, J. F., Manfredi, G., Mete, M., Colombo, E., Bramini, M., Di Marco, S., et al. (2020). Subretinally injected semiconducting polymer nanoparticles rescue vision in a rat model of retinal dystrophy. *Nat. Nanotechnol.* 15, 698–708. doi:10.1038/s41565-020-0696-3
- Mckemy, D. D., Neuhauser, W. M., and Julius, D. (2002). Identification of a cold receptor reveals a general role for TRP channels in thermosensation. *Nature* 416, 52–58. doi:10.1038/nature719
- Medina, D. L., Di Paola, S., Peluso, I., Armani, A., De Stefani, D., Venditti, R., et al. (2015). Lysosomal calcium signalling regulates autophagy through calcineurin and TFEB. *Nat. Cell Biol.* 17, 288–299. doi:10.1038/ncb3114
- Medina, D. L. (2021). Lysosomal calcium and autophagy. *Int. Rev. Cell Mol. Biol.* 362, 141–170. doi:10.1016/bs.ircmb.2021.03.002
- Melchionda, M., Pittman, J. K., Mayor, R., and Patel, S. (2016). Ca2+/H+ exchange by acidic organelles regulates cell migration *in vivo*. *J. Cell Biol.* 212, 803–813. doi:10.1083/jcb.201510019
- Menigoz, A., Ahmed, T., Sabanov, V., Philippaert, K., Pinto, S., Kerselaers, S., et al. (2016). TRPM4-dependent post-synaptic depolarization is essential for the induction of NMDA receptor-dependent LTP in CA1 hippocampal neurons. *Pflugers Arch.* 468, 593–607. doi:10.1007/s00424-015-1764-7
- Merlo, S., Spampinato, S. F., and Lim, D. (2021). Molecular aspects of cellular dysfunction in Alzheimer's disease: The need for a holistic view of the early pathogenesis. *Biomolecules* 11, 1807. doi:10.3390/biom11121807
- Michelucci, A., Pietrangeli, L., Rastelli, G., Protasi, F., Dirksen, R. T., and Boncompagni, S. (2022). Constitutive assembly of Ca2+ entry units in soleus muscle from calsequestrin knockout mice. *J. Gen. Physiol.* 154, e202213114. doi:10.1085/jgp.202213114
- Millar, F. R., Janes, S. M., and Giangreco, A. (2017). Epithelial cell migration as a potential therapeutic target in early lung cancer. *Eur. Respir. Rev.* 26, 160069. doi:10.1183/16006617.0069-2016
- Moccia, F., Antognazza, M. R., and Lodola, F. (2020). Towards novel geneless approaches for therapeutic angiogenesis. *Front. Physiol.* 11, 616189. doi:10.3389/fphys.2020.616189
- Moccia, F., Berra-Romani, R., Baruffi, S., Spaggiari, S., Signorelli, S., Castelli, L., et al. (2002). Ca2+ uptake by the endoplasmic reticulum Ca2+-ATPase in rat microvascular endothelial cells. *Biochem. J.* 364, 235–244. doi:10.1042/bj3640235
- Moccia, F., Bonetti, E., Dragoni, S., Fontana, J., Lodola, F., Romani, R. B., et al. (2012). Hematopoietic progenitor and stem cells circulate by surfing on intracellular Ca2+ waves: A novel target for cell-based therapy and anti-cancer treatment? *Curr. Signal Transd T* 7, 161–176. doi:10.2174/157436212800376672
- Moccia, F., Brunetti, V., Perna, A., Guerra, G., Soda, T., and Berra-Romani, R. (2023). The molecular heterogeneity of store-operated Ca(2+) entry in vascular endothelial cells: The different roles of Orai1 and TRPC1/TRPC4 channels in the transition from Ca(2+)-selective to non-selective cation currents. *Int. J. Mol. Sci.* 24, 3259. doi:10.3390/ijms24043259
- Moccia, F., Dragoni, S., Cinelli, M., Montagnani, S., Amato, B., Rosti, V., et al. (2013). How to utilize Ca2+ signals to rejuvenate the reparative phenotype of senescent endothelial progenitor cells in elderly patients affected by cardiovascular diseases: A useful therapeutic support of surgical approach? *BMC Surg.* 13 (Suppl. 2), S46. doi:10.1186/1471-2482-13-S2-S46
- Moccia, F. (2018). Endothelial Ca(2+) signaling and the resistance to anticancer treatments: Partners in crime. *Int. J. Mol. Sci.* 19, 217. doi:10.3390/ijms19010217

- Moccia, F., Lodola, F., Stadiotti, I., Pilato, C. A., Bellin, M., Carugo, S., et al. (2019a). Calcium as a key player in arrhythmogenic cardiomyopathy: Adhesion disorder or intracellular alteration? *Int. J. Mol. Sci.* 20, 3986. doi:10.3390/ijms20163986
- Moccia, F., Lucariello, A., and Guerra, G. (2018). TRPC3-mediated Ca(2+) signals as a promising strategy to boost therapeutic angiogenesis in failing hearts: The role of autologous endothelial colony forming cells. *J. Cell Physiol.* 233, 3901–3917. doi:10.1002/jcp.26152
- Moccia, F., Negri, S., Faris, P., Perna, A., De Luca, A., Soda, T., et al. (2021a). Targeting endolysosomal two-pore channels to treat cardiovascular disorders in the novel COronaVirus disease 2019. *Front. Physiol.* 12, 629119. doi:10.3389/fphys.2021.629119
- Moccia, F., Negri, S., Faris, P., Ronchi, C., and Lodola, F. (2022). Optical excitation of organic semiconductors as a highly selective strategy to induce vascular regeneration and tissue repair. *Vasc. Pharmacol.* 144, 106998. doi:10.1016/j.vph.2022.106998
- Moccia, F., Negri, S., Shekha, M., Faris, P., and Guerra, G. (2019b). Endothelial Ca(2+) signaling, angiogenesis and vasculogenesis: Just what it takes to make a blood vessel. *Int. J. Mol. Sci.* 20, 3962. doi:10.3390/ijms20163962
- Moccia, F., Nusco, G. A., Lim, D., Kyozyuka, K., and Santella, L. (2006). NAADP and InsP3 play distinct roles at fertilization in starfish oocytes. *Dev. Biol.* 294, 24–38. doi:10.1016/j.ydbio.2006.02.011
- Moccia, F., Zuccolo, E., Di Nezza, F., Pellavio, G., Faris, P. S., Negri, S., et al. (2021b). Nicotinic acid adenine dinucleotide phosphate activates two-pore channel TPC1 to mediate lysosomal Ca(2+) release in endothelial colony-forming cells. *J. Cell Physiol.* 236, 688–705. doi:10.1002/jcp.29896
- Montes De Oca Balderas, P., and Aguilera, P. (2015). A metabotropic-like flux-independent NMDA receptor regulates Ca2+ exit from endoplasmic reticulum and mitochondrial membrane potential in cultured astrocytes. *PLoS One* 10, e0126314. doi:10.1371/journal.pone.0126314
- Montes De Oca Balderas, P. (2022). Meeting report: Flux-independent signaling by ionotropic receptors: Unforeseen roles, complexities, and challenges. *J. Biol. Chem.* 298, 102330. doi:10.1016/j.jbc.2022.102330
- Morgan, A. J., Davis, L. C., and Galione, A. (2015). Imaging approaches to measuring lysosomal calcium. *Methods Cell Biol.* 126, 159–195. doi:10.1016/bs.mcb.2014.10.031
- Morgan, A. J., Platt, F. M., Lloyd-Evans, E., and Galione, A. (2011). Molecular mechanisms of endolysosomal Ca2+ signalling in health and disease. *Biochem. J.* 439, 349–374. doi:10.1042/BJ20110949
- Negri, S., Faris, P., Maniezi, C., Pellavio, G., Spaiardi, P., Botta, L., et al. (2021a). NMDA receptors elicit flux-independent intracellular Ca(2+) signals via metabotropic glutamate receptors and flux-dependent nitric oxide release in human brain microvascular endothelial cells. *Cell Calcium* 99, 102454. doi:10.1016/j.ceca.2021.102454
- Negri, S., Faris, P., and Moccia, F. (2021b). Endolysosomal Ca(2+) signaling in cardiovascular health and disease. *Int. Rev. Cell Mol. Biol.* 363, 203–269. doi:10.1016/bs.irmb.2021.03.001
- Negri, S., Faris, P., Soda, T., and Moccia, F. (2021c). Endothelial signaling at the core of neurovascular coupling: The emerging role of endothelial inward-rectifier K(+) (Kir2.1) channels and N-methyl-D-aspartate receptors in the regulation of cerebral blood flow. *Int. J. Biochem. Cell Biol.* 135, 105983. doi:10.1016/j.biocel.2021.105983
- Negri, S., Faris, P., Tullii, G., Vismara, M., Pellegata, A. F., Lodola, F., et al. (2022a). Conjugated polymers mediate intracellular Ca(2+) signals in circulating endothelial colony forming cells through the reactive oxygen species-dependent activation of Transient Receptor Potential Vanilloid 1 (TRPV1). *Cell Calcium* 101, 102502. doi:10.1016/j.ceca.2021.102502
- Negri, S., Scolari, F., Vismara, M., Brunetti, V., Faris, P., Terribile, G., et al. (2022b). GABA(A) and GABA(B) receptors mediate GABA-induced intracellular Ca(2+) signals in human brain microvascular endothelial cells. *Cells* 11, 3860. doi:10.3390/cells11233860
- Nelson, M. T., Cheng, H., Rubart, M., Santana, L. F., Bonev, A. D., Knot, H. J., et al. (1995). Relaxation of arterial smooth muscle by calcium sparks. *Science* 270, 633–637. doi:10.1126/science.270.5236.633
- Nesher, N., Maiolo, F., Shomrat, T., Hochner, B., and Zullo, L. (2019). From synaptic input to muscle contraction: Arm muscle cells of *Octopus vulgaris* show unique neuromuscular junction and excitation-contraction coupling properties. *Proc. Biol. Sci.* 286, 20191278. doi:10.1098/rspb.2019.1278
- Noren, N. K., Liu, B. P., Burridge, K., and Kreft, B. (2000). p120 catenin regulates the actin cytoskeleton via Rho family GTPases. *J. Cell Biol.* 150, 567–580. doi:10.1083/jcb.150.3.567
- Oksanen, M., Lehtonen, S., Jaronen, M., Goldsteins, G., Hamalainen, R. H., and Koistinaho, J. (2019). Astrocyte alterations in neurodegenerative pathologies and their modeling in human induced pluripotent stem cell platforms. *Cell Mol. Life Sci.* 76, 2739–2760. doi:10.1007/s00018-019-03111-7
- Oksanen, M., Petersen, A. J., Naumenko, N., Puttonen, K., Lehtonen, S., Gubert Olive, M., et al. (2017). PSEN1 mutant iPSC-derived model reveals severe astrocyte pathology in alzheimer's disease. *Stem Cell Rep.* 9, 1885–1897. doi:10.1016/j.stemcr.2017.10.016
- Ong, H. L., Subedi, K. P., Son, G. Y., Liu, X., and Ambudkar, I. S. (2019). Tuning store-operated calcium entry to modulate Ca(2+)-dependent physiological processes. *Biochim. Biophys. Acta Mol. Cell Res.* 1866, 1037–1045. doi:10.1016/j.bbamcr.2018.11.018
- Paillusson, S., Stoica, R., Gomez-Suaga, P., Lau, D. H. W., Mueller, S., Miller, T., et al. (2016). There's something wrong with my MAM; the ER-mitochondria Axis and neurodegenerative diseases. *Trends Neurosci.* 39, 146–157. doi:10.1016/j.tins.2016.01.008
- Patel, S., and Cai, X. (2015). Evolution of acidic Ca2+ stores and their resident Ca2+-permeable channels. *Cell Calcium* 57, 222–230. doi:10.1016/j.ceca.2014.12.005
- Patel, S. (2015). Function and dysfunction of two-pore channels. *Sci. Signal* 8, re7. doi:10.1126/scisignal.aab3314
- Patella, F., Schug, Z. T., Persi, E., Neilson, L. J., Erami, Z., Avanzato, D., et al. (2015). Proteomics-based metabolic modeling reveals that fatty acid oxidation (FAO) controls endothelial cell (EC) permeability. *Mol. Cell Proteomics* 14, 621–634. doi:10.1074/mcp.M114.005575
- Paterno, G. M., Bondelli, G., Sakai, V. G., Sesti, V., Bertarelli, C., and Lanzani, G. (2020a). The effect of an intramembrane light-actuator on the dynamics of phospholipids in model membranes and intact cells. *Langmuir* 36, 11517–11527. doi:10.1021/acs.langmuir.0c01846
- Paterno, G. M., Colombo, E., Vurro, V., Lodola, F., Cimo, S., Sesti, V., et al. (2020b). Membrane environment enables ultrafast isomerization of amphiphilic azobenzene. *Adv. Sci. (Weinh)* 7, 1903241. doi:10.1002/adv.201903241
- Peng, M., Wang, Z., Yang, Z., Tao, L., Liu, Q., Yi, L. U., et al. (2015). Overexpression of short TRPM8 variant promotes cell migration and invasion, and decreases starvation-induced apoptosis in prostate cancer LNCaP cells. *Oncol. Lett.* 10, 1378–1384. doi:10.3892/ol.2015.3373
- Pressey, J. C., and Woodin, M. A. (2021). Kainate receptor regulation of synaptic inhibition in the hippocampus. *J. Physiol.* 599, 485–492. doi:10.1113/jp279645
- Prevarskaya, N., Flourakis, M., Bidaux, G., Thebault, S., and Skryma, R. (2007). Differential role of TRP channels in prostate cancer. *Biochem. Soc. Trans.* 35, 133–135. doi:10.1042/BST0350133
- Prevarskaya, N., Skryma, R., and Shuba, Y. (2018). Ion channels in cancer: Are cancer hallmarks oncochannelopathies? *Physiol. Rev.* 98, 559–621. doi:10.1152/physrev.00044.2016
- Procino, G., Gerbino, A., Milano, S., Nicoletti, M. C., Mastrofrancesco, L., Carmosino, M., et al. (2015). Rosiglitazone promotes AQP2 plasma membrane expression in renal cells via a Ca-dependent/cAMP-independent mechanism. *Cell Physiol. Biochem.* 35, 1070–1085. doi:10.1159/000373933
- Prole, D. L., and Taylor, C. W. (2019). Structure and function of IP3 receptors. *Cold Spring Harb. Perspect. Biol.* 11, a035063. doi:10.1101/cshperspect.a035063
- Rizzuto, R., Brini, M., Murgia, M., and Pozzan, T. (1993). Microdomains with high Ca2+ close to IP3-sensitive channels that are sensed by neighboring mitochondria. *Science* 262, 744–747. doi:10.1126/science.8235595
- Rocchio, F., Tapella, L., Manfredi, M., Chisari, M., Ronco, F., Ruffinatti, F. A., et al. (2019). Gene expression, proteome and calcium signaling alterations in immortalized hippocampal astrocytes from an Alzheimer's disease mouse model. *Cell Death Dis.* 10, 24. doi:10.1038/s41419-018-1264-8
- Ronco, V., Grolla, A. A., Glasnov, T. N., Canonico, P. L., Verkhatsky, A., Genazzani, A. A., et al. (2014). Differential deregulation of astrocytic calcium signalling by amyloid- β , TNF α , IL-1 β and LPS. *Cell Calcium* 55, 219–229. doi:10.1016/j.ceca.2014.02.016
- Ronco, V., Potenza, D. M., Denti, F., Vullo, S., Gagliano, G., Tognolina, M., et al. (2015). A novel Ca2+-mediated cross-talk between endoplasmic reticulum and acidic organelles: Implications for NAADP-dependent Ca2+ signalling. *Cell Calcium* 57, 89–100. doi:10.1016/j.ceca.2015.01.001
- Ruffinatti, F., Tapella, L., Gregnani, I., Stevano, A., Chiorino, G., Canonico, P. L., et al. (2018). Transcriptional remodeling in primary hippocampal astrocytes from an alzheimer's disease mouse model. *Curr. Alzheimer Res.* 15, 986–1004. doi:10.2174/1567205015666180613113924
- Sahoo, N., Gu, M., Zhang, X., Raval, N., Yang, J., Bekier, M., et al. (2017). Gastric acid secretion from parietal cells is mediated by a Ca(2+) efflux channel in the tubulovesicle. *Dev. Cell* 41, 262–273.e6. doi:10.1016/j.devcl.2017.04.003
- Sanchez-Vazquez, V. H., Martinez-Martinez, E., Gallegos-Gomez, M. L., Arias, J. M., Pallafacchina, G., Rizzuto, R., et al. (2023). Heterogeneity of the endoplasmic reticulum Ca(2+) store determines colocalization with mitochondria. *Cell Calcium* 109, 102688. doi:10.1016/j.ceca.2022.102688
- Santello, M., Toni, N., and Volterra, A. (2019). Astrocyte function from information processing to cognition and cognitive impairment. *Nat. Neurosci.* 22, 154–166. doi:10.1038/s41593-018-0325-8
- Santulli, G., Lewis, D., Des Georges, A., Marks, A. R., and Frank, J. (2018). Ryanodine receptor structure and function in health and disease. *Subcell. Biochem.* 87, 329–352. doi:10.1007/978-981-10-7757-9_11
- Sbano, L., Bonora, M., Marchi, S., Baldassari, F., Medina, D. L., Ballabio, A., et al. (2017). TFEB-mediated increase in peripheral lysosomes regulates store-operated calcium entry. *Sci. Rep.* 7, 40797. doi:10.1038/srep40797
- Scarpellino, G., Munaron, L., Cantelmo, A. R., and Fiorio Pla, A. (2020). Calcium-permeable channels in tumor vascularization: Peculiar sensors of microenvironmental

- chemical and physical cues. *Rev. Physiol. Biochem. Pharmacol.* 182, 111–137. doi:10.1007/112_2020_32
- Schaeffer, S., and Iadecola, C. (2021). Revisiting the neurovascular unit. *Nat. Neurosci.* 24, 1198–1209. doi:10.1038/s41593-021-00904-7
- Scorza, S. I., Milano, S., Saponara, I., Certini, M., De Zio, R., Mola, M. G., et al. (2023). TRPML1-Induced lysosomal Ca(2+) signals activate AQP2 translocation and water flux in renal collecting duct cells. *Int. J. Mol. Sci.* 24, 1647. doi:10.3390/ijms24021647
- Sforza, L., Michelucci, A., Morena, F., Argentati, C., Franciolini, F., Vassalli, M., et al. (2022). Piezo1 controls cell volume and migration by modulating swelling-activated chloride current through Ca(2+) influx. *J. Cell Physiol.* 237, 1857–1870. doi:10.1002/jcp.30656
- Soda, T., Brunetti, V., Berra-Romani, R., and Moccia, F. (2023). The emerging role of N-Methyl-D-Aspartate (NMDA) receptors in the cardiovascular system: Physiological implications, pathological consequences, and therapeutic perspectives. *Int. J. Mol. Sci.* 24, 3914. doi:10.3390/ijms24043914
- Soda, T., Mapelli, L., Locatelli, F., Botta, L., Goldfarb, M., Prestori, F., et al. (2019). Hyperexcitability and hyperplasticity disrupt cerebellar signal transfer in the IB2 KO mouse model of autism. *J. Neurosci.* 39, 2383–2397. doi:10.1523/JNEUROSCI.1985-18.2019
- Tapella, L., Dematteis, G., Genazzani, A. A., De Paola, M., and Lim, D. (2023). Immortalized hippocampal astrocytes from 3xTg-AD mice, a new model to study disease-related astrocytic dysfunction: A comparative review. *Neural Regen. Res.* 18, 1672–1678. doi:10.4103/1673-5374.363192
- Tapella, L., Dematteis, G., Moro, M., Pistolato, B., Tonelli, E., Vanella, V. V., et al. (2022). Protein synthesis inhibition and loss of homeostatic functions in astrocytes from an alzheimer's disease mouse model: A role for ER-mitochondria interaction. *Cell Death Dis.* 13, 878. doi:10.1038/s41419-022-05324-4
- Tapella, L., Soda, T., Mapelli, L., Bortolotto, V., Bondi, H., Ruffinatti, F. A., et al. (2020). Deletion of calcineurin from GFAP-expressing astrocytes impairs excitability of cerebellar and hippocampal neurons through astroglial Na(+)/K(+) ATPase. *Glia* 68, 543–560. doi:10.1002/glia.23737
- Thakore, P., Pritchard, H. A. T., Griffin, C. S., Yamasaki, E., Drumm, B. T., Lane, C., et al. (2020). TRPML1 channels initiate Ca(2+) sparks in vascular smooth muscle cells. *Sci. Signal* 13, eaba1015. doi:10.1126/scisignal.aba1015
- Thebault, S., Lemonnier, L., Bidaux, G., Flourakis, M., Bavencoffe, A., Gordienko, D., et al. (2005). Novel role of cold/menthol-sensitive transient receptor potential melastatine family member 8 (TRPM8) in the activation of store-operated channels in LNCaP human prostate cancer epithelial cells. *J. Biol. Chem.* 280, 39423–39435. doi:10.1074/jbc.M503544200
- Thillaipappan, N. B., Chavda, A. P., Tovey, S. C., Prole, D. L., and Taylor, C. W. (2017). Ca(2+) signals initiate at immobile IP3 receptors adjacent to ER-plasma membrane junctions. *Nat. Commun.* 8, 1505. doi:10.1038/s41467-017-01644-8
- Tiwari, M. N., Mohan, S., Biala, Y., and Yaari, Y. (2018). Differential contributions of Ca(2+)-activated K(+) channels and Na(+)/K(+) -ATPases to the generation of the slow afterhyperpolarization in CA1 pyramidal cells. *Hippocampus* 28, 338–357. doi:10.1002/hipo.22836
- Tomilin, V. N., Mamenko, M., Zaika, O., Ren, G., Marrelli, S. P., Birnbaumer, L., et al. (2019). TRPC3 determines osmosensitive [Ca2+]i signaling in the collecting duct and contributes to urinary concentration. *PLoS One* 14, e0226381. doi:10.1371/journal.pone.0226381
- Tsagareli, M. G., and Nozadze, I. (2020). An overview on transient receptor potential channels superfamily. *Behav. Pharmacol.* 31, 413–434. doi:10.1097/FBP.0000000000000524
- Tsavalier, L., Shaper, M. H., Morkowski, S., and Laus, R. (2001). Trp-p8, a novel prostate-specific gene, is up-regulated in prostate cancer and other malignancies and shares high homology with transient receptor potential calcium channel proteins. *Cancer Res.* 61, 3760–3769.
- Vaeth, M., Kahlfuss, S., and Feske, S. (2020). CRAC channels and calcium signaling in T cell-mediated immunity. *Trends Immunol.* 41, 878–901. doi:10.1016/j.it.2020.06.012
- Vangeel, L., and Voets, T. (2019). Transient receptor potential channels and calcium signaling. *Cold Spring Harb. Perspect. Biol.* 11, a035048. doi:10.1101/cshperspect.a035048
- Venetucci, L., Denegri, M., Napolitano, C., and Priori, S. G. (2012). Inherited calcium channelopathies in the pathophysiology of arrhythmias. *Nat. Rev. Cardiol.* 9, 561–575. doi:10.1038/nrcardio.2012.93
- Verkhatsky, A., and Nedergaard, M. (2016). The homeostatic astroglia emerges from evolutionary specialization of neural cells. *Philos. Trans. R. Soc. Lond B Biol. Sci.* 371, 20150428. doi:10.1098/rstb.2015.0428
- Verkhatsky, A., Parpura, V., Rodriguez-Arellano, J. J., and Zorec, R. (2019). Astroglia in alzheimer's disease. *Adv. Exp. Med. Biol.* 1175, 273–324. doi:10.1007/978-981-13-9913-8_11
- Vetter, I. R., and Wittinghofer, A. (2001). The guanine nucleotide-binding switch in three dimensions. *Science* 294, 1299–1304. doi:10.1126/science.1062023
- Vrenken, K. S., Jalink, K., Van Leeuwen, F. N., and Middelbeek, J. (2016). Beyond ion-conduction: Channel-dependent and -independent roles of TRP channels during development and tissue homeostasis. *Biochim. Biophys. Acta* 1863, 1436–1446. doi:10.1016/j.bbamcr.2015.11.008
- Virro, V., Federici, B., Ronchi, C., Florindi, C., Sesti, V., Crasto, S., et al. (2023a). Optical modulation of excitation-contraction coupling in human-induced pluripotent stem cell-derived cardiomyocytes. *iScience* 26, 106121. doi:10.1016/j.isci.2023.106121
- Virro, V., Shani, K., Ardon, H. A. M., Zimmerman, J. F., Sesti, V., Lee, K. Y., et al. (2023b). Light-triggered cardiac microphysiological model. *Appl. Bioeng.* 7, 026108. doi:10.1063/5.0143409
- Wang, L., and Li, Q. (2018). Photochromism into nanosystems: Towards lighting up the future nanoworld. *Chem. Soc. Rev.* 47, 1044–1097. doi:10.1039/c7cs00630f
- Wang, Y., Wang, X., Yang, Z., Zhu, G., Chen, D., and Meng, Z. (2012). Menthol inhibits the proliferation and motility of prostate cancer DU145 cells. *Pathol. Oncol. Res.* 18, 903–910. doi:10.1007/s12253-012-9520-1
- Woudenberg-Vrenken, T. E., Bindels, R. J., and Hoenderop, J. G. (2009). The role of transient receptor potential channels in kidney disease. *Nat. Rev. Nephrol.* 5, 441–449. doi:10.1038/nrneph.2009.100
- Xu, H., and Ren, D. (2015). Lysosomal physiology. *Annu. Rev. Physiol.* 77, 57–80. doi:10.1146/annurev-physiol-021014-071649
- Yang, J., Zhao, Z., Gu, M., Feng, X., and Xu, H. (2019). Release and uptake mechanisms of vesicular Ca(2+) stores. *Protein Cell* 10, 8–19. doi:10.1007/s13238-018-0523-x
- Yang, Z. H., Wang, X. H., Wang, H. P., and Hu, L. Q. (2009). Effects of TRPM8 on the proliferation and motility of prostate cancer PC-3 cells. *Asian J. Androl.* 11, 157–165. doi:10.1038/aja.2009.1
- Yin, Y., Le, S. C., Hsu, A. L., Borgnia, M. J., Yang, H., and Lee, S. Y. (2019). Structural basis of cooling agent and lipid sensing by the cold-activated TRPM8 channel. *Science* 363, eaav9334. doi:10.1126/science.aav9334
- Yin, Y., Wu, M., Zubcevic, L., Borschel, W. F., Lander, G. C., and Lee, S. Y. (2018). Structure of the cold- and menthol-sensing ion channel TRPM8. *Science* 359, 237–241. doi:10.1126/science.aan4325
- Zhang, J., Wang, J., and Tian, H. (2014). Taking orders from light: Progress in photochromic bio-materials. *Mater. Horizons* 1, 169–184. doi:10.1039/c3mh00031a
- Zhang, L., and Barritt, G. J. (2004). Evidence that TRPM8 is an androgen-dependent Ca2+ channel required for the survival of prostate cancer cells. *Cancer Res.* 64, 8365–8373. doi:10.1158/0008-5472.CAN-04-2146
- Zhang, X., Cheng, X., Yu, L., Yang, J., Calvo, R., Patnaik, S., et al. (2016). MCOLN1 is a ROS sensor in lysosomes that regulates autophagy. *Nat. Commun.* 7, 12109. doi:10.1038/ncomms12109
- Zhang, X., Mak, S., Li, L., Parra, A., Denlinger, B., Belmonte, C., et al. (2012). Direct inhibition of the cold-activated TRPM8 ion channel by Gaq. *Nat. Cell Biol.* 14, 851–858. doi:10.1038/ncb2529
- Zhao, X., Liang, B., Li, C., and Wang, W. (2023). Expression regulation and trafficking of aquaporins. *Adv. Exp. Med. Biol.* 1398, 39–51. doi:10.1007/978-981-19-7415-1_3
- Zholos, A., Johnson, C., Burdya, T., and Melanaphy, D. (2011). TRPM channels in the vasculature. *Adv. Exp. Med. Biol.* 704, 707–729. doi:10.1007/978-94-007-0265-3_37
- Zhu, G., Wang, X., Yang, Z., Cao, H., Meng, Z., Wang, Y., et al. (2011). Effects of TRPM8 on the proliferation and angiogenesis of prostate cancer PC-3 cells *in vivo*. *Oncol. Lett.* 2, 1213–1217. doi:10.3892/ol.2011.410
- Zuccolo, E., Di Buduo, C., Lodola, F., Orecchioni, S., Scarpellino, G., Kheder, D. A., et al. (2018a). Stromal cell-derived factor-1 α promotes endothelial colony-forming cell migration through the Ca²⁺-dependent activation of the extracellular signal-regulated kinase 1/2 and phosphoinositide 3-kinase/AKT pathways. *Stem Cells Dev.* 27, 23–34. doi:10.1089/scd.2017.0114
- Zuccolo, E., Kheder, D. A., Lim, D., Perna, A., Nezza, F. D., Botta, L., et al. (2019). Glutamate triggers intracellular Ca(2+) oscillations and nitric oxide release by inducing NAADP- and InsP3 -dependent Ca(2+) release in mouse brain endothelial cells. *J. Cell Physiol.* 234, 3538–3554. doi:10.1002/jcp.26953
- Zuccolo, E., Laforenza, U., Ferulli, F., Pellavio, G., Scarpellino, G., Tanzi, M., et al. (2018b). Stim and Orai mediate constitutive Ca(2+) entry and control endoplasmic reticulum Ca(2+) refilling in primary cultures of colorectal carcinoma cells. *Oncotarget* 9, 31098–31119. doi:10.18632/oncotarget.25785



OPEN ACCESS

EDITED BY

Emilio Badoer,
RMIT University, Australia

REVIEWED BY

Xiang Wang,
Changzhou University, China
Eliseo A. Eugenin,
University of Texas Medical Branch at
Galveston, United States
Chiara Zurzolo,
Institut Pasteur, France

*CORRESPONDENCE

F. Pisani,
✉ francesco.pisani@uniba.it

RECEIVED 29 April 2023

ACCEPTED 11 August 2023

PUBLISHED 21 August 2023

CITATION

Capobianco DL, Simone L, Svelto M and
Pisani F (2023), Intercellular crosstalk
mediated by tunneling nanotubes
between central nervous system cells.
What we need to advance.
Front. Physiol. 14:1214210.
doi: 10.3389/fphys.2023.1214210

COPYRIGHT

© 2023 Capobianco, Simone, Svelto and
Pisani. This is an open-access article
distributed under the terms of the
[Creative Commons Attribution License
\(CC BY\)](#). The use, distribution or
reproduction in other forums is
permitted, provided the original author(s)
and the copyright owner(s) are credited
and that the original publication in this
journal is cited, in accordance with
accepted academic practice. No use,
distribution or reproduction is permitted
which does not comply with these terms.

Intercellular crosstalk mediated by tunneling nanotubes between central nervous system cells. What we need to advance

D. L. Capobianco¹, L. Simone², M. Svelto¹ and F. Pisani^{1,3*}

¹Department of Biosciences, Biotechnologies and Environment, University of Bari "Aldo Moro", Bari, Italy,

²Fondazione Istituto di Ricovero e Cura a Carattere Scientifico (IRCCS) Casa Sollievo della Sofferenza, Cancer Stem Cells Unit, San Giovanni Rotondo, Italy, ³Center for Synaptic Neuroscience and Technology, Istituto Italiano di Tecnologia, Genova, Italy

Long-range intercellular communication between Central Nervous System (CNS) cells is an essential process for preserving CNS homeostasis. Paracrine signaling, extracellular vesicles, neurotransmitters and synapses are well-known mechanisms involved. A new form of intercellular crosstalk mechanism based on Tunneling Nanotubes (TNTs), suggests a new way to understand how neural cells interact with each other in controlling CNS functions. TNTs are long intercellular bridges that allow the intercellular transfer of cargoes and signals from one cell to another contributing to the control of tissue functionality. CNS cells communicate with each other via TNTs, through which ions, organelles and other signals are exchanged. Unfortunately, almost all these results were obtained through 2D *in-vitro* models, and fundamental mechanisms underlying TNTs-formation still remain elusive. Consequently, many questions remain open, and TNTs role in CNS remains largely unknown. In this review, we briefly discuss the state of the art regarding TNTs identification and function. We highlight the gaps in the knowledge of TNTs and discuss what is needed to accelerate TNTs-research in CNS-physiology. To this end, it is necessary to: 1) Develop an *ad-hoc* TNTs-imaging and software-assisted processing tool to improve TNTs-identification and quantification, 2) Identify specific molecular pathways involved into TNTs-formation, 3) Use *in-vitro* 3D-CNS and animal models to investigate TNTs-role in a more physiological context pushing the limit of live-microscopy techniques. Although there are still many steps to be taken, we believe that the study of TNTs is a new and fascinating frontier that could significantly contribute to deciphering CNS physiology.

KEYWORDS

intercellular communication, tunneling nanotubes, central nervous system, *in-vitro* 3D model, super resolution live-cell microscopy

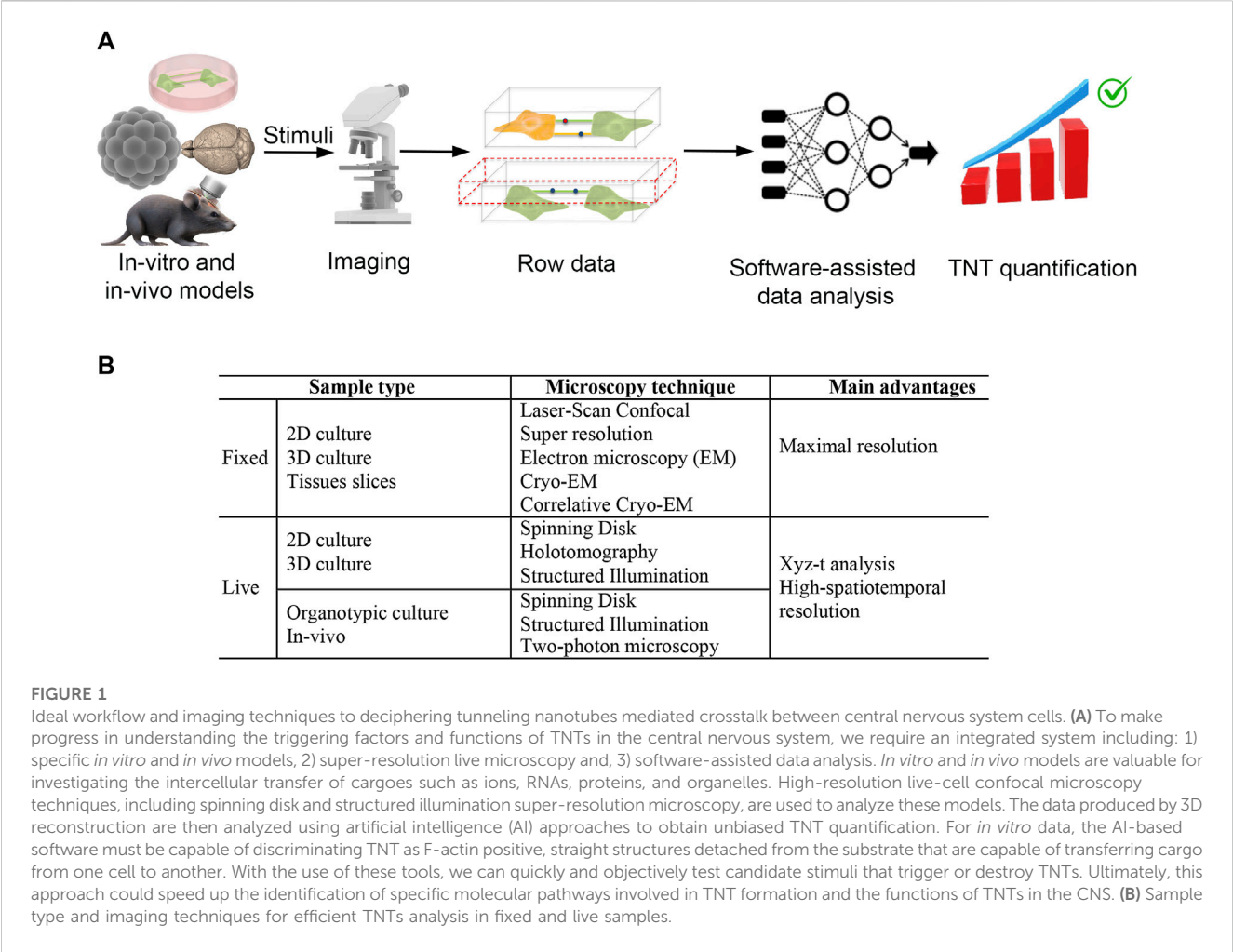
1 Introduction

Cell-to-cell communication is essential for preserving tissue functions and homeostasis. A variety of mechanisms are involved: nearby cells can communicate with each other via connexin-formed gap junctions (GJs) and synapses, while distant cells can also do so via paracrine secreted signals and extracellular vesicles.

In 2004, Rustom and colleagues discovered a new form of long-range cell-to-cell crosstalk mechanism based on long plasma membrane bridges named tunneling

TABLE 1 TNTs, in cell types of Central Nervous System.

CNS cell type	Model	Conditions	Cargoes	TNTs connected cells	TNTs identification and quantification	Software-assisted TNTs quantification	Mechanism of TNTs formation	3D-CNS or animal models	References
Brain endothelial cells	Murine brain sections	Hypoxia-Ischemia	None	Endothelial-endothelial	Confocal microscopy	No	No	Yes	Girolamo et al. (2023)
Neurons, Microglia cells	<i>In vitro</i> 2D model	Parkinson disease	α -Synuclein (α -Syn)	Neuron-microglia	Confocal microscopy	No	No	No	Chakraborty et al. (2023b)
Astrocytes, Brain Pericytes, Brain Endothelial cells.		Physiological and ischemic stroke	mitochondria	Astrocyte-pericyte. Endothelial cells-pericytes.	Confocal microscopy	No	No	No	Pisani et al. (2022)
Astrocytes	Murine models	Physiological	EGFP	Astrocytes-neurons	Immunoelectron microscopy and fluorescence microscopy.	No	No	No	Chen and Cao (2021)
Pericytes	Human Brain sections	Physiological and pathological angiogenesis	None	Pericyte-endothelial cells	Confocal microscopy	No	No	No	Errede et al. (2018)
Pericytes	Murine models	Neurovascular coupling	Ca ²⁺	Pericyte- pericyte	Live-animal two-photon microscopy	No	No	Yes	Alarcon-Martinez et al. (2020)
Microglia	<i>In vitro</i> 2D model, murine model.	Parkinson disease	α -Synuclein (α -Syn)	Microglia-microglia	Flow cytometric analysis	No	No	Yes	Scheiblich et al. (2021)
					<i>In vivo</i> two-photon imaging				
					Fluorescence microscopy				
Astrocytes	<i>In vitro</i> 2D model	Physiological	EGFP	Astrocytes-astrocytes	Live-cell confocal microscopy	No	Yes	No	Sun et al. (2012)
Neuron Astrocytes	<i>In vitro</i> 2D model	Physiological	None	Neuron-astrocytes	Differential interference contrast microscopy.	No	No	No	Wang et al. (2012)
					Fluorescent microscopy.				



nanotubes (TNTs) (Rustom et al., 2004). *In vitro*, TNTs have been described as non-adherent, actin-based cytoplasmic extensions that serve as long-distance membranous bridges. Rustom and others have demonstrated the presence of TNTs in various cell types, indicating that TNTs are a widespread cellular phenomenon crucial for long-distance cell-to-cell communication. TNTs allow the intercellular transfer not only of small molecules, such as ions, second messengers, and metabolic substrates, but also of macromolecules, including proteins and nucleic acids, and organelles. This results in a cell “support” network that plays a role in the control of tissue functions (reviewed in (2)). For instance, mounting evidence suggests that TNT-mediated intercellular mitochondrial transfer can protect recipient cells from bioenergetic deficit and apoptosis, which can be caused by pathological factors (Pisani et al., 2022).

TNTs have been observed in various cell types of the Central Nervous System (CNS) (Khattar et al., 2022), including neurons, glial cells, pericytes, and brain endothelial cells as listed in Table 1. Data suggest that TNTs could play important roles in the maintenance of neuronal networks. In this regard it has been demonstrated that TNTs contribute to the transmission of electrical signals, to the regulation of immune responses in the CNS and could play a role during brain development (Wang et al., 2010; Wang et al., 2012; Wang and Gerdes, 2012; Zurzolo, 2021; Cordero Cervantes et al., 2023). Furthermore, we have recently shown that TNTs-based crosstalk occurs between human

blood-brain barrier cells (Pisani et al., 2022). In pathological conditions affecting the CNS, such as Alzheimer’s and Parkinson’s diseases, TNTs may also play a role in the spread of pathological proteins (Abounit et al., 2016; Tardivel et al., 2016; Rostami et al., 2017; Dilna et al., 2021).

Despite the many data published on this new form of intercellular communication mechanism between neural cells, the role of TNTs in the CNS remains largely unclear. Further investigation and new tools are required to accelerate our understanding of TNTs’ role in the CNS.

In this review, we briefly discuss the state of the art regarding the identification and function of TNTs. We highlight the gaps in our knowledge of TNTs and, more importantly, what is needed, in our opinion, to accelerate the study of TNT-mediated intercellular crosstalk in the CNS (Figure 1).

2 Discussion

2.1 TNTs-identification and quantification

2.1.1 We need a rapid, automatic and operator-independent method

TNTs are described as (I) thin (20–700 nm) and straight membranous protrusions hovering over the substrate and directly

connecting two (or more) cells of either the same (homotypic) or different (heterotypic) types. They (II) contain F-actin cytoskeletal filaments and (III) are able to transfer cargo from one cell to another (Cordero Cervantes and Zurzolo, 2021).

Although some authors have reported the identification of potential TNTs markers (Jung et al., 2017), no specific markers exclusive to TNTs have been discovered to date. For this reason, morpho-functional analysis continues to be the primary standard for TNT identification and quantification.

Currently, high-resolution confocal microscopy followed by 3D-reconstruction and Z-stacks analysis, live-cell fluorescence microscopy, and analysis of intercellular transfer of cellular cargoes are the main approaches used to identify and quantify TNTs (as detailed in Table 1). These approaches are time-consuming and dependent on the researcher's expertise and interpretation. Furthermore, fixed-cell or fixed-tissue based approaches are affected by fixation procedures that tend to break TNTs.

An automatic or semi-automatic TNT identification and quantification method is mandatory to boost TNT studies. To this aim, a method aimed at developing automated detection of TNTs using Z-stacks confocal images was reported in a paper published in 2006 (Hodneland et al., 2006). More recently, a machine learning approach potentially useful for TNT quantification was developed by Smirnov and colleagues to study the dynamics of dendritic spines using live-cell microscopy data (Smirnov et al., 2018). A deep-learning artificial intelligence (AI) approach was first proposed by Ceran and colleagues for TNT analysis (Ceran et al., 2022). All these methods were able to identify only 50%–60% of human expert-identified TNTs.

For these reasons, to date, manual TNT counting based on trained investigators based on fixed and live-cell microscopy analysis remains the gold-standard method. This strongly slows the study of TNTs.

Furthermore, only phase-contrast images or plasma membrane fluorescent dyes of single-cell type culture, were used as input data in these methods. No F-actin staining, cargo tracking analysis, or intercellular transfer of cellular cargoes were investigated. Since these are three TNT-related properties that distinguish TNTs from other cell protrusions, whether these approaches are really able to automatically quantify TNTs remains elusive. We believe that taking these additional elements into account could contribute to significantly increase and improve the automatic quantification of TNTs. To achieve this objective, cell culture experiments should be conducted using co-cultures of donor and receiving cells, and the analysis should be performed using live-cell time-lapse confocal microscopy in 4D mode (xyz-t). Tracking analysis, utilizing dedicated software like TrackMate, a plugin of the free software Fiji, can assist in describing the trajectory of cargo in the xyz dimensions over time. The main challenge lies in implementing these analyses within the software design of AI-based approaches. We hope in fact that recent progress in AI-based methods will help us in this hard work. This point is crucial to accelerate the identification of molecules and stimuli that can affect or enhance the formation of TNTs, accelerating, for instance, the decoding of molecular pathways involved in TNT formation and the identification of TNT functions.

3 How cells generate TNTs is unclear

3.1 We need more molecular insights to design more TNTs-specific experiments

The formation of TNTs is thought to occur via two main mechanisms: 1) cell dislodgement, in which two cells that were initially attached to one another separate, leaving a membrane thread that develops into an actin-supported TNT, and 2) actin-driven, in which a cell forms a precursor protrusion through actin assembly that subsequently fuses with a recipient cell, forming a TNT. However, it is possible that there are other mechanisms involved in the formation of TNTs that have yet to be discovered. There are still many questions that remain unanswered in order to fully understand this process. For example, what are the actin regulators orchestrating the formation of TNTs? Do TNTs mature from a filopodia-like precursor, or is the actin-driven mechanism of TNT formation a *de novo* process? Nina Ljubojevic et al. in Ljubojevic et al. (2021).

According to imaging studies on cultured cells, TNTs can initially form from thin, actin-driven protrusions that resemble fingers (filopodia) or from a direct contact between cell bodies. The resulting TNTs maintain an intercellular distance that can be up to five hundred times greater than the TNT's thickness (hundreds of nanometers) while suspended between the cells.

A highly contentious issue is whether a TNT is open-ended or close-ended *in vivo* as well as how short and dynamic filopodia transform into long and stable TNTs, and what causes the filopodia to change into TNTs. One of the newest hypotheses for the formation of TNTs, especially the close-ended type, was recently reported by Minhyeok Chan and colleagues. In this paper, the authors found that TNTs develop from a double filopodial intercellular bridge (DFB) between distant cells. The author shows that DFB results from the dimerization of N-cadherin extracellular domains from two different filopodia of distant cells and that this bridge evolves into a closed-ended TNT. The transition from a DFB to a close-ended TNT appears to be triggered by mechanical energy accumulated in a twisted DFB. Myosin V and/or myosin II seem to play a functional role in this twisting mechanism. A specific biophysical mechanism of action was proposed, and the elastic properties of TNTs and DFB were experimentally measured (Chang et al., 2022). This intriguing paper highlights the synergistic role of F-actin/N-cadherin and myosin in TNT formation. Most recently, was found that F-actin and cadherin connection control the tensile strength and flexural strength of TNTs, respectively (Li et al., 2022). It is important to note that, before these papers, the presence of N-cadherin and Myosin 10 in TNT structures was found in neuronal TNTs through a correlative cryo-electron microscopy (EM) approach by Zurzolo's group (Sartori-Rupp et al., 2019).

Despite the conclusions proposed by Minhyeok Chan and colleagues about TNT formation being extremely intriguing, it is important to note that HEK and HeLa cells were used to produce wet data and conclusions cannot be automatically extended to CNS cells.

Several molecular players have been shown to positively or negatively regulate TNT formation, as reviewed by Ranabir Chakraborty et al. (Chakraborty et al., 2023a). However, the exact molecular pathways involved in TNT formation between

neural cells remain largely unclear (as detailed only for astrocytes in Table 1). As a result, there are currently no molecular targets that can be used to design TNT-specific interfering experiments aimed at selectively destroying TNTs while preserving other cell protrusions. This greatly hinders the identification of TNT's functions.

The only way to interfere with TNT formation currently is through the use of F-actin depolymerizing drugs such as Cytochalasin-D, Latrunculin B and Jasplakinolide. However, this treatment affects other F-actin dependent mechanisms in addition to TNT formation. Another possible approach is the use of not-in-touch coculture, which involves the use of the Transwell® system. Depending on the size-porosity of the separating membrane, not only TNTs but also other long-range intercellular trafficking mechanisms can be prevented. However, the literature is controversial and not aligned on the size-porosity required to exclusively exclude TNT-mediated intercellular trafficking.

Similarly, there is currently no possibility to specifically stimulate TNT formation. Cell stress conditions such as exposure to UV radiation (Hajek et al., 1989), oxidative stress (Wang et al., 2011), hypoxia (Desir et al., 2016; Yang et al., 2020), and other cell stressors upregulate TNT formation, but, under these conditions, mechanisms other than the formation of TNT are also induced.

In summary, the lack of specific knowledge about the molecules and pathways involved in TNT formation in neural cells, as well as the absence of TNT-specific triggering and destroying factors, are areas that need improvement to design more specific experiments aimed at isolating the specific contribute of TNTs useful at identifying TNT's functions.

4 Dynamic and structural organization of TNTs in CNS-cells: from 2D-models to *in-vivo* brain imaging

4.1 Microscopic challenges emerge

TNT-like connections have been found in human fetal brain sections between pericytes and between pericytes and endothelial cells, suggesting that these elements may play a role in the initial stages of brain vascularization (Errede et al., 2018). Fixed and live-cell experiments have shown that astrocytes, oligodendrocytes, and neurons can all form TNTs in both physiological and pathological conditions (as reviewed by Khattar and colleagues (Khattar et al., 2022)). Additionally, in recent research, we have shown that TNTs occur between human blood-brain barrier cells (Pisani et al., 2022). While these studies have demonstrated different TNT-mediated transport of cellular cargoes and stimuli in both physiological and pathological 2D *in vitro* models, conclusions regarding TNT functions remain confined to the *in vitro* model used, and whether TNTs exist in multicellular 3D-CNS models and in CNS in general remains unclear.

However, the use of 3D-CNS models such as human mini-brains and murine models generated through induced human pluripotent stem cell (iPSC) technology and cell-specific differentiation could strongly contribute to filling this gap. These models recapitulate *in vivo* tissue architecture more effectively than neural 2D-cultures [as reviewed in (Hou and Kuo, 2022; Kofman et al., 2022; Wang et al., 2023)] and could help investigate TNT functions in CNS physiology

(as detailed in Table 1). Although the use of 3D models is largely accessible for many laboratories, whether TNTs exist in these models remains unknown.

A recent technical advance in microscopy could revolutionize TNT analysis in the 3D models and in CNS slices. Zurzolo's group recently analyzed the transient external granular layer of the developing cerebellum through high-resolution, serial-sectioning, scanning electron microscopy supported by 3D-reconstruction and deep-learning approaches. This innovative approach has revealed unprecedented details about the spatial-temporal connectivity between neural cells (Cordero Cervantes et al., 2023) and could represent a new frontier for TNT identification in CNS sections. More specifically, this study highlights the potential of a newly developed software designed for tracing cell-to-cell connections in 3D samples. The software utilized for this purpose is CellWalker, which is accessible at (<https://github.com/utraf-pasteur-institute/CellWalker>). CellWalker streamlines the processing of segmented microscopy images, thereby simplifying the identification of intercellular bridges within 3D images. This could significantly aid in the identification of TNT-like structures in CNS sections.

The step forward towards demonstrating the existence of TNTs in the living CNS was published by Alarcon-Martinez and colleagues in two recent, elegant *in vivo* studies. For the first time, the authors showed that TNTs exist in the mouse retina. Specifically, they demonstrated that inter-pericyte TNTs-mediated (IP-TNTs) intercellular Ca²⁺ waves control neurovascular coupling in the retina in physiological conditions, and that this mechanism is altered in glaucoma (Alarcon-Martinez et al., 2020; Alarcon-Martinez et al., 2022).

In these papers, non-invasive live retinal imaging using two-photon laser-scanning microscopy was used to investigate IP-TNTs function *in vivo*. The authors found that IP-TNTs had an open-ended proximal side and a closed-ended terminal (end-foot) that joined with distal pericyte processes via gap junctions. They also discovered that IP-TNTs transport organelles such as mitochondria, which can move along these processes, and act as a conduit for intercellular Ca²⁺ waves, mediating communication between pericytes. These data represent the first and only available data about TNTs in the living retina.

However, the question remains: do TNTs also exist in the living brain? To investigate this possibility, specific tools and animal models are required. One useful tool is based on the expression of cell-type-specific fluorescent proteins, ion trackers, and organelle-specific fluorescent proteins in a CNS-cell type-specific manner. For example, mice that express red fluorescent protein (Ds-RED) under the control of the NG2 promoter (Cspg4) can help identify NG2-positive pericytes in the central nervous system. Another tool is the expression of the genetically encoded Ca²⁺ indicator GCaMP6 under the NG2 promoter, which enables the tracing of calcium dynamics in NG2-positive pericytes. Animal models that express a mitochondrial-specific version of Dendra2 in a cell-specific manner can also be used. These tools are commercially available from The Jackson Laboratory and were used in previous studies (Alarcon-Martinez et al., 2020; Alarcon-Martinez et al., 2022). However, it should be noted that these

animal models do not allow for the unequivocal distinction of cell types expressing the proteins of interest. Furthermore, it would be useful to have various fluorescent cargoes available, in order to discriminate cargo-specific differences in the TNTs-mediated intercellular transfer. This represents a significant obstacle for the *in vivo* study of TNTs.

What is the main limiting factor for investigating TNTs using *in vivo* approaches when animal models are available? The real limit is represented by the microscopic approaches needed to correctly describe the dynamics and structure of TNTs in the living CNS, especially in the living brain. The reason for this technical limit is intrinsic to the structure and dynamics of TNTs, which pose different microscopic challenges for visualizing their dynamics at a nanometric resolution in the brain.

TNTs are thin (20–700 nm) and highly dynamic structures. In just a few minutes, they can assemble, transport an organelle (hundreds of nanometers), or a molecule (sub-nanometers), and transfer these objects to another distant cell. How can we describe this rapid process with high spatial-temporal resolution while preserving cells from phototoxicity? Notably, phototoxicity is particularly crucial for TNT analysis, as it could induce TNT formation. This represents the main point that must be addressed in live-cell microscopy approaches useful for investigating TNTs in 2D and 3D models and *in vivo*.

The major approaches used in the literature for live-cell TNT analysis in 2D models are based on spinning-disk microscopy (SDM) approaches. This approach is widely used to describe neural complexity and functionality while preserving neurons from phototoxicity (Manzella-Lapeira et al., 2021).

Another opportunity comes from the use of holotomography (3D holographic) microscopy (HM), which is a label-free live-cell imaging approach recently reported for TNT investigation by Hans Zoellner and colleagues (Zoellner et al., 2020).

More recently, three-dimensional multi-color live-cell super-resolution imaging at high speed was achieved through the Structured Illumination Microscopy (SIM) approach. In SIM, the sample is illuminated with patterned light to minimize photon dose. After image acquisition, dedicated software analyzes the information, obtaining a reconstruction with a resolution about 2-fold higher than the diffraction limit. The spatial resolution of commercially available SIM microscopes is similar to other super-resolution microscopy techniques (e.g., STED and STORM), but the temporal resolution of SIM is better. In addition, SIM requires lower light intensity for imaging compared to STED and STORM, strongly preserving cell integrity and reducing phototoxicity more than SDM (reviewed in (Badawi and Nishimune, 2020)). Furthermore, SIM can also be used for thicker sections, such as organotypic brain slice cultures (Olenick et al., 1988) and, recently, was further improved using a rationalized deep learning approach pushing the super-resolution limit of the technique in live-imaging of subcellular processes (Qiao et al., 2023). Consequently, SIM appears to be more appropriate for investigating the high dynamicity of TNTs at a nanometric resolution. Considering the various microscopy approaches currently employed, it is evident that much remains to be done to achieve an effective analysis of TNTs *in vivo*.

5 Conclusion

Upon reviewing the current literature on TNTs-based intercellular crosstalk, it seems that AI approaches, 3D *in-vitro* and animal models, and microscopic techniques currently available, could be useful in deciphering TNT's structure, functions, and dynamics (Figure 1). In particular, super-resolution microscopy such as SIM, which is useful for analyzing live cells at nanometric resolution, could represent a great opportunity towards this aim.

Given the range of possibilities currently available, we believe that the question of whether TNTs are present in the brain could be successfully addressed in the near future. This breakthrough could represent a new frontier in neuroscience, providing valuable insight into intercellular connectivity in the brain.

Author contributions

Conceptualization: FP and MS. Writing and editing the manuscript: DC, LS, MS, and FP. All authors contributed to the article and approved the submitted version.

Funding

This work has been funded by Ministero dello Sviluppo Economico (H-STEPP F/180014/01-04/X43) to MS and FP and by Italian Minister of Health, Ricerca Corrente program 2022–2024 to LS.

Acknowledgments

We would like to thank Chiara Di Giorgio (Fondazione IRCCS Casa Sollievo della Sofferenza) for reviewing this manuscript for English language and Dr. Francesco Di Palma for bibliography research.

Conflict of interest

The authors declare that the research was conducted in the absence of any commercial or financial relationships that could be construed as a potential conflict of interest.

Publisher's note

All claims expressed in this article are solely those of the authors and do not necessarily represent those of their affiliated organizations, or those of the publisher, the editors and the reviewers. Any product that may be evaluated in this article, or claim that may be made by its manufacturer, is not guaranteed or endorsed by the publisher.

References

- Abounit, S., Bousset, L., Loria, F., Zhu, S., de Chaumont, F., Pieri, L., et al. (2016). Tunneling nanotubes spread fibrillar α -synuclein by intercellular trafficking of lysosomes. *EMBO J.* 35 (19), 2120–2138. doi:10.15252/embj.201593411
- Alarcon-Martinez, L., Shiga, Y., Villafranca-Baughman, D., Belforte, N., Quintero, H., Dotigny, F., et al. (2022). Pericyte dysfunction and loss of interpericyte tunneling nanotubes promote neurovascular deficits in glaucoma. *Proc. Natl. Acad. Sci. U. S. A.* 119 (7), e2110329119. doi:10.1073/pnas.2110329119
- Alarcon-Martinez, L., Villafranca-Baughman, D., Quintero, H., Kacerovsky, J. B., Dotigny, F., Murai, K. K., et al. (2020). Interpericyte tunnelling nanotubes regulate neurovascular coupling. *Nature* 585 (7823), 91–95. doi:10.1038/s41586-020-2589-x
- Badawi, Y., and Nishimune, H. (2020). Super-resolution microscopy for analyzing neuromuscular junctions and synapses. *Neurosci. Lett.* 715, 134644. doi:10.1016/j.neulet.2019.134644
- Ceran, Y., Ergüder, H., Ladner, K., Korenfeld, S., Deniz, K., Padmanabhan, S., et al. (2022). TNTdetect.AI: A deep learning model for automated detection and counting of tunneling nanotubes in microscopy images. *Cancers* 14 (19), 4958. doi:10.3390/cancers14194958
- Chakraborty, R., Belian, S., and Zurzolo, C. (2023a). Hijacking intercellular trafficking for the spread of protein aggregates in neurodegenerative diseases: A focus on tunneling nanotubes (TNTs). *Extracell. Vesicles Circ. Nucleic Acids* 4, 27–43. doi:10.20517/evcna.2023.05
- Chakraborty, R., Nonaka, T., Hasegawa, M., and Zurzolo, C. (2023b). Tunneling nanotubes between neuronal and microglial cells allow bi-directional transfer of α -Synuclein and mitochondria. *Cell. Death Dis.* 14 (5), 329–412. doi:10.1038/s41419-023-05835-8
- Chang, M., Lee, O. C., Bu, G., Oh, J., Yunn, N. O., Ryu, S. H., et al. (2022). Formation of cellular close-ended tunneling nanotubes through mechanical deformation. *Sci. Adv.* 8 (13), eabj3995. doi:10.1126/sciadv.abj3995
- Chen, J., and Cao, J. (2021). Astrocyte-to-neuron transportation of enhanced green fluorescent protein in cerebral cortex requires F-actin dependent tunneling nanotubes. *Sci. Rep.* 11 (1), 16798. doi:10.1038/s41598-021-96332-5
- Cordero Cervantes, D., Khare, H., Wilson, A. M., Mendoza, N. D., Coulon-Mahdi, O., Lichtman, J. W., et al. (2023). 3D reconstruction of the cerebellar germinal layer reveals tunneling connections between developing granule cells. *Sci. Adv.* 9 (14), eadf3471. doi:10.1126/sciadv.adf3471
- Cordero Cervantes, D., and Zurzolo, C. (2021). Peering into tunneling nanotubes-The path forward. *EMBO J.* 40 (8), e105789. doi:10.15252/embj.2020105789
- Desir, S., Dickson, E. L., Vogel, R. I., Thayanthi, V., Wong, P., Teoh, D., et al. (2016). Tunneling nanotube formation is stimulated by hypoxia in ovarian cancer cells. *Oncotarget* 7 (28), 43150–43161. doi:10.18632/oncotarget.9504
- Dilna, A., Deepak, K. V., Damodaran, N., Kielkopf, C. S., Kagedal, K., Ollinger, K., et al. (2021). Amyloid- β induced membrane damage instigates tunneling nanotube-like conduits by p21-activated kinase dependent actin remodeling. *Biochim. Biophys. Acta Mol. Basis Dis.* 1867 (12), 166246. doi:10.1016/j.bbdis.2021.166246
- Errede, M., Mangieri, D., Longo, G., Girolamo, F., de Trizio, I., Vimercati, A., et al. (2018). Tunneling nanotubes evoke pericyte/endothelial communication during normal and tumoral angiogenesis. *Fluids Barriers CNS* 15 (1), 28. doi:10.1186/s12987-018-0114-5
- Girolamo, F., Lim, Y. P., Virgintino, D., Stonestreet, B. S., and Chen, X. F. (2023). Inter-Alpha inhibitor proteins modify the microvasculature after exposure to hypoxia-ischemia and hypoxia in neonatal rats. *Int. J. Mol. Sci.* 24 (7), 6743. doi:10.3390/ijms24076743
- Hajek, M., Meier-Ewert, K., Wirz-Justice, A., Tobler, I., Arendt, J., Dick, H., et al. (1989). Bright white light does not improve narcoleptic symptoms. *Eur. Arch. Psychiatry Neurol. Sci.* 238 (4), 203–207. doi:10.1007/BF00381466
- Hodneland, E., Lundervold, A., Gurke, S., Tai, X. C., Rustom, A., and Gerdes, H. H. (2006). Automated detection of tunneling nanotubes in 3D images. *Cytom. Part J. Int. Soc. Anal. Cytol.* 69 (9), 961–972. doi:10.1002/cyto.a.20302
- Hou, P. S., and Kuo, H. C. (2022). Central nervous system organoids for modeling neurodegenerative diseases. *IUBMB Life* 74 (8), 812–825. doi:10.1002/iub.2595
- Jung, E., Osswald, M., Blaas, J., Wiestler, B., Sahm, F., Schmenger, T., et al. (2017). Twenty-homolog 1 drives brain colonization of gliomas. *J. Neurosci. Off. J. Soc. Neurosci.* 37 (29), 6837–6850. doi:10.1523/JNEUROSCI.3532-16.2017
- Khattar, K. E., Safi, J., Rodriguez, A. M., and Vignais, M. L. (2022). Intercellular communication in the brain through tunneling nanotubes. *Cancers* 14 (5), 1207. doi:10.3390/cancers14051207
- Kofman, S., Mohan, N., Sun, X., Ibric, L., Piermarini, E., and Qiang, L. (2022). Human mini brains and spinal cords in a dish: modeling strategies, current challenges, and prospective advances. *J. Tissue Eng.* 13, 204173142211133. doi:10.1177/20417314221113391
- Li, A., Han, X., Deng, L., and Wang, X. (2022). Mechanical properties of tunneling nanotube and its mechanical stability in human embryonic kidney cells. *Front. Cell. Dev. Biol.* 10, 955676. doi:10.3389/fcell.2022.955676
- Ljubojevic, N., Henderson, J. M., and Zurzolo, C. (2021). The ways of actin: why tunneling nanotubes are unique cell protrusions. *Trends Cell. Biol.* 31 (2), 130–142. doi:10.1016/j.tcb.2020.11.008
- Manzella-Lapeira, J., Brzostowski, J., and Serra-Vinardell, J. (2021). Studying neuronal biology using spinning disc confocal microscopy. *Methods Mol. Biol. Clifton N. J.* 2304, 265–283. doi:10.1007/978-1-0716-1402-0_14
- Olenick, J. G., Wolff, R., Nauman, R. K., and McLaughlin, J. (1988). A flagellar pocket membrane fraction from trypanosoma brucei rhodesiense: immunogold localization and nonvariant immunoprotection. *Infect. Immun.* 56 (1), 92–98. doi:10.1128/IAI.56.1.92-98.1988
- Pisani, F., Castagnola, V., Simone, L., Loiacono, F., Svelto, M., and Benfenati, F. (2022). Role of pericytes in blood-brain barrier preservation during ischemia through tunneling nanotubes. *Cell. Death Dis.* 13 (7), 582. doi:10.1038/s41419-022-05025-y
- Qiao, C., Li, D., Liu, Y., Zhang, S., Liu, K., Liu, C., et al. (2023). Rationalized deep learning super-resolution microscopy for sustained live imaging of rapid subcellular processes. *Nat. Biotechnol.* 41 (3), 367–377. doi:10.1038/s41587-022-01471-3
- Rostami, J., Holmqvist, S., Lindström, V., Sigvardson, J., Westermark, G. T., Ingelsson, M., et al. (2017). Human astrocytes transfer aggregated α -synuclein via tunneling nanotubes. *J. Neurosci. Off. J. Soc. Neurosci.* 37 (49), 11835–11853. doi:10.1523/JNEUROSCI.0983-17.2017
- Rustom, A., Saffrich, R., Markovic, I., Walther, P., and Gerdes, H. H. (2004). Nanotubular highways for intercellular organelle transport. *Science* 303 (5660), 1007–1010. doi:10.1126/science.1093133
- Sartori-Rupp, A., Cordero Cervantes, D., Pepe, A., Gousset, K., Delage, E., Corroyer-Dumont, S., et al. (2019). Correlative cryo-electron microscopy reveals the structure of TNTs in neuronal cells. *Nat. Commun.* 10 (1), 342. doi:10.1038/s41467-018-08178-7
- Scheiblich, H., Dansokho, C., Mercan, D., Schmidt, S. V., Bousset, L., Wischhof, L., et al. (2021). Microglia jointly degrade fibrillar α -synuclein cargo by distribution through tunneling nanotubes. *Cell.* 184 (20), 5089–5106.e21. doi:10.1016/j.cell.2021.09.007
- Smirnov, M. S., Garrett, T. R., and Yasuda, R. (2018). An open-source tool for analysis and automatic identification of dendritic spines using machine learning. *PloS One* 13 (7), e0199589. doi:10.1371/journal.pone.0199589
- Sun, X., Wang, Y., Zhang, J., Tu, J., Wang, X. J., Su, X. D., et al. (2012). Tunneling-nanotube direction determination in neurons and astrocytes. *Cell. Death Dis.* 3 (12), e438. doi:10.1038/cddis.2012.177
- Tardivel, M., Bégard, S., Bousset, L., Dujardin, S., Coens, A., Melki, R., et al. (2016). Tunneling nanotube (TNT)-mediated neuron-to neuron transfer of pathological Tau protein assemblies. *Acta Neuropathol. Commun.* 4 (1), 117. doi:10.1186/s40478-016-0386-4
- Wang, L., Owusu-Hammond, C., Sievert, D., and Gleeson, J. G. (2023). Stem cell-based organoid models of neurodevelopmental disorders. *Biol. Psychiatry* 93 (7), 622–631. doi:10.1016/j.biopsych.2023.01.012
- Wang, X., Bukoreshtliev, N. V., and Gerdes, H. H. (2012). Developing neurons form transient nanotubes facilitating electrical coupling and calcium signaling with distant astrocytes. *PloS One* 7 (10), e47429. doi:10.1371/journal.pone.0047429
- Wang, X., and Gerdes, H. H. (2012). Long-distance electrical coupling via tunneling nanotubes. *Biochim. Biophys. Acta* 1818 (8), 2082–2086. doi:10.1016/j.bbamem.2011.09.002
- Wang, X., Veruki, M. L., Bukoreshtliev, N. V., Hartveit, E., and Gerdes, H. H. (2010). Animal cells connected by nanotubes can be electrically coupled through interposed gap-junction channels. *Proc. Natl. Acad. Sci. U. S. A.* 107 (40), 17194–17199. doi:10.1073/pnas.1006785107
- Wang, Y., Cui, J., Sun, X., and Zhang, Y. (2011). Tunneling-nanotube development in astrocytes depends on p53 activation. *Cell. Death Differ.* 18 (4), 732–742. doi:10.1038/cdd.2010.147
- Yang, Y., Ye, G., Zhang, Y. L., He, H. W., Yu, B. Q., Hong, Y. M., et al. (2020). Transfer of mitochondria from mesenchymal stem cells derived from induced pluripotent stem cells attenuates hypoxia-ischemia-induced mitochondrial dysfunction in PC12 cells. *Neural Regen. Res.* 15 (3), 464–472. doi:10.4103/1673-5374.266058
- Zoellner, H., Paknejad, N., Cornwell, J. A., Chami, B., Romin, Y., Boyko, V., et al. (2020). Potential hydrodynamic cytoplasmic transfer between mammalian cells: cell-projection pumping. *Biophys. J.* 118 (6), 1795–1860. doi:10.1016/j.bpj.2020.03.013
- Zurzolo, C. (2021). Tunneling nanotubes: reshaping connectivity. *Curr. Opin. Cell. Biol.* 71, 139–147. doi:10.1016/j.ccb.2021.03.003



OPEN ACCESS

EDITED BY

Andrea Gerbino,
University of Bari Aldo Moro, Italy

REVIEWED BY

Claudio Bucolo,
University of Catania, Italy
Gemma Caterina Maria Rossi,
San Matteo Hospital Foundation (IRCCS), Italy

*CORRESPONDENCE

Maurizio Cammalleri
✉ maurizio.cammalleri@unipi.it

RECEIVED 30 May 2023

ACCEPTED 21 August 2023

PUBLISHED 05 September 2023

CITATION

Melecchi A, Amato R, Dal Monte M, Rusciano D, Bagnoli P and Cammalleri M (2023) Restored retinal physiology after administration of niacin with citicoline in a mouse model of hypertensive glaucoma.
Front. Med. 10:1230941.
doi: 10.3389/fmed.2023.1230941

COPYRIGHT

© 2023 Melecchi, Amato, Dal Monte, Rusciano, Bagnoli and Cammalleri. This is an open-access article distributed under the terms of the [Creative Commons Attribution License \(CC BY\)](https://creativecommons.org/licenses/by/4.0/). The use, distribution or reproduction in other forums is permitted, provided the original author(s) and the copyright owner(s) are credited and that the original publication in this journal is cited, in accordance with accepted academic practice. No use, distribution or reproduction is permitted which does not comply with these terms.

Restored retinal physiology after administration of niacin with citicoline in a mouse model of hypertensive glaucoma

Alberto Melecchi¹, Rosario Amato¹, Massimo Dal Monte^{1,2},
Dario Rusciano³, Paola Bagnoli¹ and Maurizio Cammalleri^{1,2*}

¹Department of Biology, University of Pisa, Pisa, Italy, ²Interdepartmental Research Center Nutrafood "Nutraceuticals and Food for Health", University of Pisa, Pisa, Italy, ³Research Center, Fidia Farmaceutici S.p.A, Catania, Italy

Introduction: Much interest has been addressed to antioxidant dietary supplements that are known to lower the risk of developing glaucoma or delay its progression. Among them, niacin and citicoline protect retinal ganglion cells (RGCs) from degeneration by targeting mitochondria, though at different levels. A well-established mouse model of RGC degeneration induced by experimental intraocular pressure (IOP) elevation was used to investigate whether a novel combination of niacin/citicoline has better efficacy over each single component in preserving RGC health in response to IOP increase.

Methods: Ocular hypertension was induced by an intracameral injection of methylcellulose that clogs the trabecular meshwork. Electroretinography and immunohistochemistry were used to evaluate RGC function and density. Oxidative, inflammatory and apoptotic markers were evaluated by Western blot analysis.

Results: The present results support an optimal efficacy of niacin with citicoline at their best dosage in preventing RGC loss. In fact, about 50% of RGCs were spared from death leading to improved electroretinographic responses to flash and pattern stimulation. Upregulated levels of oxidative stress and inflammatory markers were also consistently reduced by almost 50% after niacin with citicoline thus providing a significant strength to the validity of their combination.

Conclusion: Niacin combined with citicoline is highly effective in restoring RGC physiology but its therapeutic potential needs to be further explored. In fact, the translation of the present compound to humans is limited by several factors including the mouse modeling, the higher doses of the supplements that are necessary to demonstrate their efficacy over a short follow up period and the scarce knowledge of their transport to the bloodstream and to the eventual target tissues in the eye.

KEYWORDS

intraocular pressure, oxidative stress, inflammation, mitochondrial dysfunction, apoptotic cascade, electroretinography

1. Introduction

Glaucoma is a chronic optic neuropathy characterized by progressive degeneration of retinal ganglion cells (RGCs), which leads to progressive visual loss (1, 2). Elevated intraocular pressure (IOP) and the derived mechanical stress are classically considered as the main causes of RGC death. In fact, increased IOP leads to excessive production of reactive oxygen species (ROS) that plays a role in the pathogenesis of glaucoma stimulating apoptotic and inflammatory pathways and promoting RGC apoptosis. Lifestyle and dietary supplementation may influence some of the risk factors and pathophysiological mechanisms underlying glaucoma development and progression. Antioxidant, anti-inflammatory and neuroprotective properties of ingredients in the dietary regimen have shown promising results in the management of chronic degenerative ocular diseases including glaucoma. For instance, intervening on the chronic intake of active molecules such as caffeine has been recently reported to exert protective effects on RGCs through anti-inflammatory action (3). In addition, impairment of mitochondrial function by mechanical stress and decreased blood perfusion due to IOP increase is likely to affect RGC survival thus eliciting a great interest on strategies that intervene on mitochondrial dysfunction in order to delay or even halt RGC loss (4–6). Some dietary supplements targeting mitochondrial dysfunction have been demonstrated to lower the risk of developing glaucoma and potentially slow disease progression. Among them, niacin (vitamin B3 or nicotinamide, a precursor of nicotinamide adenine dinucleotide, NAD⁺) is largely present in healthy diets while citicoline (Cytidine 5'-diphosphocholine), an intermediate in the generation of phosphatidylcholine from choline, is found in small amount in only a few food groups. Although acting at different cellular levels, both compounds represent to date some of the most promising neuroprotective supplements in ophthalmology with growing evidence demonstrating their efficacy against RGC degeneration (7–10). In particular, niacin acts as a crucial regulator of mitochondrial metabolism and redox reactions (11) while citicoline stabilizes cell membranes through the synthesis of phospholipids (12) and the production of cardiolipin, thus inhibiting mitochondria-mediated apoptosis (13). In glaucoma models, diets supplemented with niacin have been demonstrated to protect RGCs from degeneration by supporting mitochondrial health and metabolism (14–16). In this respect, vitamin B3 has been included in the panel of neuroprotective strategies in glaucoma patients in which low vitamin B3 levels have been demonstrated (17). Accordingly, vitamin B3 supplementation appears to counteract RGC dysfunction. In fact, in humans, increased niacin intake is associated with a lower likelihood of glaucoma (18) and NAD precursors seem to reduce the RGC vulnerability to increased IOP (19). In addition to niacin, citicoline protection against RGC damage has been extensively demonstrated in different models of RGC injury (20, 21). At the clinical level, citicoline administration to glaucoma patients appears to slow down glaucoma progression by exerting neuroprotective effects (22, 23). Preclinical and clinical data on the efficacy of citicoline supplementation in glaucoma have been comprehensively reviewed by Grieb et al. (24). The fact that glaucomatous degeneration encompasses multiple molecular pathways with intricate interactions suggests an important role of multitarget approaches based on the use of agent combinations acting on complementary pathogenic mechanisms. For instance, oxidative stress leads to dysfunctional mitochondria, which in turn may modulate inflammatory processes, while pro-inflammatory mediators also alter mitochondrial function (25). In fact, the excess of

reactive oxygen species (ROS) not compensated by endogenous antioxidant defenses can damage lipids, DNA, and proteins leading to RGC degeneration and can also activate the release of inflammatory mediators that participate to ROS-mediated RGC apoptosis (26). To this end, dietary supplements have been recognized as a promising adjuvant therapy in glaucoma since they may counteract oxidative stress and mitochondrial dysfunction (27, 28). The fact that both niacin and citicoline target mitochondria made us to hypothesize that their association could be more effective than the action of each single molecule. Therefore, aim of this study has been the evaluation of the efficacy of a dietary supplementation with niacin and citicoline in a mouse model of ocular hypertension induced by the injection of 2% methylcellulose (MCE) into the anterior chamber (29, 30). In this model, the efficacy of niacin/citicoline, either alone or in association, has been determined on the pathological hallmarks leading to RGC death – including oxidative stress and inflammation – both converging on the apoptotic cascade that culminates in RGC loss. Further evidence on the combination efficacy on RGCs survival have been also provided by the electrophysiological assessment of RGC function (29–31).

2. Materials and methods

2.1. Animals

C57BL/6J male mice (2-month-old) were purchased from Charles River Laboratories Italy (Calco, Italy). Mice were housed in a constant environment (23 ± 1°C, 50 ± 5% humidity) with a 12 h light/dark cycle (lights on at 08.00 a.m.) and fed with a standard diet and water *ad libitum*. Before starting the study, all mice were acclimatized for 7 days to handling and tonometry. This study was carried out in compliance with the ARVO Statement for the Use of Animals in Ophthalmic and Vision Research. The present study follows the European Communities Council Directive (2010/63/UE) and the Italian guidelines for animal care (DL 26/14, permission number: 132/2019PR). The 3Rs principles for ethical use of animals in scientific research guided our efforts to reduce both the number and suffering of the animals used in the present study. A total of 60 mice with an average body weight of 20–25 g were randomly assigned to 10 different groups as reported in Table 1.

2.2. Experimental model of ocular hypertension

Ocular hypertension was induced by an intracameral injection of 2% MCE in agreement with previous studies (29, 30). MCE (M0512; Sigma Aldrich, St. Louis, MO, United States) was dissolved at 2% in sterile saline to obtain an aqueous solution with a viscosity ranging from 3,500 to 5,600 cps. Mice were anesthetized with an intraperitoneal injection of avertin (1.2% tribromoethanol and 2.4% amylene hydrate in distilled water, 0.02 mL/g body weight: Sigma-Aldrich) and injected into the anterior chamber with 5 µL of MCE in both eyes by means of a Hamilton syringe equipped with a 36-gauge needle. The needle was inserted in the iridocorneal angle at about 1 mm from ora serrata and oriented parallelly to the iris surface. After MCE injections, mice were daily monitored for any alteration in ocular tissues (e.g., cataract, corneal opacity or edema).

TABLE 1 Experimental groups.

Experimental group	MCE	Treatment	Sample size
Control		Water	6
MCE	MCE injection	Water	6
N low	MCE injection	Niacin 0.5 g/Kg/die	6
C low	MCE injection	Citicoline 0.5 g/Kg/die	6
N high	MCE injection	Niacin 2.5 g/Kg/die	6
C high	MCE injection	Citicoline 1 g/Kg/die	6
N low + C low	MCE injection	Niacin 0.5 g/Kg/die + citicoline 0.5 g/Kg/die	6
N high + C low	MCE injection	Niacin 2.5 g/Kg/die + citicoline 0.5 g/Kg/die	6
N low + C high	MCE injection	Niacin 0.5 g/Kg/die + citicoline 1 g/Kg/die	6

N: niacin; C: citicoline.

2.3. Oral supplementation with niacin and citicoline or their combination

Niacin and citicoline powders were supplied by Fidia Farmaceutici (Abano Terme, PD, Italy) and dissolved in drinking water either alone or in association. In light of pre-liminary observations showing an average daily drinking volume of 5 mL/mouse/day and assuming an average mouse body weight of 20 g, niacin was dissolved at low (2 mg/mL) or high concentration (10 mg/mL) in order to obtain a corresponding daily dosage of 0.5 g/Kg (low dose; N low) or 2.5 g/Kg (high dose; N high). Similarly, citicoline was dissolved in the drinking water at low (2 mg/mL) or high concentration (4 mg/mL) to obtain a corresponding daily dosage of 0.5 g/Kg (low dose; C low) or 1 g/Kg (high dose; C high). Niacin and citicoline doses used here are in line with those reported in previous studies (21, 32, 33). Treatments providing different dose combinations of the two components were obtained by dissolving both niacin and citicoline in the same solution at the corresponding concentration. Mice were treated 14 days before and 14 days after the induction of ocular hypertension.

2.4. IOP measurement

IOP was non-invasively assessed every day using rebound tonometry (TonoLab, Icare Finland Oy, Helsinki, Finland). Mice were gently restrained, with the probe of the tonometer aligned to the eye optical axis at a 1–2 mm distance from the cornea. After habituation, the average of 5 consecutive recordings was considered as a reliable measure of IOP.

2.5. Electroretinogram

Full field photopic ERG was recorded in control mice and in mice that received MCE, untreated or treated with niacin and citicoline either alone or in combination. Mice dark-adapted overnight were anesthetized with intraperitoneal injection of avertin and placed on a heating pad. The body temperature was maintained at 38°C using a

homeo-thermic controller. To maintain dark adaptation all handling and experiments were performed under a dim red light. ERG responses were recorded using Ag/AgCl corneal electrodes. A reference electrode was inserted on the forehead, while a ground electrode was inserted at the base of the tail. The cornea was intermittently irrigated with saline solution to prevent clouding of the ocular media. Electroretinographic recordings were made using an ERG setup (Retimax Advanced, CSO, Firenze, Italy). Following light-adaptation (10 min to 30 cd-s/m²) to suppress the rod response, photopic responses were obtained following the delivery of 10 consecutive stimuli at 3 cd-s/m² with an interstimulus interval of 3 s and averaged to minimize the noise contribution. In the photopic ERG, the photopic negative response (PhNR) was measured from the baseline (0 μV) to the trough of the negative response following the positive b-wave.

PERG responses were evoked by delivering visual stimuli consisting of black-white horizontal bars (0.05 cycles/deg. black and white bars reversing at 1 Hz presented at 98% contrast) generated on a light emitting diode display with a mean luminance of 50 cd/m² aligned at about 25 cm from the cornea surface. A total of 300 consecutive signals was averaged to reduce noise contamination. PERG responses were analyzed by measuring the N35-P50 amplitude (from the negative peak, N35, to the positive peak, P50) and the P50-N95 amplitude (from the positive peak, P50, to the negative peak, N95).

2.6. Retinal ganglion cell immunohistochemistry

After ERG recording, mice were sacrificed by an overdose of avertin and their eyeballs enucleated. Then, 6 random retinas were isolated and fixed in 4% paraformaldehyde in 0.1 M phosphate buffered saline (PBS) for 2 h at room temperature. Contralateral retinas were used for molecular analyses. Retinas were rinsed with PBS and incubated for 24 h at 4°C with the primary antibody directed to RBPMS (ABN1376, Merck, Darmstadt, Germany) diluted 1:100 in PBS containing 2% TritonX-100 and 5% BSA. Retinas were then rinsed with PBS and incubated for 2 h with FITC-conjugated anti-guinea pig secondary antibody (F6261, Merck) diluted 1:200 in PBS containing 5% BSA and 2% TritonX-100. Finally, retinas were rinsed in PBS, flat mounted on polarized glass slides with the RGC layer facing up and coverslipped with a mounting medium. Images were acquired using an epifluorescence microscope (Ni-E; Nikon-Europe, Amsterdam, Netherlands) equipped with a digital camera (DS-Fi1c camera; Nikon-Europe). The number of RBPMS immuno-positive RGCs (number of cells per mm²) was compared between the experimental groups. Quantification was performed in a masked manner, with the operator ignoring the treatment received by the donor animal.

2.7. Western blot

Isolated retinas were homogenized in RIPA lysis buffer (Santa Cruz Biotechnology, Dallas, TX, United States) containing a cocktail of protease and phosphatase inhibitors (Roche Applied Science, Indianapolis, IN, United States). Protein concentration of retinal

homogenates was quantified by Micro BCA Protein Assay (Thermo Fisher Scientific, Waltham, MA, United States). Thirty micrograms of proteins from each sample were run on 4–20% SDS-PAGE gels (Bio-Rad Laboratories, Inc., Hercules, CA, United States) before transferring samples onto polyvinylidene difluoride membranes. Membranes were blocked for 1 h with 5% skim milk and then incubated overnight at 4°C with the solutions of primary antibodies listed in Table 2 using β -actin as the loading control. Membranes were then incubated for 2 h with rabbit polyclonal anti-mouse HRP-conjugated (A9044, Sigma-Aldrich) or goat polyclonal anti-rabbit HRP-conjugated (170–6,515, Bio-Rad Laboratories, Inc.) secondary antibodies (1:5000) and developed with the Clarity Western enhanced chemiluminescence substrate (Bio-Rad Laboratories, Inc.). Images were acquired using the ChemiDoc XRS+ (Bio-Rad Laboratories, Inc.). The optical density (OD) of the bands was evaluated using the Image Lab 3.0 software (Bio-Rad Laboratories, Inc.) and data were normalized to the corresponding OD of β -actin or nuclear factor kappa-light-chain-enhancer of activated B cells (NF- κ B) p65 as appropriate.

2.8. Statistical analysis

Data were analyzed by the Shapiro–Wilk test to verify their normal distribution. Statistical analysis was carried out with Graph Pad Prism 8.0.2 software (GraphPad Software, Inc., San Diego, CA, United States). Multiple comparisons among groups were analyzed by two-way ANOVA followed by the Tukey *post hoc* test. Data are expressed as mean \pm SEM of the indicated *n* values. Differences with $p < 0.05$ were considered as significant.

3. Results

3.1. Effect of dietary supplementation with niacin and citicoline on MCE-induced IOP elevation

IOP levels were determined in both untreated and treated mice before and after MCE injection. As shown in Figure 1, during the

14 days preceding MCE injection, IOP levels were stable at about 14 mmHg with no difference between treated and untreated groups, while 24 h after the injection, IOP levels significantly increased to reach a peak at about 32 mmHg. MCE-induced ocular hypertension was maintained up to 14 days in agreement with previous findings (29, 30). Either individual or combined administration of niacin and citicoline did not influence the MCE-induced IOP elevation.

3.2. Effect of dietary supplementation with niacin and citicoline on MCE-induced RGC dysfunctional activity

The effect of niacin and citicoline administration, either alone or in combination, on MCE-induced retinal dysfunction was assessed by photopic ERG recordings, including the b-wave as a cone-driven post-receptor response and the photopic negative response (PhNR) as a RGC-related response (Figure 2A). In MCE-injected mice, the amplitude of the photopic b-wave did not display any statistical difference from the control group independent on treatment (Figure 2B). Conversely, PhNR amplitude in untreated mice receiving MCE injection, was significantly decreased by about 42% as compared to controls. Mice receiving single treatments with low dose of either niacin or citicoline displayed a PhNR amplitude comparable to that of MCE untreated mice. In contrast, single treatments with niacin or citicoline at high dose prevented the MCE-induced decrease in PhNR responses. When used in combination, either low or high dose of niacin preserved the PhNR amplitude only in the presence of citicoline at low dose, while the PhNR amplitude remained rather similar to that of MCE untreated mice in the presence of citicoline at high dose (Figure 2C).

The RGC-specific activity in each experimental group was assessed by analyzing both the positive (N35–P50) and the negative components (P50–N95) of pattern ERG (PERG) responses (Figure 3A). MCE-injected mice showed a significant decrease in both N35–P35 and P50–N95 amplitudes as compared to controls (50% and 53%, respectively), without any significant effect exerted by individual treatments with either niacin or citicoline at low dose. On the contrary, the individual treatment with niacin or citicoline at high dose partially

TABLE 2 Western blot antibodies.

Antibodies	Dilution	Source	Catalogue
Rabbit polyclonal anti-Nrf-2	1:1000	Abcam (Cambridge, UK)	ab92946
Rabbit polyclonal anti-HO-1	1:500	Abcam	ab13243
Rabbit monoclonal anti-pNF- κ B p65 (Ser 536)	1:1000	Abcam	ab76302
Rabbit polyclonal anti-NF- κ B p65	1:1000	Abcam	ab16502
Mouse monoclonal anti-IL-6	1:500	Santa Cruz Biotech	sc-57,315
Rabbit monoclonal anti-GFAP	1:5000	Abcam	ab207165
Rabbit monoclonal anti-cleaved caspase 3	1:1000	Cell Signaling Technology (Danvers, MA, United States)	9,664
Rabbit monoclonal anti-Bax	1:500	Abcam	ab182733
Rabbit polyclonal anti-Bcl-2	1:500	Abcam	ab194583
Mouse monoclonal anti-cytochrome c	1:250	BD Biosciences (San Diego, CA, United States)	556,433
Mouse monoclonal anti- β -actin	1:2500	Sigma-Aldrich	A2228

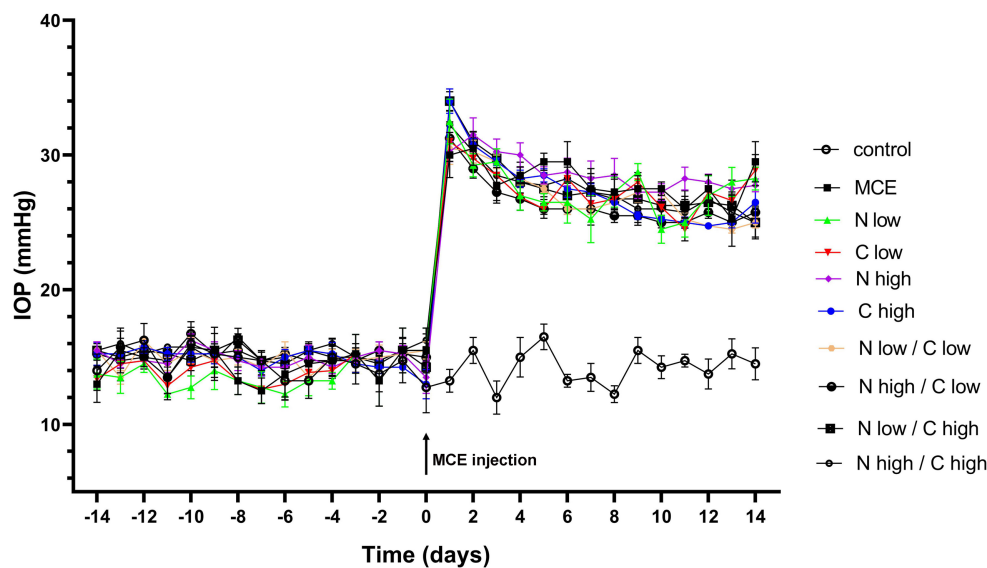


FIGURE 1

Effect of individual or combined administration of niacin and citicoline on methylcellulose (MCE)-induced ocular hypertension. Longitudinal evaluation of intraocular pressure (IOP) levels as assessed by rebound tonometry in control and MCE injected mice either untreated or treated with niacin and citicoline (individual or combined). Data are expressed as mean \pm SEM of $n = 6$ mice.

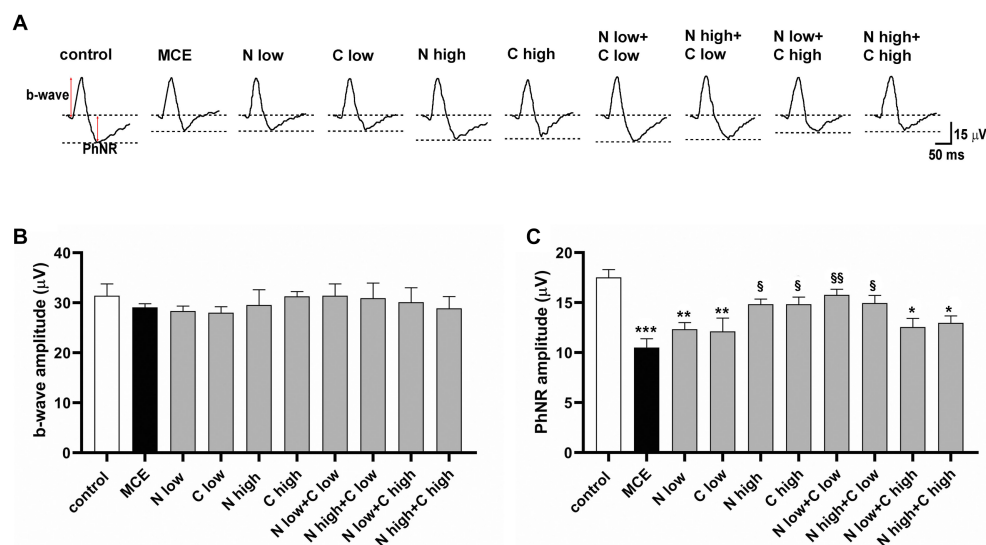


FIGURE 2

Effect of individual or combined administration of niacin with citicoline on photopic electro-retinogram (ERG). (A) Representative waveforms of photopic ERG in control and methylcellulose (MCE)-injected mice either untreated or treated with individual niacin and citicoline or their combination. (B) Mean amplitude of photopic b-wave. (C) Mean amplitude of photopic negative response (PhNR) as measured from the baseline (0 μ V) to the trough of the negative response following the positive b-wave. Data are expressed as mean \pm SEM ($n = 6$ mice for each experimental group). * $p < 0.01$, ** $p < 0.001$, and *** $p < 0.0001$ vs. control; $^{\dagger}p < 0.01$, $^{\ddagger}p < 0.001$ vs. MCE (two-way ANOVA followed by Tukey's multiple comparison post-hoc test).

prevented the MCE-induced decrease in PERG responses, which still resulted about 25% lower than in controls. Both N35-P35 and P50-N95 amplitudes were preserved to control levels following the combined administration of niacin (at either low or high dose) with citicoline at low dose. In contrast, combined administration of citicoline at high dose did not influence PERG response amplitudes, which were comparable to those of MCE untreated mice (Figures 3B,C).

3.3. Effect of dietary supplementation with niacin and citicoline on MCE-induced RGC loss

Together with RGC dysfunction, the progressive decrease in RGC density represents a hallmark of MCE-induced glaucomatous damage. After recording RGC activity, we examined whether the improved retinal function after niacin (at either doses) and citicoline at low dose

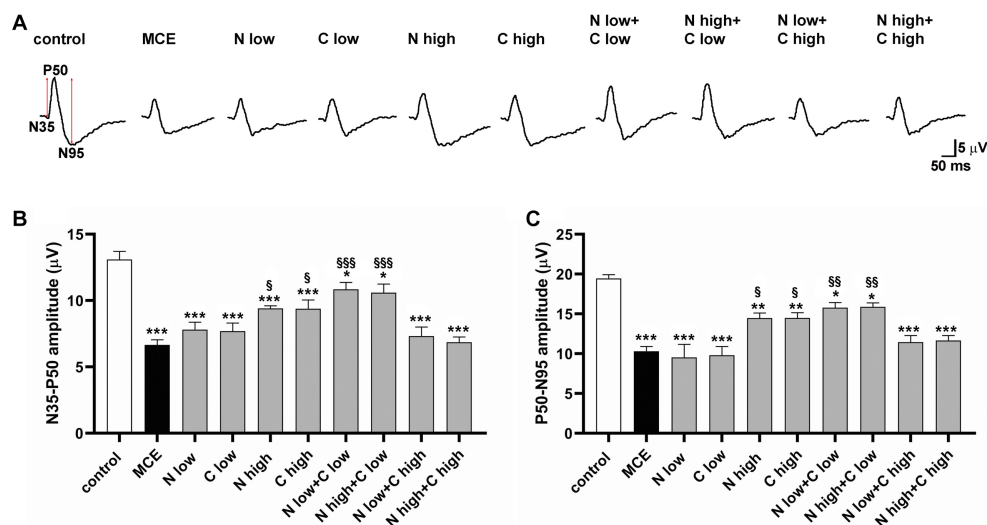


FIGURE 3

Effect of individual or combined administration of niacin and citicoline on methylcellulose (MCE)-induced dysfunctional pattern electroretinogram (PERG). (A) Representative waveforms of PERG in control and MCE-injected mice either untreated or treated with individual niacin and citicoline or their combination. (B,C) Mean amplitudes of the N35-P50 (B) and P50-N95 (C) waves. Data are expressed as mean \pm SEM ($n = 6$ mice for each experimental group). * $p < 0.05$, ** $p < 0.001$, and *** $p < 0.0001$ vs. control; § $p < 0.01$, §§ $p < 0.001$, §§§ $p < 0.0001$ vs. MCE (two-way ANOVA followed by Tukey's multiple comparison post-hoc test).

was accompanied by a reduced RGC loss by evaluating the density of RNA-binding protein with multiple splicing (RBPMS) positive RGCs in retinal flat mounts. As shown by the representative images in Figure 4A and their related quantification (Figure 4B), after MCE injection RGC density decreased by about 63% as compared to controls with no significant effects of the individual administration of niacin or citicoline at low dose. In mice receiving niacin or citicoline alone at high dose, RGC density was higher than in MCE untreated mice, but still 39% lower than in controls. The combined administration of niacin (at either doses) and citicoline at low dose preserved the RGC density to control levels. Both doses of niacin in combination with citicoline at high dose was found to slightly increase the RGC density that remained about 40% lower than in controls.

3.4. Effect of dietary supplementation with niacin and citicoline on oxidative stress and inflammatory markers

In the glaucomatous damage to RGCs, oxidative stress and inflammation represent primary events driving the progressive loss of RGC activity and viability. Retinal levels of typical markers of oxidative stress and inflammation were assessed following the individual or combined administration of niacin and citicoline to MCE-injected mice. In Figure 5, oxidative stress was evaluated by measuring protein levels of nuclear factor erythroid 2-related factor-2 (Nrf-2), a ROS-sensitive transcription factor, and the antioxidant enzyme heme oxygenase-1 [HO-1; (34)]. Protein levels of both Nrf-2 and HO-1 increased in MCE-untreated mice by about 270% and 272%, respectively, as compared with controls. Protein levels of both markers did not differ from those of MCE untreated mice after the administration of niacin or citicoline at low dose, while they were significantly decreased following the treatment with high dose of niacin (Nrf-2: -35%, HO-1: -25%) or

citicoline (Nrf-2: -34%, HO-1: -25%) as compared to MCE untreated mice. Combined administration of niacin (at either low or high dose) with citicoline at low dose further decreased oxidative stress markers to levels comparable to those in controls, whereas the combination of niacin (at either low or high dose) with citicoline at high dose only partially affected oxidative stress markers (Nrf-2: about -24%, HO-1: about -27%) as compared to MCE untreated mice.

Inflammation processes and associated glial reactivity were evaluated by measuring the protein levels of the phosphorylated form of the p65 subunit of nuclear factor kappa-light-chain-enhancer of activated B cells (pNF-kB), a master transcriptional regulator of pro-inflammatory factors including interleukin (IL)-6 (35) and the glial fibrillary acid protein (GFAP) as a gliosis marker. In untreated mice injected with MCE, the protein level of pNF-kB was significantly increased by about 92% (Figure 6A) while the protein level of IL-6 increased by about 98% (Figure 6B). The individual administration of niacin or citicoline at low dose did not influence the MCE-induced increment in pNF-kB and IL-6, while their administration at high dose significantly reduced the levels of both inflammatory markers, although they remained still higher than in controls (+40% and +45%, respectively). The combined administration of niacin with citicoline at low dose prevented the MCE-induced increase of pNF-kB and IL-6. The combination efficacy on pNF-kB increase was lost when citicoline was administered at high dose, while a slight decrement was observed on IL-6 protein levels (-19%). MCE-induced increase in GFAP protein levels (+95%) was significantly decreased by individual niacin and citicoline at high dose (-42% and -43%, respectively). Niacin (at either doses) in combination with citicoline at low dose preserved GFAP at levels similar to those in controls, while in combination with at high dose had lower efficacy on MCE-induced GFAP accumulation that remained about 55% higher than in controls (Figure 6C).

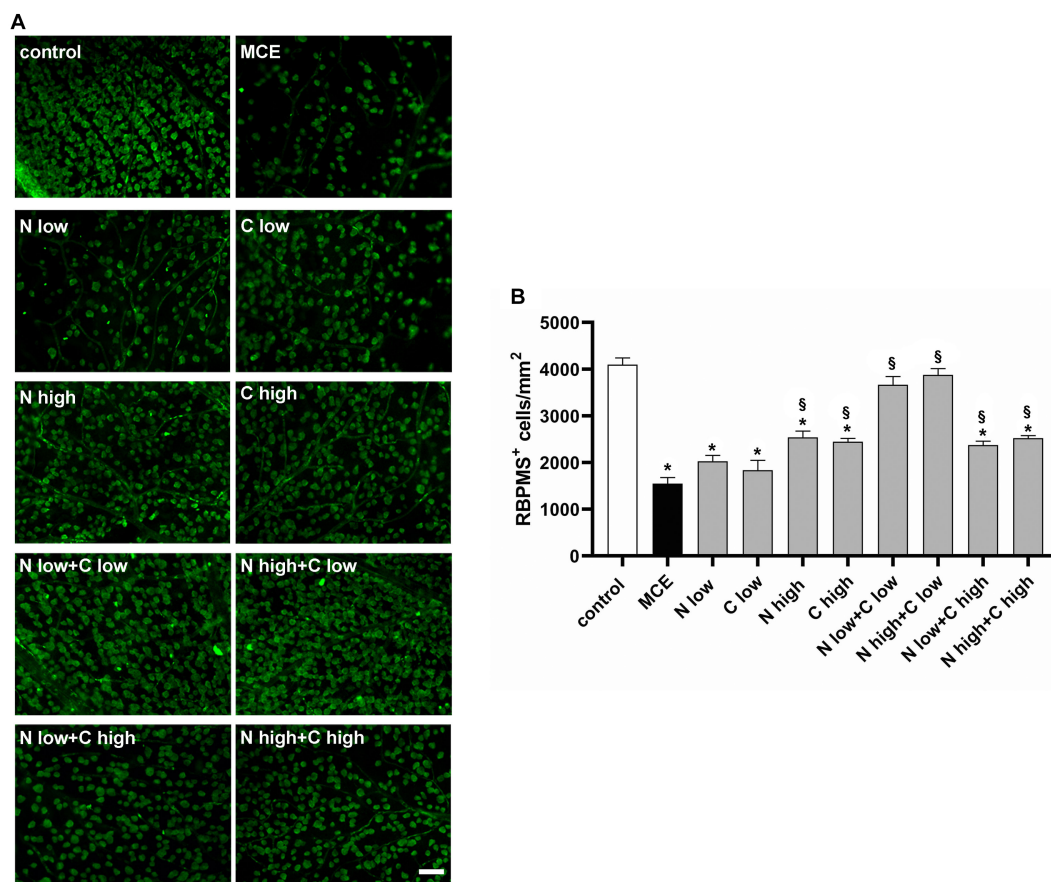


FIGURE 4

Effect of individual or combined administration of niacin and citicoline on methylcellulose (MCE)-induced retinal ganglion cell (RGC) loss. **(A)** Representative images of RNA-binding protein with multiple splicing (RBPMS) positive RGCs in whole-mount retinas of control and MCE mice either untreated or treated with individual niacin and citicoline or their combination. Scale bar: 50 μ m. **(B)** Quantitative analysis of RBPMS-positive cell density. Data are expressed as mean \pm SEM ($n = 6$ retinas for group). * $p < 0.0001$ vs. control; $^{\dagger}p < 0.0001$ vs. MCE (two-way ANOVA followed by Tukey's multiple comparison post-hoc test).

3.5. Effect of dietary supplementation with niacin and citicoline on intrinsic apoptotic pathway

Altered oxidative stress and inflammatory processes lead to progressive RGC death by triggering the apoptotic cascade in which the final executioner is the active caspase-3. As shown in Figure 7A, in MCE untreated mice, the level of caspase-3 was increased with respect to controls (+84%). It was not significantly affected by the administration of niacin or citicoline at low dose while it was drastically reduced by their administration at high dose (about -45%). Combined administration of niacin (at either low or high dose) with citicoline at low dose further decreased caspase-3 protein levels which became comparable to those in controls. Conversely, combined treatment with citicoline at high dose did not affect caspase-3 levels that remained comparable to those in untreated MCE mice. To evaluate the combination efficacy on the mitochondrial-dependent intrinsic apoptotic pathway, we assessed the ratio of pro-apoptotic Bax to anti-apoptotic Bcl-2 proteins as a major checkpoint in the intrinsic apoptotic pathway, and the retinal levels of cytochrome c, which acts as a primary trigger of the apoptotic caspase cascade. As shown in Figure 7B, the Bax/Bcl-2 ratio increased by about 300% in MCE untreated mice as compared with controls. Niacin or citicoline at low dose did not influence the MCE-induced increase in

Bax/Bcl-2 ratio, while at high dose, the ratio was reduced to about 50%. The combined administration of niacin with citicoline at low dose, further reduced the Bax/Bcl-2 ratio, reaching levels comparable to those in controls. Conversely, the Bax/Bcl-2 ratio did not significantly differ from that of MCE untreated mice after niacin combined with citicoline at high dose. The same trend of variations applies to the efficacy of the single components or their combined administration on protein levels of cytochrome c with higher efficacy of citicoline at low dose in combination with niacin at either low or high dose (Figure 7C).

4. Discussion

Increased intraocular pressure (IOP) is the main risk factor for developing glaucoma that is characterized by progressive optic nerve degeneration resulting in RGC death. Oxidative stress and inflammation work together to trigger apoptotic cell death by affecting mitochondrial dynamics. IOP elevation, characteristic of hypertensive glaucoma, was mimicked here by injecting the anterior chamber of the mouse eye with MCE, which clogs the trabecular meshwork and impairs the aqueous humor outflow. Sudden elevation of the IOP remains stable for almost 2 weeks, thus closely simulating the human hypertensive glaucoma. As shown by the present findings, a novel

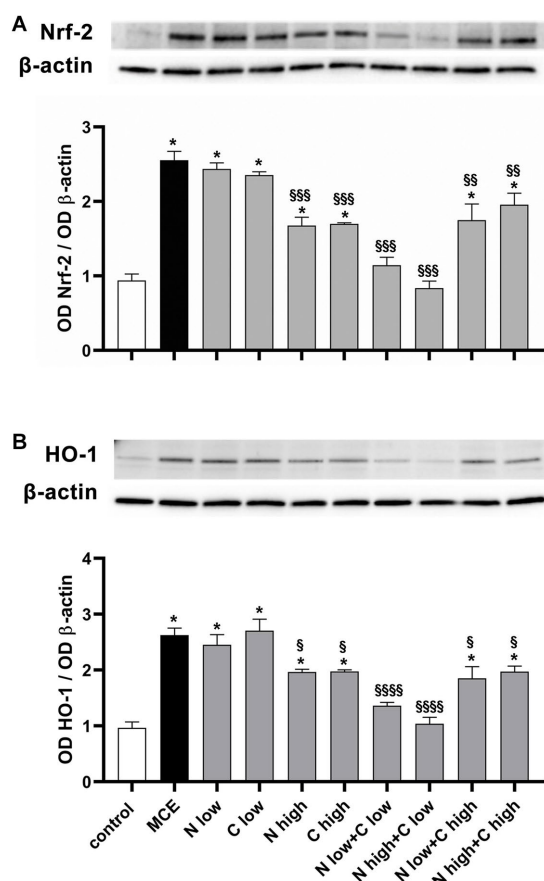


FIGURE 5

Effect of individual or combined administration of niacin and citicoline on MCE-induced oxidative stress. (A) Representative Western blots and densitometric analysis of nuclear factor erythroid 2-related factor-2 (Nrf-2) and (B) heme oxygenase-1 (HO-1) levels in control and MCE mice either untreated or treated with individual niacin and citicoline or their combination. Data are expressed as mean \pm SEM ($n = 6$ retinas for group). * $p < 0.0001$ vs. control; $^{\dagger}p < 0.01$, $^{\ddagger}p < 0.001$, and $^{\S\S\S}p < 0.0001$ vs. MCE (two-way ANOVA followed by Tukey's multiple comparison post-hoc test).

combination of niacin with citicoline has better efficacy over each single component in preserving RGC health in response to IOP increase by reducing inflammation and oxidative stress, which are the main triggers of RGC apoptotic death and retinal dysfunctional activity.

4.1. Characterization of the MCE model

Mechanic stress at the optic nerve head impairs RGC survival by activating multifactorial mechanisms among which the inflammatory cascade associated to glial cell activation triggers NF- κ B, a transcriptional factor which enters the nucleus to generate high levels of pro-inflammatory cytokines, also including IL-6 (35). The inflammatory response is closely related to increased oxidative stress by enhancing the production of oxidative metabolites through the overexpression of ROS-producing enzymes (36). On its hand, increased oxidative stress, as determined by upregulated levels of the ROS-sensitive transcriptional factor Nrf-2 and its target HO-1, promotes an intracellular signaling cascade that activates a variety of transcription factors leading to enhanced pro-inflammatory gene expression (37). Upstream the

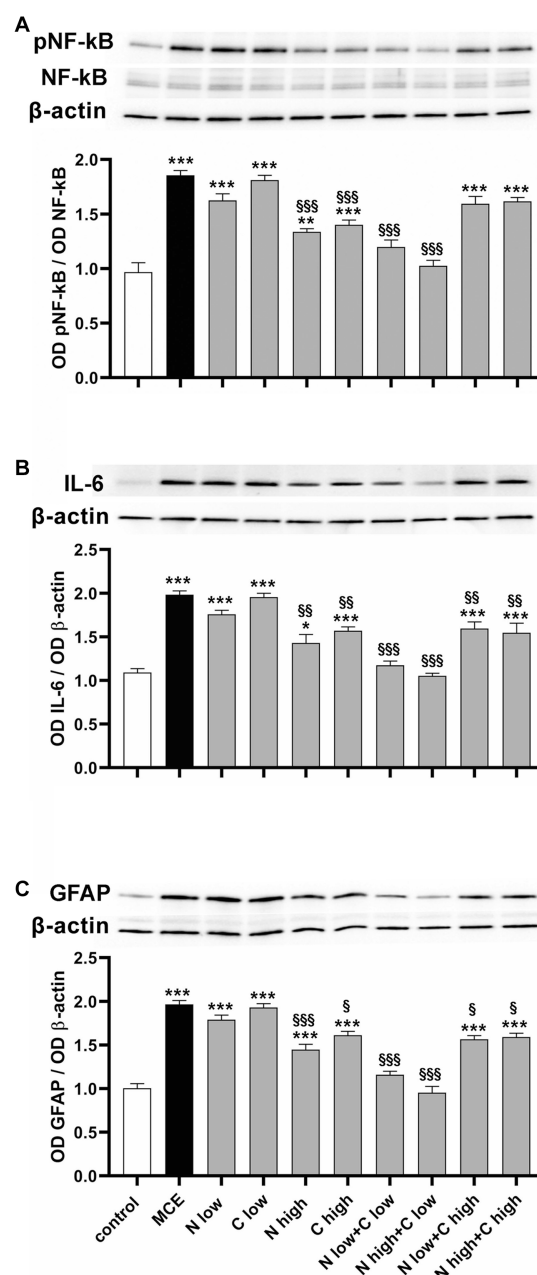


FIGURE 6

Effect of individual or combined administration of niacin and citicoline on MCE-induced inflammatory response. (A–C) Representative Western blots and densitometric analysis of the phosphorylated form of the p65 subunit of nuclear factor κ -light-chain-enhancer of activated B cells (pNF- κ B) and NF- κ B (A), interleukin (IL)-6 (B) and glial fibrillary acidic protein (GFAP; C) levels in control MCE mice either untreated or treated with individual niacin and citicoline or their combination. Data are expressed as mean \pm SEM ($n = 6$ retinas for group). * $p < 0.01$, ** $p < 0.001$, and *** $p < 0.0001$ vs. control; $^{\dagger}p < 0.01$, $^{\ddagger}p < 0.001$, and $^{\S\S\S}p < 0.001$ vs. MCE (two-way ANOVA followed by Tukey's multiple comparison post-hoc test).

IOP-associated oxidative stress, elevated mechanic stress and insufficient retinal perfusion impair mitochondrial biogenesis by affecting the activity of the electron transport chain, thus contributing to increased production of ROS finally leading to mitochondrial dysfunction and DNA alterations, eventually triggering the apoptotic cascade (38). Accordingly, we found that MCE injection leads to increased Bax/Bcl-2 ratio resulting in cytochrome c release as demonstrated by its increased

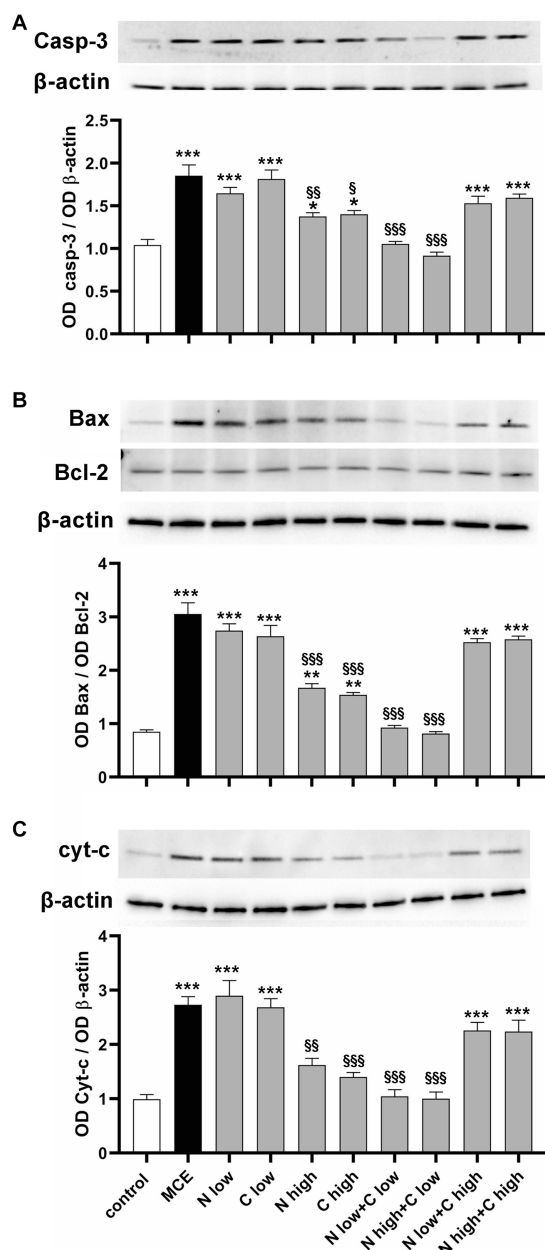


FIGURE 7

Effect of individual or combined administration of niacin and citicoline on MCE-induced apoptotic cascade. (A–C) Representative Western blots and densitometric analysis of caspase 3 (A), Bax/Bcl-2 ratio (B) and cytochrome c (C) in control and MCE mice either untreated or treated with individual niacin and citicoline or their combination. Data are expressed as mean \pm SEM ($n = 6$ retinas for group). * $p < 0.05$, ** $p < 0.001$, and *** $p < 0.0001$ vs. control; $^{\dagger}p < 0.01$, $^{\ddagger}p < 0.001$ and $^{\S}p < 0.001$ vs. MCE (two-way ANOVA followed by Tukey's multiple comparison post-hoc test).

expression. Then, activation of the apoptosis effector caspase-3 leads to a drastic decrease in immunostaining with RBPMS, a well-established marker of RGCs (39). Decreased density of RGCs is accompanied by impaired electroretinographic recordings of their activity. In fact, PhNR, a slow negative component of the photopic ERG that provides specific information about RGC activity, and PERG, an electrophysiologic response to a pattern reversing stimulus that objectively measures RGC function, are both reduced in amplitude in line with previous findings from different animal models of glaucoma with spontaneous or induced

ocular hypertension (29, 30, 33, 40–43). Alterations in PhNR and PERG are also typical of glaucoma patients in which they have been possibly related to early RGC loss (9).

4.2. Efficacy of diet supplements

The MCE model used in this study has been previously employed to assess the efficacy of treatment strategies aimed at counteracting glaucomatous RGC degeneration by acting on IOP elevation or downstream inflammatory and oxidative processes. For instance, oral administration of nutritional products based on antioxidant/anti-inflammatory components effectively counteract MCE-induced RGC degeneration independently on IOP lowering (29) at variance with topically administered melatonergic compounds, which exert a strong hypotensive effect (30). As shown by the present results, non-IOP-related mechanisms mediate the protective action of dietary supplementation with niacin and citicoline at their best dosage either alone or in combination. In particular, single administration of niacin or citicoline at doses in line with those previously reported to exert beneficial effects in preclinical models (21, 33), efficiently counteracts the major pathological signs of glaucoma at morpho/functional and molecular levels. Niacin supplementation would act by replacing the glaucoma-associated depletion of NAD^+ , a coenzyme involved in oxidative phosphorylation leading to ATP production. In fact, niacin has been shown to influence mitochondrial metabolism and its supplementation has been demonstrated to improve mitochondrial structure with the formation of more tightly folded cristae thus increasing the ATP-generating surface area (44, 45). On the other hand, citicoline exerts broader effects by elevating neurotrophin levels, ameliorating axonal transport deficits, restoring membrane integrity and improving mitochondrial function including cardiolipin synthesis that participates to ATP production (46).

4.3. Combined administration of niacin with citicoline

As also shown by the present results, the combined administration of niacin and citicoline at calibrated amounts is more effective than each single ingredient confirming the rationale for their association to limit retinal damage. This finding is in line with previous results demonstrating that the co-administration of vitamin B3 and citicoline also in combination with coenzyme Q10 is generally more effective than the single ingredients in reducing oxidation and inflammation (47). Combined efficacy of citicoline with CoQ10 has been demonstrated in many retinal pathologies including glaucoma (8). Accordingly, combined drug treatments acting by multitarget approach have been shown to be more effective compared with single-drug treatments (48). In combination, drugs could be used at doses lower than standard, thus displaying safer and more efficient activity. In the case of the MCE model of glaucoma used here, assuming that mitochondrial dysfunction mainly contributes to glaucoma-associated retinal damage and considering that mitochondrial cristae are the main target of vitamin B3, the obtained results demonstrate that the concomitant administration of niacin and citicoline has the theoretical advantage of better recovering mitochondrial health. However, the possibility that the combined efficacy of niacin and citicoline would not be limited to the improvement of mitochondrial health cannot be excluded given the broad spectrum of effects of citicoline, other

than those specifically involving mitochondrial function. For instance, citicoline, acting as a source of phosphatidylcholine, has been shown to prevent neuronal membrane breakdown and apoptosis, thus providing neuroprotection (7). Moreover, citicoline may act as a choline donor for the synthesis of neurotransmitters such as acetylcholine (46). Given the evidence of the protective efficacy of acetylcholine receptor agonists on IOP-dependent RGC degeneration (49), the possibility exists that the neuroprotective effect of citicoline might also depend on enhanced cholinergic signaling.

As also shown by the present results, the efficacy of the combined administration of niacin and citicoline depends on their relative concentration, with best efficacy of each of them at high doses when administered alone, and even better efficacy when citicoline is administered at low dose in combination with niacin at either high or low dose. Combination of niacin with citicoline at their optimal ratio consistently acts on the different players in the molecular cascade triggered by IOP elevation towards RGC morpho-functional rescue (see the schematic diagram in Figure 8). Whether the

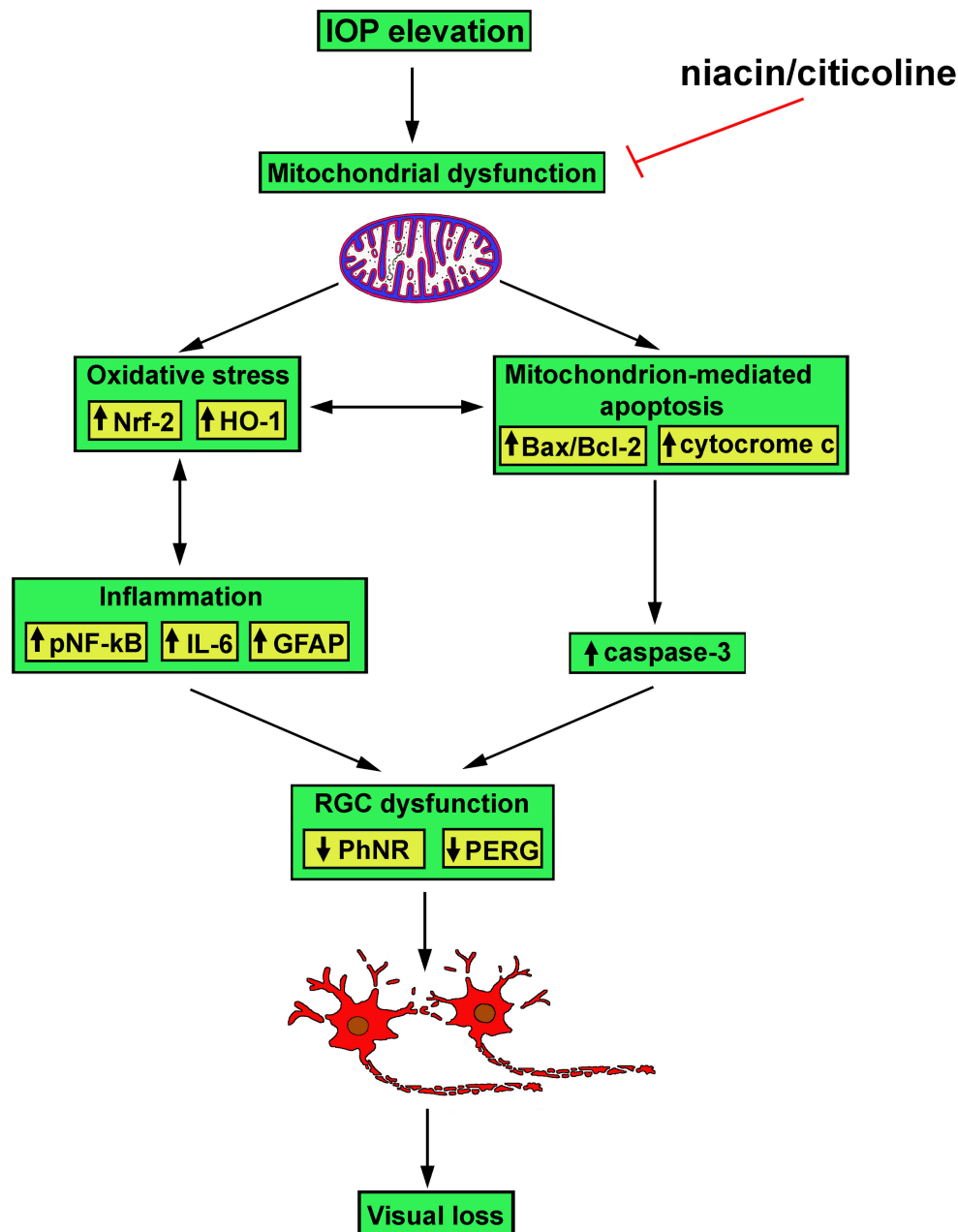


FIGURE 8

Schematic diagram depicting possible mechanisms of action of niacin and citicoline on hypertensive glaucoma. Niacin/citicoline, by intervening on dysfunctional mitochondria, would reduce oxidative stress and inflammation both resulting in preserved apoptotic cascade leading to retinal ganglion cell survival thus limiting visual loss.

combination efficacy depends on its preventive administration or rather reflects restored RGC health secondary to IOP injury remains to be answered although evidence is accumulating about lower-risk and high-benefit of dietary supplements in preventive care in respect to curative intervention (50).

The protective effects of niacin and citicoline are directly proportional to their concentration when given alone. Such effects can be improved by the association of either doses of niacin despite only in combination with low-dose citicoline. This finding is in line with the concept that low doses of two compounds that have different modes of action may provide additive effects to achieve better efficacy than high doses alone. On the other hand, the additive effect of the combination may vary according to the doses and the different proportions of each component in the combination (51). In the case of citicoline, previous evidence from a rat model of embolic stroke demonstrated that a suboptimal dose of citicoline combined with a thrombolytic therapy provided an additive efficacy on the reduction in infarct volume while increasing the dose of citicoline in the combination was less effective than its low dose (52) suggesting some kind of negative interference. We are currently unable to provide a clear explanation about the lack of combined efficacy when citicoline is given at high dose, but we can speculate about its reason. It is usually assumed that ingested citicoline is quickly hydrolyzed into cytidine and choline of which choline concentration in the plasma is much lower than cytidine thus preventing cholinergic toxicity (53). When high-dose citicoline is given in combination with niacin then choline concentration might exceed its physiological level as nicotinamide potentiates choline availability by blocking its clearance (54). Additional choline availability might derive from niacin interaction with activated phospholipase A2, which releases choline from choline-containing phospholipids (55). The final effect would be an intracellular choline accumulation beyond the level of toxicity (56). This would counterbalance the protective effect of each molecule either alone or in combination at low doses to ultimately drive apoptotic RGC death. Additionally, citicoline transport may be limited by high extracellular choline concentration with higher uptake maintained in the presence of low compared with high substrate level. Vitamin B3 diffusion, in contrast, involves high-affinity carrier-mediated mechanisms that render its transport less dependent on the substrate concentration.

4.4. Conclusion

Combination efficacy of niacin with citicoline is founded on multifactorial mechanisms of action that lead to improved mitochondrial resilience against glaucomatous stress. While drug combination is extensively studied for increasing therapy efficacy, preventing drug resistance and reducing therapy duration, less information is available on combined activity of distinct dietary supplements. In fact, supplement interactions are difficult to interpret because the variability in supplement constituents, quality, and dosage makes it difficult to dissect the efficacy of each component in respect to supplement combination.

Although the present findings suggest a potential effect of the combination in the experimental mouse model of hypertensive glaucoma, these results need to be further elucidated and reproduced in humans mostly in respect to the short follow up period in the MCE model. In this respect, the gradual increase in IOP with age associated to progressive loss of RGCs in the DBA/2J inbred mouse strain would allow us to follow for a longer time the temporal profile of RGC loss and IOP elevation (57). Additional restrictions apply on the daily doses allowed in humans that are much lower in respect to those used in animal models. Considering the different metabolism and size of a mouse, the doses used in this study are 50 to almost 260 times higher for niacin and 5 to 10 times higher for citicoline. This is justified by the fact that the insurgence of glaucoma and RGC apoptotic death occurs within 2 weeks in the mouse model as compared to decades in humans, thus much higher doses of the supplements are necessary to demonstrate their efficacy. In addition, there are many persistent gaps in our knowledge of supplement transport from the gut to the bloodstream and to the eventual target tissues in the eye. Further limitations include the difficulty to conduct large clinical trials using diet supplements to assess their impact on human health. In the case of vitamin B3, for instance, short-term clinical studies in glaucoma patients have demonstrated its efficacy in improving visual function, but additional clinical trials with longer follow-up are needed before vitamin B3 may be incorporated into clinical practice. In the case of niacin combination with citicoline, the present findings are highly suggestive of the possibility that it may become part of the adjuvant treatment of glaucoma although its therapeutic potential needs to be further explored with both preclinical and randomized clinical trials.

Data availability statement

The raw data supporting the conclusions of this article will be made available by the authors, without undue reservation.

Ethics statement

The animal study was reviewed and approved by Commission for Animal Wellbeing of the University of Pisa.

Author contributions

DR, PB, and MC: conceptualization and project administration. RA and AM: methodology, validation, and investigation. RA, AM, and MC: formal analysis and data curation. MC: resources, supervision, and funding acquisition. PB and MC: writing—original draft preparation. RA, MD, DR, PB, and MC: writing—review and editing. All authors contributed to the article and approved the submitted version.

Funding

This study was supported by funding from the Italian Ministry of Universities and Research to MC (FRA-2021/2022) and RA (FRA-2023). This study was also supported by the Italian Ministry of Universities and Research under the Department of Excellence 2023–2027 initiative. This research was also funded by the financial support of Fidia Farmaceutici S.p.A. Abano Terme, Italy.

Acknowledgments

We wish to thank Vittorio Porciatti (Bascom Palmer Eye Institute, University of Miami) for providing us with his experience in reviewing the manuscript. We also thank Eleonora Sartori and Cinzia Casella (Fidia Pharmaceuticals, Italia) for their comments on the manuscript. The authors wish to thank Tiziana Cintio for animal assistance.

References

- Harasymowycz P, Birt C, Gooi P, Heckler L, Hutnik C, Jinapriya D, et al. Medical Management of Glaucoma in the 21st century from a Canadian perspective. *J Ophthalmol*. (2016) 2016:6509809. doi: 10.1155/2016/6509809
- Jonas JB, Aung T, Bourne RR, Bron AM, Ritch R, Panda-Jonas S. Glaucoma. *Lancet*. (2017) 390:2183–93. doi: 10.1016/S0140-6736(17)31469-1
- Conti F, Lazzara F, Romano GL, Platania CBM, Drago F, Bucolo C. Caffeine protects against retinal inflammation. *Front Pharmacol*. (2022) 12:824885. doi: 10.3389/fphar.2021.824885
- Boia R, Ruzafa N, Aires ID, Pereiro X, Ambrósio AF, Vecino E, et al. Neuroprotective strategies for retinal ganglion cell degeneration: current status and challenges ahead. *Int J Mol Sci*. (2020) 21:2262. doi: 10.3390/ijms21072262
- Fu L, Kwok SS, Chan YK, Ming Lai JS, Pan W, Nie L, et al. Therapeutic strategies for attenuation of retinal ganglion cell injury in optic neuropathies: concepts in translational research and therapeutic implications. *Biomed Res Int*. (2019) 2019:8397521. doi: 10.1155/2019/8397521
- Ji MH, Kreymerman A, Belle K, Ghiam BK, Muscat SR, Mahajan VB, et al. The present and future of mitochondrial-based therapeutics for eye disease. *Transl Vis Sci Technol*. (2021) 10:4. doi: 10.1167/tvst.10.8.4
- Gandolfi S, Marchini G, Caporossi A, Scuderi G, Tomasso L, Brunoro A. Cytidine 5'-Diphosphocholine (citicoline): evidence for a neuroprotective role in glaucoma. *Nutrients*. (2020) 12:793. doi: 10.3390/nu12030793
- García-López C, García-López V, Matamoros JA, Fernández-Albarral JA, Salobrar-García E, de Hoz R, et al. The role of citicoline and coenzyme Q10 in retinal pathology. *Int J Mol Sci*. (2023) 24:5072. doi: 10.3390/ijms24065072
- Hui F, Tang J, Williams PA, McGuinness MB, Hadoux X, Casson RJ, et al. Improvement in inner retinal function in glaucoma with nicotinamide (vitamin B3) supplementation: a crossover randomized clinical trial. *Clin Exp Ophthalmol*. (2020) 48:903–14. doi: 10.1111/ceo.13818
- Williams PA, Harder JM, Cardozo BH, Foxworth NE, John SWM. Nicotinamide treatment robustly protects from inherited mouse glaucoma. *Commun Integr Biol*. (2018) 11:e1356956. doi: 10.1080/19420889.2017.1356956
- Maiese K, Chong ZZ, Hou J, Shang YC. The vitamin nicotinamide: translating nutrition into clinical care. *Molecules*. (2009) 14:3446–85. doi: 10.3390/molecules14093446
- Zweifler RM. Membrane stabilizer: citicoline. *Curr Med Res Opin*. (2002) 18:s14–7. doi: 10.1185/030077902125006079
- Secades JJ, Gareri P. Citicoline: pharmacological and clinical review, 2022 update. *Rev Neurol*. (2022) 75:S1–S89. doi: 10.33588/rn.75s05.2022311
- Bhartiya S. Niacinamide and neuroprotection: the glaucoma holy grail. *J Curr Glaucoma Pract*. (2022) 16:141–3. doi: 10.5005/jp-journals-10078-1390
- Chen TW, Wu PY, Wen YT, Desai TD, Huang CT, Liu PK, et al. Vitamin B3 provides neuroprotection via Antioxi-dative stress in a rat model of anterior ischemic optic neuropathy. *Antioxidants (Basel)*. (2022) 11:2422. doi: 10.3390/antiox11122422
- Tribble JR, Otmami A, Sun S, Ellis SA, Cimaglia G, Vohra R, et al. Nicotinamide provides neuroprotection in glaucoma by protecting against mitochondrial and metabolic dysfunction. *Redox Biol*. (2021) 43:101988. doi: 10.1016/j.redox.2021.101988

Conflict of interest

DR was an employee of Fidia Farmaceutici S.p.A.

The remaining authors declare that the research was conducted in the absence of any commercial or financial relationships that could be construed as a potential conflict of interest.

This study received funding from Fidia Farmaceutici S.p.A. The funder had the following involvement with the study: decision to publish the results.

Publisher's note

All claims expressed in this article are solely those of the authors and do not necessarily represent those of their affiliated organizations, or those of the publisher, the editors and the reviewers. Any product that may be evaluated in this article, or claim that may be made by its manufacturer, is not guaranteed or endorsed by the publisher.

- Kouassi Nzoughe J, Chao de la Barca JM, Guehlouz K, Leruez S, Coulbault L, Allouche S, et al. Nicotinamide deficiency in primary open-angle glaucoma. *Invest Ophthalmol Vis Sci*. (2019) 60:2509–14. doi: 10.1167/iov.19-27099
- Taechameekietichai T, Chansangpet S, Peerawaranun P, Lin SC. Association between daily niacin intake and glaucoma: National Health and nutrition examination survey. *Nutrients*. (2021) 13:4263. doi: 10.3390/nu13124263
- Goulart Nacácio E, Silva S, Occhiutto ML, Costa VP. The use of nicotinamide and nicotinamide riboside as an adjunct therapy in the treatment of glaucoma. *Eur J Ophthalmol*. (2023) 14:11206721231161101. doi: 10.1177/11206721231161101
- Oshitari T, Fujimoto N, Adachi-Usami E. Citicoline has a protective effect on damaged retinal ganglion cells in mouse culture retina. *Neuroreport*. (2002) 13:2109–11. doi: 10.1097/00001756-200211150-00023
- Park CH, Kim YS, Noh HS, Cheon EW, Yang YA, Yoo JM, et al. Neuroprotective effect of citicoline against KA-induced neurotoxicity in the rat retina. *Exp Eye Res*. (2005) 81:350–8. doi: 10.1016/j.exer.2005.02.007
- Oddone F, Rossetti L, Parravano M, Sbardella D, Coletta M, Ziccardi L, et al. Citicoline in ophthalmological neurodegenerative disease: a comprehensive review. *Pharmaceuticals (Basel)*. (2021) 14:281. doi: 10.3390/ph14030281
- Sahin AK, Kapti HB, Uzun A. Effect of oral citicoline therapy on retinal nerve fiber layer and ganglion cell-inner plexiform layer in patients with primary open angle glaucoma. *Int J Ophthalmol*. (2022) 15:483–8. doi: 10.18240/ijo.2022.03.17
- Grieb P, Jünemann A, Rekas M, Rejdak R. Citicoline: a food beneficial for patients suffering from or threatened with glaucoma. *Front Aging Neurosci*. (2016) 8:73. doi: 10.3389/fnagi.2016.00073
- Jassim AH, Inman DM, Mitchell CH. Crosstalk between dysfunctional mitochondria and inflammation in glaucomatous neurodegeneration. *Front Pharmacol*. (2021) 12:699623. doi: 10.3389/fphar.2021.699623
- Mahmoud AM, Wilkinson FL, Sandhu MA, Lightfoot AP. The interplay of oxidative stress and inflammation: mechanistic insights and therapeutic potential of antioxidants. *Oxidative Med Cell Longev*. (2021) 2021:1–4. doi: 10.1155/2021/9851914
- Huang CP, Lin YW, Huang YC, Tsai FJ. Mitochondrial dysfunction as a novel target for neuroprotective nutraceuticals in ocular diseases. *Nutrients*. (2020) 12:1950. doi: 10.3390/nu12071950
- Scuteri D, Rombolà L, Watanabe C, Sakurada S, Corasaniti MT, Bagetta G, et al. Impact of nutraceuticals on glaucoma: a systematic review. *Prog Brain Res*. (2020) 257:141–54. doi: 10.1016/bs.pbr.2020.07.014
- Cammalleri M, Dal Monte M, Amato R, Bagnoli P, Rusciano D. A dietary combination of forskolin with homotaurine, spearmint and B vitamins protects injured retinal ganglion cells in a rodent model of hypertensive glaucoma. *Nutrients*. (2020) 12:1189. doi: 10.3390/nu12041189
- Dal Monte M, Cammalleri M, Amato R, Pezzino S, Corsaro R, Bagnoli P, et al. A topical formulation of Melato-ninergic compounds exerts strong hypotensive and neuroprotective effects in a rat model of hypertensive glaucoma. *Int J Mol Sci*. (2020) 21:9267. doi: 10.3390/ijms21239267
- Porciatti V. Electrophysiological assessment of retinal ganglion cell function. *Exp Eye Res*. (2015) 141:164–70. doi: 10.1016/j.exer.2015.05.008

32. Chou TH, Romano GL, Amato R, Porciatti V. Nicotinamide-rich diet in DBA/2J mice preserves retinal ganglion cell met-abolic function as assessed by PERG adaptation to flicker. *Nutrients*. (2020) 12:1910. doi: 10.3390/nu12071910
33. Williams PA, Harder JM, Foxworth NE, Cochran KE, Philip VM, Porciatti V, et al. Vitamin B3 modulates mitochondrial vulnerability and prevents glaucoma in aged mice. *Science*. (2017) 355:756–60. doi: 10.1126/science.aal0092
34. Kang Q, Yang C. Oxidative stress and diabetic retinopathy: molecular mechanisms, pathogenetic role and therapeutic implications. *Redox Biol*. (2020) 37:101799. doi: 10.1016/j.redox.2020.101799
35. Liu T, Zhang L, Joo D, Sun SC. NF- κ B signaling in inflammation. *Signal Transduct Target Ther*. (2017) 2:17023. doi: 10.1038/sigtrans.2017.23
36. Morgan MJ, Liu ZG. Crosstalk of reactive oxygen species and NF- κ B signaling. *Cell Res*. (2011) 21:103–15. doi: 10.1038/cr.2010.178
37. Pizzino G, Irrera N, Cucinotta M, Pallio G, Mannino F, Arcoraci V, et al. Oxidative stress: harms and benefits for human health. *Oxidative Med Cell Longev*. (2017) 2017:8416763. doi: 10.1155/2017/8416763
38. Liu H, Liu H, Prokosch V. The relationship between mitochondria and Neurodegeneration in the eye: a review. *Appl Sci*. (2021) 11:7385. doi: 10.3390/app11167385
39. Rodriguez AR, de Sevilla Müller LP, Brecha NC. The RNA binding protein RBPMS is a selective marker of ganglion cells in the mammalian retina. *J Comp Neurol*. (2014) 522:1411–43. doi: 10.1002/cne.23521
40. Blanco R, Martinez-Navarrete G, Pérez-Rico C, Valiente-Soriano FJ, Avilés-Trigueros M, Vicente J, et al. A chronic ocular-hypertensive rat model induced by injection of the sclerosant agent polidocanol in the aqueous humor outflow pathway. *Int J Mol Sci*. (2019) 20:3209. doi: 10.3390/ijms20133209
41. Lazzara F, Amato R, Platania CBM, Conti F, Chou TH, Porciatti V, et al. 1 α ,25-dihydroxyvitamin D3 protects retinal ganglion cells in glaucomatous mice. *J Neuroinflamm*. (2021) 18:206. doi: 10.1186/s12974-021-02263-3
42. Porciatti V, Chou TH. Using noninvasive electrophysiology to determine time windows of neuroprotection in optic neuropathies. *Int J Mol Sci*. (2022) 23:5751. doi: 10.3390/ijms23105751
43. Zhang J, Li L, Huang H, Fang F, Webber HC, Zhuang P, et al. Silicone oil-induced ocular hypertension and glaucomatous neurodegeneration in mouse. *elife*. (2019) 8:e45881. doi: 10.7554/eLife.45881
44. Afzal N, Lederer WJ, Jafri MS, Mannella CA. Effect of crista morphology on mitochondrial ATP output: a computational study. *Curr Res Physiol*. (2021) 4:163–76. doi: 10.1016/j.crphys.2021.03.005
45. Hazim RA, Paniagua AE, Tang L, Yang K, Kim KKO, Stiles L, et al. Vitamin B3, nicotinamide, enhances mitochondrial metabolism to promote differentiation of the retinal pigment epithelium. *J Biol Chem*. (2022) 298:102286. doi: 10.1016/j.jbc.2022.102286
46. Faiq MA, Wollstein G, Schuman JS, Chan KC. Cholinergic nervous system and glaucoma: from basic science to clinical applications. *Prog Retin Eye Res*. (2019) 72:100767. doi: 10.1016/j.preteyeres.2019.06.003
47. Mastropasqua L, Agnifili L, Ferrante C, Sacchi M, Figus M, Rossi GCM, et al. Citicoline/coenzyme Q10/vitamin B3 fixed combination exerts synergistic protective effects on neuronal cells exposed to oxidative stress. *Nutrients*. (2022) 14:2963. doi: 10.3390/nu14142963
48. Maneu V, Lax P, De Diego AMG, Cuenca N, García AG. Combined drug triads for synergic neuroprotection in retinal degeneration. *Biomed Pharmacother*. (2022) 149:112911. doi: 10.1016/j.biopha.2022.112911
49. Iwamoto K, Birkholz P, Schipper A, Mata D, Linn DM, Linn CL. A nicotinic acetylcholine receptor agonist prevents loss of retinal ganglion cells in a glaucoma model. *Invest Ophthalmol Vis Sci*. (2014) 55:1078–87. doi: 10.1167/iops.13-12688
50. Rautiainen S, Manson JE, Lichtenstein AH, Sesso HD. Dietary supplements and disease prevention – a global overview. *Nat Rev Endocrinol*. (2016) 12:407–20. doi: 10.1038/nrendo.2016.54
51. Santana-Gálvez J, Cisneros-Zevallos L, Jacobo-Velázquez DA. A practical guide for designing effective nutraceutical combinations in the form of foods, beverages, and dietary supplements against chronic degenerative diseases. *Trends Food Sci Technol*. (2019) 88:179–93. doi: 10.1016/j.tifs.2019.03.026
52. Andersen M, Overgaard K, Meden P, Boysen G, Choi SC. Effects of citicoline combined with thrombolytic therapy in a rat embolic stroke model. *Stroke*. (1999) 30:1464–71. doi: 10.1161/01.STR.30.7.1464
53. López-Coviella I, Agut J, Savci V, Ortiz JA, Wurtman RJ. Evidence that 5'-cytidinediphosphocholine can affect brain phospholipid composition by increasing choline and cytidine plasma levels. *J Neurochem*. (1995) 65:889–94. doi: 10.1046/j.1471-4159.1995.65020889.x
54. Köppen A, Klein J, Holler T, Löffelholz K. Synergistic effect of nicotinamide and choline administration on extracellular choline levels in the brain. *J Pharmacol Exp Ther*. (1993) 266:720–5.
55. Boulanger Y, Labelle M, Khiat A. Role of phospholipase a(2) on the variations of the choline signal intensity observed by 1H magnetic resonance spectroscopy in brain diseases. *Brain Res Brain Res Rev*. (2000) 33:380–9. doi: 10.1016/S0165-0173(00)00037-0
56. Synoradzki K, Grieb P. Citicoline: a superior form of choline? *Nutrients*. (2019) 11:1569. doi: 10.3390/nu11071569
57. Amato R, Cammalleri M, Melecchi A, Bagnoli P, Porciatti V. Natural history of glaucoma progression in the DBA/2J model: early contribution of Müller cell gliosis. *Cells*. (2023) 12:1272. doi: 10.3390/cells12091272



OPEN ACCESS

EDITED BY

Giovanna Valenti,
University of Bari Aldo Moro, Italy

REVIEWED BY

Valerio Magnaghi,
University of Milan, Italy

*CORRESPONDENCE

Michele Maffia
✉ michele.maffia@unisalento.it

[†]These authors have contributed equally to this work and share first authorship

RECEIVED 22 June 2023

ACCEPTED 16 October 2023

PUBLISHED 03 November 2023

CITATION

Greco M, Munir A, Musarò D, Coppola C and Maffia M (2023) Restoring autophagic function: a case for type 2 diabetes mellitus drug repurposing in Parkinson's disease. *Front. Neurosci.* 17:1244022. doi: 10.3389/fnins.2023.1244022

COPYRIGHT

© 2023 Greco, Munir, Musarò, Coppola and Maffia. This is an open-access article distributed under the terms of the [Creative Commons Attribution License \(CC BY\)](#). The use, distribution or reproduction in other forums is permitted, provided the original author(s) and the copyright owner(s) are credited and that the original publication in this journal is cited, in accordance with accepted academic practice. No use, distribution or reproduction is permitted which does not comply with these terms.

Restoring autophagic function: a case for type 2 diabetes mellitus drug repurposing in Parkinson's disease

Marco Greco^{1†}, Anas Munir^{1,2†}, Debora Musarò¹, Chiara Coppola^{1,2} and Michele Maffia^{1*}

¹Department of Biological and Environmental Science and Technology, University of Salento, Lecce, Italy, ²Department of Mathematics and Physics "E. De Giorgi", University of Salento, Lecce, Italy

Parkinson's disease (PD) is a predominantly idiopathic pathological condition characterized by protein aggregation phenomena, whose main component is alpha-synuclein. Although the main risk factor is ageing, numerous evidence points to the role of type 2 diabetes mellitus (T2DM) as an etiological factor. Systemic alterations classically associated with T2DM like insulin resistance and hyperglycemia modify biological processes such as autophagy and mitochondrial homeostasis. High glucose levels also compromise protein stability through the formation of advanced glycation end products, promoting protein aggregation processes. The ability of antidiabetic drugs to act on pathways impaired in both T2DM and PD suggests that they may represent a useful tool to counteract the neurodegeneration process. Several clinical studies now in advanced stages are looking for confirmation in this regard.

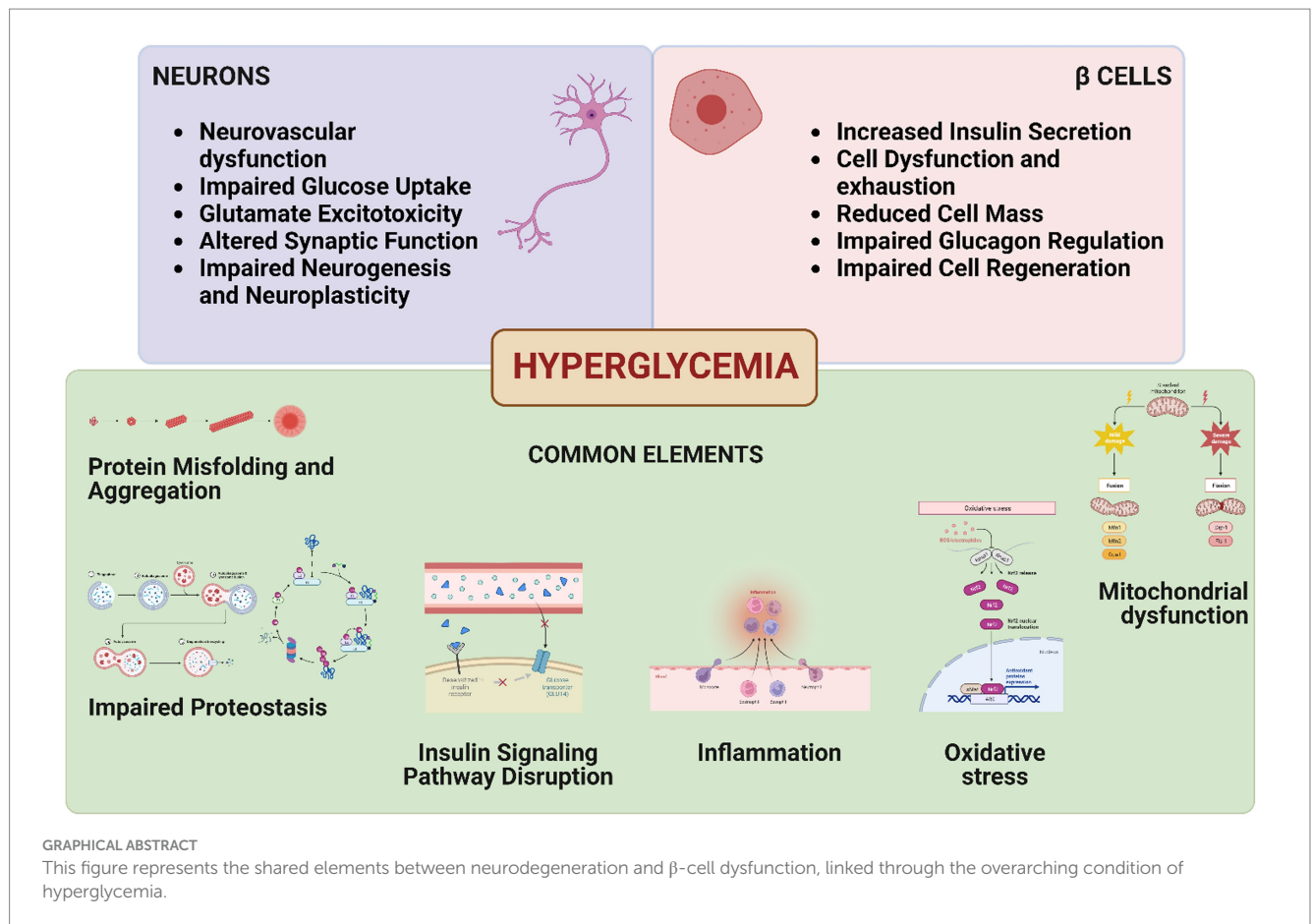
KEYWORDS

type 2 diabetes mellitus, Parkinson's disease, alpha-synuclein, islet amyloid peptide protein, insulin-resistance, autophagy, hyperglycemia

1. Introduction

Parkinson's disease (PD) is an irreversible and progressive neurological condition that affects 8.5 million people worldwide ([World Health Organization, 2022](#)), with an incidence expected to double by 2040 ([Dorsey and Bloem, 2018](#)). PD classically involves midbrain structures, causing the depletion of the residing dopaminergic neuronal population and a predominantly motor symptomatology. The disease belongs to the class of proteinopathies and, apart from 5% of genetically linked cases, it is considered idiopathic ([Reed et al., 2019](#)).

Proteinopathies are chronic conditions characterized by an imbalance between protein synthesis and degradation ([Bayer, 2015](#)). This imbalance, which is caused by ageing, mitochondrial dysfunction, oxidative stress, inflammation and alterations in post-translational processes (PTMs), is responsible for protein aggregation and Lewy bodies formation at the neuronal level in PD. Type 2 diabetes mellitus (T2DM) is another proteinopathy with an alarming prevalence rate of 536 million worldwide, characterized by peripheral insulin resistance, high blood glucose levels and increased insulin secretion, which in time lead to a diminishment of β -cell functionality and number ([Sun et al., 2022](#)). Furthermore, these disease symptoms when sustained cause mitochondrial dysfunction, inflammation, and protein misfolding.



An association between type 2 diabetes mellitus (T2DM) and PD has long been advocated (Sandyk, 1993), and subsequently strengthened by a better understanding of the underlying pathologically involved pathways. Numerous population-based studies have failed to unequivocally confirm the hypothesis of a causal relationship, with often contradictory conclusions requiring further investigation (Driver et al., 2008; Cereda et al., 2011, 2012; Schernhammer et al., 2011; Savica et al., 2012; Lu et al., 2014; Pagano et al., 2018). However, because of the brain requirement of insulin and the similar signaling mechanisms in the two body districts, impaired insulin release or uptake can contribute to both T2DM and PD pathogenesis. Both the conditions share pathophysiological elements like chronic inflammation, lysosomal and mitochondrial dysfunction, whose molecular bases are associated with a loss in glucose metabolism (Burbulla et al., 2017; Ma et al., 2017). Moreover, insulin signaling has been shown to be involved in several mechanisms regulating apoptosis and oxidative stress prevention, with a profound role as neuroprotective agent (Duarte et al., 2008; Serhan et al., 2020; Gayen et al., 2022).

Furthermore, the dysfunction of glucose metabolism, typical of T2DM has been demonstrated as an early marker of PD (Dunn et al., 2014). Another important process that is impacted in both diseases is the cellular recycling and degradation mechanism of autophagy, which is interestingly both disturbed and contributes to the overwhelming aggregation of proteinaceous Lewy bodies and amyloid plaques in PD and T2DM, respectively (Hou et al., 2020). Moreover, mutations in autophagy-related genes (ARGs) also inherently impair the autophagic flux in both the diseases (Simón-Sánchez et al., 2009; Cui and Li, 2023). In view of this, a limited

number of studies have demonstrated that the activation of pathways like the mammalian target of rapamycin (mTOR) can restore autophagy, alleviating symptoms in *in vitro* and *in vivo* models of the two diseases (Pupyshev et al., 2021; Cui and Li, 2023). Targeting autophagy, therefore, presents a lucrative drug target common to both disorders.

2. Protein aggregation as a two-way connection

It has long been known, thanks to the pioneering observations of Polymeropoulos and co-workers first, Spillantini and colleagues later, that Lewy bodies in PD, initially localized in the *substantia nigra pars compacta*, are predominantly composed of alpha-synuclein (aS) protein (Polymeropoulos et al., 1997; Spillantini et al., 1997). It was subsequently discovered by Fujiwara et al. (2002) that aggregates were mainly composed of the phospho-Ser129 form of the protein (Fujiwara et al., 2002). The loss of function of the protein because of its aggregation has several consequences in dopaminergic neurons, it being involved in the modulation of neurotransmitter synthesis and, once incorporated into vesicles, also in their transport and release (Abeliovich et al., 2000; Cabin et al., 2002). Interactors of aS include tyrosine 3-monooxygenase (TH), the rate-limiting dopamine biosynthetic enzyme (Perez et al., 2002), dopamine decarboxylase (Tehrani et al., 2006), protein phosphatase 2A (PP2A) (Qu et al., 2018), vesicle membranes (Jao et al., 2004) and SNARE proteins (Burré et al., 2014). An important but still poorly understood

interactor of aS is the Kir6.2 (internal rectifier potassium channel 6.2) subunit of the ATP-sensitive potassium (KATP) channel and its associated sulfonylurea receptor 1 (SUR1). This interaction modulates dopamine release by reducing it (Vidal-Martinez et al., 2018; Choudhury et al., 2022).

A similar function for the protein was observed by Geng and colleagues in pancreatic β -cell, where it has been shown to act as a regulator of the release of insulin-containing vesicles, in response to glucose concentration (Geng et al., 2007). Aggregation is observed in these cells during T2DM; the major component of which is islet amyloid polypeptide (IAPP) (Cooper et al., 1987), although immunoreactivity for phospho-Ser129-aS has also been observed (Martinez-Valbuena et al., 2018).

The fibrillation process of aS passes through the formation of oligomeric structures which are neurotoxic formations able to pierce membranes and spread. At this point, the protein can be internalised by other cells or flow through the cerebrospinal fluid (CSF) to the bloodstream (Menéndez-González et al., 2018; Karpowicz et al., 2019). A role for aS active internalization process seems to be played by surface prion protein (PrP), expressed both at the nervous and pancreatic levels, where it modulates insulin and glucose homeostasis through metal interaction (Ashok and Singh, 2018; Jucker and Walker, 2018; De Riccardis et al., 2019). Recently, Martinez-Valbuena et al. (2021) have found the presence of cytoplasmic aggregates containing IAPP and phospho-Ser129-aS interacting with PrP in human *post-mortem* pancreatic tissues (Martinez-Valbuena et al., 2021). This offers a new perspective towards a two-way connection between the pathogenesis of T2DM and PD.

3. Insulin resistance and the impairment of autophagic processes

A persistent condition associated with T2DM is insulin resistance, which determines a loss of glycemic control mechanisms in peripheral organs. The brain, however, is capable of managing its own glucose requirements independently of insulin, although new evidence is casting doubt on this assumption (García-Cáceres et al., 2016; Kleinridders, 2016; Pomytkin et al., 2018). Therefore, in the brain, insulin resistance results mainly in an altered signaling pathway.

Encephalic insulin receptors are predominantly expressed in neurons, where they play a role in modulating dendritic and synaptic plasticity, being most highly expressed at these levels (Sportelli et al., 2020). The hormone is associated with a plethora of activities in the brain, such as learning, memory, cognitive functions (Craft et al., 1993), neurotransmitter release (de Bartolomeis et al., 2023), neuroprotection, neuronal proliferation, migration, and differentiation (Roger and Fellows, 1980; Schubert et al., 2003; Xu et al., 2004; Sousa-Nunes et al., 2011). These activities are all modulated by the binding of insulin to its receptors and the activation of their downstream pathways, for instance, Raf-1/MAPK/ERK or PI3K/protein kinase B (AKT) (Arnold et al., 2018). These effectors then modulate mTOR activity, promote protein synthesis activating ribosomal protein S6 kinase (S6K) (Huang et al., 2019), inhibiting the eukaryotic translation initiation factor 4E-binding protein 1 (4E-BP1) (Le Bacquer et al., 2007), while activating transcription factors like forkhead box protein O1 (FoxO1) (Tsai et al., 2003), sterol regulatory element-binding protein (SREBP) and carbohydrate-responsive element-binding protein (ChREBP) (Iizuka et al., 2004; Suzuki et al., 2010).

The mTOR protein, a central element of the mTORC1 and mTORC2 complexes, modulated by the PI3K/AKT pathway, regulates the autophagic process. Alterations in this mechanism are associated with protein aggregation and reduction in ATP/ADP and NAD⁺/NADH ratios (Heras-Sandoval et al., 2014; Steinberg and Carling, 2019; Katsyuba et al., 2020). A 2010 study found high amounts of autophagosomes with permeabilized lysosomes, indicating a shunted lysosomal-mediated autophagosome clearance contributing to disease onset in *post-mortem* PD brain (Dehay et al., 2010). This, in addition to the high levels of autophagic markers that colocalize with aS in Lewy bodies, such as microtubule-associated proteins 1A/1B light chain 3B (LC3) in its lipidated form LC3-II and ubiquitin-binding protein p62 (sequestosome-1), provides important evidence for a failure of the autophagic process during the disease (Alvarez-Erviti et al., 2010; Fellner et al., 2021).

4. Hyperglycemia compromises cellular proteostasis

An impaired protein degradation, although sufficient to alter cellular proteostasis, is not the only event observed during T2DM. Increased level of circulating glucose also has detrimental effects on cellular homeostasis and protein function. An engulfment of the glycolytic pathway diverts glucose towards the polyol pathway (Du et al., 2003). Then, the sustained activity of aldose reductase and sorbitol dehydrogenase causes the depletion of NADPH and NAD⁺, which impairs the capability of the cell to restore reduced glutathione (GSH) levels and causes inhibition of GAPDH (Mathebula, 2015; Lutchmansingh et al., 2018). The accumulation of triose phosphates results in methylglyoxal (MG) formation, an α -keto reactive aldehyde, and then to advanced glycation end products (AGEs) (Strom et al., 2021). Hyperglycemia also impairs the hexosamine pathway, increasing UDP-N-acetylglucosamine levels and altering PTMs (Du et al., 2000; Del Coco et al., 2023). As the MG detoxification is mainly mediated by the highly conserved glutathione-dependent glyoxalase I/II (GloI/II) system, a reduction in intracellular levels of GSH is toxic for the cells (Blair et al., 1979; Yadav et al., 2005). Altered glycosylation and glycation processes involve both aS and IAPP, promoting their aggregation and impairing their degradation (Vicente Miranda et al., 2017; Milordini et al., 2020).

5. Mitochondrial dysfunction as a fatal consequence

Insulin resistance and hyperglycemia cause mitochondria dysfunction, with ROS increase and loss in Ca²⁺ homeostasis further contributing to AGEs formation (Soejima et al., 1996). Mitochondria are responsible for cellular energy metabolism, regulating also proliferation (Diers et al., 2012), apoptosis (Wang and Youle, 2009), protein degradation (Liao et al., 2020), neurotransmitter transport, uptake and recycle (Varoqui and Erickson, 1996; Gasnier, 2000; Vos, 2010). Their dysfunction is strongly related to inflammation, which in the brain is supported by microglia through the release of pro-inflammatory cytokines.

Hyperglycemia causes alterations in the organelle morphology, triggering fission processes (Wang et al., 2012). Mitophagy, a selective form of autophagy, is responsible for the removal of damaged mitochondria; during this process, organelles are labelled for

degradation by PTEN-induced putative kinase 1 (PINK1), E3 ubiquitin-protein ligase Parkin, Ubiquitin and Sequestosome-1 (Lewis and Lewis, 1915; Palikaras et al., 2018). An important role in mitochondria homeostasis is held by DJ-1 protein; it acts as a transcription factor and an antioxidant and modulates chaperones, proteases, and mitochondria activity. DJ-1 functions are modulated by its oxidative state in the cell (Canet-Avilés et al., 2004; Hao et al., 2010; Wilson, 2011; Takahashi-Niki et al., 2017).

Finally, DJ-1 has a key role in repairing MG-related damages, with a recent study demonstrating glyoxalase and weak deglyoxalase activity for the protein (Mazza et al., 2022). Mutations in PINK1, Parkin and DJ-1 are correlated with the onset of monogenic forms of PD (Guadagnolo et al., 2021). This emphasizes how mitophagy and organelle homeostasis are crucial for cell well-being, and how glycemic dyshomeostasis can induce PD.

6. Autophagy and hyperglycemia as new drug targets

The pharmacological approach to PD is merely symptomatic, therefore the identification of a trigger capable of inducing the pathology, and its medication, stand to represent a new complementary route of intervention. Hyperglycemia, hyperinsulinemia, hypercholesterolemia, inflammation, mitochondrial dyshomeostasis, oxidative stress, alteration of protein-degrading pathways, and aggregation are all potential targets to be exploited.

Several widely used antidiabetic and hypoglycemic drugs are currently undergoing pharmaceutical trials in various studies on cohorts of PD patients with a perspective of drug repurposing (Table 1).

In line with this premise, this review focuses on the compilation of a list of main drugs initially developed for treating hyperglycemia in the context of diabetes, but the activation of whose principal molecular pathways is potentially beneficial in the context of PD. The knowledge of these drugs from a pharmacokinetic and toxicological point of view has great advantages, allowing for drastically shortened trial times.

6.1. Metformin

Metformin is considered the first-line treatment for T2DM since the early 2000s, according to the guidelines of the International Diabetes Foundation (IDF Clinical Guidelines Task Force, 2006), but it is currently also considered a prime candidate for PD therapy. It inhibits hepatic gluconeogenesis, increases peripheral insulin sensitivity and glucagon-like peptide 1 (GLP-1) secretion, promoting peripheral glucose uptake, and reducing its bowel absorption at the same time. The mechanism of action is thought to be mainly through the inhibition of complex I of the mitochondrial transport chain, lowering ATP levels and indirectly activating the cellular metabolic state sensor AMPK (Zhou et al., 2016; Bahne et al., 2018; Baker et al., 2021; Drzewoski and Hanefeld, 2021). This increases fatty acid oxidation, reduces ROS production, and inhibits mTORC1 activating autophagic pathways and lysosomal biogenesis (Amin et al., 2019; Ma et al., 2023). Metformin also activates several downstream interactors including Bcl-1, CREB and PGC1, that promote cell viability and rescue mitochondrial defects,

increasing their mass and improving their function (Kang et al., 2017; de Maraño et al., 2022). Finally, by modulation of Nrf2, FoxO3 and NF- κ B activity, it exerts a protective effect in astrocytes and microglia (Ryu et al., 2018, 2020; Zhou et al., 2021).

In recent years, metformin has shown neuroprotective effects in both *in vitro* and *in vivo* models of PD, in the latter case by decreasing the loss of dopaminergic neurons and reducing motor symptoms, countering phospho-Ser129- α S aggregation in several ways. Pérez-Revuelta and colleagues have observed that metformin promotes the activity of PP2A, an enzyme of primary importance in reducing intracellular levels of phospho-Ser129- α S (Pérez-Revuelta et al., 2014; Greco et al., 2021); PP2A activity has indeed been shown to inhibit mTOR, promoting autophagy. Experiments in *C. elegans* and murine models of PD have both confirmed the effect of metformin in lowering phospho-Ser129- α S levels through an evolutionarily conserved mechanism (Pérez-Revuelta et al., 2014; Katila et al., 2017; Saewanee et al., 2021). Finally, metformin shows anti-glycating properties, acting as a scavenger of the aldehydic part of MG, preventing the accumulation of AGEs in subjects with T2DM (Kinsky et al., 2016).

6.2. GLP-1 agonists

Secreted by intestinal cells in response to food intake, especially carbohydrates, GLP-1 acts on several organs regulating glucose homeostasis. It stimulates insulin secretion from pancreatic β -cells in a glucose-dependent manner, reduces the secretion of glucagon, slows down gastric emptying, reduces the perception of hunger and thirst, and enhances peripheral glucose uptake (Hira et al., 2021).

Studies have shown that GLP-1 can inhibit mTOR stimulating autophagy in pancreatic β -cells and neurons. The binding of GLP-1 with its ubiquitously expressed membrane receptor GLP-1R triggers activation of the PI3K/AKT pathway. Subsequently, several downstream actors such as GSK3- β , FoxO1, NF- κ B and Nrf2 exert cytoprotective effects (Buteau et al., 2006; Dai et al., 2013; Park et al., 2018; Costantino and Paneni, 2019; Li et al., 2020).

Interestingly, GLP-1R presence has been observed in the dopaminergic neuron of the encephalic area postrema, known for its role in modulating autonomic and reward responses, but also addiction mechanisms. GLP-1 seems therefore to be involved, at least in this specific region of the nervous system, in the modulation of dopamine synthesis and release (Yamamoto et al., 2003; Jensen et al., 2020).

Among the most important GLP-1R artificial agonists are exenatide, liraglutide, lixisenatide, semaglutide and NLY01. This class of molecules, found to be neuroprotective in mouse models treated with 6-OHDA or MPTP, is now a subject of interest for human use (Aviles-Olmos et al., 2013; Aslan et al., 2014; Jalewa et al., 2017). Promising results have been observed, with early-PD patients responding better to the treatment and showing motor and cognitive improvements (Athauda et al., 2019).

6.3. Glitazones

Glitazones, which includes pioglitazone, lobeglitazone and rosiglitazone are a class of oral antidiabetic drugs used in patients where first-line therapies fail to achieve glycemic control. Exerting their effect as agonists of the peroxisome proliferator-activated

TABLE 1 Clinical trials on anti-diabetic drugs in PD.

Drug	Molecule class	Anti-diabetic mechanisms of action	Clinical studies	ClinicalTrials.gov identifier	Status	Sponsor/ collaborators
Metformin	Biguanides	Inhibition of hepatic gluconeogenesis (Madiraju et al., 2018; Agius et al., 2020) Restoration of peripheral insulin sensitivity and glucose uptake (Li et al., 2011; Rueggsegger et al., 2019b) Reduction of intestinal absorption of glucose (Horakova et al., 2019; Sansome et al., 2020) Modulation of GLP-1 release (Amadi et al., 2021; Lee C. B. et al., 2021) Modulation of lipid metabolism by reducing LDL cholesterol and triglycerides levels (Han et al., 2019; Hu et al., 2021; Tarry-Adkins et al., 2021; Xing et al., 2022) Anti-inflammatory and antioxidant effect (Tian et al., 2019; Luo et al., 2020)	Clinical study to evaluate the possible efficacy of metformin in patients with Parkinson's disease	NCT05781711	Phase 2 – Recruiting	Tanta University, Tanta, Egypt
Exenatide	GLP-1 agonists	Stimulation of GLP-1 receptors (Helmstädter et al., 2020; Sterling et al., 2020; Angarita et al., 2021; Cardoso et al., 2023) Promotion of insulin secretion (Yaribeygi et al., 2019) Pro-survival effect on β -cells (Tanday et al., 2022; Zhou et al., 2022) Inhibition of glucagon release (Bai et al., 2022) Slowing of gastric emptying (Geyer et al., 2019; Shang et al., 2021; Jensterle et al., 2023) Loss of appetite (Yamamoto et al., 2003; Jensen et al., 2020; Kadouh et al., 2020) Reduction of weight (Kadouh et al., 2020; Lee S. E. et al., 2021; Arastu et al., 2022; Borlaug et al., 2023) Anti-inflammatory and antioxidant effect (Sterling et al., 2020; Martins et al., 2022; Meurot et al., 2022; Luna-Marco et al., 2023)	Exenatide once weekly over 2 years as a potential disease modifying treatment for Parkinson's disease	NCT04232969	Phase 3 – Active, not recruiting	University College, London, United Kingdom
			Trial of exenatide for Parkinson's disease	NCT01971242	Phase 2 – Completed	University College, London, United Kingdom
			Exenatide treatment in Parkinson's disease	NCT04305002	Phase 2 – Active, not recruiting	Center for Neurology, Stockholm, Sweden Karolinska Institutet, Solna, Sweden
			Effects of exenatide on motor function and the brain	NCT03456687	Phase 1 – Completed	University of Florida, Gainesville, FL, United States National Institute of Neurological Disorders and Stroke (NINDS), Bethesda, MD, United States
Liraglutide	GLP-1 agonists		Safety and efficacy of liraglutide in Parkinson's disease	NCT02953665	Phase 2 – Completed	Cedars Sinai Medical Center, Los Angeles, CA, United States The Cure Parkinson's Trust, London, United Kingdom Novo Nordisk A/S, Bagsværd, Denmark
Semaglutide			GLP1R in Parkinson's disease	NCT03659682	Phase 2 – Not yet recruiting	Oslo University Hospital, Oslo, Norway
NLY01			A clinical study of NLY01 in patient's with early Parkinson's disease	NCT04154072	Phase 2 – Active, not recruiting	Neuraly, Inc., Gaithersburg, MD, United States

(Continued)

TABLE 1 (Continued)

Drug	Molecule class	Anti-diabetic mechanisms of action	Clinical studies	ClinicalTrials.gov identifier	Status	Sponsor/ collaborators
Pioglitazone	Thiazolidinediones	PPAR γ agonist effect (Soliman et al., 2019; Nazreen, 2021) Inhibition of hepatic gluconeogenesis (Rahimi et al., 2020; Asakawa et al., 2023) Promotion of fat cells maturation (Yu et al., 2023) Promotion of fat deposition into peripheral tissues (Lee et al., 2023; Liu et al., 2023) Promotion of HDL cholesterol levels increase and triglycerides levels decrease (Alam et al., 2019; Lian and Fu, 2021) Restoration of insulin sensitivity (Al-Muzafar et al., 2021; Fiorentino et al., 2021) Anti-inflammatory effect (Radwan and Hasan, 2019; Pakravan et al., 2022)	Pioglitazone in Early Parkinson's Disease	NCT01280123	Phase 2 – Completed	University of Rochester, Rochester, NY, United States National Institute of Neurological Disorders and Stroke (NINDS), Bethesda, MD, United States Michael J. Fox Foundation for Parkinson's Research, New York, NY, United States
Insulin	Hormone	Reduction in hematic glucose levels (Rahman et al., 2021) Increase in peripheral glucose uptake via GLUTs transporters translocation toward plasma membrane (Turner et al., 2020) Suppression of hepatic gluconeogenesis and promotion of glycogen synthesis (Rahman et al., 2021) Promotion of protein synthesis (Khalid et al., 2021) Inhibition of lipolysis and promotion of fatty acid synthesis and storage (Ahmed et al., 2021; Grabner et al., 2021) Ketone bodies formation inhibition (Garcia et al., 2020) Inhibition of catabolic processes (Batista et al., 2021)	Intranasal Insulin in Parkinson's Disease	NCT04251585	Phase 2 – Recruiting	HealthPartners Neuroscience Center, Saint Paul, MN, United States
			Intranasal Insulin and Glutathione as an Add-On Therapy in Parkinson's Disease	NCT05266417	Phase 2 – Recruiting	Gateway Institute for Brain Research, Fort Lauderdale, FL, United States
			Treatment of Parkinson Disease and Multiple System Atrophy Using Intranasal Insulin	NCT02064166	Phase 2 – Completed	Peter Novak, Boston, MA, United States University of Massachusetts, Worcester, MA, United States

Studies that have passed the completion date and whose status has not been verified for more than 2 years are not reported. Information extracted from clinicaltrials.gov, access date 07-10-2023.

receptor PPAR γ , a transcription factor of the nuclear ligand-activated receptor family, they increase tissues' insulin sensitivity (Nanjan et al., 2018).

PPAR γ induces the expression of a plethora of genes related to carbohydrate and lipid metabolism; at an encephalic level, expressed mainly in regions controlling reward and movement mechanisms such as the basal ganglia it has neuroprotective, with antioxidant, anti-inflammatory and anti-apoptotic properties (Warden et al., 2016; Villapol, 2018; Sonne et al., 2023). These effects, also linked to the downstream NF- κ B signaling pathway activation, appear to be able to attenuate cognitive decline in various neurological diseases and neurodegenerative conditions (Delerive et al., 1999; Behl et al., 2021).

In several *in vivo* studies in PD-induced mice models, PPAR γ agonists have shown a protective effect on dopaminergic neurons,

with an improvement in motor symptoms. This is probably due to an inhibition of MAO-B, COX-1, COX-2 and iNOS activity, which reduce inflammation and preserve mitochondrial function and morphology (Xing et al., 2007; Quinn et al., 2008; Barbiero et al., 2014).

6.4. Insulin

The neuromodulatory, neurotrophic, and neuroprotective properties of insulin on the encephalon are well-known, therefore, its use in neurodegenerative contexts presents several potential beneficial effects (Yang et al., 1981; Shah and Hausman, 1993; Shuaib et al., 1995). However, two problems have hindered this approach until recently: the poor permeability of the blood–brain barrier (BBB) to its passage (Margolis and Altszuler, 1967) and the effect on hematic

glycemia when parenterally administered. Therefore, new formulations have been studied to circumvent this problem; the most promising is via inhalation which exploits the permeability of the cribriform plate, shortening drug delivery to the target site and allowing precise modulation of administration. Several *in vivo* studies on murine PD models have demonstrated the efficacy of the molecule in this form and its neuroprotective activity (Fine et al., 2020; Iravanpour et al., 2021). Rajasekar and colleagues have shown how the use of intranasal insulin in mice treated with streptozocin was able to improve insulin-signaling cascade and attenuate neuroinflammation, neuronal loss, and protein aggregation. This was explained to be due to the modulation of NF- κ B and PI3K/Akt pathway (Rajasekar et al., 2017).

Indeed, when intranasal insulin is administered, a canonical activation of PI3K/AKT and MAPK pathways is observed. From a neuroprotective perspective, there is an increased hypoxia-inducible factor-1 (HIF-1) activity, resulting in angiogenesis and endothelial proliferation (Zelzer, 1998). Furthermore, altered insulin signalling is associated with reduced mitochondrial fusion processes at the expense of organelle fission, resulting in increased ROS and reduced ATP levels (Kelley et al., 2002; Bach et al., 2003; Jheng et al., 2012).

Ruegsegger and colleagues demonstrated the ability of intranasal insulin to counteract these processes through the observation of an increase in the MFN1, MFN2, and OPA1 proteins, and a decrease in the DRP1 protein, involved in mitochondrial fusion and fission, respectively, (Ruegsegger et al., 2019a). Moreover, insulin also regulates mitochondrial quality control mechanisms by restoring the compromised activity of PINK1 and DJ-1. This appears particularly beneficial in brain areas of high mitochondrial activity such as the hypothalamus, and hippocampus (Onphachanh et al., 2017; Ruegsegger et al., 2019a; Su et al., 2020). Finally, insulin contributes to the removal of aggregates by promoting PP2A activity, which inhibits mTOR1 and dephosphorylates ULK1, initiating the autophagic process (Axe et al., 2008).

A 2018 clinical interventional study conducted at the University of Massachusetts on 15 patients for 4 weeks, involving intranasal administration of insulin, showed encouraging results. In this study, an improvement in motor performance, visuospatial memory, and verbal fluency was observed in PD subjects compared to placebo, due to a better ability to draw on mnemonic data (Novak et al., 2019).

7. Conclusion

To date, multiple pieces of evidence link T2DM to the onset of PD and other proteinopathies. The absence of cures for such medical conditions and the expected increase in their incidence in the coming years is driving clinical research. Hyperglycemia and insulin resistance, with the resulting protein aggregation, oxidative stress, and mitochondria dysfunction represent important and promising common medical targets, justifying interest in antidiabetic drugs, albeit the apparently different clinical settings. A large body of evidence on the efficacy of such drugs on pathways known to

be involved in proteostasis and disrupted in PD exists. The data gathered in *in vivo* and *in vitro* models, together with the results of clinical trials leads to the view that the use of antidiabetic drugs, in combination with the current symptomatic medications is extremely encouraging.

Author contributions

MG and AM conceptualized and drafted the original article, then revised it once in its final form. DM wrote a section of the manuscript and prepared the graphical abstract. CC performed data curation. MM funded the publication process, contributed to conception and revised its final form. All authors contributed to the article and approved the submitted version.

Funding

This research was funded by: (i) Italian Ministry of University and Research thanks to the PRIN 2017 project (MIUR) prot. 2017J92TM5 “enhancement of autophagy for the therapy of liver diseases” and to the innovative PhD position made available to AM; (ii) Apulia Region thanks to the post-doc position of the POC PUGLIA FESR ESF 2014/2020 entitled “PaRTiRe - Parkinson’s research through the voice” “Riparti project” made available to MG; (iii) Concorde Project, with grant PNRA18_0 0071_Prot. 20891.21-11-2019, assigned to Michele Samaja, Department of Health Sciences, University of Milan, Milan, Italy. We must also thank the “Alessia Pallara” Foundation for its constant economic support to our Physiology Lab at University of Salento.

Acknowledgments

The authors would like to thank Antonio Danieli for his constant support.

Conflict of interest

The authors declare that the research was conducted in the absence of any commercial or financial relationships that could be construed as a potential conflict of interest.

Publisher’s note

All claims expressed in this article are solely those of the authors and do not necessarily represent those of their affiliated organizations, or those of the publisher, the editors and the reviewers. Any product that may be evaluated in this article, or claim that may be made by its manufacturer, is not guaranteed or endorsed by the publisher.

References

- Abeliovich, A., Schmitz, Y., Fariñas, I., Choi-Lundberg, D., Ho, W.-H., Castillo, P. E., et al. (2000). Mice lacking α -Synuclein display functional deficits in the nigrostriatal dopamine system. *Neuron* 25, 239–252. doi: 10.1016/S0896-6273(00)80886-7
- Agius, L., Ford, B. E., and Chachra, S. S. (2020). The metformin mechanism on gluconeogenesis and AMPK activation: the metabolite perspective. *Int. J. Mol. Sci.* 21:3240. doi: 10.3390/ijms21093240

- Ahmed, B., Sultana, R., and Greene, M. W. (2021). Adipose tissue and insulin resistance in obese. *Biomed. Pharmacother.* 137:111315. doi: 10.1016/j.biopha.2021.111315
- Alam, F., Islam, M. A., Mohamed, M., Ahmad, I., Kamal, M. A., Donnelly, R., et al. (2019). Efficacy and safety of pioglitazone monotherapy in type 2 diabetes mellitus: a systematic review and Meta-analysis of randomised controlled trials. *Sci. Rep.* 9:5389. doi: 10.1038/s41598-019-41854-2
- Al-Muzafar, H. M., Alshehri, F. S., and Amin, K. A. (2021). The role of pioglitazone in antioxidant, anti-inflammatory, and insulin sensitivity in a high fat-carbohydrate diet-induced rat model of insulin resistance. *Brazilian J. Med. Biol. Res.* 54:e10782. doi: 10.1590/1414-431x2020e10782
- Alvarez-Erviti, L., Rodriguez-Oroz, M. C., Cooper, J. M., Caballero, C., Ferrer, I., Obeso, J. A., et al. (2010). Chaperone-mediated autophagy markers in Parkinson disease brains. *Arch. Neurol.* 67, 1464–1472. doi: 10.1001/archneurol.2010.198
- Amadi, J. A., Amadi, P. U., Njoku, U. C., and Osuoha, J. O. (2021). Potentiation of incretin hormones and modulation of metabolic enzymes as possible mechanisms behind the insulin sensitizing effects of cabbage-metformin treatment. *Transl. Res.* 230, 44–54. doi: 10.1016/j.trsl.2020.10.008
- Amin, S., Lux, A., and O'Callaghan, F. (2019). The journey of metformin from glycaemic control to mTOR inhibition and the suppression of tumour growth. *Br. J. Clin. Pharmacol.* 85, 37–46. doi: 10.1111/bcp.13780
- Angarita, G. A., Matuskey, D., Pittman, B., Costeines, J. L., Potenza, M. N., Jastreboff, A. M., et al. (2021). Testing the effects of the GLP-1 receptor agonist exenatide on cocaine self-administration and subjective responses in humans with cocaine use disorder. *Drug Alcohol Depend.* 221:108614. doi: 10.1016/j.drugalcdep.2021.108614
- Arastu, N., Cummins, O., Uribe, W., and Neme, E. C. (2022). Efficacy of subcutaneous semaglutide compared to placebo for weight loss in obese, non-diabetic adults: a systematic review & meta-analysis. *Int. J. Clin. Pharm.* 44, 852–859. doi: 10.1007/s11096-022-01428-1
- Arnold, S. E., Arvanitakis, Z., Macauley-Rambach, S. L., Koenig, A. M., Wang, H.-Y., Ahima, R. S., et al. (2018). Brain insulin resistance in type 2 diabetes and Alzheimer disease: concepts and conundrums. *Nat. Rev. Neurol.* 14, 168–181. doi: 10.1038/nrneurol.2017.185
- Asakawa, M., Takagi, N., Hamada, D., Yamasaki, Y., and Katsuta, H. (2023). Efficacy of 3 months of additional pioglitazone treatment in type 2 diabetes patients with alcoholic fatty liver disease. *Diabetol. Int.* 14, 243–251. doi: 10.1007/s13340-023-00619-z
- Ashok, A., and Singh, N. (2018). Prion protein modulates glucose homeostasis by altering intracellular iron. *Sci. Rep.* 8:6556. doi: 10.1038/s41598-018-24786-1
- Aslan, I. R., Ranadive, S. A., Valle, I., Kollipara, S., Noble, J. A., and Vaisse, C. (2014). The melanocortin system and insulin resistance in humans: insights from a patient with complete POMC deficiency and type 1 diabetes mellitus. *Int. J. Obes.* 38, 148–151. doi: 10.1038/ijo.2013.53
- Athauda, D., Maclagan, K., Budnik, N., Zampieri, L., Hibbert, S., Aviles-Olmos, I., et al. (2019). Post hoc analysis of the exenatide-PD trial-factors that predict response. *Eur. J. Neurosci.* 49, 410–421. doi: 10.1111/efn.14096
- Aviles-Olmos, I., Dickson, J., Kefalopoulou, Z., Djamshidian, A., Ell, P., Soderlund, T., et al. (2013). Exenatide and the treatment of patients with Parkinson's disease. *J. Clin. Invest.* 123, 2730–2736. doi: 10.1172/JCI68295
- Axe, E. L., Walker, S. A., Manifava, M., Chandra, P., Roderick, H. L., Habermann, A., et al. (2008). Autophagosome formation from membrane compartments enriched in phosphatidylinositol 3-phosphate and dynamically connected to the endoplasmic reticulum. *J. Cell Biol.* 182, 685–701. doi: 10.1083/jcb.200803137
- Bach, D., Pich, S., Soriano, F. X., Vega, N., Baumgartner, B., Oriola, J., et al. (2003). Mitofusin-2 determines mitochondrial network architecture and mitochondrial metabolism. *J. Biol. Chem.* 278, 17190–17197. doi: 10.1074/jbc.M212754200
- Bahne, E., Sun, E. W. L., Young, R. L., Hansen, M., Sonne, D. P., Hansen, J. S., et al. (2018). Metformin-induced glucagon-like peptide-1 secretion contributes to the actions of metformin in type 2 diabetes. *JCI Insight* 3:e93936. doi: 10.1172/jci.insight.93936
- Bai, C., Wang, Y., Niu, Z., Guan, Y., Huang, J., Nian, X., et al. (2022). Exenatide improves hepatocyte insulin resistance induced by different regional adipose tissue. *Front. Endocrinol.* 13:1012904. doi: 10.3389/fendo.2022.1012904
- Baker, C., Retzik-Stahr, C., Singh, V., Plomondon, R., Anderson, V., and Rasouli, N. (2021). Should metformin remain the first-line therapy for treatment of type 2 diabetes? *Ther. Adv. Endocrinol. Metab.* 12:204201882098022. doi: 10.1177/2042018820980225
- Barbiero, J. K., Santiago, R. M., Persike, D. S., da Silva Fernandes, M. J., Tonin, F. S., da Cunha, C., et al. (2014). Neuroprotective effects of peroxisome proliferator-activated receptor alpha and gamma agonists in model of parkinsonism induced by intranigral 1-methyl-4-phenyl-1,2,3,6-tetrahydropyridine. *Behav. Brain Res.* 274, 390–399. doi: 10.1016/j.bbr.2014.08.014
- Batista, T. M., Haider, N., and Kahn, C. R. (2021). Defining the underlying defect in insulin action in type 2 diabetes. *Diabetologia* 64, 994–1006. doi: 10.1007/s00125-021-05415-5
- Bayer, T. A. (2015). Proteinopathies, a core concept for understanding and ultimately treating degenerative disorders? *Eur. Neuropsychopharmacol.* 25, 713–724. doi: 10.1016/j.euroneuro.2013.03.007
- Behl, T., Madaan, P., Sehgal, A., Singh, S., Sharma, N., Bhatia, S., et al. (2021). Elucidating the neuroprotective role of PPARs in Parkinson's disease: a neoteric and prospective target. *Int. J. Mol. Sci.* 22:10161. doi: 10.3390/ijms221810161
- Blair, J. B., James, M. E., and Foster, J. L. (1979). Adrenergic control of glucose output and adenosine 3':5'-monophosphate levels in hepatocytes from juvenile and adult rats. *J. Biol. Chem.* 254, 7579–7584. doi: 10.1016/S0021-9258(18)35983-0
- Borlaug, B. A., Kitzman, D. W., Davies, M. J., Rasmussen, S., Barros, E., Butler, J., et al. (2023). Semaglutide in HFpEF across obesity class and by body weight reduction: a prespecified analysis of the STEP-HFpEF trial. *Nat. Med.* 29, 2358–2365. doi: 10.1038/s41591-023-02526-x
- Burbulla, L. F., Song, P., Mazzulli, J. R., Zampese, E., Wong, Y. C., Jeon, S., et al. (2017). Dopamine oxidation mediates mitochondrial and lysosomal dysfunction in Parkinson's disease. *Science* 357, 1255–1261. doi: 10.1126/science.aam9080
- Burré, J., Sharma, M., and Südhof, T. C. (2014). α -Synuclein assembles into higher-order multimers upon membrane binding to promote SNARE complex formation. *Proc. Natl. Acad. Sci.* 111:E4274–83. doi: 10.1073/pnas.1416598111
- Buteau, J., Spatz, M. L., and Accili, D. (2006). Transcription factor FoxO1 mediates glucagon-like Peptide-1 effects on pancreatic β -cell mass. *Diabetes* 55, 1190–1196. doi: 10.2337/db05-0825
- Cabin, D. E., Shimazu, K., Murphy, D., Cole, N. B., Gottschalk, W., McIlwain, K. L., et al. (2002). Synaptic vesicle depletion correlates with attenuated synaptic responses to prolonged repetitive stimulation in mice lacking α -Synuclein. *J. Neurosci.* 22, 8797–8807. doi: 10.1523/JNEUROSCI.22-20-08797.2002
- Canet-Avilés, R. M., Wilson, M. A., Miller, D. W., Ahmad, R., McLendon, C., Bandyopadhyay, S., et al. (2004). The Parkinson's disease protein DJ-1 is neuroprotective due to cysteine-sulfenic acid-driven mitochondrial localization. *Proc. Natl. Acad. Sci.* 101, 9103–9108. doi: 10.1073/pnas.0402959101
- Cardoso, L. E. M., Marinho, T. S., Martins, F. F., Aguilá, M. B., and Mandarim-de-Lacerda, C. A. (2023). Treatment with semaglutide, a GLP-1 receptor agonist, improves extracellular matrix remodeling in the pancreatic islet of diet-induced obese mice. *Life Sci.* 319:121502. doi: 10.1016/j.lfs.2023.121502
- Cereda, E., Barichella, M., Cassani, E., Caccialanza, R., and Pezzoli, G. (2012). Clinical features of Parkinson disease when onset of diabetes came first: a case-control study. *Neurology* 78, 1507–1511. doi: 10.1212/WNL.0b013e3182553cc9
- Cereda, E., Barichella, M., Pedrollo, C., Klersy, C., Cassani, E., Caccialanza, R., et al. (2011). Diabetes and risk of Parkinson's disease. *Diabetes Care* 34, 2614–2623. doi: 10.2337/dc11-1584
- Choudhury, S. P., Bano, S., Sen, S., Suchal, K., Kumar, S., Nikolajeff, F., et al. (2022). Altered neural cell junctions and ion-channels leading to disrupted neuron communication in Parkinson's disease. *NPJ Park. Dis.* 8:66. doi: 10.1038/s41531-022-00324-9
- Cooper, G. J., Willis, A. C., Clark, A., Turner, R. C., Sim, R. B., and Reid, K. B. (1987). Purification and characterization of a peptide from amyloid-rich pancreases of type 2 diabetic patients. *Proc. Natl. Acad. Sci.* 84, 8628–8632. doi: 10.1073/pnas.84.23.8628
- Costantino, S., and Paneni, F. (2019). GLP-1-based therapies to boost autophagy in cardiometabolic patients: from experimental evidence to clinical trials. *Vasc. Pharmacol.* 115, 64–68. doi: 10.1016/j.vph.2019.03.003
- Craft, S., Dagogo-Jack, S. E., Wiethop, B. V., Murphy, C., Nevins, R. T., Fleischman, S., et al. (1993). Effects of hyperglycemia on memory and hormone levels in dementia of the Alzheimer type: a longitudinal study. *Behav. Neurosci.* 107, 926–940. doi: 10.1037/0735-7044.107.6.926
- Cui, K., and Li, Z. (2023). Identification and analysis of type 2 diabetes-mellitus-associated autophagy-related genes. *Front. Endocrinol.* 14:1164112. doi: 10.3389/fendo.2023.1164112
- Dai, Y., Mehta, J. L., and Chen, M. (2013). Glucagon-like Peptide-1 receptor agonist Liraglutide inhibits Endothelin-1 in endothelial cell by repressing nuclear factor-kappa B activation. *Cardiovasc. Drugs Ther.* 27, 371–380. doi: 10.1007/s10557-013-6463-z
- de Bartolomeis, A., De Simone, G., De Prisco, M., Barone, A., Napoli, R., Beguinot, F., et al. (2023). Insulin effects on core neurotransmitter pathways involved in schizophrenia neurobiology: A meta-analysis of preclinical studies. Implications for the treatment. *Mol. Psychiatry*. doi: 10.1038/s41380-023-02065-4 [Epub ahead of print].
- de Marañón, A. M., Díaz-Pozo, P., Canet, F., Díaz-Morales, N., Abad-Jiménez, Z., López-Domènech, S., et al. (2022). Metformin modulates mitochondrial function and mitophagy in peripheral blood mononuclear cells from type 2 diabetic patients. *Redox Biol.* 53:102342. doi: 10.1016/j.redox.2022.102342
- De Riccardis, L., Rizzo, F., Urso, E., Garzarelli, V., Intini, V., Greco, M., et al. (2019). Physiological role of prion protein in copper homeostasis and angiogenic mechanisms of endothelial cells. *Euro Biotech J.* 3, 57–70. doi: 10.2478/ebjt-2019-0007
- Dehay, B., Bové, J., Rodríguez-Muela, N., Perier, C., Recasens, A., Boya, P., et al. (2010). Pathogenic lysosomal depletion in Parkinson's disease. *J. Neurosci.* 30, 12535–12544. doi: 10.1523/JNEUROSCI.1920-10.2010
- Del Cocio, L., Greco, M., Inguscio, A., Munir, A., Danieli, A., Cossa, L., et al. (2023). Blood metabolite profiling of Antarctic expedition members: an ¹H NMR spectroscopy-based study. *Int. J. Mol. Sci.* 24:8459. doi: 10.3390/ijms24098459
- Delerive, P., De Bosscher, K., Besnard, S., Vanden Berghe, W., Peters, J. M., Gonzalez, F. J., et al. (1999). Peroxisome proliferator-activated receptor α negatively

regulates the vascular inflammatory gene response by negative cross-talk with transcription factors NF- κ B and AP-1. *J. Biol. Chem.* 274, 32048–32054. doi: 10.1074/jbc.274.45.32048

Diers, A. R., Broniowska, K. A., Chang, C.-F., and Hogg, N. (2012). Pyruvate fuels mitochondrial respiration and proliferation of breast cancer cells: effect of monocarboxylate transporter inhibition. *Biochem. J.* 444, 561–571. doi: 10.1042/BJ20120294

Dorsey, E. R., and Bloem, B. R. (2018). The Parkinson pandemic—a call to action. *JAMA Neurol.* 75:9. doi: 10.1001/jamaneurol.2017.3299

Driver, J. A., Smith, A., Buring, J. E., Gaziano, J. M., Kurth, T., and Logroscino, G. (2008). Prospective cohort study of type 2 diabetes and the risk of Parkinson's disease. *Diabetes Care* 31, 2003–2005. doi: 10.2337/dc08-0688

Drzewoski, J., and Hanefeld, M. (2021). The current and potential therapeutic use of metformin—the good old drug. *Pharmaceuticals*. 14:122. doi: 10.3390/ph14020122

Du, X.-L., Edelstein, D., Rossetti, L., Fantus, I. G., Goldberg, H., Ziyadeh, F., et al. (2000). Hyperglycemia-induced mitochondrial superoxide overproduction activates the hexosamine pathway and induces plasminogen activator inhibitor-1 expression by increasing Sp1 glycosylation. *Proc. Natl. Acad. Sci.* 97, 12222–12226. doi: 10.1073/pnas.97.22.12222

Du, X., Matsumura, T., Edelstein, D., Rossetti, L., Zsengeller, Z., Szabó, C., et al. (2003). Inhibition of GAPDH activity by poly (ADP-ribose) polymerase activates three major pathways of hyperglycemic damage in endothelial cells. *J. Clin. Invest.* 112, 1049–1057. doi: 10.1172/JCI18127

Duarte, A. I., Santos, P., Oliveira, C. R., Santos, M. S., and Rego, A. C. (2008). Insulin neuroprotection against oxidative stress is mediated by Akt and GSK-3 β signaling pathways and changes in protein expression. *Biochim. Biophys. Acta-Mol. Cell Res.* 1783, 994–1002. doi: 10.1016/j.bbamcr.2008.02.016

Dunn, L., Allen, G. F., Mamais, A., Ling, H., Li, A., Duberley, K. E., et al. (2014). Dysregulation of glucose metabolism is an early event in sporadic Parkinson's disease. *Neurobiol. Aging* 35, 1111–1115. doi: 10.1016/j.neurobiolaging.2013.11.001

Fellner, L., Gabassi, E., Haybaeck, J., and Edenhofer, F. (2021). Autophagy in α -synucleinopathies — an overstrained system. *Cells* 10:3143. doi: 10.3390/cells10113143

Fine, J. M., Stroebel, B. M., Faltesek, K. A., Terai, K., Haase, L., Knutzen, K. E., et al. (2020). Intranasal delivery of low-dose insulin ameliorates motor dysfunction and dopaminergic cell death in a 6-OHDA rat model of Parkinson's disease. *Neurosci. Lett.* 714:134567. doi: 10.1016/j.neulet.2019.134567

Fiorrentino, T. V., Monroy, A., Kamath, S., Sotero, R., Cas, M. D., Daniele, G., et al. (2021). Pioglitazone corrects dysregulation of skeletal muscle mitochondrial proteins involved in ATP synthesis in type 2 diabetes. *Metabolism* 114:154416. doi: 10.1016/j.metabol.2020.154416

Fujiwara, H., Hasegawa, M., Dohmae, N., Kawashima, A., Masliah, E., Goldberg, M. S., et al. (2002). α -Synuclein is phosphorylated in synucleinopathy lesions. *Nat. Cell Biol.* 4, 160–164. doi: 10.1038/ncb748

García, E., Shalaurou, I., Matyus, S. P., Oskardmay, D. N., Otvos, J. D., Dullaart, R. P. F., et al. (2020). Ketone bodies are mildly elevated in subjects with type 2 diabetes mellitus and are inversely associated with insulin resistance as measured by the lipoprotein insulin resistance index. *J. Clin. Med.* 9:321. doi: 10.3390/jcm9020321

García-Cáceres, C., Quarta, C., Varela, L., Gao, Y., Gruber, T., Legutko, B., et al. (2016). Astrocytic insulin signaling couples brain glucose uptake with nutrient availability. *Cells* 166, 867–880. doi: 10.1016/j.cell.2016.07.028

Gasnier, B. (2000). The loading of neurotransmitters into synaptic vesicles. *Biochimie* 82, 327–337. doi: 10.1016/S0300-9084(00)00221-2

Gayen, M., Benoit, M. R., Fan, Q., Hudobenko, J., and Yan, R. (2022). The CX3CL1 intracellular domain exhibits neuroprotection via insulin receptor/insulin-like growth factor receptor signaling. *J. Biol. Chem.* 298:102532. doi: 10.1016/j.jbc.2022.102532

Geng, X., Li, L., Bottino, R., Balamurugan, A. N., Bertera, S., Densmore, E., et al. (2007). Antidiabetic sulfonylurea stimulates insulin secretion independently of plasma membrane K ATP channels. *Am. J. Physiol. Metab.* 293, E293–E301. doi: 10.1152/ajpendo.00016.2007

Geyer, M. C., Sullivan, T., Tai, A., Morton, J. M., Edwards, S., Martin, A. J., et al. (2019). Exenatide corrects postprandial hyperglycaemia in young people with cystic fibrosis and impaired glucose tolerance: a randomized crossover trial. *Diabetes. Obes. Metab.* 21, 700–704. doi: 10.1111/dom.13544

Grabner, G. F., Xie, H., Schweiger, M., and Zechner, R. (2021). Lipolysis: cellular mechanisms for lipid mobilization from fat stores. *Nat. Metab.* 3, 1445–1465. doi: 10.1038/s42255-021-00493-6

Greco, M., Spinelli, C. C., De Riccardis, L., Buccolieri, A., Di Giulio, S., Musarò, D., et al. (2021). Copper dependent modulation of α -Synuclein phosphorylation in differentiated SH5Y5 neuroblastoma cells. *Int. J. Mol. Sci.* 22:2038. doi: 10.3390/ijms22042038

Guadagnolo, D., Piane, M., Torrisi, M. R., Pizzuti, A., and Petrucci, S. (2021). Genotype-phenotype correlations in monogenic Parkinson disease: a review on clinical and molecular findings. *Front. Neurol.* 12:648588. doi: 10.3389/fneur.2021.648588

Han, Y., Xie, H., Liu, Y., Gao, P., Yang, X., and Shen, Z. (2019). Effect of metformin on all-cause and cardiovascular mortality in patients with coronary artery diseases: a

systematic review and an updated meta-analysis. *Cardiovasc. Diabetol.* 18:96. doi: 10.1186/s12933-019-0900-7

Hao, L.-Y., Giasson, B. I., and Bonini, N. M. (2010). DJ-1 is critical for mitochondrial function and rescues PINK1 loss of function. *Proc. Natl. Acad. Sci.* 107, 9747–9752. doi: 10.1073/pnas.0911175107

Helmstädter, J., Frenis, K., Filippou, K., Grill, A., Dib, M., Kalinovic, S., et al. (2020). Endothelial GLP-1 (glucagon-like Peptide-1) receptor mediates cardiovascular protection by Liraglutide in mice with experimental arterial hypertension. *Arterioscler. Thromb. Vasc. Biol.* 40, 145–158. doi: 10.1161/atv.0000615456.97862.30

Heras-Sandoval, D., Pérez-Rojas, J. M., Hernández-Damián, J., and Pedraza-Chaverri, J. (2014). The role of PI3K/AKT/mTOR pathway in the modulation of autophagy and the clearance of protein aggregates in neurodegeneration. *Cell. Signal.* 26, 2694–2701. doi: 10.1016/j.cellsig.2014.08.019

Hira, T., Trakooncharoenvit, A., Taguchi, H., and Hara, H. (2021). Improvement of glucose tolerance by food factors having glucagon-like Peptide-1 releasing activity. *Int. J. Mol. Sci.* 22:6623. doi: 10.3390/ijms22126623

Horakova, O., Kroupova, P., Bardova, K., Buresova, J., Janovska, P., Kopecky, J., et al. (2019). Metformin acutely lowers blood glucose levels by inhibition of intestinal glucose transport. *Sci. Rep.* 9:6156. doi: 10.1038/s41598-019-42531-0

Hou, X., Watzlawik, J. O., Fiesel, F. C., and Springer, W. (2020). Autophagy in Parkinson's disease. *J. Mol. Biol.* 432, 2651–2672. doi: 10.1016/j.jmb.2020.01.037

Hu, D., Guo, Y., Wu, R., Shao, T., Long, J., Yu, B., et al. (2021). New insight into metformin-induced cholesterol-lowering effect crosstalk between glucose and cholesterol homeostasis via ChREBP (carbohydrate-responsive element-binding protein)-mediated PCSK9 (Proprotein convertase Subtilisin/Kexin type 9) regulation. *Arterioscler. Thromb. Vasc. Biol.* 41, e208–e223. doi: 10.1161/ATVBAHA.120.315708

Huang, Y., Wan, Z., Wang, Z., and Zhou, B. (2019). Insulin signaling in *Drosophila melanogaster* mediates A β toxicity. *Commun. Biol.* 2:13. doi: 10.1038/s42003-018-0253-x

IDF Clinical Guidelines Task Force (2006). Global guideline for type 2 diabetes: recommendations for standard, comprehensive, and minimal care. *Diabet. Med.* 23, 579–593. doi: 10.1111/j.1464-5491.2006.01918.x

Iizuka, K., Bruck, R. K., Liang, G., Horton, J. D., and Uyeda, K. (2004). Deficiency of carbohydrate response element-binding protein (ChREBP) reduces lipogenesis as well as glycolysis. *Proc. Natl. Acad. Sci.* 101, 7281–7286. doi: 10.1073/pnas.0401516101

Iravanpour, F., Dargahi, L., Rezaei, M., Haghighi, M., Heidari, R., Valian, N., et al. (2021). Intranasal insulin improves mitochondrial function and attenuates motor deficits in a rat 6-OHDA model of Parkinson's disease. *CNS Neurosci. Ther.* 27, 308–319. doi: 10.1111/cns.13609

Jalewa, J., Sharma, M. K., Gengler, S., and Hölscher, C. (2017). A novel GLP-1/GIP dual receptor agonist protects from 6-OHDA lesion in a rat model of Parkinson's disease. *Neuropharmacology* 117, 238–248. doi: 10.1016/j.neuropharm.2017.02.013

Jao, C. C., Der-Sarkissian, A., Chen, J., and Langen, R. (2004). Structure of membrane-bound α -synuclein studied by site-directed spin labeling. *Proc. Natl. Acad. Sci.* 101, 8331–8336. doi: 10.1073/pnas.0400553101

Jensen, M. E., Galli, A., Thomsen, M., Jensen, K. L., Thomsen, G. K., Klausen, M. K., et al. (2020). Glucagon-like peptide-1 receptor regulation of basal dopamine transporter activity is species-dependent. *Neurochem. Int.* 138:104772. doi: 10.1016/j.neuint.2020.104772

Jensterle, M., Ferjan, S., Ležaič, L., Sočan, A., Goričar, K., Zalete, K., et al. (2023). Semaglutide delays 4-hour gastric emptying in women with polycystic ovary syndrome and obesity. *Diabetes Obes. Metab.* 25, 975–984. doi: 10.1111/dom.14944

Jheng, H.-F., Tsai, P.-J., Guo, S.-M., Kuo, L.-H., Chang, C.-S., Su, I.-J., et al. (2012). Mitochondrial fission contributes to mitochondrial dysfunction and insulin resistance in skeletal muscle. *Mol. Cell. Biol.* 32, 309–319. doi: 10.1128/MCB.05603-11

Jucker, M., and Walker, L. C. (2018). Propagation and spread of pathogenic protein assemblies in neurodegenerative diseases. *Nat. Neurosci.* 21, 1341–1349. doi: 10.1038/s41593-018-0238-6

Kadouch, H., Chedid, V., Halawi, H., Burton, D. D., Clark, M. M., Khemani, D., et al. (2020). GLP-1 analog modulates appetite, taste preference, gut hormones, and regional body fat Stores in Adults with obesity. *J. Clin. Endocrinol. Metab.* 105, 1552–1563. doi: 10.1210/clinem/dgz140

Kang, H., Khang, R., Ham, S., Jeong, G. R., Kim, H., Jo, M., et al. (2017). Activation of the ATF2/CREB-PGC-1 α pathway by metformin leads to dopaminergic neuroprotection. *Oncotarget* 8, 48603–48618. doi: 10.18632/oncotarget.18122

Karpowicz, R. J., Trojanowski, J. Q., and Lee, V. M.-Y. (2019). Transmission of α -synuclein seeds in neurodegenerative disease: recent developments. *Lab. Invest.* 99, 971–981. doi: 10.1038/s41374-019-0195-z

Katila, N., Bhurtel, S., Shadfar, S., Srivastav, S., Neupane, S., Ojha, U., et al. (2017). Metformin lowers α -synuclein phosphorylation and upregulates neurotrophic factor in the MPTP mouse model of Parkinson's disease. *Neuropharmacology* 125, 396–407. doi: 10.1016/j.neuropharm.2017.08.015

Katsyuba, E., Romani, M., Hofer, D., and Auwerx, J. (2020). NAD⁺ homeostasis in health and disease. *Nat. Metab.* 2, 9–31. doi: 10.1038/s42255-019-0161-5

- Kelley, D. E., He, J., Menshikova, E. V., and Ritov, V. B. (2002). Dysfunction of mitochondria in human skeletal muscle in type 2 diabetes. *Diabetes* 51, 2944–2950. doi: 10.2337/diabetes.51.10.2944
- Khalid, M., Alkaabi, J., Khan, M. A. B., and Adem, A. (2021). Insulin signal transduction perturbations in insulin resistance. *Int. J. Mol. Sci.* 22:8590. doi: 10.3390/ijms22168590
- Kinsky, O. R., Hargraves, T. L., Anumol, T., Jacobsen, N. E., Dai, J., Snyder, S. A., et al. (2016). Metformin scavenges methylglyoxal to form a novel imidazolinone metabolite in humans. *Chem. Res. Toxicol.* 29, 227–234. doi: 10.1021/acs.chemrestox.5b00497
- Kleinridders, A. (2016). Deciphering brain insulin receptor and insulin-like growth factor 1 receptor Signalling. *J. Neuroendocrinol.* 28. doi: 10.1111/jne.12433
- Le Bacquer, O., Petroulakis, E., Pagliarunga, S., Poulin, F., Richard, D., Cianflone, K., et al. (2007). Elevated sensitivity to diet-induced obesity and insulin resistance in mice lacking 4E-BP1 and 4E-BP2. *J. Clin. Invest.* 117, 387–396. doi: 10.1172/JCI29528
- Lee, C. B., Chae, S. U., Jo, S. J., Jerng, U. M., and Bae, S. K. (2021). The relationship between the gut microbiome and metformin as a key for treating type 2 diabetes mellitus. *Int. J. Mol. Sci.* 22:3566. doi: 10.3390/ijms22073566
- Lee, E., Korf, H., and Vidal-Puig, A. (2023). An adipocentric perspective on the development and progression of non-alcoholic fatty liver disease. *J. Hepatol.* 78, 1048–1062. doi: 10.1016/j.jhep.2023.01.024
- Lee, S. E., Lee, N. Y., Kim, S. H., Kim, K.-A., and Kim, Y. S. (2021). Effect of liraglutide 3.0mg treatment on weight reduction in obese antipsychotic-treated patients. *Psychiatry Res.* 299:113830. doi: 10.1016/j.psychres.2021.113830
- Lewis, M. R., and Lewis, W. H. (1915). Mitochondria (and other cytoplasmic structures) in tissue cultures. *Am. J. Anat.* 17, 339–401. doi: 10.1002/aja.1000170304
- Li, Z., Li, S., Wang, N., Xue, P., and Li, Y. (2020). Liraglutide, a glucagon-like peptide-1 receptor agonist, suppresses osteoclastogenesis through the inhibition of NF- κ B and MAPK pathways via GLP-1R. *Biomed. Pharmacother.* 130:110523. doi: 10.1016/j.biopha.2020.110523
- Li, X., Zhang, N., Li, Y., Shi, Y., Li, D., Xie, Y., et al. (2011). Effects of metformin and rosiglitazone on peripheral insulin resistance and β -cell function in obesity: a double-blind, randomized, controlled study. *J. Int. Med. Res.* 39, 358–365. doi: 10.1177/147323001103900203
- Lian, J., and Fu, J. (2021). Pioglitazone for NAFLD patients with prediabetes or type 2 diabetes mellitus: a meta-analysis. *Front. Endocrinol.* 12:615409. doi: 10.3389/fendo.2021.615409
- Liao, P.-C., Wolken, D. M. A., Serrano, E., Srivastava, P., and Pon, L. A. (2020). Mitochondria-associated degradation pathway (MAD) function beyond the outer membrane. *Cell Rep.* 32:107902. doi: 10.1016/j.celrep.2020.107902
- Liu, J., Wang, D., Xie, Z., Ding, L., Li, S., Ma, X., et al. (2023). Combination of pioglitazone and metformin actions on liver lipid metabolism in obese mice. *Biomol. Ther.* 13:1199. doi: 10.3390/biom13081199
- Lu, L., Fu, D., Li, H., Liu, A., Li, J., and Zheng, G. (2014). Diabetes and risk of Parkinson's disease: an updated Meta-analysis of case-control studies. *PLoS One* 9:e85781. doi: 10.1371/journal.pone.0085781
- Luna-Marco, C., de Marañon, A. M., Hermo-Argibay, A., Rodriguez-Hernandez, Y., Hermenejildo, J., Fernandez-Reyes, M., et al. (2023). Effects of GLP-1 receptor agonists on mitochondrial function, inflammatory markers and leukocyte-endothelium interactions in type 2 diabetes. *Redox Biol.* 66:102849. doi: 10.1016/j.redox.2023.102849
- Luo, X., Hu, R., Zheng, Y., Liu, S., and Zhou, Z. (2020). Metformin shows anti-inflammatory effects in murine macrophages through dicer/microribonucleic acid-34a-5p and microribonucleic acid-125b-5p. *J. Diabetes Investig.* 11, 101–109. doi: 10.1111/jdi.13074
- Lutchmansingh, F. K., Hsu, J. W., Bennett, F. I., Badaloo, A. V., McFarlane-Anderson, N., Gordon-Strachan, G. M., et al. (2018). Glutathione metabolism in type 2 diabetes and its relationship with microvascular complications and glycemia. *PLoS One* 13:e0198626. doi: 10.1371/journal.pone.0198626
- Ma, Z., Liu, Z., Li, X., Zhang, H., Han, D., Xiong, W., et al. (2023). Metformin collaborates with PINK1/Mfn2 overexpression to prevent cardiac injury by improving mitochondrial function. *Biology* 12:582. doi: 10.3390/biology12040582
- Ma, L.-Y., Lv, Y.-L., Huo, K., Liu, J., Shang, S.-H., Fei, Y.-L., et al. (2017). Autophagy-lysosome dysfunction is involved in A β deposition in STZ-induced diabetic rats. *Behav. Brain Res.* 320, 484–493. doi: 10.1016/j.bbr.2016.10.031
- Madiraju, A. K., Qiu, Y., Perry, R. J., Rahimi, Y., Zhang, X.-M., Zhang, D., et al. (2018). Metformin inhibits gluconeogenesis via a redox-dependent mechanism in vivo. *Nat. Med.* 24, 1384–1394. doi: 10.1038/s41591-018-0125-4
- Margolis, R. U., and Altszuler, N. (1967). Insulin in the cerebrospinal fluid. *Nature* 215, 1375–1376. doi: 10.1038/2151375a0
- Martinez-Valbuena, I., Amat-Villegas, I., Valenti-Azcarate, R., del Carmona-Abellán, M. M., Marcilla, I., Tuñón, M. T., et al. (2018). Interaction of amyloidogenic proteins in pancreatic β cells from subjects with synucleinopathies. *Acta Neuropathol.* 135, 877–886. doi: 10.1007/s00401-018-1832-0
- Martinez-Valbuena, I., Valenti-Azcarate, R., Amat-Villegas, I., Marcilla, I., Martí-Andrés, G., Caballero, M.-C., et al. (2021). Mixed pathologies in pancreatic β cells from subjects with neurodegenerative diseases and their interaction with prion protein. *Acta Neuropathol. Commun.* 9:64. doi: 10.1186/s40478-021-01171-0
- Martins, F. F., Marinho, T. S., Cardoso, L. E. M., Barbosa-da-Silva, S., Souza-Mello, V., Aguilá, M. B., et al. (2022). Semaglutide (GLP-1 receptor agonist) stimulates browning on subcutaneous fat adipocytes and mitigates inflammation and endoplasmic reticulum stress in visceral fat adipocytes of obese mice. *Cell Biochem. Funct.* 40, 903–913. doi: 10.1002/cbf.3751
- Mathebula, S. D. (2015). Polyol pathway: a possible mechanism of diabetes complications in the eye. *African Vis. Eye Heal.* 74:5. doi: 10.4102/aveh.v74i1.13
- Mazza, M. C., Shuck, S. C., Lin, J., Moxley, M. A., Termini, J., Cookson, M. R., et al. (2022). DJ-1 is not a deglycase and makes a modest contribution to cellular defense against methylglyoxal damage in neurons. *J. Neurochem.* 162, 245–261. doi: 10.1111/jnc.15656
- Menéndez-González, M., Padilla-Zambrano, H., Tomás-Zapico, C., and García, B. (2018). Clearing extracellular alpha-Synuclein from cerebrospinal fluid: a new therapeutic strategy in Parkinson's disease. *Brain Sci.* 8:52. doi: 10.3390/brainsci8040052
- Meurot, C., Martin, C., Sudre, L., Breton, J., Bougault, C., Rattenbach, R., et al. (2022). Liraglutide, a glucagon-like peptide 1 receptor agonist, exerts analgesic, anti-inflammatory and anti-degradative actions in osteoarthritis. *Sci. Rep.* 12:1567. doi: 10.1038/s41598-022-05323-7
- Milordini, G., Zacco, E., Percival, M., Puglisi, R., Dal Piaz, F., Temussi, P., et al. (2020). The role of glycation on the aggregation properties of IAPP. *Front. Mol. Biosci.* 7:104. doi: 10.3389/fmolb.2020.00104
- Nanjan, M. J., Mohammed, M., Prashantha Kumar, B. R., and Chandrasekar, M. J. N. (2018). Thiazolidinediones as antidiabetic agents: a critical review. *Bioorg. Chem.* 77, 548–567. doi: 10.1016/j.bioorg.2018.02.009
- Nazreen, S. (2021). Design, synthesis, and molecular docking studies of thiazolidinediones as PPAR- γ agonists and thymidylate synthase inhibitors. *Arch. Pharm. (Weinheim)*. 354:e2100021. doi: 10.1002/ardp.202100021
- Novak, P., Pimentel Maldonado, D. A., and Novak, V. (2019). Safety and preliminary efficacy of intranasal insulin for cognitive impairment in Parkinson disease and multiple system atrophy: a double-blinded placebo-controlled pilot study. *PLoS One* 14:e0214364. doi: 10.1371/journal.pone.0214364
- Onphachanh, X., Lee, H. J., Lim, J. R., Jung, Y. H., Kim, J. S., Chae, C. W., et al. (2017). Enhancement of high glucose-induced PINK1 expression by melatonin stimulates neuronal cell survival: involvement of MT 2/Akt/NF- κ B pathway. *J. Pineal Res.* 63:e12427. doi: 10.1111/jpi.12427
- Pagano, G., Polychronis, S., Wilson, H., Giordano, B., Ferrara, N., Niccolini, F., et al. (2018). Diabetes mellitus and Parkinson disease. *Neurology* 90, e1654–e1662. doi: 10.1212/WNL.0000000000005475
- Pakravan, G., Peymani, M., Abedpoor, N., Safaiejad, Z., Yadegari, M., Derakhshan, M., et al. (2022). Antiapoptotic and anti-inflammatory effects of Ppary agonist, pioglitazone, reversed dox-induced cardiotoxicity through mediating of miR-130a downregulation in C57BL/6 mice. *J. Biochem. Mol. Toxicol.* 36:e23041. doi: 10.1002/jbt.23041
- Palikaras, K., Lionaki, E., and Tavernarakis, N. (2018). Mechanisms of mitophagy in cellular homeostasis, physiology and pathology. *Nat. Cell Biol.* 20, 1013–1022. doi: 10.1038/s41556-018-0176-2
- Park, S. W., Mansur, R. B., Lee, Y., Lee, J.-H., Seo, M. K., Choi, A. J., et al. (2018). Liraglutide activates mTORC1 signaling and AMPA receptors in rat hippocampal neurons under toxic conditions. *Front. Neurosci.* 12:756. doi: 10.3389/fnins.2018.00756
- Perez, R. G., Waymire, J. C., Lin, E., Liu, J. J., Guo, F., and Zigmond, M. J. (2002). A role for α -Synuclein in the regulation of dopamine biosynthesis. *J. Neurosci.* 22, 3090–3099. doi: 10.1523/JNEUROSCI.22-08-03090.2002
- Pérez-Revuelta, B. I., Hettich, M. M., Ciociaro, A., Rotermund, C., Kahle, P. J., Krauss, S., et al. (2014). Metformin lowers Ser-129 phosphorylated α -synuclein levels via mTOR-dependent protein phosphatase 2A activation. *Cell Death Dis.* 5, e1209. doi: 10.1038/cddis.2014.175
- Polymeropoulos, M. H., Lavedan, C., Leroy, E., Ide, S. E., Dehejia, A., Dutra, A., et al. (1997). Mutation in the α -Synuclein gene identified in families with Parkinson's disease. *Science* 276, 2045–2047. doi: 10.1126/science.276.5321.2045
- Pomytkin, I., Costa-Nunes, J. P., Kasatkin, V., Veniaminova, E., Demchenko, A., Lyundup, A., et al. (2018). Insulin receptor in the brain: mechanisms of activation and the role in the CNS pathology and treatment. *CNS Neurosci. Ther.* 24:763. doi: 10.1111/cns.12866
- Pupyshev, A. B., Tenditnik, M. V., Ovsyukova, M. V., Akopyan, A. A., Dubrovina, N. I., and Tikhonova, M. A. (2021). Restoration of Parkinson's disease-like deficits by activating autophagy through mTOR-dependent and mTOR-independent mechanisms in pharmacological and transgenic models of Parkinson's disease in mice. *Bull. Exp. Biol. Med.* 171, 425–430. doi: 10.1007/s10517-021-05242-z
- Qu, J., Yan, H., Zheng, Y., Xue, F., Zheng, Y., Fang, H., et al. (2018). The molecular mechanism of alpha-Synuclein dependent regulation of protein phosphatase 2A activity. *Cell. Physiol. Biochem.* 47, 2613–2625. doi: 10.1159/000491657
- Quinn, L. P., Crook, B., Hows, M. E., Vidgeon-Hart, M., Chapman, H., Upton, N., et al. (2008). The PPAR γ agonist pioglitazone is effective in the MPTP mouse model of

Parkinson's disease through inhibition of monoamine oxidase B. *Br. J. Pharmacol.* 154, 226–233. doi: 10.1038/bjp.2008.78

Radwan, R. R., and Hasan, H. F. (2019). Pioglitazone ameliorates hepatic damage in irradiated rats via regulating anti-inflammatory and antifibrogenic signalling pathways. *Free Radic. Res.* 53, 748–757. doi: 10.1080/10715762.2019.1624742

Rahimi, M., Sajadimajd, S., Mahdian, Z., Hemmati, M., Malekhtabati, P., Bahrami, G., et al. (2020). Characterization and anti-diabetic effects of the oligosaccharide fraction isolated from *Rosa canina* in STZ-induced diabetic rats. *Carbohydr. Res.* 489:107927. doi: 10.1016/j.carres.2020.107927

Rahman, M. S., Hossain, K. S., Das, S., Kundu, S., Adegoke, E. O., Rahman, M. A., et al. (2021). Role of insulin in health and disease: an update. *Int. J. Mol. Sci.* 22:6403. doi: 10.3390/ijms22126403

Rajasekar, N., Nath, C., Hanif, K., and Shukla, R. (2017). Intranasal insulin administration ameliorates Streptozotocin (ICV)-induced insulin receptor dysfunction, Neuroinflammation, Amyloidogenesis, and memory impairment in rats. *Mol. Neurobiol.* 54, 6507–6522. doi: 10.1007/s12035-016-0169-8

Reed, X., Bandrés-Ciga, S., Blauwendraat, C., and Cookson, M. R. (2019). The role of monogenic genes in idiopathic Parkinson's disease. *Neurobiol. Dis.* 124, 230–239. doi: 10.1016/j.nbd.2018.11.012

Roger, L. J., and Fellows, R. E. (1980). Stimulation of ornithine decarboxylase activity by insulin in developing rat brain. *Endocrinology* 106, 619–625. doi: 10.1210/endo-106-2-619

Rueggsegger, G. N., Manjunatha, S., Summer, P., Gopala, S., Zabeilski, P., Dasari, S., et al. (2019a). Insulin deficiency and intranasal insulin alter brain mitochondrial function: a potential factor for dementia in diabetes. *FASEB J.* 33, 4458–4472. doi: 10.1096/fj.201802043R

Rueggsegger, G. N., Vanderboom, P. M., Dasari, S., Klaus, K. A., Kabiraj, P., McCarthy, C. B., et al. (2019b). Exercise and metformin counteract altered mitochondrial function in the insulin-resistant brain. *JCI Insight* 4:e130681. doi: 10.1172/jci.insight.130681

Ryu, Y.-K., Go, J., Park, H.-Y., Choi, Y.-K., Seo, Y. J., Choi, J. H., et al. (2020). Metformin regulates astrocyte reactivity in Parkinson's disease and normal aging. *Neuropharmacology* 175:108173. doi: 10.1016/j.neuropharm.2020.108173

Ryu, Y.-K., Park, H.-Y., Go, J., Choi, D.-H., Kim, Y.-H., Hwang, J. H., et al. (2018). Metformin inhibits the development of l-DOPA-induced dyskinesia in a murine model of Parkinson's disease. *Mol. Neurobiol.* 55, 5715–5726. doi: 10.1007/s12035-017-0752-7

Saewanee, N., Praputpittaya, T., Malaiwong, N., Chalorak, P., and Meemon, K. (2021). Neuroprotective effect of metformin on dopaminergic neurodegeneration and α -synuclein aggregation in *C. elegans* model of Parkinson's disease. *Neurosci. Res.* 162, 13–21. doi: 10.1016/j.neures.2019.12.017

Sandyk, R. (1993). The relationship between diabetes mellitus and Parkinson's disease. *Int. J. Neurosci.* 69, 125–130. doi: 10.3109/00207459309003322

Sansome, D. J., Xie, C., Veefald, S., Horowitz, M., Rayner, C. K., and Wu, T. (2020). Mechanism of glucose-lowering by metformin in type 2 diabetes: role of bile acids. *Diabetes. Obes. Metab.* 22, 141–148. doi: 10.1111/dom.13869

Savica, R., Grossardt, B. R., Ahlskog, J. E., and Rocca, W. A. (2012). Metabolic markers or conditions preceding Parkinson's disease: a case-control study. *Mov. Disord.* 27, 974–979. doi: 10.1002/mds.25016

Schernhammer, E., Hansen, J., Rugbjerg, K., Wermuth, L., and Ritz, B. (2011). Diabetes and the risk of developing Parkinson's disease in Denmark. *Diabetes Care* 34, 1102–1108. doi: 10.2337/dc10-1333

Schubert, M., Brazil, D. P., Burks, D. J., Kushner, J. A., Ye, J., Flint, C. L., et al. (2003). Insulin receptor Substrate-2 deficiency impairs brain growth and promotes tau phosphorylation. *J. Neurosci.* 23, 7084–7092. doi: 10.1523/JNEUROSCI.23-18-07084.2003

Serhan, A., Aerts, J. L., Boddeke, E. W. G. M., and Kooijman, R. (2020). Neuroprotection by insulin-like growth Factor-1 in rats with ischemic stroke is associated with microglial changes and a reduction in Neuroinflammation. *Neuroscience* 426, 101–114. doi: 10.1016/j.neuroscience.2019.11.035

Shah, B. H., and Hausman, R. E. (1993). Effect of insulin on GABAergic development in the embryonic chick retina. *Dev. Brain Res.* 72, 151–158. doi: 10.1016/0165-3806(93)90180-I

Shang, P., Baker, M., Banks, S., Hong, S.-I., and Choi, D.-S. (2021). Emerging nondopaminergic medications for Parkinson's disease: focusing on A2A receptor antagonists and GLP1 receptor agonists. *J. Mov. Disord.* 14, 193–203. doi: 10.14802/jmd.21035

Shuaib, A., Ijaz, M. S., Waqar, T., Voll, C., Kanthan, R., Miyashita, H., et al. (1995). Insulin elevates hippocampal GABA levels during ischemia. This is independent of its hypoglycemic effect. *Neuroscience* 67, 809–814. doi: 10.1016/0304-4522(95)00093-X

Simón-Sánchez, J., Schulte, C., Bras, J. M., Sharma, M., Gibbs, J. R., Berg, D., et al. (2009). Genome-wide association study reveals genetic risk underlying Parkinson's disease. *Nat. Genet.* 41, 1308–1312. doi: 10.1038/ng.487

Soejima, A., Inoue, K., Takai, D., Kaneko, M., Ishihara, H., Oka, Y., et al. (1996). Mitochondrial DNA is required for regulation of glucose-stimulated insulin secretion in a mouse pancreatic Beta cell line, MIN6. *J. Biol. Chem.* 271, 26194–26199. doi: 10.1074/jbc.271.42.26194

Soliman, E., Behairy, S. F., El-maraghy, N. N., and Elshazly, S. M. (2019). PPAR- γ agonist, pioglitazone, reduced oxidative and endoplasmic reticulum stress associated with L-NAME-induced hypertension in rats. *Life Sci.* 239:117047. doi: 10.1016/j.lfs.2019.117047

Sonne, J., Reddy, V., and Beato, M. R. (2023). *Neuroanatomy, Substantia Nigra*. Treasure Island: StatPearls Publishing.

Sousa-Nunes, R., Yee, L. L., and Gould, A. P. (2011). Fat cells reactivate quiescent neuroblasts via TOR and glial insulin relays in *Drosophila*. *Nature* 471, 508–512. doi: 10.1038/nature09867

Spillantini, M. G., Schmidt, M. L., Lee, V. M.-Y., Trojanowski, J. Q., Jakes, R., and Goedert, M. (1997). α -Synuclein in Lewy bodies. *Nature* 388, 839–840. doi: 10.1038/42166

Sportelli, C., Urso, D., Jenner, P., and Chaudhuri, K. R. (2020). Metformin as a potential neuroprotective agent in prodromal Parkinson's disease—viewpoint. *Front. Neurol.* 11, 1–10. doi: 10.3389/fneur.2020.00556

Steinberg, G. R., and Carling, D. (2019). AMP-activated protein kinase: the current landscape for drug development. *Nat. Rev. Drug Discov.* 18, 527–551. doi: 10.1038/s41573-019-0019-2

Sterling, J. K., Adetunji, M. O., Guttha, S., Bargoud, A. R., Uyhazi, K. E., Ross, A. G., et al. (2020). GLP-1 receptor agonist NLY01 reduces retinal inflammation and neuron death secondary to ocular hypertension. *Cell Rep.* 33:108271. doi: 10.1016/j.celrep.2020.108271

Strom, A., Strassburger, K., Schmuck, M., Shevalye, H., Davidson, E., Zivehe, F., et al. (2021). Interaction between magnesium and methylglyoxal in diabetic polyneuropathy and neuronal models. *Mol. Metab.* 43:101114. doi: 10.1016/j.molmet.2020.101114

Su, C.-J., Shen, Z., Cui, R.-X., Huang, Y., Xu, D.-L., Zhao, F.-L., et al. (2020). Thioredoxin-interacting protein (TXNIP) regulates Parkin/PINK1-mediated Mitophagy in dopaminergic neurons under high-glucose conditions: implications for molecular links between Parkinson's disease and diabetes. *Neurosci. Bull.* 36, 346–358. doi: 10.1007/s12264-019-00459-5

Sun, H., Saeedi, P., Karuranga, S., Pinkepank, M., Ogurtsova, K., Duncan, B. B., et al. (2022). IDF diabetes atlas: global, regional and country-level diabetes prevalence estimates for 2021 and projections for 2045. *Diabetes Res. Clin. Pract.* 183:109119. doi: 10.1016/j.diabres.2021.109119

Suzuki, R., Lee, K., Jing, E., Biddinger, S. B., McDonald, J. G., Montine, T. J., et al. (2010). Diabetes and insulin in regulation of brain cholesterol metabolism. *Cell Metab.* 12, 567–579. doi: 10.1016/j.cmet.2010.11.006

Takahashi-Niki, K., Niki, T., Iguchi-Ariga, S. M. M., and Ariga, H. (2017). Transcriptional regulation of DJ-1. *Adv. Exp. Med. Biol.* 2017, 89–95. doi: 10.1007/978-981-10-6583-5_7

Tanday, N., Lafferty, R. A., Flatt, P. R., and Irwin, N. (2022). Beneficial metabolic effects of recurrent periods of beta-cell rest and stimulation using stable neuropeptide Y1 and glucagon-like peptide-1 receptor agonists. *Diabetes. Obes. Metab.* 24, 2353–2363. doi: 10.1111/dom.14821

Tarry-Adkins, J. L., Grant, I. D., Ozanne, S. E., Reynolds, R. M., and Aiken, C. E. (2021). Efficacy and side effect profile of different formulations of metformin: a systematic review and Meta-analysis. *Diabetes Ther.* 12, 1901–1914. doi: 10.1007/s13300-021-01058-2

Tehrani, R., Montoya, S. E., Van Laar, A. D., Hastings, T. G., and Perez, R. G. (2006). Alpha-synuclein inhibits aromatic amino acid decarboxylase activity in dopaminergic cells. *J. Neurochem.* 99, 1188–1196. doi: 10.1111/j.1471-4159.2006.04146.x

Tian, R., Li, R., Liu, Y., Liu, J., Pan, T., Zhang, R., et al. (2019). Metformin ameliorates endotoxemia-induced endothelial pro-inflammatory responses via AMPK-dependent mediation of HDAC5 and KLF2. *Biochim. Biophys. Acta Mol. Basis Dis.* 1865, 1701–1712. doi: 10.1016/j.bbdis.2019.04.009

Tsai, W.-C., Bhattacharyya, N., Han, L.-Y., Hanover, J. A., and Rechler, M. M. (2003). Insulin inhibition of transcription stimulated by the Forkhead protein Foxo1 is not solely due to nuclear exclusion. *Endocrinology* 144, 5615–5622. doi: 10.1210/en.2003-0481

Turner, M. C., Martin, N. R. W., Player, D. J., Ferguson, R. A., Wheeler, P., Green, C. J., et al. (2020). Characterising hyperinsulinemia-induced insulin resistance in human skeletal muscle cells. *J. Mol. Endocrinol.* 64, 125–132. doi: 10.1530/JME-19-0169

Varoqui, H., and Erickson, J. D. (1996). Active transport of acetylcholine by the human vesicular acetylcholine transporter. *J. Biol. Chem.* 271, 27229–27232. doi: 10.1074/jbc.271.44.27229

Vicente Miranda, H., Szegő, É. M., Oliveira, L. M. A., Breda, C., Darendeliloglu, E., de Oliveira, R. M., et al. (2017). Glycation potentiates α -synuclein-associated neurodegeneration in synucleinopathies. *Brain* 140, 1399–1419. doi: 10.1093/brain/awx056

Vidal-Martinez, G., Yang, B., Vargas-Medrano, J., and Perez, R. G. (2018). Could α -Synuclein modulation of insulin and dopamine identify a novel link between Parkinson's disease and diabetes as well as potential therapies? *Front. Mol. Neurosci.* 11:465. doi: 10.3389/fnmol.2018.00465

Villapol, S. (2018). Roles of peroxisome proliferator-activated receptor gamma on brain and peripheral inflammation. *Cell. Mol. Neurobiol.* 38, 121–132. doi: 10.1007/s10571-017-0554-5

- Vos, M. (2010). Synaptic mitochondria in synaptic transmission and organization of vesicle pools in health and disease. *Front. Synaptic Neurosci.* 2:139. doi: 10.3389/fnsyn.2010.00139
- Wang, W., Wang, Y., Long, J., Wang, J., Haudek, S. B., Overbeek, P., et al. (2012). Mitochondrial fission triggered by hyperglycemia is mediated by ROCK1 activation in podocytes and endothelial cells. *Cell Metab.* 15, 186–200. doi: 10.1016/j.cmet.2012.01.009
- Wang, C., and Youle, R. J. (2009). The role of mitochondria in apoptosis. *Annu. Rev. Genet.* 43, 95–118. doi: 10.1146/annurev-genet-102108-134850
- Warden, A., Truitt, J., Merriman, M., Ponomareva, O., Jameson, K., Ferguson, L. B., et al. (2016). Localization of PPAR isotypes in the adult mouse and human brain. *Sci. Rep.* 6:27618. doi: 10.1038/srep27618
- Wilson, M. A. (2011). The role of cysteine oxidation in DJ-1 function and dysfunction. *Antioxid. Redox Signal.* 15, 111–122. doi: 10.1089/ars.2010.3481
- World Health Organization (2022). Parkinson Disease. Available at: <https://www.who.int/news-room/fact-sheets/detail/parkinson-disease> (Accessed June 14, 2023).
- Xing, H., Liang, C., Wang, C., Xu, X., Hu, Y., and Qiu, B. (2022). Metformin mitigates cholesterol accumulation via the AMPK/SIRT1 pathway to protect osteoarthritis chondrocytes. *Biochem. Biophys. Res. Commun.* 632, 113–121. doi: 10.1016/j.bbrc.2022.09.074
- Xing, B., Liu, M., and Bing, G. (2007). Neuroprotection with pioglitazone against LPS insult on dopaminergic neurons may be associated with its inhibition of NF- κ B and JNK activation and suppression of COX-2 activity. *J. Neuroimmunol.* 192, 89–98. doi: 10.1016/j.jneuroim.2007.09.029
- Xu, Q.-G., Li, X.-Q., Kotecha, S. A., Cheng, C., Sun, H. S., and Zochodne, D. W. (2004). Insulin as an in vivo growth factor. *Exp. Neurol.* 188, 43–51. doi: 10.1016/j.expneurol.2004.03.008
- Yadav, S. K., Singla-Pareek, S. L., Ray, M., Reddy, M. K., and Sopory, S. K. (2005). Methylglyoxal levels in plants under salinity stress are dependent on glyoxalase I and glutathione. *Biochem. Biophys. Res. Commun.* 337, 61–67. doi: 10.1016/j.bbrc.2005.08.263
- Yamamoto, H., Kishi, T., Lee, C. E., Choi, B. J., Fang, H., Hollenberg, A. N., et al. (2003). Glucagon-like Peptide-1-responsive catecholamine neurons in the area Postrema link peripheral glucagon-like Peptide-1 with central autonomic control sites. *J. Neurosci.* 23, 2939–2946. doi: 10.1523/JNEUROSCI.23-07-02939.2003
- Yang, J. W., Raizada, M. K., and Fellows, R. E. (1981). Effects of insulin on cultured rat brain cells: stimulation of ornithine decarboxylase activity. *J. Neurochem.* 36, 1050–1057. doi: 10.1111/j.1471-4159.1981.tb01699.x
- Yaribeygi, H., Sathyapalan, T., and Sahebkar, A. (2019). Molecular mechanisms by which GLP-1 RA and DPP-4i induce insulin sensitivity. *Life Sci.* 234:116776. doi: 10.1016/j.lfs.2019.116776
- Yu, P., Wang, W., Guo, W., Cheng, L., Wan, Z., Cheng, Y., et al. (2023). Pioglitazone-enhanced brown fat whitening contributes to weight gain in diet-induced obese mice. *Exp. Clin. Endocrinol. Diabetes.* doi: 10.1055/a-2178-9113 [Epub ahead of print].
- Zelzer, E. (1998). Insulin induces transcription of target genes through the hypoxia-inducible factor HIF-1 α /ARNT. *EMBO J.* 17, 5085–5094. doi: 10.1093/emboj/17.17.5085
- Zhou, Y., Ma, X.-Y., Han, J.-Y., Yang, M., Lv, C., Shao, Y., et al. (2021). Metformin regulates inflammation and fibrosis in diabetic kidney disease through TNC/TLR4/NF- κ B/miR-155-5p inflammatory loop. *World J. Diabetes* 12, 19–46. doi: 10.4239/wjd.v12.i1.19
- Zhou, S., Sun, Y., Xing, Y., Wang, Z., Wan, S., Yao, X., et al. (2022). Exenatide ameliorates hydrogen peroxide-induced pancreatic β -cell apoptosis through regulation of METTL3-mediated m6A methylation. *Eur. J. Pharmacol.* 924:174960. doi: 10.1016/j.ejphar.2022.174960
- Zhou, Z., Tang, Y., Jin, X., Chen, C., Lu, Y., Liu, L., et al. (2016). Metformin inhibits advanced glycation end products-induced inflammatory response in murine macrophages partly through AMPK activation and RAGE/NF κ B pathway suppression. *J. Diabetes Res.* 2016, 1–10. doi: 10.1155/2016/4847812



OPEN ACCESS

EDITED BY

Andrea Gerbino,
University of Bari Aldo Moro, Italy

REVIEWED BY

Ioannis Tsamedidis,
Aristotle University of Thessaloniki,
Greece
Maria Giulia Lionetto,
University of Salento, Italy

*CORRESPONDENCE

Alessia Remigante,
✉ aremigante@unime.it

[†]These authors have contributed equally
to this work

[†]These authors shared senior authorship

RECEIVED 28 September 2023

ACCEPTED 22 November 2023

PUBLISHED 04 December 2023

CITATION

Remigante A, Spinelli S, Patanè GT,
Barreca D, Straface E, Gambardella L,
Bozzuto G, Caruso D, Falliti G, Dossena S,
Marino A and Morabito R (2023), AAPH-
induced oxidative damage reduced anion
exchanger 1 (SLC4A1/AE1) activity in
human red blood cells: protective effect
of an anthocyanin-rich extract.
Front. Physiol. 14:1303815.
doi: 10.3389/fphys.2023.1303815

COPYRIGHT

© 2023 Remigante, Spinelli, Patanè,
Barreca, Straface, Gambardella, Bozzuto,
Caruso, Falliti, Dossena, Marino and
Morabito. This is an open-access article
distributed under the terms of the
[Creative Commons Attribution License
\(CC BY\)](https://creativecommons.org/licenses/by/4.0/). The use, distribution or
reproduction in other forums is
permitted, provided the original author(s)
and the copyright owner(s) are credited
and that the original publication in this
journal is cited, in accordance with
accepted academic practice. No use,
distribution or reproduction is permitted
which does not comply with these terms.

AAPH-induced oxidative damage reduced anion exchanger 1 (SLC4A1/AE1) activity in human red blood cells: protective effect of an anthocyanin-rich extract

Alessia Remigante^{1*†}, Sara Spinelli^{1†}, Giuseppe Tancredi Patanè¹,
Davide Barreca¹, Elisabetta Straface², Lucrezia Gambardella²,
Giuseppina Bozzuto³, Daniele Caruso⁴, Giuseppe Falliti⁴,
Silvia Dossena⁵, Angela Marino^{1†} and Rossana Morabito^{1†}

¹Department of Chemical Biological, Pharmaceutical and Environmental Sciences, University of Messina, Messina, Italy, ²Biomarkers Unit, Center for Gender-Specific Medicine, Istituto Superiore di Sanità, Rome, Italy, ³National Center for Drug Research and Evaluation, Istituto Superiore di Sanità, Rome, Italy, ⁴Complex Operational Unit of Clinical Pathology of Papardo Hospital, Messina, Italy, ⁵Institute of Pharmacology and Toxicology, Paracelsus Medical University, Salzburg, Austria

Introduction: During their lifespan in the bloodstream, red blood cells (RBCs) are exposed to multiple stressors, including increased oxidative stress, which can affect their morphology and function, thereby contributing to disease.

Aim: This investigation aimed to explore the cellular and molecular mechanisms related to oxidative stress underlying anion exchanger 1 activity (band 3, SLC4A1/AE1) in human RBCs. To achieve this aim, the relationship between RBC morphology and functional and metabolic activity has been explored. Moreover, the potential protective effect of an anthocyanin-enriched fraction extracted from *Callistemon citrinus* flowers was studied.

Methods: Cellular morphology, parameters of oxidative stress, as well as the anion exchange capability of band 3 have been analyzed in RBCs treated for 1 h with 50 mM of the pro-oxidant 2,2'-azobis (2-methylpropionamide)-dihydrochloride (AAPH). Before or after the oxidative insult, subsets of cells were exposed to 0.01 µg/mL of an anthocyanin-enriched fraction for 1 h.

Results: Exposure to AAPH caused oxidative stress, exhaustion of reduced glutathione, and over-activation of the endogenous antioxidant machinery, resulting in morphological alterations of RBCs, specifically the formation of acanthocytes, increased lipid peroxidation and oxidation of proteins, as well as abnormal distribution and hyper-phosphorylation of band 3. Expected, oxidative stress was also associated with a decreased band 3 ion transport activity and an increase of oxidized haemoglobin, which led to abnormal clustering of band 3. Exposure of cells to the anthocyanin-enriched fraction prior to, but not after, oxidative stress efficiently counteracted oxidative stress-related alterations. Importantly, protection of band3 function from oxidative stress could only be achieved in intact cells and not in RBC ghosts.

Conclusion: These findings contribute a) to clarify oxidative stress-related physiological and biochemical alterations in human RBCs, b) propose anthocyanins as natural antioxidants to neutralize oxidative stress-related

modifications, and 3) suggest that cell integrity, and therefore a cytosolic component, is required to reverse oxidative stress-related pathophysiological derangements in human mature RBCs.

KEYWORDS

oxidative stress, erythrocytes, anthocyanins, anion, exchange, methemoglobin

1 Introduction

Human red blood cells (RBC) have maximized their functional capacity to transport and deliver oxygen to tissues and cells of the body through the progressive loss of the cytoplasmic organelles, including nuclei, which occurs during their maturation process from erythroid precursors to reticulocytes, and ultimately, to mature biconcave RBCs (Moras et al., 2017). As a result, each mature RBC encloses about 250–270 hemoglobin million copies, which account for 98% of the cytosolic proteome (D'Alessandro and Zolla, 2017). At full oxygen saturation, mature RBCs can carry up to 1 billion molecules of oxygen/cell (Mohanty et al., 2014). Therefore, the major endogenous source of intracellular reactive species in RBCs is the slow auto-oxidation of haemoglobin, which produces non-functional methaemoglobin and superoxide radicals that rapidly dismutate to form hydrogen peroxide (H_2O_2) (Fujii et al., 2021). In addition, exogenous reactive molecules can be released in the bloodstream by macrophages, neutrophils, and endothelial cells (Pretini et al., 2019). Oxidative damage to any of the biological macromolecules (Akki et al., 2018; Akki et al., 2022) of RBCs can affect the integrity and stability of their cellular structure and their functional and metabolic activity (Xiong et al., 2013; Vona et al., 2019; D'Alessandro et al., 2021). Lipid peroxidation is one of the most damaging reactions of free radicals in RBCs. It is well documented that lipid peroxidation is the outcome of the oxidation of membrane polyunsaturated fatty acids (PUFA), which interferes with the canonical structure and physiological functions of the RBC plasma membrane. These oxidative events generate hydroperoxides and secondary products that ultimately result in structural disruption of cell-surface lipid bilayer and protein carbonylation and/or protein thiol oxidation of plasma membrane-bound proteins (Pandey and Rizvi, 2011; Contreras-Puentes et al., 2019; Zhang et al., 2019; Amezcaga et al., 2020; Akki et al., 2022; Remigante and Morabito, 2022).

Since RBCs are larger than the diameter of capillaries in the micro-circulation, they have to deform and squeeze into blood capillaries to deliver oxygen to the cells and tissues of the body as needed (Ebrahimi and Bagchi, 2022). In this context, oxidative damage to the plasma membrane as well as cytoskeletal proteins impairs the rheologic properties of circulating RBCs (Mazzulla et al., 2015). These abnormalities include i) decreased deformability, ii) increased membrane micro-viscosity, and iii) increased RBC aggregation (Maruyama et al., 2022). There is a number of investigations showing that injury at the level of the plasma membrane and cytoskeletal proteins impairs RBC deformability. To name just a few examples, Jiang and co-authors proved that increased spectrin glycosylation induced by augmented intracellular oxidative stress condition led to deformability abnormalities in rat diabetic RBCs, which is not surprising, as diabetes generates oxygen free radicals (Jiang et al., 1990). Additionally, a recent study performed

by Spinelli and collaborators demonstrated that oxidative stress related to natural aging impaired human RBCs deformability, resulting in structural rearrangements of the membrane cytoskeleton-associated proteins spectrin, ankyrin, and protein 4.1, and increased tyrosine phosphorylation of plasma membrane-bound band 3 protein (Vallese et al., 2022). Band 3 (SLC4A1/AE1) (Remigante et al., 2022b), the most abundant RBC membrane protein, possesses two different cytosolic domains (Arakawa et al., 2015). At high oxygen saturation, the N-terminal domain can serve as an inhibitory docking site for glycolytic enzymes. On the contrary, at low oxygen saturation, deoxyhemoglobin competes with the glycolytic enzymes and displaces them from the plasma membrane to boost glycolysis and stimulate both ATP and 2,3-diphosphoglycerate production. Prolonged oxidant stress, for example, during RBC storage in blood banks, triggers proteolysis of the band 3 N-terminal domain, thus provoking the loss of this RBC oxygen-dependent metabolic modulation pathway (Mandal et al., 2003; Rinalducci et al., 2012; Matte et al., 2013). Moreover, oxidative stress-related events are well known to cross-link band 3 dimers and tetramers and, also, band 3 and haemoglobin, thus leading to the formation of high molecular mass aggregates (Rinalducci et al., 2012). On the other hand, the C-terminal domain contains the anion-transport functional region that mediates the chloride-bicarbonate exchange across the RBC membrane (Reithmeier et al., 2016). Membrane ionic transport systems, including band 3, are involved in the maintenance of cellular homeostasis during exposure to stressors and are therefore accurately regulated to respond to stress conditions (Remigante et al., 2021a).

To cope with the oxidative stress effects, RBCs have developed extensive endogenous antioxidant machinery involving both non-enzymatic antioxidants, such as glutathione, and enzymatic antioxidants, including catalase, superoxide dismutase, peroxiredoxin-2, and glutathione peroxidase (Martemucci et al., 2022). Also, natural secondary metabolites with antioxidant properties might play a protective function in this context. Multiple polyphenol-rich extracts of plant origin have been proven as an excellent and workable alternative for supporting intracellular antioxidant defense during elevated oxidative stress owing to their activity as ROS scavengers and/or inhibitors (Niedzwiecki et al., 2016; Kouka et al., 2017; Philip et al., 2019; Luo et al., 2021; Monjotin et al., 2022). By definition, antioxidants are molecules capable of inhibiting and/or quenching free radical reactions in order to delay or prevent cellular injury. In this context, an anthocyanin-enriched fraction extracted from *Callistemon citrinus* (Curtis, sheels), which is an ornamental and medicinal plant from the *Myrtaceae* family, showed antioxidant power *in vitro* and in cell-based assays (Lagana et al., 2020). Anthocyanins are water-soluble pigments belonging to the polyphenol class of compounds and are responsible for conferring red colors to flowers. The study of the constituents of

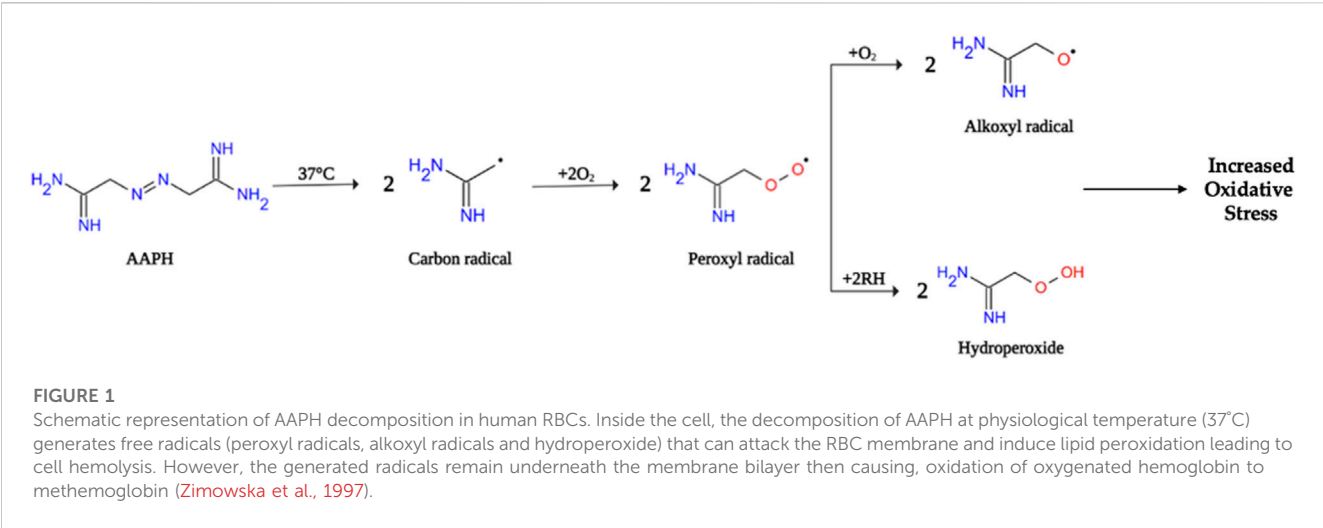


TABLE 1 Identification and quantification of anthocyanin profile of the anthocyanin-enriched fraction by RP-HPLC-DAD analysis. Results are expressed as mean \pm SD of three independent experiments (n = 3), and are quantified as mg cyanidin-3-O-glucoside equivalents (CyG) per 100 gr of dry extract (DE).

PEAK	Compound	Rt (min)	mg CyG/100 g DE
1	Cyanidin 3,5-O-diglucoside	17.8	305.13 \pm 2.82
2	Peonidin-3,5-O-diglucoside	20.3	172.06 \pm 1.10
3	Cyanidin-3-O-glucoside	22.5	43.07 \pm 0.61
4	Cyanidin-coumaroylglucoside-pyruvic acid	25.3	9.75 \pm 0.17

therapeutic plants is of great value and essential for identifying novel antioxidants (Larayetan et al., 2017; Maury et al., 2020; Nishikito et al., 2023). However, the molecular mechanisms underlying the antioxidant action of polyphenol compounds in human RBCs have not yet been fully clarified and are still a matter of considerable debate.

Among the various cell-based models of oxidative stress, 2,2'-azobis (2-methylpropionamide)-dihydrochloride (AAPH)-stimulated RBCs represent a useful system to study oxidative stress-related pathological states affecting the integrity of human RBC and leading to multi-organ dysfunction, such as haemolytic anemia, vaso-occlusion, chronic inflammation, and tissue damage (Zheng et al., 2016) (Figure 1). Thus, the present investigation aimed to explore the cellular and molecular mechanisms related to oxidative stress underlying anion exchanger 1 (band 3) activity in human RBCs. To achieve this aim, the relationship between RBC morphology, integrity, and functional activity has been explored. Moreover, the potential protective effect of an anthocyanin-enriched fraction extracted from *Callistemon citrinus* flowers was studied.

2 Results

2.1 Determination and quantification of phenolic compounds

An acidified ethanolic extract from *Callistemon citrinus* flowers was submitted to reverse phase high performance liquid

chromatography coupled with diode array detection (RP-HPLC-DAD). The compounds found in the anthocyanin-enriched fraction are reported in Table 1. The inspection of UV spectra recorded between 200 and 800 nm, and simultaneous detection by diode array performed at 260, 290, 330, 370, and 520 nm only showed the presence of anthocyanin compounds in significant amounts, which was in agreement with literature data previously published by our group (Lagana et al., 2020), in particular: cyanidin-3,5-O-diglucoside (cyanin, 1); peonidin-3,5-O-diglucoside (peonin, 2); cyanidin-3-O-glucoside (3) and cyanidin-coumaroylglucoside-pyruvic acid (4). The most abundant compound was, by far, cyanidin-3,5-O-diglucoside (305.13 \pm 2.82 mg/100 g DE) followed by peonidin-3,5-O-diglucoside and cyanidin-3-O-glucoside (172.06 \pm 1.10 and 43.07 \pm 0.61 mg/100 g DE, respectively), while the last compound (cyanidin-coumaroylglucoside-pyruvic acid) was present in significantly lower amount with respect to the other derivatives (9.75 \pm 0.17 mg/100 g DE). Peak identity was confirmed by comparing their retention times and absorption spectra with those of pure ($\geq 99\%$) commercially available standards and comparison with literature data.

2.2 Anthocyanin-enriched fraction prevents cell shape modifications in AAPH-Incubated RBCs

In the present investigation, the first step was to assay a broad range of concentrations (from 0.01 μ g/mL to 100 μ g/mL) of an

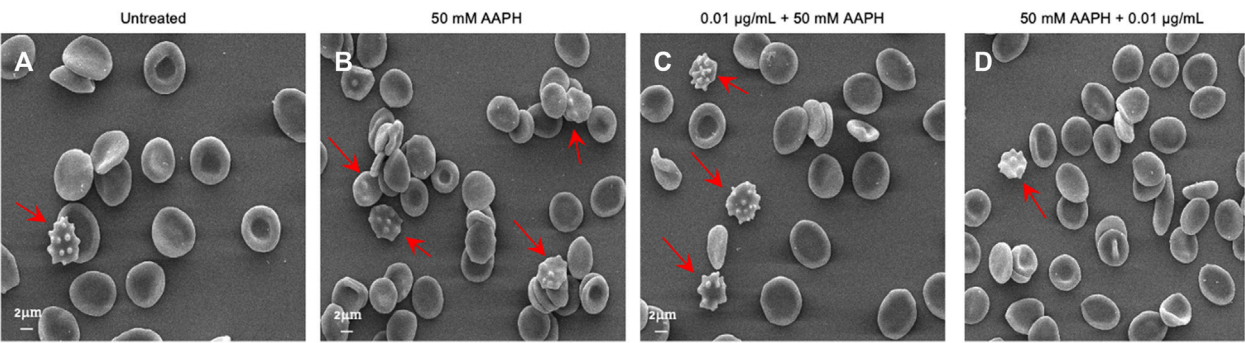


FIGURE 2
Evaluation of RBC morphology. Representative SEM images showing human RBCs with a canonical biconcave shape (A) untreated cells; (B) acanthocytes (arrows) after treatment with 50 mM AAPH (for 1 h, at 37°C); (C). Pre-incubation with anthocyanin-enriched fraction (0.01 µg/mL for 1 h, at 37°C) still showed a remarkable cell morphology modification. On the contrary, (D) post-treatment with anthocyanin-enriched fraction (0.01 µg/mL for 1 h, at 37°C) attenuated the morphological changes compared to 50 mM AAPH exposure. Magnification 1,500x.

TABLE 2 Percentage of morphological alterations in RBCs left untreated or treated as reported. Data are presented as means ± S.E.M. from three independent experiments, where ns, not statistically significant versus untreated and 50 mM AAPH; ****p* < 0.001 versus untreated; *p* < 0.001 versus 50 mM AAPH, one-way ANOVA followed by Bonferroni’s multiple comparison post-hoc test.

Experimental conditions	Acanthocytes
Untreated	5% ± 1
50 mM AAPH	23% ± 3***
0.01 µg/mL Extract + 50 mM AAPH	21% ± 0.1 ^{ns}
50 mM AAPH + 0.01 µg/mL Extract	9% ± 0.5 ^{ns}

anthocyanin-enriched fraction as well as different incubation time intervals (30 min, 1 h, and 2 h), to exclude any damage in terms of haemolysis, lipid peroxidation, and protein oxidation, including the production of MetHb, which could be potentially provoked by direct exposure of RBCs to the extract (Supplementary Figure S1). This experimental procedure points to the importance of carefully establishing the proper concentration and incubation time for testing novel potential antioxidant compounds in cell-based assays. Based on these considerations, we selected a 1 h pre- and post-treatment with 0.01 µg/mL anthocyanin-enriched fraction, in order to estimate its potential antioxidant capacity.

Based on these results, as shown in Figure 2, treatment for 1 h at 37°C with 50 mM AAPH provoked morphological changes in human RBCs. Indeed, in these experimental conditions, 23% of acanthocytes (surface blebs) were reported by scanning electron microscopy analysis. However, in samples pre-incubated with 0.01 µg/mL anthocyanin-enriched fraction (for 1 h, at 37°C) and then treated with 50 mM AAPH (1 h, at 37°C), the percentage of morphologically modified cells was reduced to 21%. Therefore, the generation of acanthocytes was not completely avoided by the pre-treatment with the anthocyanin-enriched fraction (Table 2). On the contrary, in human RBCs incubated with 50 mM AAPH and then exposed to 0.01 µg/mL anthocyanin-enriched fraction, we only noticed 9% of acanthocytes.

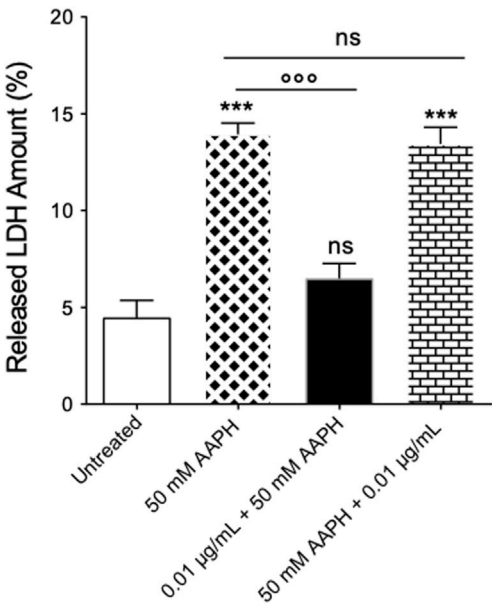
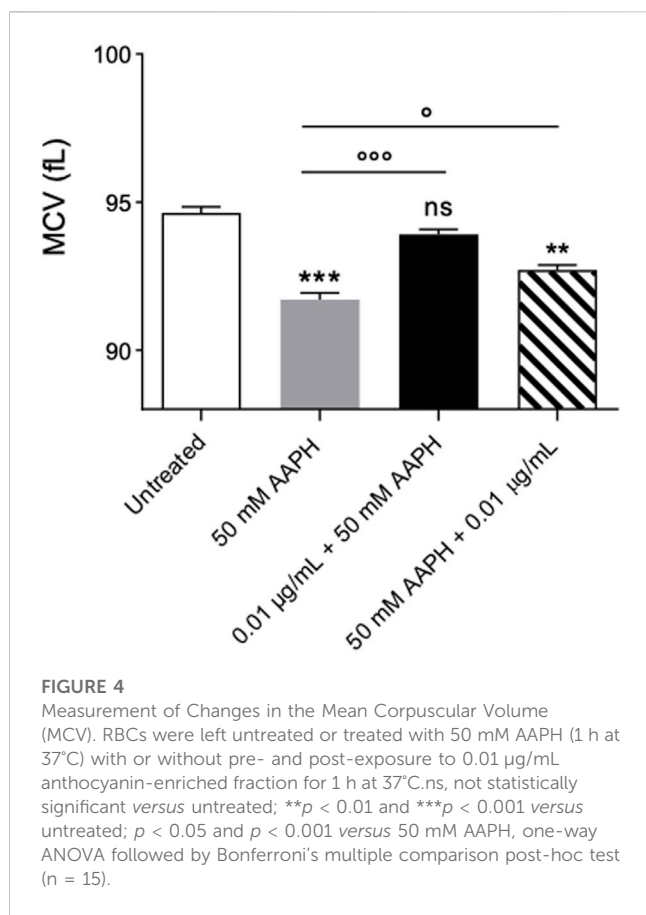


FIGURE 3
Determination of released LDH amount. Released LDH amounts were detected in RBCs left untreated or incubated with 50 mM AAPH (1 h at 37°C) with or without pre- and post-exposure to the anthocyanin-enriched fraction (0.01 µg/mL) for 1 h at 37°C. ns, not statistically significant versus control (untreated) cells and 50 mM AAPH; ****p* < 0.001 versus untreated; *p* < 0.001 versus 50 mM AAPH, one-way ANOVA followed by Tukey’s test (*n* = 3).

2.3 Determination of released lactate dehydrogenase (LDH) amount

As expected, in RBCs treated with 50 mM AAPH (1 h at 37 °C), a moderate (about 1.8-fold) increase of released LDH was observed compared to cells left untreated (Figure 3). However, pre-exposure of cells to 0.01 µg/mL anthocyanin-enriched fraction (1 h at 37 °C) significantly decreased the amount of LDH released. On the contrary, in RBCs first exposed to 50 mM AAPH (1 h at 37°C)



and then incubated with the anthocyanin-enriched fraction (0.01 µg/mL for 1 h at 37°C), the LDH amount released was not different compared to that measured in RBCs treated with 50 mM AAPH. The anthocyanin-enriched fraction alone did not affect the released LDH amount (data not shown).

2.4 Measurements of the mean corpuscular volume (MCV)

Figure 4 reports MCV values measured in left untreated RBCs or treated with 50 mM AAPH (1 h, at 37°C) with or without pre- or post-treatment with anthocyanin-enriched fraction (0.01 µg/mL) for 1 h at 37°C. This parameter is a surrogate measure of the average cellular size. In human RBCs treated with 50 mM AAPH, MCV was significantly lower than those measured in untreated cells. On the contrary, the MCV values in RBCs pre-treated with anthocyanin-enriched fraction were statistically higher than those measured in 50 mM AAPH-treated cells. Instead, the post-treatment with anthocyanin extract was ineffective. Anthocyanin-enriched fraction alone did not affect such parameter.

2.5 Oxidative stress assessment

2.5.1 Evaluation of intracellular ROS levels

The measurement of ROS levels was performed by flow cytometry in RBCs that were left untreated or, alternatively,

exposed to 50 mM AAPH for 1 h at 37°C with or without pre- or post-exposure to the anthocyanin extract (0.01 µg/mL) for 1 h at 37°C. Figure 5A displays the intracellular ROS levels. Blood samples incubated with AAPH showed a significant increase of intracellular ROS levels compared to untreated samples. In samples exposed to the anthocyanin extract before or after exposure to AAPH, ROS levels were significantly reduced. Notably, in samples first treated with AAPH and successively exposed to the anthocyanin extract, ROS levels did not differ from those of control RBCs. As expected, in RBCs exposed to 20 mM H₂O₂ for 1 h at 25°C, the intracellular ROS content was significantly higher than that of control RBCs, whereas the anthocyanin extract (0.01 µg/mL) alone did not affect the production of intracellular ROS (data not shown).

2.5.2 Measurement of thiobarbituric-acid-reactive substances (TBARS) levels

Figure 5B shows the TBARS levels in RBCs left untreated or, alternatively, treated with 50 mM AAPH for 1 h at 37°C with or without pre- or post-exposure to the anthocyanin extract (0.01 µg/mL) for 1 h at 37°C. As expected, TBARS levels of RBCs treated with 20 mM H₂O₂ for 1 h were significantly higher than those of untreated RBCs. In parallel, in RBCs pre-incubated with the anthocyanin extract and then treated with AAPH, TBARS production, although significantly reduced compared to RBCs treated with AAPH alone, remained significantly elevated compared to control values. Conversely, in RBCs first incubated with AAPH and then exposed to the anthocyanin extract, TBARS levels were not significantly different from control values. Of note, anthocyanin extract alone did not affect TBARS levels (data not shown).

2.5.3 Measurement of total sulfhydryl group content

Figure 5C displays the total content of sulfhydryl groups in RBCs left untreated or treated with either the oxidizing compound NEM (2 mM for 1 h at 25°C) as the positive control or 50 mM AAPH for 1 h at 37°C with or without pre- or post-treatment with the anthocyanin extract (0.01 µg/mL) for 1 h at 37°C. NEM incubation led to a significant reduction in sulfhydryl group content compared to control values. Sulfhydryl groups were also significantly reduced in AAPH-treated RBCs. Pre- and post-treatment with the anthocyanin extract completely restored the total levels of sulfhydryl groups. Noteworthy, the anthocyanin extract alone did not induce oxidation of sulfhydryl groups (data not shown).

2.5.4 Evaluation of methemoglobin (MetHb) levels

Figure 5D displays the MetHb levels measured in RBCs left untreated or treated with 50 mM AAPH for 1 h at 37°C with or without pre- or post-treatment with the anthocyanin extract (0.01 µg/mL) for 1 h at 37°C, or alternatively, exposed to the well-known MetHb-forming compound NaNO₂ (4 mM for 1 h at 25°C). Methemoglobin levels measured after treatment with NaNO₂ were significantly higher than those detected in untreated RBCs. Alongside, MetHb levels measured after exposure to AAPH were significantly higher than those measured in untreated cells, while both pre- and post-treatment with the anthocyanin extract significantly reduced the production of MetHb levels. The anthocyanin extract alone did not affect MetHb levels.

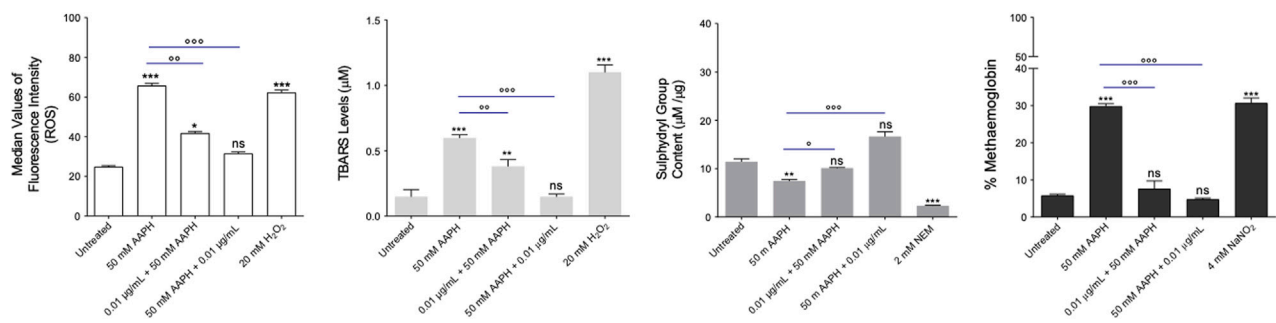


FIGURE 5

Evaluation of oxidative stress. **(A)** Detection of ROS levels. ROS levels were detected in RBCs left untreated or treated with 50 mM AAPH for 1 h at 37°C with or without pre- or post-exposure to the anthocyanin extract (0.01 µg/mL) for 1 h at 37°C. 20 mM H₂O₂ (1 h at 37°C) was used as the positive control. ns, not statistically significant *versus* control (untreated); ****p* < 0.001 *versus* control, *p* < 0.01 and *p* < 0.001 *versus* 50 mM AAPH, one-way ANOVA followed by Bonferroni's post-hoc test (*n* = 15). **(B)** Estimation of TBARS levels. TBARS levels (µM) were detected in RBCs left untreated or treated with 50 mM AAPH for 1 h at 37°C with or without pre- or post-exposure to the anthocyanin extract (0.01 µg/mL) for 1 h at 37°C. 20 mM H₂O₂ (1 h at 37°C) was used as the positive control. ns, not statistically significant *versus* control; ***p* < 0.01 and ****p* < 0.001 *versus* control; *p* < 0.01 and *p* < 0.001 *versus* 50 mM AAPH, one-way ANOVA followed by Bonferroni's post-hoc test (*n* = 15). **(C)** Evaluation of sulphydryl group content (µM TNB/µg protein) was detected in RBCs left untreated and in RBCs treated with 50 mM AAPH for 1 h at 37°C with or without pre-or post-exposure to the anthocyanin extract (0.01 µg/mL) for 1 h at 37°C. NEM (2 mM for 1 h at 37°C) was used as a positive control. ns, not statistically significant *versus* control; ****p* < 0.001 *versus* control, *p* < 0.01 and *p* < 0.001 *versus* 50 mM AAPH, one-way ANOVA followed by Bonferroni's post-hoc test (*n* = 15). **(D)** Determination of MetHb (%) levels. MetHb levels were detected in RBCs left untreated or incubated with 50 mM AAPH (1 h, 37°C) with or without pre- or post-exposure to the anthocyanin extract (0.01 µg/mL) for 1 h at 37°C. NaNO₂ (4 mM for 1 h at 37°C) was used as the positive control. ns, not statistically significant; ****p* < 0.001 *versus* control; *p* < 0.001 *versus* 50 mM AAPH, one way ANOVA followed by Bonferroni's post-hoc test (*n* = 15).

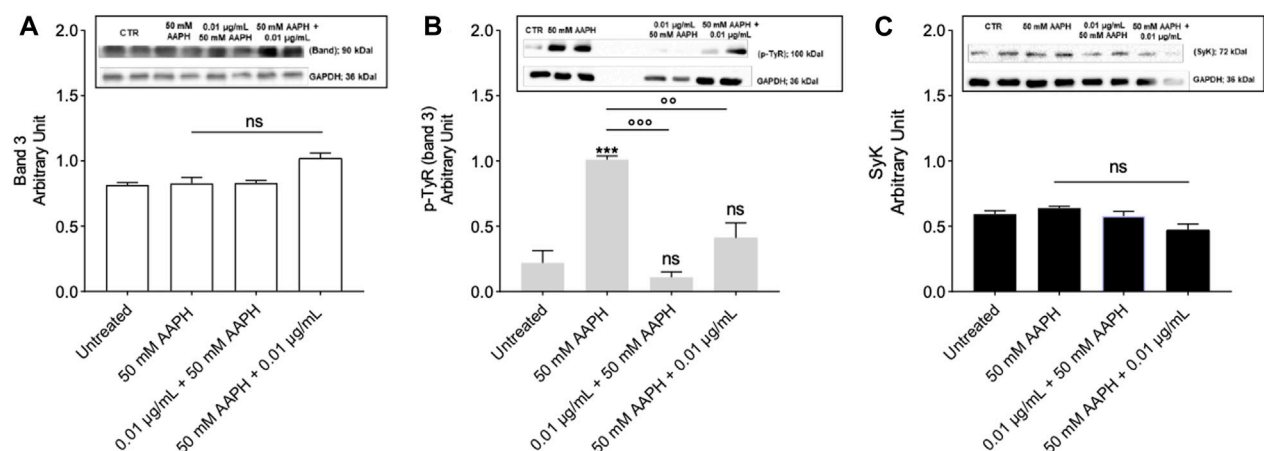


FIGURE 6

Measurement of Protein Levels by Western blot Analysis. **(A)** Band 3 levels in human RBCs left untreated or exposed to 50 mM AAPH for 1 h at 37°C with or without exposure to 0.01 µg/mL anthocyanin-enriched fraction for 1 h at 37°C; ns not statistically significant *versus* control (untreated), one-way ANOVA followed by Bonferroni's multiple comparison post-hoc test (*n* = 3). **(B)** p-Tyr (tyrosine) levels in RBCs left untreated or exposed to 50 mM AAPH for 1 h at 37°C with or without exposure to 0.01 µg/mL anthocyanin-enriched fraction for 1 h at 37°C. ns, not statistically significant; ****p* < 0.001 *versus* untreated; *p* < 0.01 and *p* < 0.001 *versus* 50 mM AAPH, one-way ANOVA followed by Bonferroni's multiple comparison post-hoc test (*n* = 3). **(C)** SyK levels in RBCs left untreated or exposed to 50 mM AAPH for 1 h at 37°C with or without exposure to 0.01 µg/mL anthocyanin-enriched fraction for 1 h at 37°C; ns not statistically significant *versus* control, one way ANOVA followed by Bonferroni's post-hoc test (*n* = 3).

2.6 Detection of protein expression by western blotting analysis

2.6.1 Detection of band 3 protein levels

Figure 6A shows the levels of band 3 in human RBCs treated with 50 mM AAPH for 1 h at 37°C with or without pre-exposure to 0.01 µg/mL anthocyanin extract for 1 h at 37°C. In all conditions

tested, band 3 levels were not significantly different with respect to those determined in untreated RBCs.

2.6.2 Detection of band 3 tyrosine phosphorylation and SyK kinase levels

Figure 6B reports both tyrosine phosphorylation (p-Tyr) levels of band 3 and SyK kinase levels in human RBCs incubated with 50 mM

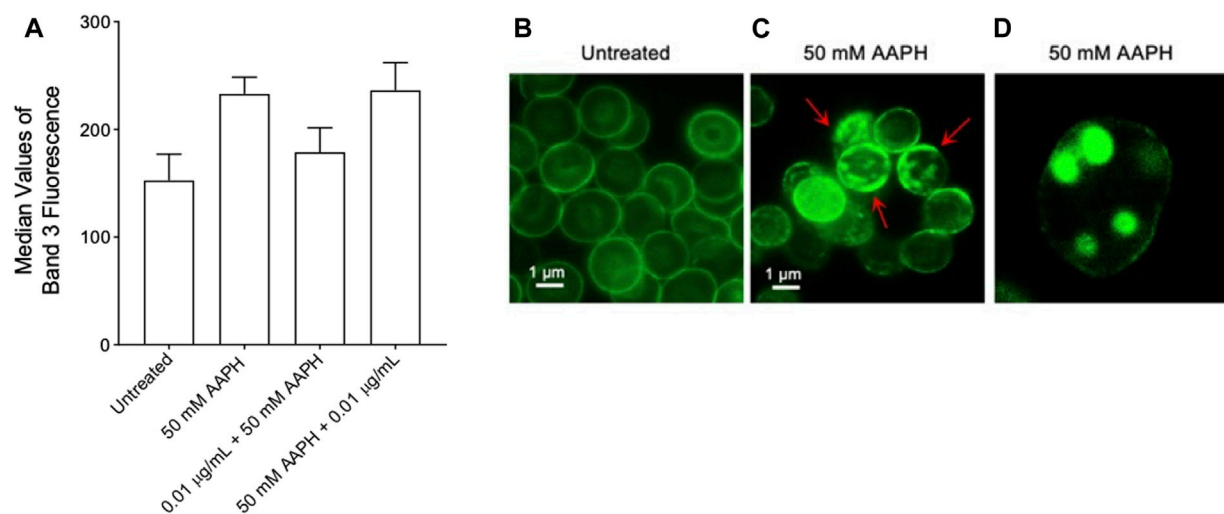


FIGURE 7

Flow cytometry immunofluorescence of band 3 levels. Red blood cells were left untreated or treated with 50 mM AAPH for 1 h at 37°C, with or without pre- and post-exposure to 0.01 µg/mL anthocyanin-enriched fraction for 1 h at 37°C. (A) Histograms reporting median values of fluorescence intensity. (B–D) Flow cytometry immunofluorescence representative micrographs showing band 3 distribution in untreated RBCs and RBCs treated with 50 mM AAPH. Samples were observed with a $\times 100$ objective. (B) Significant morphological changes in 50 mM AAPH-treated RBCs were reported (red arrows). (C) Hemichromes formation is reported (7,000 \times magnification). ns, not statistically significant versus untreated, ANOVA followed by Bonferroni's multiple comparison post-test ($n = 10$).

AAPH for 1 h at 37°C with or without pre-incubation with the anthocyanin-enriched fraction (0.01 µg/mL) for 1 h at 37°C. Exposure of RBCs to AAPH caused an intense band 3 phosphorylation (Figure 6B). Importantly, treatment with the anthocyanin-enriched fraction before or after exposure to 50 mM AAPH prevented the increase of tyrosine phosphorylation of band 3 (Figure 6B). Anthocyanin-enriched fraction alone did not significantly affect tyrosine phosphorylation levels (data not shown). In parallel, Syk kinase, which is responsible for the phosphorylation of band 3, was detected (Figure 6C). No Syk kinase expression changes were detected in human RBCs treated with 50 mM AAPH, or alternatively, exposed to the anthocyanin-enriched fraction before or after exposure to AAPH. Also, anthocyanin-enriched fraction alone did not significantly modify Syk kinase expression (data not shown).

2.7 Band 3 exposition level determination by flow cytometry analysis

Expression levels of band 3 (median values of fluorescence obtained by flow cytometry) observed in human RBCs exposed to the anthocyanin-enriched fraction or to AAPH were comparable to those reported in untreated RBCs (Figure 7A). Although data were not statistically significant, an increased exposition of band 3 was detected in human RBCs treated with 50 mM AAPH for 1 h at 37°C with respect to untreated cells. Representative immunofluorescence images of band 3 distribution in untreated cells (left panel) and in 50 mM AAPH-treated RBCs (middle and right panels) are shown, respectively. Results demonstrated that band 3 was mainly clustered (red arrows) in acanthocytes after 50 mM AAPH treatment with respect to untreated RBCs (Figure 8B). Moreover, band 3 exposition was not altered by the anthocyanin-enriched fraction given alone (data not shown).

2.8 Measurement of SO_4^{2-} uptake through band 3 in intact RBCs

Figure 8 shows the SO_4^{2-} uptake as a function of time in RBCs untreated and in RBCs treated with 50 mM AAPH for 1 h at 37°C with or without pre- or post-treatment with 0.01 µg/mL anthocyanin-enriched fraction for 1 h at 37°C. In untreated samples, SO_4^{2-} uptake gradually increased and reached equilibrium within 45 min ($0.057 \pm 0.001 \text{ min}^{-1}$). Blood samples treated with the anthocyanin-enriched fraction alone showed a rate constant of SO_4^{2-} uptake not significantly different with respect to control (data not shown). On the contrary, the rate constant ($0.046 \pm 0.001 \text{ min}^{-1}$) in RBCs treated with AAPH was significantly decreased with respect to control ($***p < 0.001$). Notably, in RBCs pre-incubated with the anthocyanin-enriched fraction and then treated with 50 mM AAPH, the rate constant ($0.060 \pm 0.001 \text{ min}^{-1}$) was significantly higher ($p < 0.001$) than that of RBCs treated with AAPH alone and was not significantly different with respect to control (Table 3). In contrast, in RBCs first incubated with AAPH and then treated with the anthocyanin-enriched fraction, the rate constant ($0.041 \pm 0.001 \text{ min}^{-1}$) was not significantly different with respect to that of RBCs treated with AAPH alone (Table 3). SO_4^{2-} uptake via band 3 was almost totally blocked by DIDS (10 µM) applied at the beginning of incubation in SO_4^{2-} medium ($0.04 \pm 0.001 \text{ min}^{-1}$, $***p < 0.001$, Table 3). In addition, the SO_4^{2-} amount internalized by AAPH-treated RBCs after 45 min of incubation in SO_4^{2-} medium was significantly lower than untreated (Table 3). Conversely, the SO_4^{2-} amount internalized by RBCs pre-incubated with the anthocyanin-enriched fraction and then exposed to AAPH was not significantly different compared to that measured in untreated RBCs (Table 3). In DIDS-treated samples, the SO_4^{2-} amount internalized was significantly lower than that of both untreated and treated RBCs ($***p < 0.001$, Table 3).

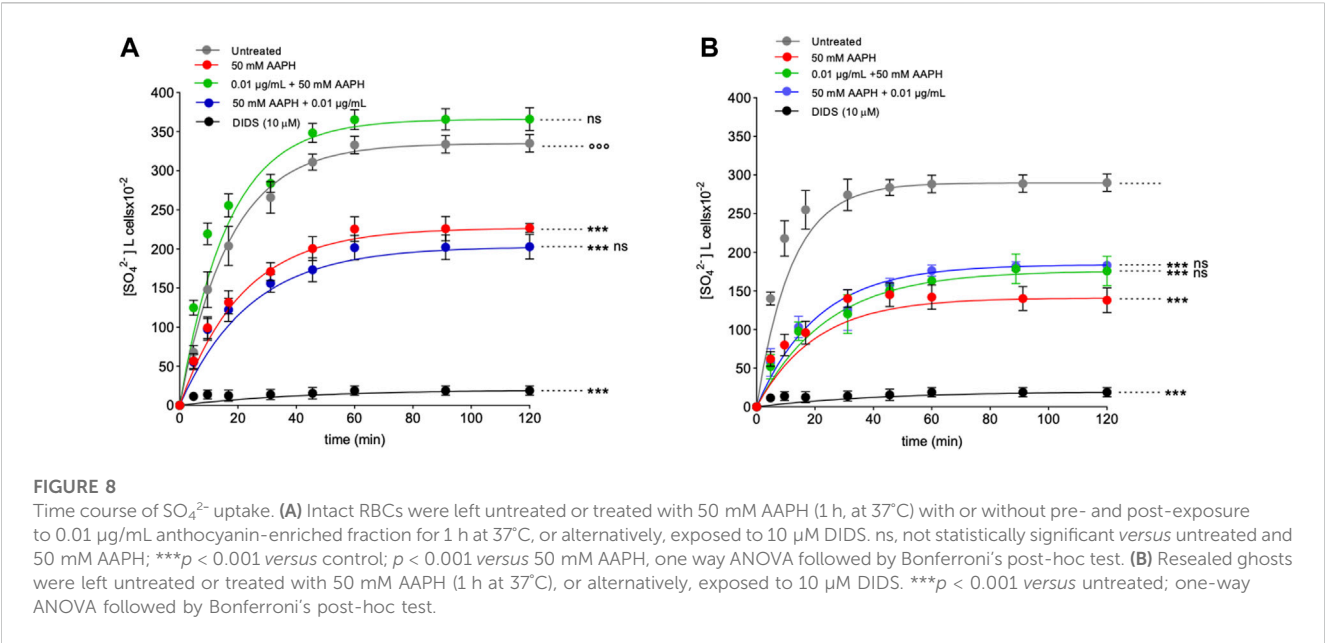


TABLE 3 Rate constant of SO_4^{2-} uptake and amount of SO_4^{2-} trapped in human RBCs untreated and RBCs treated as indicated. Results are presented as means \pm SEM, from separate experiments (n), where ns, not statistically significant versus untreated and/or 50 mM AAPH; *** $p < 0.001$ versus untreated (intact RBCs, or alternatively, in resealed ghosts); $p < 0.001$ versus 50 mM AAPH, one-way ANOVA followed by Bonferroni's multiple comparison post-hoc test.

Experimental conditions	Rate constant (min ⁻¹)	TIME (min)	n	SO_4^{2-} amount trapped after 45 min of incubation IN SO_4^{2-} medium [SO ₄ ²⁻] I cells x 10 ⁻²
INTACT RBCS				
Untreated	0.057 \pm 0.001	17.16	10	311 \pm 8.95
50 mM AAPH	0.046 \pm 0.001***	21.44	10	200 \pm 10.25***
0.01 $\mu\text{g/mL}$ Extract + 50 mM AAPH	0.060 \pm 0.003 ^{ns}	16.43	10	348 \pm 18.65 ^{ns}
50 mM AAPH + 0.01 $\mu\text{g/mL}$ Extract	0.041 \pm 0.002 ^{ns,***}	23.8	10	173 \pm 11.37 ^{ns,***}
10 μM DIDS	0.024 \pm 0.001***	41.66	10	15.5 \pm 0.37***
RESEALED GHOSTS				
Untreated	0.049 \pm 0.001***	12.01	10	284 \pm 0.35
50 mM AAPH	0.082 \pm 0.002***	20.40	10	142.3 \pm 0.50***
0.01 $\mu\text{g/mL}$ Extract + 50 mM AAPH	0.048 \pm 0.002 ^{***, ns}	20.62	10	158.05 \pm 0.42 ^{***,ns}
50 mM AAPH + 0.01 $\mu\text{g/mL}$ Extract	0.041 \pm 0.002 ^{***, ns}	23.87	10	150.05 \pm 0.32 ^{***,ns}
10 μM DIDS	0.023 \pm 0.001***	43.47	10	14.3 \pm 0.29***

2.8.1 Measurement of SO_4^{2-} uptake through band 3 in resealed ghosts

Figure 8B reports the time course of SO_4^{2-} uptake in resealed ghosts. The rate constant of SO_4^{2-} uptake (0.082 \pm 0.002 min⁻¹, Table 3) in RBCs treated with 50 mM AAPH (1 h, at 37°C) was significantly decreased with respect to untreated RBCs (0.049 \pm 0.001, *** $p < 0.001$, Table 3). SO_4^{2-} uptake via band 3 was almost totally blocked by DIDS applied at the beginning of incubation in SO_4^{2-} medium (0.024 \pm 0.001 min⁻¹, *** $p < 0.001$, Table 3). In

addition, the SO_4^{2-} amount internalized by AAPH-treated RBCs after 45 min of incubation in SO_4^{2-} medium was significantly lower than the control (Table 3). In DIDS-treated samples, the SO_4^{2-} amount internalized was significantly lower than both untreated and treated RBCs (*** $p < 0.001$, Table 3). In RBCs pre-incubated with the anthocyanin extract and then treated with 50 mM AAPH, the rate constant (0.048 \pm 0.001 min⁻¹) was not different than that of RBCs treated with 50 mM AAPH alone and was significantly different with respect to control (Table 3). In parallel, in RBCs

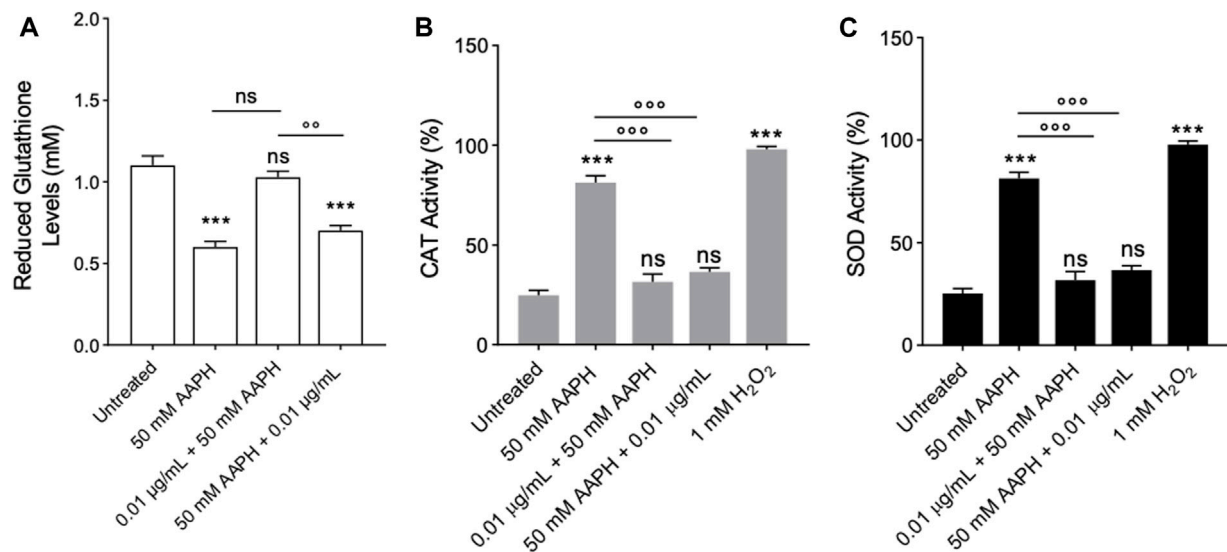


FIGURE 9

Evaluation of Endogenous Antioxidant Activity. Red blood cells were treated with 50 mM AAPH for 1 h at 37°C with or without pre- and post-treatment with the anthocyanin-enriched fraction (1 h at 37°C). (A) ns, not statistically significant versus untreated RBCs and 50 mM AAPH; *** $p < 0.001$ versus untreated; $p < 0.01$ versus pre-treatment, one-way ANOVA followed by Tukey's test. (n = 8). (B) CAT activity and (C) SOD activity. ns, not significant versus untreated RBCs; *** $p < 0.001$ versus untreated RBCs; $p < 0.001$ versus 50 mM AAPH, one-way ANOVA followed by Bonferroni's multiple comparison post-hoc test (n = 8).

first incubated with 50 mM AAPH and then treated with the anthocyanin-enriched fraction, the rate constant ($0.041 \pm 0.001 \text{ min}^{-1}$) was not significantly different with respect to that of human RBCs treated with 50 mM AAPH alone (Table 3). SO_4^{2-} uptake via band 3 was almost totally blocked by DIDS applied at the beginning of incubation in SO_4^{2-} medium ($0.023 \pm 0.001 \text{ min}^{-1}$, *** $p < 0.001$, Table 3). In addition, the SO_4^{2-} amount internalized by AAPH-treated RBCs after 45 min of incubation in SO_4^{2-} medium was significantly lower than untreated cells (Table 3). Also, the SO_4^{2-} amount internalized by RBCs pre- and post-incubated with the anthocyanin-enriched fraction and exposed to 50 mM AAPH was significantly different compared to that measured in untreated RBCs (Table 3). In DIDS-treated samples, the SO_4^{2-} amount internalized was significantly lower than that of both untreated and treated RBCs (*** $p < 0.001$, Table 3).

2.9 Assessment of the Endogenous Antioxidant Activity

2.9.1 Determination of reduced glutathione (GSH) levels

Figure 9A reports the GSH levels measured in human RBCs treated with 50 mM AAPH for 1 h at 37°C with or without pre- and post-treatment with the enriched anthocyanin fraction (0.01 µg/mL for 1 h at 37°C). The reduced GSH levels measured after incubation with AAPH were significantly lower (~45%) than those detected in untreated RBCs. Nevertheless, pre-incubation with the anthocyanin-enriched fraction completely restored the GSH content. On the contrary, in human RBCs first exposed to 50 mM AAPH (1 h at 37°C) and then treated with the anthocyanin-enriched fraction (0.01 µg/mL for 1 h at 37°C), the

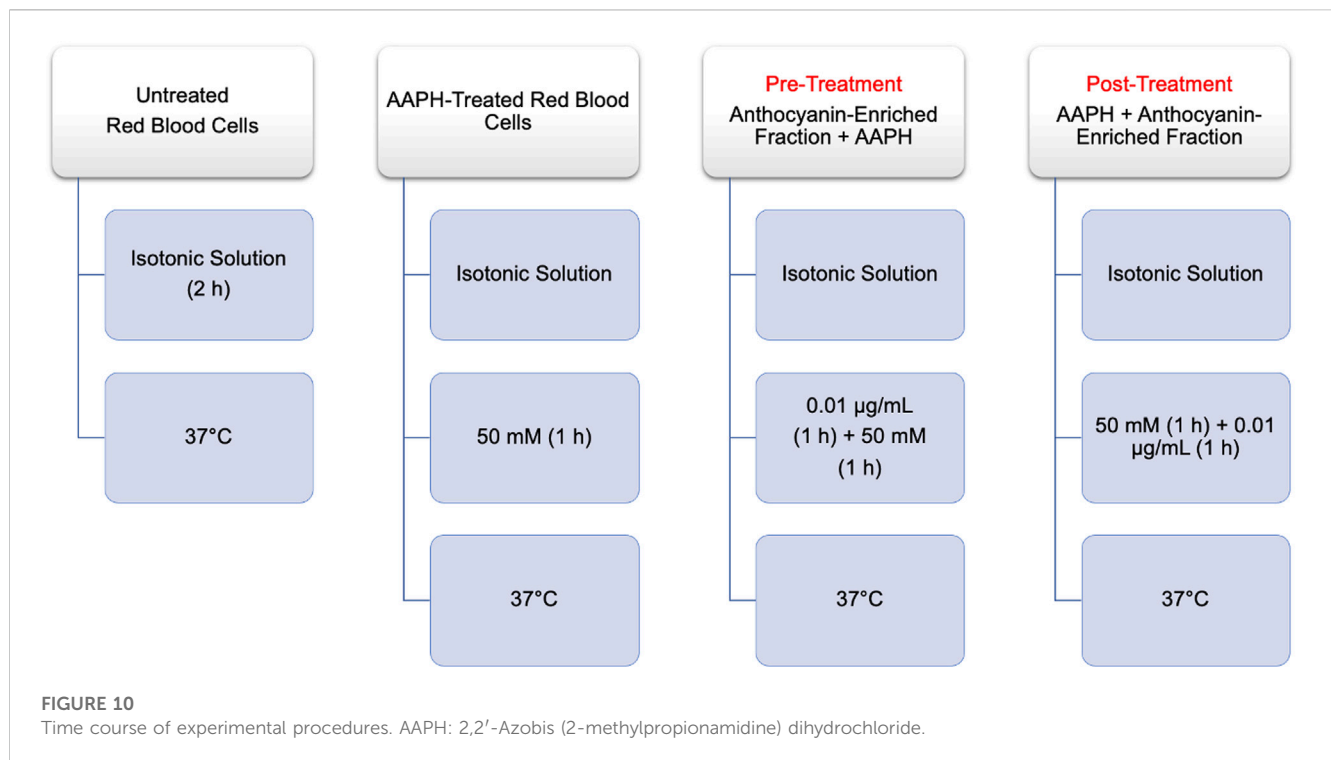
GSH content was not different compared to that measured in RBCs treated with 50 mM AAPH. The anthocyanin-enriched fraction alone did not significantly modify the GSH levels (data not shown).

2.9.2 Catalase (CAT) activity assay

Catalase was assayed in human RBCs untreated or treated with 50 mM AAPH for 1 h at 37°C with or without pre- or post-treatment with the anthocyanin-enriched fraction (0.01 µg/mL) for 1 h at 37°C. The treatment with AAPH provoked an increased CAT activity compared to cells left untreated, which was consistent with an elevated oxidative stress (Figure 10A). Unlike, the pre- and post-incubation with anthocyanin-enriched fraction (0.01 µg/mL for 1 h at 37°C) reduced the CAT activity to control values (Figure 9B). Exposure to 1 mM H_2O_2 for 30 min at 25°C has been considered as a positive control. As expected, CAT activity in human RBCs treated with H_2O_2 was significantly higher than that of control RBCs, whereas anthocyanin-enriched fraction alone did not significantly modify CAT activity (data not shown).

2.9.3 Superoxide dismutase (SOD) activity assay

In Figure 9C, the SOD activity was measured in human RBCs untreated or treated with 50 mM AAPH for 1 h at 37°C with or without pre- or post-treatment with the anthocyanin-enriched fraction (0.01 µg/mL) for 1 h at 37°C. In AAPH-treated RBCs, SOD activity was found significantly increased compared to the cells left untreated. On the contrary, both pre- and post-incubation with the anthocyanin extract resulted in a significant inhibition of SOD activity with respect to AAPH-treated cells. As expected, SOD activity in RBCs treated with 1 mM H_2O_2 (30 min at 25°C) was significantly higher than that of control RBCs. Anthocyanin-enriched fraction did not significantly modify SOD activity when given alone (data not shown).



3 Discussion

Red blood cells are the most numerous cells of the human blood. Their discoid donut-like shape is essential for their physiological functions as it enhances cellular flexibility and favours a high cellular surface area-to-volume ratio, thus allowing efficient gas (O_2 and CO_2 , respectively) exchange from the lungs to the tissues and *vice versa* (Sicinska, 2018). However, these cells are constantly exposed to stressors during their 120-day lifespan, resulting in biochemical and structural modifications. These alterations could impair the ability of the RBCs to transport oxygen and eventually trigger their removal from the blood circulation (Kuhn et al., 2017). The processes triggering RBC removal have been partly investigated. As many of these processes involve the increase of oxidative stress levels, the present investigation aimed to explore the cellular and molecular mechanisms underlying oxidative stress in human AAPH-stimulated RBCs. To achieve this aim, the relationship between RBC morphology and functional activity has been explored.

Plant-based antioxidant compounds could help reduce the effect of increased ROS levels and the resultant oxidative stress and can boost the endogenous antioxidant system against oxidizing molecules, thus playing a crucial role in the prevention of oxidative stress-related pathological states (Ugusman et al., 2023). In this context, the potential protective activity of an anthocyanin-enriched fraction extracted from *Callistemon citrinus* flowers (Table 1) for counteracting oxidative stress events was also studied. An interesting issue concerning the benefits of phytochemicals in human health is their combined administration. Combinations of several phytochemicals can cause a change in both final biological effects and bioavailability of each component. These combinations can improve or reduce the benefits conferred by individual bioactive compounds, as well as

may induce facilitation/competition for cellular absorption and transport (Wang et al., 2011). Synergistic interactions between antioxidants can be explained by the theory of antioxidant regeneration: one antioxidant protects another antioxidant from oxidative degradation or isomerization by its own oxidation. In this context, Bendokas and collaborators stated that a complex mixture of anthocyanin metabolites in the plasma rather than a single type of anthocyanins may cause beneficial effects in humans (Bendokas et al., 2020).

The possible beneficial effect has been assayed by applying the extract either before treatment of RBCs with the established pro-oxidant AAPH (pre-treatment) or after treatment with AAPH (post-treatment). Although multiple investigations reported the beneficial properties of extracts of plant origin, the anthocyanin effects on oxidative stress events in human RBCs have not yet been fully investigated.

The susceptibility of RBCs to AAPH exposure was investigated in terms of morphological changes by scanning electron microscopy (SEM). The images (Figure 2) revealed significant changes in the cellular shape, as the canonical biconcave shape was lost in a notable number of cells, which displayed surface blebs known as acanthocytes. However, post-treatment with the anthocyanin-enriched fraction attenuated the morphological modifications (Figure 2), with a significant reduction of the acanthocyte percentage. The morphology of circulating RBCs has a fundamental influence on the rheological properties of the blood (Gyawali et al., 2012; Gyawali et al., 2015). The cell integrity, one of the major determinants of blood rheological properties, implies that human RBCs are capable of reversible deformation in the different conditions of shear in the bloodstream. In this context, LDH release is commonly considered as a marker of loss of cell membrane integrity in response to elevated oxidant stress levels. This enzyme is

normally compartmentalized within the RBCs, but its activity is significantly increased in the extra-cellular side as a result of cellular damage (Franca et al., 2014; Morabito et al., 2014). To better explore this characteristic, the amount of released LDH was also quantified. As expected, in human RBCs treated with 50 mM AAPH a moderate increase in released LDH was detected (Figure 3). However, the pre-exposure to the anthocyanin-enriched fraction significantly decreased the released LDH amount, which returned to control values. Conversely, in RBCs first exposed to 50 mM AAPH and then incubated with the anthocyanin-enriched fraction, the amount of released LDH was not different compared to that measured in 50 mM AAPH-treated RBCs, but was significantly higher than that of untreated RBCs. These results indicate that anthocyanins can prevent but not reverse an oxidative stress-induced loss of cell membrane integrity. Red blood cells membrane mechanical properties can be remodeled by oxidative stress, thus resulting in a reduction of deformability, or alternatively, in altered permeability of the phospholipid bilayer, which, in turn, limits plasma membrane ability to counter osmotic variations (Spinelli et al., 2023). Among the main determinants of RBC deformability (Maruyama et al., 2022), the mean corpuscular volume (MCV, as a measure of cellular size) was considered. Our results demonstrated that pre-treatment with the anthocyanin-enriched fraction reverted the cell size reduction provoked by exposure to AAPH (Figure 4). The reduced membrane surface area following oxidative stress was confirmed by both reduced cell size (MCV) and the presence of acanthocytes (Figure 4).

It is interesting to point out that oxidative stress events, as well as oxidative stress-related diseases (Remigante et al., 2021b; Zuccolini et al., 2022), are associated with RBC shrinkage (Rinalducci et al., 2011). In β -thalassemic RBCs, a pro-oxidant environment favours the abnormal band 3 clusterization, inhibition of the Ca-ATPase pump, and activation of Ca-permeable unselective cation channels (Crupi et al., 2010; Voskou et al., 2015). The consequent increase in intracellular Ca^{2+} activates the K^+/Cl^- co-transporter (KCC), which causes the leakage of K^+ from the cell and results in cellular shrinkage and impaired deformability. An increase in intracellular calcium also activates calpain and some caspases that can degrade and/or crosslink cytoskeletal proteins and lead to eryptosis (De Franceschi et al., 2013). Eryptosis mimics the programmed cell death of nucleated cells (apoptosis). This phenomenon is characterized by a gradual increase in membrane phospholipid asymmetry and ATP consumption, which results in the externalization of phosphatidylserine to the outer leaflet of the plasma membrane (Yasin et al., 2003; Bosman et al., 2011). The externalization of phosphatidylserine on the surface of eryptotic cells can have two pathophysiological consequences: on one hand, it starts the RBC phagocytosis; on the other hand, it favours RBC adherence to vascular endothelial cells, which express phosphatidylserine receptors. Exposure to AAPH did not induce the translocation of phosphatidylserine at the outer plasma membrane leaflet (Supplementary Figure S2), thus demonstrating that, in this model of acute oxidative stress, human RBCs remain in an early and vital phase of the oxidizing process. Human RBCs may respond to any form of insult by changing their morphology following alterations in the biochemical composition of the plasma membrane. Red blood cells are extremely susceptible to ROS-induced injury because of their high polyunsaturated fatty acid

content and their abundance in iron (Fe^{2+})-rich haemoglobin. The latter acts as a catalyst in redox reactions and lipid peroxidation, resulting in TBARS as the final product (Pandey and Rizvi, 2010). Also, RBCs often undergo plasma membrane protein oxidation (Tsamesidis et al., 2020). Therefore, the oxidation of protein sulfhydryl groups is a typical indicator of oxidative damage at the protein level in human RBCs. These phenomena could alter plasma membrane properties and, consequently, cell shape. Since ROS generated during cellular metabolism cause the oxidation of macromolecules, the effects of the anthocyanin extract on the intracellular ROS content have been evaluated. Our results show that both pre- and post-treatment with the anthocyanin-enriched fraction induced a reduction of ROS generation induced by AAPH (Figure 5A). Also, pre- and post-treatment with the anthocyanin-enriched fraction avoided the lipid peroxidation of plasma membranes caused by AAPH (Figure 5B) and protected RBC protein sulfhydryl groups from oxidative injury (Figure 5C). These results demonstrate the antioxidant capacity of anthocyanins. These plant-derived components properly protect both the lipid and protein components of RBC membrane from oxidative injury, and may act as scavengers for neutralizing both reactive species and free radicals. These data are in line with what was previously reported by other authors (Heo and Lee, 2005; Fernandes et al., 2013; Speer et al., 2020; Hu J. et al., 2023; Hu X. et al., 2023).

Band 3 (SLC4A1/AE1) is the dominant integral transmembrane protein in the human RBCs (Mohandas and Gallagher, 2008). This protein plays different important functions, such as a) maintenance of anion homeostasis through the C-terminal domain that carries out $\text{Cl}^-/\text{HCO}_3^-$ exchange across the plasma membrane (Reithmeier et al., 2016), b) maintenance of cell shape because of the binding between the plasma membrane and cytoskeletal structures (Vallese et al., 2022), and c) maintenance of the interaction of some cytosolic proteins with the plasma membrane through the N-terminal domain that extends into the intracellular side. In particular, this region of band 3 competitively binds both haemoglobin and glycolytic enzymes (Issaian et al., 2021). The band 3 function can be investigated via the measurement of the rate constant for sulfate (SO_4^{2-}) uptake (Morabito et al., 2016; Morabito et al., 2017a; Morabito et al., 2017b; Morabito et al., 2018; Remigante et al., 2020; Remigante et al., 2022c; Remigante et al., 2022d; Remigante et al., 2022e), which is slower and more easily measurable than the physiological uptake of Cl^- or HCO_3^- (Jennings, 1976; Romano and Passow, 1984; Morabito et al., 2019a; Crupi et al., 2019). This methodological approach is as a valid tool to study the impact of oxidative stress on mature RBCs homeostasis (Morabito et al., 2016; Morabito et al., 2019a; Remigante et al., 2019; Remigante et al., 2022a; Remigante et al., 2023b; Perrone et al., 2023). Based on this background, SO_4^{2-} uptake through band 3 was measured in mature RBCs after exposure to AAPH with or without pre- and post-treatment with the anthocyanin-enriched fraction. In RBCs incubated with AAPH, the rate constant for SO_4^{2-} uptake was decreased compared to the untreated cells (Figure 7A; Table 3). The finding that increased oxidative stress caused functional alterations of band 3 activity in mature RBCs has been demonstrated also in other cell-based models of oxidative stress. To name just an example, Morabito and collaborators have demonstrated that not haemolytic concentrations of H_2O_2

(300 μ M, for 30 min, at 37°C) induced a reduction of band 3 transport efficiency (Morabito et al., 2017b). Such a reduction, which was associated with significant oxidative stress, could be attenuated by a short-time pre-exposure of mature RBCs to low (10 μ M, for 10 min at 37°C) H_2O_2 concentrations. The pre-exposure induces RBCs to adapt to a mild and transient oxidative stress and allows for an increased endurance to a subsequent stronger oxidant condition. Such an adaptation response, known as pre-conditioning, did not involve the phosphorylation (p-Tyr) pathways of band 3 but is mediated by the increase of CAT activity. In fact, this strategy enabled RBCs to improve the endogenous antioxidant defence performance, in order to provide a better protection against oxidative injury (Morabito et al., 2017b). Although no alterations in band 3 protein expression were reported in RBCs treated with AAPH with or without exposure to the anthocyanin-enriched fraction (Figure 7A), the pre-exposure of RBCs previously treated with AAPH to the anthocyanin-enriched fraction totally restored the rate constant for SO_4^{2-} uptake (Figure 7A; Table 3). On the contrary, the post-treatment did not enable recovery of the rate constant of SO_4^{2-} uptake (Figure 7A; Table 3).

Based on data hitherto showed, we can confirm that the anthocyanin extract displays a beneficial effect on the anionic exchange and could play a crucial role in counteracting oxidative stress-related functional modifications in mature RBCs. In elevated oxidative stress conditions, phosphorylation of proteins acts a crucial role in the modulation of the plasma membrane elasticity, resulting in the deformability of mature RBCs. For instance, tyrosine phosphorylation of the band 3 cytoplasmic domain breaks the interaction between band 3 and ankyrin, which connects the cytoskeleton spectrin to the plasma membrane, and induces metabolic changes via the reduction of anion transport (Cilek et al., 2023). The redox regulation of band 3 (p-Tyr) phosphorylation requires the action of two specific enzymes, Lyn, which allows for tyrosine 359 phosphorylation, and Syk, which allows for tyrosine 8 and 21 phosphorylation (Brunati et al., 2000; Bordin et al., 2009; Marchetti et al., 2020). It is well established that post-translation modifications (Costa et al., 2020) can impair cytoskeleton (spectrin)-band 3 binding and provoke modifications in the deformability and cell shape of mature RBCs (Lin and Brown, 2005). In this regard, AAPH-caused oxidative stress provoked a significant increase of band 3 tyrosine phosphorylation. However, both pre- and post-treatment with the anthocyanin-enriched fraction avoided these post-translational modifications (Figure 6B). Overall, no alteration in the Syk kinase expression levels was shown after treatment with AAPH with or without pre- and post-incubation with the anthocyanin-enriched fraction (Figure 6C). The oxidation of the band 3 cytoplasmic domain is likely induced by the increase of the intracellular ROS production. Elevation of ROS allows for Syk docking to band 3 and suppresses the action of the tyrosine phosphatases (Pantaleo et al., 2016; Pantaleo et al., 2017). It is well known that the binding site for oxidized haemoglobin (MetHb) is also located in the band 3 N-terminal cytoplasmic domain (Mollan et al., 2013). In RBCs, the production of ROS favours the haemoglobin denaturation, resulting in the release of heme iron (Reeder, 2023). This process can be auto-catalytic, thus leading to ever-increasing oxidative stress. To better explore the molecular relationship between band 3 and oxidized haemoglobin, MetHb levels were assayed. Our findings showed that

exposure to AAPH increased the levels of MetHb in mature RBCs (Figure 5D). These modifications can initiate a cascade of biochemical and/or structural changes, including the release of micro-particles containing both hemichromes and clustering of band 3 regions (Low et al., 1985; Mannu et al., 1995; Pantaleo et al., 2016). When intracellular oxidants are produced in excess, the balance between antioxidant and pro-oxidant capacity can be modified. Here, band 3 clusters could facilitate the recognition by antibodies directed against aging cells, thus triggering the premature removal of senescent RBCs from circulation before the physiological end of their 120-day life span. Interestingly, both pre- and post-treatment with the anthocyanin-enriched fraction prevented AAPH-induced MetHb production (Figure 5D). As mentioned above, another special feature of RBC oxidation is the band 3 clustering process. To better clarify band 3 distribution in conditions of elevated oxidative stress, the exposition of this protein was investigated by immunofluorescence analysis. Data displayed that, following exposure to AAPH, band 3 re-arranged in surface blebs, thus leading to the formation of clustered band 3 (Figures 8C,D). In particular, Figure 8C shows an aggregation of fluorescent bodies, most probably caused by the association between band 3 and MetHb. These data confirmed that MetHb binding to the C-terminus domain of band 3 induces clustering of band 3, thus leading to hemichromes formation. Yet, despite this, band 3 exposition levels were recovered in RBCs pre- and post-treated the anthocyanin-enriched fraction (Figure 8A).

To confirm the hypothesis that intracellular content could be involved in the AAPH-induced oxidative stress response, we measured band 3 exchange capability in resealed ghosts, which are composed of reconstituted plasma membranes but deprived of intracellular cytoplasmic content. Resealed ghosts represent a valid tool for investigating band 3 activity as well as its interaction with cytoplasmic proteins (Morabito et al., 2016). In resealed ghosts, the exposure to AAPH induced a reduction of the rate constant of SO_4^{2-} uptake with respect to untreated ghosts (Figure 7B; Table 3), thus suggesting that the prime target of AAPH seems to be the lipid component of the plasma membrane. The pre- and post-treatment with the anthocyanin-enriched fraction did not restore the anion exchange capability through band 3 (Figure 5B). In these experimental conditions, human RBCs were deprived of intracellular cytoplasmic content, including methaemoglobin reductase. Normally, this enzyme converts methaemoglobin back to haemoglobin (Kuma, 1981). As demonstrated, haemoglobin is also able to bind the N-terminal domain of band 3 and supports the anion exchange activity. However, the lack of methaemoglobin reductase in AAPH-treated resealed RBCs did not allow for such a conversion, resulting in an altered band 3 function (Figure 7B). The data obtained indicate that the anthocyanin-enriched fraction may protect the enzyme activity, including that of methaemoglobin reductase, in order to reduce excessive oxidative stress levels. Not surprisingly, mature RBCs are equipped with a battery of different antioxidant mechanisms, a combination of both antioxidant enzymes and non-enzymatic compounds, to inactivate the oxidizing species (Moller et al., 2023). Such efficient detoxification system keeps RBCs functional for 120 days in the bloodstream. Antioxidant enzymes possess an excellent free radical scavenging capacity and play crucial roles in mature RBCs (Ulanczyk et al., 2020). Glutathione is the main non-enzymatic endogenous antioxidant. This molecule affects the pentose

phosphate pathway through the glutathione reductase enzyme, which generates NADP, as a result of the reduction of GSSG with NADPH + H⁺. In human RBCs, the reduced GSH amount displays a wide inter-individual variability from 0.4 to 3.0 mM. However, it has been widely demonstrated that different factors, including oxidative stress-related diseases, can alter reduced GSH levels (van 'T Erve et al., 2013; Bertelli et al., 2021; Ferrera et al., 2021; Remigante et al., 2023a). The data obtained confirmed that exposure to AAPH reduced (~45%) GSH levels (Figure 9). The anthocyanin-enriched fraction exhibited a double response on the damaged RBCs. On one hand, the pre-incubation of human RBCs with the anthocyanin-enriched fraction completely restored GSH levels (Figure 9A). On the other hand, the post-incubation did not revert the effects of the oxidizing agent. However, these findings are in line with those reported in a former investigation (Lagana et al., 2020), which demonstrates that an anthocyanin-enriched fraction is able to scavenge different free radical species. This has been demonstrated via Electron Transfer and Hydrogen Atom Transfer reaction-based assays.

Antioxidant enzymes can work together to scavenge excessive ROS levels and maintain the redox balance in mature RBCs. For example, the SOD enzyme catalyses the dismutation of harmful O₂^{•-} into O₂ and H₂O₂. The H₂O₂ generated can then be decomposed into nontoxic H₂O and O₂ by means of other antioxidant enzymes such as catalase (CAT). In this regard, both SOD and CAT activity were investigated. The activity of both enzymes was much higher in RBCs incubated with AAPH than in untreated cells, which could reflect the activation of the endogenous antioxidant defense system to suppress the production of free radicals (Figures 9B,C). However, increased SOD and CAT activity failed to counterbalance the free radical rise, as demonstrated by the increase in lipid peroxidation levels as well as protein oxidation (Figures 5B,C). In this context, pre-exposure of RBCs to the anthocyanin-enriched fraction significantly prevented the upregulation in both SOD and CAT activity reported in AAPH-treated cells (Figures 9B,C). Both upregulation in CAT and SOD activity and concomitant substantial elevation of oxidative stress levels could reflect exhaustion of the endogenous antioxidant battery. These biochemical modifications may induce significant damage to the plasma membrane lipid components as well as protein structures. As a result, the membrane mechanical properties could be altered, resulting in a reduction of fluidity and deformability or altered permeability of the phospholipid bilayer, which, in turn, reduces the ability of the plasma membrane to withstand osmotic changes (Spinelli et al., 2023). These data indicate that anthocyanins might behave synergistically with the endogenous antioxidant machinery to counteract oxidative stress events in mature RBCs and preserve cellular integrity.

4 Materials and methods

4.1 Preparation of anthocyanin-enriched fraction of acidified ethanolic extract from *Callistemon citrinus* flowers

Flowers of *Callistemon citrinus* were collected from local nurseries in Messina (Italy), hair dried until they reached a moisture content lower than 2%, powdered with a mortar, and

used for the extraction of anthocyanins. A total of 1 g of powder was extracted several times with a 1:10 (w/v) acetic acid:ethanol:water (1:70:29, v/v/v) mixture. The volume obtained was concentrated to 5.0 mL with a rotary evaporator, extracted again, and concentrated, followed by a solid phase extraction (SPE) by a SupelcleanTM LC-18 SPE cartridge (Supelco Ltd., Bellefonte, PA, USA). The final elution has been performed with an acetic acid:ethanol:water (1:70:29, v/v/v) mixture. The anthocyanin-rich fraction was dried with a yield of ~21%. The powder obtained was stored in the dark at 4°C.

4.2 Anthocyanin profile characterization by RP-HPLC-DAD

Qualitative and quantitative determination of anthocyanins was carried out using a Shimadzu system, consisting of an LC-10AD pump system, a vacuum degasser, a quaternary solvent mixing, an SPD-M10A diode array detector, and a Rheodyne 7725i injector. The chromatographic separation was carried out using a Luna Omega PS C18 column (150 × 2.1 mm, 5 μm; Phenomenex) with solvent A (formic acid 0.1%) and solvent B (acetonitrile), according to the following gradient elution program: 0–3 min, 0% B; 3–9 min, 3% B; 9–24 min, 12% B; 24–30 min, 20% B; 30–33 min, 20% B; 33–43 min, 30% B; 43–63 min, 50% B; 63–66 min, 50% B; 66–76 min, 60% B; 76–81 min, 60% B; 81–86 min, 0% B, and equilibrated 4 min for a total run time of 90 min. The flow rate, injection volume, and column temperature were 0.4 mL/min, 5 μL, and 25 °C, respectively. UV-visible spectra of anthocyanins were recorded between 220 and 800 nm wavelength and chromatograms were acquired at 260, 290, 330, 370, and 520 nm wavelength to detect the eventual presence of different polyphenols classes. The peak identity was confirmed by comparing retention times and UV-visible spectra with those reported in the literature and with authentic standards when commercially available. Due to the presence of poly-glycosylated and polymeric anthocyanins, the anthocyanin content was expressed as cyanidin-3-O-glucoside equivalents/100 g of dry extract (DE) by using an external calibration curve made with a reference standard.

4.3 Solutions and chemicals for RBC sample processing

All chemicals were purchased from Sigma (Milan, Italy). Regarding stock solutions, 4,4'-diisothiocyanatostilbene-2,2'-disulfonate (DIDS, 10 mM) and 2,2'-Azobis (2-methylpropionamidine) dihydrochloride (AAPH, 0.5 M) were dissolved in dimethyl sulfoxide (DMSO); N-ethylmaleimide (NEM, 310 mM) was dissolved in ethanol. H₂O₂ experimental solution was obtained by diluting a 30% w/v stock solution in distilled water. Both ethanol and DMSO never exceeded 0.001% v/v in the experimental solutions and were previously tested on RBCs to exclude possible haemolytic damage.

4.4 Preparation of human RBCs

The experiments were carried out on male (mean age 53 ± 5 years) and female (mean age 54 ± 5 years) non-smoking donors.

Following the rules of good medical practice, the nature and purpose of the study were explained to all participants who then gave their informed consent. All donors had stopped taking aspirin or NSAIDs at least 1 week before the start of the study. To exclude the interference of sex hormones with the aggregation of red blood cells, only menopausal women who had not taken hormone replacement therapy were enrolled. Whole human blood was collected in test tubes containing ethylenediaminetetraacetic acid (EDTA). Red blood cells were washed in isotonic solution (NaCl 150 mM, 4-(2-hydroxyethyl)-1-piperazineethanesulfonic acid (HEPES) 5 mM, glucose 5 mM, pH 7.4, osmotic pressure 300 mOsm/kgH₂O) and centrifuged (Neya 16R, 1,200×g, 5 min) to discard both plasma and buffy coat. Then, RBCs were suspended to different haematocrits in isotonic solution according to the experimental tests. The experimental design shown in [Figure 2](#) was applied.

4.5 Analysis of cell shape by scanning electron microscopy (SEM)

RBCs samples were left untreated or exposed to a 50 mM AAPH-containing isotonic solution for 1 h at 37°C with or without pre- or post-incubation with 0.01 µg/mL *Callistemon citrinus* extract for 1 h at 37°C. Next, RBCs were collected, plated on poly-L-lysine-coated slides, and fixed with 2.5% glutaraldehyde in 0.1 M cacodylate buffer (pH 7.4) at room temperature for 20 min. Then, samples were post-fixed with 1% OsO₄ in 0.1 M sodium cacodylate buffer and dehydrated via a graded series of ethanol solutions from 30% to 100%. Then, absolute ethanol was gradually substituted by a 1:1 solution of hexamethyldisilazane (HMDS)/absolute ethanol and successively by pure HMDS. As a further step, HMDS was completely removed and samples were dried in a desiccator. Dried samples were mounted on stubs, coated with gold (10 nm), and analysed by a Cambridge 360 scanning electron microscopy (Leica Microsystems, Wetzlar, Germany), as formerly described ([Straface et al., 2002](#)). The number of RBCs with an altered shape (acanthocytes) was evaluated by counting ≥ 500 cells (50 RBCs for each different SEM field with a magnification of 3,000x) from samples in triplicate.

4.6 Determination of lactate dehydrogenase (LDH) release

To evaluate the amount of lactate dehydrogenase (LDH) released, the human RBCs were left untreated or treated with 50 mM AAPH for 1 h at 37°C with or without pre- or post-treatment with the anthocyanin-enriched fraction (0.01 µg/mL) for 1 h at 37°C. The RBCs were centrifuged at 1,200 ×g for 10 min to save the supernatant. The latter was used for the determination of the amount of LDH released and was homogenized by sonication and centrifuged at 14,000×g for 10 min. The amount of LDH released has been quantified as lactate conversion to pyruvate using nicotinamide adenine dinucleotide (NAD⁺) as a hydride acceptor. LDH activity is directly proportional to the absorbance decrease at 340 nm wavelength. The amount of LDH released has been expressed as % of the maximum amount of LDH in an untreated sample.

4.7 Measurements of mean corpuscular volume (MCV)

Mean corpuscular volume (MCV) is the average volume of RBCs. It has been measured by automated haematology analyser (BC-6800 PLUS, Medical Systems, Milan, Italy) in left untreated RBCs or treated with 50 mM AAPH (1 h, at 37°C) with or without pre- or post-treatment with anthocyanin-enriched fraction (0.01 µg/mL) for 1 h, at 37°C. Such parameter was calculated from haematocrit and RBC count, as follows: $MCV \text{ in fl} = (Hct \text{ [in L/L]} / RBC \text{ [in } \times 10^{12}/L]) \times 1,000$.

4.8 Assessment of oxidative stress parameters

4.8.1 Detection of reactive oxygen species (ROS) levels

To evaluate intracellular ROS content, RBCs, left untreated or exposed to AAPH-containing solution (for 1 h, at 37°C) with or without pre- or post-treatment with anthocyanin-enriched fraction (0.01 µg/mL, for 1 h, at 37°C) were incubated in Hanks' balanced salt solution, pH 7.4, containing dihydrorhodamine 123 (DHR 123; Molecular Probes) and then analyzed with a FACScan flow cytometer (Becton-Dickinson, Mountain View, CA, USA). At least 20,000 events were acquired. The median values of fluorescence intensity histograms were used to provide a semi-quantitative analysis of ROS production ([Lucantoni et al., 2006](#)).

4.8.2 Measurement of TBARS levels

Thiobarbituric-acid-reactive substances (TBARS) levels were measured as reported by Mendanha and collaborators ([Mendanha et al., 2012](#)). TBARS are derived from the reaction between thiobarbituric acid (TBA) and malondialdehyde (MDA), which is the end-product of lipid peroxidation. Red blood cells were incubated with 50 mM AAPH for 1 h at 37°C with or without pre- or post-incubation with the anthocyanin extract (0.01 µg/mL) for 1 h at 37°C. Successively, samples were centrifuged (Neya 16R, 1,200 ×g, 5 min) and suspended in isotonic solution. Samples (1.5 mL) were treated with 10% (w/v) trichloroacetic acid (TCA) and centrifuged (Neya 16R, 3,000 ×g, 10 min). TBA (1% in 0.5 mM NaOH hot solution, 1 mL) was added to the supernatant and the mixture was incubated at 95°C for 30 min. At last, TBARS levels were obtained by subtracting 20% of the absorbance at 453 nm from the absorbance at 532 nm (Onda Spectrophotometer, UV-21). Results are indicated as µM TBARS levels ($1.56 \times 10^5 \text{ M}^{-1} \text{ cm}^{-1}$ M extinction coefficient).

4.8.3 Measurement of total -SH content

Measurement of total -SH groups was carried out according to the method of Aksenov and Markesbery ([Aksenov and Markesbery, 2001](#)). In short, RBCs were left untreated or exposed to an isotonic AAPH-containing solution for 1 h at 37°C with or without pre- or post incubation with the anthocyanin extract (0.01 µg/mL) for 1 h at 37°C. Next, RBCs were centrifuged (Neya 16R, 1,200 ×g, 5 min) and a 100 µL sample was haemolysed in 1 mL of distilled water. A 50 µL aliquot of the haemolysis product was added to 1 mL of phosphate-buffered saline (PBS, pH 7.4) containing EDTA (1 mM).

Then, the addition of 5,5'-Dithiobis (2-nitrobenzoic acid) (DTNB, 10 mM, 30 μ L) initiated the reaction and the samples were incubated for 30 min at 25°C protected from light. Control samples without cell lysate or DTNB were processed in parallel. After incubation, sample absorbance was measured at 412 nm (Onda spectrophotometer, UV-21) and 3-thio-2-nitro-benzoic acid (TNB) levels were detected after subtraction of blank absorbance determined on samples containing only DTNB. To achieve full oxidation of -SH groups as the positive control, an aliquot of RBCs was incubated with 2 mM NEM for 1 h at 25°C (Morabito et al., 2015; Morabito et al., 2016). Data were normalised to protein content and results reported as μ M TNB/mg protein.

4.8.4 Measurement of methaemoglobin (MetHb) levels

The MetHb content was determined as reported by Naoum and collaborators (Naoum and Magaly Da Silva, 2004). This assay is based on MetHb and (oxy)-hemoglobin (Hb) determination by spectrophotometry at 630 and 540 nm wavelength, respectively. After incubation with 50 mM AAPH for 1 h at 37°C with or without pre- or post-treatment with the anthocyanin extract (0.01 μ g/mL) for 1 h at 37°C, 25 μ L of RBCs resuspended were lysed in 1975 μ L hypotonic buffer (2.5 mM NaH_2PO_4 , pH 7.4, 4°C). Then, samples were centrifuged (13,000 \times g, 15 min, 4°C; Eppendorf) to remove plasma membranes and the absorbance of the supernatant was measured (BioPhotometer Plus; Eppendorf). To induce a complete haemoglobin (Hb) oxidation, a sample of RBCs was incubated for 1 h at 25°C with 4 mM NaNO_2 , a well-known MetHb-forming compound. The percentage (%) of MetHb was determined as follows: % MetHb = $(\text{OD } 630/\text{OD } 540) \times 100$ (OD), where OD is the optical density.

4.9 Preparation of RBC membranes

Cell plasma membranes were processed as described by Pantaleo and collaborators (Pantaleo et al., 2016). Blood samples were suspended in hypotonic cold solution (2.5 mM NaH_2PO_4) containing a protease inhibitor mixture and were centrifuged (Eppendorf, 4°C, 18,000 \times g, 10 min) to discard haemoglobin. Plasma membranes were then solubilized with SDS (1% v/v) and put on ice for 20 min. The supernatant containing the solubilized plasma membrane proteins was finally conserved at -80°C.

4.9.1 SDS-PAGE preparation and western blotting analysis

Red blood cell plasma membranes were heated for 10 min at 95°C after dissolving in Laemmli buffer (Laemmli, 1970). The proteins were separated using SDS-polyacrylamide gel electrophoresis and transferred to a polyvinylidene fluoride membrane by maintaining a constant voltage for 2 h. Membranes were blocked for 1 h at 25°C in BSA and incubated at 4°C with the primary antibodies diluted in TBST (mouse monoclonal anti-band 3, B9277, Sigma-Aldrich, Milan, Italy, 1:1,000; mouse monoclonal anti-P-Tyr antibody (tyrosine), T1325, Sigma-Aldrich, Milan, Italy, 1:1,000; and rabbit monoclonal anti-Syk, SAB4500552, Sigma-Aldrich, Milan, Italy, 1:500). Successively, membranes were incubated with peroxidase-conjugated goat anti-mouse/rabbit IgG

secondary antibodies (A9044/A0545, Sigma-Aldrich, Milan, Italy) diluted 1:10,000/1:20,000 in TBST solution for 1 h at 25°C. To quantify the protein in equal amounts, a mouse monoclonal anti-GAPDH antibody (SC-32233, Santa Cruz Biotechnology, Italy, 1:10,000 in TBST), was incubated with the same membrane, as reported by Yeung and co-authors (Yeung and Stanley, 2009). A system of chemiluminescence detection (Super Signal West Pico Chemiluminescent Substrate, Pierce Thermo Scientific, Rockford, IL, USA) was employed to obtain the signal for image analysis (Image Quant TL, v2003). The intensity of protein bands was determined by densitometry (Bio-Rad ChemiDoc™ XRS+).

4.10 Analytical cytology

Red blood cells were left untreated or exposed to an AAPH-containing isotonic solution for 1 h at 37°C with or without pre- or post-incubation with the anthocyanin extract (0.01 μ g/mL) for 1 h at 37°C. Next, RBCs were fixed with 3.7% formaldehyde in PBS (pH 7.4) for 10 min at room temperature and then washed in the same buffer. Cells were then permeabilized with 0.5% Triton X-100 in PBS for 5 min at room temperature. After washing with PBS, samples were incubated with a mouse monoclonal anti-band 3 antibody (Sigma, Milan, Italy) for 30 min at 37°C, washed, and then incubated with a fluorescein isothiocyanate (FITC)-labeled anti-mouse antibody (Sigma, Milan, Italy) for 30 min at 37°C (Giovannetti et al., 2012). Cells incubated with the secondary antibody given alone were used as the negative control. Samples were analyzed by an Olympus BX51 Microphot fluorescence microscope or by a FACScan flow cytometer (Becton Dickinson, Mountain View, CA, USA) equipped with a 488 nm argon laser. At least 20,000 events have been acquired. The median values of fluorescence intensity histograms are given to provide a semiquantitative analysis. Fluorescence intensity values were normalised for those of untreated erythrocytes and expressed in %.

4.11 Measurement of SO_4^{2-} uptake

4.11.1 Control condition

The anion exchange through band 3 was determined as the uptake of SO_4^{2-} in RBCs, as described elsewhere (Romano and Passow, 1984; Romano et al., 1998; Morabito et al., 2018; Morabito et al., 2019b). Briefly, after washing, RBCs were suspended in 35 mL SO_4^{2-} medium (composition in mM: Na_2SO_4 118, HEPES 10, glucose 5, pH 7.4, osmotic pressure 300 mOsm/kgH₂O) and incubated at 25°C for 5, 10, 15, 30, 45, 60, 90, and 120 min. After each incubation time, DIDS (10 μ M), which is an inhibitor of band 3 activity (Jessen et al., 1986), was added to 5 mL sample aliquots, which were kept on ice. To eliminate SO_4^{2-} from the external medium, samples were washed three times in cold isotonic solution and centrifuged (Neya 16R, 4°C, 1,200 \times g, 5 min). Distilled water was added to the cell pellet to induce osmotic lysis and perchloric acid (4% v/v) was used to precipitate proteins. After centrifugation (Neya 16R, 4°C, 2,500 \times g, 10 min), the supernatant, which contained SO_4^{2-} trapped by erythrocytes during the fixed incubation times, was subjected to the turbidimetric analysis. To this end, 500 μ L of the supernatant were sequentially mixed to 500 μ L glycerol diluted in distilled water (1:1), 1 mL 4 M NaCl, and 500 μ L

1.24 M $\text{BaCl}_2 \cdot 2\text{H}_2\text{O}$. Finally, the absorbance of each sample was measured at 425 nm (Spectrophotometer, UV-21, Onda Spectrophotometer, Carpi, Modena, Italy). A calibrated standard curve, which was obtained in a separate experimental set by precipitating known SO_4^{2-} concentrations, was used to convert the absorbance into $[\text{SO}_4^{2-}] \text{ L cells} \times 10^{-2}$. The rate constant of SO_4^{2-} uptake (min^{-1}) was derived from the following equation: $C_t = C_\infty (1 - e^{-rt}) + C_0$, where C_t , C_∞ , and C_0 indicate the intracellular SO_4^{2-} concentrations measured at time t , ∞ , and 0, respectively, e represents the Neper number (2.7182818), r indicates the rate constant of the process, and t is the specific time at which the SO_4^{2-} concentration was measured. The rate constant is the inverse of the time needed to reach ~63% of total SO_4^{2-} intracellular concentration (Romano et al., 1998). Results are reported as $[\text{SO}_4^{2-}] \text{ L cells} \times 10^{-2}$ and represent the SO_4^{2-} micromolar concentration internalized by 5 mL erythrocytes suspended to 3% haematocrit.

4.11.2 Experimental conditions

After treatment with AAPH (50 mM) for 1 h at 37 °C proceeded or followed by 1 h incubation with or without the anthocyanin extract (0.01 $\mu\text{g/mL}$ at 37°C), RBCs (3% haematocrit) were centrifuged (Neya 16R, 4°C, 1,200 $\times g$, 5 min) and suspended in the SO_4^{2-} -containing supernatant. The rate constant of SO_4^{2-} uptake was then determined as described for the control condition.

4.12 Preparation of resealed ghosts and SO_4^{2-} uptake measurement

Resealed ghosts were prepared from human RBCs as described by Morabito and co-authors (Morabito et al., 2016; Morabito et al., 2020). In short, RBC samples were washed, suspended in 35 mL of cold hypo-osmotic buffer (NaH_2PO_4 2.5 mM, HEPES 5 mM, pH 7.4), and incubated for 10 min at 0 °C. Successively, the intracellular haemoglobin was discarded by multiple centrifugations (Neya 16R, 4 °C, 13,000 $\times g$, 30 min). The supernatant was replaced by 35 mL of isotonic resealing medium (NaCl 145 mM, HEPES 5 mM, glucose 5 mM, pH 7.4, 300 mOsm/kg $_{\text{H}_2\text{O}}$, 37°C). The plasma membranes were then incubated for 45 min at 37°C to allow for the correct resealing. Finally, resealed ghosts, which contained ~10% of the total haemoglobin, were treated with AAPH (50 mM) for 1 h at 37°C preceded or followed by incubation with or without the anthocyanin-enriched fraction (0.01 $\mu\text{g/mL}$) for 1 h at 37°C. The SO_4^{2-} uptake was measured according to the protocol described above for intact RBCs.

4.13 Assessment of the Endogenous Antioxidant Activity

4.13.1 Determination of reduced glutathione (GSH) levels

After treatment with 50 mM AAPH for 1 h at 37 °C with or without pre- or post-treatment with the anthocyanin-enriched fraction (0.01 $\mu\text{g/mL}$ for 1 h at 37 °C), RBC samples were centrifuged at 1,200 $\times g$ for 10 min to discard the supernatant. Each sample was homogenized by sonication and an aliquot was withdrawn and diluted with an equal volume of 5-sulfosalicylic acid solution (5%) to accomplish sample

deproteinization. Samples were then centrifuged at 13,000 $\times g$ for 10 min. Intracellular reduced glutathione (GSH) levels were assayed according to Alisik and collaborators (Alisik et al., 2019). The quantification was performed by a standard curve obtained with pure GSH. Results are indicated as mM GSH. Both AAPH and the anthocyanin-enriched fraction did not interfere with the determination of GSH levels.

4.13.2 Catalase (CAT) activity assay

Catalase (CAT) activity was evaluated by the catalase assay kit (MAK381, Sigma-Aldrich, Milan, Italy), according to the manufacturer's instructions. RBCs were exposed to 50 mM AAPH for 1 h at 37°C with or without pre- or post-incubation with the anthocyanin extract (0.01 $\mu\text{g/mL}$) for 1 h at 37 °C. As the positive control, cells were exposed to 20 mM H_2O_2 for 30 min. After each treatment, the incubation medium was discarded and cells were washed in PBS 1X. Subsequently, cells were lysed in 0.2 mL catalase assay buffer and centrifuged at 10,000 for 15 min at 4 °C. The supernatant (50 μL) was incubated with 12 μL of 20 mM H_2O_2 for 30 min at 25 °C. Stop solution (10 μL) and developer reaction mix (50 μL) were added and the samples were incubated for 10 min at 25 °C. CAT activity was determined by reading the absorbance at 570 nm wavelength (Fluostar Omega, BMG Labtech, Ortenberg, Germany) after subtracting the background.

4.13.3 Superoxide dismutase (SOD) activity assay

Superoxide dismutase (SOD) activity was evaluated by a specific assay (CS0009, Sigma-Aldrich, Milan, Italy), according to the manufacturer's instructions. RBCs were exposed to 50 mM AAPH for 1 h at 37 °C with or without pre- or post-incubation with the anthocyanin extract (0.01 $\mu\text{g/mL}$) for 1 h at 37°C. As the positive control, cells were exposed to 20 mM H_2O_2 for 30 min. Subsequently, cells were lysed in 1:5 distilled water. The lysate was collected in 0.5 mL tubes and centrifuged at 10,000 $\times g$ for 10 min at 4°C. The supernatant (20 μL) was transferred to a 96-well plate. Then, 20 μL dilution buffer, 160 μL WST solution and 20 μL xanthine oxidase solution were sequentially added. The samples were incubated for 1 h at 25 °C and SOD activity was determined by reading the absorbance at 450 nm wavelength (Fluostar Omega, BMG Labtech, Ortenberg, Germany) after subtracting the background.

4.14 Experimental data and statistics

All data are expressed as arithmetic mean \pm SEM. For statistical analysis and graphics, GraphPad Prism (version 8.0, GraphPad Software, San Diego, CA, USA) and Excel (Version 2019; Microsoft, Redmond, WA, USA) software were used. Significant differences between mean values were determined by one-way analysis of variance (ANOVA) followed by Bonferroni's post-hoc test. Statistically significant differences were assumed at $p < 0.05$; (n) corresponds to the number of independent measurements.

5 Conclusion

In conclusion, exposure of RBCs to AAPH increased oxidative stress levels, resulting in morphological alterations, namely, the formation of acanthocytes, increased lipid peroxidation and

oxidation of proteins, as well as abnormal distribution and hyperphosphorylation of band 3. Expected, AAPH incubation was also associated with a decrease of the band 3 functional activity and an increased amount of oxidized haemoglobin, which led to abnormal clustering of band 3. Finally, exposure to AAPH provoked both the consumption of reduced GSH and the over-activation of the endogenous antioxidant machinery, represented by catalase and superoxide dismutase. Pre-treatment of RBCs with an anthocyanin-enriched fraction effectively prevented all these oxidative stress-related alterations to a significant extent. In contrast, exposure of RBCs to the antioxidant compounds after the oxidative insult was less effective. These results reveal that most oxidative stress-associated modifications in RBCs are irreversible, but early implementation of natural antioxidant compounds can prevent or neutralize oxidative stress.

Indeed, exposure of RBCs to the anthocyanin fraction prior to, but not after, oxidative stress could protect band 3 function from oxidative stress-dependent inhibition. However, this effect can only be observed in intact RBCs but not in RBC ghosts, pointing to the fact that cellular integrity and preservation of a cytosolic component are essential prerequisites for the prevention of oxidative stress-related functional alterations in RBCs. In addition, the present study provides mechanistic insights into the different benefits deriving from the use of naturally occurring anthocyanins against oxidative stress on a cellular level. Taking into account that oxidative stress is involved in a large number of pathologies, new biomarkers of oxidative stress with diagnostic and monitoring potential are needed. In this regard, blood can be obtained from patients with minimally-invasive procedures, reflects the physiological states of peripheral tissues and cells, and could be considered as a remarkable source of oxidative stress biomarkers. In particular, we propose band 3 (SLC4A1/AE1) activity as a novel oxidative stress biomarker. Further studies (*ex vivo*) are needed to clarify the mechanisms underlying the oxidative stress events on RBC homeostasis, including potential effects on the interaction between band 3 and the cytoskeletal proteins ankyrin and spectrin, their possible post-translation modifications, as well as the mechanisms by which metabolism of RBCs regulates the transport systems of gas exchange.

Data availability statement

The original contributions presented in the study are included in the article/**Supplementary Materials**, further inquiries can be directed to the corresponding author.

Ethics statement

The studies involving humans were approved by the Institutional Review Board (or Ethics Committee) of University of Messina (prot.52-22). The studies were conducted in accordance

with the local legislation and institutional requirements. The participants provided their written informed consent to participate in this study.

Author contributions

AR: Conceptualization, Data curation, Formal Analysis, Supervision, Validation, Writing—original draft, Writing—review and editing. SS: Investigation, Methodology, Writing—review and editing. GP: Investigation, Writing—review and editing. DB: Data curation, Investigation, Methodology, Writing—review and editing. ES: Data curation, Investigation, Methodology, Writing—review and editing. LG: Investigation, Methodology, Writing—review and editing. GB: Investigation, Methodology, Writing—review and editing. DC: Investigation, Writing—review and editing. GF: Investigation, Writing—review and editing. SD: Writing—review and editing. AM: Writing—review and editing. RM: Supervision, Writing—review and editing.

Funding

The author(s) declare financial support was received for the research, authorship, and/or publication of this article. This scientific work was supported by Italian Research Ministry (PRIN2022YRBE8B).

Conflict of interest

The authors declare that the research was conducted in the absence of any commercial or financial relationships that could be construed as a potential conflict of interest.

Publisher's note

All claims expressed in this article are solely those of the authors and do not necessarily represent those of their affiliated organizations, or those of the publisher, the editors and the reviewers. Any product that may be evaluated in this article, or claim that may be made by its manufacturer, is not guaranteed or endorsed by the publisher.

Supplementary material

The Supplementary Material for this article can be found online at: <https://www.frontiersin.org/articles/10.3389/fphys.2023.1303815/full#supplementary-material>

References

- Akki, R., Siracusa, R., Cordaro, M., Remigante, A., Morabito, R., Errami, M., et al. (2022). Adaptation to oxidative stress at cellular and tissue level. *Arch. Physiol. Biochem.* 128, 521–531. doi:10.1080/13813455.2019.1702059
- Akki, R., Siracusa, R., Morabito, R., Remigante, A., Campolo, M., Errami, M., et al. (2018). Neuronal-like differentiated SH-SY5Y cells adaptation to a mild and transient H(2) O(2) -induced oxidative stress. *Cell Biochem. Funct.* 36, 56–64. doi:10.1002/cbf.3317

- Aksenov, M. Y., and Markesbery, W. R. (2001). Changes in thiol content and expression of glutathione redox system genes in the hippocampus and cerebellum in Alzheimer's disease. *Neurosci. Lett.* 302, 141–145. doi:10.1016/s0304-3940(01)01636-6
- Alisik, M., Neselioglu, S., and Erel, O. (2019). A colorimetric method to measure oxidized, reduced and total glutathione levels in erythrocytes. *J. Laboratory Med.* 43, 269–277. doi:10.1515/labmed-2019-0098
- Amezaga, J., Ugartemendia, G., Larraioz, A., Bretana, N., Iruretagoyena, A., Camba, J., et al. (2020). Altered levels of desaturation and omega-6 fatty acids in breast cancer patients' red blood cell membranes. *Metabolites* 10, 469. doi:10.3390/metabo10110469
- Arakawa, T., Kobayashi-Yurugi, T., Alguel, Y., Iwanari, H., Hatae, H., Iwata, M., et al. (2015). Crystal structure of the anion exchanger domain of human erythrocyte band 3. *Science* 350, 680–684. doi:10.1126/science.aaa4335
- Bendokas, V., Stanys, V., Mazeikiene, I., Trumbeckaite, S., Baniene, R., and Liobikas, J. (2020). Anthocyanins: from the field to the antioxidants in the body. *Antioxidants (Basel)* 9, 819. doi:10.3390/antiox9090819
- Bertelli, S., Remigante, A., Zuccolini, P., Barbieri, R., Ferrera, L., Picco, C., et al. (2021). Mechanisms of activation of LRRC8 volume regulated anion channels. *Cell Physiol. Biochem.* 55, 41–56. doi:10.33594/000000329
- Bordin, L., Fiore, C., Bragadin, M., Brunati, A. M., and Clari, G. (2009). Regulation of membrane band 3 Tyr-phosphorylation by proteolysis of p72(Syk) and possible involvement in senescence process. *Acta Biochim. Biophys. Sin. (Shanghai)* 41, 846–851. doi:10.1093/abbs/gmp071
- Bosman, G. J., Cluitmans, J. C., Groenen, Y. A., Werre, J. M., Willekens, F. L., and Novotny, V. M. (2011). Susceptibility to hyperosmotic stress-induced phosphatidylserine exposure increases during red blood cell storage. *Transfusion* 51, 1072–1078. doi:10.1111/j.1537-2995.2010.02929.x
- Brunati, A. M., Bordin, L., Clari, G., James, P., Quadroni, M., Baritono, E., et al. (2000). Sequential phosphorylation of protein band 3 by Syk and Lyn tyrosine kinases in intact human erythrocytes: identification of primary and secondary phosphorylation sites. *Blood* 96, 1550–1557. doi:10.1182/blood.v96.4.1550.h8001550_1550_1557
- Cilek, N., Ugurel, E., Goksel, E., and Yalcin, O. (2023). Signaling mechanisms in red blood cells: a view through the protein phosphorylation and deformability. *J. Cell Physiol.* doi:10.1002/jcp.30958
- Contreras-Puentes, N., Rodriguez-Cavallo, E., and Mendez-Cuadro, D. (2019). Membrane protein carbonylation of Plasmodium falciparum infected erythrocytes under conditions of sickle cell trait and G6PD deficiency. *Mol. Biochem. Parasitol.* 227, 5–14. doi:10.1016/j.molbiopara.2018.11.003
- Costa, R., Remigante, A., Civello, D. A., Bernardinelli, E., Szabo, Z., Morabito, R., et al. (2020). O-GlcNAcylation suppresses the ion current IClswell by preventing the binding of the protein IClN to α -integrin. *Front. Cell Dev. Biol.* 8, 607080. doi:10.3389/fcell.2020.607080
- Crupi, M., Romano, L., Romano, P., Venza, M., Venza, I., and Teti, D. (2010). Erythrocytes anion transport and oxidative change in beta-thalassemias. *Cell Biol. Int.* 34, 655–662. doi:10.1042/CBI20090472
- Crupi, R., Morabito, R., Remigante, A., Gugliandolo, E., Britti, D., Cuzzocrea, S., et al. (2019). Susceptibility of erythrocytes from different sources to xenobiotics-induced lysis. *Comp. Biochem. Physiol. C Toxicol. Pharmacol.* 221, 68–72. doi:10.1016/j.cbpc.2019.03.008
- D'alessandro, A., Fu, X., Kanas, T., Reis, J. A., Culp-Hill, R., Guo, Y., et al. (2021). Donor sex, age and ethnicity impact stored red blood cell antioxidant metabolism through mechanisms in part explained by glucose 6-phosphate dehydrogenase levels and activity. *Haematologica* 106, 1290–1302. doi:10.3324/haematol.2020.246603
- D'alessandro, A., and Zolla, L. (2017). Proteomic analysis of red blood cells and the potential for the clinic: what have we learned so far? *Expert Rev. Proteomics* 14, 243–252. doi:10.1080/14789450.2017.1291347
- De Franceschi, L., Bertoldi, M., Matte, A., Santos Franco, S., Pantaleo, A., Ferru, E., et al. (2013). Oxidative stress and beta-thalassemia erythroid cells behind the molecular defect. *Oxid. Med. Cell Longev.* 2013, 985210. doi:10.1155/2013/985210
- Ebrahimi, S., and Bagchi, P. (2022). A computational study of red blood cell deformability effect on hemodynamic alteration in capillary vessel networks. *Sci. Rep.* 12, 4304. doi:10.1038/s41598-022-08357-z
- Fernandes, I., Marques, F., De Freitas, V., and Mateus, N. (2013). Antioxidant and antiproliferative properties of methylated metabolites of anthocyanins. *Food Chem.* 141, 2923–2933. doi:10.1016/j.foodchem.2013.05.033
- Ferrera, L., Barbieri, R., Picco, C., Zuccolini, P., Remigante, A., Bertelli, S., et al. (2021). TRPM2 oxidation activates two distinct potassium channels in melanoma cells through intracellular calcium increase. *Int. J. Mol. Sci.* 22, 8359. doi:10.3390/ijms22168359
- Franca, E. L., Ribeiro, E. B., Scherer, E. F., Cantarini, D. G., Pessoa, R. S., Franca, F. L., et al. (2014). Effects of Momordica charantia L. on the blood rheological properties in diabetic patients. *Biomed. Res. Int.* 2014, 840379. doi:10.1155/2014/840379
- Fujii, J., Homma, T., Kobayashi, S., Warang, P., Madkaikar, M., and Mukherjee, M. B. (2021). Erythrocytes as a preferential target of oxidative stress in blood. *Free Radic. Res.* 55, 562–580. doi:10.1080/10715762.2021.1873318
- Giovannetti, A., Gambardella, L., Pietraforte, D., Rosato, E., Giammarioli, A. M., Salsano, F., et al. (2012). Red blood cell alterations in systemic sclerosis: a pilot study. *Cell Physiol. Biochem.* 30, 418–427. doi:10.1159/000339035
- Gyawali, P., Richards, R. S., Bwititi, P. T., and Nwose, E. U. (2015). Association of abnormal erythrocyte morphology with oxidative stress and inflammation in metabolic syndrome. *Blood Cells Mol. Dis.* 54, 360–363. doi:10.1016/j.bcmd.2015.01.005
- Gyawali, P., Richards, R. S., and Uba Nwose, E. (2012). Erythrocyte morphology in metabolic syndrome. *Expert Rev. Hematol.* 5, 523–531. doi:10.1586/ehm.12.47
- Heo, H. J., and Lee, C. Y. (2005). Strawberry and its anthocyanins reduce oxidative stress-induced apoptosis in PC12 cells. *J. Agric. Food Chem.* 53, 1984–1989. doi:10.1021/jf048616l
- Hu, J., Li, X., Wu, N., Zhu, C., Jiang, X., Yuan, K., et al. (2023a). Anthocyanins prevent AAPH-induced steroidogenesis disorder in leydig cells by counteracting oxidative stress and StAR abnormal expression in a structure-dependent manner. *Antioxidants (Basel)* 12, 508. doi:10.3390/antiox12020508
- Hu, X., Yang, Y., Tang, S., Chen, Q., Zhang, M., Ma, J., et al. (2023b). Anti-aging effects of anthocyanin extracts of Sambucus canadensis caused by targeting mitochondrial-induced oxidative stress. *Int. J. Mol. Sci.* 24, 1528. doi:10.3390/ijms24021528
- Issaian, A., Hay, A., Dzieciatkowska, M., Roberti, D., Perrotta, S., Darula, Z., et al. (2021). The interactome of the N-terminus of band 3 regulates red blood cell metabolism and storage quality. *Haematologica* 106, 2971–2985. doi:10.3324/haematol.2020.278252
- Jennings, M. L. (1976). Proton fluxes associated with erythrocyte membrane anion exchange. *J. Membr. Biol.* 28, 187–205. doi:10.1007/BF01869697
- Jessen, F., Sjöholm, C., and Hoffmann, E. K. (1986). Identification of the anion exchange protein of Ehrlich cells: a kinetic analysis of the inhibitory effects of 4,4'-diisothiocyanato-2,2'-stilbene-disulfonic acid (DIDS) and labeling of membrane proteins with 3H-DIDS. *J. Membr. Biol.* 92, 195–205. doi:10.1007/BF01869388
- Jiang, Z. Y., Woollard, A. C., and Wolff, S. P. (1990). Hydrogen peroxide production during experimental protein glycation. *FEBS Lett.* 268, 69–71. doi:10.1016/0014-5793(90)80974-n
- Kouka, P., Priftis, A., Stagos, D., Angelis, A., Stathopoulos, P., Xinos, N., et al. (2017). Assessment of the antioxidant activity of an olive oil total polyphenolic fraction and hydroxytyrosol from a Greek Olea europea variety in endothelial cells and myoblasts. *Int. J. Mol. Med.* 40, 703–712. doi:10.3892/ijmm.2017.3078
- Kuhn, V., Diederich, L., Keller, T. C. S. T., Kramer, C. M., Luckstadt, W., Panknin, C., et al. (2017). Red blood cell function and dysfunction: redox regulation, nitric oxide metabolism, anemia. *Antioxid. Redox Signal* 26, 718–742. doi:10.1089/ars.2016.6954
- Kuma, F. (1981). Properties of methemoglobin reductase and kinetic study of methemoglobin reduction. *J. Biol. Chem.* 256, 5518–5523. doi:10.1016/s0021-9258(19)69231-8
- Laemmli, U. K. (1970). Cleavage of structural proteins during the assembly of the head of bacteriophage T4. *Nature* 227, 680–685. doi:10.1038/227680a0
- Lagana, G., Barreca, D., Smeriglio, A., Germano, M. P., D'angelo, V., Calderaro, A., et al. (2020). Evaluation of anthocyanin profile, antioxidant, cytoprotective, and anti-angiogenic properties of Callistemon citrinus flowers. *Plants (Basel)* 9, 1045. doi:10.3390/plants9081045
- Larayat, R. A., Okoh, O. O., Sadimenko, A., and Okoh, A. I. (2017). Terpene constituents of the aerial parts, phenolic content, antibacterial potential, free radical scavenging and antioxidant activity of Callistemon citrinus (Curtis) Skeels (Myrtaceae) from Eastern Cape Province of South Africa. *BMC Complement. Altern. Med.* 17, 292. doi:10.1186/s12906-017-1804-2
- Lin, L. C., and Brown, F. L. (2005). Dynamic simulations of membranes with cytoskeletal interactions. *Phys. Rev. E Stat. Nonlin Soft Matter Phys.* 72, 011910. doi:10.1103/PhysRevE.72.011910
- Low, P. S., Waugh, S. M., Zinke, K., and Drenckhahn, D. (1985). The role of hemoglobin denaturation and band 3 clustering in red blood cell aging. *Science* 227, 531–533. doi:10.1126/science.2578228
- Lucantoni, G., Pietraforte, D., Matarrese, P., Gambardella, L., Metere, A., Paone, G., et al. (2006). The red blood cell as a biosensor for monitoring oxidative imbalance in chronic obstructive pulmonary disease: an ex vivo and in vitro study. *Antioxid. Redox Signal* 8, 1171–1182. doi:10.1089/ars.2006.8.1171
- Luo, J., Si, H., Jia, Z., and Liu, D. (2021). Dietary anti-aging polyphenols and potential mechanisms. *Antioxidants (Basel)* 10, 283. doi:10.3390/antiox10020283
- Mandal, D., Baudin-Creuz, V., Bhattacharyya, A., Pathak, S., Delaunay, J., Kundu, M., et al. (2003). Caspase 3-mediated proteolysis of the N-terminal cytoplasmic domain of the human erythroid anion exchanger 1 (band 3). *J. Biol. Chem.* 278, 52551–52558. doi:10.1074/jbc.M306914200
- Mann, F., Arese, P., Cappellini, M. D., Fiorelli, G., Cappadoro, M., Giribaldi, G., et al. (1995). Role of hemichrome binding to erythrocyte membrane in the generation of band-3 alterations in beta-thalassemia intermedia erythrocytes. *Blood* 86, 2014–2020. doi:10.1182/blood.v86.5.2014.bloodjournal8652014
- Marchetti, G., Dessi, A., Dallochio, R., Tsamesidis, I., Pau, M. C., Turrini, F. M., et al. (2020). Syk inhibitors: new computational insights into their intraerythrocytic action in plasmodium falciparum malaria. *Int. J. Mol. Sci.* 21, 7009. doi:10.3390/ijms21197009

- Martemucci, G., Portincasa, P., Di Ciaula, A., Mariano, M., Centonze, V., and D'Alessandro, A. G. (2022). Oxidative stress, aging, antioxidant supplementation and their impact on human health: an overview. *Mech. Ageing Dev.* 206, 111707. doi:10.1016/j.mad.2022.111707
- Maruyama, T., Hieda, M., Mawatari, S., and Fujino, T. (2022). Rheological abnormalities in human erythrocytes subjected to oxidative inflammation. *Front. Physiol.* 13, 837926. doi:10.3389/fphys.2022.837926
- Matte, A., Bertoldi, M., Mohandas, N., An, X., Bugatti, A., Brunati, A. M., et al. (2013). Membrane association of peroxiredoxin-2 in red cells is mediated by the N-terminal cytoplasmic domain of band 3. *Free Radic. Biol. Med.* 55, 27–35. doi:10.1016/j.freeradbiomed.2012.10.543
- Maury, G. L., Rodriguez, D. M., Hendrix, S., Arranz, J. C. E., Boix, Y. F., Pacheco, A. O., et al. (2020). Antioxidants in plants: a valorization potential emphasizing the need for the conservation of plant biodiversity in Cuba. *Antioxidants (Basel)* 9, 1048. doi:10.3390/antiox9111048
- Mazzulla, S., Schella, A., Gabriele, D., Baldino, N., Sesti, S., Perrotta, E., et al. (2015). Oxidation of human red blood cells by a free radical initiator: effects on rheological properties. *Clin. Hemorheol. Microcirc.* 60, 375–388. doi:10.3233/CH-141841
- Mendanha, S. A., Anjos, J. L., Silva, A. H., and Alonso, A. (2012). Electron paramagnetic resonance study of lipid and protein membrane components of erythrocytes oxidized with hydrogen peroxide. *Braz J. Med. Biol. Res.* 45, 473–481. doi:10.1590/s0100-879x2012007500050
- Mohandas, N., and Gallagher, P. G. (2008). Red cell membrane: past, present, and future. *Blood* 112, 3939–3948. doi:10.1182/blood-2008-07-161166
- Mohanty, J. G., Nagababu, E., and Rifkind, J. M. (2014). Red blood cell oxidative stress impairs oxygen delivery and induces red blood cell aging. *Front. Physiol.* 5, 84. doi:10.3389/fphys.2014.00084
- Mollan, T. L., Banerjee, S., Wu, G., Parker Siburt, C. J., Tsai, A. L., Olson, J. S., et al. (2013). α -Hemoglobin stabilizing protein (AHSP) markedly decreases the redox potential and reactivity of α -subunits of human HbA with hydrogen peroxide. *J. Biol. Chem.* 288, 4288–4298. doi:10.1074/jbc.M112.412064
- Moller, M. N., Orrico, F., Villar, S. F., Lopez, A. C., Silva, N., Donze, M., et al. (2023). Oxidants and antioxidants in the redox biochemistry of human red blood cells. *ACS Omega* 8, 147–168. doi:10.1021/acsomega.2c06768
- Monjot, N., Amiot, M. J., Fleurentin, J., Morel, J. M., and Raynal, S. (2022). Clinical evidence of the benefits of phytonutrients in human healthcare. *Nutrients* 14, 1712. doi:10.3390/nu14091712
- Morabito, R., Dossena, S., La Spada, G., and Marino, A. (2014). Heavy metals affect nematocysts discharge response and biological activity of crude venom in the jellyfish *Pelagia noctiluca* (Cnidaria, Scyphozoa). *Cell Physiol. Biochem.* 34, 244–254. doi:10.1159/000362979
- Morabito, R., Falliti, G., Geraci, A., Spada, G. L., and Marino, A. (2015). Curcumin protects -sh groups and sulphate transport after oxidative damage in human erythrocytes. *Cell Physiol. Biochem.* 36, 345–357. doi:10.1159/000430256
- Morabito, R., Remigante, A., Cavallaro, M., Taormina, A., La Spada, G., and Marino, A. (2017a). Anion exchange through band 3 protein in canine leishmaniasis at different stages of disease. *Pflugers Arch.* 469, 713–724. doi:10.1007/s00424-017-1974-2
- Morabito, R., Remigante, A., Di Pietro, M. L., Giannetto, A., La Spada, G., and Marino, A. (2017b). SO_4^{2-} uptake and catalase role in preconditioning after H_2O_2 -induced oxidative stress in human erythrocytes. *Pflugers Arch.* 469, 235–250. doi:10.1007/s00424-016-1927-1
- Morabito, R., Remigante, A., and Marino, A. (2019a). Melatonin protects band 3 protein in human erythrocytes against H_2O_2 -induced oxidative stress. *Molecules* 24, 2741. doi:10.3390/molecules24152741
- Morabito, R., Remigante, A., and Marino, A. (2019b). Protective role of magnesium against oxidative stress on SO_4^{2-} uptake through band 3 protein in human erythrocytes. *Cell Physiol. Biochem.* 52, 1292–1308. doi:10.33594/000000091
- Morabito, R., Remigante, A., Spinelli, S., Vitale, G., Trichilo, V., Loddo, S., et al. (2020). High glucose concentrations affect band 3 protein in human erythrocytes. *Antioxidants (Basel)* 9, 365. doi:10.3390/antiox9050365
- Morabito, R., Romano, O., La Spada, G., and Marino, A. (2016). H_2O_2 -Induced oxidative stress affects SO_4^{2-} transport in human erythrocytes. *PLoS One* 11, e0146485. doi:10.1371/journal.pone.0146485
- Morabito, R., Remigante, A., Arcuri, B., Marino, A., Giammanco, M., and La Spada, G. M. A. (2018). Effect of cadmium on anion exchange capability through Band 3 protein in human erythrocytes. *J. Biol. Res.* 91, 1–7. doi:10.4081/jbr.2018.7203
- Moras, M., Lefevre, S. D., and Ostuni, M. A. (2017). From erythroblasts to mature red blood cells: organelle clearance in mammals. *Front. Physiol.* 8, 1076. doi:10.3389/fphys.2017.01076
- Naoum, P. C. R. J., and Magaly Da Silva, M. (2004). Cinética plasmática de uma microemulsão rica em colesterol em pacientes com beta talassemia menor. *Rev. Bras. Hematol. Hemoter.* 26, 19–22. doi:10.1590/s1516-84842004000400014
- Niedzwiecki, A., Roomi, M. W., Kalinsky, T., and Rath, M. (2016). Anticancer efficacy of polyphenols and their combinations. *Nutrients* 8, 552. doi:10.3390/nu8090552
- Nishikito, D. F., Borges, A. C. A., Laurindo, L. F., Otoboni, A., Direito, R., Goulart, R. A., et al. (2023). Anti-inflammatory, antioxidant, and other health effects of dragon fruit and potential delivery systems for its bioactive compounds. *Pharmaceutics* 15, 159. doi:10.3390/pharmaceutics15010159
- Pandey, K. B., and Rizvi, S. I. (2010). Markers of oxidative stress in erythrocytes and plasma during aging in humans. *Oxid. Med. Cell Longev.* 3, 2–12. doi:10.4161/oxim.3.1.10476
- Pandey, K. B., and Rizvi, S. I. (2011). Biomarkers of oxidative stress in red blood cells. *Biomed. Pap. Med. Fac. Univ. Palacky. Olomouc Czech Repub.* 155, 131–136. doi:10.5507/bp.2011.027
- Pantaleo, A., Ferru, E., Pau, M. C., Khadjavi, A., Mandili, G., Matte, A., et al. (2016). Band 3 erythrocyte membrane protein acts as redox stress sensor leading to its phosphorylation by p (72) Syk. *Oxid. Med. Cell Longev.* 2016, 6051093. doi:10.1155/2016/6051093
- Pantaleo, A., Kesely, K. R., Pau, M. C., Tsamesidis, I., Schwarzer, E., Skorokhod, O. A., et al. (2017). Syk inhibitors interfere with erythrocyte membrane modification during P falciparum growth and suppress parasite egress. *Blood* 130, 1031–1040. doi:10.1182/blood-2016-11-748053
- Perrone, P., Spinelli, S., Mantegna, G., Notarale, R., Straface, E., Caruso, D., et al. (2023). Mercury chloride affects band 3 protein-mediated anionic transport in red blood cells: role of oxidative stress and protective effect of olive oil polyphenols. *Cells* 12, 424. doi:10.3390/cells12030424
- Philip, P., Sagaspe, P., Taillard, J., Mandon, C., Constans, J., Pourtau, L., et al. (2019). Acute intake of a grape and blueberry polyphenol-rich extract ameliorates cognitive performance in healthy young adults during a sustained cognitive effort. *Antioxidants (Basel)* 8, 650. doi:10.3390/antiox8120650
- Pretini, V., Koenen, M. H., Kaestner, L., Fens, M., Schiffelers, R. M., Bartels, M., et al. (2019). Red blood cells: chasing interactions. *Front. Physiol.* 10, 945. doi:10.3389/fphys.2019.00945
- Reeder, B. J. (2023). Globin associated oxidative stress. *Antioxidants (Basel)* 12, 1077. doi:10.3390/antiox12051077
- Reithmeier, R. A., Casey, J. R., Kalli, A. C., Sansom, M. S., Alguel, Y., and Iwata, S. (2016). Band 3, the human red cell chloride/bicarbonate anion exchanger (AE1, SLC4A1), in a structural context. *Biochim. Biophys. Acta* 1858, 1507–1532. doi:10.1016/j.bbame.2016.03.030
- Remigante, A., and Morabito, R. (2022). Cellular and molecular mechanisms in oxidative stress-related diseases. *Int. J. Mol. Sci.* 23, 8017. doi:10.3390/ijms23148017
- Remigante, A., Morabito, R., and Marino, A. (2019). Natural antioxidants beneficial effects on anion exchange through band 3 protein in human erythrocytes. *Antioxidants (Basel)* 9, 25. doi:10.3390/antiox9010025
- Remigante, A., Morabito, R., and Marino, A. (2021a). Band 3 protein function and oxidative stress in erythrocytes. *J. Cell Physiol.* 236, 6225–6234. doi:10.1002/jcp.30322
- Remigante, A., Morabito, R., Spinelli, S., Trichilo, V., Loddo, S., Sarikas, A., et al. (2020). D-galactose decreases anion exchange capability through band 3 protein in human erythrocytes. *Antioxidants (Basel)* 9, 689. doi:10.3390/antiox9080689
- Remigante, A., Spinelli, S., Basile, N., Caruso, D., Falliti, G., Dossena, S., et al. (2022a). Oxidation stress as a mechanism of aging in human erythrocytes: protective effect of quercetin. *Int. J. Mol. Sci.* 23, 7781. doi:10.3390/ijms23147781
- Remigante, A., Spinelli, S., Marino, A., Pusch, M., Morabito, R., and Dossena, S. (2023a). Oxidative stress and immune response in melanoma: ion channels as targets of therapy. *Int. J. Mol. Sci.* 24, 887. doi:10.3390/ijms24010887
- Remigante, A., Spinelli, S., Pusch, M., Sarikas, A., Morabito, R., Marino, A., et al. (2022b). Role of SLC4 and SLC26 solute carriers during oxidative stress. *Acta Physiol. (Oxf)* 235, e13796. doi:10.1111/apha.13796
- Remigante, A., Spinelli, S., Straface, E., Gambardella, L., Caruso, D., Falliti, G., et al. (2022c). Açai (*Euterpe oleracea*) extract protects human erythrocytes from age-related oxidative stress. *Cells* 11, 2391. doi:10.3390/cells11152391
- Remigante, A., Spinelli, S., Straface, E., Gambardella, L., Caruso, D., Falliti, G., et al. (2022d). Antioxidant activity of quercetin in a H_2O_2 -induced oxidative stress model in red blood cells: functional role of band 3 protein. *Int. J. Mol. Sci.* 23, 10991. doi:10.3390/ijms231910991
- Remigante, A., Spinelli, S., Straface, E., Gambardella, L., Russo, M., Cafeo, G., et al. (2023b). Mechanisms underlying the anti-aging activity of bergamot (*Citrus bergamia*) extract in human red blood cells. *Front. Physiol.* 14, 1225552. doi:10.3389/fphys.2023.1225552
- Remigante, A., Spinelli, S., Trichilo, V., Loddo, S., Sarikas, A., Pusch, M., et al. (2022e). D-Galactose induced early aging in human erythrocytes: role of band 3 protein. *J. Cell Physiol.* 237, 1586–1596. doi:10.1002/jcp.30632
- Remigante, A., Zuccolini, P., Barbieri, R., Ferrera, L., Morabito, R., Gavazzo, P., et al. (2021b). NS-11021 modulates cancer-associated processes independently of BK channels in melanoma and pancreatic duct adenocarcinoma cell lines. *Cancers (Basel)* 13, 6144. doi:10.3390/cancers13236144
- Rinalducci, S., D'Amici, G. M., Blasi, B., Vaglio, S., Grazzini, G., and Zolla, L. (2011). Peroxiredoxin-2 as a candidate biomarker to test oxidative stress levels of stored red

- blood cells under blood bank conditions. *Transfusion* 51, 1439–1449. doi:10.1111/j.1537-2995.2010.03032.x
- Rinalducci, S., Ferru, E., Blasi, B., Turrini, F., and Zolla, L. (2012). Oxidative stress and caspase-mediated fragmentation of cytoplasmic domain of erythrocyte band 3 during blood storage. *Blood Transfus.* 10 (2), s55–s62. doi:10.2450/2012.009S
- Romano, L., and Passow, H. (1984). Characterization of anion transport system in trout red blood cell. *Am. J. Physiol.* 246, C330–C338. doi:10.1152/ajpcell.1984.246.3.C330
- Romano, L., Peritore, D., Simone, E., Sidoti, A., Trischitta, F., and Romano, P. (1998). Chloride-sulphate exchange chemically measured in human erythrocyte ghosts. *Cell Mol. Biol. (Noisy-le-grand)* 44, 351–355.
- Sicinska, P. (2018). Di-n-butyl phthalate, butylbenzyl phthalate and their metabolites induce haemolysis and eryptosis in human erythrocytes. *Chemosphere* 203, 44–53. doi:10.1016/j.chemosphere.2018.03.161
- Speer, H., D'cunha, N. M., Alexopoulos, N. I., Mckune, A. J., and Naumovski, N. (2020). Anthocyanins and human health-A focus on oxidative stress, inflammation and disease. *Antioxidants (Basel)* 9, 366. doi:10.3390/antiox9050366
- Spinelli, S., Straface, E., Gambardella, L., Caruso, D., Falliti, G., Remigante, A., et al. (2023). Aging injury impairs structural properties and cell signaling in human red blood cells; açai berry is a keystone. *Antioxidants (Basel)* 12, 848. doi:10.3390/antiox12040848
- Straface, E., Rivabene, R., Masella, R., Santulli, M., Paganelli, R., and Malorni, W. (2002). Structural changes of the erythrocyte as a marker of non-insulin-dependent diabetes: protective effects of N-acetylcysteine. *Biochem. Biophys. Res. Commun.* 290, 1393–1398. doi:10.1006/bbrc.2002.6340
- Tsamesidis, I., Perio, P., Pantaleo, A., and Reybier, K. (2020). Oxidation of erythrocytes enhance the production of reactive species in the presence of artemisinin. *Int. J. Mol. Sci.* 21, 4799. doi:10.3390/ijms21134799
- Ugusman, A., Hui, C. K., and Wan Ahmad, W. a.N. (2023). Editorial: benefits of bioactive plant-based compounds supplementation on cardiovascular and metabolic health. *Front. Nutr.* 10, 1197450. doi:10.3389/fnut.2023.1197450
- Ulanczyk, Z., Grabowicz, A., Cecerska-Heryc, E., Sleboda-Taront, D., Krytkowska, E., Mozolewska-Piotrowska, K., et al. (2020). Dietary and lifestyle factors modulate the activity of the endogenous antioxidant system in patients with age-related macular degeneration: correlations with disease severity. *Antioxidants (Basel)* 9, 954. doi:10.3390/antiox9100954
- Vallese, F., Kim, K., Yen, L. Y., Johnston, J. D., Noble, A. J., Cali, T., et al. (2022). Architecture of the human erythrocyte ankyrin-1 complex. *Nat. Struct. Mol. Biol.* 29, 706–718. doi:10.1038/s41594-022-00792-w
- Van 't Erve, T. J., Wagner, B. A., Ryckman, K. K., Raife, T. J., and Buettner, G. R. (2013). The concentration of glutathione in human erythrocytes is a heritable trait. *Free Radic. Biol. Med.* 65, 742–749. doi:10.1016/j.freeradbiomed.2013.08.002
- Vona, R., Gambardella, L., Cittadini, C., Straface, E., and Pietraforte, D. (2019). Biomarkers of oxidative stress in metabolic syndrome and associated diseases. *Oxid. Med. Cell Longev.* 2019, 8267234. doi:10.1155/2019/8267234
- Voskou, S., Aslan, M., Fanis, P., Phylactides, M., and Kleanthous, M. (2015). Oxidative stress in beta-thalassaemia and sickle cell disease. *Redox Biol.* 6, 226–239. doi:10.1016/j.redox.2015.07.018
- Wang, S., Meckling, K. A., Marccone, M. F., Kakuda, Y., and Tsao, R. (2011). Synergistic, additive, and antagonistic effects of food mixtures on total antioxidant capacities. *J. Agric. Food Chem.* 59, 960–968. doi:10.1021/jf1040977
- Xiong, Y., Li, Y., Xiong, Y., Zhao, Y., Tang, F., and Wang, X. (2013). Cluster of erythrocyte band 3: a potential molecular target of exhaustive exercise-induced dysfunction of erythrocyte deformability. *Can. J. Physiol. Pharmacol.* 91, 1127–1134. doi:10.1139/cjpp-2013-0145
- Yasin, Z., Witting, S., Palascak, M. B., Joiner, C. H., Rucknagel, D. L., and Franco, R. S. (2003). Phosphatidylserine externalization in sickle red blood cells: associations with cell age, density, and hemoglobin F. *Blood* 102, 365–370. doi:10.1182/blood-2002-11-3416
- Yeung, Y. G., and Stanley, E. R. (2009). A solution for stripping antibodies from polyvinylidene fluoride immunoblots for multiple reprobing. *Anal. Biochem.* 389, 89–91. doi:10.1016/j.ab.2009.03.017
- Zhang, L., Wang, X., Cueto, R., Effi, C., Zhang, Y., Tan, H., et al. (2019). Biochemical basis and metabolic interplay of redox regulation. *Redox Biol.* 26, 101284. doi:10.1016/j.redox.2019.101284
- Zheng, L., Dong, H., Su, G., Zhao, Q., and Zhao, M. (2016). Radical scavenging activities of Tyr-Trp-Cys- and Met-Gly and their protective effects against AAPH-induced oxidative damage in human erythrocytes. *Food Chem.* 197, 807–813. doi:10.1016/j.foodchem.2015.11.012
- Zimowska, W., Motyl, T., Skierski, J., Balasinska, B., Ploszaj, T., Orzechowski, A., et al. (1997). Apoptosis and Bcl-2 protein changes in L1210 leukaemic cells exposed to oxidative stress. *Apoptosis* 2, 529–539. doi:10.1023/a:1026490631930
- Zuccolini, P., Ferrera, L., Remigante, A., Picco, C., Barbieri, R., Bertelli, S., et al. (2022). The VRAC blocker DCPIB directly gates the BK channels and increases intracellular Ca(2+) in melanoma and pancreatic duct adenocarcinoma cell lines. *Br. J. Pharmacol.* 179, 3452–3469. doi:10.1111/bph.15810



OPEN ACCESS

EDITED BY

Andrea Gerbino,
University of Bari Aldo Moro, Italy

REVIEWED BY

Pooja Kaushik,
Jamia Hamdard University, India
Ciro Menale,
University of Naples Federico II, Italy

*CORRESPONDENCE

Marika Cordaro,
✉ cordarom@unime.it

[†]These authors share first authorship

RECEIVED 13 October 2023

ACCEPTED 15 December 2023

PUBLISHED 05 January 2024

CITATION

Interdonato L, Marino Y, Impellizzeri D, D'Amico R, Siracusa R, Fusco R, Cammilleri G, Pantano L, Modafferi S, Abdelhameed AS, Fritsch T, Rashan LJ, Cuzzocrea S, Calabrese V, Cordaro M and Di Paola R (2024), Autophagy machinery plays an essential role in traumatic brain injury-induced apoptosis and its related behavioral abnormalities in mice: focus on *Boswellia Sacra* gum resin. *Front. Physiol.* 14:1320960. doi: 10.3389/fphys.2023.1320960

COPYRIGHT

© 2024 Interdonato, Marino, Impellizzeri, D'Amico, Siracusa, Fusco, Cammilleri, Pantano, Modafferi, Abdelhameed, Fritsch, Rashan, Cuzzocrea, Calabrese, Cordaro and Di Paola. This is an open-access article distributed under the terms of the [Creative Commons Attribution License \(CC BY\)](#). The use, distribution or reproduction in other forums is permitted, provided the original author(s) and the copyright owner(s) are credited and that the original publication in this journal is cited, in accordance with accepted academic practice. No use, distribution or reproduction is permitted which does not comply with these terms.

Autophagy machinery plays an essential role in traumatic brain injury-induced apoptosis and its related behavioral abnormalities in mice: focus on *Boswellia Sacra* gum resin

Livia Interdonato^{1†}, Ylenia Marino^{1†}, Daniela Impellizzeri¹, Ramona D'Amico¹, Rosalba Siracusa¹, Roberta Fusco¹, Gaetano Cammilleri², Licia Pantano², Sergio Modafferi³, Ali S. Abdelhameed⁴, Tilman Fritsch⁵, Luay J. Rashan⁶, Salvatore Cuzzocrea¹, Vittorio Calabrese³, Marika Cordaro^{7*} and Rosanna Di Paola⁸

¹Department of Chemical and Biological, Pharmaceutical and Environmental Sciences, University of Messina, Messina, Italy, ²Chemistry Department, Istituto Zooprofilattico Sperimentale Della Sicilia, Palermo, Italy, ³Department of Biomedical and Biotechnological Sciences, University of Catania, Catania, Italy, ⁴Department of Pharmaceutical Chemistry, College of Pharmacy, King Saud University, Riyadh, Saudi Arabia, ⁵NAM-Institute, Salzburg, Austria, ⁶Medicinal Plants Division, Research Center, Dhofar University, Salalah, Oman, ⁷Department of Biomedical, Dental and Morphological and Functional Imaging University of Messina, Messina, Italy, ⁸Department of Veterinary Sciences, University of Messina, Messina, Italy

Traumatic brain injury (TBI) is described as a structural damage or physiological disturbance of brain function that occurs after trauma and causes disability or death in people of all ages. New treatment targets for TBI are being explored because current medicines are frequently ineffectual and poorly tolerated. There is increasing evidence that following TBI, there are widespread changes in autophagy-related proteins in both experimental and clinical settings. The current study investigated if *Boswellia Sacra* Gum Resin (BSR) treatment (500 mg/kg) could modulate post-TBI neuronal autophagy and protein expression, as well as whether BSR could markedly improve functional recovery in a mouse model of TBI. Taken together our results shows for the first time that BSR limits histological alteration, lipid peroxidation, antioxidant, cytokines release and autophagic flux alteration induced by TBI.

KEYWORDS

TBI, autophagy, apoptosis, behavioral, *Boswellia sacra*

1 Introduction

With more than 1.7 million new cases each year and 60% of all trauma-related deaths in the U.S., TBI is a significant public health issue. TBI causes secondary brain injury, which sets off a chain reaction of pathophysiological events that cause neuronal cell death, brain edema, and neurological impairments. These events include oxidative stress, autophagy, inflammation, and apoptosis. However, there are currently no viable treatments for TBI

patients undergoing clinical intervention. Understanding the pathophysiological mechanisms following TBI and locating new therapeutic methods are thus crucial and urgent (Zeng et al., 2020). The latter indicates delayed and perhaps reversible molecular and cellular pathophysiological pathways that start shortly after the first injury and may last for months or years (Bramlett and Dietrich, 2007; Wu and Lipinski, 2019). Despite the fact that most current research has focused on the earliest cellular and molecular events, experimental and clinical data indicate that central nervous system (CNS) trauma-mediated pathophysiological changes may persist for years, causing chronic post-mitotic cell loss and activation of microglia and astrocytes as well as chronic functional deficits (Ramlackhansingh et al., 2011). A growing database of research shows that substantial changes in autophagy-related proteins occur after TBI in both experimental and clinical settings (Zeng et al., 2020). Neurological impairments and mortality are mostly caused by cell death following neurotrauma. Even though CNS damage affects many different cell types, including neurons and oligodendrocytes, the mechanisms of neuronal cell death have received most of the attention. Multiple cell death mechanisms exist in the damaged CNS after trauma such as apoptosis and autophagy (Stoica and Faden, 2010; Schoch et al., 2012). Long-lived cytosolic proteins and damaged organelles increase a defective autophagic machinery that could lead to apoptosis. The transfer of the desired components to the lysosome includes a series of sequential steps, including the creation of a double membrane, elongation, and ultimately vesicle maturation. The morphology of apoptotic cell is the best way to explain it. Cell rounding, membrane blebbing, cytoskeletal collapse, cytoplasmic condensation and fragmentation, nuclear pyknosis, chromatin condensation and fragmentation, and the development of membrane-encased apoptotic bodies—bodies that are quickly phagocytosed by macrophages or nearby cells—are its distinguishing features (Ghavami et al., 2014). It is interesting that the Bcl-2 family of proteins and other regulatory elements such as AMP-activated protein kinase (AMPK) that are shared by both apoptosis and autophagy (Pattinire et al., 2005). The variety of cell death routes, which have overlapping and different molecular causes, as well as the limited therapeutic window for some types of neuronal cell death, are barriers to effective therapy against neurotrauma-induced neuronal cell death (Faden, 2002).

At present time, there are no effective therapies available for TBI patients receiving clinical intervention. Oral supplementation with vegetal bioactive compounds shows promise in delaying the irreversible course in this discouraging situation (Stacchiotti and Corsetti, 2020). However, given that the “one-drug, one-target” approach to treating the complex pathophysiology of traumatic brain injury (TBI) has not proven to be effective in clinical settings, traditional medicinal herbs or plants could have a pleiotropic effects and may offer a viable therapeutic supplementation (Di Paolo et al., 2019). Various substances have been employed thus far to control autophagic activity after traumatic brain injury. For instance, apocynin, quercetin, luteolin, polyphenols baicalin and more are found in a wide variety of fruits and vegetables as a modulator of TBI-related neuronal injury (Zeng et al., 2020). The botanical name for frankincense is *Boswellia sacra* Fluck, and it is a member of the Burseraceae family. The majority of these *Boswellia* species’ chemical components are comparable. The

most widely used type of *Boswellia* in Arab nations is *Boswellia sacra*, often known as “*Omani Luban*” which has long been used to cure a variety of illnesses (Al-Yahya et al., 2020; Alyahya and Asad, 2020). Acetyl-11-keto-beta-boswellic acid (AKBA) and 11-keto-beta-boswellic acid (KBA), which have been investigated for their possible pharmacological and therapeutic qualities, are the two most powerful anti-inflammatory boswellic acids found in *Boswellia* (Asad and Alhomoud, 2016). The bioactive phytoconstituents of *boswellia*, boswellic acids and pentacyclic triterpenoids have demonstrated encouraging outcomes in both experimental and clinical research. It is thought to be a potentially useful natural pharmacophoric molecule that could be important for finding anti-inflammatory and therapeutic drugs (Iram et al., 2017). It is traditionally used to cure stomach, skin, ear, and throat infections, to relieve menstruation pain, cardiovascular and neurological issues, etc. It is also chewed as a mouth freshener in many nations. Additionally, goods derived from *Boswellia* oleo gum resin are sold all over the world for a variety of purposes (Hamidpour et al., 2013; Liu et al., 2018; Mojaverrostami et al., 2018). In this study, we examined the neuroprotective effects of *Boswellia Sacra Resin* (BSR) against apoptosis TBI-induced with a particularly attention to autophagic flux modulation.

2 Materials and methods

2.1 Reagents and gases

Acetone, acetonitrile, and formic acid (purity > 99.9%) were purchased from Sigma Aldrich (Amsterdam, Holland); hydrochloric acid was purchased from Carlo Erba (Milan, Italy). The standard solutions (purity > 99.9%) at 1,000 mg L⁻¹ of gallic acid, catechin, caffeic acid, syringic acid, rutin, ellagic, hesperidin, ferulic acid, myricetin, quercetin, apigenin, naringenin and kaempferol were purchased from Sigma-Aldrich S. r.l. (Milan, Italy); chlorogenic acid was purchased from VWR (Milan, Italy). Apigenin and kaempferol were dissolved in aqueous solution at pH > 8.

2.2 Sample extraction

The sample extraction was carried out according to protocols previously reported (Puigventos et al., 2015). In brief, 0.1 g of sample was weighted and added to 10 mL of acetone/water/hydrochloridric acid solution (70:29:0.1 v/v/v). The mixture was sonicated for 30 min. Subsequently, the mixture was centrifugated for 15 min at 3,500 rpm, and the supernatant filtered with 0.45 µm nylon filters and stored at -4°C until the analysis.

2.3 Materials

Oleo gum resins were collected from verified *Boswellia sacra* Fluck trees of Wadi Doka (Najdi type resin) on the plateau region north of Salalah during 2023. The sample was collected by traditional method. This region experiences a desert climate, with low rainfall (<100 mm annually) and sharp temperature variations throughout the day. The oleo gum resin was authenticated by

comparison with preserved voucher samples stored at the Herbarium of Nizwa University, Oman. Unless otherwise stated, all compounds were purchased from Sigma-Aldrich.

2.4 LC-HRMS conditions and validation of the method

The chromatographic separations were carried out as reported before with a Raptor C18 column (2.1 mm × 100 mm, 1.7 μm) (Cammilleri et al., 2023). The mobile phase consisted of eluent A: H₂O + formic acid 1%, eluent B: acetonitrile + formic acid 1% for a total run time of 14 min with a flow rate of 0.3 mL min⁻¹.

As a mass spectrometer, a Q Exactive™ Plus Hybrid Quadrupole-Orbitrap™ (Thermo Fisher Scientific, California, United States) was employed. The Full MS scan/dd-MS²-SIM mode was used to collect all data. The resolution of the Orbitrap was adjusted to 70,000 FWHM (scan range 100–1,000 m/z). For a maximum injection period of 200 ms, the automatic gain control (AGC) was set to 3 × 10⁶ ions. The product ions were discovered by raising the normalized collision energy until the precursor ions were completely fragmented. Each analyte was assigned a normalized collision energy (NCE) value. The retention time (tR), accurate mass, and distinctive fragmentation were used to identify the analytes. Each day before the study, an external calibration for mass accuracy was done. The Thermo Xcalibur™ version 4.0 software was used to record and expound on acquisition data. The method's performance was evaluated for linearity, specificity, and trueness in compliance with Commission Decision 2002/657. The limits of detection and quantification (LODs and LOQs) were determined by the 3σ and 10σ approach. The linearity test yielded good results for all analytes tested ($r^2 > 0.993$). Trueness by recovery yielded values ranging between 80% and 105%. The polyphenols concentrations were expressed as μg/Kg.

2.5 Extraction of the Boswellia sacra gum resin (BSR) acid fraction

The particle size of the harvested oleo gum of Boswellia sacra resin (BSR) was reduced to a coarse powder with a mortar and a pestle for 2 hours. A fine powder was produced with an electrical grinder. 200 g were placed into a 5,000 mL bottom flask, 2 L of distilled water were added. A hydro distillation with a Clevenger type apparatus was performed under atmospheric pressure. The resulting essential oil was collected (14.2 mL). After 6–8 h no further increase of essential oil was observed. The remaining mixture was filtered (Whatman filter paper, grades 1,2 and 3), the residue was washed out with hot water 3–4 times. The filtrate was cold down to 0°C to obtain a precipitate. After 60 min the precipitate was collected and washed out several times with cold distilled water, dried under vacuo and powdered with the electrical grinder. To reduce the water content below the powder was transferred into a desiccator and this is followed by sieving the powder into a very fine mesh at 40°C for 5 days. The final particle size (3–5 mm) the resulting BSR acid fraction (80 g) was produced by grinding the material at a temperature below 0°C.

2.6 HPLC analysis of BSR for pentacyclic triterpenic acids

For chemical characterization of the BSR acid fraction, eight pentacyclic triterpenic acids (PTA), alpha-boswellic acid (alpha-BA), acetyl-alpha-boswellic acid (alpha-ABA), beta-boswellic acid (beta-BA), acetyl-Beta-boswellic acid (B-ABA), 11-keto-beta-boswellic acid (KBA), acetyl-11-keto-beta-boswellic acid (AKBA), lupeolic acid (LA), and acetyl-lupeolic acid (ALA), were quantified by HPLC analysis. For detailed information please see our previous work (Schmiech et al., 2019).

2.7 Animals

CD1 male mice (8-week-old, 18–24 g) were acquired from Envigo (Milan, Italy) and located in a controlled environment and provided with standard rodent chow (Teklad standard diet acquire from Envigo) and water available *ad libitum*. They were housed 5 mice/cage and maintained in a 12:12 h light–dark cycle at 21°C ± 1°C and 50% ± 5% humidity. The University of Messina Review Board for animal care (OPBA) approved the study (P.R. 89126.8).

2.8 Experimental design and groups

The controlled impactor device Impact One™ Stereotaxic impactor for controlled cortical impact (CCI) (Leica, Milan, Italy) was used to create a cortical contusion on the exposed cortex after a craniotomy (tip diameter: 4 mm; cortical contusion depth: 3 mm; impact velocity: 1.5 m/s). The clinical symptoms and weight of the animals were monitored daily and recorded. Sham mice underwent the identical surgical procedure but were not injured (Impellizzeri et al., 2017; Fusco et al., 2020; Campolo et al., 2021).

Mice were divided as following:

- Sham + vehicle group: mice were subjected to the surgical procedures as above except that the impact was not applied, and animals were treated o. s. with vehicle (data not shown).
- Sham + BSR: mice were subjected to the surgical procedures as above except that the impact was not applied, and animals were treated o. s. with 500 mg/kg on BSR in saline 1 h after TBI medical procedures.
- TBI: mice were subjected to CCI plus administration of vehicle (saline).
- TBI + BSR: As for the TBI + vehicle group but BSR was administered o. s. at 500 mg/kg in saline 1 h after TBI.

Taking into account that there is no discernible difference between the Sham and Sham + BSR groups we choose to shown in the figures Sham + BSR group. The animals of the first set of experiment were sacrificed 24 h after TBI induction. The animal of the second group pf experiment were sacrificed 30 days after TBI induction, and they received every days for 30 days starting 1 h after the damage orally administration of BSR at the dose of 500 mg/kg (see [Supplementary Material](#) for experimental design graph).

2.9 Behavioural analysis

30 days after the trauma induction, a designed group of animals underwent behavioural testing. Mice were moved to the behaviour testing room 30 min before the first trial started so they could become accustomed to the environment. Based on behavioural tests that were used to keep the environment as uniform as feasible, animals were trained to use the equipment before every recording. The behavioural tests were conducted by three distinct trustworthy experts who were blinded to the animals' damage state. Below a brief description of tests.

2.9.1 Force swimming test (FST)

The method is based on that which Porsolt et al. described (Porsolt et al., 1979). Briefly, FST is used to assess depressive-like conditions. Mice are placed in an impenetrable, transparent tank filled with water, and their movement behaviour related to escape is recorded. In this experiment, for 6 minutes, each mouse was gently placed in the cylinder, and the duration of floating was recorded. During the final 4-min of the test, immobility was examined (Genovese et al., 2021).

2.9.2 Open field test (OFT)

The OFT, created by Calvin S. Hall, is an experiment that measures a rodent's general locomotor activity levels, anxiety, and exploratory willingness. Each mouse in this experiment was trained before being put in the centre of the box, where activity was then recorded for 5 minutes of exploration (Prut and Belzung, 2003).

2.9.3 Elevated plus maze (EPM)

Utilizing the Elevated Plus Maze (EPM) test, rodents' anxiety-related behaviour is evaluated. The EPM device is made up of a core region, two oppositely positioned open arms, two oppositely positioned closed arms, with an elevated "+"-shaped maze. A video camera set above the maze records the subjects' actions while they freely navigate it, and their actions are then analysed. After training, it was counted how many times the mice entered each arm and how long they spent in open arms (Pellow et al., 1985).

2.9.4 Morris Water Maze (MWM)

Hippocampal-dependent spatial learning and memory were assessed using the MWM test (Zhao et al., 2017; Siebold et al., 2020). Following a training session, a mouse was placed in the water in each of the three separate quadrants and given 1 minute to swim there. The platform was taken away for the test 1 day following the navigation experiment. It was noted how much time was spent in the target quadrant.

2.9.5 Novel object recognition (NOR)

The NOR test was used to determine whether mice had a natural tendency to spend time studying unfamiliar or familiar objects. Mice were placed in the box for 5 min after a training session, during which the examiner replaced one of the familiar objects with a novel one at random. Each object's total amount of mouse exploration time was recorded (Siracusa et al., 2017; Pan et al., 2018).

2.10 Histological brain analysis

After the experiment, brain tissue was removed, fixed at room temperature in buffered formaldehyde solution (10% in phosphate buffered saline), dehydrated by graduated ethanol, and then embedded in paraffin. Light microscopy was used to examine tissue sections that were 7 μ m thick after being deparaffinized with xylene and stained with haematoxylin/eosin (Bio-Optica, Milan, Italy). The number of damaged neurons was counted, and the grey matter's histopathologic alterations were graded on a 6-point scale: No lesion was found, 1; 1–5 eosinophilic neurons were present in the Gray matter, 2; 5–10 eosinophilic neurons were present, 3; more than 10 eosinophilic neurons were present, 4; a small infarction (less than one third of the grey matter area), 5; a moderate infarction (one third to one half of the Gray matter area); and 6, a large infarction (more than half of the grey matter area). To determine a final score for each mouse, the results from every part of each brain were averaged. The slices were then analysed by a blinded histopathologist using an optical microscope using a Leica DM6 microscope (Leica Microsystems Spa, Milan, Italy) (Petrosino et al., 2017).

2.11 Cytokines measurement

Using commercially available enzyme-linked immunosorbent assay (ELISA) kits (R&D Systems, Minneapolis, MN, United States) in accordance with the manufacturer's instructions, TNF- α , IL-1 β , and IL-6 levels from brain were measured as previously described (Cordaro et al., 2020a).

2.12 Antioxidants and malondialdehyde measurement

The supernatant of the brain tissue homogenate was centrifuged (14,000 rpm at 4°C for 30 min) as previously described (Marklund and Marklund, 1974; Rajasankar et al., 2009). ELISA kits (R&D Systems, Minneapolis, MN, United States) were used to measure superoxide dismutase (SOD) and glutathione (GSH-Px) levels. The test procedure was described in detail in the manufacturer's manuals. Levels of malondialdehyde in brain tissue were determined as an indicator of lipid peroxidation (Ohkawa et al., 1979). Briefly, brain tissues were weighed and homogenized in a 1.15% (wt/vol) KCl solution. 100 μ L aliquots of homogenate were then removed and added to a reaction mixture containing 200 μ L 8.1% (wt/vol) lauryl sulfate, 1.5 mL 20% (vol/vol) acetic acid (pH 3.5), 1.5 mL 0.8% (wt/vol) thiobarbituric acid, and 700 μ L distilled water. Samples were then boiled for 1 hour at 95°C and centrifuged at 3000g for 10 min. The absorbance of the supernatant was measured spectrophotometrically at 532 nm. MDA levels were expressed as nmol/mg of tissue (Di Paola et al., 2009; Genovese et al., 2022).

2.13 Apoptosis and autophagy detection

The level of mRNA expression of apoptosis-related cytokines caspase-3, caspase-8, caspase-9, Bax, Bcl-2, and cytochrome c and

autophagy markers such as Beclin-1, LC3 AMPK and p62 were determined using real-time quantitative RT polymerase chain reaction (RT-PCR) as previously described (Liu and Saint, 2002; Hu et al., 2011; Wang et al., 2013; Ze et al., 2014; Wang et al., 2022): Caspase-8 Forward primer ATCTGCTGTATCCCAGC Reverse primer AGGCACTCCTTTCTGGAAGTTAC; Caspase-9 Forward primer GCGGTGGTGAGCAGAAAGA Reverse primer CCTGGG AAGGTGGAGTAGGA; Caspase-3 Forward primer CTGACTGGA AAGCCGAACTC Reverse primer GACTGGATGAACCACGAC CC; Bax Forward primer GGATGCGTCCACCAAGAAG Reverse primer CAAAGTAGAAGAGGGCAACCAC; Bcl-2 Forward primer TGTGGTCCATCTGACCTCC Reverse primer ACA TCTCCCTGTTGACGCTCT; Cytochrome c Forward primer CATCCCTTGACATCGTGCTT Reverse primer GGGTAGTCT GAGTAGCGTCGTG; LC3 Forward primer AACGTAGGCACC CACATAGG Reverse primer GAAGAGACTGCCCTGACAC; Beclin1 Forward primer GAACTCTGGAGGTCTCGCT Reverse primer CACCCAGGCTCGTTCTACC; p62 Forward primer AGT CCAGAATTCCTGCCTGA Reverse primer TTCATTGGCTT CACATGAA; adenosine monophosphate (AMP) activated protein kinase (AMPK) Forward primer GTGATCAGCACTCCG ACAGA Reverse primer TCTCTGGCTTCAGGTCCCTA; β -actin Forward primer AATGTGTCCGTCGTGGATCTGA Reverse primer AGTGTAGCCCAAGATGCCCTTC.

2.14 Western Blots

Cytosolic extracts were prepared as previously described (Cordaro et al., 2017; Di Paola et al., 2021a; Di Paola et al., 2021b). The following primary antibodies were used: anti-Bax (1:500; SCB, B-9 sc-7480), anti-Bcl-2 (1:500; SCB, C-2 sc-7382), Beclin-1 (1:500; SCB, sc-48381) and LC3 (1:500; SCB, sc-271625) in 1× PBS, 5% w/v non-fat dried milk, 0.1% Tween-20 at 4°C overnight (Impellizzeri et al., 2016a; Paterniti et al., 2017; Cordaro et al., 2018; Cordaro et al., 2020b; Crupi et al., 2020). Blots were further probed with an anti- β -actin protein antibody (1:500; SCB) for the cytosolic fraction to make sure that they were loaded with an equivalent number of proteins (Di Paola et al., 2016a; Cordaro et al., 2020c). As directed by the manufacturer, signals were evaluated using an enhanced chemiluminescence (ECL) detection system reagent (Thermo, Monza, Italy) (Akki et al., 2018; Remigante et al., 2022). Using BIORAD ChemiDoc TM XRS + software and densitometry, the relative expression of the protein bands was measured and standardized to the levels of β -actin and lamin A/C (Paterniti et al., 2015; Di Paola et al., 2016b; Esposito et al., 2016; Siracusa et al., 2018; Peritore et al., 2020).

2.15 Statistical evaluation

The data in this study are presented as the average \pm SEM and represent at least three experiments conducted on various days. N denotes the number of animals utilized in in vivo experiments. The G*Power 3.1 software (Die Heinrich-Heine-Universität Düsseldorf, Düsseldorf, Germany) was employed to calculate the number of animals used in in vivo research. A competent histopathologist examined the data, without knowledge of the treatments. In all the

statistical studies, GraphPad Software Prism 9 (La Jolla, CA, United States) was used. One-way ANOVA was used to examine the data, and then a Bonferroni post-hoc test for multiple comparisons was used. A p -value of 0.05 or less was regarded as significant. In figure: ns $p > 0.05$; * $p \leq 0.05$; ** $p \leq 0.01$; *** $p \leq 0.001$; **** $p \leq 0.0001$.

3 Results

3.1 Polyphenols contents and HPLC-MS/MS analysis in BSR

The polyphenols contents found in the B. Sacra samples followed the order Petunidin > Pelargonidin > Cyanidin > Myricetin > Quercetin. Among the anthocyanins, a high presence of Petunidin (925.85 $\mu\text{g/Kg}$) (Figure 1A) was found, followed by Pelargonidin (2.36 $\mu\text{g/Kg}$) (Figure 1D) and Cyanidin (0.56 $\mu\text{g/Kg}$) (Figure 1E). Myricetin (47.10 $\mu\text{g/Kg}$) (Figure 1B) and Quercetin (1.78 $\mu\text{g/Kg}$) (Figure 1C) were the only flavonols detected. No cinnamate esters, hydroxycinnamic acids and other sub-classes of polyphenols were found. For chemical characterization of the BSR acid fraction were quantified by HPLC analysis eight pentacyclic triterpenic acids: alpha-boswellic acid (alpha-BA), acetyl-alpha-boswellic acid (alpha-ABA), beta-boswellic acid (beta-BA), acetyl-Beta-boswellic acid (B-ABA), 11-keto-beta-boswellic acid (KBA), acetyl-11-keto-beta-boswellic acid (AKBA), lupeolic acid (LA), and acetyl-lupeolic acid (ALA) (Figure 1F).

3.2 Effects of BSR on memory performance, locomotor activity changes brought on by TBI, and spatial learning

The MWM test was used to determine whether BSR could help with memory problems brought on by TBI. When compared to the controls, TBI-subjected animals took longer to find the platform during training (Figure 2A). In addition, the injured animal spent less time throughout the probe experiment in the target quadrant of the platform (Figure 2B). The escape latency was dramatically decreased (Figure 2A) and the duration spent in the target quadrant was increased (Figure 2B) after oral administration of BSR at a dose of 500 mg/kg, demonstrating an improvement in the cognitive deficiencies brought on by the trauma. We evaluated any shortcomings in their social interaction and exploratory behaviour using the NOR (Figure 2C) test. In this test, we discovered that after TBI, the amount of number of contacts were statistically reduced (Figure 2C). The administration of BSR, on the other hand, considerably improves the memory function harmed by trauma. The EPM test was also applied to mice to evaluate risk-taking behaviours and post-injury anxiety. According to the bibliography, fictitious animals spend more time in open arms whereas injured animals spend more time in closed arms, which also lowers the number of entries. However, compared to the TBI group, the animals that got oral BSR treatment spent longer time in the open arms and made more entrances (Figure 2D). The OFT was utilized to assess locomotor activity further. We found that following TBI injuries, mice spent less time in the centre and made fewer crossings, in contrast to

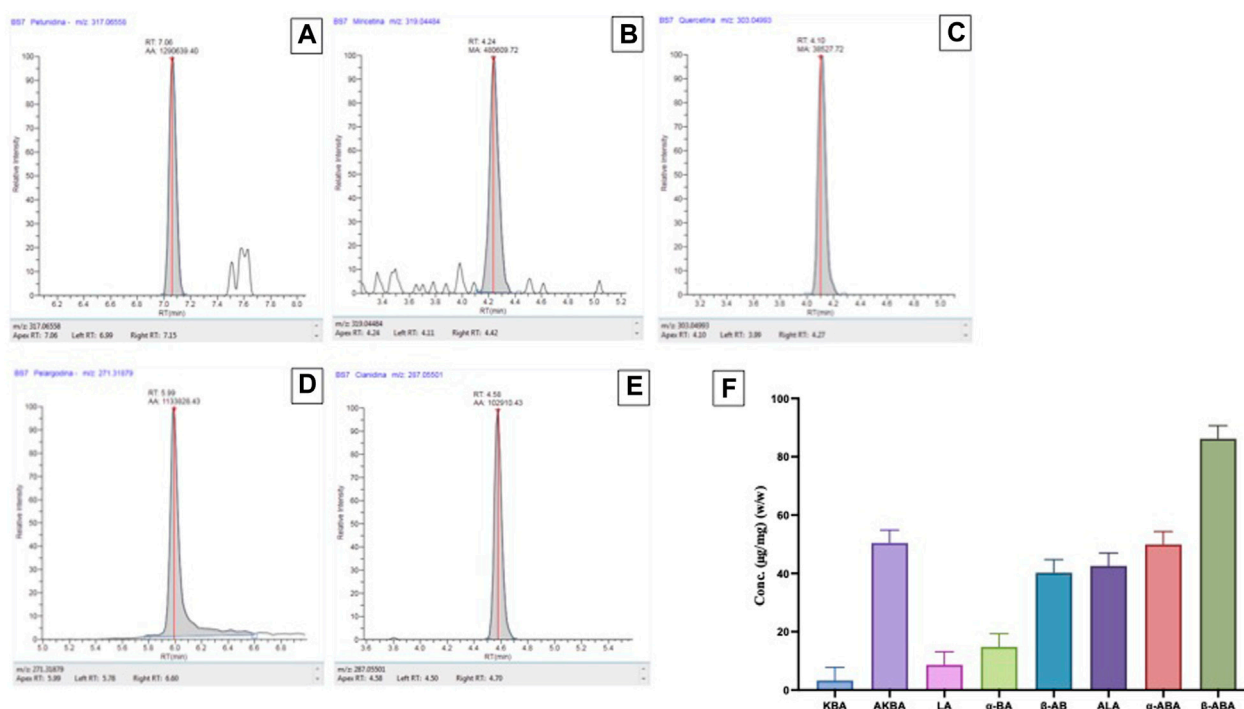


FIGURE 1

Polyphenols contents found in the BSR. Chromatogram of a B. Sacra sample analyzed by the LC-HRMS method. (A) = Petunidin; (B) = Myricetin; (C) = Quercetin; (D) = Pelargonidin; (E) = Cyanidin. HPLC (F) analysis for pentacyclic triterpenic acids: alpha-boswellic acid (alpha-BA), acetyl-alpha-boswellic acid (alpha-ABA), beta-boswellic acid (beta-BA), acetyl-Beta-boswellic acid (B-ABA), 11-keto-beta-boswellic acid (KBA), acetyl-11-keto-beta-boswellic acid (AKBA), lupeolic acid (LA), and acetyl-lupeolic acid (ALA).

sham animals. In this case, BSR was successful in resuming locomotor activity and the frequency of crossings (Figure 2E).

3.3 BSR limits histological alteration induced by TBI

Histological analysis of a brain sample taken from the TBI group 24 h after the TBI injury revealed significant tissue damage, inflammation, and architectural alterations when compared to brain from the sham group (Figures 3A, A' for sham; Figures 3B, B' for TBI, see histological score 3D). When administered at a dose of 500 mg/kg, BSR significantly lessened the severity of brain injury when compared to the TBI group (Figures 3C, C' see histological score Figure 3D).

3.4 BSR administration modulates lipid peroxidation, antioxidant, and cytokines release

Given the high concentration of polyunsaturated fatty acids in the brain, lipid peroxidation is the main manifestation of oxidative stress following TBI. Comparing the TBI group to the sham mice, we discovered that there was a considerably higher level of lipid peroxidation that was significantly attenuated following oral administration of BSR (Figure 4A). The cell is shielded from oxidative stress by enzymes that neutralize superoxide and H_2O_2 .

The primary defensive enzymes against superoxide radicals are GSH-Px and SOD (Cordaro et al., 2021a; Cordaro et al., 2021b). Oxidative stress impairs mitochondria's ability to function and move to synaptic areas, which causes synaptic dysfunction and neurodegeneration. After controlled cortical impact, we observed lower levels of SOD (Figure 4B) and GSH-Px (Figure 4C) compared to sham mice, according to the literature. Following oral administration of BSR at a dose of 500 mg/kg, physiological levels were practically replete. Cytokines storm promotes the inflammatory response by activating microglia and increasing the synthesis of chemokines, and preclinical models show that TBI causes neuronal injury with these raised levels (Ahmad et al., 2013; Gugliandolo et al., 2018). We used ELISA kits to measure the levels of TNF- α (Figure 4D), IL-6 (Figure 4E), and IL-1 β (Figure 4F). While the sham group had only trace quantities of this cytokine, brain samples from TBI mice had a substantial increase in all cytokines that was significantly reduced after oral administration of BSR at the dose of 500 mg/kg.

3.5 BSR limits neuronal death TBI

The discovery that caspase-mediated programmed cell death plays a significant role in secondary brain injury raises the possibility of a connection between pathogenic molecular pathways and healing (Jarrahi et al., 2020). For this reason, we made RT-PCR for Caspase-3 (Figure 5A), Caspase-8 (Figure 5B), Caspase-9 (Figure 5C), Bax (Figure 5D), Bcl-2 (Figure 5E), and Cytochrome

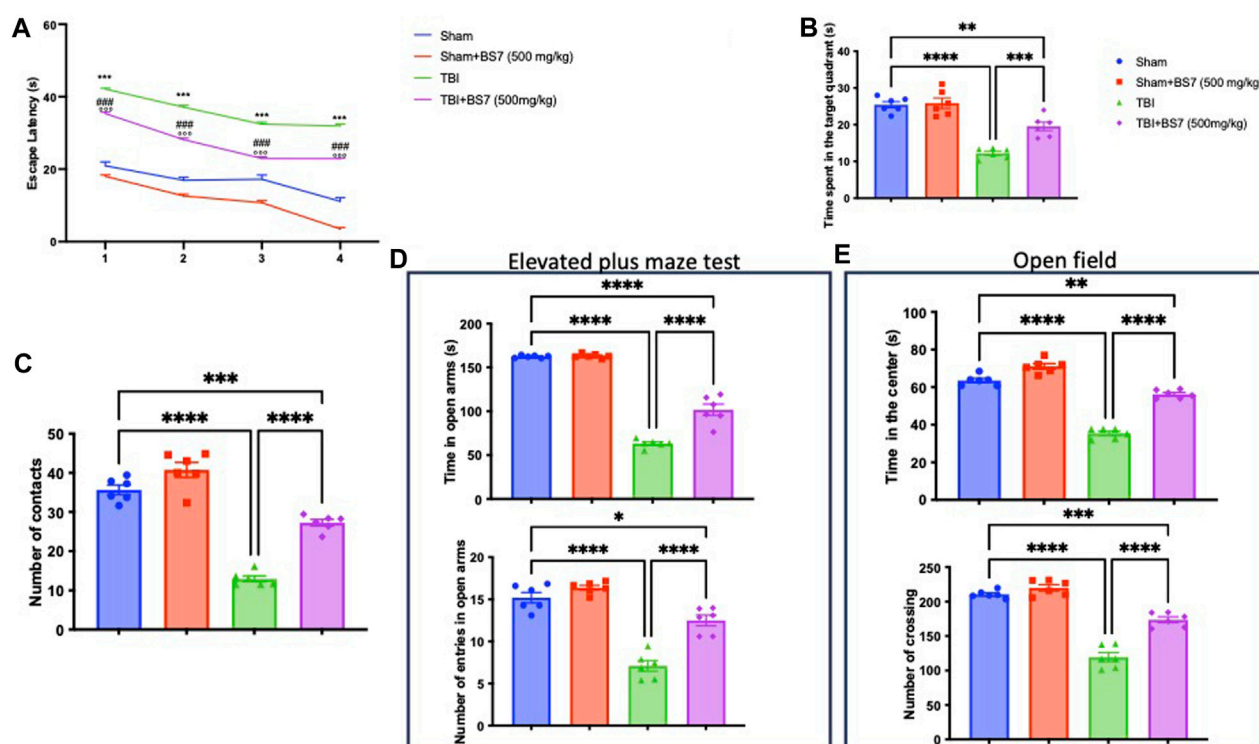


FIGURE 2

Effects of BSR on spatial learning, memory function, anxiety, and locomotor activity. Morris Water Maze training (A) and probe (B); novel object recognition (C); elevated plus maze test (D); Open field (E). As showed in panel 2, BSR administration significantly improve behavior recovery in terms of spatial learning, memory function, anxiety, and locomotor activity after TBI. The graphs are representative of at least three experiments performed on different experimental days. Each data is expressed as mean \pm S.E.M. from $n = 6$ male mice for each group. TBI + BS7 vs Sham.

C (Figure 5F). We found a significantly increase in apoptosis in animal subjected to the injury compared with the sham group except for BCL-2 in which we found a decrease of this expression. The same trend was also observed by western blot analysis of Bax and Bcl-2 (Figure 5G). On the other hand after BSR administration at the dose of 500 mg/kg all the expression of apoptotic marker were brought back to physiological levels.

3.6 BSR stimulate autophagic flux

Previous study demonstrates that the administration of Boswellia was able to stimulates autophagic flux in an experimental model of rotenone-induced neurotoxicity (Shadfar et al., 2022). In our work we found after RT-PCR analysis that after TBI there were an increase in autophagic flux as demonstrate by AMPK (Figure 6A), Beclin-1 (Figure 6B), LC3 (Figure 6C) and p62 (Figure 6D) compared to the control animals. The same trend was also observed by western blot analysis of Beclin-1 and LC3 (Figure 6E). Additionally, The single oral administration of BSR at the dose of 500 mg/kg significantly increased autophagic flux.

4 Discussion

TBI is regarded as a serious health issue that frequently results in mortality and disability and places a significant burden on medical

resources. The development of therapeutic methods to treat brain injury was not very rapid. Neuroprotection and neurorecovery are still the primary therapeutic approaches in development, aside from conservative care (Zhang et al., 2014). Studies have shown that secondary cell death, which may eventually make up as much as 40% of the total tissue loss, affects the prognosis after a TBI and so presents a significant pharmacological target for neuroprotective treatment (Smith et al., 2000). Since the dawn of medicine, natural compounds made from plants have been employed in healing. The phytochemicals have undergone substantial evaluation for drug development in recent decades. However, only a small number of these plant species have undergone thorough scientific scrutiny. Therefore, research into the bioactivities of these plants and phytochemicals is necessary. Even now, several of these historically utilized herbs and compounds produced from plants are still useful pharmacologically. One such healing plant is the Burseraceae genus *Boswellia Sacra*. Typically, triterpenoidal principles, essential oils, and carbohydrates make up the normal oleo-gum resin. Boswellic acids include β -boswellic acid, 11-keto- β -boswellic acid, and acetyl-11-keto- β -boswellic acid make up most of the oleo-gum resin. It is safe to use up to oral doses of 1,000 mg/kg in rats, as revealed by Al-Yahya and colleagues, who also showed that the methanolic extract of *Boswellia sacra* oleo gum resin did not create any significant effect on the kidney and liver with repeated dose administration for 28 days (Al-Yahya et al., 2020). Another study assessed the oral and intraperitoneal toxicity of boswellic acids in mice, rats, and monkeys for acute, subacute, and chronic effects. Boswellic acids were discovered to be safe up to the 2.0 g/kg investigated dosing levels

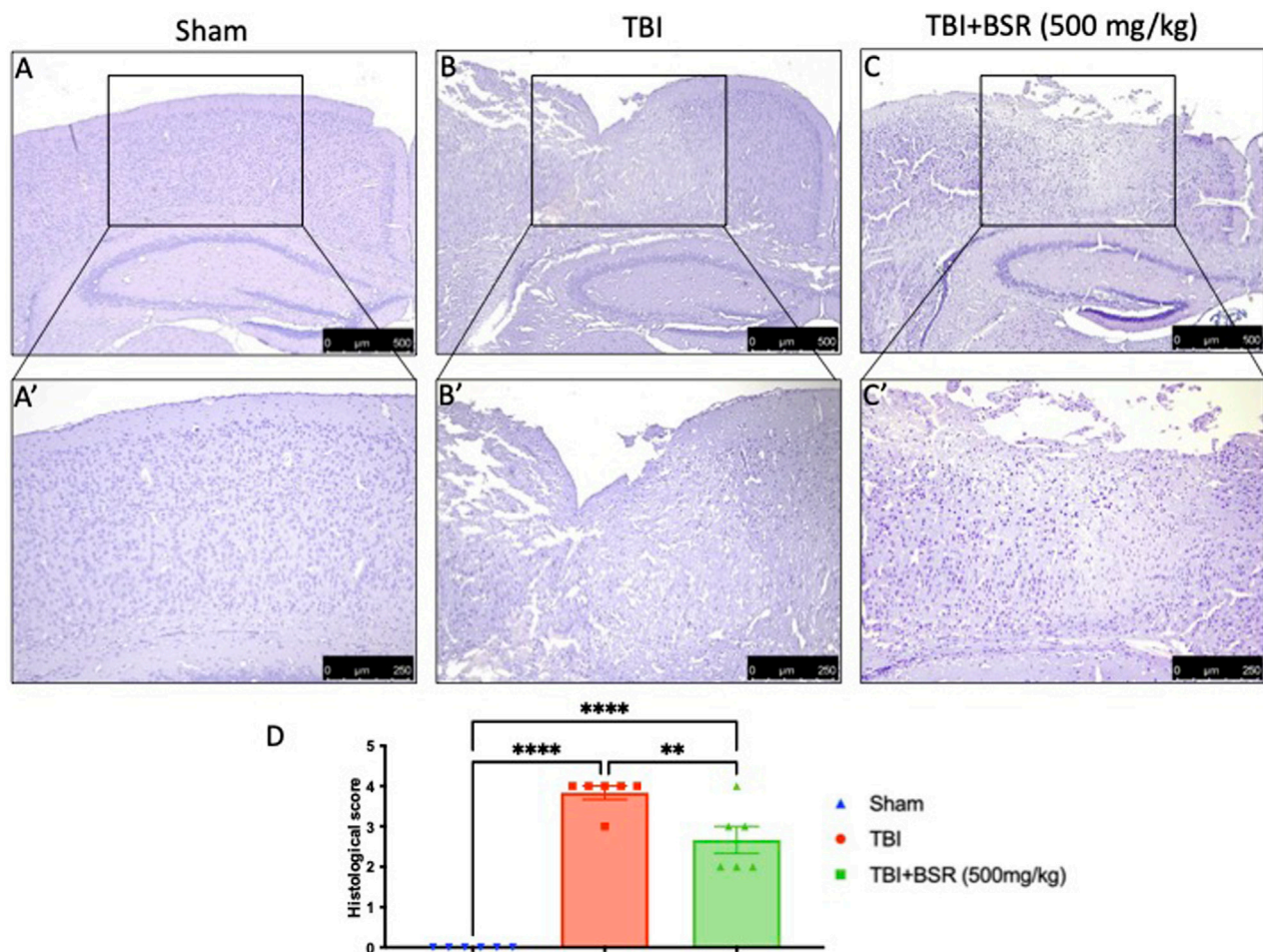


FIGURE 3

BSR limits histological alteration induced by TBI. Representative images of histological structure of: Sham (A) and higher magnification (A') TBI (B) and higher magnification (B') and TBI + BSR (C) and higher magnification (C'); histological score (D). The figures are representative of at least three experiments performed on different experimental days. Each data is expressed as mean \pm S.E.M. from $n = 6$ male mice for each group.

(Khan et al., 2016). With this background in our mind we want to elucidate the molecular pathways by which BSR could have a neuroprotective effects in an experimental model of TBI. It is common practice to examine the prevalent clinical problem in people using animal models of trauma. After a controlled cortical impact, animals that lead to neurological diseases such seizures and deteriorated memory and learning. In our investigation, a single oral dose of BSR at the dose of 500 mg/kg given 1 hour after trauma induction was able to reduce post-traumatic stress disorder symptoms such anxiety and altered locomotor activity while also improving spatial learning and memory. CCI is a consolidated models of brain trauma that induce a significantly alteration in histological architecture (Campolo et al., 2014; Impellizzeri et al., 2016b; Cordaro et al., 2016; Impellizzeri et al., 2017; Gugliandolo et al., 2018; Fusco et al., 2020; Cordaro et al., 2021a; Cordaro et al., 2021b). In our study we found that in the mice subjected to the trauma the perilesional area revealed considerable tissue damage, inflammation, and architecture alterations 24 h after TBI injury that was significantly reduced after the administration of BSR at the dose of 500 mg/kg. A common underlying cause of many neuropathologies is the overproduction of reactive oxygen species (ROS), reactive nitrogen species (RNS), and cytokines which have been demonstrated to harm a

variety of cellular components, including proteins, lipids, and DNA. Superoxide dismutase (SOD) and reduced glutathione (GSH), two endogenous defensive enzyme systems, can be overwhelmed by free radicals, especially superoxide ($O_2^{\cdot-}$), and non-radicals such hydrogen peroxide (H_2O_2) (Slemmer et al., 2008). In our study we found a significantly increase in lipid peroxidation as well as in pro inflammatory cytokines in animals subjected to the injury compared to the control group and a significantly reduction in physiological antioxidant system as demonstrated by the analysis of SOD and GSH-Px. On the other hands, a single oral administration of BSR, have been significantly limited these alterations. The three main types of cell death are necrosis, apoptosis, and autophagy. Apoptosis, in contrast to necrosis, is a tightly controlled and energy-intensive process that can be started by the original necrosis. We concentrated on apoptosis and autophagy because there were no specific ways to identify necrosis. The pathophysiology of brain injury in the TBI model heavily depends on apoptosis. The relative amounts of these genes, Bcl-2 and Caspases, which are commonly regarded as the most significant apoptotic regulators, influence the fate of cells (Zhang et al., 2014). In our study we found a significantly increase in apoptotic pathway as demonstrated by the increase in Caspase-3, Caspase-8, Caspase-9,

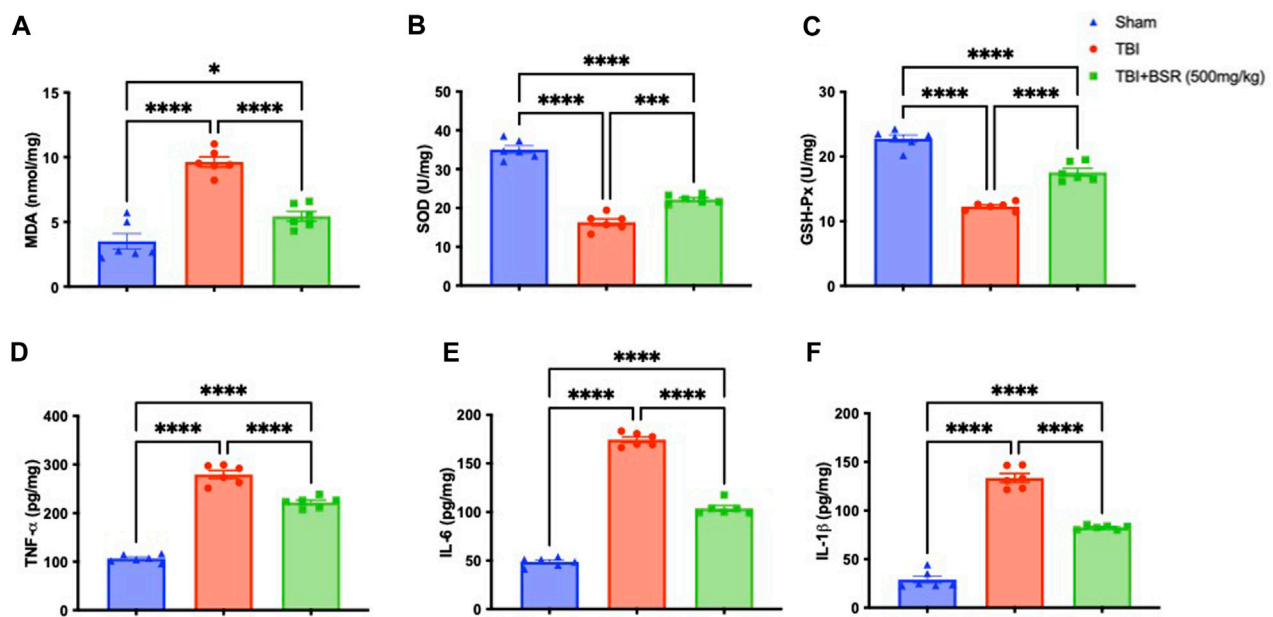


FIGURE 4

Effects of BSR administration on lipid peroxidation, antioxidant enzymes and cytokines release. MDA (A), SOD (B) and GSH-Px activity (C) TNF-α (D), IL-6 (E), and IL-1β (F). The graph is representative of at least three experiments performed on different experimental days. Each data is expressed as mean \pm S.E.M. from $n = 6$ male mice for each group.

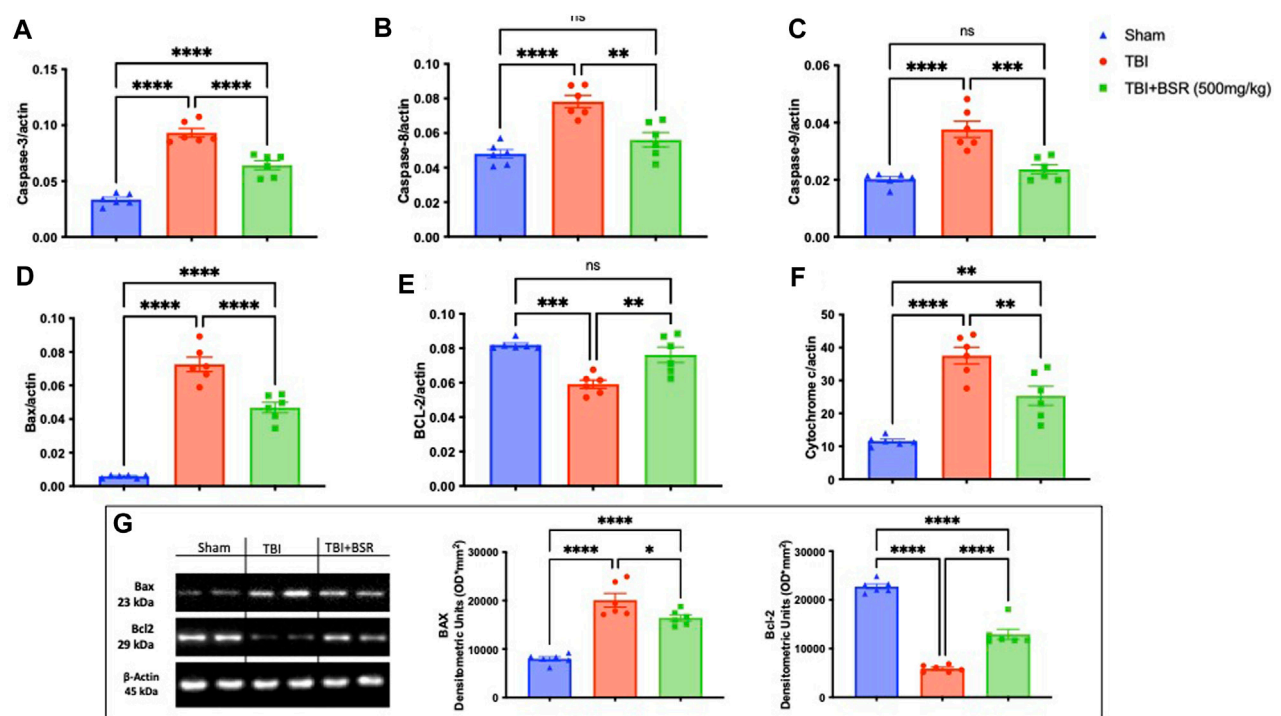
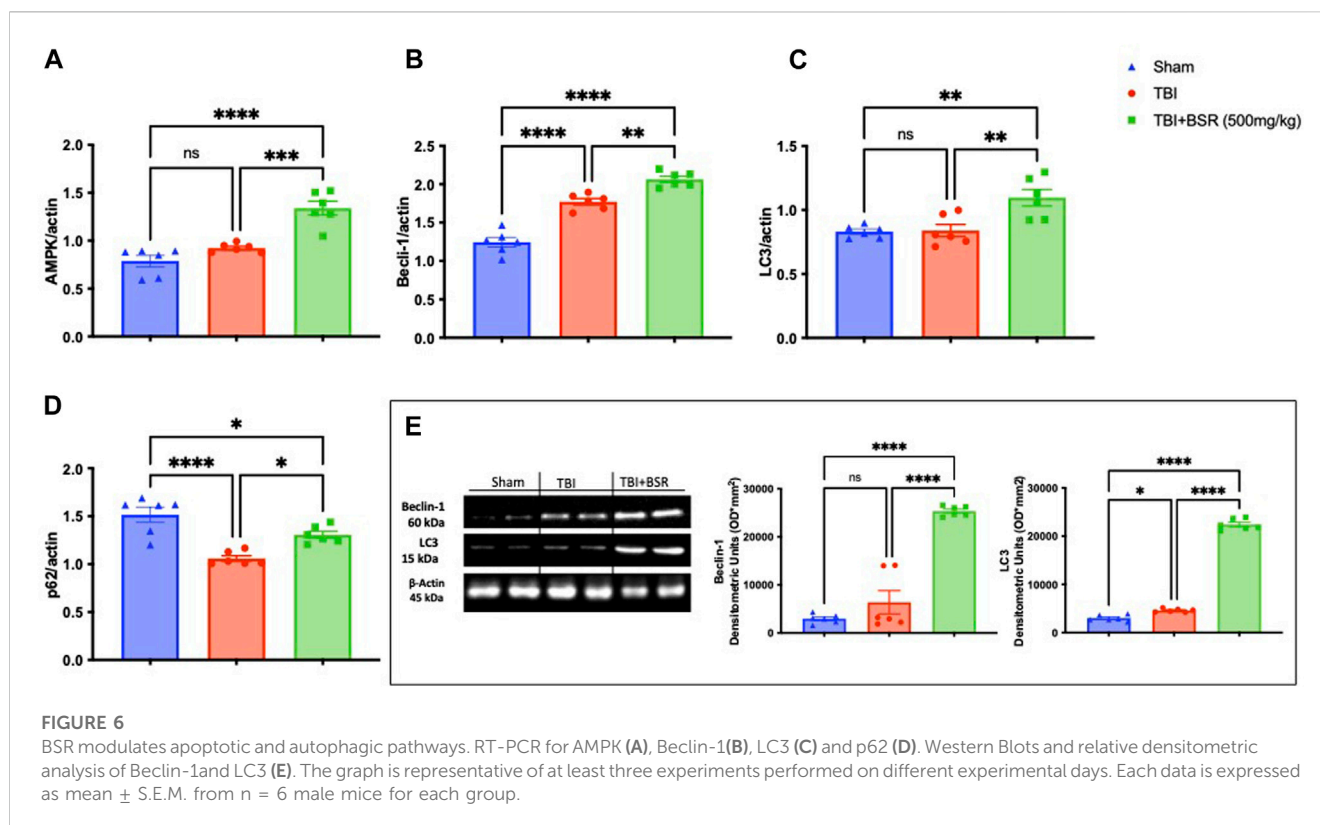


FIGURE 5

BSR reduced apoptosis TBI-induced. RT-PCR for Caspase-3 (A), Caspase-8 (B), Caspase-9 (C), Bax (D), Bcl-2 (E), and Cytochrome C (F); Western Blots and relative densitometric analysis of Bax and BCL-2 (G). The graphs are representative of at least three experiments performed on different experimental days. Each data is expressed as mean \pm S.E.M. from $n = 6$ male mice for each group.



Bcl-2 and Cytochrome C (and obviously in a decrease of Bcl-2) founded in mice subjected to the trauma compared to the control group. After the single administration of BSR we found an important return to the physiological levels of the apoptotic pathway. Numerous and various experimental models of brain injury, including trauma, show increased autophagy (Wang et al., 2013). It is unknown, though, whether autophagy plays a beneficial or harmful function in the recovery of brain-damaged neuronal tissue (Raghupathi, 2004). It is likely that the function of autophagy following brain damage depends on the cell's ability to react to the accumulation of broken or dysfunctional macromolecules and organelles. Enhancing autophagy would probably be advantageous if the increase in autophagic capacity is minimal (Zhang et al., 2005). Although maintaining ATP homeostasis and controlling metabolism are two of AMPK's most well-known jobs, it has recently been suggested that AMPK also controls cell apoptosis or survival under stressful circumstances. Independently of the stimuli, AMPK activation can induce the autophagic process (Villanueva-Paz et al., 2016). Moreover, its well known that the increasing of microtubule-associated protein light chain 3 (LC3)-III and beclin-1, while a decreasing in p62 are autophagy markers demonstrating that autophagic activity is persistently activated after TBI in a controlled cortical impact (CCI) system model of TBI *in vivo* and *in vitro* (Liu et al., 2008; Au et al., 2017; Sebastiani et al., 2017). In our study we found a physiological activation of autophagic flux that were significantly improved after BSR administration as demonstrated by the analysis of AMPK, Beclin-1 and LC3. Additionally, cytoplasmic organoids are ubiquitinated by the adaptor protein p62 before being

transported to the autophagosome and destroyed by the autolysosome. As a result, the downregulation of p62 points to an autophagic flux (Klionsky et al., 2016). According to bibliography, in our work we found a decrease in p62 in the animals subjected to the trauma compared to the control group that were significantly restored after BSR administration at the dose of 500 mg/kg.

5 Conclusion

Acute neuroprotective treatments try to stop the molecular chain reaction that results in damage after TBI. Although neuroprotection is a key strategy for treating this injury, no efficient neuroprotective medications have been discovered from TBI clinical trials to date. However, additional research is required to fully understand the cascade of events that starts with the impact and continues throughout the patient's life. Using natural substances is the only way to completely avoid all the negative effects of pharmacological therapy. Future directions of our research could include testing BSR on many components of trauma that have not yet been considered to see if it can function on several fronts due to the special combination of this molecule.

Data availability statement

The original contributions presented in the study are included in the article/Supplementary Material, further inquiries can be directed to the corresponding author.

Ethics statement

The animal study was approved by the Messina Review Board for animal care (OPBA). The study was conducted in accordance with the local legislation and institutional requirements.

Author contributions

LI: Methodology, Writing-review and editing. YM: Methodology, Writing-original draft. DI: Investigation, Writing-original draft. RD: Investigation, Writing-original draft. RS: Investigation, Writing-original draft. RF: Investigation, Writing-original draft. GC: Formal Analysis, Writing-review and editing. LP: Formal Analysis, Writing-original draft. AA: Formal Analysis, Writing-original draft. TF: Formal Analysis, Writing-original draft. SM: Formal Analysis, Writing-original draft. LR: Formal Analysis, Writing-original draft. SC: Funding acquisition, Resources, Writing-original draft. VC: Funding acquisition, Resources, Writing-original draft. MC: Conceptualization, Writing-original draft. RD: Project administration, Supervision, Writing-review and editing.

Funding

The author(s) declare financial support was received for the research, authorship, and/or publication of this article. This research has been conducted with funds from “Piano di incentivi per la Ricerca, Linea Intervento 2 PIACERI,

2020–2022”, University of Catania, Italy; and Researchers Supporting Project number (RSPD2024R750). King Saud University, Riyadh, Saudi Arabia”.

Conflict of interest

The authors declare that the research was conducted in the absence of any commercial or financial relationships that could be construed as a potential conflict of interest.

The author(s) declared that they were an editorial board member of Frontiers, at the time of submission. This had no impact on the peer review process and the final decision.

Publisher's note

All claims expressed in this article are solely those of the authors and do not necessarily represent those of their affiliated organizations, or those of the publisher, the editors and the reviewers. Any product that may be evaluated in this article, or claim that may be made by its manufacturer, is not guaranteed or endorsed by the publisher.

Supplementary material

The Supplementary Material for this article can be found online at: <https://www.frontiersin.org/articles/10.3389/fphys.2023.1320960/full#supplementary-material>

References

- Ahmad, A., Crupi, R., Campolo, M., Genovese, T., Esposito, E., and Cuzzocrea, S. (2013). Absence of TLR4 reduces neurovascular unit and secondary inflammatory process after traumatic brain injury in mice. *PLoS One* 8 (3), e57208. doi:10.1371/journal.pone.0057208
- Akki, R., Siracusa, R., Morabito, R., Remigante, A., Campolo, M., Errami, M., et al. (2018). Neuronal-like differentiated SH-SY5Y cells adaptation to a mild and transient H(2) O(2) -induced oxidative stress. *Cell. Biochem. Funct.* 36 (2), 56–64. doi:10.1002/cbf.3317
- Al-yahya, A. A. I., and Asad, M. (2020). Repeated 28-DAY oral dose study on Boswellia sacra oleo gum resin extract for testicular toxicity in rats. *J. Ethnopharmacol.* 258, 112890. doi:10.1016/j.jep.2020.112890
- Al-Yahya, A. A. I., Asad, M., Sadaby, A., and Alhussaini, M. S. (2020). Repeat oral dose safety study of standardized methanolic extract of Boswellia sacra oleo gum resin in rats. *Saudi J. Biol. Sci.* 27 (1), 117–123. doi:10.1016/j.sjbs.2019.05.010
- Asad, M., and Alhomoud, M. (2016). Proulcerogenic effect of water extract of Boswellia sacra oleo gum resin in rats. *Pharm. Biol.* 54 (2), 225–230. doi:10.3109/13880209.2015.1028553
- Au, A. K., Aneja, R. K., Bayir, H., Bell, M. J., Janesko-Feldman, K., Kochanek, P. M., et al. (2017). Autophagy biomarkers beclin 1 and p62 are increased in cerebrospinal fluid after traumatic brain injury. *Neurocrit Care* 26 (3), 348–355. doi:10.1007/s12028-016-0351-x
- Bramlett, H. M., and Dietrich, W. D. (2007). Progressive damage after brain and spinal cord injury: pathomechanisms and treatment strategies. *Prog. Brain Res.* 161, 125–141. doi:10.1016/S0079-6123(06)61009-1
- Cammilleri, G., Calabrese, V., Pantano, L., Brunone, M., Galluzzo, F. G., Pulvirenti, A., et al. (2023). Polyphenols of white lupin (*Lupinus albus* L.) seeds cultivated in Southern Italy by a LC-HRMS method. *Nat. Prod. Res.*, 1–5. doi:10.1080/14786419.2023.2245535
- Campolo, M., Crupi, R., Cordaro, M., Cardali, S. M., Ardizzzone, A., Casili, G., et al. (2021). Co-ultra PEALut enhances endogenous repair response following moderate traumatic brain injury. *Int. J. Mol. Sci.* 22 (16), 8717. doi:10.3390/ijms22168717
- Campolo, M., Esposito, E., Ahmad, A., Di Paola, R., Paterniti, I., Cordaro, M., et al. (2014). Hydrogen sulfide-releasing cyclooxygenase inhibitor ATB-346 enhances motor function and reduces cortical lesion volume following traumatic brain injury in mice. *J. Neuroinflammation* 11, 196. doi:10.1186/s12974-014-0196-1
- Cordaro, M., Cuzzocrea, S., and Crupi, R. (2020c). An update of palmitoylethanolamide and luteolin effects in preclinical and clinical studies of neuroinflammatory events. *Antioxidants (Basel)* 9 (3), 216. doi:10.3390/antiox9030216
- Cordaro, M., D'Amico, R., Morabito, R., Fusco, R., Siracusa, R., Peritore, A. F., et al. (2021b). Physiological and biochemical changes in NRF2 pathway in aged animals subjected to brain injury. *Cell. Physiol. Biochem.* 55 (2), 160–179. doi:10.33594/000000353
- Cordaro, M., Fusco, R., D'Amico, R., Siracusa, R., Peritore, A. F., Gugliandolo, E., et al. (2020b). Cashew (*anacardium occidentale* L.) nuts modulate the Nrf2 and NLRP3 pathways in pancreas and lung after induction of acute pancreatitis by cerulein. *Antioxidants (Basel)* 9 (10), 992. doi:10.3390/antiox9100992
- Cordaro, M., Impellizzeri, D., Paterniti, I., Bruschetta, G., Siracusa, R., De Stefano, D., et al. (2016). Neuroprotective effects of Co-UltraPEALut on secondary inflammatory process and autophagy involved in traumatic brain injury. *J. Neurotrauma* 33 (1), 132–146. doi:10.1089/neu.2014.3460
- Cordaro, M., Paterniti, I., Siracusa, R., Impellizzeri, D., Esposito, E., and Cuzzocrea, S. (2017). KU0063794, a dual mTORC1 and mTORC2 inhibitor, reduces neural tissue damage and locomotor impairment after spinal cord injury in mice. *Mol. Neurobiol.* 54 (4), 2415–2427. doi:10.1007/s12035-016-9827-0
- Cordaro, M., Scuto, M., Siracusa, R., D'Amico, R., Filippo Peritore, A., Gugliandolo, E., et al. (2020a). Effect of N-palmitoylethanolamine-oxazoline on comorbid neuropsychiatric disturbance associated with inflammatory bowel disease. *FASEB J.* 34 (3), 4085–4106. doi:10.1096/fj.201901584RR
- Cordaro, M., Siracusa, R., Crupi, R., Impellizzeri, D., Peritore, A. F., D'Amico, R., et al. (2018). 2-Pentadecyl-2-Oxazoline reduces neuroinflammatory environment in the MPTP model of Parkinson disease. *Mol. Neurobiol.* 55 (12), 9251–9266. doi:10.1007/s12035-018-1064-2

- Cordaro, M., Trovato Salinaro, A., Siracusa, R., D'Amico, R., Impellizzeri, D., Scuto, M., et al. (2021a). Hidrox roles in neuroprotection: biochemical links between traumatic brain injury and alzheimer's disease. *Antioxidants (Basel)* 10 (5), 818. doi:10.3390/antiox10050818
- Crupi, R., Cordaro, M., Cuzzocrea, S., and Impellizzeri, D. (2020). Management of traumatic brain injury: from present to future. *Antioxidants (Basel)* 9 (4), 297. doi:10.3390/antiox9040297
- Di Paola, D., Capparucci, F., Lanteri, G., Cordaro, M., Crupi, R., Siracusa, R., et al. (2021b). Combined toxicity of xenobiotics bisphenol A and heavy metals on zebrafish embryos (*Danio rerio*). *Toxics* 9 (12), 344. doi:10.3390/toxics9120344
- Di Paola, D., Iaria, C., Capparucci, F., Cordaro, M., Crupi, R., Siracusa, R., et al. (2021a). Aflatoxin B1 toxicity in zebrafish larva (*Danio rerio*): protective role of hericium erinaceus. *Toxins (Basel)* 13 (10), 710. doi:10.3390/toxins13100710
- Di Paola, R., Cordaro, M., Crupi, R., Siracusa, R., Campolo, M., Bruschetta, G., et al. (2016b). Protective effects of ultramicrozoned palmitoylethanolamide (PEA-um) in myocardial ischemia and reperfusion injury *in vivo*. *Shock* 46 (2), 202–213. doi:10.1097/SHK.0000000000000578
- Di Paola, R., Crisafulli, C., Mazzon, E., Genovese, T., Paterniti, I., Bramanti, P., et al. (2009). Effect of PD98059, a selective MAPK3/MAPK1 inhibitor, on acute lung injury in mice. *Int. J. Immunopathol. Pharmacol.* 22 (4), 937–950. doi:10.1177/039463200902200409
- Di Paola, R., Impellizzeri, D., Fusco, R., Cordaro, M., Siracusa, R., Crupi, R., et al. (2016a). Ultramicrozoned palmitoylethanolamide (PEA-um[®]) in the treatment of idiopathic pulmonary fibrosis. *Pharmacol. Res.* 111, 405–412. doi:10.1016/j.phrs.2016.07.010
- Di Paolo, M., Papi, L., Gori, F., and Turillazzi, E. (2019). Natural products in neurodegenerative diseases: a great promise but an ethical challenge. *Int. J. Mol. Sci.* 20 (20), 5170. doi:10.3390/ijms20205170
- Esposito, E., G. B., et al. (2016). A new co-micronized composite containing palmitoylethanolamide and polydatin shows superior oral efficacy compared to their association in a rat paw model of carrageenan-induced inflammation. *Eur. J. Pharmacol.* 782, 107–118. doi:10.1016/j.ejphar.2016.03.033
- Faden, A. I. (2002). Neuroprotection and traumatic brain injury: theoretical option or realistic proposition. *Curr. Opin. Neurol.* 15 (6), 707–712. doi:10.1097/01.wco.0000044767.39452.bf
- Fusco, R., Gugliandolo, E., Siracusa, R., Scuto, M., Cordaro, M., D'Amico, R., et al. (2020). Formyl peptide receptor 1 signaling in acute inflammation and neural differentiation induced by traumatic brain injury. *Biol. (Basel)* 9 (9), 238. doi:10.3390/biology9090238
- Genovese, T., Impellizzeri, D., D'Amico, R., Fusco, R., Peritore, A. F., Di Paola, D., et al. (2022). Role of bevacizumab on vascular endothelial growth factor in apolipoprotein E deficient mice after traumatic brain injury. *Int. J. Mol. Sci.* 23 (8), 4162. doi:10.3390/ijms23084162
- Genovese, T., Siracusa, R., Fusco, R., D'Amico, R., Impellizzeri, D., Peritore, A. F., et al. (2021). Atrazine inhalation causes neuroinflammation, apoptosis and accelerating brain aging. *Int. J. Mol. Sci.* 22 (15), 7938. doi:10.3390/ijms22157938
- Ghavam, S., Shojaei, S., Yeganeh, B., Ande, S. R., Jangamreddy, J. R., Mehrpour, M., et al. (2014). Autophagy and apoptosis dysfunction in neurodegenerative disorders. *Prog. Neurobiol.* 112, 24–49. doi:10.1016/j.pneurobio.2013.10.004
- Gugliandolo, E., D'Amico, R., Cordaro, M., Fusco, R., Siracusa, R., Crupi, R., et al. (2018). Neuroprotective effect of artesunate in experimental model of traumatic brain injury. *Front. Neurol.* 9, 590. doi:10.3389/fneur.2018.00590
- Hamidpour, R., Hamidpour, S., Hamidpour, M., and Shahleri, M. (2013). Frankincense (*Boswellia* species): from the selection of traditional applications to the novel phytotherapy for the prevention and treatment of serious diseases. *J. Tradit. Complement. Med.* 3 (4), 221–226. doi:10.4103/2225-4110.119723
- Hu, R., Zheng, L., Zhang, T., Gao, G., Cui, Y., Cheng, Z., et al. (2011). Molecular mechanism of hippocampal apoptosis of mice following exposure to titanium dioxide nanoparticles. *J. Hazard Mater* 191 (1–3), 32–40. doi:10.1016/j.jhazmat.2011.04.027
- Impellizzeri, D., Campolo, M., Bruschetta, G., Crupi, R., Cordaro, M., Paterniti, I., et al. (2016b). Traumatic brain injury leads to development of Parkinson's disease related pathology in mice. *Front. Neurosci.* 10, 458. doi:10.3389/fnins.2016.00458
- Impellizzeri, D., Cordaro, M., Bruschetta, G., Crupi, R., Pascali, J., Alfonsi, D., et al. (2016a). 2-pentadecyl-2-oxazoline: identification in coffee, synthesis and activity in a rat model of carrageenan-induced hindpaw inflammation. *Pharmacol. Res.* 108, 23–30. doi:10.1016/j.phrs.2016.04.007
- Impellizzeri, D., Cordaro, M., Bruschetta, G., Siracusa, R., Crupi, R., Esposito, E., et al. (2017). N-Palmitoylethanolamine-Oxazoline as a new therapeutic strategy to control neuroinflammation: neuroprotective effects in experimental models of spinal cord and brain injury. *J. Neurotrauma* 34 (18), 2609–2623. doi:10.1089/neu.2016.4808
- Iram, F., Khan, S. A., and Husain, A. (2017). Phytochemistry and potential therapeutic actions of Boswellia acids: a mini-review. *Asian Pac. J. Trop. Biomed.* 7 (6), 513–523. doi:10.1016/j.apjtb.2017.05.001
- Jarrahi, A., Braun, M., Ahluwalia, M., Gupta, R. V., Wilson, M., Munie, S., et al. (2020). Revisiting traumatic brain injury: from molecular mechanisms to therapeutic interventions. *Biomedicines* 8 (10), 389. doi:10.3390/biomedicines8100389
- Khan, M. A., Ali, R., Parveen, R., Najmi, A. K., and Ahmad, S. (2016). Pharmacological evidences for cytotoxic and antitumor properties of Boswellia acids from Boswellia serrata. *J. Ethnopharmacol.* 191, 315–323. doi:10.1016/j.jep.2016.06.053
- Klionsky, D. J., Abdelmohsen, K., Abe, A., Abedin, M. J., Abeliovich, H., Acevedo Arozena, A., et al. (2016). Guidelines for the use and interpretation of assays for monitoring autophagy (3rd edition). *Autophagy* 12, 1–222. doi:10.1080/15548627.2015.1100356
- Liu, C. L., Chen, S., Dietrich, D., and Hu, B. R. (2008). Changes in autophagy after traumatic brain injury. *J. Cereb. Blood Flow. Metab.* 28 (4), 674–683. doi:10.1038/sj.jcbfm.9600587
- Liu, W., and Saint, D. A. (2002). Validation of a quantitative method for real time PCR kinetics. *Biochem. Biophys. Res. Commun.* 294 (2), 347–353. doi:10.1016/S0006-291X(02)00478-3
- Liu, X., Machado, G. C., Eyles, J. P., Ravi, V., and Hunter, D. J. (2018). Dietary supplements for treating osteoarthritis: a systematic review and meta-analysis. *Br. J. Sports Med.* 52 (3), 167–175. doi:10.1136/bjsports-2016-097333
- Marklund, S., and Marklund, G. (1974). Involvement of the superoxide anion radical in the autoxidation of pyrogallol and a convenient assay for superoxide dismutase. *Eur. J. Biochem.* 47 (3), 469–474. doi:10.1111/j.1432-1033.1974.tb03714.x
- Mojaverrostami, S., Bojnordi, M. N., Ghasemi-Kasman, M., Ebrahimzadeh, M. A., and Hamidabadi, H. G. (2018). A review of herbal therapy in multiple sclerosis. *Adv. Pharm. Bull.* 8 (4), 575–590. doi:10.15171/apb.2018.066
- Ohkawa, H., Ohishi, N., and Yagi, K. (1979). Assay for lipid peroxides in animal tissues by thiobarbituric acid reaction. *Anal. Biochem.* 95 (2), 351–358. doi:10.1016/0003-2697(79)90738-3
- Pan, Z., Cui, M., Dai, G., Yuan, T., Li, Y., Ji, T., et al. (2018). Protective effect of anthocyanin on neurovascular unit in cerebral ischemia/reperfusion injury in rats. *Front. Neurosci.* 12, 947. doi:10.3389/fnins.2018.00947
- Paterniti, I., Campolo, M., Siracusa, R., Cordaro, M., Di Paola, R., Calabrese, V., et al. (2017). Liver X receptors activation, through TO901317 binding, reduces neuroinflammation in Parkinson's disease. *PLoS One* 12 (4), e01. doi:10.1371/journal.pone.0174470
- Paterniti, I., Di Paola, R., Campolo, M., Siracusa, R., Cordaro, M., Bruschetta, G., et al. (2015). Palmitoylethanolamide treatment reduces retinal inflammation in streptozotocin-induced diabetic rats. *Eur. J. Pharmacol.* 769, 313–323. doi:10.1016/j.ejphar.2015.11.035
- Pattingre, S., Tassa, A., Qu, X., Garuti, R., Liang, X. H., Mizushima, N., et al. (2005). Bcl-2 antiapoptotic proteins inhibit Beclin 1-dependent autophagy. *Cell* 122 (6), 927–939. doi:10.1016/j.cell.2005.07.002
- Pellow, S., Chopin, P., File, S. E., and Briley, M. (1985). Validation of open:closed arm entries in an elevated plus-maze as a measure of anxiety in the rat. *J. Neurosci. Methods* 14 (3), 149–167. doi:10.1016/0165-0270(85)90031-7
- Peritore, A. F., Crupi, R., Scuto, M., Gugliandolo, E., Siracusa, R., Impellizzeri, D., et al. (2020). The role of annexin A1 and formyl peptide receptor 2/3 signaling in chronic corticosterone-induced depression-like behaviors and impairment in hippocampal-dependent memory. *CNS Neurol. Disord. Drug Targets* 19 (1), 27–43. doi:10.2174/1871527319666200107094732
- Petrosino, S., Campolo, M., Impellizzeri, D., Paterniti, I., Allarà, M., Gugliandolo, E., et al. (2017). 2-Pentadecyl-2-Oxazoline, the oxazoline of pea, modulates carrageenan-induced acute inflammation. *Front. Pharmacol.* 8, 308. doi:10.3389/fphar.2017.00308
- Porsolt, R. D., Bertin, A., Blavet, N., Deniel, M., and Jalfre, M. (1979). Immobility induced by forced swimming in rats: effects of agents which modify central catecholamine and serotonin activity. *Eur. J. Pharmacol.* 57 (2–3), 201–210. doi:10.1016/0014-2999(79)90366-2
- Prut, L., and Belzung, C. (2003). The open field as a paradigm to measure the effects of drugs on anxiety-like behaviors: a review. *Eur. J. Pharmacol.* 463 (1–3), 3–33. doi:10.1016/S0014-2999(03)01272-X
- Puigventos, L., Navarro, M., Alechaga, É., Núñez, O., Saurina, J., Hernández-Cassou, S., et al. (2015). Determination of polyphenolic profiles by liquid chromatography-electrospray-tandem mass spectrometry for the authentication of fruit extracts. *Anal. Bioanal. Chem.* 407 (2), 597–608. doi:10.1007/s00216-014-8298-2
- Raghupathi, R. (2004). Cell death mechanisms following traumatic brain injury. *Brain Pathol.* 14 (2), 215–222. doi:10.1111/j.1750-3639.2004.tb00056.x
- Rajasankar, S., Manivasagam, T., and Surendran, S. (2009). Ashwagandha leaf extract: a potential agent in treating oxidative damage and physiological abnormalities seen in a mouse model of Parkinson's disease. *Neurosci. Lett.* 454 (1), 11–15. doi:10.1016/j.neulet.2009.02.044
- Ramlackhansingh, A. F., Brooks, D. J., Greenwood, R. J., Bose, S. K., Turkheimer, F. E., Kinnunen, K. M., et al. (2011). Inflammation after trauma: microglial activation and traumatic brain injury. *Ann. Neurol.* 70 (3), 374–383. doi:10.1002/ana.22455
- Remigante, A., Spinelli, S., Straface, E., Gambardella, L., Caruso, D., Falliti, G., et al. (2022). Açai (*Euterpe oleracea*) extract protects human erythrocytes from age-related oxidative stress. *Cells* 11 (15), 2391. doi:10.3390/cells11152391

- Schmiech, M., Lang, S. J., Werner, K., Rashan, L. J., Syrovets, T., and Simmet, T. (2019). Comparative analysis of pentacyclic triterpenic acid compositions in oleogum resins of different boswellia species and their *in vitro* cytotoxicity against treatment-resistant human breast cancer cells. *Molecules* 24 (11), 2153. doi:10.3390/molecules24112153
- Schoch, K. M., Madathil, S. K., and Saatman, K. E. (2012). Genetic manipulation of cell death and neuroplasticity pathways in traumatic brain injury. *Neurotherapeutics* 9 (2), 323–337. doi:10.1007/s13311-012-0107-z
- Sebastiani, A., Gözl, C., Sebastiani, P. G., Bobkiewicz, W., Behl, C., Mittmann, T., et al. (2017). Sequestosome 1 deficiency delays, but does not prevent brain damage formation following acute brain injury in adult mice. *Front. Neurosci.* 11, 678. doi:10.3389/fnins.2017.00678
- Shadfar, S., Khanal, S., Bohara, G., Kim, G., Sadigh-Eteghad, S., Ghavami, S., et al. (2022). Methanolic extract of boswellia serrata gum protects the nigral dopaminergic neurons from rotenone-induced neurotoxicity. *Mol. Neurobiol.* 59 (9), 5874–5890. doi:10.1007/s12035-022-02943-y
- Siebold, L., Krueger, A. C., Abdala, J. A., Figueroa, J. D., Bartnik-Olson, B., Holshouser, B., et al. (2020). Cosyntropin attenuates neuroinflammation in a mouse model of traumatic brain injury. *Front. Mol. Neurosci.* 13, 109. doi:10.3389/fnmol.2020.00109
- Siracusa, R., Impellizzeri, D., Cordaro, M., Crupi, R., Esposito, E., Petrosino, S., et al. (2017). Anti-inflammatory and neuroprotective effects of Co-UltraPEALut in a mouse model of vascular dementia. *Front. Neurol.* 8, 233. doi:10.3389/fneur.2017.00233
- Siracusa, R., Paterniti, I., Cordaro, M., Crupi, R., Bruschetta, G., Campolo, M., et al. (2018). Neuroprotective effects of temsirolimus in animal models of Parkinson's disease. *Mol. Neurobiol.* 55 (3), 2403–2419. doi:10.1007/s12035-017-0496-4
- Slemmer, J. E., Shacka, J. J., Sweeney, M. I., and Weber, J. T. (2008). Antioxidants and free radical scavengers for the treatment of stroke, traumatic brain injury and aging. *Curr. Med. Chem.* 15 (4), 404–414. doi:10.2174/092986708783497337
- Smith, F. M., Raghupathi, R., MacKinnon, M. A., McIntosh, T. K., Saatman, K. E., Meaney, D. F., et al. (2000). TUNEL-positive staining of surface contusions after fatal head injury in man. *Acta Neuropathol.* 100 (5), 537–545. doi:10.1007/s004010000222
- Stacchiotti, A., and Corsetti, G. (2020). Natural compounds and autophagy: allies against neurodegeneration. *Front. Cell. Dev. Biol.* 8, 555409. doi:10.3389/fcell.2020.555409
- Stoica, B. A., and Faden, A. I. (2010). Cell death mechanisms and modulation in traumatic brain injury. *Neurotherapeutics* 7 (1), 3–12. doi:10.1016/j.nurt.2009.10.023
- Villanueva-Paz, M., Cotán, D., Garrido-Maraver, J., Oropesa-Ávila, M., de la Mata, M., Delgado-Pavón, A., et al. (2016). AMPK regulation of cell growth, apoptosis, autophagy, and bioenergetics. *Exp. Suppl.* 107, 45–71. doi:10.1007/978-3-319-43589-3_3
- Wang, P., Zhou, X., Cui, D., Ouyang, T., Chen, W., et al. (2022). A single bout of exhaustive treadmill exercise increased AMPK activation associated with enhanced autophagy in mice skeletal muscle. *Clin. Exp. Pharmacol. Physiol.* 49 (4), 536–543. doi:10.1111/1440-1681.13632
- Wang, Y. J., Huang, L. Q., Jiang, C., and Shen, Y. (2013). Cloning and bioinformatics analysis of chorismate mutase gene from *Salvia miltiorrhiza*. *Zhongguo Zhong Yao Za Zhi* 38 (11), 1697–1702.
- Wu, J., and Lipinski, M. M. (2019). Autophagy in neurotrauma: good, bad, or dysregulated. *Cells* 8 (7), 693. doi:10.3390/cells8070693
- Ze, Y., Hu, R., Wang, X., Sang, X., Ze, X., Li, B., et al. (2014). Neurotoxicity and gene-expressed profile in brain-injured mice caused by exposure to titanium dioxide nanoparticles. *J. Biomed. Mater. Res. A* 102 (2), 470–478. doi:10.1002/jbm.a.34705
- Zeng, Z., Zhang, Y., Jiang, W., He, L., and Qu, H. (2020). Modulation of autophagy in traumatic brain injury. *J. Cell. Physiol.* 235 (3), 1973–1985. doi:10.1002/jcp.29173
- Zhang, M., Shan, H., Chang, P., Wang, T., Dong, W., Chen, X., et al. (2014). Hydrogen sulfide offers neuroprotection on traumatic brain injury in parallel with reduced apoptosis and autophagy in mice. *PLoS One* 9 (1), e87241. doi:10.1371/journal.pone.0087241
- Zhang, X., Chen, Y., Jenkins, L. W., Kochanek, P. M., and Clark, R. S. B. (2005). Bench-to-bedside review: apoptosis/programmed cell death triggered by traumatic brain injury. *Crit. Care* 9 (1), 66–75. doi:10.1186/cc2950
- Zhao, P., Zhou, R., Zhu, X. Y., Liu, G., Zhao, Y. P., Ma, P. S., et al. (2017). Neuroprotective effects of lycium barbarum polysaccharide on focal cerebral ischemic injury in mice. *Neurochem. Res.* 42 (10), 2798–2813. doi:10.1007/s11064-017-2293-x

Frontiers in Physiology

Understanding how an organism's components work together to maintain a healthy state

The second most-cited physiology journal, promoting a multidisciplinary approach to the physiology of living systems - from the subcellular and molecular domains to the intact organism and its interaction with the environment.

Discover the latest Research Topics

[See more →](#)

Frontiers

Avenue du Tribunal-Fédéral 34
1005 Lausanne, Switzerland
frontiersin.org

Contact us

+41 (0)21 510 17 00
frontiersin.org/about/contact

